Studies of viral and cellular proteins involved in herpes simplex virus type-1 egress

Md Firoz Ahmed

This dissertation is submitted for

the degree of Doctor of Philosophy at

the University of Cambridge

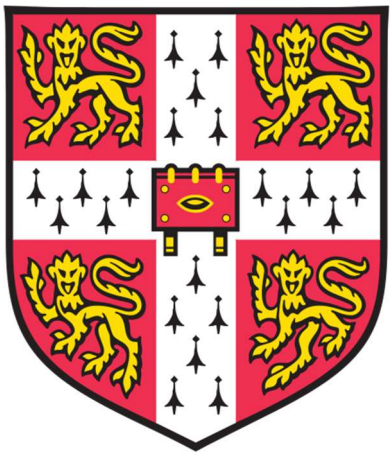

Hughes Hall

August 2018

This thesis is dedicated to my parents

late MD BADRUL ISLAM and

MOST MOMENA KHATUN

Table of contents

Declaration

This dissertation is the result of my own work and includes nothing which is the outcome of work done in collaboration except where specifically mentioned in the text. This thesis contains approximately 50,000 words and 95 figures.

August 2018 Md Firoz Ahmed

Acknowledgements

First and foremost, I would like to thank my supervisor Dr. Colin Crump for allowing me as a PhD student in his lab. Colin has always been very supportive and guided me throughout the whole time both for research and personal hard times. Without his care, inspiration and innovative ideas I would have been lost in the infinity.

Furthermore, I would like to thank all the past and present members of the Crump lab as well as the Virology division. Many of you helped me during my difficult and crucial moments of my research. Others provided me knowledge on their culture, different ways of looking at life and ideas about innovative future. Anna, Gareth, Lucy, Aminu, Luca, Fred, Ed, Myra, Mike G, Mike N, Tim, Sophia, Selina, Sabastine thank you all guys! Thanks to Heather for her technical knowledge in many things, Viv and Susanna for continuous supply of various cell lines over the past four years. Big thanks to Daniel and Rintaro for teaching me some important research techniques. Special thanks to Laura for being always very kind and supportive throughout my PhD.

I would also like to thank Dr. Stephen Graham, my mentor for his feedback on when to stop and what to plan next. I enjoyed the joined lab meeting sessions with Rupert Beale's and Michael Weekes' lab on Monday morning (!) and also some random meetings with the Graham group.

My dad had always been the source of my confidence in reaching my targets, he used to say "I know you can do it", and my mom has always been my 'dream-maker'. I came this far in life considering those two things as my asset but unfortunately, I lost my dad last year. I will never have the chance to share thousands of stories I saved for him over the past four years, I won't able to explain how much it takes to do a PhD and I will never be able to say "Thank you" Abba (dad) I did it because you thought I could do it. I am thankful to my mom for bringing me into existence, shaping and guiding me, and dreaming about me and my future.

A BIG THANKS to my wife Dr. Nusrat Jahan my soul-mate and soon-to-be-mom of our upcoming son (Nashwan Wariyaan Ahmed). Living in a foreign country would never had been so easy without a supportive partner like her. She also had a tough time as she lost her mother a month after I lost my dad. Beside all her hard times she tried to ease my stresses with her sweet smile and love.

Lastly, I would like to thank my funding body the Commonwealth Scholarship Commissions in the UK.

Abstract

The egress pathway of herpes simplex virus-1 (HSV-1) is a complicated process mediated by co-ordinated activity of several virus glycoproteins. The virions are first assembled and enveloped at trans-Golgi-network (TGN) or endosome membranes and then travel through a guided pathway that is directed towards the cell adherent points for secretion. Once secreted the vast majority of virions remain associated with the extracellular membrane of cells and very few free virions are released into the culture medium (<1%). The mechanisms that mediate both the targeted secretion of newly assembled virions at cell contact points and post-secretion attachment of virions with the extracellular surface of cells are poorly understood, and were the topics of this research.

In this thesis, an HSV-1 passage mutant of increased virion secretion phenotype had been studied. Genome sequencing of the mutant virus identified mutations in three viral envelope proteins. Study of recombinant viruses that were constructed based on those three mutations revealed that a single amino acid change in glycoprotein I (gI) of glycine to arginine at residue 39 is responsible for the increased release of virus. The result suggests the principal effect of this mutation is to modify the secretory pathway used by virions during their release from infected cells. Data also suggests a role of gC in the attachment of virions to the extracellular surface of cells after egress.

In the context of HSV-1 envelopment and egress glycoprotein E (gE), which forms a heterodimeric complex with gI (gE/gI), is known to be important. The gE/gI complex has been shown to interact with many tegument proteins and have a redundant role in secondary envelopment. The gE/gI complex has been also proposed to colocalise with various cellular components and sort the nascent virions to cell contact points. However, there is little understanding of the cellular proteins that gE/gI interact with, or the mechanisms that mediate targeted secretion of virions. This research has identified a novel interactome of gE/gI by mass-spectrometric analysis utilising stable isotope labelling with amino acids in cell culture (SILAC) medium. Among the cellular interactome obtained, Nipsnap1 was validated by co-precipitation assays from both infected and transfected cells, and furthermore using cell free systems, suggesting gE and Nipsnap1 directly interact. Nipsnap1 and its homologue Nipsnap2 have been proposed to contribute in vesicle transport and membrane fusion in cells. Using CRISPR-Cas9 technology these proteins were knocked out in a keratinocyte cell line (HaCaT)

to investigate their role in HSV-1 egress. However, little or no effect on HSV-1 egress could be observed upon loss of either or both of these proteins suggesting the biological significance of gE-Nipsnap1 interaction may not be directly linked to any egress function of gE/gI. Two further interesting 'hits' from the gE/gI interactome were interferon-induced transmembrane protein type-2 (IFITM2), a virus restriction factor, and Myoferlin that has a putative role in endocytic vesicle recycling. This study could validate gE-Myoferlin interaction and co-localisation in infected or transfected cells however, functional significance of this interaction remains to be determined.

Overall, the research of this thesis has provided a better understanding of the role of the gE/gI complex in HSV-1 egress and investigated the role of some interesting cellular proteins in the context of virion egress.

Abbreviations

ACV	Acyclovir
APP	Amyloid precursor proteins
ASFV	African swine fever virus
BAC	Bacterial artificial chromosome
CA	Cell-associated
CAM	Chloramphenicol
Cas9	CRISPR associated protein 9
Cav-1	Caveolin 1
COP	Coat protein (e.g., COPI, COPII)
CRISPR	Clustered Regularly Interspaced Short Palindromic Repeats
CT	C terminus
CVSC	Capsid vertex specific component
DAB	Diaminobenzidine
DAPI	4,6-diamidino-2-phenylindole
DMSO	dimethyl sulphoxide
DNA	Deoxyribonucleic acid
DTT	Dithiothreitol
Dyn-2	Dynamin 2
DYSF	Dysferlin
E. coli	*Escherichia coli*
E/β	Early (gene)
EBV	Epstein-barr virus
EE	Early endosome
EGFR	Epidermal growth factor receptor
ER	Endoplasmic reticulum
ESCRT	Endosomal sorting complexes required for transport
EXPH5	Exophilin 5
EYFP	Enhanced yellow fluorescent protein
FDA	Food and Drug Administration
Fer	Ferlin
FHV	Feline Herpes Virus
g	Glycoprotein (e.g., gE, gI, gD)

GAG	Glycosaminoglycan
GFP	Green fluorescent protein
GST	Glutathione S-transferase
h pi/hpi	Hour post infection
h/ hr	Hours
HCF	Host cell factor
HCMV/HHV-5	Human cytomegalovirus/ human herpesvirus 5
HCV	Hepatitis C virus
HHV	Human herpesvirus
HSV	Herpes simplex virus
HVEM	Herpesvirus entry mediator
ICP	Infected cell protein
IE/α	Immediate early (gene)
IFITM	Interferon induced transmembrane
IGFR-1	Insulin growth factor receptor-1
IgG	Immunoglobulin G
IL-	Interleukin (e.g., IL-6)
INM	Inner nuclear membrane
IP	Immunoprecipitation
KAN	Kanamycin
KDa	Kilo-Dalton
KSHV/HHV-8	Kaposi's sarcoma-associated virus/human herpesvirus-8
L/γ	Late (gene)
lacZ	β-galactosidase gene
LAMP1	Lysosome-associated membrane glycoprotein 1
LE	Late endosome
LPS	Lipopolysaccharides
LYS	Lysis (buffer)
MAb	Monoclonal antibody
MBV	Multivesicular bodies
MOI	Multiplicity of infection
MQW	Milli-Q water (ultrapure water)
mRNA	Messenger RNA
MS	Mass spectrometry
MTOC	Microtubule organising centre

MW	Molecular weight
MYOF	Myoferlin
NEC	Nuclear egress complex
NEU	Neutralisation (buffer)
NF-κB	Nuclear factor-kappa B
NGS	Next generation sequencing
NHEJ	Non-homologous end joining
nm	Nanometre
NPC	Nuclear pore complex
NST	Nocistatin
NT	N terminus
oHSV	Oncolytic HSV
ONM	Outer nuclear membrane
OTOF	Otoferlin
PACS-1	Phosphofurin acidic cluster sorting protein 1
PBS	Phosphate-buffer saline
PCR	Polymerase chain reaction
PFU	Plaque-forming unit
PKC	Protein kinase C
PKD	Protein kinase D
PM	Plasma membrane
PRR	Pattern recognition receptor
PrV	Pseudorabies virus
RES	Resuspension (buffer)
RNA	Ribonucleic acid
RNAP II	RNA polymerase II
RVFV	Rift Valley fever virus
SDS-PAGE	Sodium dodecyl sulfate polyacrylamide gel electrophoresis
SH3	Src (Sarcoma) homology 3
SILAC	S isotope labelling by/with amino acids in cell culture
siRNA	Small interfering RNA
SNAP	SyNaptosomal associated protein
SNARE	Soluble NSF(N-ethylmaleimide-sensitive factor) attachment protein receptor
STYL4	Synaptotagmin-like protein 4

Sup	Supernatant
Syts	Synaptotagmins
TEM	Transmission electron microscopy
TGN	*trans*-Golgi network
TRPV-6	Transient receptor potential vanilloid channel 6
UL or US	Unique long or unique short
VEGFR	Vascular endothelial growth factor receptor
vhs	Virion host shut-off
VP	Virion polypeptide
VSV	Vesicular stomatitis virus
VZV	Varicella-zoster virus
WT	Wild type
ZO-1	Zonula Occludens-1
γ1	Leaky-late
γ2	True-late

List of figures

Chapter 1

Chapter 2

Chapter 7

Chapter 8

Chapter 9

List of tables

1. Introduction

1.1 Introduction to the *Herpesviridae*

Herpesviridae is a large family of DNA viruses that contain pathogens of a wide range of hosts including humans. The members of this family are commonly known as herpesviruses.

1.1.1 Classification

Herpesviruses are structurally complex DNA viruses that belong to the family *Herpesviridae*, which is further subdivided into alpha- (α), beta- (β) and gamma- (γ) *Herpesvirinae* subfamilies (Minson et al., 2000). There are nine known human herpes viruses (HHV) (Table 1.1) and they share common structural features (Strauss and Strauss, 2008). All of them bear a large double-stranded linear DNA within an icosahedral capsid which is surrounded by a lipid bilayer membrane. Primary infection by these viruses usually occurs in childhood with mild symptoms (e.g. fever and rash) to no symptoms at all. Subsequently, the virus becomes latent in specific cell types (e.g. neurons of the sensory nervous system for human alphaherpesviruses) and can be reactivated to produce recurrent disease.

1.1.2 Important biological properties

Members of the family *Herpesviridae* share four important biological properties; (i) They express various enzymes (e.g. thymidine kinase) important for metabolism of nucleic acid, synthesis of DNA (e.g. DNA helicase/primase) and protein processing (e.g. protein kinases), (ii) The viral genome is synthesised and the capsid is assembled in the nucleus whereas the envelope is obtained in the cytoplasm, (iii) During a productive lytic infection cycle they destroy the infected cell, and (iv) They are capable of establishing latent infections in their hosts and can become reactivated in response to cellular stresses.

1.1.3 *Alphaherpesvirinae* subfamily

The *Alphaherpesvirinae* comprises of three human viruses; HSV-1, HSV-2 and VZV. Although genetically very different, HSV-1 and HSV-2 are able to cause similar disease symptoms in humans, for example cold sores, genital infection, keratoconjunctivitis, and encephalitis. VZV on the other hand primarily causes chickenpox during primary infection and shingles upon reactivation. Pseudorabies virus (PrV) is another alphaherpesvirus that causes disease in pigs and has been extensively researched.

Table 1.1 | Characteristics of the human herpesviruses

Sub-Family	Example	Pathology	Trans-Mission	Target Cells
Alpha (α)				
HHV-1	Herpes simplex virus-1 (HSV-1)	Oral herpes, genital herpes, keratitis, encephalitis, gingivostomatitis etc	Oral or sexual	Infect mucosal epithelial cells Latent in neurons
HHV-2	Herpes simplex virus-2 (HSV-2)	Genital herpes, may cause oral herpes	Oral or sexual	
HHV-3	Varicella-zoster virus (VZV)	Chickenpox and shingles	Respiratory	
Beta (β)				
HHV-5	Human cytomegalovirus (HCMV)	Congenital cytomegalovirus infection may cause hepatosplenomegaly, rash, retinitis and central nervous system damage. Life threatening to immunocompromised patients	Saliva, urine, breast milk	Infect various cell types e.g., epithelial cells, endothelial cells, smooth muscle cells and fibroblasts Latent in Monocytes
HHV-6A	Roseolovirus	Roseola	Saliva or respiratory	Infect and latent in T-cells
HHV-6B	Roseolovirus			
HHV-7	Roseolovirus			
Gamma (γ)				
HHV-4	Epstein-Barr virus (EBV)	Infectious mononucleosis. Associated with Burkitt's lymphoma, Hodgkin disease, nasopharyngeal carcinoma	Saliva, transfusion, tissue transplantation	Infect epithelial cells and B cells Latent in B cells
HHV-8	Kaposi's sarcoma-associated herpesvirus (KSHV)	Kaposi's sarcoma, effusion lymphoma	Sexual contact, saliva	Infect lymphocyte and other tissue Latent in B cells

1.1.4 *Betaherpesvirinae* subfamily

This group includes the human viruses; HCMV, HHV-6A, HHV-6B and HHV-7. HCMV is well studied as it is a significant problem in immunocompromised and organ transplant patients, and in infants. Murid herpesvirus 1 (murine CMV) is studied as a model for HCMV infection. HHV-6A is associated with neuroinflammatory disease patients and may also cause roseola whereas HHV-6B is the cause of common childhood illness roseola infantum (high fever and pink rash). Although less frequent HHV-7 causes a similar kind of disease condition in children like HHV-6B.

1.1.5 *Gammaherpesvirinae* subfamily

Among the gammaherpesviruses EBV (causes Burkitt's lymphoma and infectious mononucleosis) and KSHV (causes Kaposi's sarcoma) are the best studied viruses in this group. These viruses can induce lymphoproliferative diseases, and tumours, and can remain latent in lymphocytes. Because of the similarities in viral structure, infectivity and latency, Murid herpesvirus 4 is often used as a model system to study genetics of KSHV.

1.2 Human herpes virus-1 (HHV-1)

1.2.1 Disease, treatment and therapeutic potential of HSV-1

HHV-1, commonly known as herpes simplex virus 1 (HSV-1), is a highly contagious host-adapted pathogen that causes a wide variety of disease conditions in human. The virus is transmitted by direct human to human contact and about 30-100% of the adult population aged over 20 is seropositive for HSV-1 (reviewed in Cunningham et al., 2006). The virus primarily causes cold sores and occasionally genital herpes. However, it may lead to more severe disease conditions like encephalitis or keratitis in some cases. An infected individual can shed the virus through body secretions such as tears, saliva, and genital fluids (Beauman, 2005), and direct contact of the infected body part or fluid of active lesions promotes virion transmission. Humans are the only known hosts for HSV-1 and depending on virus strain, virus entry site and host immune response, HSV-1 infection can be mild/asymptotic to life-threatening. HSV-

1 like most other herpes viruses of the α-subfamily can establish latency in sensory ganglia and cause lifelong infection in its host (Shukla and Spear, 2001).

Although treatment can lessen disease symptoms there is no cure for HSV. Currently acyclovir (ACV) or its derivatives are used to target viral DNA replication, however these drugs are ineffective in clearing latent infections. Other drugs like cidofovir or foscarnet can be used to treat HSV infections but these drugs frequently exhibit severe toxicity towards host cells hence are the second line of therapeutic options. Unfortunately, there is a growing problem of ACV resistance and this together with increasing numbers of immunocompromised patients worldwide warrants continued research to aid the development of effective and safe drugs against HSV.

Interestingly, HSV can be modified for therapeutic purposes. First of all, HSV has a cytolytic life cycle in the majority of cells infected by this virus, although while it can infect a variety of human cells infections are usually self-limiting. Additionally, the non-essential genes of HSV-1 can be replaced either to increase cytolytic potential, and/or to modify its envelope glycoproteins to alter cell tropism (Sanchala et al., 2017). This has allowed the generation of oncolytic HSV (oHSV) capable of eliminating target cancer cells. Recently, talimogene laherparepvec (T-VEC) an engineered HSV has been approved as the world's first oncolytic viro-therapeutic agent for the treatment of melanoma by the US Food and Drug Administration (FDA) (Killock, 2015; Johnson et al., 2015).

1.2.2 HSV-1 structure

A mature HSV-1 virion is approximately 175-225 nm in diameter and composed of four characteristic components; the core, capsid, tegument and envelope (Figure 1.1) (Grunewald et al., 2003). Viral DNA is contained in the core protected in an icosahedral capsid, with DNA-filled capsids generally referred to as nucleocapsids. The nucleocapsid is then surrounded by tegument proteins and finally wrapped by a phospholipid bilayer envelope. Individual virions are also thought to carry some viral and cellular messenger RNAs (mRNAs) and various cellular proteins that help viral replication and transport process (Loret et al., 2008; Sciortino et al., 2002; Stegen et al., 2013). The essential stages of the virus life cycle: attachment, entry, spread and egress are controlled by the proteins found in the viral capsid, teguments and envelope (Table 1.2).

HSV-1 can be grown in many standard mammalian cell types in culture and is easily titred as plaque-forming units (PFU) on cell culture monolayers. The particle-to-PFU ratio for wild type HSV-1 is commonly around 10:1, although this can vary due to differences in virus preparation (Brown and MacLean, 1998; Harland and Brown, 1998; Watson et al., 1963). Beside producing infectious virions during an HSV-1 infection many particles are released as defective virions due to damage or inappropriate virus maturation, lysis of cells before morphogenesis is complete, or as light particles. Light particles do not contain a capsid or virus DNA but are tegument proteins wrapped in a membrane and hence unable to cause infection (Dargan and Subak-Sharpe, 1997). However, light particles could function in the delivery of tegument and envelope proteins to surrounding cells to induce or suppress host responses.

Table 1.2 | List of proteins that are found in different layers of the HSV-1 particle

Capsid	Tegument	Envelope
pUL6, pUL17, pUL18 (VP23), pUL19 (VP5), VP24, pUL25, pUL35 (VP26), pUL38 (VP19c)	pUL7, pUL11, pUL13 (VP18.8), pUL14, pUL16, pUL21, pUL23 (TK), pUL36 (VP1/2), pUL37, pUL41 (vhs), pUL46 (VP11/12), pUL47 (VP13/14), pUL48 (VP16), pUL49 (VP22), pUL50, pUL51, pUL55, ICP0, ICP4, ICP34.5, pUS2, pUS3, pUS10, pUS11	pUL1 (gL), pUL10 (gM), pUL20, pUL22 (gH), pUL27 (gB), pUL43, pUL44 (gC), pUL45, pUL49.5 (gN) pUL53 (gK), pUL56, pUS4 (gG), pUS5 (gJ), pUS6 (gD), pUS7 (gI), pUS8 (gE), pUS9

1.2.2.1 The core

The HSV-1 core consists of a single piece of double stranded DNA (Figure 1.1 c). The DNA is linear, ~152 kb long with ~68% G+C content and has unique long (UL) and unique short (US) regions flanked by terminal and internal repeats (Roizman et al., 1979, Sheldrick and Berthelot, 1975). The genome of HSV-1 encodes over 80 protein-coding open reading frames of which ~65 genes are contained with the UL and ~15 genes are contained within the US region (Roizman et al., 2013).

1.2.2.2 The capsid

The capsid of HSV-1 is 15 nm thick, 125 nm in diameter and is composed of 162 capsomers arranged in a T = 16 icosahedral symmetry (Newcomb et al., 1993; Schrag et al., 1989). Mature capsids are composed of eight proteins; VP5, VP19C, VP23, VP24, VP26, pUL6, pUL17, and pUL25 (Newcomb et al., 2001). VP5 is the major capsid protein (955 copies per virion) and makes up both the 150 hexons and 11 of the 12 penton capsomers. VP26 is also found in great numbers (900 copies per virion) and is located at the distal hexon tips in the capsid. VP19c and VP23 are found in triplexes whereas pUL17 and pUL25 form a complex found near pentons on capsids (often referred to as the capsid-vertex specific component (CVSC). Twelve copies of pUL6 form a ring at a unique vertex in the capsid for DNA entry and exit. VP24 is a protease that initially forms part of the capsid scaffold and plays a role during DNA encapsidation (Sheaffer et al., 2000).

1.2.2.3 The tegument

The HSV-1 tegument is asymmetrical in structure and can be viewed as more capsid-associated inner tegument and less capsid-associated outer tegument. Proteins found in the tegument can act immediately after the initiation of infection and before expression of any viral gene. At least 24 virus-encoded tegument proteins are recruited into HSV-1 virions and they play various roles during the virus life cycle (Loret et al., 2008). Tegument proteins are added to the virion both in the nucleus and cytoplasm (Bucks et al., 2007; Read et al., 2007; Mettenleiter, 2002 and 2004,). Other than pUS3, VP1/2, pUL37, ICP0 and ICP4 tegument proteins, the rest are considered as outer tegument proteins (Delboy and Nicola, 2011; Loret and Lippé, 2012; Reynolds et al., 2002). However, little is known about the structure of the tegument and location of specific proteins within this complex structural domain, although super-resolution microscopy studies have begun to shed light on this (Laine et al., 2015). The tegument proteins shown to be present in HSV-1 particles are listed in Table 1.2.

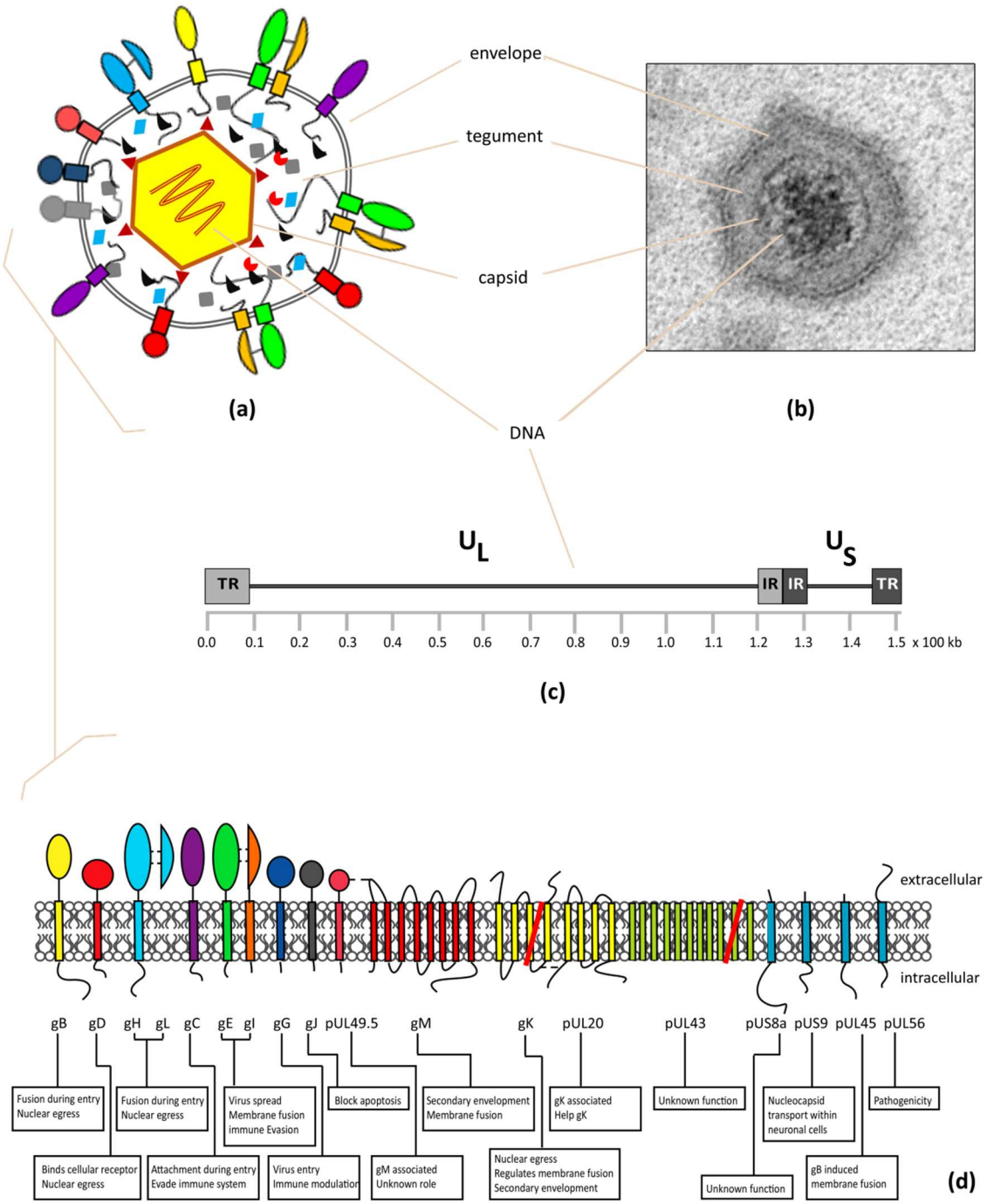

Figure 1.1 | HSV-1 virion morphology, genome and envelope proteins. (a) Structure of the HSV-1 virion as shown by a schematic diagram, (b) transmission electron microscopy (TEM) image of a virion, (c) HSV-1 genome with unique long (UL) and unique short region flanked by terminal repeat (TR) and internal repeat (IR) regions and (d) HSV-1 membrane proteins with known and putative functions. The transmembrane domains are predicted regions. For gK either three or four transmembrane domains and for pUL43 either ten or eleven transmembrane domains have been predicted. Dotted lines indicate membrane protein interactions.

1.2.2.4 The envelope

The HSV-1 tegument coated nucleocapsid is enclosed by a host cell membrane derived, viral glycoprotein (g) bearing envelope. Within the envelope at least 13 virus-encoded proteins including gB, gC, gD, gE, gH, gI, gJ, gK, gG, gL and gM have been identified (Figure 1.1 d) (Loret et al., 2008; Mettenleiter, 2004). The life cycle of HSV-1 depends on proper functioning of its envelope glycoproteins (Spear and Longnecker, 2003; Mettenleiter, 2002 and 2004). Some of those glycoproteins (gB, gD and gH/L that are the core entry factors) are essential while others are non-essential (Cai et al., 1988; Ligas and Johnson, 1988; Forrester et al., 1992; Roop et al., 1993). To cause infection HSV-1 must bind to specific receptors on the cell to enter. Deletion of any of the essential glycoproteins from the virus inhibits its entry in to the cell therefore, the incorporation of these glycoproteins on to naïve virions is important. On the other hand, deletion of some non-essential glycoproteins can cause a delay in virus entry, envelopment or egress and can alter the pathway of virion secretion. Therefore, a balanced co-ordination between essential and non-essential glycoproteins is expected to play a critical role during the virus life cycle. Some of the published functions of individual envelope proteins are shown in Figure 1.1.

1.2.2.5 Significance of envelope glycoproteins in HSV-1 life cycle

HSV-1 envelope glycoproteins contribute to various aspect of the virus life cycle, with many of them having multiple functions. The currently known and proposed functions of the glycoproteins are listed on Table 1.3, although new functions will undoubtedly come to light with current and future research.

Table 1.3 | Summary of known and predicted functions of HSV-1 envelope glycoproteins

Glycoprotein (encoding gene)	Known or predicted function(s)	References
gB (UL27)	Virion attachment Fusion of viral and cellular membranes Nuclear egress Syncytia formation (with gK)	Eisenberg et al., 2012; Wisner et al., 2009; Melancon et al., 2005
gC (UL44)	Virion attachment Prevention of complement-mediated cell lysis and virus neutralisation	Herold et al., 1991; Yeh et al., 2011
gD (US6)	Virus entry Inhibits apoptosis Nuclear egress	Eisenberg et al., 2012; Zhou et al., 2003
gE (US8)	gI associated Virion envelopment Directional transport of virion Regulate membrane fusion Evasion of host immune system by utilising its FcR, located in the ectodomain when in complex with gI	Dingwell and Johnson, 1998; Howard et al., 2013; Ndjamen et al., 2014
gG (US4)	Virion entry Bind to chemokines (CC and CXC) and modulate their function	Tran et al., 2000; Viejo-Borbolla et al., 2012
gH (UL22)	gL associated Virion entry/fusion Nuclear egress	Eisenberg et al., 2012; Farnsworth et al., 2007a
gI (US7)	See gE	
gJ (US5)	Inhibits apoptosis	Jerome et al., 2001
gK (UL53)	pUL20 associated Nuclear egress Assists gB-mediated virus-induced cell fusion Secondary envelopment	Jayachandra et al., 1997; Melancon et al., 2005
gL (UL1)	See gH	
gM (UL10)	gN associated Intracellular targeting of membrane proteins Secondary envelopment Membrane fusion regulator	Leege et al., 2009; Ren et al., 2012
gN (UL49.5)	gM associated gM maturation and fusion activity modulation	Striebinger et al., 2016; Mach et al., 2007; El Kasmi and Lippé, 2015

1.2.3 HSV-1 life cycle

HSV-1 begins its life cycle by attaching to a target cell and fusing its envelope to the host cell membrane. Subsequently, the viral capsid is transported to the nuclear pore and viral DNA is delivered in to the host cell nucleus (Cheshenko et al., 2003). A temporally regulated set of viral genes (immediate early, early and late) are then expressed which allows viral replication, transcription and protein synthesis. Next, viral DNA is packaged in to newly formed capsids and the resulting nucelocapsids likely associate with a few tegument proteins and then undergo egress from the nucleus by budding at the inner nuclear membrane, to form a primary enveloped virion in the perinuclear space, followed by fusion with the outer nuclear membrane. The nucleocapsids then collect the full complement of tegument proteins in the cytoplasm and become enveloped by budding/wrapping at membrane compartments derived from endosomal compartments and/or the *trans*-Golgi-network (TGN) (reviewed in Johnson and Baines, 2011; Hollinshead et al., 2012). Release of the mature virions occurs by fusion of the virus-containing vesicles with the plasma membrane in a poorly understood mechanism (Figure 1.2). These different stages are described in more detail below.

1.2.3.1 Attachment

Viruses initially attach to host cell surface receptors prior to entry. HSV-1 envelope proteins gC and gB attach to glycosaminoglycan (GAG) chains of host cell surface heparan sulphate. However, the interaction of these glycoproteins with GAGs is not an absolute requirement for attachment as mutant viruses lacking either one or both of these GAG-binding activities are still able to infect cells in culture (Cai et al., 1988; Herold et al., 1991). In viruses lacking gC the GAG-binding activity of gB can take over the attachment function although overall binding of virion to cell surfaces decreases (Shukla and Spear, 2001).

1.2.3.2 Entry and uncoating

HSV-1 can enter into its target cell via direct fusion with the plasma membrane and/or fusion within an acidic or neutral endosome depending on the cell type (Koyama and Uchida, 1987; Wittels and Spear, 1991). The process of entry is dependent on gB, gD, gH and gL envelope glycoproteins and mutant viruses lacking these proteins are entry defective (Cai et al., 1988; Ligas and Johnson, 1988; Roop et al., 1993). After initial attachment, gD interacts with at-

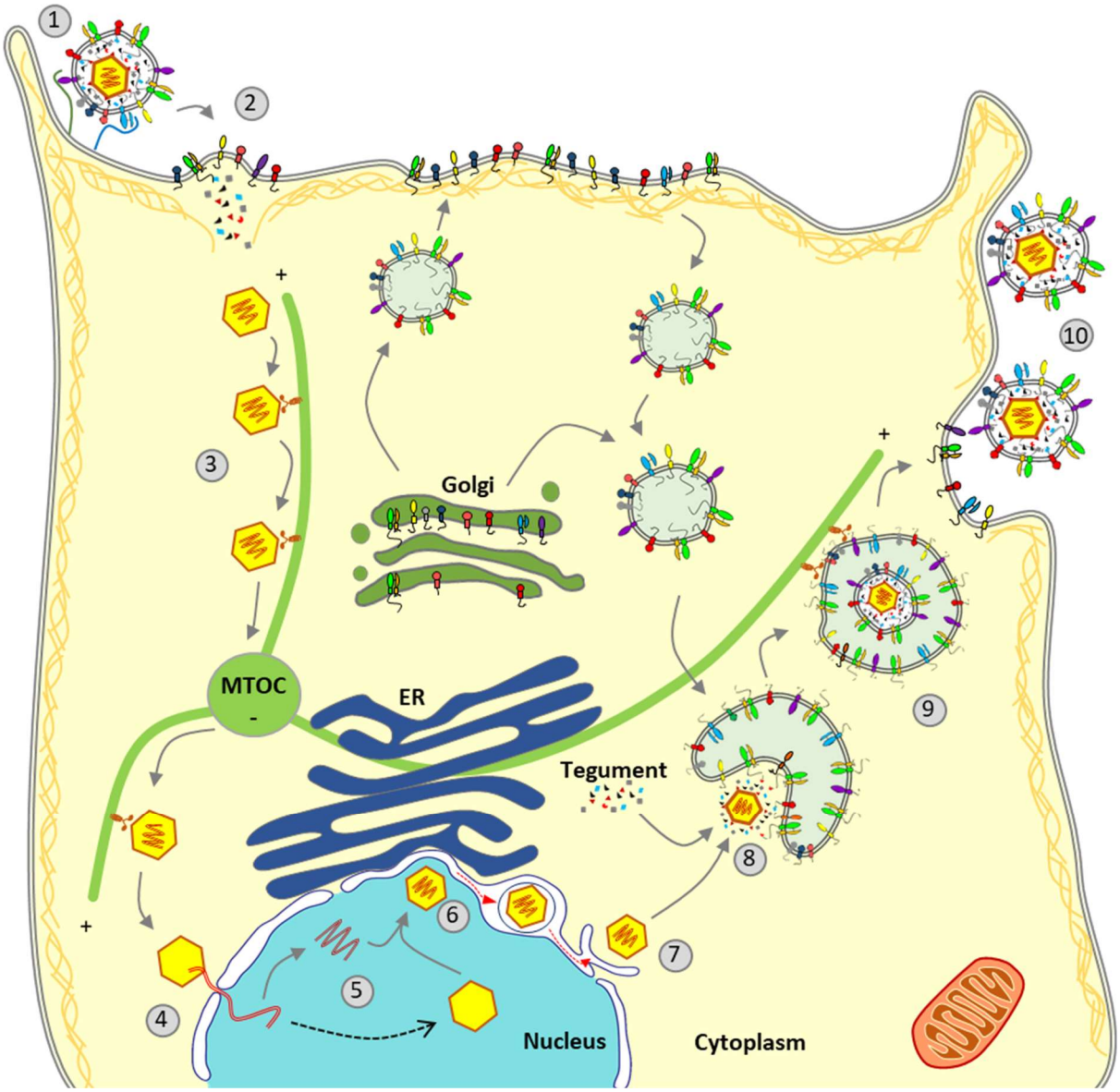

Figure 1.2 | Overview of HSV-1 life cycle. 1. gB and gC binding to heparan sulphate mediate virion attachment to host cell. 2. gD binding to entry receptors promotes fusion complex formation by gB, gH/gL for nucleocapsid delivery to the cytosol. 3. Nucleocapsid is transported towards the nucleus. 4. Nucleocapsid docks onto the nuclear pore and injects viral DNA into the nucleus. 5. Viral DNA is transcribed into mRNA by host cell DNA-dependent RNA polymerase II and which is translated by cellular machinery and viral DNA is replicated by viral DNA polymerase. 6. Capsid assembles in the nucleus, genome packaging and nucleocapsid transport to the perinuclear space by primary envelopment. 7. Nucleocapsid is released in the cytoplasm after fusion of the perinuclear virion with the outer nuclear membrane. 8. Nucleocapsid recruits tegument proteins and becomes enveloped by TGN/endosome derived membrane. 9. Enveloped particle-loaded vesicles transported to the cell membrane for egress. 10. Vesicles fuse with plasma membrane to release the virion to the extracellular milieu.

least one of three entry receptors; herpesvirus entry mediator (HVEM), nectin-1 and 3-O sulphated heparan sulphate (Ligas and Johnson, 1988; Montgomery et al., 1996; Shukla et al., 1999; Shukla et al., 2000). The binding event changes the conformation of gD which then forms a complex with the gH/gL heterodimer (Atanasiu et al., 2010; Krummenacher et al., 2005). Consequently, gB interacts with the gH/gL complex (Atanasiu et al., 2007) and forms the fusion machinery which effects penetrartion of the host cell membrane. Other glycoproteins such as gG have also been proposed to play role in virus entry. Mutant viruses lacking gG were able to infect neighbouring cells through the basal surface but failed to do so thorough the apical surface of polarised epithelial cells in culture (Tran et al., 2000). Fusion of the viral envelope with cell membranes releases the tegumented nucleocapsids into the cytoplasm (Maurer et al., 2008; Sodeik et al., 1997). The capsids are thought to shed most of their tegument proteins rapidly upon entry and bind to dynein motors for transportation along microtubules towards the microtubule organising centre (MTOC) (Sodeik et al., 1997). The entry process has also been shown to trigger intracellular calcium influx, which in turn stimulates downstream signalling to promote viral capsid transport along the microtubules towards nuclear pores (Cheshenko et al., 2003). Some tegument proteins (such as VP1/2), which remain attached to nucleocapsids, are thought to aid this process (Copeland et al., 2009). The capsid then docks onto nuclear pore complex (NPC) and releases viral DNA into the nucleus.

1.2.3.3 Viral gene expression

HSV-1 DNA encodes at least 80 proteins that are translated in a temporally controlled fashion that is regulated by both viral and cellular factors (Roizman et al., 2013). The genes expressed can be grouped as immediate early (IE/α), early (E/β) and late (L/γ), with late genes often classified as early/late (γ1) and true late (γ2) (Figure 1.3). Immediately after entry, the virion tegument protein VP16 (also called α-TIF) binds to host cell factor-1 (HCF-1) and enters the nucleus as a VP16-HCF-1 complex (La et al., 1999) which binds to cellular Oct-1 protein and initiates transcription of IE genes (ICP0, ICP4, ICP22, ICP27 and ICP47). These gene products promote expression of E and L genes, inhibit host transcription, aid splicing and transport of viral RNA, and facilitate viral protein synthesis. Viral genes are transcribed by host RNA polymerase II (RNAP II) (Alwine et al., 1974), which can be modulated by viral gene products for selective and efficient expression of viral genes (Fox et al., 2017). At 2-4 hours post

infection (hpi) when sufficient IE proteins are synthesised (Boehmer and Lehman, 1997), transcription of E genes is initiated. At least 13 E gene products are known and most of them are directly or indirectly involved in viral DNA replication. Though stimulated by viral DNA synthesis some γ1 gene can also express in the absence of DNA replication whereas γ2 gene expression strictly requires viral DNA replication to occur beforehand. Approximately, 60 genes are considered as late genes.

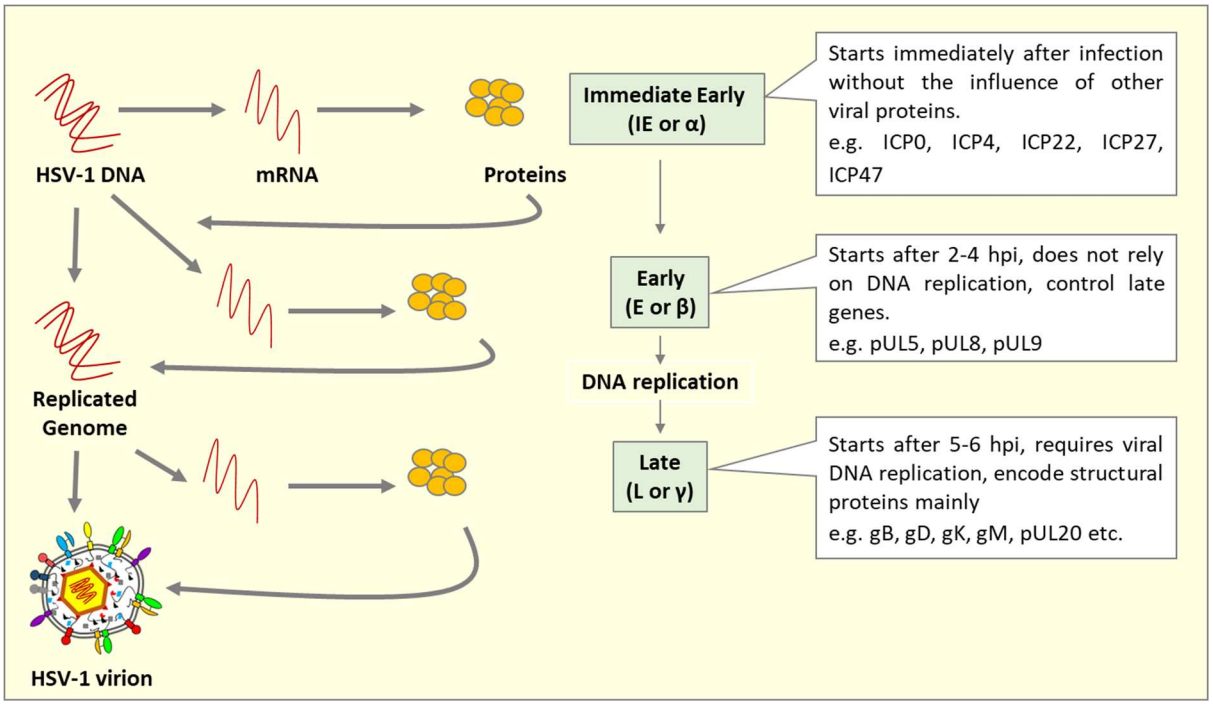

Figure 1.3 | Outline of herpesvirus productive replication cycle. Immediate-early gene products act on early genes. Early genes are also transcribed from the viral genome and these gene products help in viral DNA replication and late gene expression. Late gene products mostly contribute to the formation of the viral particle.

In addition to enhancing transcription of its own genes, HSV-1 can selectively hijack host ribosomes and control viral protein synthesis during lytic infection. Virion host shut-off (vhs) (pUL41) is an example of a tegument protein that is delivered to the cytoplasm by the virus after its entry. The protein can selectively degrade both cellular and viral mRNA by its endoribonuclease activity. It is thought to target actively translating mRNAs by directly binding to the cellular translation initiation factor eIF4H (Feng et al., 2001). The early vhs activity is thought to favour viral translation by reducing competition for the translation

machinery while later in infection vhs is considered to promote the transition between different classes of viral genes (IE, E and L) by increasing mRNA turnover (Esclatine et al., 2004; Taddeo and Roizman, 2006). During late stage of infection, the RNase activity of vhs is reduced by the tegument proteins VP16 and VP22 which is thought to facilitate incorporation of vhs into the tegument of naïve virions. (Lam et. al., 1996; Taddeo et al., 2007).

1.2.3.4 Genome replication

Replication of HSV-1 DNA occurs simultaneously in the infected cell nucleus in a number of stages and the process involves seven viral proteins. The replication begins at one of the three viral origin(s) of replication (Ori) sequences, OriL in the UL region or one of the two copies of OriS in the repeat regions. Interestingly, deletion of either oriL or both copies of oriS have demonstrated little or no effect on viral replication *in vitro*, suggesting that oriL and oriS are functionally redundant (Igarashi et al., 1993; Polvino-Bodnar et al., 1987). However, studies in mouse models proposed important roles of oriL in HSV-1 latency (Balliet and Schaffer, 2006). The DNA synthesis starts with the distortion of the AT-rich origin spacer region by the Origin binding protein pUL9 and the single-stranded DNA binding protein ICP8 (pUL29) (Makhov et al., 2003). Afterwards, pUL5/pUL8/pUL52 helicase-primase complexes are recruited to promote origin unwinding (helicase function) and generate small RNA primers to initiate DNA replication (primer function) (Muylaert et al., 2011). Viral DNA intermediates are formed by rolling circle or recombinational mechanisms by the HSV-1 polymerase holoenzyme (Skaliter and Lehman, 1994; Wikinson and Weller, 2003). The holoenzyme consists of a large catalytic and a small auxiliary subunit derived from UL30 and UL42 genes respectively (Lehman and Boehmer, 1999). Viral DNA synthesis is seen as early as 3 hpi, with maximum rate of DNA synthesis between 7-10 hpi (Weller and Coen, 2012).

1.2.3.5 Capsid assembly and packaging of DNA

In an HSV-1 infected cell nucleus three different capsid types are found in varying numbers. Firstly, precursor procapsids are formed which become matured and give rise to more stable forms of capsid type A, B and C. The A, B and C capsid shells share common features although their internal contents vary from each other. A substantial amount of viral DNA and removal of the majority of the internal scaffold proteins are necessary for a capsid to become an infectious virion. Capsid type A (incomplete DNA packaging) and B (lacks viral DNA) are deficient in either one or both of the characteristics and hence considered as abortive (Roos et

al., 2009). Capsid type C bears the correct amount of both viral DNA and scaffold proteins and becomes a mature virion (Perdue et al., 1976). *In vitro*, expression of VP5, VP19c, VP21, VP22a, VP23, VP24 and VP26 has been shown to reconstitute capsid assembly (Tatman et al., 1994). The Capsid assembly process is thought to begin with the interaction of pUL6 and VP5 (Newcomb et al., 2001). A condensation interaction among VP5 with the scaffold proteins pUL26 (VP21-VP24) and VP22a help the formation of a partial procapsid shell. Further interaction of triplex proteins VP19c and VP23 convert the partial shells into a virus procapsid (Newcomb et al., 1996). With the initiation of viral DNA packaging into the procapsid, pUL26 undergoes autocleavage, separating the N-terminal VP24 protease and C-terminal VP21 scaffold domain. This cleavage also converts the shape of the procapsid into a polyhedral and angular capsid which becomes icosahedral with 150 hexons (VP5), 12 pentons (VP5) and 320 triplexes (VP19c and VP23) (Newcomb et al., 1996).

DNA encapsidation occurs in the nucleus of infected cells and begins with the interaction of a set of viral proteins with newly synthesised viral DNA. At least seven viral proteins are essential for the cleavage and packaging stage: the two CVSC proteins (pUL17 and pUL25), pUL6, pUL15, pUL28, pUL32 and pUL33. Deletion of any of these proteins results in maturation defects in HSV-1 and only B capsids are formed (Cockrell et al., 2011). The UL32 gene product has been reported to transport the assembled capsids to DNA encapsidation sites (Lamberti and Weller, 1998). pUL15, pUL28 and pUL33 act as a terminase complex which docks onto the pUL6 portal to bind, scan and cleave viral DNA at specific positions. pUL17 and pUL25 help to keep DNA in the capsid through stabilisation of the DNA filled capsid structure (Lamberti and Weller, 1998). The DNA-filled capsid (termed nucleocapsid) is then associated with a limited number of tegument proteins and egresses from the nucleus by budding.

1.2.3.6 Egress pathway

Once packaging is complete, nucleocapsids travel to the cytoplasm for maturation and egress. At least three different mechanisms have been postulated about how HSV-1 traverses the nuclear envelope and gains access to the cytoplasm for final maturation followed by exit. Firstly, the single-envelopment or luminal model suggests virions present in the perinuclear space between the inner and outer nuclear membranes (INM and ONM), which is contiguous with the lumen of the endoplasmic reticulum, exit the cell using the secretory pathway without

the need for de-envelopment and re-envelopment (Campadelli-Fiume, 2007; Enquist et al., 1998). However, if viral glycoproteins are artificially re-targeted to the ER they can no longer be incorporated into virions, suggesting the perinuclear particles are not the mature virions and so an alternative mechanism of HSV-1 egress is likely to occur (Skepper et al., 2001). Additionally, EM analysis of the mature and perinuclear HSV-1 particles showed difference in their morphology (Granzow et al., 2001), also biochemical analysis detected the pUL31/pUL34 complex in the perinuclear virions but not in the mature virions (Hagen et al., 2015). These and many other studies suggest that during maturation and egress HSV-1 loses its perinuclear envelope and acquire an envelope from post-ER cytoplasmic compartments. Hence, a second hypothesis, the envelopment-deenvelopment-reenvelopment (dual envelopment) model has been proposed and is widely accepted (Figure 1.4). In this model the nucleocapsid buds through the INM forming a primary enveloped particle in the perinuclear space (Klupp et al., 2007; Mou et al., 2007; Kato et al., 2008), then becomes de-enveloped by fusion with the ONM (Reynolds et al., 2002; Farnsworth et al., 2007a; Wisner et al., 2009) and finally re-enveloped (secondary envelopment) in the cytoplasm to complete the process of virion maturation (Hollinshead et al., 2012; Albecka et al., 2016) (described in detail below). A third mechanism based on electron microscopy (EM) observations hypothesised that the dilation of nuclear pores could allow egress of viral capsids from the nucleus (Leuzinger et al., 2005). However, this hypothesis lacks biochemical or genetic experimental evidence and was not supported by other researchers, particularly because nuclear pores normally only allow transport of cargo up to 36 nm in size (Pante and Kann, 2002) whereas the HSV-1 nucleocapsid is 125 nm and the morphological integrity of nuclear pores appear unaffected until very late stages of infection (Hofemeister and O'hare, 2008; Mettenleiter and Minson, 2006).

1.2.3.6.1 Primary envelopment

In the dual envelopment model, HSV-1 pUL31 and pUL34 form the nuclear egress complex (NEC) (Klupp et al., 2007), which interacts with nucleocapsids to drive their budding through the INM in to the perinuclear region for primary envelopment. During this process the nuclear lamina (lamins A, B and C), a meshwork of dense microfilaments providing structural rigidity to the nucleus, acts as a barrier to the capsids and need to be disrupted. In addition to local disruption of the lamina by pUL31 and pUL34, several other viral and cellular mechanisms likely to contribute this process. During HSV-1 infection, two protein kinase C (PKC) isoforms (PKCδ and PKCα) are thought to phosphorylate lamin B (Leach and Roller, 2010) whereas the

virally encoded pUS3 kinase can phosphorylate lamin A and lamin C (Mou et al., 2007). Phosphorylation is thought to cause a thinning of the lamina due to reduced binding efficiency of the lamina to their target receptors on the INM (Morris et al., 2007; Leach et al., 2007; Leach and Roller, 2010). The interaction of pUL31 and pUL34 with lamin A and C may also prevent or reduce lamin-lamin binding and contribute to lower density of lamina meshwork (Reynolds et al., 2004; Leach and Roller, 2010). Localisation of pUL31 and pUL34 to NEC has been also shown to be regulated by pUL13 kinase activity, in either a pUS3-dependent or -independent mechanism (Kato et al., 2008).

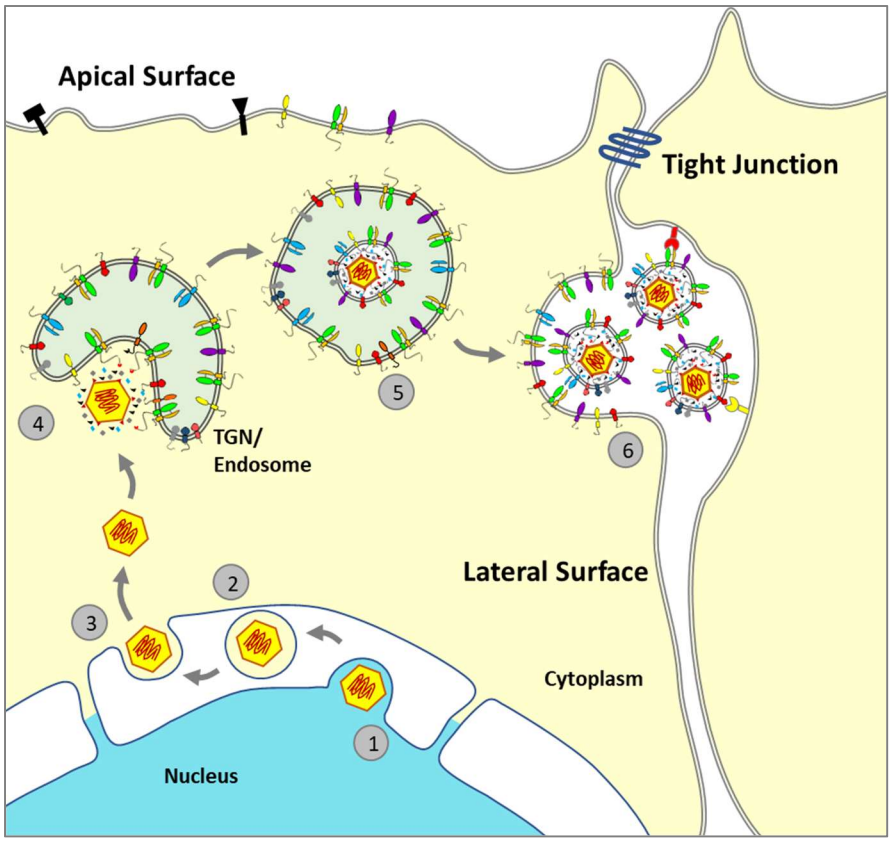

Figure 1.4 | HSV-1 egress pathway. 1. Viral nucleocapsid passes through the nuclear lamina and interacts with the INM. 2. The nucleocapsid buds in to the perinuclear space for primary envelopment. 3. The primary envelope fuses with the ONM for de-envelopment of the nucleocapsid. 4. The capsid acquires tegument proteins and undergoes secondary envelopment by budding/wrapping at membranes derived from the TGN/endosomes. 5. Cargo vesicles carry the virion towards the cell-to-cell contact points, 6. Fusion of the cargo vesicle with the plasma membrane releases the virion at the cell junction where the particles remain attached utilising envelope glycoproteins and/or enters a neighbouring cell.

Beside lamina disruption during nuclear egress, pUL31/pUL34 has been also proposed to select C-capsids specifically by interacting with the higher copy number of pUL25 present on C-compared to A- or B-capsids (Newcomb et al., 2006; Sheaffer et al., 2001; Yang and Baines, 2011; Yang et al., 2014). Importantly pUL31/pUL34 also induces membrane curvature for primary envelopment (Klupp et al., 2007; Mou et al., 2009; Roller et al., 2010; Hagen et al., 2015; Zeev-Ben-Mordehai et al., 2015). Interestingly, deletion of either UL31 or UL34 gene can still produce cytosolic virions but in severely reduced number, suggesting other mechanism of nuclear egress can take place during infection (Chang et al., 1997; Fuchs et al., 2002; Klupp et al., 2000; Roller et al., 2000; Ye and Roizman, 2000). However, no role of pUL31/pUL34 has been noted for during secondary envelopment and these proteins are not incorporated into mature virions.

HSV-1 gB, gD, gM and gH/gL have been reported to be present in the INM and perinuclear virions although a direct involvement of these envelope protein during primary envelopment has not been documented (Baines et al., 2007; Fransworth et al., 2007a; Padula et al., 2009; Stannard et al., 1996; Torrissi et al., 1992). The NEC possibly interacts with gM and gD in the INM and pUL34 is thought to bind gD either recruiting it or retaining it into INM. Whether or not these glycoproteins play partial roles in connecting the INM to the nucleocapsid during primary envelopment is unknown. For HSV-1, the entry glycoproteins gB and gH have been proposed to play an active role during de-envelopment, suggesting they are incorporated into the perinuclear virion (Farnsworth et al., 2007a) (detailed in section below).

1.2.3.6.2 De-envelopment

The perinuclear virion rapidly fuses with the ONM releasing the de-enveloped nucleocapsid into the cytoplasm and leaving behind the NEC proteins by a mechanism which is poorly understood (Reynolds et al., 2002). The process of fusion to ONM for de-envelopment has been proposed to engage the same fusogenic protein complex of gB, gD and gH/gL heterodimer that is required during virion entry into the cell (Wisner et al., 2009; Baines et al., 2007; Farnsworth et al., 2007a; Torrisi et al., 1992). Although there is no evidence for a role of gD during de-envelopment, a mutant virus lacking both gB and gH has been shown to accumulate in large numbers in perinuclear regions often observed in large INM derived vesicles termed ‘herniations’ that project into the nucleoplasm (Farnsworth et al., 2007a). Formation of such herniations is also seen with the deletion of pUS3 (Reynolds et al., 2002; Ryckman and Roller,

2004). pUS3 may act in multiple ways to promote de-envelopment, including the phosphorylation of pUL31 and the gB cytoplasmic domain. Inhibition of the kinase activity of pUS3 also enhances herniations and reduces de-envelopment (Wisner et al., 2009; Mou et al., 2009).

However, the potential role of gB and gH/gL in de-envelopment is unclear and alternative mechanisms for de-envelopment can occur. For example, a mutant virus lacking both gB and gD did not demonstrate a deficiency in nuclear egress (Johnson et al., 2011), making it difficult to rationalise a direct fusion role of gB and gH/gL in de-envelopment because gB is widely believed to be the fusogen. Additionally, PrV double deletion mutants lacking any two of gB, gH and gD showed no defects in nucleocapsid egress into the cytoplasm (Klupp et al., 2008). Whether gB and gH play some sort of redundant, facilitatory role in HSV-1 nuclear egress, and what activity they play in this process remains to be determined.

1.2.3.6.3 Tegument acquisition

HSV-1 capsids are released into the cytoplasm with only a limited number of tegument proteins associated (e.g. pUS3) and rest of the tegument proteins are added to the virion before or during secondary envelopment. The assembly of the tegument layer involves a complex and intricate network where tegument proteins interact with each other, with capsid proteins and also with envelope proteins. Because of the complexity of tegument interactions, functional redundancy is common in the network. Tegumentation is thought to begin in the nucleus with at least some tegument proteins (pUS3, VP1/2, pUL37, ICP0, ICP4, vhs, VP16, and VP22) proposed to associate with nucleocapsids in the nucleoplasm or with perinuclear virions. However, with the possible exception of pUS3 that has a clear function during nuclear egress, the actual acquisition sites for the rest of these proteins is a matter of dispute (reviewed in Johnson and Baines, 2011). One of the first tegument proteins likely to be associated with the nucleocapsid is VP1/2, which has been shown to directly interact with VP5 and/or pUL25 (component of CVSC) (Cardone et al., 2012; Coller et al., 2007). Once such scaffolds are formed other tegument proteins can be recruited, either sequentially or via redundant interactions with each other, and this process is likely to continue until secondary envelopment is complete (Figure 1.5).

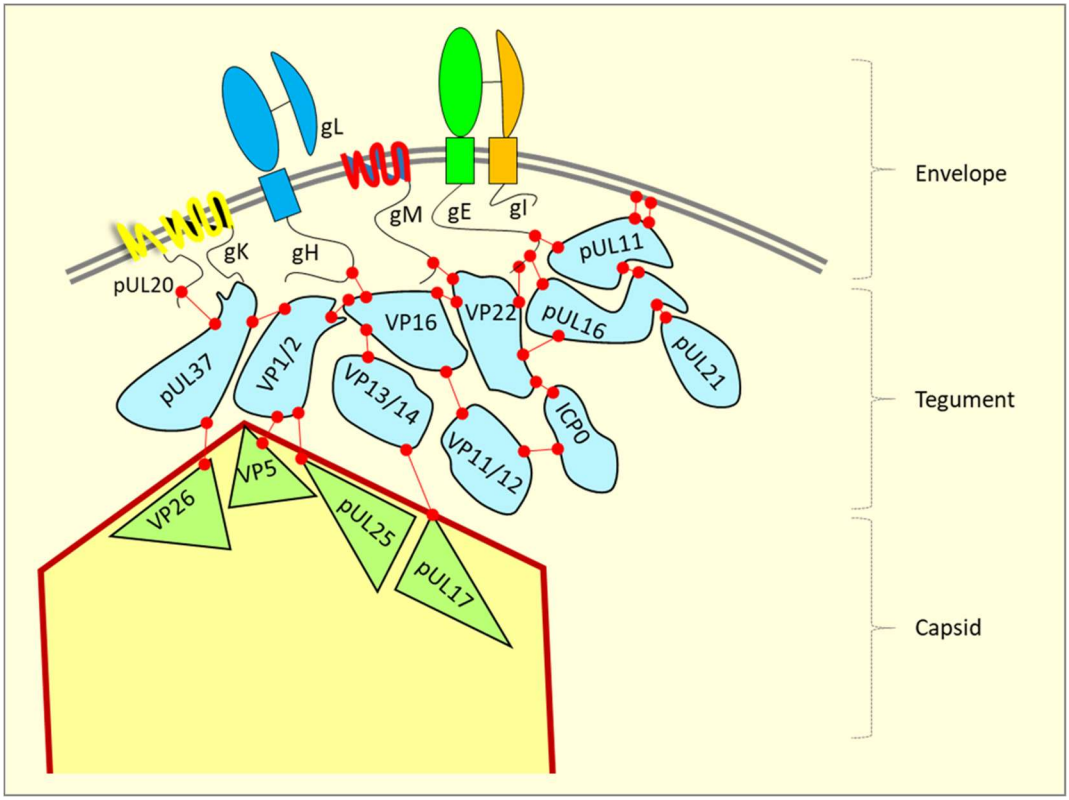

Figure 1.5 | Interaction network of tegument proteins with capsid and envelope glycoproteins. The tegument assembles via a complex network of protein-protein interactions during secondary envelopment. Only a subset of tegument proteins and their known interactions are shown.

1.2.3.6.4 Secondary envelopment

The final stage of virion maturation is to become re-enveloped by budding into, or wrapping at, cytoplasmic membrane by a process called secondary envelopment. Though the exact site of this process has not been confirmed, experimental data shows the lipid composition of mature virion envelope is similar to that of Golgi-derived membrane (van Genderen et al., 1994). Other studies based on immunological techniques have also suggested that the secondary envelopment process occurs in the TGN (Granzow et al., 2001). Alternatively, the virus has been reported to be re-enveloped in endocytic membranes which are abundant and more available in the cell than the smaller TGN (Hollinshead et al., 2012; Albecka et al., 2016).

Another study in this regard hypothesised multivesicular bodies are important in HSV-1 envelopment (Calistri et al., 2007). Endosomal sorting complexes required for transport (ESCRT) components are also shown to be involved in secondary envelopment as inhibiting the activity of the ESCRT protein Vps4 caused accumulation of nucleocapsids in the cytoplasm, which failed to become enveloped (Crump et al., 2007). During late stages of infection HSV-1 dramatically rearranges the Golgi, TGN and endocytic vesicles distributing them throughout the cytoplasm. This makes it difficult to determine where in the cell secondary envelopment happens, and the disruption of the normal pathways of secretory and endocytic transport by virus infection suggests the normal definitions of subcellular compartments may not be completely applicable to infected cells (Campadelli et al., 1993). Many studies to determine the precise sites of herpesvirus envelopment have utilised electron microscopy-based techniques, which only provides a static snapshot of this highly dynamic event, and many of the intracellular trafficking compartments like the TGN, Golgi and endosomes can be difficult to distinguish as they tend to cluster around the microtubule organising centre (MTOC). However, HSV-1 has been co-fractionated with both TGN and endosomes (Harley et al., 2001) suggesting capsids are wrapped at different sites depending on where in cell they meet the envelope.

Envelope proteins are required for secondary envelopment as they interact with capsid or tegument proteins to connect the membrane to capsids, and there is substantial evidence of envelope protein involvement in virion envelopment including gB (Johnson et al., 2011), gD, gE and gI (Farnsworth et al., 2003), gM (Ren et al., 2012), gK (Melancon et al., 2005) and pUL20 (Foster et al., 2004). However, deletion of a single glycoprotein (gB, gC, gD, gE, gH, gI, or gL) often has little or no effect on secondary envelopment, and deletion of two or three glycoproteins together is often required to cause more substantial defects in secondary envelopment. For example, mutant viruses lacking gB and gD were shown to be defective for cytoplasmic envelopment, and similar defects were observed with deletion of the cytoplasmic tails of gE and gD or gE and gM (Brack et al., 2000; Farnsworth et al., 2007a and b; Johnson et al., 2011). Likewise, triple deletion of gD, gE and gI caused large aggregates of unenveloped capsids surrounded by layers of tegument proteins to accumulate in the cytoplasm (Farnsworth et al., 2003). Studies with gK and pUL20 deletion viruses also demonstrated large accumulations of cytoplasmic capsids that are unenveloped (Foster et al., 2004; Melancon et

al., 2005; Lau and Crump, 2015) suggesting their importance in secondary envelopment, possibly by interacting with tegument or other glycoproteins.

Tegument proteins also play a significant role in secondary envelopment in linking the glycoprotein studded envelope to the nucleocapsid. For example mutant viruses lacking VP22 have been shown to incorporate less gD or gE/gI into the virion (Duffy et al., 2006), and a VP22 mutant that is unable to interact with gE/gI localises differently and does not accumulate in perinuclear regions (Stylianou et al., 2009) suggesting that VP22 interacts with gE/gI and gD to promote envelopment in the cytoplasm. Evidence also suggests VP22 interacts with gM (Maringer et al., 2012), pUL11 with gD and gE (Farnsworth et al., 2007b), pUL16 with gE (Chadha et al., 2012), VP16 with gB, gD and gH (Gross et al., 2003; Kamen et al., 2005; Zhu and Courtney, 1994), and pUL37 with gK (Jambunathan et al., 2014). It is interesting to note that tegument and glycoproteins by themselves are able to complete the secondary envelopment process, and the nucleocapsid is not necessary, as observed by the production of light particles of HSV-1, which appear to contain all tegument and envelope proteins but are devoid of capsid proteins (McLauchlan and Rixon, 1992; Szilagyi and Cunningham, 1991).

1.2.3.6.5 Directed virion secretion

Once secondary envelopment is complete the virion is contained in a large vesicle which interacts with cellular microtubule motors and moves towards the cell surface (Radtke et al., 2010). The virion-loaded vesicle membrane likely contains viral membrane proteins with their sorting motifs facing towards the cytoplasm and ecto-domains inside the vesicle lumen, although whether all or just some of the viral membrane proteins are present on the vesicle membrane is unclear. The virion-loaded vesicles eventually fuse with the plasma membrane to release the virions outside of the cell. Clearly, vesicle fusion with the plasma membrane will not involve the fusion activity of the viral entry glycoprotein as the fusion domains are on the opposite (luminal) side of the vesicle membrane. However, the cytoplasmic tails of certain viral membrane proteins are thought to interact with cellular mediators of vesicle fusion and exocytosis. In HSV-1 and PrV cellular regulators of vesicle transport and fusion including Rab GTPases 3A, 6A, 8a and 11a, the microtubule motor kinesin-1 and the soluble N-ethylmaleimide-sensitive factor activating protein receptor (SNARE)-family vesicle fusion protein synaptosomal-associated protein 25 (SNAP-25) have been shown to be co-trafficked with viral tegument and glycoproteins to egress sites (Hogue et al., 2014; Saksena et al., 2009).

Knockdown of selected Rab molecules (6A, 10 and 13) was shown to be somewhat inhibitory for HSV-1 replication (Griffiths et al., 2013). Specifically, Rab6A is known to involve in membrane transport from the Golgi to the plasma membrane and has been shown to be important for HSV-1 capsid envelopment, suggesting Rab6A-mediated trafficking to plasma membrane is important for targeting glycoproteins to virion assembly compartments (Hollinshead et al., 2012; Johns et al., 2014). Protein kinase D (PKD), which is a membrane trafficking mediator that can control the departure of secretory cargo from TGN, has also been shown to be important for HSV-1 egress (Rémillard-Labrosse et al., 2009). Furthermore, myosin Va (MYO5a) is activated upon HSV-1 infection and has been proposed to facilitate the transport of virion- and glycoprotein-loaded vesicles through the cortical actin network to the plasma membrane (Roberts and Baines, 2010).

After fusion of the virion-containing vesicle with the plasma membrane, the majority of the progeny virions remain attached to the host cell surface rather than becoming free particles in the extracellular medium, at least in cultured cell monolayers (Mingo et al., 2012). In polarised epithelial cells virions are preferentially delivered to the lateral surfaces and cell junctions where they become concentrated (Johnson et al., 2001). Viral glycoproteins are thought to mediate remodelling of TGN or endosomal compartments to direct the targeting of virion secretion. The gE/gI complex has been proposed to function with other HSV proteins within TGN subdomains to promote virion assembly and subsequent egress to cell junctions (Johnson and Huber, 2002). Such directed secretion is thought to promote cell-to-cell spread of virions and help bypass detection by the host immune system. When gE was deleted, HSV-1 was shown to be secreted more randomly from the apical surface of infected cells rather than at cell junctions, contributing less cell-to-cell spread (Johnson et al., 2001; Wisner et al., 2000; McMillan and Johnson, 2001).

Studies using the non-polarised Vero cell line reported similarly directed virion egress at adherent surfaces of cell-cell or cell-culture plate contacts (Mingo et al., 2012). However, other studies in non-polarised HEp-2 cell line conducted at late time point of infection (17 h) reported a random release of virion (Johnson et al., 2001). Such differences could be either due to cell line specific factors that control vesicle transport and fusion or due to the time post infection used in these studies: in Vero cells by 12 hpi virions were found to have already transfered into neighbouring un-infected cells (Mingo et al., 2012), and thus 17 h is quite a late time point to

study directed virion egress. Because non-polarised cells do not form strong cell-to-cell junctions, the state of being adherent to a substrate (e.g. plastic culture dishes) or more loosely attached to neighbouring cells may suffice to stimulate directional virion egress in some cell types, and the process could be linked to the organisation of the cytoskeleton and specific cell surface attachment proteins.

Directed egress of alphaherpesivrus is also seen in neurons where upon reactivation of latent HSV-1 the newly synthesised particles are transported in an anterograde direction from the neuronal cell body along the axon to the axon tip and spread to other neurons or epithelial cells. Currently two models describe the axonal transport of virus particles: the 'Married model' when virions are enveloped in the neuron cell body and transported as complete particles along the axon, and the 'Separate model' when virion capsid and glycoprotein containing envelope are transported separately and secondary envelopment occurs at axon termini (Kratchmarov et al., 2013). Studies have shown HSV-1 gE/gI and pUS9 promote anterograde transport of capsids, other glycoproteins, and enveloped virions (Ch'ng and Enquist, 2005; Snyder et al., 2008; Lyman et al., 2007). The cytoplasmic domain of both gE and pUS9 has been also shown to interact with kinesin motors to transport glycoprotein containing vesicles along axons (Howard et al., 2013; Kramer et al., 2012). The gE/gI complex and pUS9 seem to cooperate with each other in this process as deletion of gE, gI or pUS9 was shown to reduce axonal transport of virion capsids and glycoproteins (Saksena et al., 2015). Additionally, a pUS9 deletion showed a marked defect in virus assembly and egress in the axon terminus inhibiting epithelial cell transfer (Saksena et al., 2015). Similarly, deletion of the ecto-domain of gE/gI contributed to partial inhibition of capsid transport along axons, and deletion of both gE and pUS9 completely blocked axonal transport of capsids and virion spread (Howard et al., 2013; Howard et al., 2014).

1.2.3.7 Spread of virus

The progeny HSV-1 particles released into the extracellular space at or near cell contact points can directly spread to adjacent cells in a process termed cell-to-cell transmission. Alternatively, an indirect transmission mechanism can occur where the virions are released from the surface of the producing cells and diffuse in the extracellular matrix to infect both adjacent and distal cells. This mechanism is seen in most wild-type (sometimes termed syn^+ in the literature) strains. However, the extracellular virions that infect distal cells can be targeted by host

neutralising antibodies. Alternatively, HSV-1 can spread to neighbouring cells directly by forming syncytia (sometimes termed syn$^-$), a process whereby viral glycoproteins expressed on the infected cell surface induce an uninfected cell to fuse with it, by a mechanism thought to be similar but not identical to that of virus entry during primary infection (Roizman and Sears, 1996; Spear, 1993). Studies have demonstrated that HSV-1 gB, gD, and gH/gL are essential for both free virus particle entry and syncytia formation, and viruses lacking any of these glycoproteins are defective in both processes (Cai et al., 1988; Forrester et al., 1992; Ligas and Johnson 1988; Roop et al., 1993).

Despite having no role in the entry of free virus, several other HSV-1 envelope proteins have been shown to be important for cell-to-cell spread, including the gE/gI complex, pUS9, gG, gM, and pUL45 (Farnsworth and Johnson, 2006; Wisner et al., 2000; Polcicova et al., 2005; Balan et al., 1994; Haanes et al., 1994; Carmichael et al., 2018; Kim et al., 2013). The gE/gI complex has been shown to localise to cell-to-cell junctions and has therefore been proposed to assist virion spread across cell junctions in both epithelial cells and neurons (Dingwell et al., 1995 and 1998; Johnson et al., 1988). Deletion of gE from HSV-1 was shown to markedly reduce plaque size on infected cell monolayers suggesting cell-to-cell spread is hampered (Maringer et al., 2012; Balan et al., 1994; Wisner et al., 2000). pUS9 has been proposed to regulate the microtubule-based transport of virion-containing vesicles to the cell surface in neurons. The role of other HSV-1 envelope proteins in cell-to-cell spread is unclear and may be specific to the spread of syncytial strains. HSV-1 can also induce filopodia formation in infected cells, which may help the spread of released virions still attached to the extracellular surface of cells (Clement et al., 2006; Roop et al., 1993). Studies have shown that HSV trafficking along filopodia is mediated by myosin-dependent F-actin retrograde flow (Lehmann et al., 2005).

1.3 Intracellular Protein Trafficking Compartments

Eukaryotic cells are highly compartmentalised which enables efficient separation of functions in different organelles. Cell materials can shuttle outward (exo-) and inward (endo-) utilising two major cellular pathways (Figure 1.6). In the exocytic pathway, proteins are co-translationally inserted into the lumen or membrane of the endoplasmic reticulum (ER) and then transported from the ER to the *cis*-Golgi apparatus within membranous vesicles. The

proteins become post-translationally modified as they are transported forward through medial and *trans*-Golgi to the TGN and eventually packaged into secretory vesicles to be either secreted into the extracellular matrix or presented on the plasma membrane. Vesicular transport also occurs from the Golgi and TGN to endosomes and lysosomes, or back to the ER (reviewed in Tokarev et al., 2009). In the endocytic pathway, proteins are internalised from the extracellular environment/plasma membrane in endocytic vesicles which fuse with early endosomes. From here cargo/receptors can be transported back to the plasma membrane either directly, or via the recycling endosome, or remain in the endosome as it matures into a late endosomes/multivesicular bodies (MVB) and become degraded by fusion with a lysosome (reviewed in Tokarev et al., 2009).

There are several mechanisms of endocytosis which are generally divided into the well-studied clathrin-dependent pathway or the less well understood variety of clathrin-independent pathways (Doherty and McMahon, 2009; Hansen and Nichols 2009). There is also much cross-talk between exocytic and endocytic pathways with vesicle transport between most if not all compartments of the secretory and endocytic pathways that can occur bi-directionally (Stoorvogel et al., 2002; Ghosh et al., 2003). Furthermore, in polarised cells the distinct apical and basolateral domains have somewhat independent secretory and endocytic pathways between the TGN and plasma membrane, although there is also cross-talk between these pathways, for example endocytic vesicles from apical surface can incorporate into basolateral early endosomes and be recycled to the basolateral plasma membrane (Mostov et al., 2000). Cell organelles communicate with each other utilising vesicular transport where cargo-loaded vesicles are released from donor compartment utilising coat and adaptor proteins (Bonifacino and Glick, 2004). The well-characterised vesicle coats are clathrin, coat protein I (COPI) and coat protein 2 (COPII) which are utilised in different transport steps. COPI- and COPII- coated vesicles mediate transport from the ER and the Golgi whereas clathrin-coated vesicles mediate transport from the TGN and plasma membrane. Once vesicles are formed, the coats are dissociated and the vesicles are transported towards their target membrane with the guidance of Rab GTPase family proteins (Stenmark, 2009). Upon reaching their target site the vesicles dock on to a tethering complex and SNARE proteins help fusion of those vesicles to the membrane.

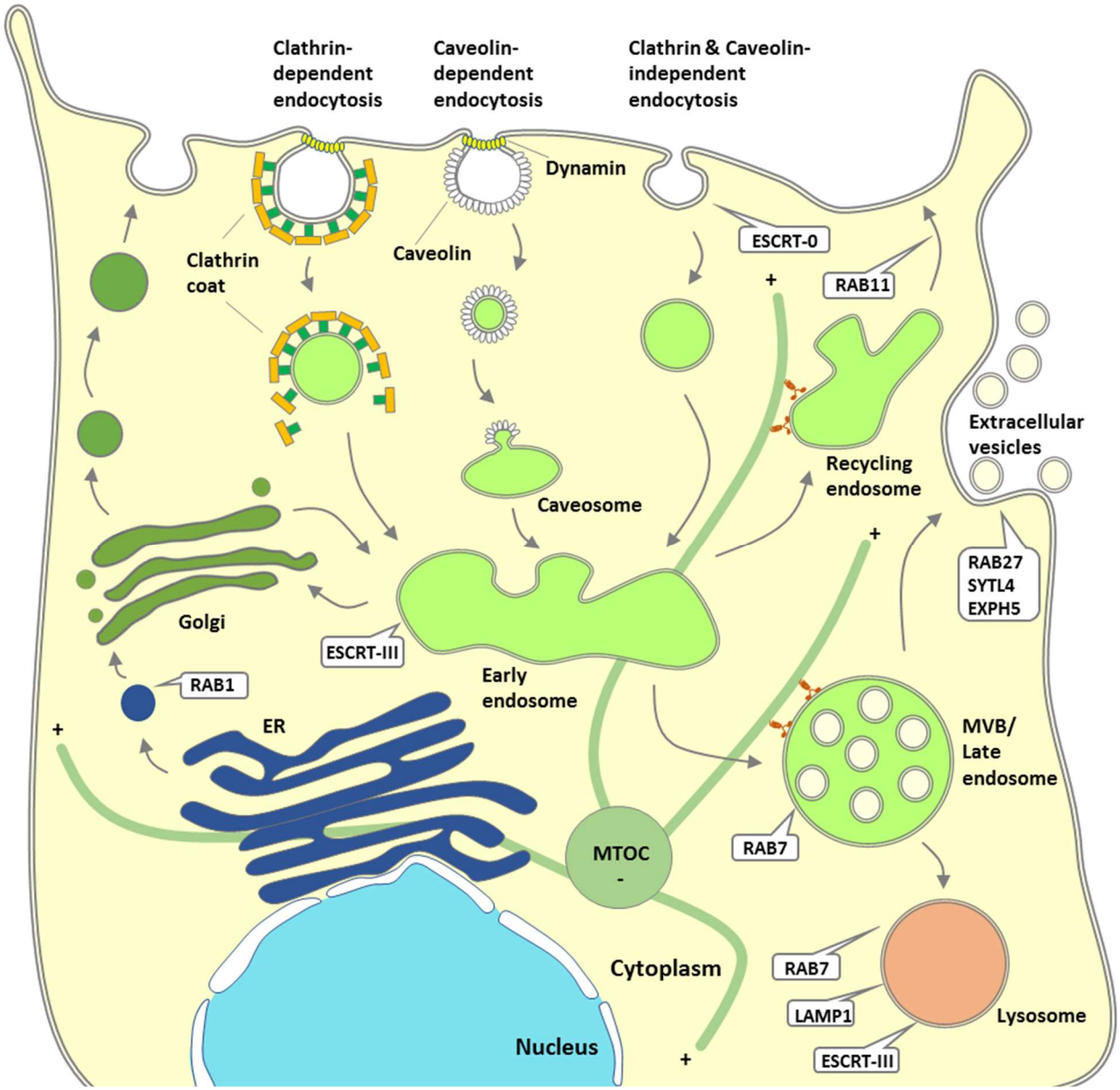

Figure 1.6 | Overview of secretory and endocytic trafficking pathways. Molecules from the extracellular milieu are taken up by either clathrin- or caveolin- dependent, or independent pathways. Endocytic vesicles fuse with early endosome (EE) and from there cargo is sorted for either recycling or degradation. Proteins mentioned in the box have demonstrated/proposed functions in the indicated transport steps. ER: endoplasmic reticulum, MVB: multivesicular body, ESCRT: endosomal sorting complexes required for transport, LAMP1 lysosome-associated membrane glycoprotein 1, EXPH5: exophilin, STYL4: synaptotagmin-like protein 4.

1.4 Overview of viral and cellular proteins relevant to this thesis

The primary focus of this thesis was to understand the role of HSV-1 gE/gI complex during virion secretion and the following host proteins were investigated as potential interactors of gE/gI.

1.4.1 The gE/gI complex of HSV-1

Much of this thesis focuses on the gE/gI complex of HSV-1, which was identified as a Fc-binding heterodimer (Baucke and Spear, 1979; Johnson and Feenstra, 1987; Johnson et al., 1988). gI and gE are encoded by US7 and US8 genes respectively. Full length gI is composed of 383 amino acids, whereas full length gE contains 550 amino acids and these proteins have a predicted molecular mass of 40 KDa, and 59 KDa respectively (Uniprot:Q702Y4 and Uniprot:P04488). However, both proteins become glycosylated (three potential N-linked glycosylation sites in the gI sequence and two in the gE sequence), contributing to higher molecular mass of both proteins (Chapman et al., 1999). Early studies with US7 and US8 genes suggested that the glycosylated products are ~65 KDa and ~80 KDa respectively (Baucke and Spear, 1979; Longnecker et al., 1987; Sullivan and Smith, 1988, Collins and Johnson, 2003), although the observed molecular mass for each protein can vary due to differences in glycan chain processing depending on the cell type. Both gE and gI are type-I membrane glycoproteins with extended N-terminal ecto-domains (residues 1-419 and 1-266 respectively) that contain a short signal sequence at their N-terminus that is co-translationally cleaved during translocation across the ER membrane, a single transmembrane domains (residues 420-440 and 267-289 respectively) and relatively long C-terminal cytoplasmic tails (residues 441-550 and 289-383 respectively) (Figure 1.7). The Fc-binding domain within the N-terminal domain of gE (residues 213–390) has been shown to be a β-sheet rich, Ig-like domain by X-ray crystallography, and this domain of gE can bind Fc in the absence of other gE or gI domains (Sprague et al., 2006).

When co-expressed gE and gI form a heterodimeric complex in infected and transfected cells as well as in virus particles. The gI binding site on gE has been predicted to be between 235-264 amino acid residues (Dubin et al., 1994; Basu et al., 1995), although protease cleavage studies on gE have revealed that the N-terminal 1-188 residues of mature gE ectodomain forms a stable complex with gI (Rizvi and Raghavan, 2001). The gE interaction site within gI is not known but the domain of gI that has been predicted to be important for IgG binding is between amino acids 128-145 (Basu et al., 1997). Although gE alone can bind to the Fc region of human IgG, the affinity is 100 times less strong compared to that of gE/gI complex (Sprague et al., 2004). However, gI alone is not able to interact with IgG molecules (Basu et al., 1997). The IgG binding activity of gE/gI ectodomain has been shown to involve in immune evasion and viral pathogenesis (Ndjamen et al. 2014).

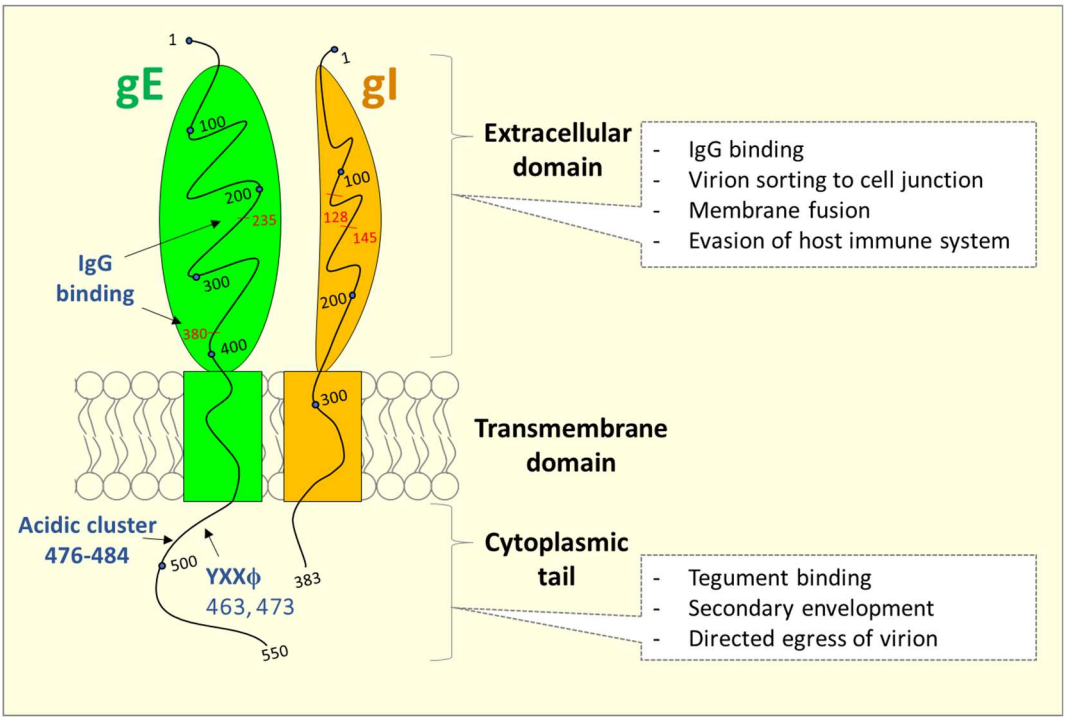

Figure 1.7 | Cartoon of the HSV-1 gE/gI complex and it's proposed functions. HSV-1 gE and gI form a heterodimeric complex and the extracellular domain can act as a Fc receptor. The IgG binding site on gE and gI have been predicted. Both extracellular- and cytoplasmic domains of the gE/gI complex exhibit some important functions in the virus life cycle as have been indicated.

At the lateral surfaces of the cell the gE/gI extracellular domain has been proposed to interact with cellular receptors to promote entry of the virus into neighbouring uninfected cells. However, fusion of the virion envelope with the recipient cell requires HSV gD, gB, and gH/gL and is unlikely to directly involve gE/gI (McMillan and Johnson, 2001). The interaction between gC and heparin sulphate has also been shown to trigger pUL16 release from the capsid possibly by interacting with gE ectodomain because pUL16 also binds to gE CT-domain (Yeh et al., 2011; Meckes and Wills, 2008). Such a trigger may facilitate capsid uncoating and/or activate the fusion apparatus for virus entry (Figure 1.8).

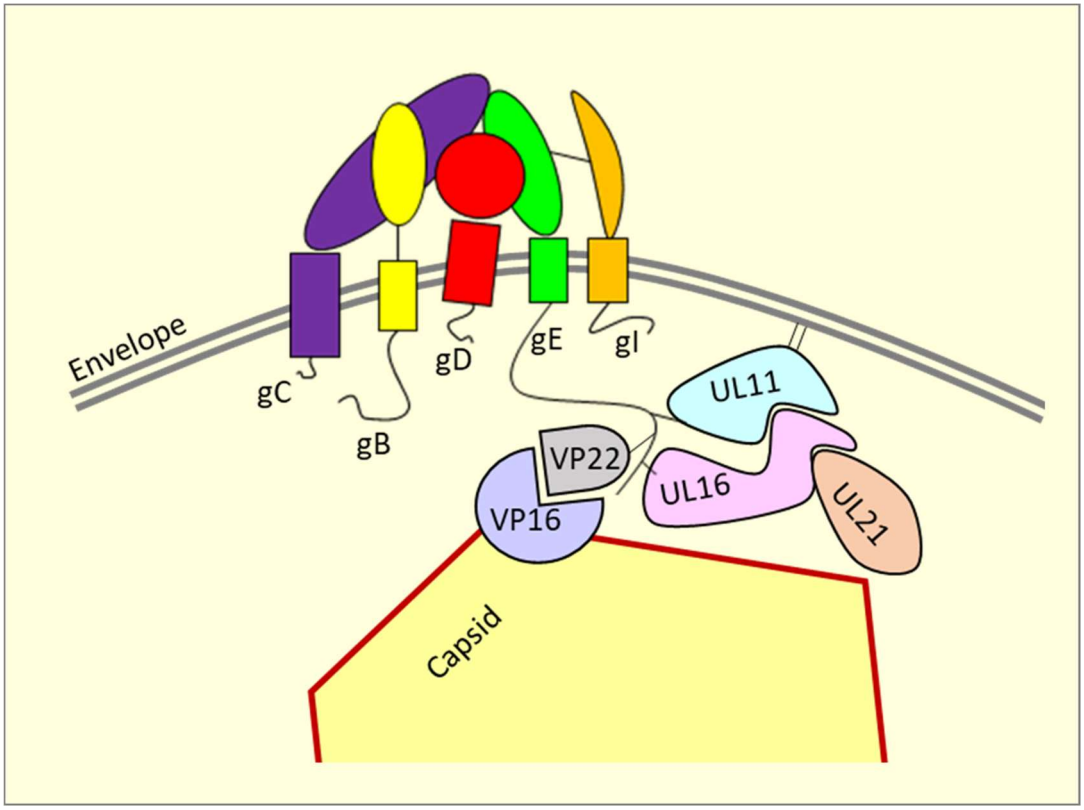

Figure 1.8 | Cartoon of HSV-1 gE/gI complex together with potential viral protein interactions. The CT-domain of gE has been proposed to bind pUL11, pUL16 and pUL49 (VP22) whereas the ectodomain is thought to send signals to pUL16 during virion attachment mediated by gC-heparan sulphate binding. (Adapted from Yeh et al., 2011).

As has been mentioned previously, the gE/gI complex has a role during secondary envelopment of the virion, albeit redundant with other viral envelop proteins. The process of secondary envelopment of HSV may involve distinct phases of gE/gI involvement. A number of tegument proteins (VP22, pUL11, pUL16, pUL21) have been found to interact with gE/gI complex and these interactions may be important for processing, transport, and function of gE (Maringer et al., 2012; Farnsworth et al., 2007b; Han et al., 2012). Additionally, gE/gI accumulation in the TGN is thought to be facilitated by the interaction between the cytoplasmic domain of gE and proteins of cellular sorting machinery such as phosphofurin acidic cluster sorting protein 1 (PACS-1) and clathrin adapters (McMillan and Johnson, 2001). The cytoplasmic dileucine motif of gI is thought to assist in these trafficking processes such as endocytosis, localisation to the TGN and basolateral sorting (Wisner and Johnson, 2004; reviewed in McMillan and Johnson, 2001). In cells infected with a gI deletion virus both gE and TGN46 remained trapped in the TGN suggesting that gI plays an important role in the localisation of gE (McMillan and Johnson, 2001). gE may also interact with pUS9 forming a tripartite complex important for the recruitment of kinesin motors and virion egress in neurons (Howard et al., 2013; reviewed in Johnson and Baines 2011).

In epithelial cells gE and gI expressed by recombinant adenovirus vectors were found to become accumulated at lateral surfaces rather than on apical or basal surfaces (Dingwell and Johnson, 1998). Mutant viruses lacking gE are unable to be targeted to cell junctions and so spread poorly from cell-to-cell in polarised epithelial cell line (Johnson et al., 2001). In non-polarised cells however, gE/gI and other glycoproteins such as gB, gD and gH have been found to accumulate at sack-like areas of the plasma membrane at the basal surfaces of the cell prior to HSV-1 particles being released at these specific sites. In these non-polarised cells, gE deleted viruses showed increased viral egress from the sack-like sites (Mingo et al., 2012; Wisner and Johnson, 2004). gE/gI deletion mutants form smaller plaques in Vero cell monolayers and in vivo studies also suggest that gE is important for the virus to spread from primary infection sites to sensory ganglia and from infected ganglia back to epithelial cells (Dingwell et al., 1995; Dingwell et al., 1995; Johnson et al., 2001; McGraw and Friedman, 2009; Mingo et al., 2012; Saldanha et al., 2000).

1.4.2 IFITM

Interferon induced transmembrane (IFITM) proteins are type II transmembrane proteins in vertebrates with a conserved cytosolic loop (reviewed in Bailey et al., 2014). IFITMs have been demonstrated to restrict the replication of many enveloped and non-enveloped viruses (Alber and Staeheli, 1996; Zhu and Liu, 2003; Huang et al., 2011). So far, five IFITMs (IFITM1, 2, 3, 5 and 10) have been identified in humans, among which IFITM1-3 can act as restriction factors for many viruses because of their capacity to block viral entry. For example, IFITM1 has been reported to restrict vesicular stomatitis virus (VSV), IFITM1 and IFITM3 inhibit Zika virus, IFITM2 and 3 are reported to restrict Rift Valley fever virus (RVFV), and IFITM3 is reported to restrict both hepatitis C virus (HCV) and influenza A virus (Savidis et al., 2016; Alber and Staeheli, 1996; Mudhasani et al., 2013; Zhu and Liu, 2003; Desai et al., 2014). However, an inhibitory effect of IFITMs on DNA virus replication has only been demonstrated for African swine fever virus (ASFV), with overexpression of IFITM 2 and 3 in Vero cells suggested to directly affect ASFV entry/uncoating (Muñoz-Moreno et al., 2016). Although the exact mechanisms of virus inhibition by IFITMs are not known, these proteins are thought to either modify endosomal or lysosomal compartments or alter the rate of intracellular vesicle trafficking thereby rendering the host environment inhospitable for virus replication (Feeley et al., 2011; Huang et al., 2011). Interestingly, IFITMs have been suggested to have a pro-viral role for HCMV during viral morphogenesis because knock down of IFITM proteins inhibited HCMV replication, whereas HSV-1 was unaffected (Xie et al., 2015).

1.4.3 Nipsnap

Nipsnap1 and Nipsnap2 (GBAS) proteins are member of evolutionarily well-conserved protein family with unclear functions in the cell. The other members of the family include Nipsnap3 and Nipsnap4. All these proteins have a 4-nitrophenylphosphatase (NIP) domain and a non-neuronal SNAP-25-like protein homology domain. SNAP-25 is a neuronal SNARE protein that is involved in docking and fusion of synaptic vesicles to the plasma membrane and therefore Nipsnaps have been proposed to be involved in vesicle trafficking in cells (Seroussi et al., 1998; Lee et al., 2002). However, a vesicle trafficking role of Nipsnap1 and 2 has yet to be formally shown. Nipsnap1 has been shown to bear a mitochondrial targeting sequence at its N terminal region and interact with mitochondrial translocation machinery (Mootha et al., 2003; Tummala et al., 2010). Nipsnap1 and 2 have over 66% sequence identity (Figure 1.9) and likewise Nipsnap3 and 4 are 87% identical, although the Nipsnap1 amino acid sequence is only ~22% identical to that of Nipsnap3 and 4.

Both Nipsnap1 and 2 have a predicted molecular weight of 33 KDa. However, full-length Nipsnap1 (33 KDa) has been shown to become truncated at the N terminus and generate a mature protein of 29 KDa (Behrends et al., 2010; Nautiyal et al., 2010; Okuda-Ashitaka et al., 2012; Tummala et al., 2010). Nipsnap1 has been shown to be expressed in brain, spinal cord, heart, liver and kidney, whereas Nipsnap2 was identified in brain but can also be found in other tissues (Okuda-Ashitaka et al., 2012; Nautiyal et al., 2010; Seroussi et al., 1998; Schoeber et al., 2008; Okuda-Ashitaka et al., 2012; Tummala et al., 2010; Wang et al., 1998). Nipsnap3 and 4 have been shown to be expressed in brain, muscle, and testis (Buechler et al., 2004; Lee et al., 2002). Nipsnap1 and Nipsnap2 have both been detected in the inner membrane space of mitochondria, however a fraction of both proteins can also be detected in the outer membrane of mitochondria, and in the cytoplasm as they can interact with cytosolic protein P62/SQSTM1 (Yamamoto et al., 2017 (a) and (b); Shanmughapriya et al., 2015).

The exact physiological role of Nipsnap1 and 2 proteins are yet to be determined though a number of functions have been predicted for Nipsnap1. Recent discoveries suggest Nipsnap1 can interact with 1) the neuropeptide nocistatin (NST) and possibly play role in pain transmission (Okuda-Ashitaka et al., 2012), 2) the transient receptor potential vanilloid channel 6 (TRPV-6) and modulate TRPV6-mediated Ca^{2+} entry (Schoeber et al., 2008) and 3) the branched-chain α-keto acid (BCKA) dehydrogenase enzyme complex possibly to provide structural stability to the protein (Nautiyal et al., 2010). On the other hand, amyloid precursor protein (APP) has been shown to bind and modulate the level of Nipsnap1 in cells (Tummala et al., 2010). Nipsnap1 may also act as negative regulators for multiple ATG8 family members thereby affecting autophagy (Behrends et al., 2010). Nipsnap1 and 2 has been also shown to exert a positive role in pattern recognition receptor (PRR) induced signalling and NF-κB activity in response to lipopolysaccharides (LPS) (Yamamoto et al., 2017a).

```
Program: needle
Aligned sequences: 2
# 1: NIPSNAP1
# 2: NIPSNAP2
# Identity:     196/296 (66.2%)
# Similarity:   229/296 (77.4%)

NIPSNAP1          1 MAPRLCSISVTARRLLGGPGPR-AGDVASAAA----------ARFYSKD     38
                    .|.|:|...|.. ||.:...||          ....::.
NIPSNAP2          1 ----------MAARVLRARGAAWAGGLLQRAAPCSLLPRLRTWTSSSNRS     40

NIPSNAP1         39 NEGSWFRSLFVHKVDPRKDAHSTLLSKKETSNLYKIQFHNVKPEYLDAYN     88
                    .|.||.:||||.||||||||||.||:|||||||||:||||||||.|:|||
NIPSNAP2         41 REDSWLKSLFVRKVDPRKDAHSNLLAKKETSNLYKLQFHNVKPECLEAYN     90

NIPSNAP1         89 SLTEAVLPKLHLDEDYPCSLVGNWNTWYGEQDQAVHLWRFSGGYPALMDC    138
                    .:.:.||||:|.|:.|||:|||.||||||||||||||:.||||||.:.
NIPSNAP2         91 KICQEVLPKIHEDKHYPCTLVGTWNTWYGEQDQAVHLWRYEGGYPALTEV    140

NIPSNAP1        139 MNKLKNNKEYLEFRRERSQMLLSRRNQLLLEFSFWNEPQPRMGPNIYELR    188
                    ||||:.|||:||||:.||.|||||:||||||||||||.||.||||||||
NIPSNAP2        141 MNKLRENKEFLEFRKARSDMLLSRKNQLLLEFSFWNEPVPRSGPNIYELR    190

NIPSNAP1        189 TYKLKPGTMIEWGNNWARAIKYRQENQEAVGGFFSQIGELYVVHHLWAYK    238
                    :|:|:|||||||||.|||||::||:..||||||||||:||:|||||||:
NIPSNAP2        191 SYQLRPGTMIEWGNYWARAIRFRQDGNEAVGGFFSQIGQLYMVHHLWAYR    240

NIPSNAP1        239 DLQSREETRNAAWRKRGWDENVYYTVPLVRHMESRIMIPLKISPLQ        284
                    |||:||:.|||||.|.||:|.|||||||::.||||||||||.||||
NIPSNAP2        241 DLQTREDIRNAAWHKHGWEELVYYTVPLIQEMESRIMIPLKTSPLQ        286
```

Figure 1.9 | Similarity between human Nipsnap1 and Nipsnap2 protein sequence. Human Nipsnap1 and 2 protein sequences were copied from Uniprot (http://www.uniprot.org) database (ID Q9BPW8 and O75323 respectively) and run on the 'EMBOSS Needle' program (https://www.ebi.ac.uk/Tools/psa/emboss_needle/) for comparative analysis.

1.4.4 Myoferlin and other ferlins

Myoferlin (MYOF) is a 235 KDa protein (2061 aa) that belongs to the evolutionarily conserved ferlin protein family. The other members of the family are dysferlin (DYSF), and otoferlin (OTOF). The ferlins are type II membrane proteins characterised by multiple C2 domains (second constant sequence of 'classical' protein kinase C (PKC) isoform) facing the cytoplasm and a C terminal transmembrane domain (Chapman, 2002; Achanzar and Ward, 1997; Davis *et al.,* 2002; Bansal and Campbell, 2004; Doherty and McNally, 2003). MYOF, which has ~60% amino acid similarity to DYSF, has been proposed to contain six C2 domains and additional Src-homology-3 (SH3) domains (Figure 1.10) (Doherty et al., 2008; Pangršič et al., 2012; Davis et al., 2000). The C2 domains in the ferlin protein family are thought to act the

same way as has been predicted for membrane associated synaptotagmins (Syts), which is to trigger exocytosis in response to increasing Ca^{2+} (Chapman *et al.,* 2002; Davis et al., 2002; Bansal and Campbell, 2004; Doherty and McNally, 2003; Therrien et al., 2009). However, C2 domains can also interact with phosphatidylserine, zwitterionic lipids, and phosphotyrosines in a Ca^{2+} -dependent or -independent manner (Cho and Stahelin, 2006; Rizo and Sudhof, 1998; Fernandez-Chacon *et al.,* 2001; Davis *et al.,* 2002; Chapman *et al.,* 2002). Overall, the ferlin protein family is thought to participate in the regulation of membrane fusion events in cells (Bansal and Campbell, 2004; Doherty and McNally, 2003; McNeil and Kirchhausen, 2005). The role of ferlin-specific domains FerI, FerA and FerB are not known (Glover and Brown, 2007).

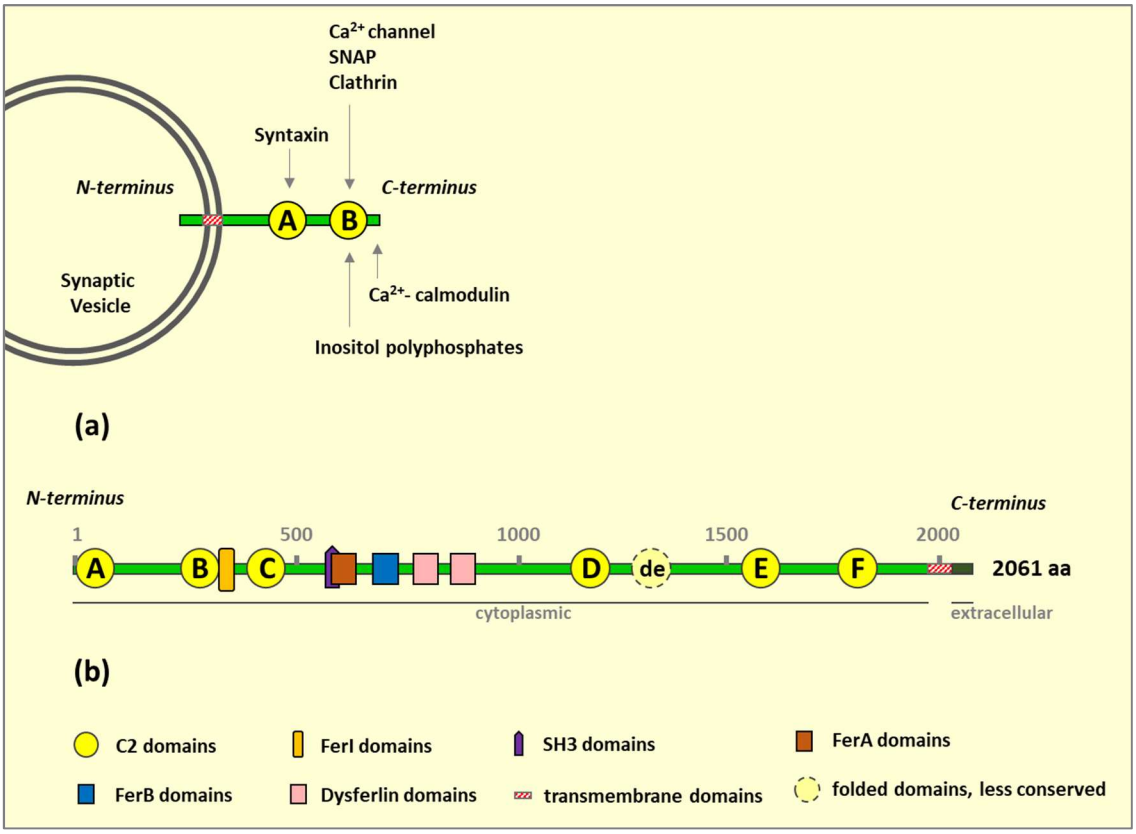

Figure 1.10 | Synaptotagmin and myoferlin structure. (a) Synaptotagmin is a small transmembrane protein with two C2 domains found on synaptic vesicles. (b) Myoferlin is a 2061 amino acid long protein with six C2 domains, some Fer (I, A, B) domains, a SH3 domain and dysferlin domains.

MYOF is expressed in skeletal muscle sarcolemma and can also be found in spleen, kidney, lung, heart and other muscle tissues (Britton et al., 2000; Davis et al., 2000). Within a cell MYOF can be found in the nucleus, the nuclear membrane, cytosolic vesicles and also in the plasma membrane (Davis et al., 2000). Human MYOF has been proposed to take part in different cellular processes like myoblast fusion, endocytosis, growth factor receptor stability and cell membrane repair (Doherty et al., 2008; Bernatchez et al., 2007 and 2009; Demonbreun et al., 2010). During myoblast fusion MYOF binds directly with EHD2, a member of Eps15 homology domain (EH domain) protein family implicated in endocytosis and endosome recycling to the plasma membrane (Doherty et al., 2008; Posey et al., 2011).

In endothelial cell signalling MYOF has been shown to modulate vascular endothelial growth factor/vascular endothelial growth factor receptor (VEGF/VEGFR-2) by stabilising VEGFR-2 (Bernatchez et al., 2007). In cancer cells MYOF has been shown to stabilise epidermal growth factor receptor (EGFR) to control EGF/EGFR signalling (Turtoi et al., 2013). Likewise, MYOF binds to the insulin growth factor receptor-1 (IGFR-1) (Demonbreun et al., 2010). Figure 1.11 outlines the proposed role of MYOF in endocytosis: in the absence of MYOF endocytic vesicle recycling and fusion with the plasma membrane slows down leading to an increased chance of receptors being targeted to the lysosomal degradation pathway (Doherty et al., 2008; Demonbreun et al., 2010). MYOF has been also shown to co-localise with the tight junction protein zonula occludens-1 (ZO-1), and siRNA knock down of MYOF contributed to a loss of cell adhesion of airway epithelial cells (Leung et al., 2012). Conversely, in breast cancer cells MYOF depletion has been shown to increase phosphorylation of focal adhesion kinase and paxillin, and enhance cell-matrix adhesion (Blackstone et al., 2015). MYOF has also been proposed to contribute to both clathrin-dependent and caveolin-mediated endocytosis, and it can be observed to co-localise with dynamin 2 and caveolin 1. The SH3 domain in MYOF has been shown to form a complex with dynamin-2 and VEGFR-2 (Bernatchez et al., 2007). This indicates a potential role of MYOF in both membrane fission in addition to the proposed role in vesicle fusion events (Doherty et al., 2008; Bernatchez et al., 2009). Therefore, the roles of MYOF may be diverse and cell type dependent.

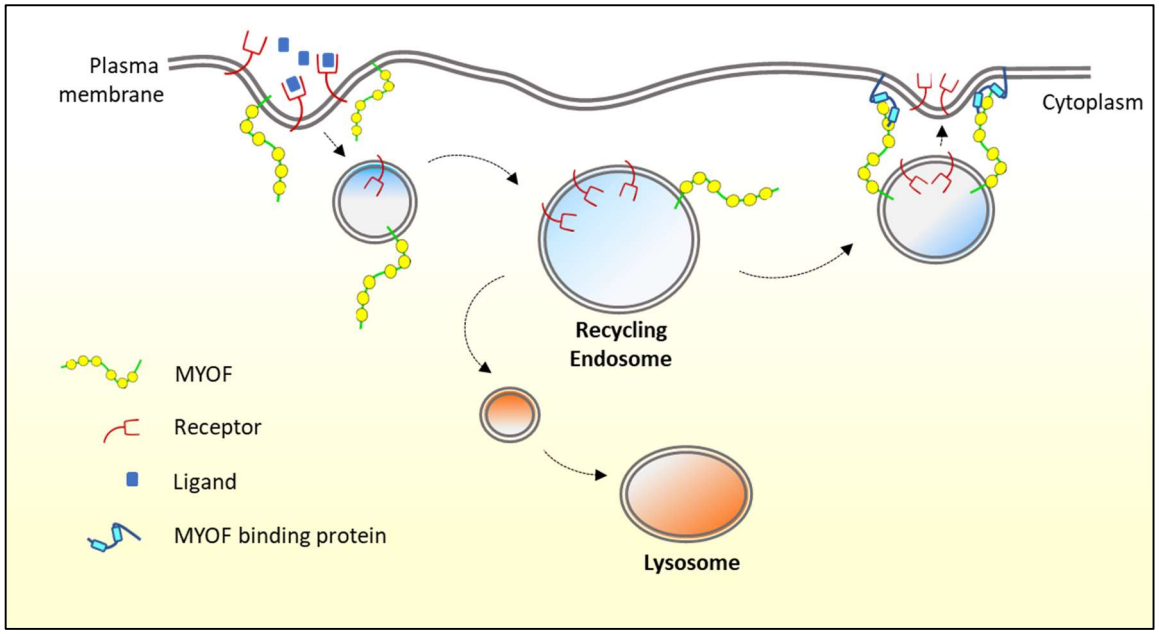

Figure 1.11 | Model for the role of myoferlin during receptor endocytosis. Myoferlin is thought to be an important regulator of bidirectional membrane turnover events (endocytosis and exocytosis). Myoferlin seems to protect the surface receptors and in the absence of myoferlin surface receptors follow degradative pathways.

1.5 Aims of this thesis

The aims of this thesis were to provide further understanding of the egress mechanism of HSV-1 with specific interest in identifying cellular proteins assisting in these processes. The research was divided into two major parts. The first section involved characterisation of an HSV-1 passage mutant selected for increased release into cell culture medium and identification of viral genes and mutations responsible for the observed release phenotype of the strain. In the second section of the thesis, screens and functional validation experiments were conducted to investigate cellular proteins that interact with the HSV-1 gE/gI complex and understand their potential roles in virion replication and egress.

2. Studying an HSV-1 passage mutant to understand what factor leads to increase virion secretion property during infection

2.1 Introduction

HSV-1 egress is the outcome of a series of intricate events. In cell culture models of infection, most progeny virus particles remain cell-associated and very few particles are present in the cell culture medium until late stages (15 hpi) of infection (Newcomb and Brown, 2012; Abaitua et al., 2013). This is thought to be at least partly due to newly secreted virions becoming or remaining attached to the extracellular surface of the plasma membrane after they are secreted from the producing cell. Additionally, virions have been shown to be delivered to cell-to-cell contact points, which is thought to help mediate rapid spread to neighbouring cells and evade the host immune system (Al-Mubarak et al., 2004; Johnson and Huber 2002; Johnson et al., 2001; Collins and Johnson, 2003). The trapping of viruses at the cell junctions, whether or not they are physically attached to the plasma membrane, is likely to also contribute towards fewer virions being secreted into the culture medium. The effect of successful cell-to-cell spread of virus can be observed on cell-culture monolayers by the formation of distinctive plaques. Virus cell-association, targeted virion secretion to cell contacts, and consistent plaque spread all rely on proper functioning of viral envelope glycoproteins during infection (Abaitua et al., 2013; Spear and Longnecker, 2003; Mettenleiter, 2002 and 2004).

The studies in this thesis have been mainly conducted using the KOS strain of HSV-1. The KOS strain was originally isolated from a lip lession of Kendall O. Smith and is commonly used for laboratory studies (Smith, 1964). The KOS strain was chosen for this study because an isolate of this strain that had cloned as a bacterial artificial chromosome (BAC) was already available in laboratory. To investigate viral activities that contribute to the cell-associated nature of HSV-1, the KOS strain was serially passaged in the laboratory by repeatedly collecting cell free virus from culture medium of infected cells and using this to infect fresh cells. After twenty-two passages, a plaque purified isolate was generated that was found to secrete substantially more infectious virus into the culture medium of infected cells compared to the parental strain. The aim of this chapter was to characterise the passage mutant strain to understand it's genetic changes, identify the mutation(s) that may contribute to the altered phenotype and generate recombinant viruses containing individual or multiple mutations that

were observed in the passage mutant for further studies on the mechanism of virus release from infected cells.

2.2 Results

2.2.1 Assessing the proportion of cell-associated virus for different HSV-1 strains

HSV-1 is generally considered to be predominantly cell-associated. To investigate whether the proportion of infectious virus present as cell-associated virus or free extracellular virions in the culture medium varies between different strains of HSV-1, two cell lines commonly used for HSV-1 research, Vero (primate kidney epithelial) and HaCaT (human keratinocyte), were infected with four different wild type (WT) laboratory strains of HSV-1: KOS, StH2, Sc16, Strain 17 (S17) and a clinical isolate MG at 10 plaque forming unit (PFU)/cell. At 18 hpi culture supernatants were carefully collected and cellular debris was removed by two consecutive centrifugation steps. Cells were harvested by scraping in fresh medium, and cell-associated virus was released by freeze-thawing the samples. The amount of infectious virus present in cell-associated and supernatant fractions was determined by plaque assay on Vero cell monolayers (Figure 2.1 a). The proportion of infectious virus released into the culture medium was determined as supernatant titre divided by total titre (cell-associated titre plus supernatant titre) (Figure 2.1 b). For all strains of HSV-1 the majority of infectious virus was present in the cell-associated fractions for both cell types (>99% in most conditions). This demonstrates that relatively little infectious virus is released from infected cells into the medium (<1%) by late stages of the HSV-1 replication cycle in both of these cell types, irrespective of the strain of WT HSV-1. One exception to this was the SC16 strain in HaCaT cells where the percentage of virus release reached ~3% (Figure 2.1 b), although subsequent experiments suggested this value was aberrantly high. These findings are consistent with previous research demonstrating that the majority of the HSV-1 particles remain attached to the extracellular surface of the plasma membrane after egress (Mingo et al., 2012).

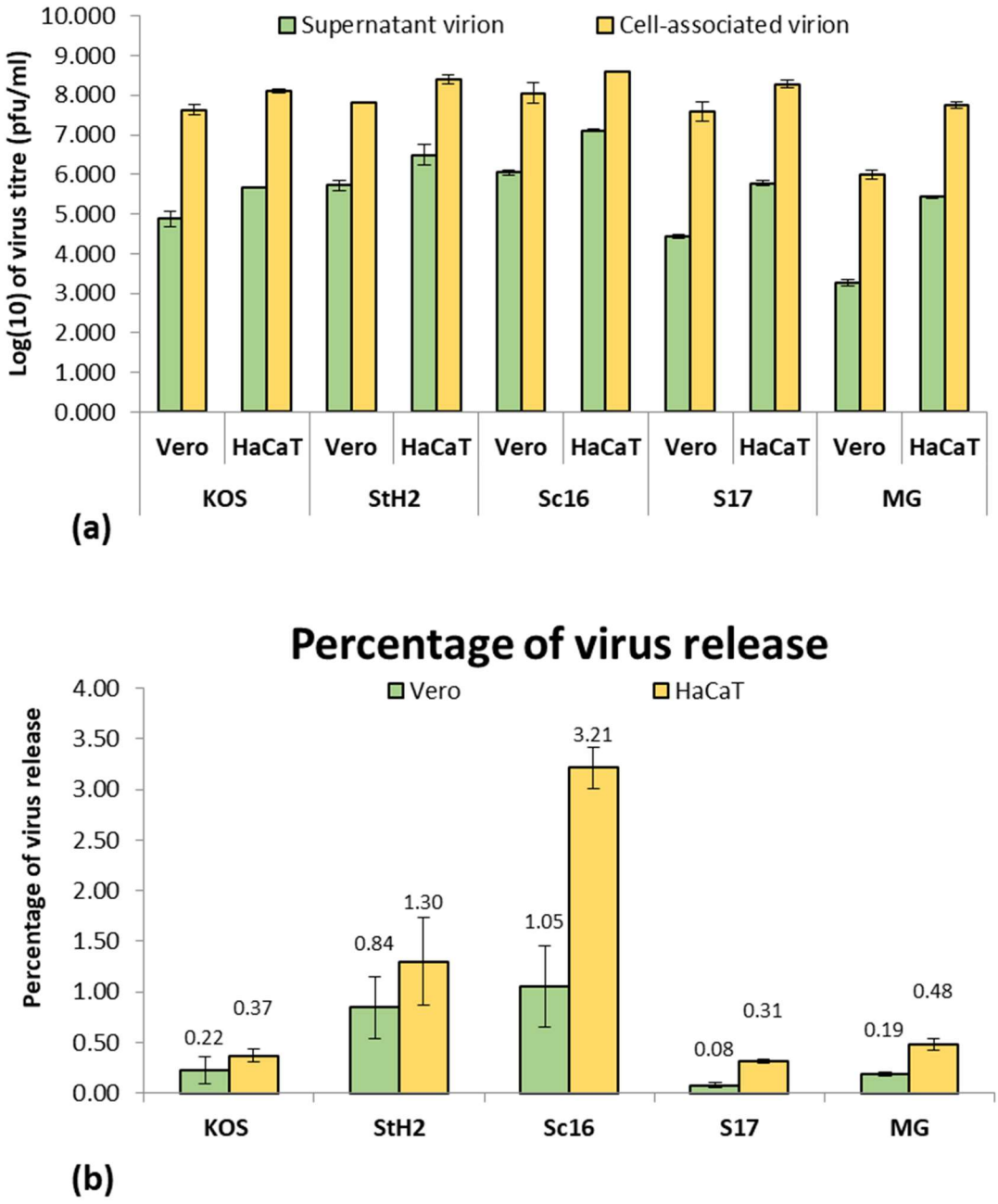

Figure 2.1 | Growth assay of different WT HSV-1 strains on different cell lines. Vero and HaCaT cell lines were infected with KOS, StH2, Sc16, S17 and MG strains of WT HSV-1 viruses at 10 PFU/cell. Cell-associated and supernatant virus fractions were harvested at 18 hpi and infectious titres were determined by plaque assay in Vero cells. (a) log(10) value of the cell-associated and supernatant virus titre and (b) percentage of released virus titre (supernatant titre/(cell-associated titre+supernatant titres)x100) on the cell lines utilized. Error bars represent standard errors of the means of 3 biological replicates.

2.2.2 Isolation of an HSV-1 strain with enhanced virion release into the cell culture medium

To select for HSV-1 variants that releases a greater proportion of virions into the medium of cultured cells a serial passage of WT HSV-1 (strain KOS) was conducted by infecting COS-7 cell monolayers at low (0.01 PFU/cell) multiplicity of infection (MOI), incubating for 2-3 days and then using the media from the infected cells, clarified of cell debris by centrifugation, to innoculate fresh COS-7 monolayers (Figure 2.2).

The relative amounts of cell-associated and supernatant virus produced by virus stocks at different passage numbers was measured and compared to that of the WT strain. At 22 passages the virus population demonstrated a marked increase in the proportion of infectivity present in the culture media. A single plaque-purified isolate was generated from this passaged population (V22a). The serial passage and plaque purification were conducted by Susanne Bell prior to commencing this research.

To investigate the release properties of the cloned passage mutant, the V22a isolate and the parental WT KOS strain were used to infect Vero, COS-7, HeLa, HaCaT, HFF-hTERT and A549 cells. At 18 hpi infectious virus titres present in the supernatant and cell-associated samples were determined by plaque assay on Vero cell monolayers (Figure 2.3 a and b). Both of the viruses replicated efficiently in all cell lines with the exception of HeLa cells where both the viruses grew relatively poorly, and HaCaT cells where the V22a strain showed poorer growth than WT. A substantial increase in the proportion of total infectious virus released into the media was observed for V22a compared to WT HSV-1 in all cell lines, with an approximate 18-fold increase for HFF-hTERT, 31-fold increase for COS-7, 30-fold increase for Vero, 11-fold increase for both HaCaT and A549 cell lines. However, on HeLa cells only 1.6-fold increase in virion release was observed (Figure 2.3 c).

It could be argued that the greater amount of infectious virus in the supernatant fraction of the V22a strain is due to a lower particle:PFU ratio compared to the WT HSV-1. If this was the case, then the V22a strain would have been expected to show a correspondingly similar increase in the amounts of cell-associated virus infectivity compared to WT. However, as can be seen in Figure 2.3 b, there was not a consistently greater total infectious virus titre produced for V22a compared to WT in the different cell lines, with some cell types showing lower total infectivity but higher released infectivity for V22a than WT, suggesting a decrease in particule:PFU ratio is unlikely to be the reason for these observations. To investigate this further, additional techniques such as qPCR (to quantify viral genome), and electron microscopy or immunofluorescence microscopy (to quantify virus particle numbers) could be conducted to determine genome:PFU and particle:PFU ratios for supernatant fractions of V22a compared to WT virus more directly.

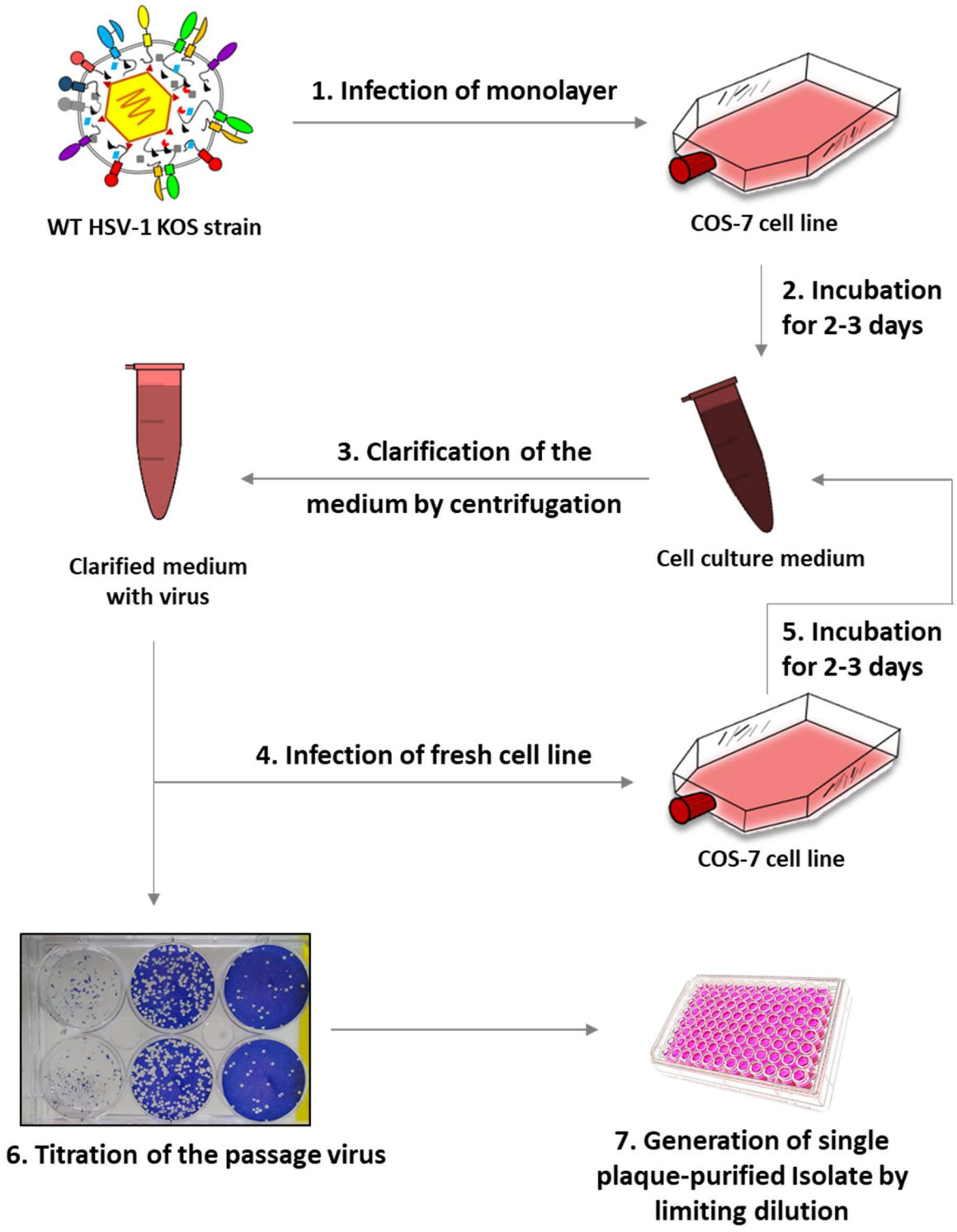

Figure 2.2 | Generation of a virus strain with increased secretion by serial passage of infected cell supernatant. A COS-7 cell monolayer was infected with low MOI (0.01 PFU/cell) of WT HSV-1 KOS strain. Viruses released in the supernatant was clarified and transferred to fresh cells periodically. Passaged virus stocks were titred on Vero cells at various intervals until a population of sufficiently increased secretion was achieved. From the population, single plaque-purified V22a passage mutant was isolated by limiting dilution.

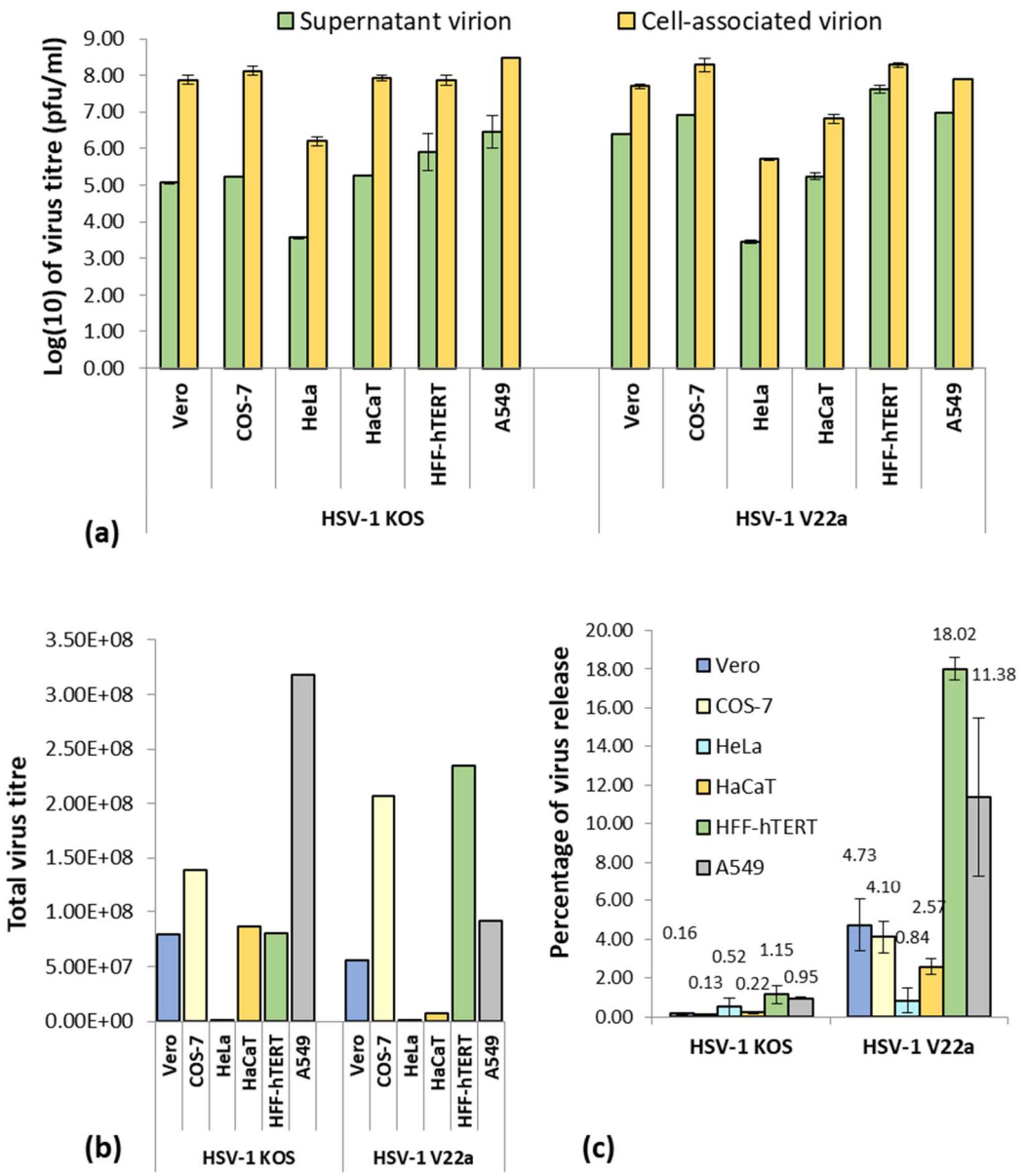

Figure 2.3 | Growth and release properties of HSV-1 strains on different cell lines. Vero, COS-7, HeLa, HaCaT, HFF-hTERT and A549 cells were infected with WT HSV-1 strain KOS and the passage mutant V22a. At 18 hpi supernatant media and cell-associated virus samples were collected, and virus titres were determined by plaque assay on Vero cells. (a) log(10) value of the cell-associated and supernatant virus titre, (b) total amount of virus being made on individual cell line and (c) percentage of virus release titre. Each experiment was repeated at least three times. Data presented here is from a single representative experiment containing duplicate samples. Error bars indicate standard error of the two biological replicates.

To understand the possible genetic changes in the V22a strain that could cause the increased virus release, viral genome sequences were obtained by next-generation sequencing (NGS) using DNA isolated from cells infected with WT or V22a. NGS and sequence analysis was kindly performed by Rory Bowden (University of Oxford, UK). Greater than 2 million reads were mapped to the HSV-1 genome (Strain 17 reference sequence; NC_001806.2) for both samples, giving 95.7% and 93.7% coverage for WT and V22a respectively. Alignment and pairwise comparison analysis of the consensus sequences demonstrated a 2890 bp deletion and 27 single nucleotide differences in the V22a sequence compared to the parental WT HSV-1 (KOS strain). The deletion (corresponding to nucleotides 94889-97778 in NC_001806.2) spans the majority of the UL43 and UL44 genes, which encode a multi-pass transmembrane protein of unclear function (pUL43) and glycoprotein C (gC) respectively. This deletion leaves only the first 30 codons of UL43 and the last 22 codons of UL44, which could conceivably result in the expression of a short fusion protein of the N terminus of pUL43 and the C terminus of gC (MLRNDSHRAVSPEDGQGRVDDGRPHLACVG^VLVVTAIVYVVRTSQSRQRHRR). Out of the single nucleotide differences there were 11 intergenic, 10 non-synonymous and 6 synonymous changes (Table 2.1). The intergenic changes will not translate into protein and the synonymous changes will incorporate the same amino acid into the protein. Of the non-synonymous mutations UL16 (A→V), UL38 (A→V) and US12 (V→G) are relatively conservative changes which would be predicted to have little effect on overall protein activity. Among the other viral genes with a coding sequence difference UL12, UL30 and UL52 encode non-structural proteins involved in DNA replication and so are unlikely to be directly involved in virion egress. ICP4 is the major viral transcription factor and has no reported role in virus assembly or egress, although ICP4 is present in the tegument. VP16 is a tegument protein that is essential for virion assembly, although has no reported role in post-assembly virus egress, and the amino acid alteration is relatively conservative (A→T).

The glycoprotein I (gI), an envelope glycoprotein that forms a complex with gE, which is known to facilitate virion egress and deliver virions for secretion at cell-junctions (McMillan and Johnson, 2001), acquired a non-synonymous point mutation (G→R) at codon 39. Regarding the two deleted proteins pUL43 has no known function and it is unclear whether this protein is a virion component, while gC has heparin-sulphate binding activity and functions as an attachment factor for virus binding to cells during entry (Herold et al., 1991; Shukla and Spear, 2001), and hence could also function to tether secreted virions to the cell surface after egress. Taken together, the deletion of pUL43 and gC, as well as the point mutation gI were considered the best candidates for contributing to the increased release phenotype of the V22a strain.

Table 2.1 | Single nucleotide differences between HSV-1 WT (KOS strain) and passaged isolate (V22a). Sequencing reads were mapped to nucleotides 9214-145585 of the Strain 17 HSV-1 reference sequence (NC_001806.2); this sequence comprises the unique long (UL), internal repeat (RL-RS) and unique short (US) regions of the HSV-1 genome. All numbering refers to NC_001806.2.

Position	KOS WT	V22a	KOS WT codon	V22a codon	Type	Protein position	Amino acid change	Gene name	Product
11333	C	T	CTG	TTG	Synonymous	Codon 115	-	UL3	Nuclear phosphoprotein
26690	A	G	TCG	CCG	Nonsynonymous	Codon 67	$S_{67}P$	UL12	5'-to-3' exonuclease
31265	G	A	GCG	GTG	Nonsynonymous	Codon 11	$A_{11}V$	UL16	Tegument protein
46606	C	T	NA	NA	Intergenic	-	-	-	-
54670	G	A	CTG	TTG	Synonymous	Codon 376	-	UL27	Glycoprotein B
64189	C	T	TTC	TTT	Synonymous	Codon 461	-	UL30	DNA polymerase
64502	G	A	GCC	ACC	Nonsynonymous	Codon 566	$A_{566}T$	UL30	DNA polymerase
84925	C	T	GCG	GTG	Nonsynonymous	Codon 132	$A_{132}V$	UL38	Capsid triplex protein
103253	G	A	NA	NA	Intergenic	-	-	-	-
105032	C	T	GCT	ACT	Nonsynonymous	Codon 17	$A_{17}T$	UL48	Tegument protein VP16
105429	G	A	NA	NA	Intergenic	-	-	-	-
109682	C	T	CGC	TGC	Nonsynonymous	Codon 212	$R_{212}C$	UL52	DNA primase
129733	G	A	CTG	TTG	Synonymous	Codon 467	-	RS1	ICP4
130043	C	T	GCG	GCA	Synonymous	Codon 363	-	RS1	ICP4
130791	C	A	CGA	CTA	Nonsynonymous	Codon 114	$R_{114}L$	RS1	ICP4
130822	C	T	GCG	ACG	Nonsynonymous	Codon 104	$A_{104}T$	RS1	ICP4
131644	G	A	NA	NA	Intergenic	-	-	-	-
131652	C	T	NA	NA	Intergenic	-	-	-	-
131666	T	C	NA	NA	Intergenic	-	-	-	-
131739	G	A	NA	NA	Intergenic	-	-	-	-
139903	G	A	GGG	AGG	Nonsynonymous	Codon 39	$G_{39}R$	US7	Glycoprotein I
143921	C	T	NA	NA	Intergenic	-	-	-	-
145255	G	C	NA	NA	Intergenic	-	-	-	-
145260	C	A	NA	NA	Intergenic	-	-	-	-
145297	T	C	NA	NA	Intergenic	-	-	-	-
145350	A	C	GTG	GGG	Nonsynonymous	Codon 78	$V_{78}G$	US12	ICP47
145529	C	T	GGG	GGA	Synonymous	Codon 18	-	US12	ICP47

2.2.3 Plaque size analysis of WT and V22a viruses

During HSV-1 infection the majority of newly assembled viruses are thought to be delivered to cell junctions allowing rapid spread to the neighbouring cells and bypassing the effect of virus neutralising antibodies. The simplest way to study cell-to-cell transmission in cell culture is to study plaque formation by the virus under a semi-solid medium (e.g. containing carboxymethyl cellulose), which is commonly conducted using Vero cells. The overall diameter of plaques can reflect several cumulative processes, such as capacity of a virus to enter the cells, replicate, assemble properly, be secreted at cell junctions via appropriate intracellular transport pathways, interact with the uninfected cells at the junctions and penetrate these cells (Dingwell et al., 1994; Johnson et al., 2001; Mettenleiter et al., 2009; Abaitua et al., 2013). To understand whether the increased secretion of the V22a passage mutant affects cell-to-cell spread, the plaque formation capacity of V22a compared to parental WT virus was tested on Vero cell monolayers. At 3 days post infection the plaques were fixed and stained with toluidine blue, the plates were scanned and plaques were measured using Photoshop. As shown in Figure 2.4, no noticeable difference was observed for plaque size between V22a and WT. This indicates the increased secretion of the V22a passage mutant does not impact the ability of the virus to spread between cells and produce plaques, at least in the Vero cell line.

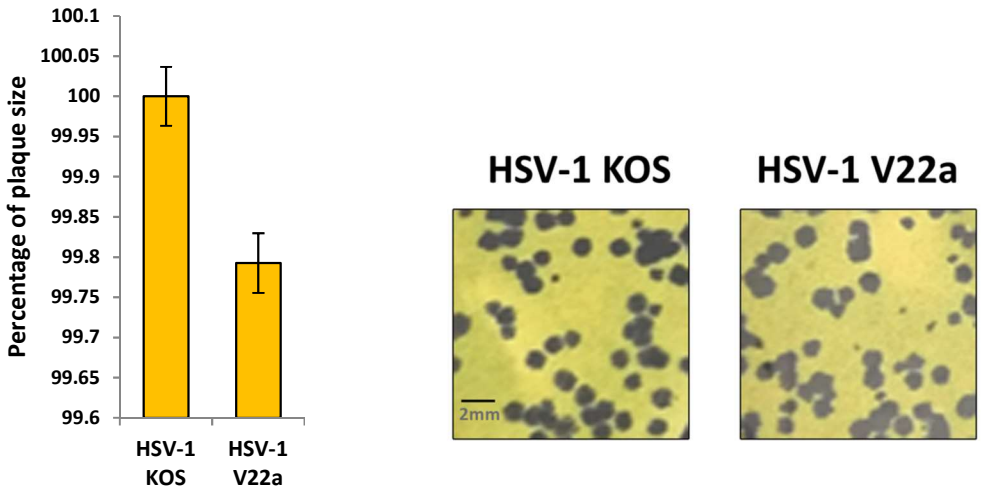

Figure 2.4 | Plaque size comparison of HSV-1 WT and V22a on Vero cells. Monolayers of Vero cells were infected with HSV-1 WT (KOS) or V22a viruses. After 3 days the cells were fixed and stained with toluidine blue and washed with water. The plates were scanned and diameters of the plaques were measured in Photoshop. Data shows average diameter of 60 plaques in percentage normalised to the average plaque diameter of the WT virus. Error bars indicate standard error of 60 plaques measured diameter. The pictures on the right shows areas toluidine blue stained plates (colour inverted in Photoshop for better illustration). Scale bar indicates 2 mm in length.

2.2.4 Protein expression profile of V22a passage mutant

The expression of a range of viral envelope glycoproteins in the V22a passage mutant compared to WT HSV-1 was investigated. Vero cells were infected with HSV-1 WT (KOS) or V22a and cell lysates were prepared at 18 hpi and analysed by WB using a range of monoclonal antibodies. gB, gD, gE and gH were expressed in both WT and V22a to broadly similar levels, whereas gC expression was completely absent in V22a infected cells, as expected due to the large deletion in the gene coding for gC (UL44). Interestingly gI, which has a single amino acid difference between WT and V22a (G39R), appeared to be expressed at a very low level in V22a-infected cells (Figure 2.5 a). The poor expression of gI was consistent and observed using two independent monoclonal antibodies (MAb-CC7 and MAb-CC8) (Figure 2.5 b). These observations suggest that the single mutation in gI in V22a (i.e., gIG39R) causes this glycoprotein to be less stable.

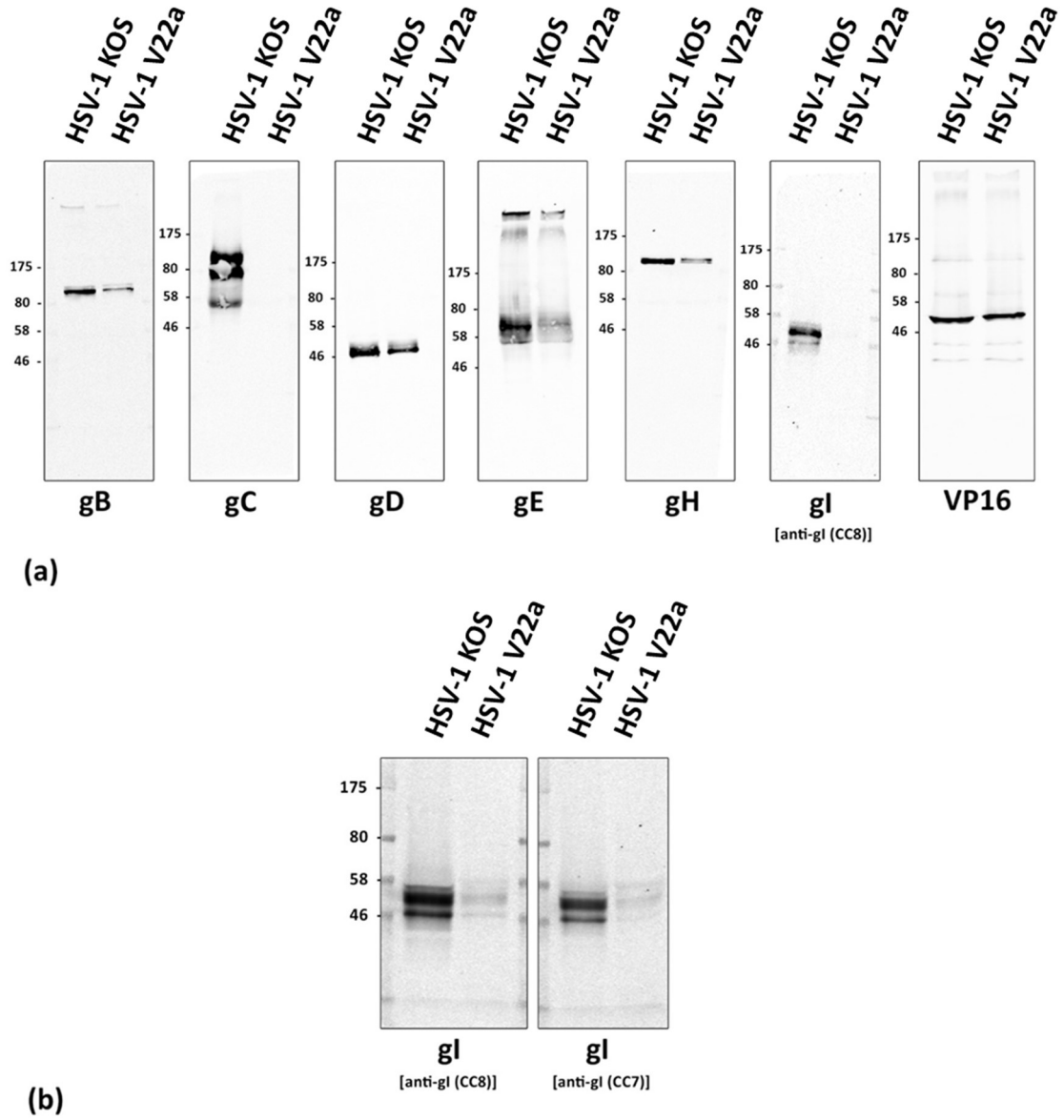

Figure 2.5 | Viral protein expression in cells infected with HSV-1 WT and V22a viruses. Vero cells were infected with HSV-1 WT or V22a viruses at 5 PFU/cell and cell lysates were prepared at 18 hpi, separated by SDS-PAGE and analysed by WB with antibodies indicated. (a) Shows expression of gB, gC, gD, gE, gH, gI and VP16 and (b) shows expression of gI utilising two different anti-gI antibodies (MAb-CC7 and MAb-CC8) in WT and V22a virus-infected cell lysates. Molecular mass markers (in KDa) indicated on left.

2.2.5 Immunofluorescence microscopy analysis of viral proteins expression

To investigate the expression of different HSV-1 proteins in infected cells by immunofluorescence (IF) microscopy, HFF-hTERT cells were infected with the HSV-1 WT and V22a strains. Cells were fixed at 18 hpi and probed with monoclonal antibodies to various HSV-1 proteins together with a rabbit polyclonal anti-HSV antiserum as a control for infection levels. As shown in Figure 2.6, no signal could be detected with an anti-gC antibody for the V22a-infected cells as expected. Surprisingly, a much higher expression of gI was noted in the V22a strain, despite clearly reduced proteins levels being observed in WB using the same anti-gI (MAb-CC8) antibody. The most logical explanation for an increased signal for V22a gI (gIG39R) in IF may be due to a greater exposure of the monoclonal antibody binding epitope in gIG39R despite there being less protein. The fluorescence signals for the other proteins tested (gB, gD, gE, gG, gH/gL and VP16) were similar in V22a-infected cells to that of WT with no observable difference in expression level or localisation. Unfortunately, the loss of pUL43 expression could not be confirmed by IF or WB due to the lack of suitable anti-pUL43 antibody.

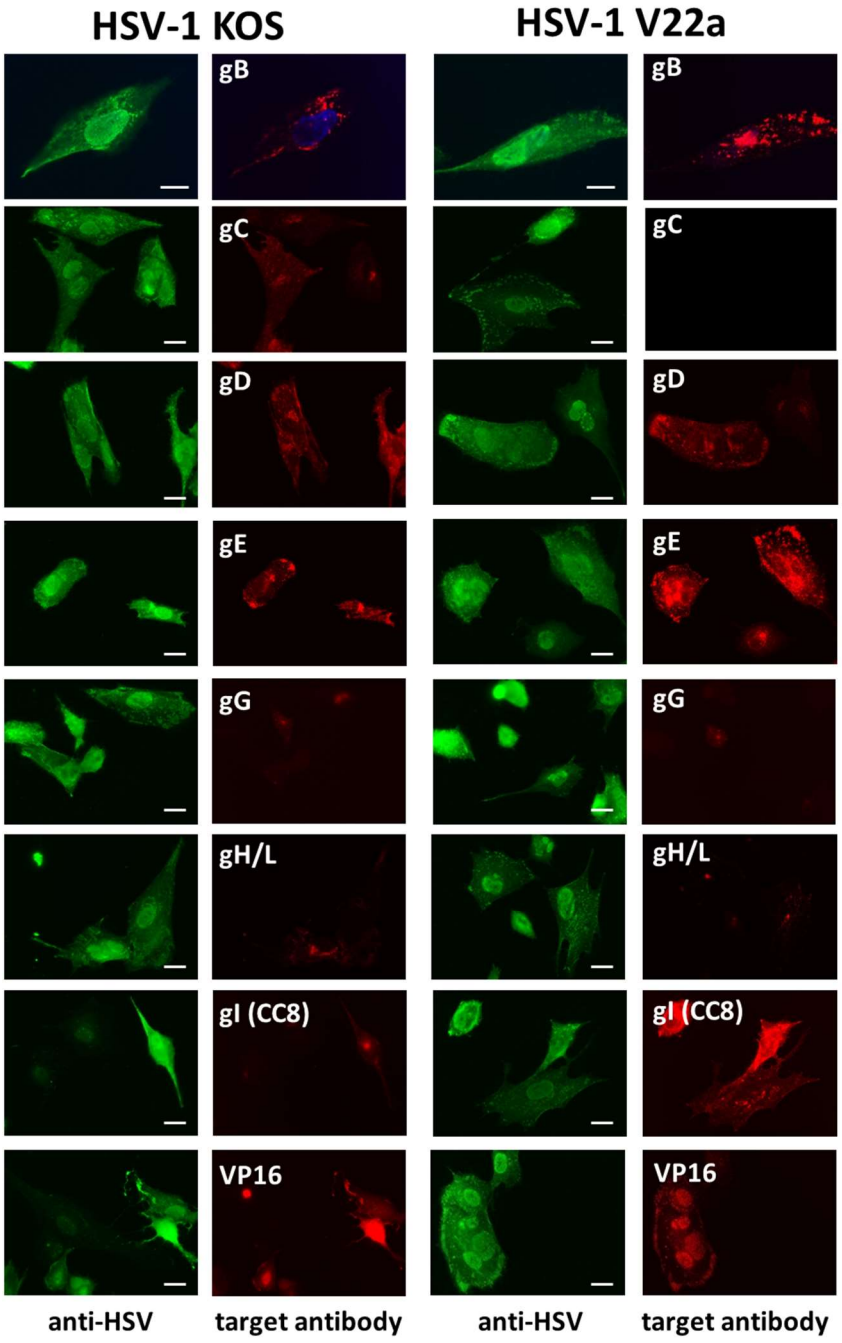

Figure 2.6 | Immunofluorescence microscopy analysis of HSV-1 WT (KOS) and V22a infected cells. Monolayers of HFF-hTERT cells grown on coverslips were infected with WT (left) and V22a passage mutant (right) at 5 MOI. At 18 hpi cells were fixed and permeabilised before staining with anti-HSV (shown in green) and target antibodies (shown in red). Images were taken using an Olympus IX-81 inverted fluorescence microscope using a 60x oil immersion lens. Blue: staining of nuclei with DAPI (4,6-diamidino-2-phenylindole). Scale bar indicates 20 μm.

2.2.6 Generation of pUL43, gC and gI recombinant viruses

Of the nine viral genes with altered protein coding in the V22a strain (Table 2.1), changes to viral membrane proteins were considered to be the most likely to affect HSV-1 egress or cell-association. Therefore, recombinant viruses were constructed expressing gI with the glycine residue at position 39 mutated to arginine (gIG39R) or lacking the expression of pUL43 (ΔpUL43) or gC (ΔgC) by inserting three tandem stop codons in frame after codon 53 of UL43 or after codon 36 of UL44 respectively (Figure 2.7). Additionally, all double and triple combinations of these mutations (ΔpUL43-gIG39R (gIG39R added on ΔpUL43 backbone); ΔgC-gIG39R (gIG39R added on ΔgC backbone); ΔpUL43-ΔgC (ΔgC added on ΔpUL43 backbone); ΔpUL43-ΔgC-gIG39R (gIG39R added on ΔpUL43-ΔgC backbone) were made. Furthermore, recombinant viruses lacking expression of functional gI (ΔgI) or it's binding partner gE (ΔgE) were generated by inserting 3 tandem stop codons in frame after codon 20 for both US7 and US8. These viruses were made to compare their life cycle and protein expression with that of gIG39R. Fluorescently-labelled viruses were constructed by inserting the coding sequence for EYFP at the C terminus of gI in a WT or gIG39R virus backbone and also on a backbone already containing mTurquoise-tagged VP26 (at the N terminus of VP26, replacing the first 4 codons). The rationale for making a gI^{EYFP} virus was to be able to determine the localisation of the protein in infected cells in an antibody epitope-independent manner, and immunoprecipitate the protein with GFP-Trap beads. All the recombinant viruses were generated in a BAC-cloned HSV-1 KOS genome using the Red-recombination method (Gierasch et al., 2006; Tischer et al., 2010).

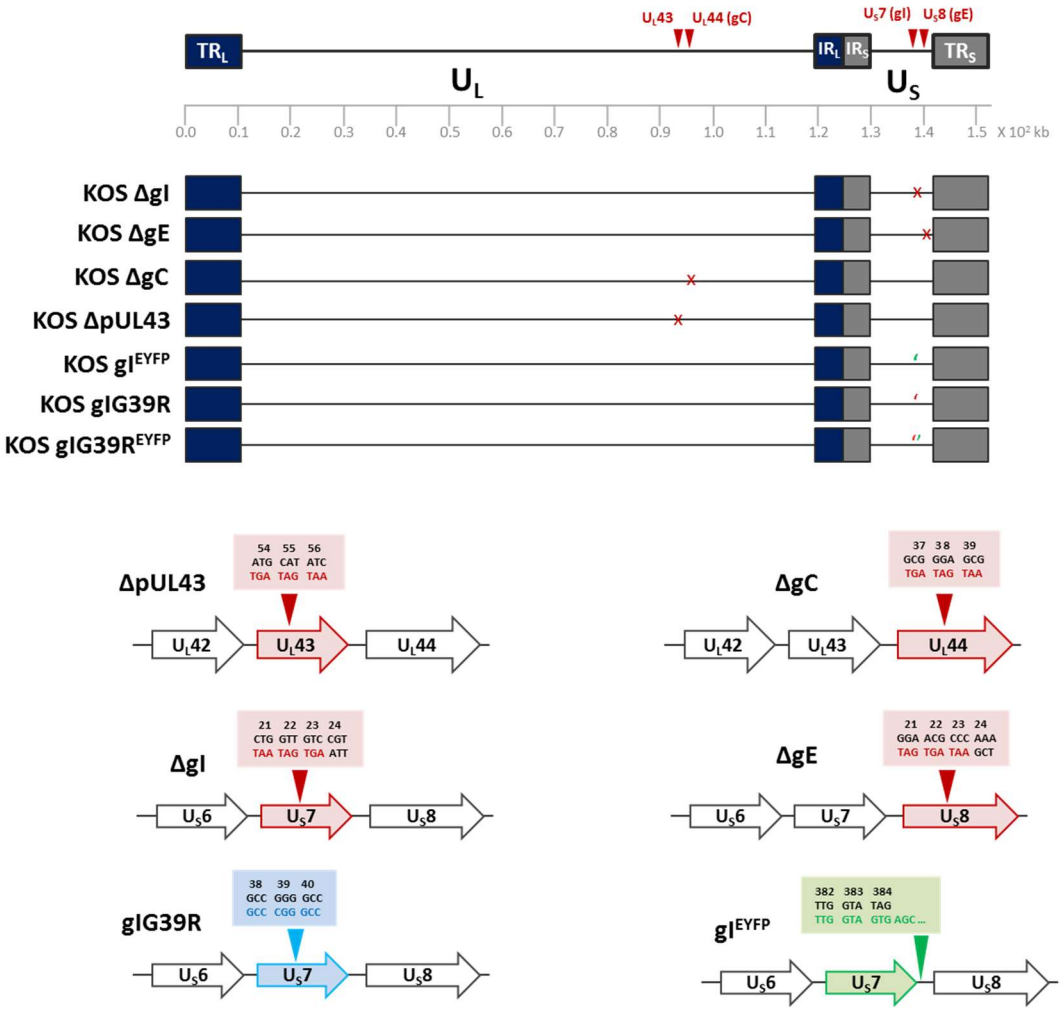

Figure 2.7 | Schematic representation of HSV-1 genome and the deletion mutants. BAC-cloned WT HSV-1 (KOS strain) was modified using the Red-recombination system to generate the indicated changes to the viral genome.

The single mutant ΔgC and ΔpUL43 strains were previously constructed in the lab and verified by DNA sequencing (by S. Bell and S.Y.K. Lau respectively). To confirm the correct insertion of the gIG39R mutation in the recombinant viruses, viral genomes were isolated from cells infected with recombinant virus stocks, the gI gene was amplified by PCR and sequenced. When compared to the NCBI database it confirmed the desired mutation in all the gIG39R mutant constructs (Figure 2.8). However, one other difference was observed between the gI sequence from all the new recombinant BAC viruses generated containing the gIG39R mutation when compared to the gI sequence from the WT KOS strain (sequenced by NGS) at amino acid position 198. All the recombinant BAC viruses had an asparagine codon, whereas the lab WT KOS sequence had a serine codon. Analysis of other KOS sequences on the GenBank database showed the same variation, with some sequences showing S at position 198 (GenBank: CAF24821.1, SBS69812.1) and others showing N at position 198 (e.g. GenBank: ASM47819.1). This suggests there is some variation within different isolates of the KOS strain and that the N at position 198 was already present in the parent BAC-cloned KOS strain used to generate all recombinant viruses.

Figure 2.8 | Confirmation of gIG39R mutation introduction in the recombinant virus constructs. HSV-1 WT, gIG39R, ΔpUL43-gIG39R-ΔgC, ΔpUL43-gIG39R, ΔgC-gIG39R and gIG39R^{EYFP} viral DNA from infected HaCaT cell were collected, the US7 gene region amplified by PCR and sent for sequencing. All the gIG39R mutants had the same G→R mutation at amino acid position 39 of the protein as shown in the representative alignment figure in red.

2.2.7 Comparison of viral protein expression of the recombinant viruses by WB

To investigate differences in viral protein expression by the recombinant viruses constructed and to recapitulate the protein changes observed in the V22a passage strain, Vero cells were infected with parental HSV-1 KOS-BAC (WT) or the recombinant viruses containing the gIG39R, ΔpUL43 and ΔgC mutations individually or in each double or the triple combination. Infected cell lysates were collected at 18 hpi and analysed by WB. Figure 2.9 illustrates that all viruses containing the ΔgC mutation do not express any detectable gC. Expression of VP16, gB, gD, gE, gG, and gH appeared similar for all the mutant viruses as compared to WT infection. However, all viruses harbouring the gIG39R mutation demonstrated a substantial reduction in the expression of gI, similar to the results observed in the V22a virus (Figure 2.5). The same observation was made with both gI-specific monoclonal antibodies (MAb-CC7 and MAb-CC8) suggesting the reduced detection of gI is not due to the gIG39R mutation affecting antibody recognition as it seems unlikely a single amino acid change would affect the binding of two independent monoclonal antibodies similarly. The expression of pUL43 could not be investigated due to a lack of appropriate antibodies.

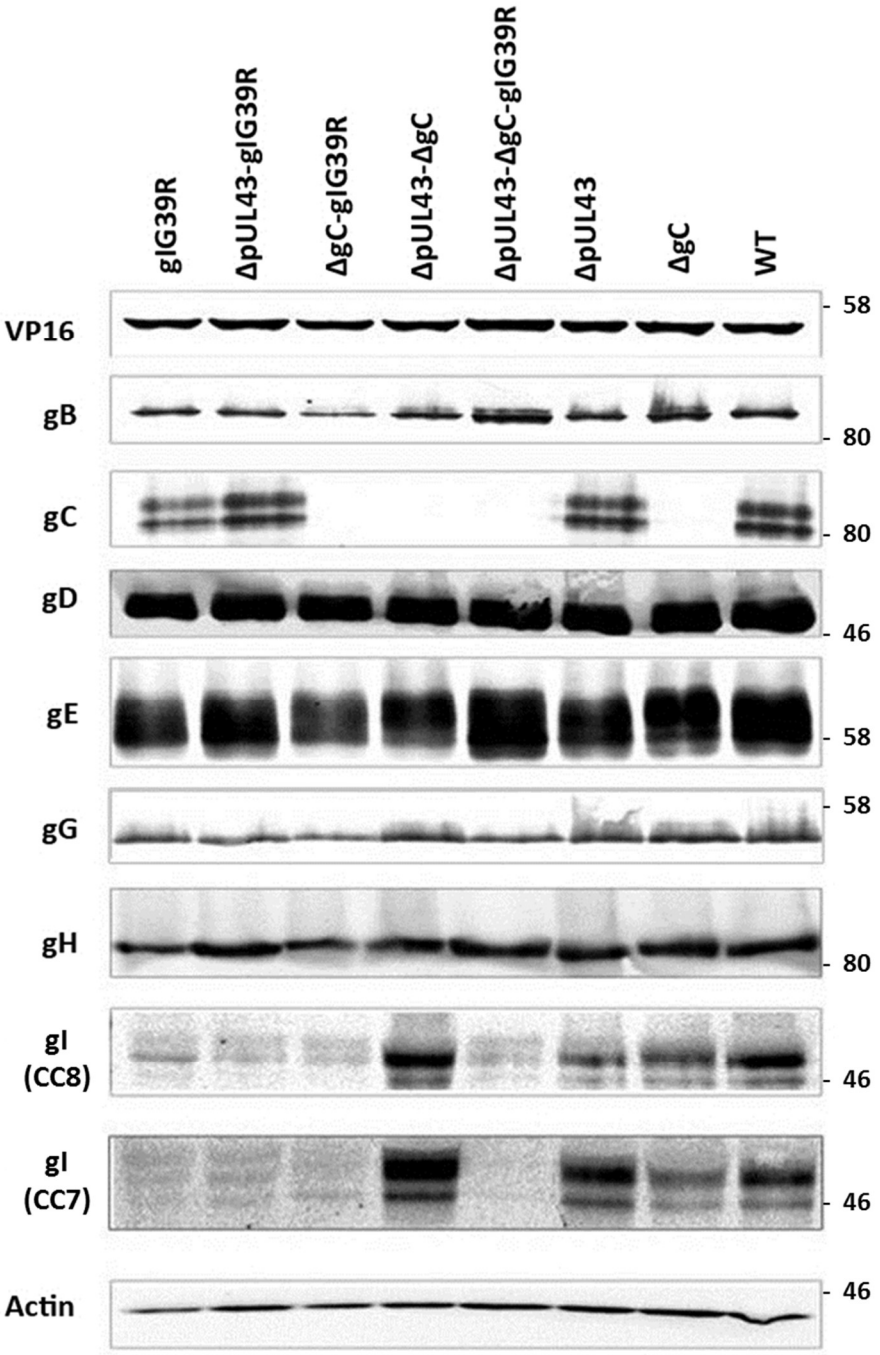

Figure 2.9 | Protein expression profiles of mutant viruses. Vero cells were infected with gIG39R, ΔpUL43-gIG39R, ΔgC-gIG39R, ΔpUL43-ΔgC, ΔpUL43-gIG39R-ΔgC, ΔpUL43, ΔgC and WT HSV-1 (KOS-BAC) viruses. At 18 hpi cells were lysed and proteins were separated by SDS-PAGE and then immunoblotted and tested for the expression of VP16, gB, gD, gC, gE, gG, gH, gI and actin. Numbers to the right indicate positions of molecular mass markers in KDa

2.2.8 Comparison of viral protein expression and localisation for the recombinant virus by immunofluorescence

To investigate the expression of different HSV-1 proteins among different recombinant viruses by IF microscopy HFF-hTERT cells were infected at 1 PFU/cell with WT, gIG39R, ΔgC and ΔpUL43 viruses for 8 h. The cells were fixed and stained for gC, gE, gI and anti-HSV antibody as a control of infection. Figure 2.10 shows images for the single mutant viruses (gIG39R, ΔgC and ΔpUL43). Similar to observations with the V22a passage mutant infected cells, the signal intensity of gI was greater in cells infected with the gIG39R virus compared to WT or the other mutants, despite the lower level of gI protein expression observed by WB data (Figure 2.9). The increased signal intensity with the gI antibody was consistently observed for all recombinant viruses containing the gIG39R mutant (Figure 2.11). The mutation of gI in each of these recombinant viruses was independently generated and confirmed by sequencing suggesting the increased signal intensity is due to the G39R mutation and not a secondary change to the sequence of gI (Figure 2.8). Furthermore, a similar increase of signal intensity was observed with the independent gI monoclonal antibody (MAb-CC7), with weak signals in WT-infected cells but stronger signals in gIG39R-infected cells (Figure 2.12). The expression of gE and gI by the ΔgE and ΔgI recombinant viruses was also tested by IF (Figure 2.13), which confirmed deletion of the targeted genes from the recombinant viruses. Interestingly with ΔgE virus-infected cells an increased signal intensity was also observed for gI compared to WT-infected cells. This suggests the epitopes for the gI antibodies tested are normally masked by interaction with its binding partner gE, and that perhaps the G39R mutation alters gI conformation to increase the accessibility of these epitopes in IF assays.

The dual fluorescent virus expressing mTurquoise-tagged VP26 (capsid) and EYFP-tagged gI was also analysed by fluorescence microscopy. HFF-hTERT cells were infected with ^{mTQ}VP26-gI^{EYFP} at 1 MOI for 8 h and then the cells were fixed. As shown in Figure 2.14 strong signals were observed in the nucleus for ^{mTQ}VP26 and in a perinuclear location reminiscent of the Golgi/TGN for gI^{EYFP}, as expected for a capsid protein and envelope glycoprotein respectively. In addition, small puncta near the cell periphery that were positive for both VP26 (in red) and gI (in green) were observed, suggesting EYFP-tagged gI becomes incorporated into enveloped virions.

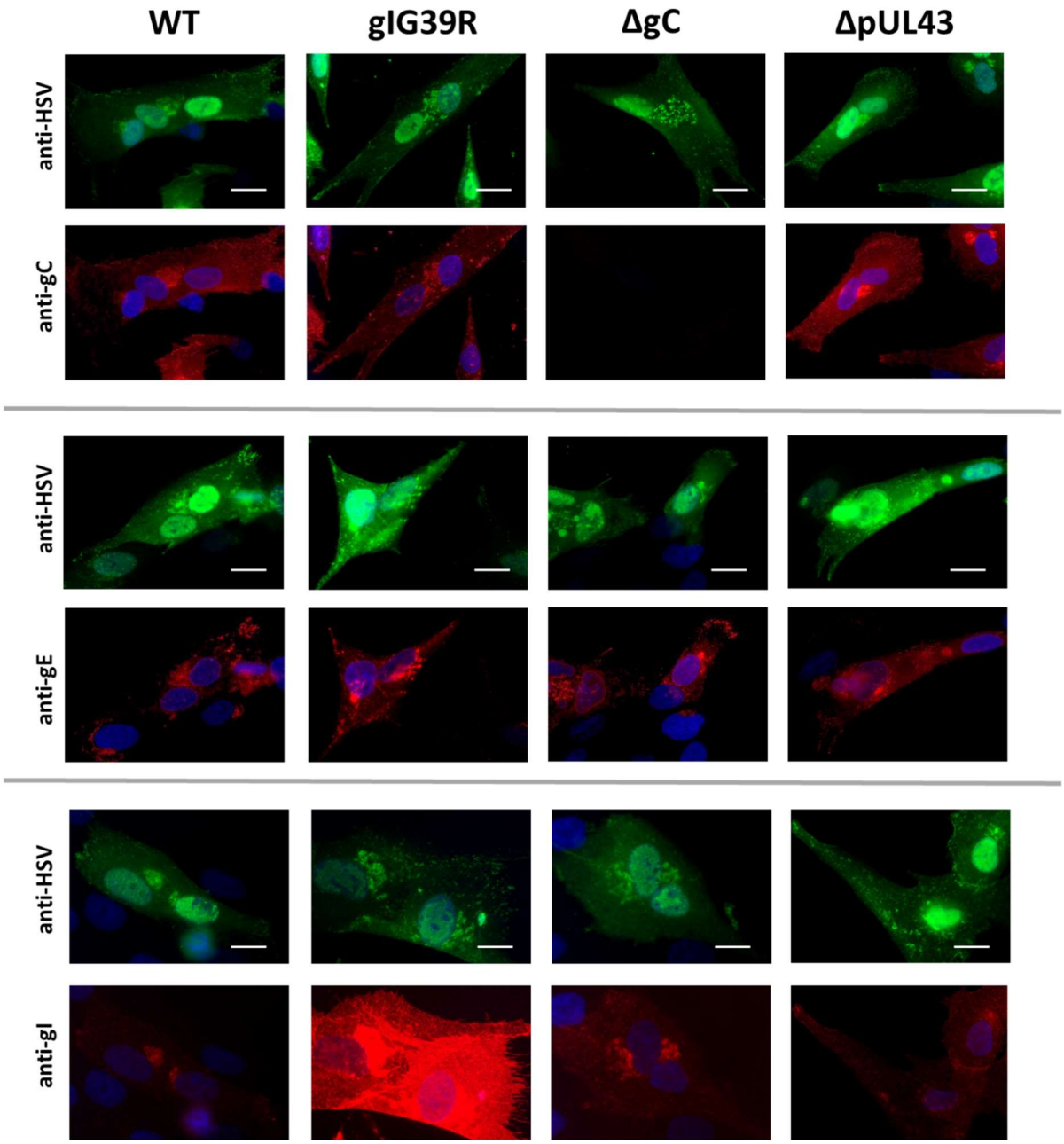

Figure 2.10 | Immunofluorescence assay to compare protein expression for single mutant viruses. Monolayers of HFF-hTERT cells grown on cover slips were infected with HSV-1 WT, gIG39R, ΔgC and ΔpUL43 viruses at 1 PFU/cell. At 8 hpi cells were fixed and permeabilised and were treated with anti- gC, gE and gI (MAb-CC8), antibodies together with anti-HSV antiserum. Images were taken using an Olympus IX-81 inverted fluorescence microscope using a 60x oil immersion lens. Blue: staining of nuclei with DAPI. Scale bar indicates 20 μm.

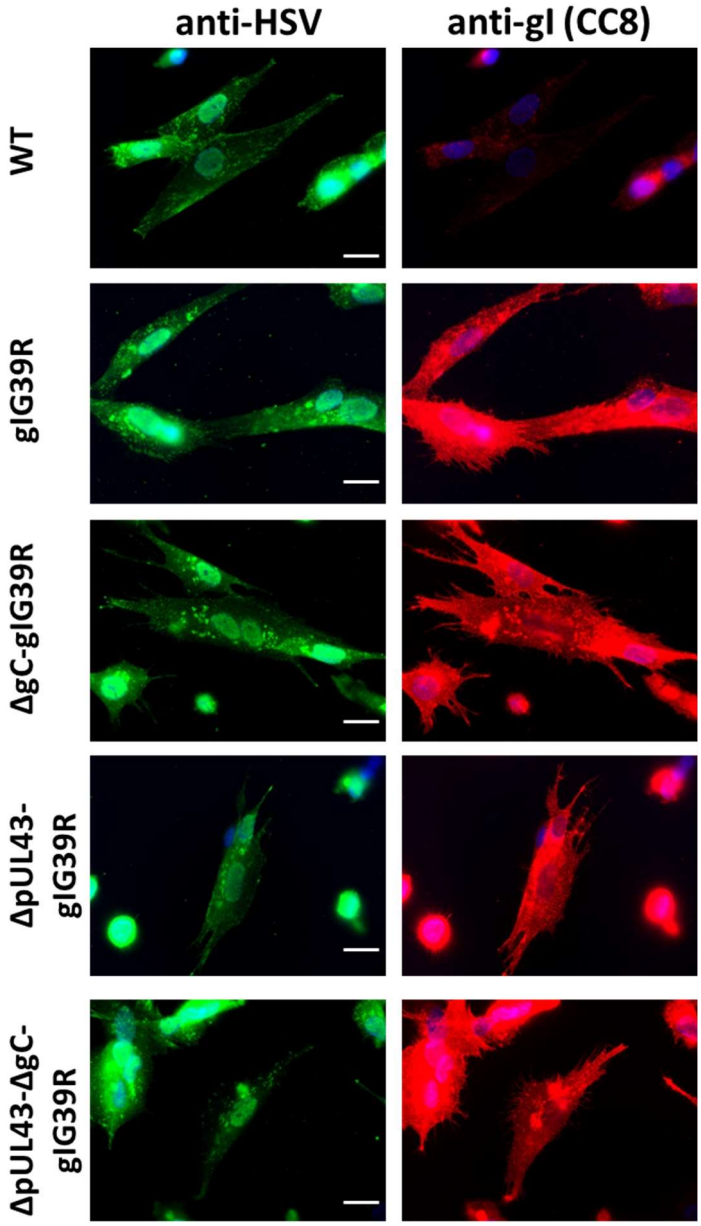

Figure 2.11 | Immunofluorescence to compare signal intensity for all independent recombinant viruses containing the gIG39R mutation. Monolayers of HFF-hTERT cells grown on cover slips were infected with HSV-1 WT, gIG39R, ΔgC-gIG39R, ΔpUL43-gIG39R and ΔgC-ΔpUL43-gIG39R viruses at 1 PFU/cell. After 8 h cells were fixed and permeabilised and were treated with polyclonal anti-HSV (green) and anti-gI (MAb-CC8, red) antibodies. Images were taken at the same exposure using an Olympus IX-81 inverted fluorescence microscope using a 60x oil immersion lens. Blue: staining of nuclei with DAPI. Scale bar indicates 20 μm.

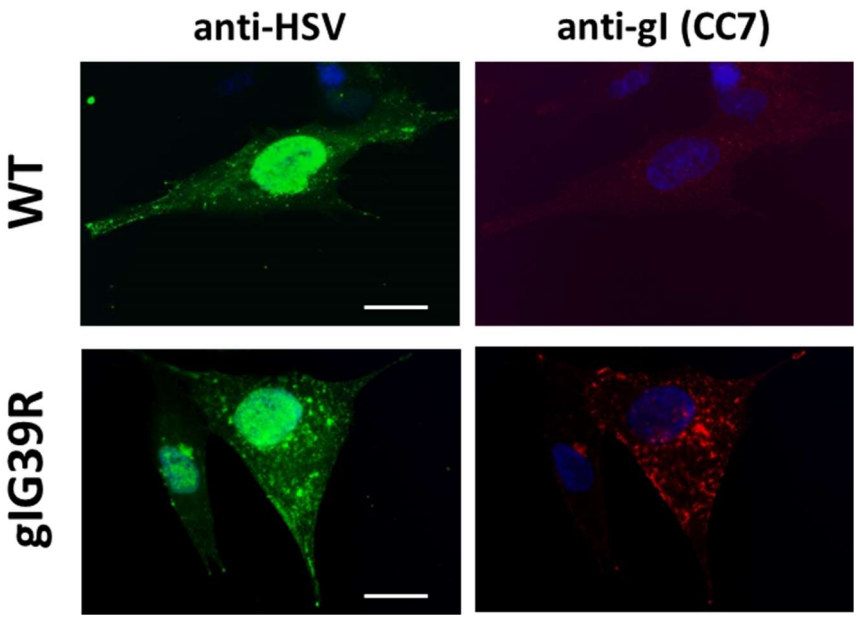

Figure 2.12 | Immunofluorescence to compare signal intensity for anti-gI (CC7) antibody in detecting gI in cells infected with WT and gIG39R viruses. Monolayers of HFF-hTERT cells grown on cover slips were infected with HSV-1 WT and gIG39R at 1 PFU/cell. After 8 h cells were fixed and permeabilised. Subsequently the cells were treated with polyoclonal anti-HSV (green) together with anti-gI (CC7) antibody (red). Images were taken at the same exposure using an Olympus IX-81 inverted fluorescence microscope using a 60x oil immersion lens. Blue: staining of nuclei with DAPI. Scale bar indicates 20 µm.

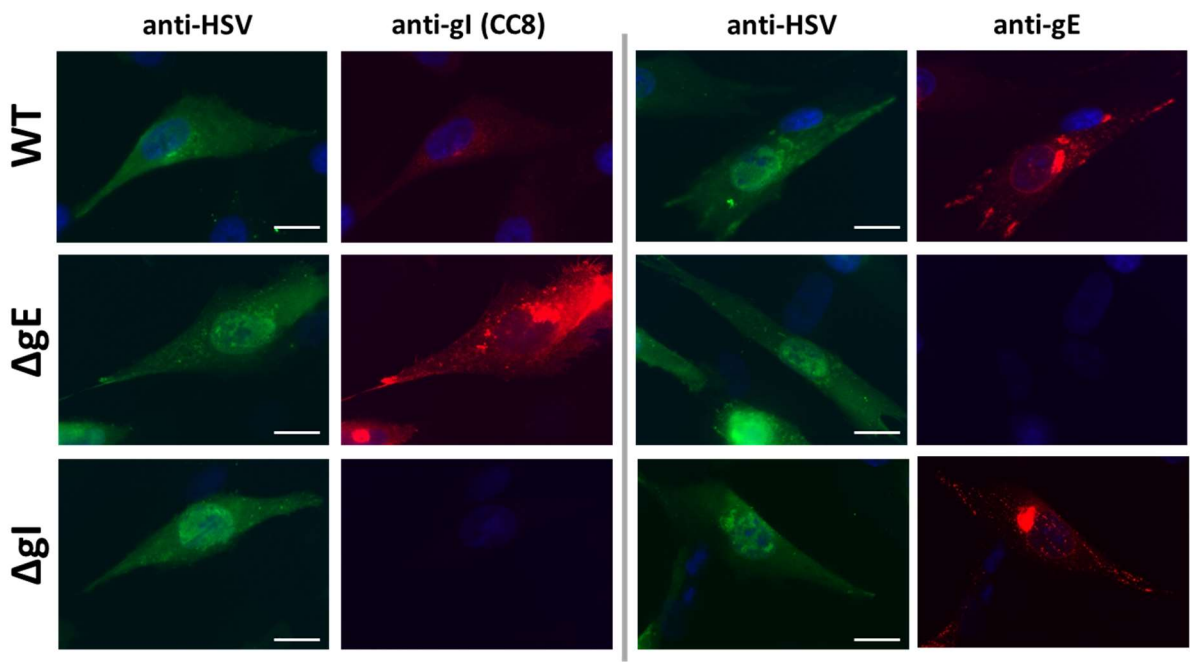

Figure 2.13 | Immunofluorescence analysis of gE and gI deletion viruses. Monolayers of HFF-hTERT cells grown on cover slips were infected with HSV-1 WT, ΔgE, and ΔgI viruses at 1 PFU/cell. After 8 h cells were fixed and permeabilised and were treated with polyclonal anti-HSV (green) together with anti-gI (MAb-CC8) or anti-gE antibodies (red). Images were taken using an Olympus IX-81 inverted fluorescence microscope using a 60x oil immersion lens. Blue: staining of nuclei with DAPI. Scale bar indicates 20 µm.

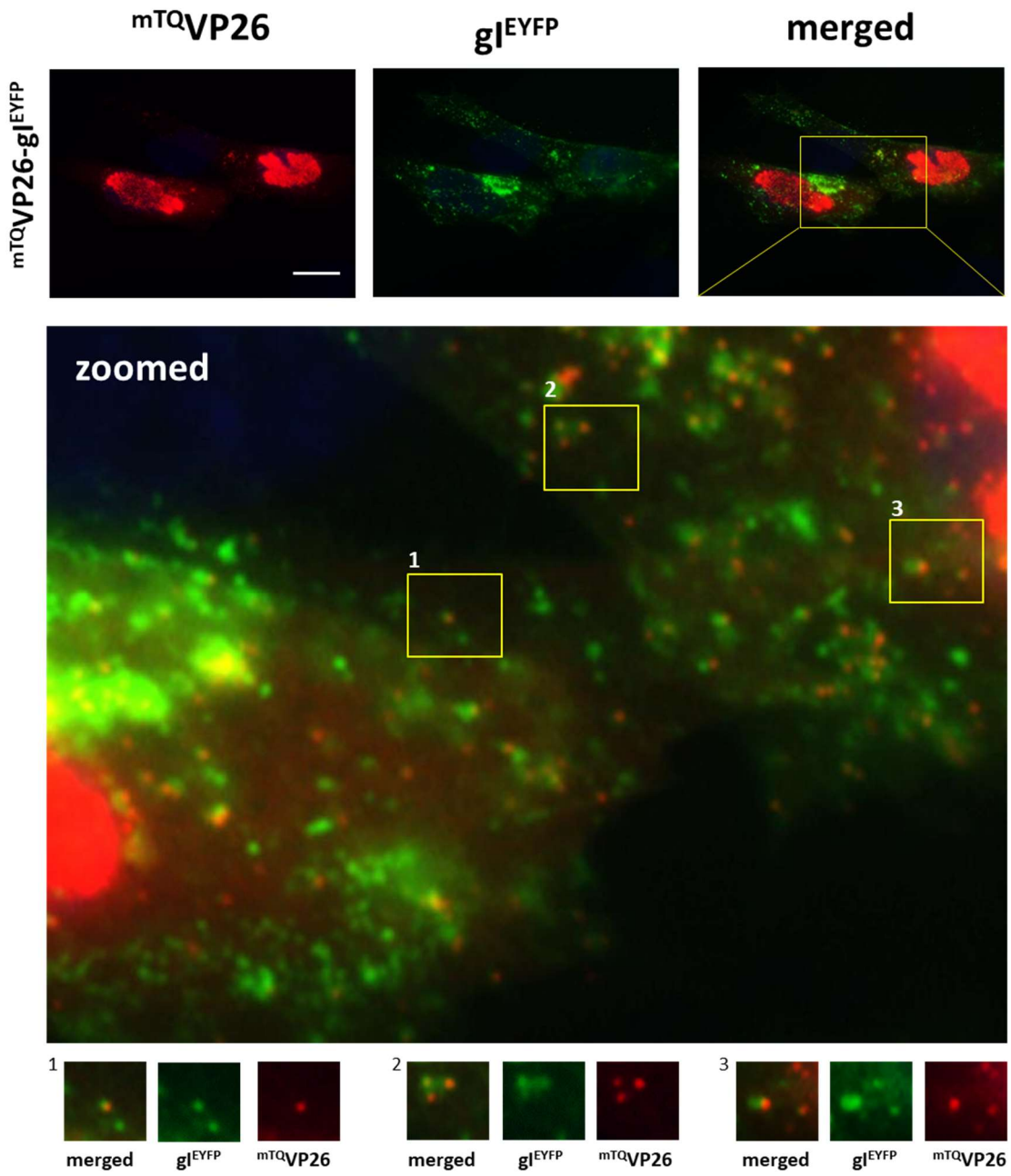

Figure 2.14 | Fluorescence microscopy images of ^{mTQ}VP26-gI^{EYFP} infected cells. Monolayers of HFF-hTERT cells grown on cover slips were infected with the ^{mTQ}VP26-gI^{EYFP} recombinant virus at 1 PFU/cell. After 8 h cells were fixed. Images were taken using an Olympus IX-81 inverted fluorescence microscope using a 60x oil immersion lens. Yellow boxes in the zoomed panel indicate HSV-1 particles positive for both VP26 (in red) and gI (in green). These selected areas are also shown separately in the bottom panel. Scale bar indicates 20 μm.

2.2.9 Replication and release of the recombinant viruses

To investigate the effect on virus replication and release into the medium of the various combinations of mutations in the newly generated recombinant viruses, Vero, HFF-hTERT and HaCaT cells were infected with each recombinant virus. At 18 hpi cell-associated (CA) and culture medium supernatant (Sup) were collected. The amount of infectious virus present in each sample was determined by plaque assays and the proportion of virus released was calculated. All viruses containing the gIG39R mutation demonstrated a greater proportion of virus released into the culture medium compared to WT (KOS-BAC) virus (Figure 2.15). An increase in the proportion of released virus was also observed for a virus lacking gI expression (ΔgI) in all three cell lines, and similarly for a virus lacking gE expression (ΔgE) in HaCaT and Vero cell lines, although surprisingly not in the HFF-hTERT cell line. The deletion of pUL43 appeared to have no obvious effect on HSV-1 replication or release either individually or in combination with any other mutation. On Vero cells, a marginal increase due to the ΔpUL43 mutation was suggested by these data, for example ΔpUL43-gIG39R and ΔgC-ΔpUL43-gIG39R released more virus than the gIG39R or ΔgC-gIG39R viruses. However, such potential effects of loss of pUL43 were small and not consistent between viruses or cell lines. The deletion of functional gC had little effect on virion secretion when alone or in combination with ΔpUL43, but loss of gC enhanced the release of virus into the culture media when in combination with the gIG39R mutation for both HFF-hTERT and HaCaT cells. Overall, these data suggest that the gIG39R mutation is primarily responsible for causing the greater release of infectious virus into culture medium observed for the passaged strain V22a, with the loss of gC increasing the magnitude of this effect in at least some cell types.

The replication and release properties of WT, gIG39R, ΔgE and ΔgI viruses over the course of a single cycle of HSV-1 replication were analysed by infecting HaCaT cells at 10 PFU/cell and harvesting cell-associated and culture medium fractions separately at 2, 6, 9, 12 and 24 hpi. The replication rate of all three mutant viruses was indistinguishable from WT HSV-1, as shown by the cell-associated titres, all of which plateau by around 12 hpi (Figure 2.16 a). All three mutant viruses (gIG39R, ΔgI and ΔgE) secreted more infectious virus into the cell culture medium compared to WT HSV-1 throughout the replication cycle, with the greatest difference being evident during the logarithmic growth phase (6-12 h) with up to 100-fold increase in the amount of virus released into the medium. The amount of infectious virus present in the culture medium was more similar between the viruses at 24 hpi, with approximately 3-fold more virus

released for the mutant viruses compared to WT, although by this late stage post infection the cytopathic effect leading to cell damage/lysis would likely have a greater contribution than at earlier time points.

Replication and release properties of WT, gIG39R, ΔgE, ΔgI, ΔgC and ΔgC-gIG39R viruses were further analysed in HFF-hTERT cells. The cell line was infected with 5 PFU/cell viruses and cell-associated and culture medium fractions were harvested separately at 2, 6, 9, 12 and 24 hpi. The replication rate of gIG39R, ΔgE and ΔgI viruses were indistinguishable from WT HSV-1 (Figure 2.16 b). However, the ΔgC virus showed slight attenuation in terms of replication and surprisingly the ΔgC-gIG39R seemed to replicate more rapidly, with higher titres at 6, 9 and 12 h compared to WT (Figure 2.16 c). As seen with HaCaT cell line, cell-associated titres of all the viruses plateaued by around 12 hpi. For all the viruses, the amount of released virions were maximum during the log phase of growth. The ΔgC-gIG39R virus secreted the highest amount of infectious virus into the cell culture medium, followed by gIG39R and then ΔgI viruses, with all these gI mutant viruses releasing more than WT. The ΔgE and ΔgC virus secreted less infectious virus than the WT. The differences in secretion of ΔgE viruses in HaCaT and HFF-hTERT is surprising and indicates there may be a cell type specific differences in the requirement of gE and gI for virus release.

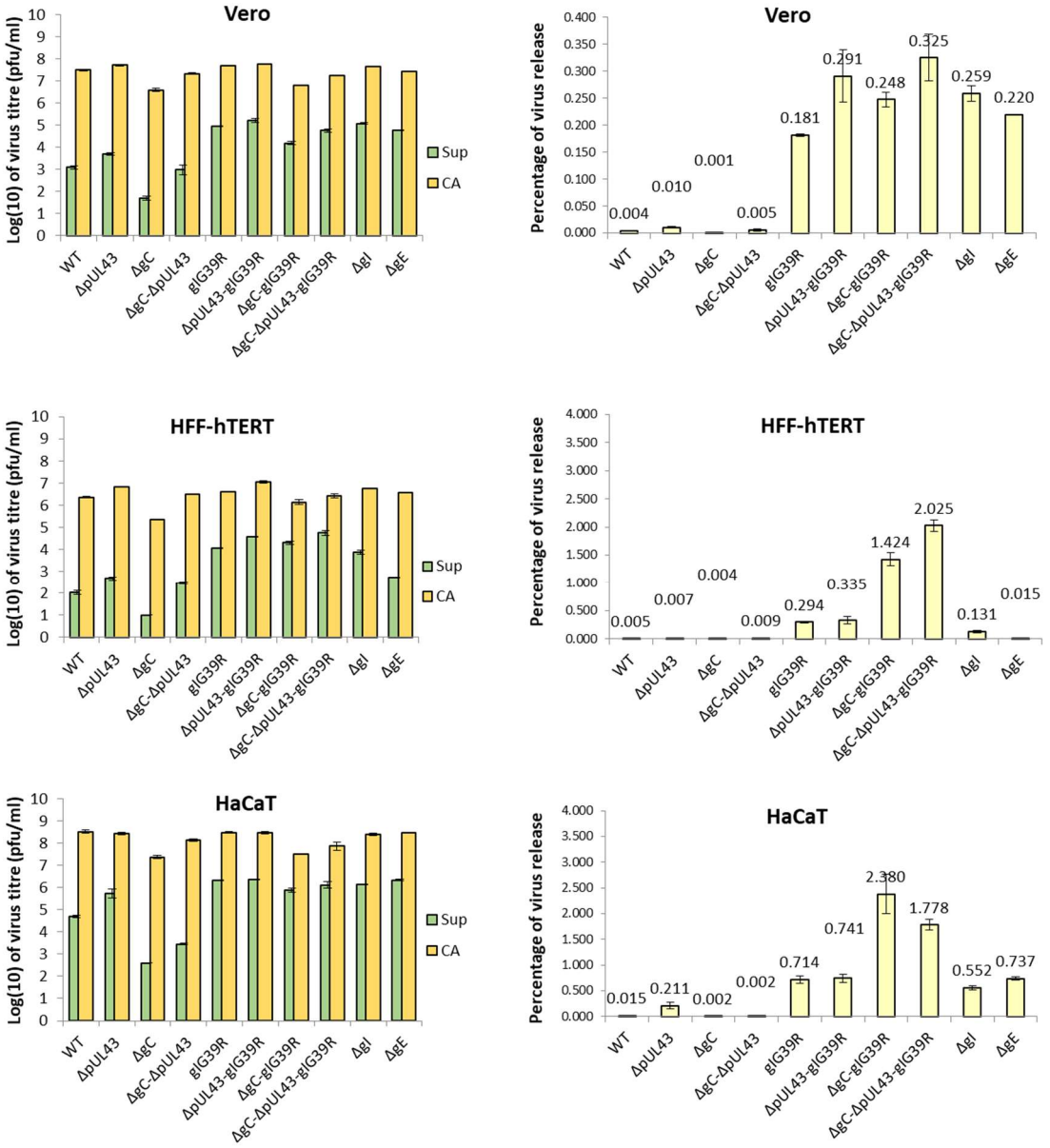

Figure 2.15 | Release assay of recombinant viruses on different cell lines. Growth assay of HSV-1 WT (KOS-BAC), ΔpUL43, ΔgC, ΔpUL43-ΔgC, gIG39R, ΔpUL43-gIG39R, ΔgC-gIG39R, ΔpUL43-gIG39R-ΔgC, ΔgI and ΔgE viruses was conducted on Vero, HFF-hTERT and HaCaT cell lines. Cells were infected with 10 MOI of the viruses and at 10 hpi supernatant (Sup) medium and cell-associated (CA) virus samples were collected. Samples were titred by plaque assay on Vero cells. Each experiment was repeated at least three times. Data presented here is from a single representative experiment containing duplicate sample set. Error bars indicate standard error of two biological replicates.

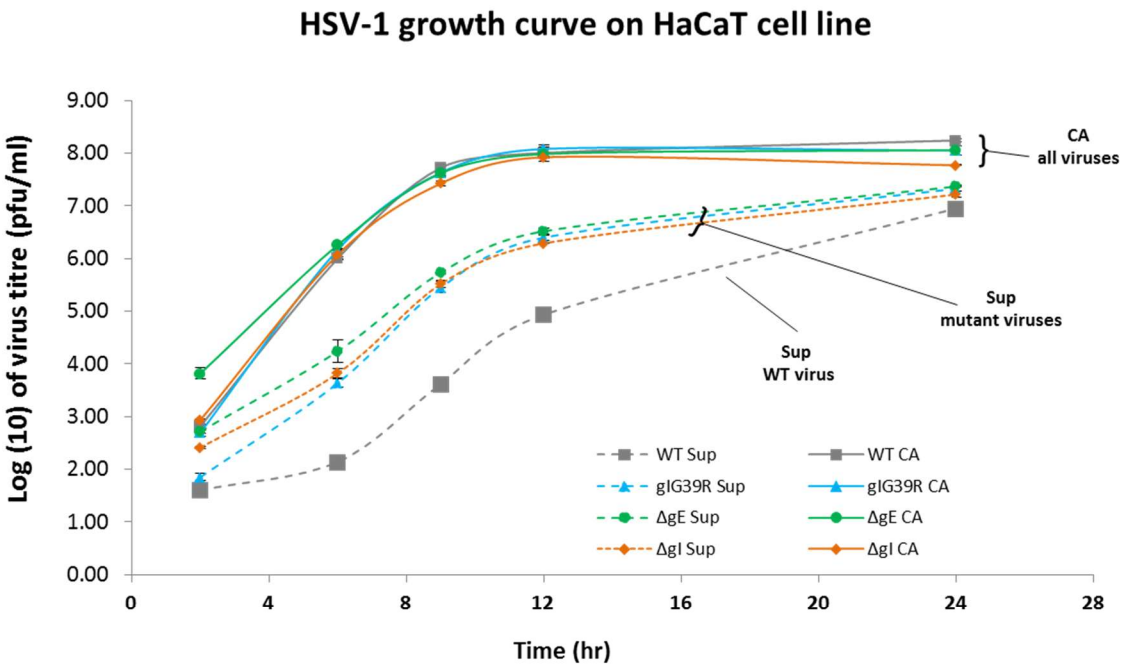
HSV-1 growth curve on HaCaT cell line
Log (10) of virus titre (pfu/ml)
Time (hr)
CA
all viruses
Sup
mutant viruses
Sup
WT virus
WT Sup
gIG39R Sup
ΔgE Sup
Δgl Sup
WT CA
gIG39R CA
ΔgE CA
Δgl CA

(a)

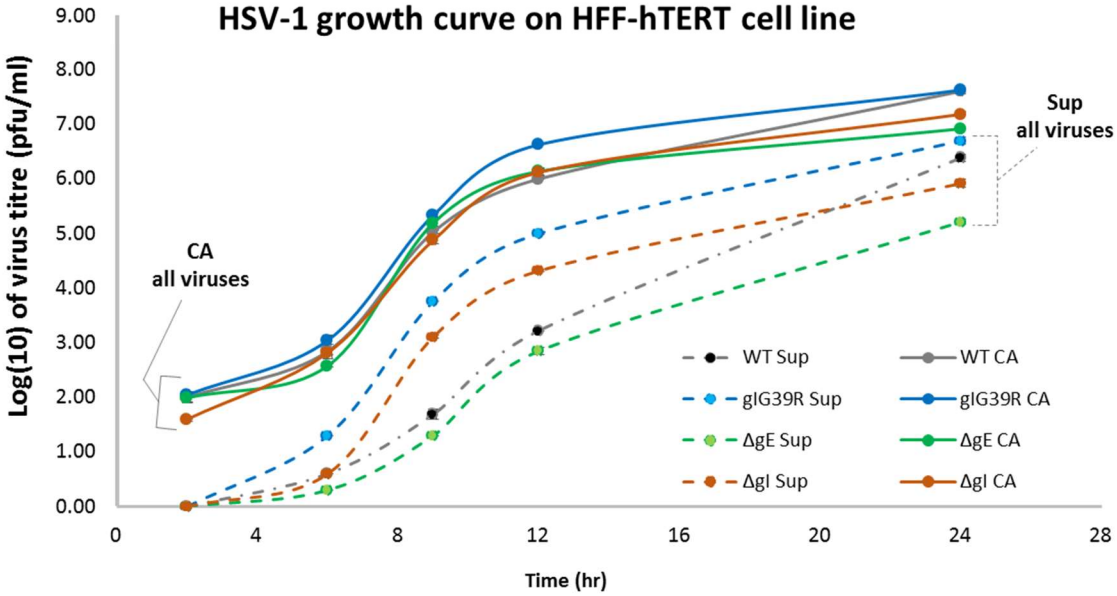
HSV-1 growth curve on HFF-hTERT cell line
Log(10) of virus titre (pfu/ml)
Time (hr)
CA
all viruses
Sup
all viruses
WT Sup
gIG39R Sup
ΔgE Sup
Δgl Sup
WT CA
gIG39R CA
ΔgE CA
Δgl CA

(b)

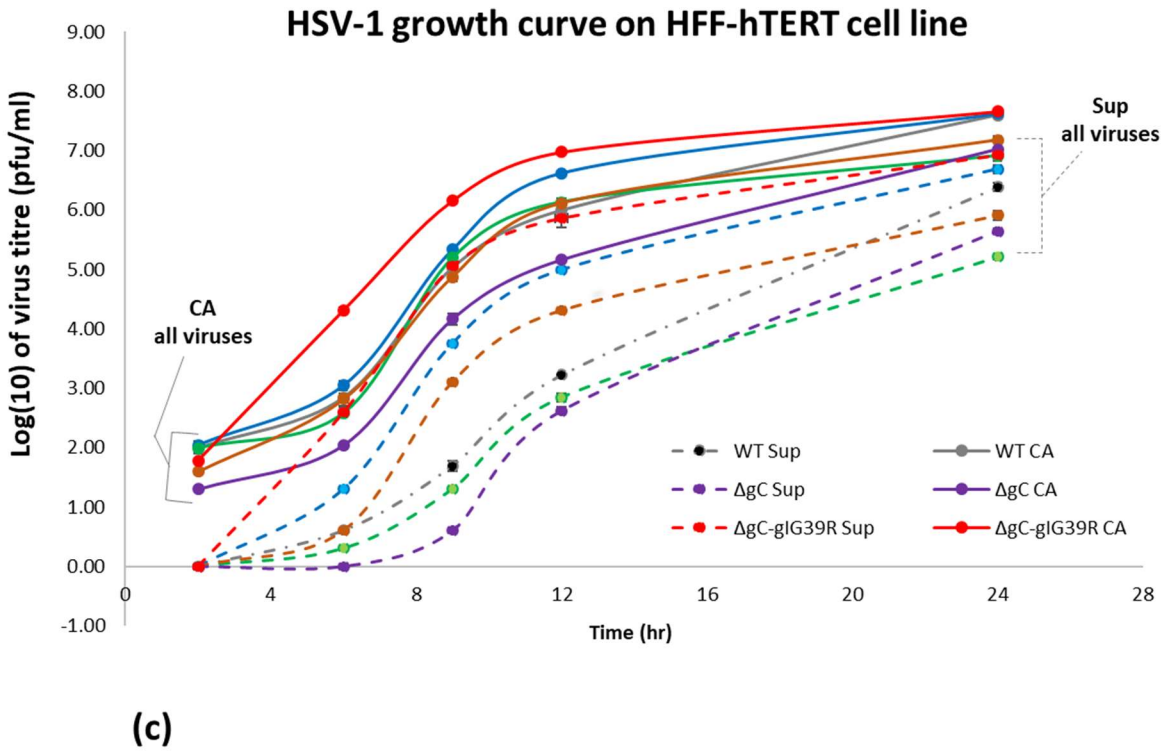

(c)

Figure 2.16 | Release assay and growth curves of recombinant viruses on different cell lines. Single step growth curves for WT, gIG39R, ΔgE, and ΔgI viruses (a) at high MOI (10 PFU/cell) on the HaCaT cell line, (b) at high MOI (5 PFU/cell) on the HFF-hTERT cell line and (c) for ΔgC and ΔgC-gIG39R viruses at high MOI (5 PFU/cell) on the HFF-hTERT cell line. Supernatant (Sup) medium and cell-associated (CA) virus samples were collected at 2, 6, 9, 12 and 24 hpi for growth curves. Samples were titred by plaque assay on Vero cells. Each assay was repeated at least three times. Data presented here is from a single representative experiment containing duplicate sample set. Error bars indicate standard error of two biological replicates.

2.2.10 Analysis of plaque size of the recombinant viruses

As mentioned above plaques reflect the capacity of a virus to infect, multiply and spread to neighbouring uninfected cells. A mutant virus that is defective in one or more of these processes may produce plaques of different morphology. Firstly, plaques formation on Vero cell monolayers was analysed for WT and the recombinant viruses containing all combinations of gIG39R, ΔpUL43 and ΔgC mutations. After incubation for 3 days under semi-solid medium, cells were stained, plaques scanned and images processed with Photoshop to measure plaque sizes. As shown in Figure 2.17 pUL43 deletion does not seem to affect plaque size whereas the gIG39R mutation seemed to reduce plaque size by ~20% compared to the WT plaques. Interestingly gC deletion seemed to marginally increase plaque size by at least 14%, and this phenotype appears dominant to the reduction in plaque size caused by the gIG39R mutation because viruses containing both mutations have similarly larger plaques as ΔgC alone. The increased plaque size in the absence of gC expression could reflect a reduction in 'stickiness' of the virions due to reduced interaction with extracellular heparin sulphate allowing easier diffusion to neighbouring cells. This is similar to suggestions made in previous studies which also demonstrated increased plaque size for a gC null virus (Laquerre et al., 1998; Mårdberg et al., 2004).

Deletion or mutation of gE is well established as causing severely reduced plaque size of HSV-1 (Wisner et al., 2000; Han et al., 2012; Maringer et al., 2012; Balan et al., 1994; Dingwell et al., 1995). To compare defects in plaque formation capacity caused by deletion of gE or gI with the gIG39R mutation, plaque size analysis for these recombinant viruses and WT were compared using monolayers of Vero, HFF-hTERT and HaCaT cells. Of these cell lines, only Vero cells produce plaques that can be easily observed by toluidine blue staining, therefore HaCaT and HFF-hTERT samples were fixed and stained with a HSV specific antibody followed by HRP-conjugated secondary antibody and developed with a diaminobenzidine (DAB) peroxidase reaction. As shown in Figure 2.18, gIG39R produces plaques with ~20% reduced diameter on monolayers of Vero and HFF-hTERT cells and ~65% reduced diameter on monolayers of HaCaT cell line compared to WT plaques on the same cell lines. Greater reductions in plaque diameter were observed for the ΔgI virus, and even further reductions for the ΔgE virus in all three cell lines. These data indicate that gE activity is more important for mediating cell-to-cell spread than gI, and suggests that gE that is not in complex with gI retains

some level of function to promote plaque formation. The expression of gIG39R, despite reduced expression levels, enables more efficient plaque formation than the complete absence of gI, particularly in Vero and HFF-hTERT cells. Furthermore, it would appear that release of infectious virus into the culture medium and plaque formation have different requirements for gE and gI function; for example, gIG39R mutation and loss of gE expression demonstrate a similar level of increased virus secretion into culture medium but loss of gE has a more profound effect on plaque size than the gIG39R mutation.

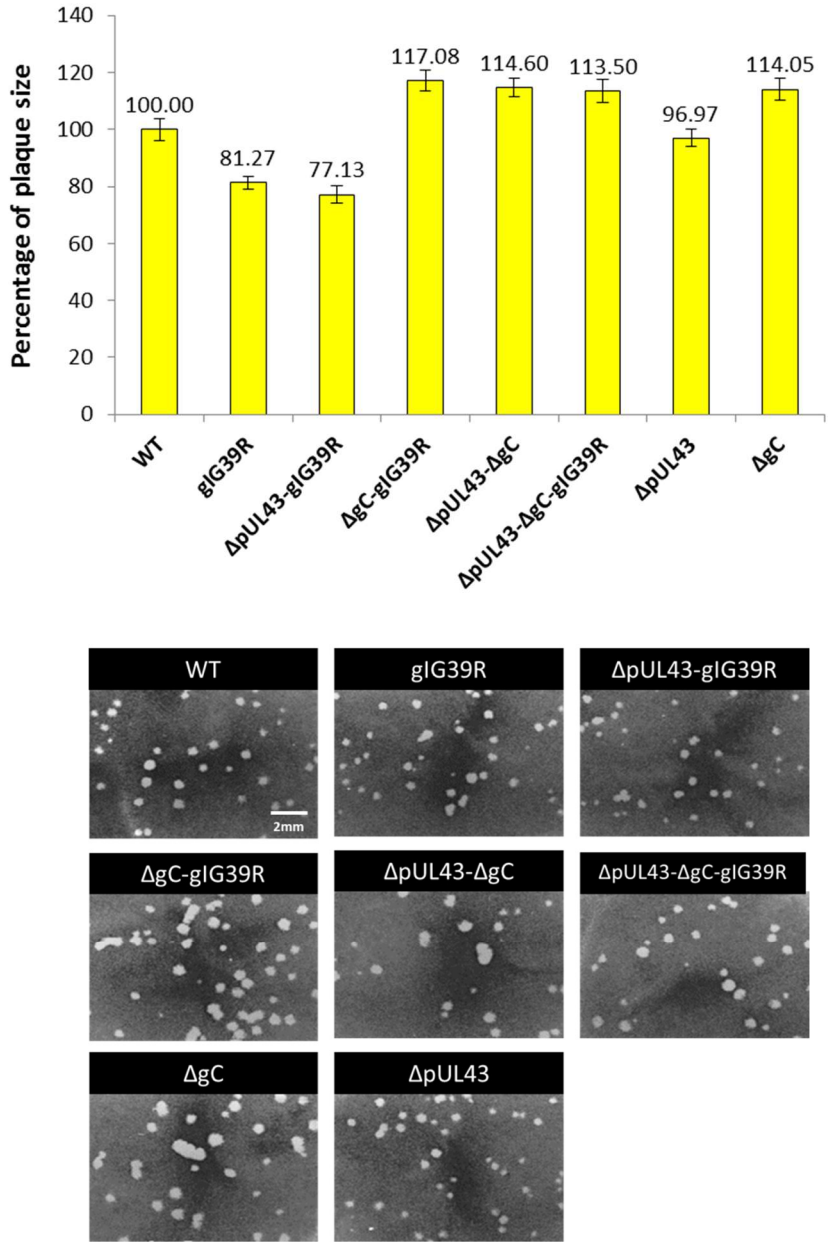

Figure 2.17 | Plaque size comparison of all gIG39R, ΔgC and ΔpUL43 recombinant viruses on Vero cell. Monolayers of Vero cells were infected with HSV-1 WT, gIG39R ΔpUL43-gIG39R, ΔgC-gIG39R, ΔpUL43-ΔgC, ΔpUL43-ΔgC-gIG39R, ΔgC and ΔpUL43 viruses. After 3 days the cells were fixed and stained with toluidine blue. The plates were then scanned and diameters of the plaques were measured in Photoshop. Data shows the average of 60 plaques diameter, normalised to WT (set as 100%) and error bars indicate standard error. Representative images of plaques for each virus are shown. White scale bar indicates 2 mm.

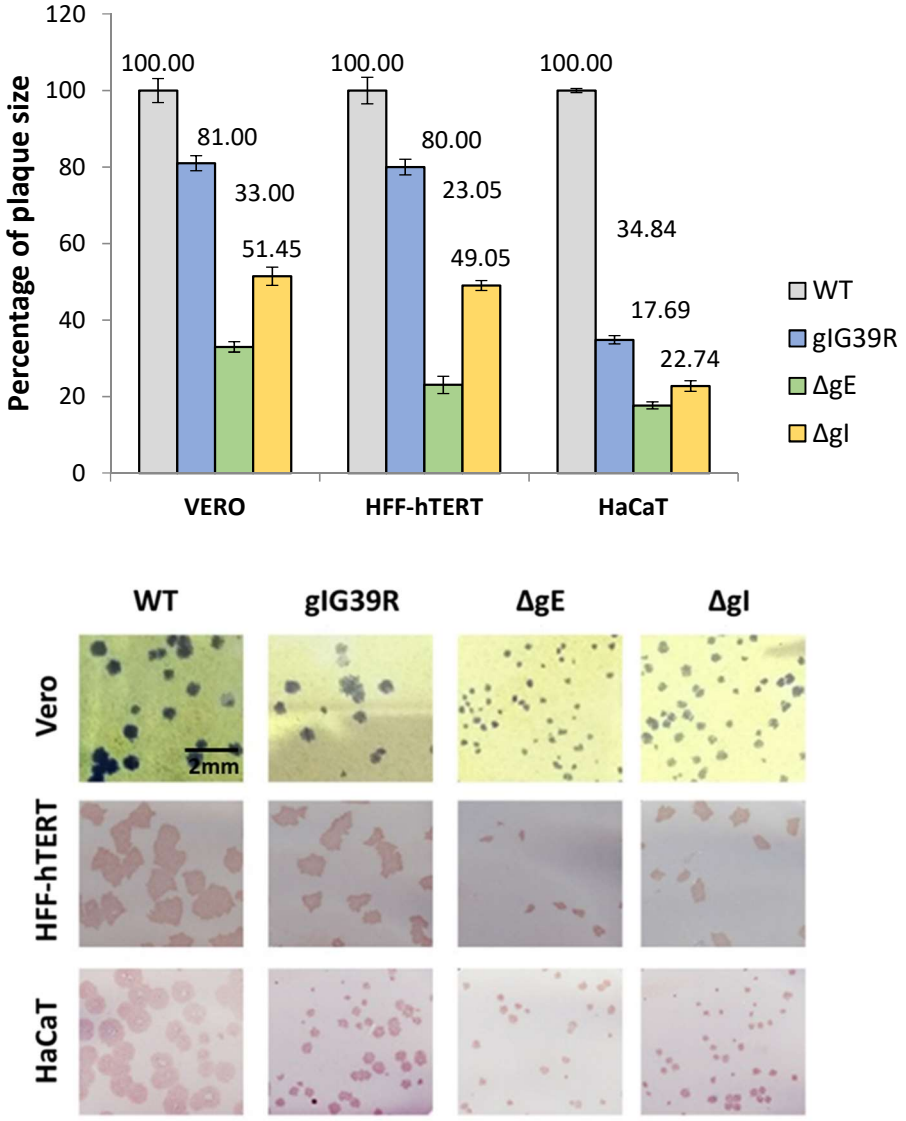

Figure 2.18 | Plaque size comparison of gE and gI mutant viruses on Vero, HFF-hTERT and HaCaT cells. Monolayers of cells were infected with HSV-1 WT, gIG39R mutant, ΔgE or ΔgI viruses. After 3 days the cells were fixed and either stained with toluidine blue (Vero cells, colour shown has been inverted) or antibody-dependent DAB peroxidase reaction. The plates were then scanned and diameters of the plaques were measured in Photoshop. Data shows average of 60 plaques diameter normalised to WT (set as 100%) and error bars indicate standard error. Representative images of plaques for each virus are shown. Black scale bar indicates 2 mm.

2.2.11 Effect of cell density on release of the mutant viruses

During WT virus infection, the gE/gI complex has been shown to target the secretion of virions to cell junctions rather than to the apical surface in polarised cells (Johnson et al., 2001). These data above demonstrate that loss of the gE/gI complex causes greater release of virions into the culture medium, possibly due to increased virus secretion at medium-exposed cell surfaces rather than cell-to-cell contacts. Therefore, the effect of gE and gI mutations on virion egress were investigated in the absence of cell-to-cell contact points. To achieve this goal HFF-hTERT and Vero cells were seeded at varying subconfluent densities and were infected with WT, gIG39R, ΔgE and ΔgI viruses. At 10 hpi cell-associated and released virus fractions were collected and titred on Vero cells. The percentage of release for the all the viruses was then calculated. Interestingly the proportion of WT virion secretion into the culture medium was essentially unchanged irrespective of cell density for HFF-hTERT cells (Figure 2.19 a) although in Vero cells a slight decrease in virion secretion was noticed with increasing cell density (Figure 2.19 b). The gIG39R and ΔgI viruses demonstrated increased virus secretion at all cell densities compared to WT in both cell types, with the percentage of virus release reducing with increasing cell density. The same was observed for ΔgE virus in Vero cells but as shown above in HFF-hTERT cells the ΔgE virus had little-to-no increase in virus secretion compared to WT at higher cell densities, although did show a marginal increase in release at low cell densities. One explanation for these data is that the majority of WT virus particles are secreted at the basal cell membrane that is adhered to the cell culture dish, and that only a relatively small proportion of virus is released at medium- exposed surfaces of cells, so there are relatively few virions that can become ‘trapped’ between cells as the cell density increases. For viruses with disrupted gE/gI complex more virions are secreted at exposed cell surfaces, and thus more are present as free virions in the culture medium, but these medium-exposed virions are more easily ‘trapped’ as cell density increases. Overall virus secretion was more sensitive to cell density in Vero cells, which may be explained by the fact that HFF-hTERT cells are large flat fibroblasts that make few lateral cell contacts whereas Vero cells form more packed monolayers. The difference in the secretion of ΔgE between HFF-hTERT and Vero cells is difficult to explain but could reflect the different cell morphologies of these cell lines, or differences in the potential cellular binding partners for gE between these human and monkey cells.

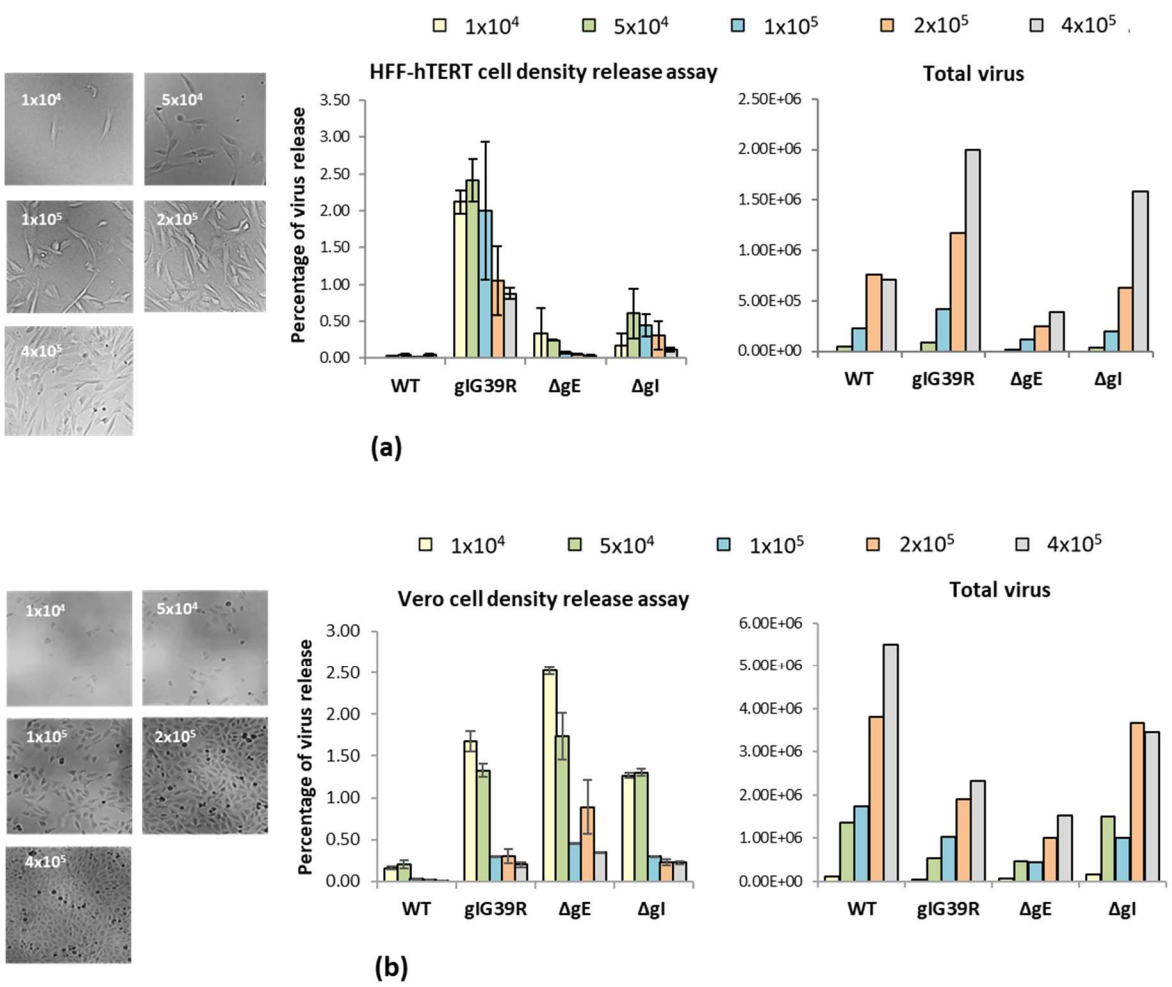

Figure 2.19 | HSV-1 release assay with increasing cell density. (a) HFF-hTERT and (b) Vero cells were seeded at different densities ($1x10^4$, $5x10^4$, $1x10^5$, $2x10^5$ and $4x10^5$) and infected the following day with WT, gIG39R, ΔgE and ΔgI viruses. Images of cells were taken before infection (left). At 10 hpi cell-associated and supernatant virions were collected and titred on Vero cell monolayers. Plaques were counted at 72 hpi to calculate percentage of virus release. Data indicates average of two independent biological replicates. Error bars indicate standard error of two biological replicates.

2.2.12 Complementation assays

To investigate whether the increased release of HSV-1 into the culture medium when the gE/gI complex is disrupted can be suppressed by supplying the missing WT gE or gI protein in *trans*, complementation assays were performed. Initially, cells stably expressing gE or gI were made by transducing HaCaT cells using a lentivirus transduction system and selected populations tested for transgene expression by IF (Figure 2.20 a). The majority of HaCaT-gI cells (80%) were positive for gI expression although gE expression was only detected in approximately 50% of the HaCaT-gE cells. The level of gE and gI protein expression in these stable cells was compared between mock infected cells and cells infected with WT, ΔgE and ΔgI viruses (Figure 2.20 b). The expression of both gE and gI in the stable cell lines was substantially lower than expression from the viral genome. In mock-infected HaCaT-gE cells, the majority of the gE protein appeared to be immature, whereas when these cells were infected with ΔgE virus the cell line which expressed gE appeared to be more similar to the size of mature gE. This is similar to the difference in gE observed between WT and ΔgI-infected cells suggesting the efficient maturation of gE requires gI expression. To understand whether this low-level expression of gE or gI can alter the virus release phenotype of gE or gI deletion viruses, parental, gE expressing and gI expressing HaCaT cell lines were infected with WT, ΔgE or ΔgI viruses and the medium and cell-associated samples were collected at 6 hpi infection and infectious virus determined by plaque assay (Figure 2.20 c). This time point was used as it is a relatively early stage of virus assembly and release which may be more sensitive to gE and gI levels. The release of ΔgE and ΔgI viruses was greater than WT HSV-1 in parental HaCaT cells as previously observed. In HaCaT-gE cells the proportion of ΔgE virus secretion was slightly lower than the proportion of ΔgE virus released in the parental HaCaT cell line. This was more apparent in the gI-HaCaT cell line with approximately 3-fold lower release of ΔgI virus compared to the same infection in parental HaCaT cells, although the release of ΔgI virus was still ~5-fold higher than WT HSV-1 in the HaCaT-gI cells. These data suggest that the relatively low expression level of gE and gI in the stably cell lines can somewhat compensate for the loss of these proteins in the control virion secretion. The effects were modest however, likely due to the low expression levels of gE and gI in these cell lines.

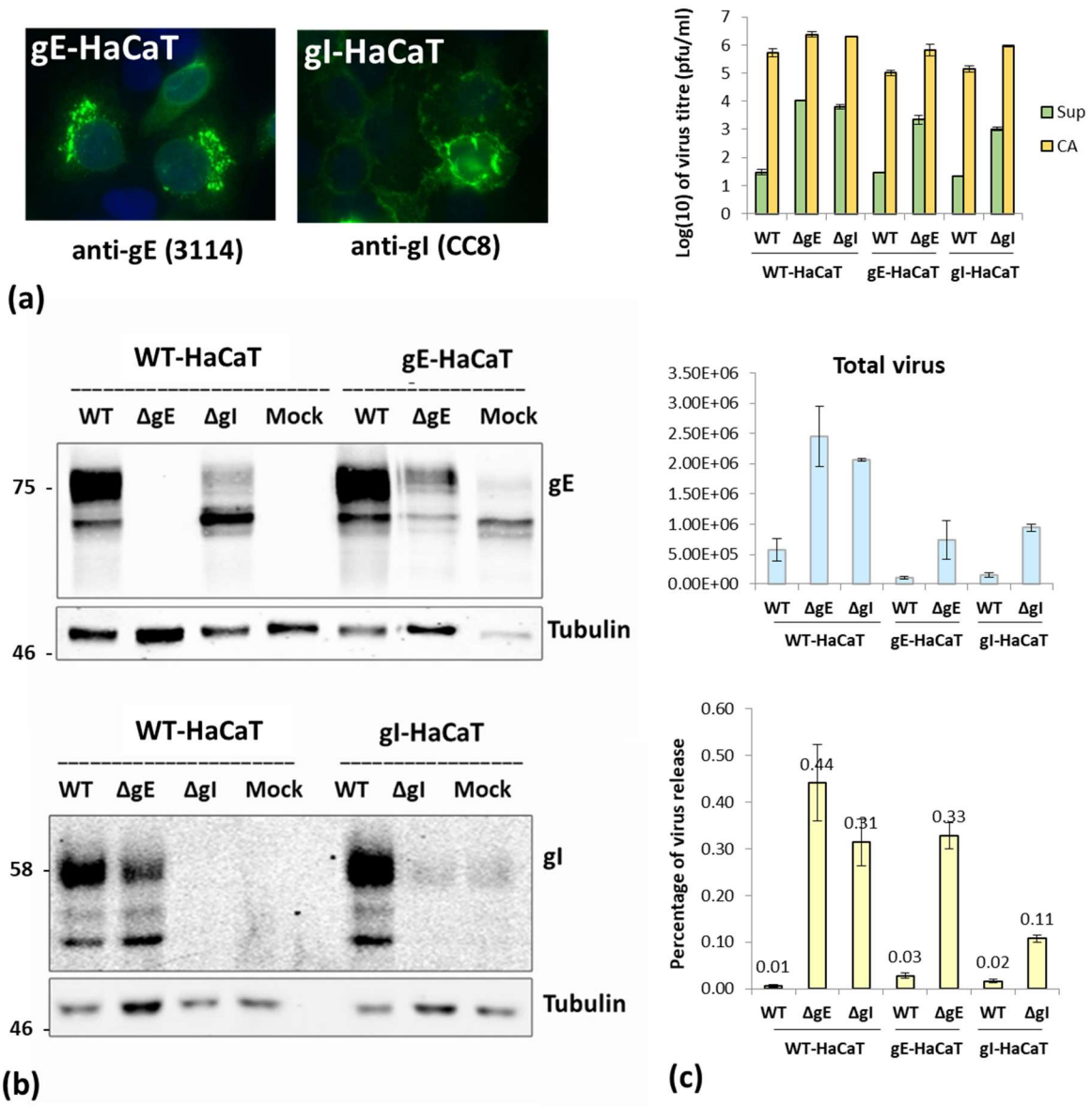

Figure 2.20 | gE and gI expression and HSV-1 release assay in complementing HaCaT cell lines. HaCaT cells were transduced with lentivirus vectors to generate cell populations stably expressing gE or gI. (a) gE and gI expression HaCaT cell lines detected by IF, (b) parental and gE or gI HaCaT cells were infected either with HSV-1 WT, ΔgE or ΔgI at 10 PFU/cell and expression of gE and gI detected by WB at 6 hpi. (c) Cell-associated (CA) and supernatant (Sup) virus samples were collected from WT and gE- or gI- HaCaT cells infected with HSV-1 WT, ΔgE or ΔgI viruses at 10 hpi and titred on Vero cell to calculate the percentage of virus release. Data indicates average of two independent biological replicates. Error bars indicate standard error of two biological replicates.

As an alternative strategy, co-infection experiments were performed. HaCaT cells were infected with WT, gIG39R, ΔgE, or ΔgI viruses, co-infected with ΔgE and ΔgI viruses or mock infected, harvested at 6 hpi and protein expression analysed by WB. Figure 2.21 (a) indicates that both gE and gI were efficiently expressed in cells co-infected with ΔgE and ΔgI, and there was less immature gE in the co-infected samples than ΔgI or gIG39R infected samples. This suggests that gI and gE expressed from co-infection with ΔgE and ΔgI can form a complex. The ability of co-infection to complement virus secretion phenotypes was investigated by co-infecting cells with ΔgE together with gI or gIG39R and the relative virus release compared to infection with each individual virus (Figure 2.21 b). Consistent with earlier results, in single virus infection samples substantially more gIG39R, ΔgE and ΔgI virus was released from HaCaT cells than WT HSV-1. However, the amount of virus released from cells infected with ΔgE in combination with either gIG39R or ΔgI was substantially lower than the single deletion or gIG39R mutant viruses. These data suggest virus secretion from cells can be controlled by WT gE/gI complexes even when the functional proteins are expressed from different virus genomes, and further indicates that the gIG39R mutant protein is not acting in a dominant negative capacity.

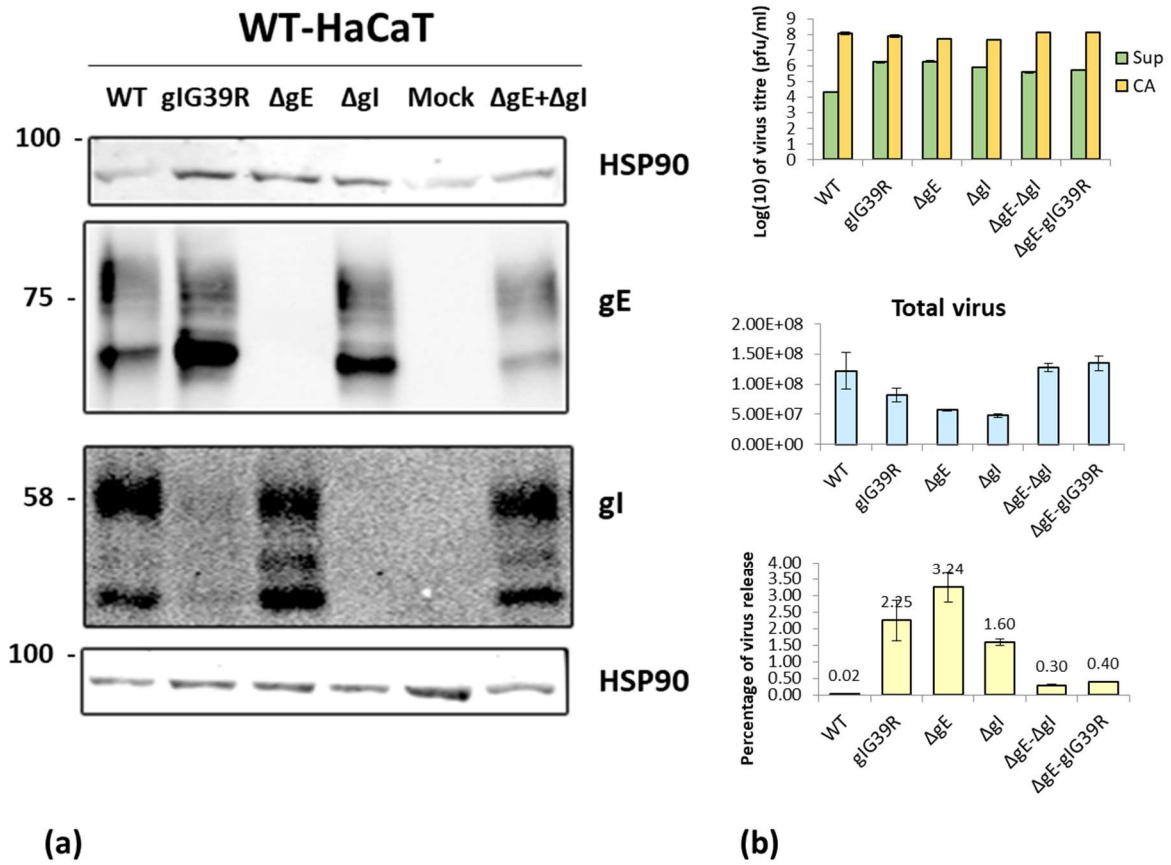

Figure 2.21 | Release assay and expression of gE and gI during co-infection. (a) HaCaT cells were infected either with WT, gIG39R, ΔgE, ΔgI or co-infected with both ΔgE and ΔgI, viruses. After 6 hpi the cells were lysed and gE, gI expression was checked by WB. (b) HaCaT cells were infected either with WT, gIG39R, ΔgE, ΔgI or co-infected with both ΔgE and ΔgI or ΔgE and gIG39R viruses. At 10 hpi cell-associated (CA) and supernatant (Sup) virus samples were collected and titred on Vero cell to calculate percentage of virus release. Data indicates average of two independent biological replicates. Error bars indicate standard error of two biological replicates.

2.3 Discussion

The widely accepted notion that HSV-1 is highly cell-associated virus came from the observation that very few particles are found in the cell culture medium and virions are observed to remain attached to the cell surface of the infected cells (Newcomb and Brown, 2010; Abaitua et al., 2013). In agreement with this, release assay experiments demonstrated <1% of infectious virus is present in the culture medium after a single round of virus replication for all WT HSV-1 strains tested in nearly all conditions. The passage mutant V22a exhibited an increase in the proportion of virus release from all the infected cells, although this was less evident in HeLa cell possibly because HSV-1 replicates poorly in this cell line. The V22a also replicated more poorly than WT in HaCaT cells suggesting one or more of the mutations in V22a affects an aspect of the virus lifecycle other than egress in this cell line. Construction of recombinant viruses in the parental WT strain genetic background to recapitulate the genetic defects observed in V22a (gIG39R and deletion of UL43 and UL44) identified the gIG39R mutation as the primary cause of the increased virus release phenotype. Additionally, deletion of gC on top of gIG39R mutation increases virion secretion even further in human cell lines. Interestingly, the gIG39R mutation caused a severe reduction in protein expression observed by WB although IF experiments showed substantially higher signals for gIG39R than WT gI with all anti-gI antibodies tested. The most logical explanation for these findings is that the epitopes within gI that are the binding sites for the anti-gI antibodies are masked either by the 3-dimensional structure of native gI or because of an interaction with gE within the gE/gI complex. The G39R mutation presumably causes a sufficient change to gI structure to expose the antibody binding sites, possibly by disrupting its interaction with gE.

The gIG39R virus produced smaller plaques most noticeably on HaCaT cell line than the WT HSV-1 as did the ΔgE and ΔgI viruses irrespective of strain differences. This was consistent with the observations made by previous researchers for gE and gI deletion viruses (Wisner et al., 2000; Dingwell et al., 1994). Overall, the differences in plaque size indicate that the gE/gI function is required for proper release of the virion to the cell contact points which allows efficient spread of the virions to neighbouring cells. Also, gE is more important in mediating virion delivery to the cell junction than gI. Furthermore, appearance of slightly bigger plaque with all ΔgC viruses on cultured monolayers could indicate that gC-HS interaction might have a role on the viruses that have recently egressed (Laquerre et al., 1998; Mårdberg et al., 2004).

Even though HFF-hTERT and Vero cells are nonpolarised and don't form tight junctions with cell-density-release-assay, WT HSV-1 virions were possibly delivered to the adherent junctions. Lack of cell-contact points in with lower cell-densities resulted in increased secretion of the gE and gI mutant/deletion viruses possibly in a random manner from the cell surface because of misdirectional/abnormal virion secretion pathways. In Vero cells HSV-1 has been reported to egress at sites that are adherent either with plastic or neighbouring cells (Mingo et al., 2012). This study also supports the same hypothesis for both Vero and HFF-hTERT cell line. Such cell density experiments in HaCaT cell line is difficult to perform given the nature of the cells to remain in a cluster.

3. The G39R mutation in gI destabilises the gE/gI complex in HSV-1 and dysregulates virion egress

3.1 Introduction

In the previous chapter, it was observed that a single amino acid change in glycoprotein I (G39R) identified in the V22a passage mutant is primarily responsible for the increased virion secretion phenotype of this virus. A similar phenotype was also observed in viruses lacking expression of gE or gI. This suggests the G39R mutation might have affected the functionality of gE/gI complex.

Glycoprotein I is encoded by the US7 gene of HSV-1 virus. It is a type 1 transmembrane protein and is almost always found in complex with gE in infected cells (Hanke et al., 1990; Bell et al., 1990). Although gI has been proposed to partially contribute to virion envelopment its function largely depends on the presence of gE (Farnsworth et al., 2003). Various roles of gE during HSV replication have been proposed but similarly such functions appear to mostly depend on its ability to remain in complex with gI. The gE/gI complex actively participates during various steps of virus life cycle. The cytoplasmic tail of gE contains tyrosine-based (YXXΦ) trafficking motifs, and the cytoplasmic tail of gI contains a putative dileucine motif, which are thought to help these proteins to localise to the TGN and endocytose from plasma membrane (Alconada et al., 1996; Alconada et al., 1999; Olson and Grose, 1998; Olson and Grose, 1997). A cluster of acidic amino acids in the cytoplasmic tail of gE, which likely undergoes phosphorylation, is also thought to control gE/gI trafficking (Alconada et al., 1996; Edson, 1993; Wisner et al., 2000) The accumulation of gE/gI in TGN or endosomal compartments likely aids virion assembly through the interaction of this complex with tegument proteins, including VP22 and pUL11 that interact with the gE cytoplasmic tail. Once secondary envelopment is complete, gE/gI is thought to help transport virion-containing vesicles to the cell junctions to release the newly assembled virions in proximity to neighbouring cells. In addition, the ecto-domain of the gE/gI complex has been suggested to bind a putative receptor present on the cell junctions of uninfected cells, which may facilitate rapid virion spread (Dingwell and Johnson, 1998). The ecto-domain of gE/gI complex can also act as an Fc receptor to inhibit antibody response (Ndjamen et al., 2014). However, deletion of either of these proteins does not noticeably inhibit virus replication with only a minor defect in envelopment is suggested (Johnson et al., 2001). This may be due to redundancy within the secondary envelopment process as mutant viruses

lacking gB and gE/gI or gD and gE/gI do show substantial defects in secondary envelopment, presumably due to a loss of interaction between tegument and envelope proteins (Farnsworth et al., 2003; Johnson et al., 2011; Mingo et al., 2012; Wisner and Johnson, 2004).

The overall aim of this chapter was to understand the mechanism behind the observed phenotype caused by the gIG39R mutation by comparing it with ΔgE and ΔgI viruses and investigating the fate of gE, gI and the gE/gI complex.

3.2 Results

3.2.1 Time dependent expression of gE and gI in WT and mutant viruses

As shown in Chapter 2, the gIG39R recombinant virus demonstrated lower expression levels of gI compared to WT virus at a late stage post infection in Vero cells (18 h; Figure 2.9). To investigate whether the effect of the G39R mutation on protein levels varies at different stages of virus replication or shows cell-type dependence Vero, HFF-hTERT and HaCaT cell lines were infected with WT, gIG39R, ΔgE and ΔgI viruses and infected cell pellets were collected at 3, 6, 8, 10, 12 and 24 hpi. Protein expression levels were analysed by WB with antibodies specific for gE, gI, VP16 and tubulin. As can be seen in Figure 3.1 the expression of gI was severely reduced by the G39R mutation at all time points and in all three cell lines tested. Surprisingly, the gI expression levels in ΔgE-infected cells were greater than gIG39R-infected samples in all three cell types, albeit lower than WT HSV-1-infected samples. This suggests the G39R mutation has a greater destabilising effect on gI than loss of its binding partner gE. The expression levels of gE were broadly similar between gIG39R and ΔgI -infected samples, showing little difference compared to WT-infected samples in Vero cells, a marginal decrease in HFF-hTERT cells and reduced expression as well as a shift to a faster migrating product in HaCaT cells. This suggests a somewhat cell type-dependent effect on gE expression and/or glycosylation when the expression of gI is reduced or lost. Comparing the WT gE expression among the three different cell lines also indicates gE has different processing and maturation characteristics in the different cell types.

A parallel comparison of gI expression in three different cell lines revealed that there are also cell type specific differences in terms of glycosylation/maturation of this protein (Figure 3.2). In the HaCaT cell line gI appeared as three bands with a major species the top-most band

(presumably mature gI) and then two immature bands of different intensity. With HFF-hTERT cells however only two bands for gI were observed where the immature band was very faint and the intermediate species observed in HaCaT cells was missing. In Vero cells the mature gI band showed a lower molecular weight than mature gI in HFF-hTERT and HaCaT cells, although the immature band appeared to be the same molecular weight in all three cell lines. The G39R mutant of gI is barely detectable in all the cell lines with only mature gI being detectable. Interestingly, the molecular mass for gI detected (~58 KDa) in this thesis was much lower than what was proposed (~65 KDa) in the earlier studies (Sullivan and Smith, 1988; Collins and Johnson, 2003). This could be because of differences in the cell lines, antibodies, polyacrylamide gel comosition or protein molecular weight standards used in different experiments. As can be observed in Figure 3.2, different apparent molecular weight species can be observed for glycoproteins expressed in different cell lines, and so it is possible differences in glycosylation could explain the different molecular weight observed here than in previous publications. This study utilised two independent mouse monoclonal anti-gI antibodies (MAb-CC7 and MAb-CC8) that were generated and validated in the laboratory, and both these antibodies recognise gI at the same position on membrane (Figure 2.5 and 2.9).

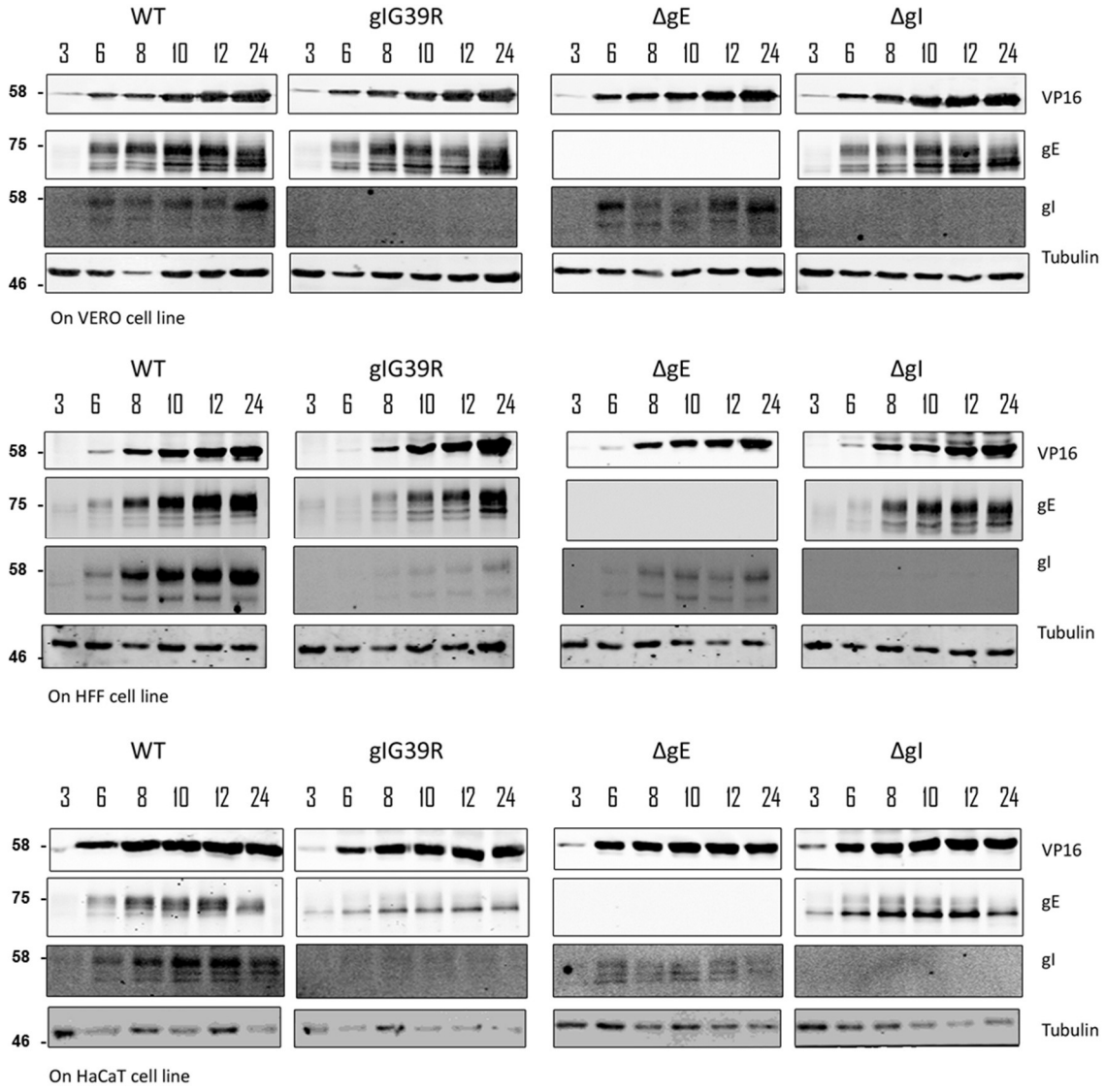

Figure 3.1 | Protein expression profiles of WT, gIG39R, ΔgE and ΔgI mutant viruses on different cell lines. Vero, HFF-hTERT and HaCaT cells were infected with HSV-1 WT, gIG39R, ΔgE and ΔgI viruses at 10 PFU/cell. At 3, 6, 8, 10, 12 and 24 hpi cells were lysed and proteins were separated by SDS-PAGE and immunoblotted, and tested for the expression of VP16, gE, gI and tubulin as indicated in the figure. Left panel indicates molecular mass of proteins in KDa.

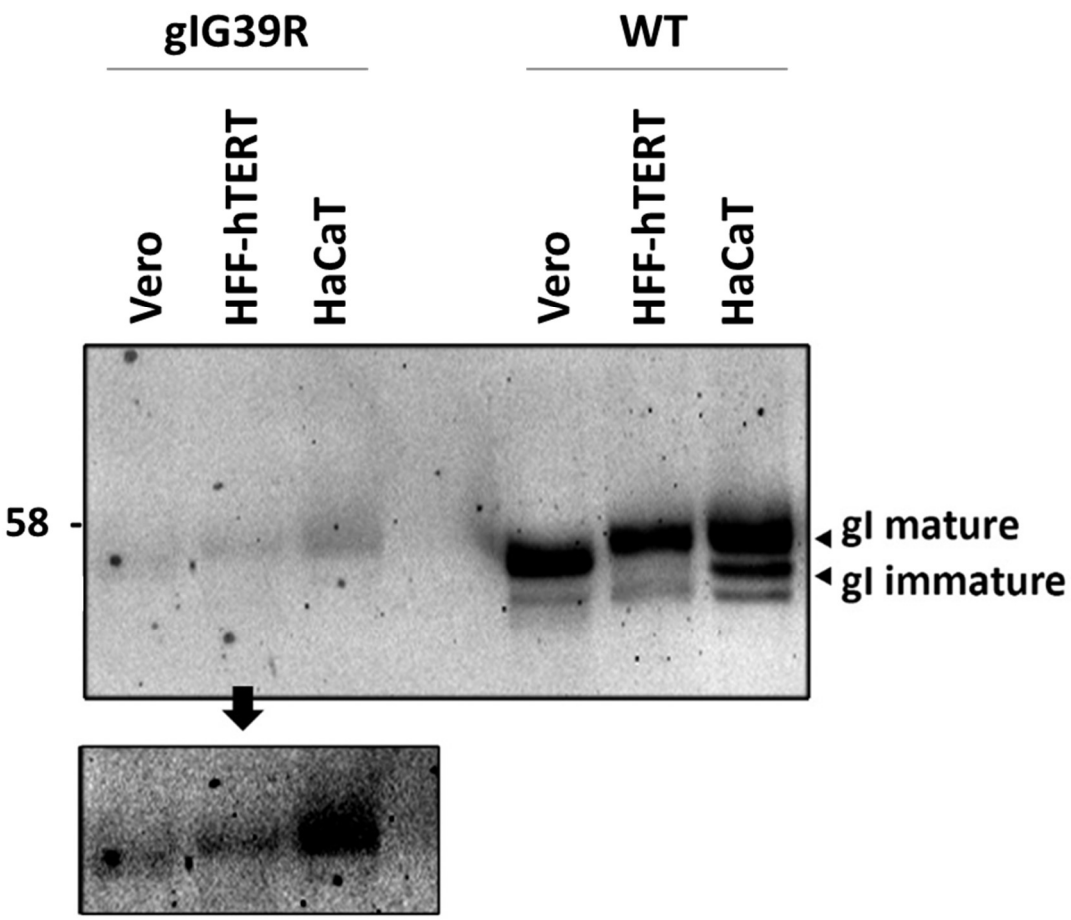

Figure 3.2 | Direct comparison of gI and gIG39R expression in different cell lines. Vero, HFF-hTERT and HaCaT cells were infected with HSV-1 WT and gIG39R viruses. At 16 hpi cells were lysed and proteins were separated by SDS-PAGE, immunoblotted, and tested for the expression of gI using anti-gI (MAb-CC8) antibody. Left panel indicates molecular mass of protein in KDa.

3.2.2 Analysis of interaction between gE and gI in WT and mutant virus infected cells

To investigate whether fluorescent-tagging of gI at the C terminus with EYFP may stabilise gI, lysates from HaCaT cells infected with the gI^{EYFP} and $gIG39R^{EYFP}$ were tested by WB (Figure 3.3). Surprisingly, using an antibody that recognises EYFP suggested there was some stabilisation of gIG39R when tagged with EYFP, whereas using a gI-specific antibody suggested the $gIG39R^{EYFP}$ had similarly reduced expression levels as observed for the untagged gIG39R protein above (Figure 3.3). The discrepancy between the two antibodies may reflect different binding affinities of these antibodies for their targets. Expression of gE was lower in the $gIG39R^{EYFP}$-infected samples, similar to that seen with untagged gIG39R virus infection in HaCaT cells.

To investigate the effect of the G39R mutation in gI on the interaction between gE and gI, immunoprecipitation (IP) experiments were conducted using two anti-gE monoclonal antibodies, MAb-3114 that recognises gE independently of gI and MAb-3063 that recognises gE in a gI-dependent manner (presumably via a conformational epitope that is better exposed in the gE/gI complex) (Collins and Johnson, 2003; Maringer et al., 2012), as well as two anti-gI monoclonal antibodies MAb-CC7 and MAb-CC8 that were generated in the laboratory. HaCaT cells were infected with WT, gIG39R, ΔgE and ΔgI viruses and cell lysates were prepared at 16 hpi. The lysates were incubated separately with each antibody followed by protein A/G beads. The samples were then analysed by WB with antibodies specific to gE (MAb-3114) or gI (MAb-CC8). Figure 3.4 (a) demonstrates that in WT HSV-1 infected samples both gE and gI were efficiently pulled-down by MAb-3063 whereas MAb-3114 pulled-down gE efficiently but only weak signals were observed for gI. This suggests that there may be pools of gE either in complex with gI or free of gI. Alternatively, MAb-3114 antibodies may compete with gI for gE binding, thus displacing the majority of gI from the immunoprecipitated complex. In gIG39R-infected samples gE was still efficiently pulled-down by the MAb-3114 antibody whereas only low levels of gE were pulled-down by MAb-3063 and no detectable gI was present in either sample. Similar results were seen for ΔgI infected samples, which showed efficient IP of gE by MAb-3114 but very low levels of gE in MAb-3063 pull downs. As observed in Figure 3.4 expression levels of gI were reduced in gIG39R-infected samples to a greater extent than in ΔgE samples. The IP experiments conducted with the two gI antibodies (MAb- CC8 and CC7) are shown in Figure 3.4 (b).

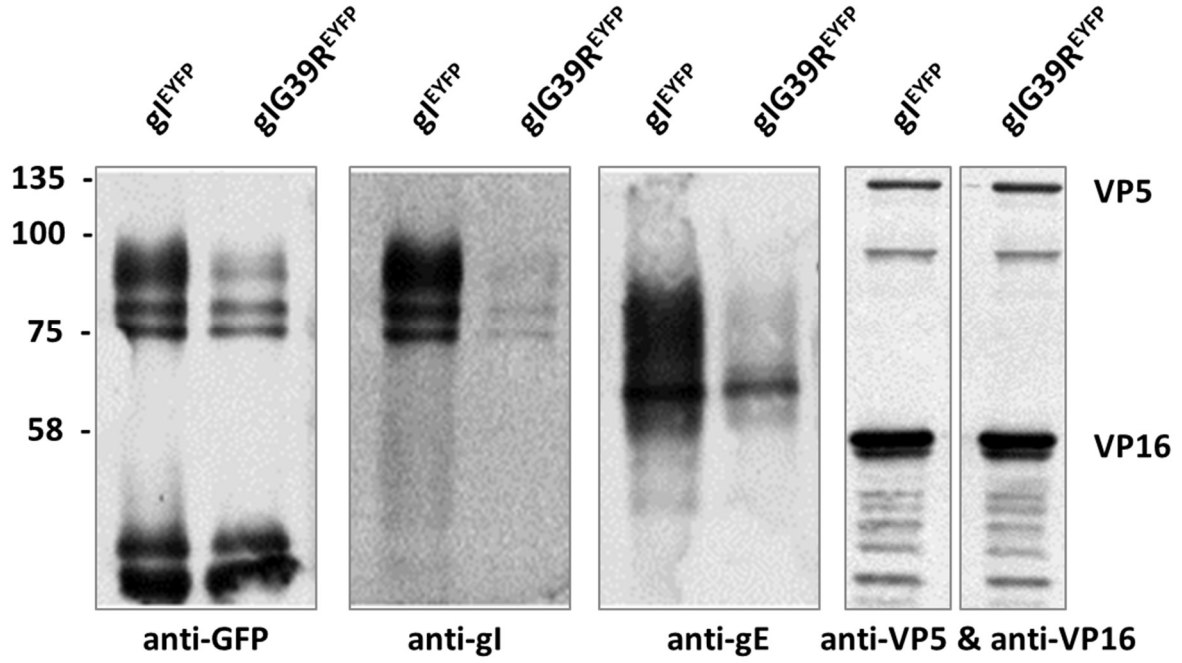

Figure 3.3 | Protein expression analysis for the gI^{EYFP}-tagged viruses. HaCaT cells were infected with HSV-1 gI^{EYFP} and gIG39R^{EYFP} viruses at 10 PFU/cell. At 16 hpi the cells were lysed. The protein samples were then separated by SDS-PAGE and immunoblotted for EYFP, gI, gE, VP5 and VP16 as indicated. Left panel indicates molecular mass of proteins in KDa.

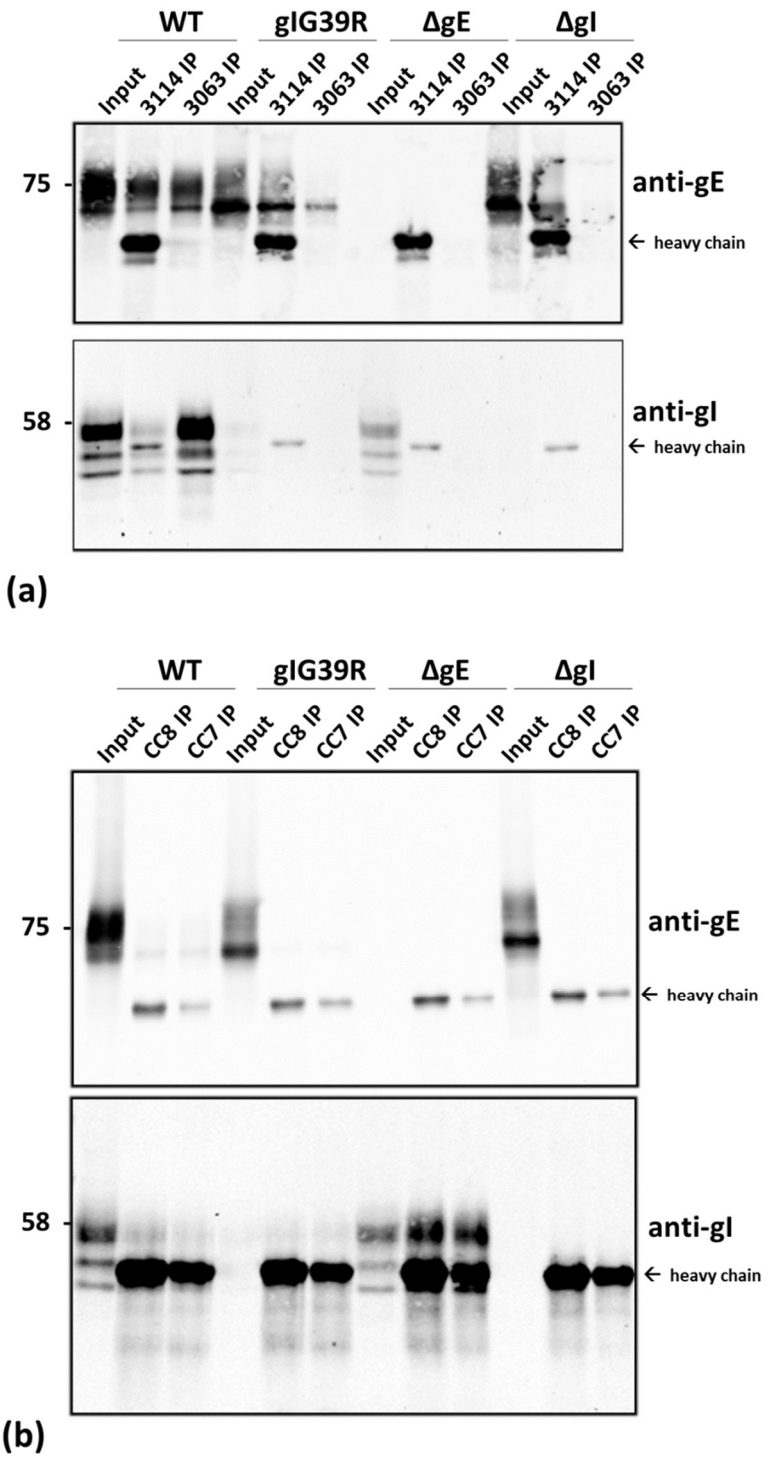

Figure 3.4 | Immunoprecipitation analysis of infected cells using antibodies recognising free gE, gE/gI and free gI. HaCaT cells were infected with HSV-1 WT, gIG39R, ΔgE and ΔgI viruses at 10 PFU/cell. 16 hpi cells were lysed and an IP was carried out using antibodies that recognise (a) gE (MAb-3114), gE/gI (MAb-3063) and (b) gI (MAb- CC8 and CC7). Proteins were then separated by SDS-PAGE and immunoblotted for gE and gI (MAb-CC8) as indicated. Left panel indicates molecular mass of proteins in KDa.

Only very weak signals that were barely above background were observed for gI IP from the WT-infected cell lysates whereas in ΔgE-infected samples substantially more gI was seen in the IP samples for both the antibodies, even though there was lower overall gI expression. This indicates that the binding site for both CC8 and CC7 antibodies may reside within the gE/gI binding region as they appear to be masked in the complex. Therefore, in the absence of any gE both antibodies could efficiently pull down gI present in the sample whereas with WT infection because most or all gI is in complex with gE, little to no gI was pulled-down by these antibodies. Consistent with this, the gI IP samples showed very weak signals for gE in WT-infected samples. Given the very low expression level of gI in gIG39R-infected cells and none in ΔgI-infected cells, it is unsurprising that both gI antibodies did not pull down any gI or gE from the samples infected with either of these viruses.

To understand whether overexpression of gIG39R by transfection could promote gE/gIG39R complex formation, HEK293T cells were co-transfected with either gE and gI or gE and gIG39R expression plasmids. After 22 h the cells were lysed and an IP experiment was carried out using MAb-3063 antibody to pull-down any functional gE/gI complex present in the cell lysates. Both gE and gI were pulled-down from WT gI expressing samples, whereas very little gE and no detectable gI was pulled-down from gIG39R expressing samples suggesting gIG39R does not form a complex with gE (Figure 3.5).

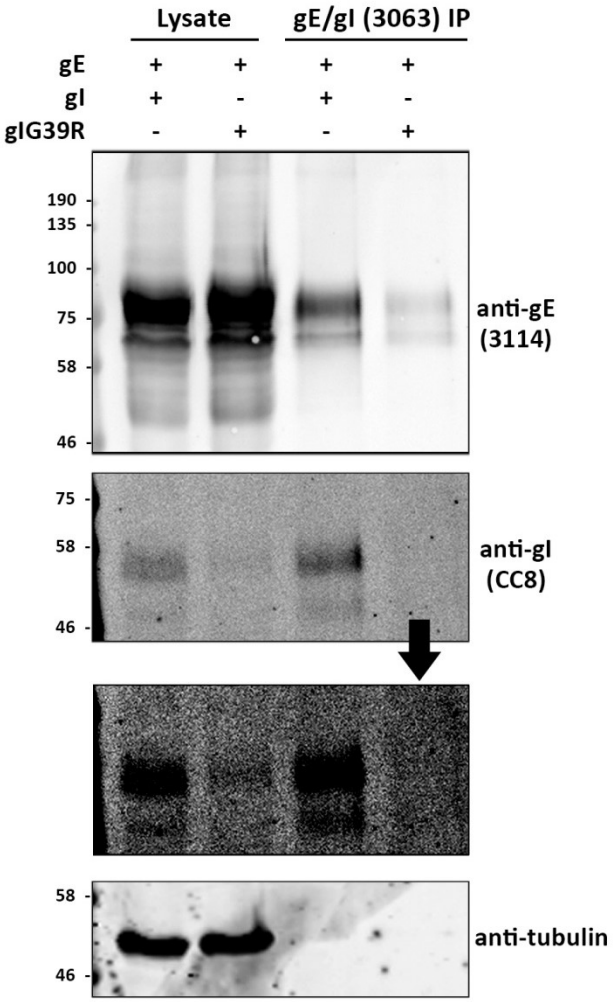

Figure 3.5 | Immunoprecipitation analysis of transfected cells. HEK293T cells were co-transfected with HSV-1 gE and gI or gE and gIG39R encoding plasmids. 22 h post-transfection cells were lysed and an IP was carried out using anti-gE/gI (MAb-3063) antibody. Proteins were then separated by SDS-PAGE and immunoblotted for gE and gI (MAb-CC8) as indicated. Left panel indicates molecular mass of proteins in KDa.

3.2.3 Immunofluorescence microscopy analysis of gE, gI localisation in cells

To further investigate gE/gI complex formation the expression and localisation of gE, gI and the gE/gI complex were analysed by IF microscopy. HFF-hTERT cells were infected with WT, gIG39R and ΔgI viruses and then fixed at 3, 6, 9, and 12 hpi and co-stained with monoclonal antibodies to HSV-1 gE (MAb-3114; IgG2a) and gE/gI (MAb-3063; IgG1) (Figure 3.6). In WT-infected cells antibodies showed overlapping signals predominantly in a perinuclear compartment from 6 h onwards, with noticeable signal at the cell periphery by 12 h. Staining was also observed around the nuclear rim for MAb-3114 but not MAb-3063 suggesting that some gE localises to the nuclear membrane in a gI-independent manner. In cells infected with either gIG39R or ΔgI viruses, MAb-3114 showed very similar expression and localisation as in WT virus-infected cells, whereas only weak signals were detected for MAb-3063 in gIG39R-infected cells and these were further reduced in ΔgI samples. These data further demonstrate that the G39R mutation in gI inhibits the formation of the gE/gI complex, although the fact that higher signal levels were detected for MAb-3063 in gIG39R-infected samples than ΔgI suggests the G39R mutant gI can still partially associate with gE. Furthermore, thiese data suggest that loss of gI interaction does not affect gE subcellular localisation.

In the previous chapter it was observed that anti-gI antibodies give very poor signal in IF in WT-infected cells compared to gIG39R or ΔgE-infected cells (Figure 2.10-2.13), even though WT virus expresses more gI as detected by WB (Figure 2.9). To understand the discrepancy between gI detection in WB and IF approaches further, HFF-hTERT cells were infected with viruses expressing WT or G39R mutated gI either as untagged protein or fused to EYFP at the C terminus (WT, gIG39R, gI^{EYFP} and $gIG39R^{EYFP}$ viruses), fixed at 3, 6 and 8 hpi and stained with anti-gI (MAb-CC8). As can be seen in Figure 3.7, WT-infected cells demonstrate a very weak signal for gI antibody staining, whereas with gIG39R infection shows a much stronger signal from 6 h onwards. The same observations were made for the EYFP-tagged viruses, with the addition that gI expression levels could be more directly observed because every copy of gI should be fused to EYFP: for the gI^{EYFP} virus a robust signal for EYFP was observed but with a corresponding weak signal for the gI antibody, whereas a weak EYFP signal intensity coupled with a strong signal for the gI antibody was observed for the $gIG39R^{EYFP}$ virus (Figure 3.8). These data on cells infected with the EYFP-tagged gI viruses also demonstrate that the anti-gI antibody can recognise its target epitope efficiently in IF.

Overall these data support the notion that the G39R mutation in the extracellular domain of gI inhibits interaction of gI with gE, thereby releasing gI from the complex so that it becomes accessible to antibody detection in IF. These data also suggest that in WT HSV-1 infection there is little free gI within cells, but that some free gE is present within infected cells, for example in the nuclear membrane.

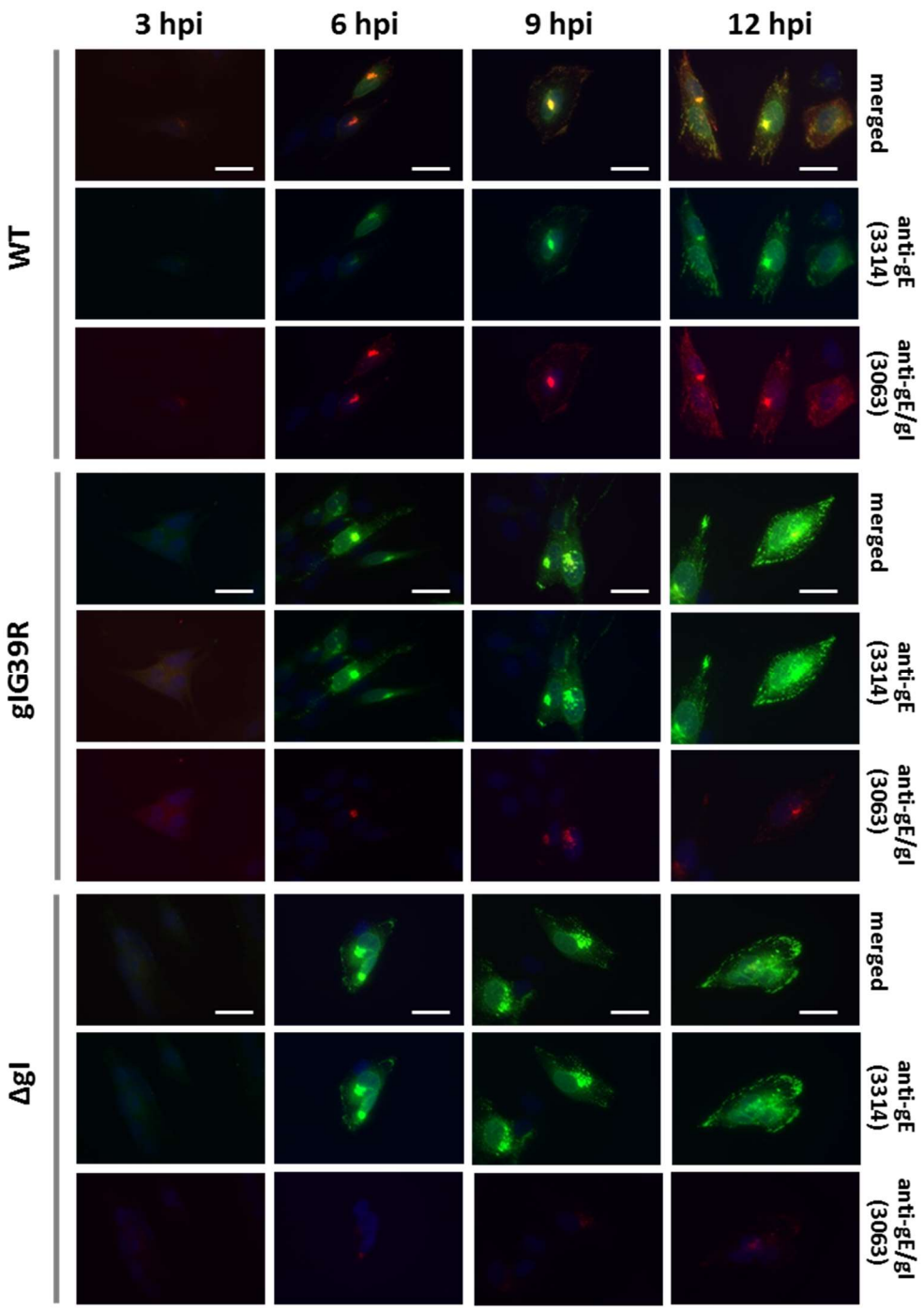

Figure 3.6 | Time course analysis of gE and gE/gI expression in infected cells by immunofluorescence. HFF-hTERT cells were infected with HSV-1 WT, gIG39R or ΔgI at 1 PFU/cell, fixed at 3, 6, 9 and 12 hpi, and labelled with anti-gE (MAb-3114) (green), anti-gE/gI (MAb-3063) (red) antibodies. Images were taken using an Olympus IX-81 inverted fluorescence microscope using a 60x oil immersion lens. Blue: staining of nuclei with DAPI. Scale bar indicates 20 μm.

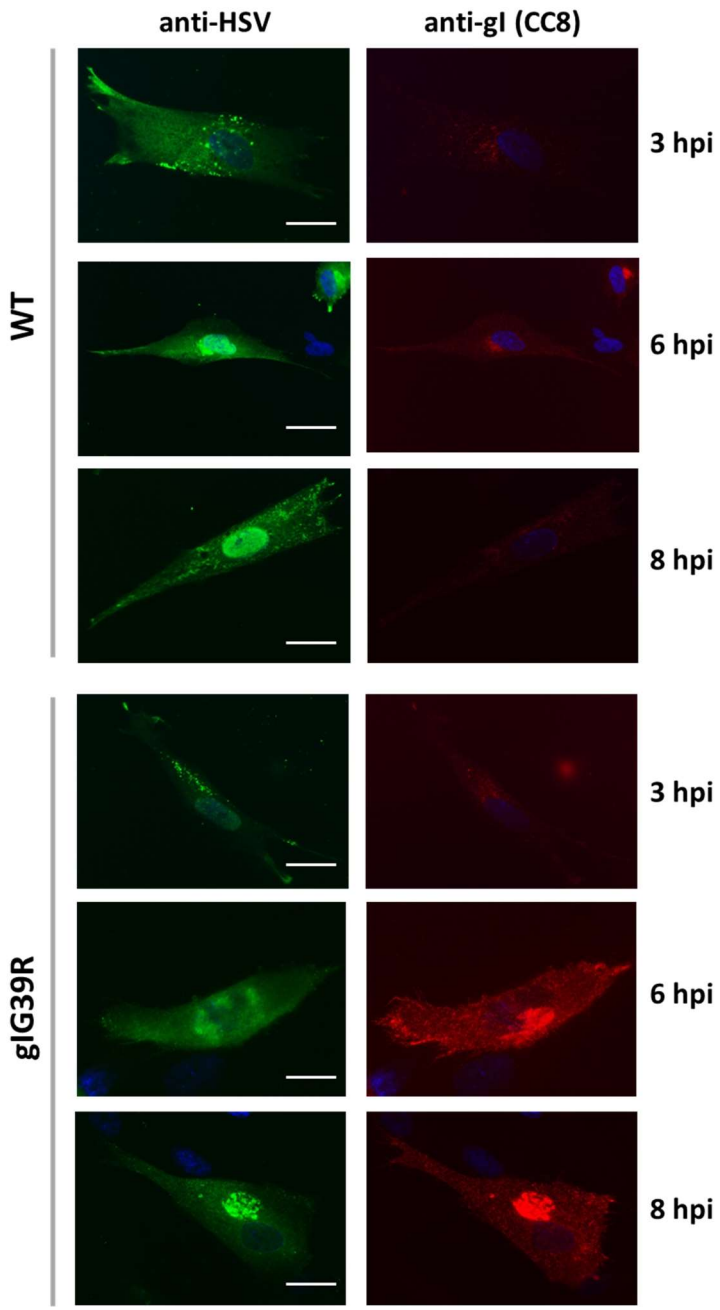

Figure 3.7 | Time course analysis of gI expression in infected cells by immunofluorescence. HFF-hTERT cells were infected with HSV-1 WT or gIG39R at 1 PFU/cell fixed after 3, 6 and 8 hpi and labelled with anti-gI (MAb-CC8) (red), anti-HSV (green) antibodies. Images were taken using an Olympus IX-81 inverted fluorescence microscope using a 60x oil immersion lens. Blue: staining of nuclei with DAPI. Scale bar indicates 20 µm.

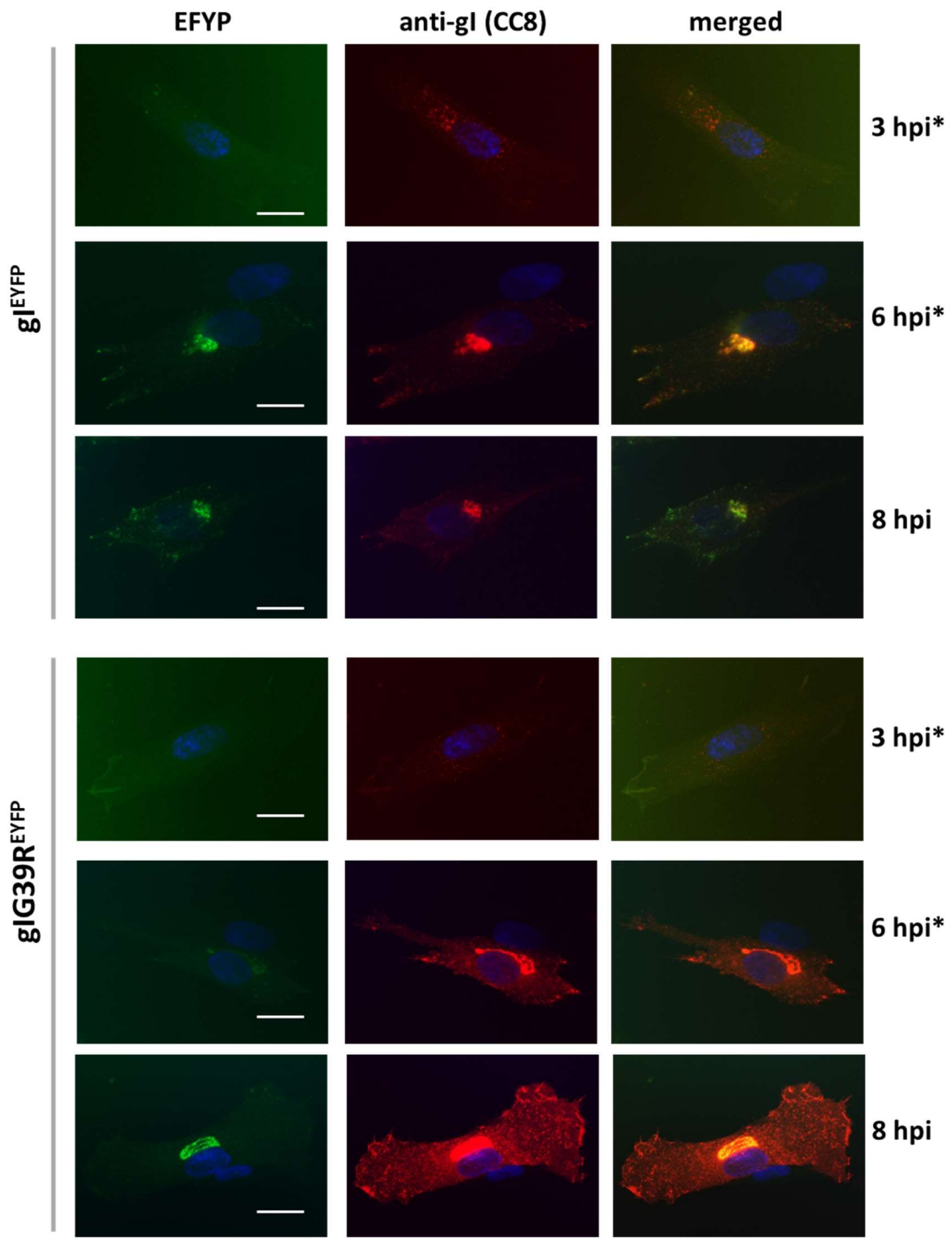

Figure 3.8 | Time course analysis of EYFP-tagged gI expression profile in infected cells by immunofluorescence. HFF-hTERT cells were infected with HSV-1 gI^{EYFP} or $gIG39R^{EYFP}$ at 1 PFU/cell and cells were fixed after 3, 6 and 8 hpi and labelled with anti-gI (MAb-CC8) (red) and nucleus (blue). Images were taken using an Olympus IX-81 inverted fluorescence microscope at using a 60x oil immersion lens. Blue: staining of nuclei with DAPI. *Images taken at 2x longer exposure for all channels except 8 hpi images. Scale bar indicates 20 µm.

3.2.4 The Fc receptor is abolished in gE and gI mutants

The ecto-domain of the gE/gI complex functions as an Fc receptor (FcR) and is known to efficiently bind human and rabbit IgG (Ndjamen et al., 2014; Johnson et al., 1988). The binding site for the Fc domain is thought to be within gE and this gE-Fc interaction is facilitated by gI (Basu et al., 1997; Dubin et al., 1994; Basu et al., 1995). To investigate the effect of the gIG39R mutant on Fc receptor activity HFF-hTERT cells were infected with WT, gIG39R, ΔgE, or ΔgI viruses and fixed at 12hpi. Cells were permeabilised and incubated with non-specific rabbit IgG together with mouse monoclonal antibodies to HSV-1 gD and gE, followed by subtype or species-specific fluorescently-labelled secondary antibodies. As can be seen in Figure 3.9 a strong signal was observed for rabbit IgG that co-localised with gE in WT-infected cells, demonstrating a strong Fc receptor activity. However, only very faint signals could be observed for rabbit IgG in gIG39R and ΔgI-infected cells, and no signal above background was detected with ΔgE-infected cells. These data indicate that the abolishment of gE/gI complex due to the G39R mutation or deletion of gI severely attenuates the Fc binding activity of gE, although some residual Fc receptor activity remains in the absence of gI. The simplest explanation of these observations is that the conformation of gE necessary to interact with Fc domains is stabilised in the gE/gI complex, although a small fraction of gE molecules fold sufficiently well to bind to antibody Fc domains in a gI-independent manner.

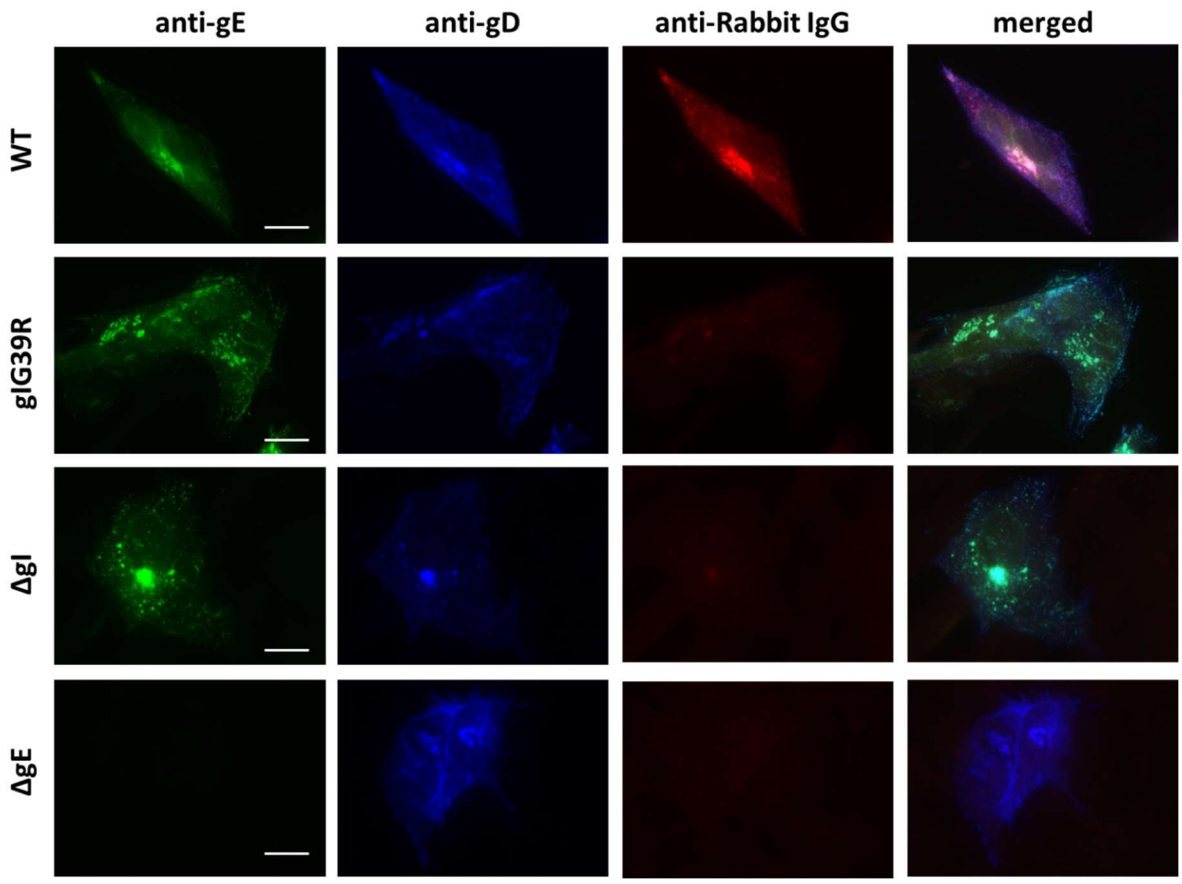

Figure 3.9 | Fc receptor activity in cells infected with WT and gE or gI mutant viruses. HFF-hTERT cells were infected with HSV-1 WT, gIG39R, ΔgE or ΔgI at 1 PFU/cell. The cells were fixed at 12 hpi, and stained with gE, gD, non-specific rabbit IgG antibodies. Images were taken using an Olympus IX-81 inverted fluorescence microscope using a 60x oil immersion lens. Scale bar indicates 20 μm.

3.2.5 Effects of gIG39R mutation on the localisation of gE and gI to virion assembly sites

During virion assembly HSV-1 glycoprotein-containing TGN/endosomal vesicles wrap around the tegument-surrounded nucleocapsids. To investigate the impact of the G39R mutation on gI and gE localisation during the virion assembly stage of infection, HFF-hTERT cells were infected with HSV-1 gI^{EYFP} and $gIG39R^{EYFP}$ viruses, fixed at 10 hpi and stained for gE and the inner tegument protein VP1/2 as a marker for cytoplasmic nucleocapsids (Figure 3.10). EYFP-tagged WT gI and gE localise to the same intracellular compartments including VP1/2 positive puncta, which indicates assembling or assembled virus particles. However, in $gIG39R^{EYFP}$-infected cells the mutant gI protein appeared to be more retained on the plasma membrane and showed less co-localisation with gE in intracellular compartments. However, some particles were still observed bearing gE, $gIG39R^{EYFP}$ and VP1/2 suggesting mutant gI (gIG39R) can still be incorporated into assembling virions.

To investigate the impact of the G39R mutation on the localisation of gE and gI with another envelope protein, gD, HFF-hTERT cells were infected with either WT or gIG39R viruses, fixed at 10 hpi and were stained for gD, gE and VP1,2 (Figure 3.11). In this setup gE and gD showed extensive co-localisation for both viruses indicating gIG39R mutation does not affect localisation of gE with other glycoproteins such as gD. This suggests gE can still be incorporated into virions efficiently when not in complex with gI.

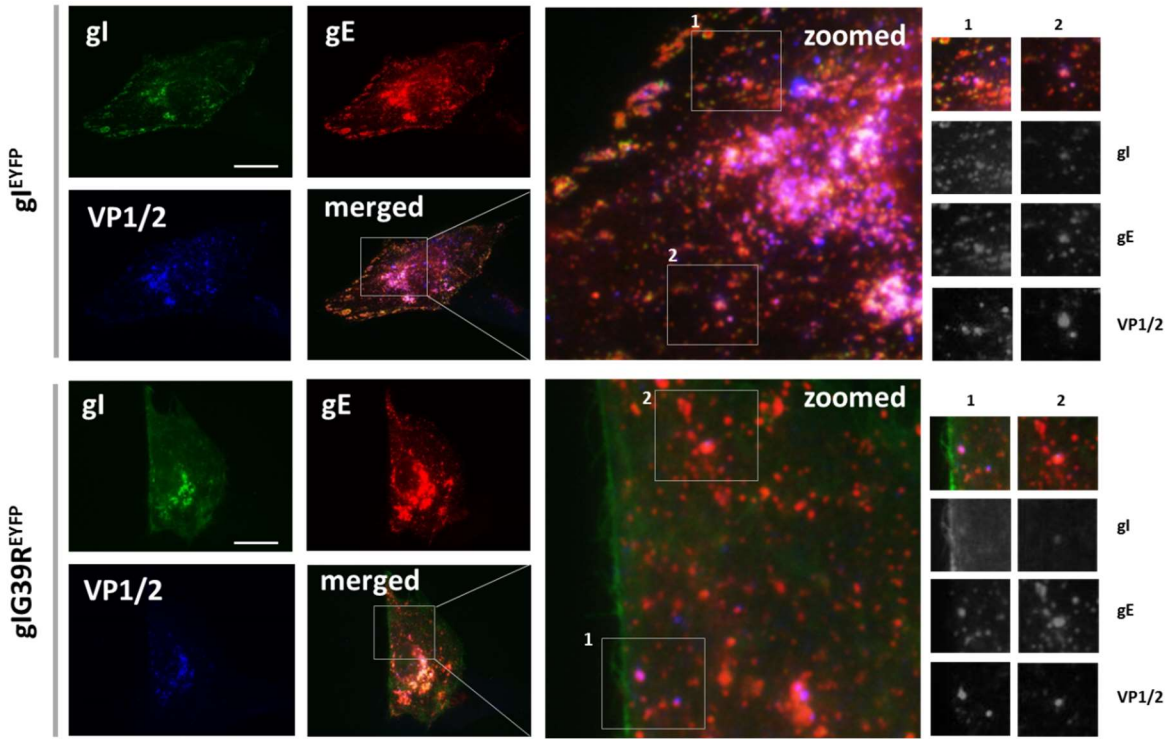

Figure 3.10 | gE, gI and VP1/2 localisation in the cells infected with gI^{EYFP} recombinant viruses. HFF-hTERT cells were infected with gI^{EYFP} or gIG39R^{EYFP} viruses at 1 PFU/cell, cells were fixed after 10 hpi, and labelled with anti-gI (MAb-CC8) (green), anti-gE (MAb-3114) (red), and anti-VP1/2 (blue). Images on the right panel indicate selected areas from the zoomed panel to show possible co-localisation of the indicated proteins. Images were taken using an Olympus IX-81 inverted fluorescence microscope using a 60x oil immersion lens. Scale bar indicates 20 µm.

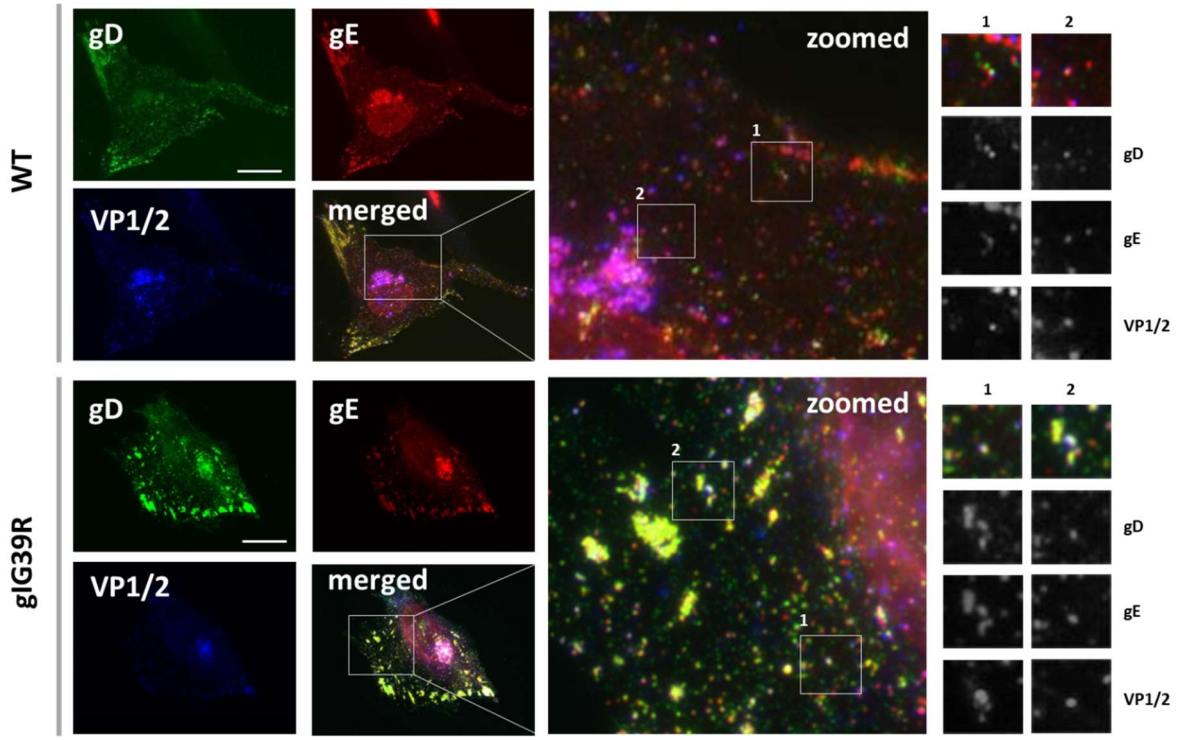

Figure 3.11 | gD, gE and VP1/2 localisation in the cells infected with WT and gIG39R viruses. HFF-hTERT cells were infected with WT or gIG39R viruses at 1 PFU/cell, cells were fixed after 10 hpi. The cells were labelled with gD (green), gE (MAb-3114) (red) and VP1/2 (blue). Images on the right panel indicate selected areas from the zoomed panel to show possible co-localisation of the indicated proteins. Images were taken using an Olympus IX-81 inverted fluorescence microscope using a 60x oil immersion lens. Scale bar indicates 20 µm.

3.2.6 Packaging of viral proteins in recombinant viruses

Packaging of HSV-1 proteins into virion involves an intricate series of interactions between envelope proteins, tegument proteins and capsids at the assembly sites. Data presented above suggests the stability and subcellular localisation of gI appears to be at least partially dependent on interaction with gE. To investigate whether the G39R mutation in gI or deletion of gE or gI affects the packaging of viral proteins during virion assembly, viruses were purified by Ficoll gradient from the culture medium of WT, gIG39R, ΔgE and ΔgI -infected HaCaT cells. Initially, the purity and relative protein content of virion preparations was assessed by commassie blue staining of SDS-PAGE (Figure 3.12). No differences could be observed for the major viral protein species although protein levels were lower for the ΔgI sample indicating fewer virus particles present in this sample. Purified virus preparations were then analysed by WB using various amounts of samples to facilitate more accurate comparison, and tested for VP5, gB, gE, gI, VP16 and VP22 incorporation (Figure 3.13 a). Estimates of the amount of each protein being incorporated into the virion was calculated in 'LI-COR Image Studio Lite' software. The values were normalised to the level of VP5 to determine the percentage of incorporation of other proteins into the virion (Figure 3.13 b). The packaging of gE showed a modest increase in both the gIG39R and ΔgI viruses compared to WT. The incorporation of gI was greatly reduced in both ΔgE and gIG39R viruses, which possibly reflects the reduced localisation of gI to assembly sites as observed by IF microscopy as well as reduced total gI protein levels observed by WB in infected cells lysates for these mutant viruses. These data fit with the notion that incorporation of gI into virions is more efficient when it is in complex with gE and that gI incorporation is more dependent on gE than gE is on gI. The incorporation of gI into ΔgE virions may reflect a passive mechanism due to a level of saturation of the cellular endomembrane system by viral membrane proteins including gI late in infection. The incorporation of the tegument proteins VP16 and VP22 showed a little difference between any of the viruses despite VP22 being a well-established interactor of the cytoplasmic domain of gE (Stylianou et al., 2009; Maringer et al., 2012).

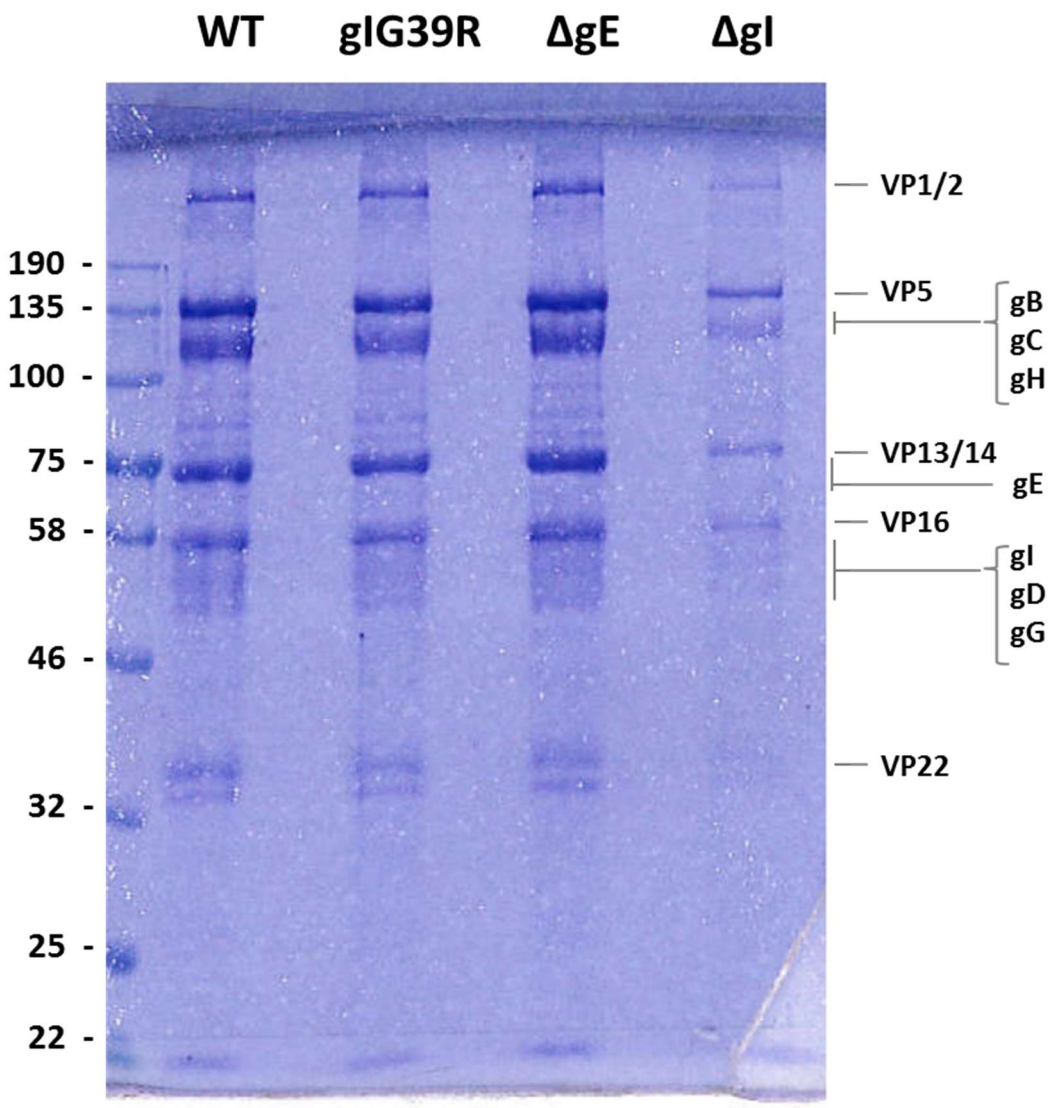

Figure 3.12 | Protein expression profiles of purified virions. HaCaT cells were infected with HSV-1 WT, gIG39R, ΔgE and ΔgI viruses at MOI of 0.01 and after 3 dpi viruses were purified by Ficoll gradient. 10 µL of purified virus particles were loaded to separate the virion proteins by SDS-PAGE and the gel was stained with Coomassie Brilliant Blue. The expected positions of major capsid, tegument and envelope proteins are indicated on the right. Left panel indicates molecular mass of proteins in KDa.

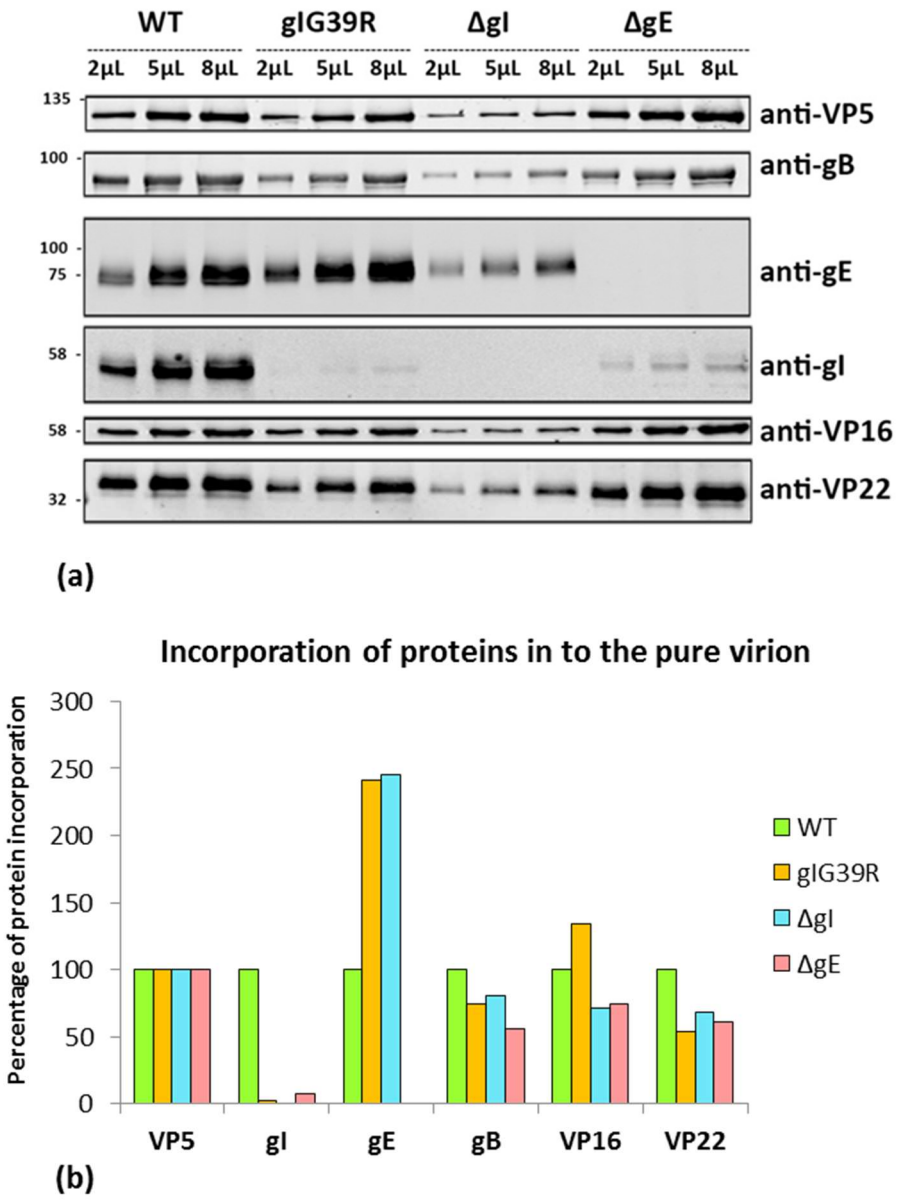

Figure 3.13 | Analysis of protein incorporation into purified virions. Gradient purified WT ($1.52x10^{10}$ PFU/ml), gIG39R ($7.4x10^{9}$ PFU/ml), ΔgI ($1.8x10^{9}$ PFU/ml) and ΔgE ($1.5x10^{10}$ PFU/ml) virions were loaded on SDS-PAGE at 2, 5, 8 µL volume, transferred to nitrocellulose by WB and probed with the antibodies indicated in the figure. The amount of protein incorporation (8µL lane for ΔgI was considered against 2µL lane for the rests) was analysed in 'LI-COR Image Studio Lite' software. The packaging levels were calculated by dividing the amount of protein detected in purified virions (normalised for VP5) by the amount of protein detected in purified WT virion (normalised for VP5). Left panel indicates molecular mass of proteins in KDa.

3.2.7 Transmission electron microscopy (TEM)

To investigate the effects of mutation or deletion of gE and gI on virion morphogenesis and secretion at the ultrastructural level, HaCaT and HFF-hTERT cells were infected with WT, gIG39R, ΔgE and ΔgI viruses at 5 PFU/cell and processed for TEM analysis at 15 hpi. For each infected cell samples, multiple Images were taken for areas highlighting virion envelopment and egress. As can be seen in Figure 3.14 for HaCaT and HFF-hTERT cells intracellular enveloped virions were seen for all the mutant viruses as well as extracellular virus particles. Many extracellular particles were cell-associated or in cell-junctions for all viruses in both cell lines. Overall there were no noticeable defects in virion morphogenesis or egress. Even though the mutant viruses released more infectious viruses into the culture medium than WT HSV-1, the number was still less than 5% of the total number of infectious virions that remained cell-associated. This relatively small increase in secretion (in terms of total virus yield) likely makes observing any difference in virion localisation due to the increased virion secretion difficult to detect by TEM. Conducting such TEM studies using cells that form more extensive cell-cell junctions, such as polarised epithelial cells, may shed more light on potential changes in virion secretion patterns caused by mutations that disrupt gE/gI function.

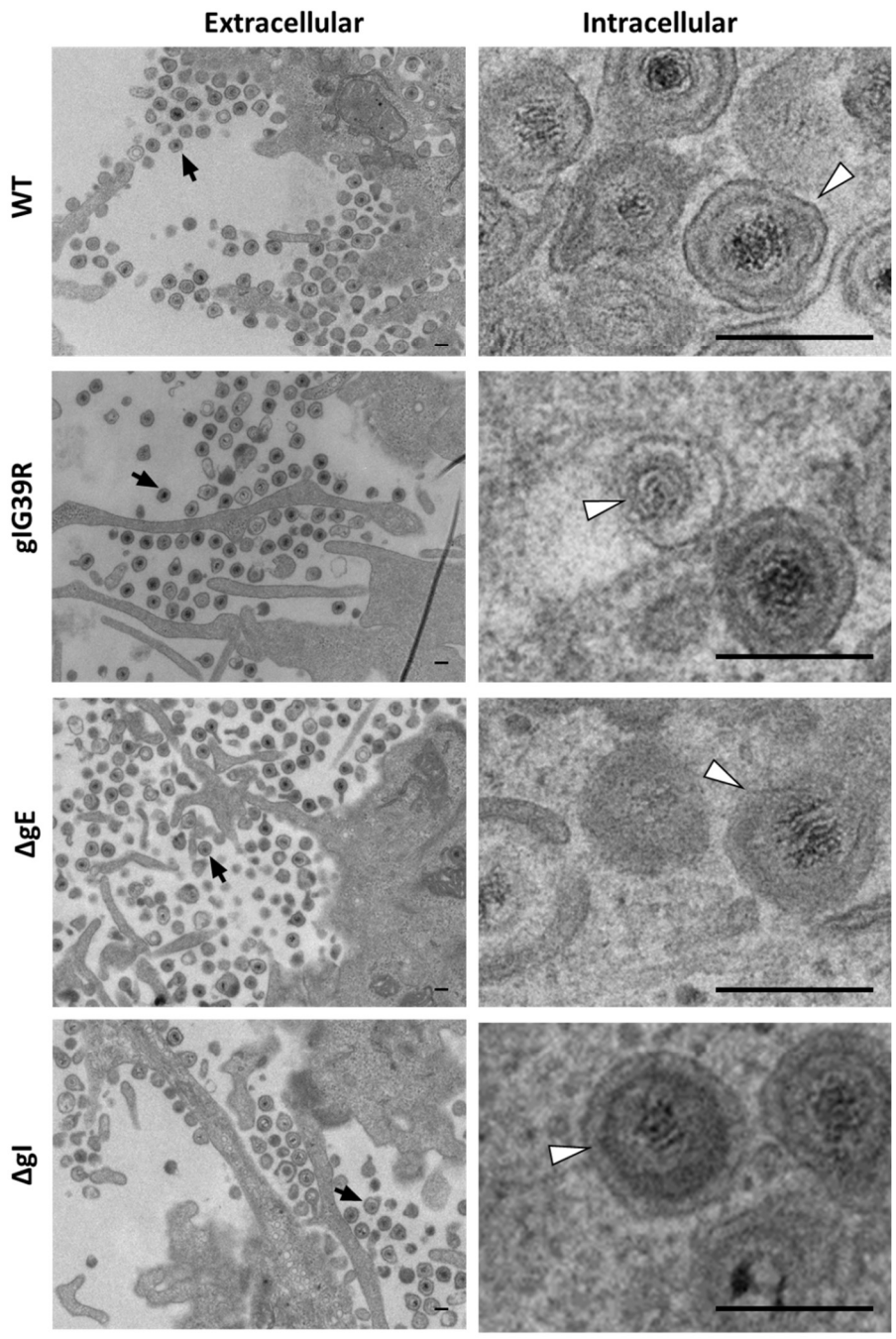

(a)

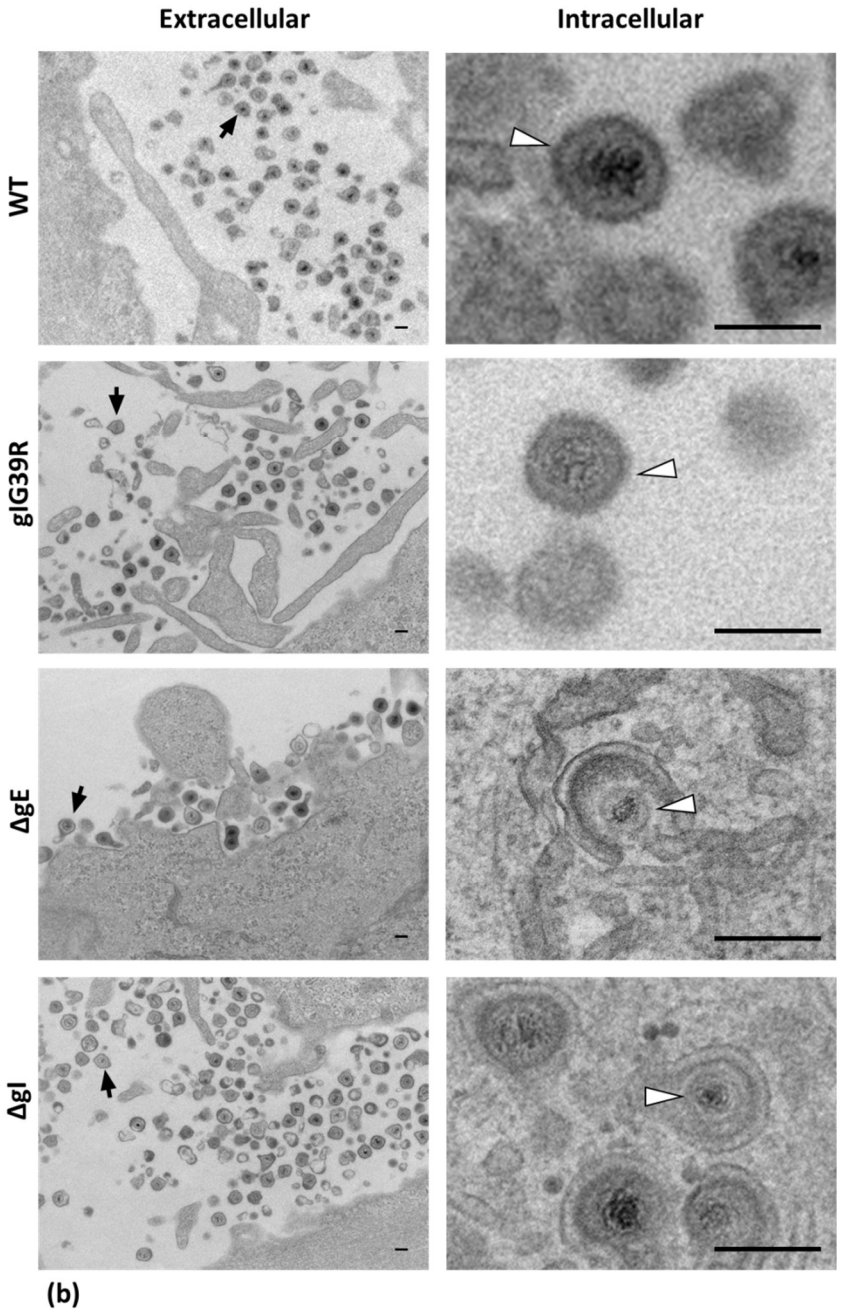

Figure 3.14 | Ultrastructural morphology of cells infected with WT, gIG39R, ΔgE and ΔgI viruses. (a) HaCaT and (b) HFF-hTERT cells were infected with HSV-1 WT, gIG39R, ΔgE or ΔgI virus at MOI of 5 PFU/cell and processed for electron microscopy at 15 hpi. Extracellular virions are marked with black arrow, intracellular capsids are marked with white arrow heads. Scale bars: 250 nm.

3.3 Discussion

The primary aim of this chapter was to understand the significance of gIG39R in V22a mutant that was identified in the first chapter and further characterise the effects of this mutation.

Protein expression profile of infected cell lysates and purified virions clearly indicate that the gIG39R virus essentially functions like a ΔgI virus. Although small amounts of gI proteins are made by the gIG39R virus, these do not seem to form any functional complex with gE, as shown by IP and IF experiments with a conformational antibody that specifically recognises the gE/gI complex (MAb-3063). Maturation of gE appears to be affected in HaCaT cells when it is unable to form complex with gI, suggesting that transport along the secretory pathway and associated post-translational modification in the ER and Golgi of gE relies upon interaction with gI. Alternatively, mature gE may be degraded more rapidly in the absence of each other. The same appears true for gI in infected HaCaT cells, albeit to a lesser extent, as the proportion of mature gI appears lower in ΔgE-infected cells compared to WT. However, these differences in maturation or stability are not so evident in HFF-hTERT or Vero cells, and so maybe a cell type specific effect. The gI-specific monoclonal antibodies used in this work do not appear to work well in the presence of gE, suggesting their epitopes are masked in the gE/gI complex, shown in both IP and IF analysis of cells infected with WT virus. The masking effect of gE on the gI MAb epitopes was also seen in IF experiments where much greater signal levels were observed for gI staining when gE was either absent (ΔgE virus) or unable to interact with gI (gIG39R virus), despite substantially reduced expression levels of gI in these circumstances. In WT-infected cells gI was found to be almost always in complex with gE as the anti-gI antibodies could pull-down very small amount of gI in IP experiments and provided very little signal in IF. The anti-gE (MAb-3114) antibody on the other hand showed good signals for gE in IF and could pull-down gE but not enough gI (compared to the pull-down efficiency of MAb-3063) suggesting that free gE is present in the cells without forming a complex with gI. Additionally, the appearance of gE around the nuclear membrane in IF experiments possibly suggests that free gE could have a role in the nuclear membrane or in ER, whereas gE that exits the ER is primarily in complex with gI. The exact binding site on gI for gE is currently unknown, although data presented here suggest the region around the G39 residue may be important. The IgG binding sites for the Fc-receptor function of gE and gI have been suggested (Basu et al., 1995 and 1997; Dubin et al., 1994), although it has been also proposed that gI

might not be part of the Fc binding domain but rather its presence mediates conformational changes in gE for better Fc receptor activity (Dubin et al., 1994). Data presented in this thesis show that the formation of the gE/gI complex is necessary for Fc binding however it does not distinguish between whether gI has a direct role in binding IgG or functions in stabilising the appropriate conformation of the Fc-binding region on gE. Figure 3.15 represents these interpretations of these data regarding the effect of the gIG39R mutation on gE/gI complex in terms of interaction of various antibodies.

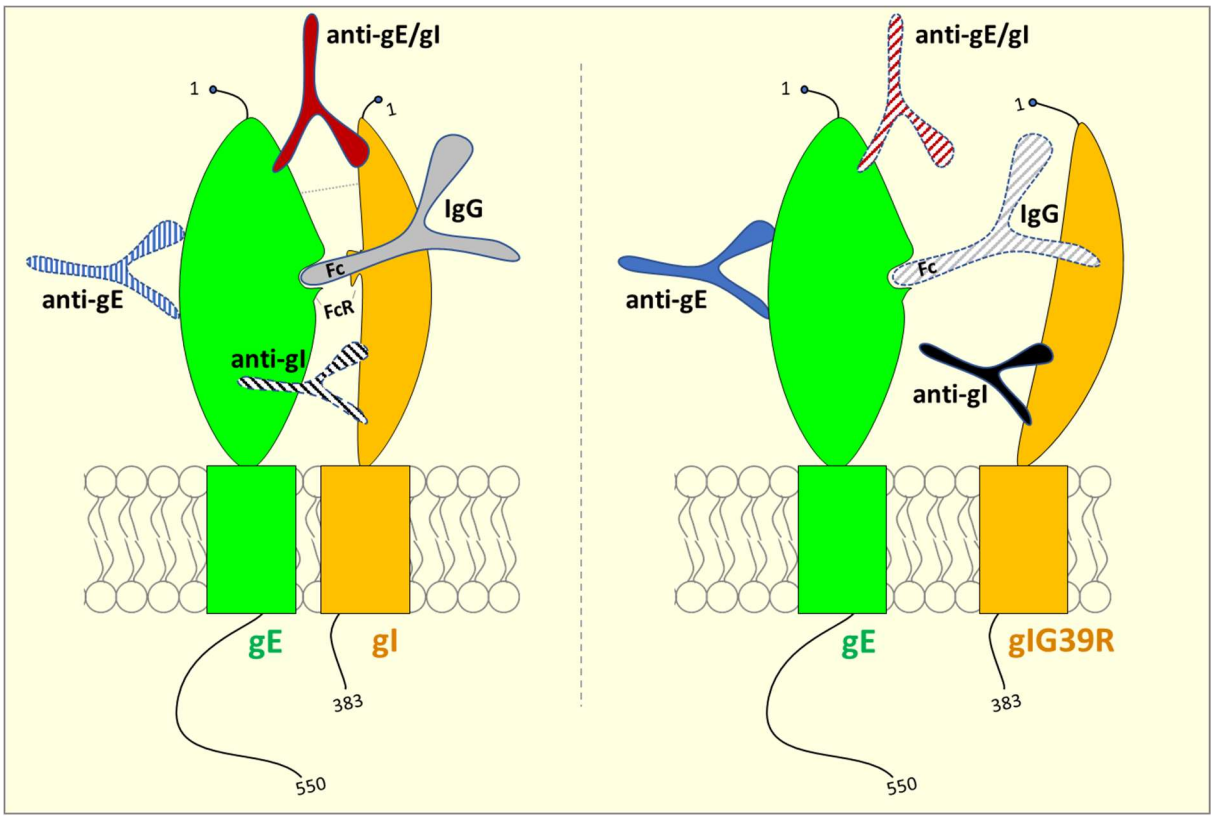

Figure 3.15 | Cartoon of gIG39R-mediated alteration of gE/gI complex for target antibody interactions. The gE/gI complex can bind anti-gE/gI antibody and act as potential Fc receptor for IgG. It may also bind to anti-gE antibody. However, it interacts poorly with anti-gI antibodies. The presence of gIG39R mutation disrupts the gE/gI complex enabling gE to bind strongly to anti-gE but poorly to anti-gE/gI and IgG (poor FcR function) and gIG39R binds strongly to anti-gI antibodies. Strong antibody interactions are shown in solid colour whereas poor interactions are shown in dash colour and lines.

4. Identification of binding partners of the gE/gI complex during HSV-1 infection

4.1 Introduction

During HSV-1 assembly viral glycoproteins will need to interact with different cellular proteins for a variety of functions. The gE/gI complex is proposed to be important, though not essential, for secretion of virions at cell junctions as well as helping connect the envelope to the underlying tegument. Specifically, the cytoplasmic tail of gE has been shown to directly or indirectly interact with many tegument proteins (pUL11, pUL16, pUL21 and pUL49) (Maringer et al., 2012; Farnsworth et al., 2007b; Han et al., 2012) and hence forms part of the network of protein interactions that mediate HSV-1 envelopment. Figure 4.1 represents the putative interactions of gE/gI with tegument and cell-junction targeting proteins during secondary envelopment and transport of virion loaded vesicles to the plasma membrane for fusion. The gE/gI complex of newly released virions has also been proposed to interact with an unknown receptor of neighbouring uninfected cells at the junction (Dingwell and Johnson, 1998).

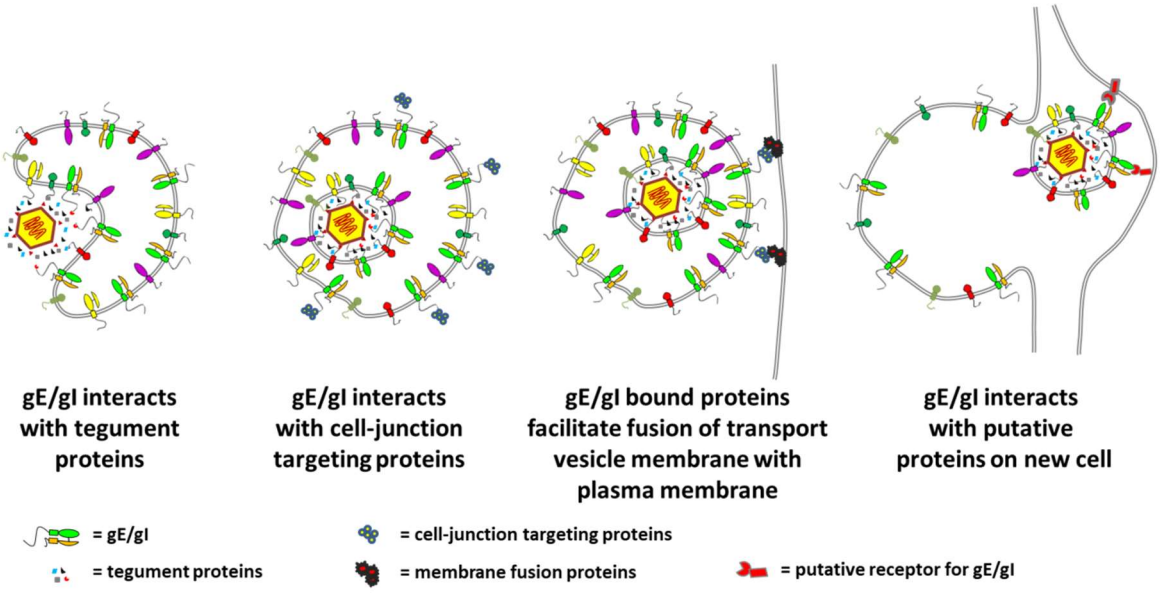

Figure 4.1 | Schematic representation of the potential roles of HSV-1 gE/gI complex during envelopment, egress and spread.

Studies have reported that the gE/gI complex accumulates in the TGN during infection and at late time points gE/gI and TGN46 are redistributed to cell junctions co-localising with β-catenin (Farnsworth et al., 2006; Wisner et al., 2004; McMillan et al., 2001), although the interpretation of these data may have been complicated by the Fc-binding activity of gE/gI. The gE/gI complex is thought to interact with cytosolic adaptor molecules involved in vesicle formation and transport like the clathrin adaptor AP-1 and PACS-1 due to the presence of consensus binding motifs for these cellular proteins in the cytoplasmic domain of gE (Gu et al., 2001; Wan et al., 1998). However, there is little direct evidence of specific cellular interactors of gE/gI and this has not been investigated by quantitative proteomic studies of gE/gI binding partners in the context of HSV-1. Such studies could provide an insight of cellular and viral interactome of the complex which would help understand the mechanism of targeted HSV-1 virion egress to the cell junction.

Immunoprecipitation techniques to precipitate a target protein using highly specific antibodies enable direct and indirect binding partners of the target protein to be co-precipitated from a reaction mixture. Such isolated protein complexes then can be analysed by mass spectrometry (MS) to identify the binding partners of the target proteins. To facilitate identification of specific interactors above the ‘noise’ of background non-specific interactors, a technique known as stable isotope labelling of amino acids in cell culture (SILAC) is commonly used. SILAC is a mass spectrometry-based approach that allows the abundance of proteins to be directly compared in up to 3 samples in parallel through the simultaneous detection of peptides with the identical amino acid sequence but that differ in molecular weight due to differences in the incorporation of non-radioactive isotopic labelled amino acids into proteins in living cells (Ong and Mann, 2005). The technique depends on metabolic incorporation of 'light' (L), ‘medium’ (M) or 'heavy' (H) amino acids (usually lysine and arginine) that differ in their content of ‘heavy’ isotopes of carbon and nitrogen (C13 and N15) into cellular proteins. To enable this, cells are grown in the L-, M- or H-labelled medium for a minimum of five cell doubling times to ensure the vast majority of proteins from these cells are fully labelled with respective R and K amino acids, which can be detected by MS.

In this chapter, SILAC-labelled HaCaT cells were infected with different HSV-1 viruses to perform IP of the gE/gI complex followed by MS analysis. Potential interactors were validated to select candidate gE/gI binding partners that may regulate for virion egress.

4.2 Results

4.2.1 gE/gI immunoprecipitation from SILAC-labelled HaCaT cells for mass spectrometric analysis

To identify the cellular proteins that interact with gE/gI complex during infection, an IP experiment on SILAC-labelled cells was performed. Initially, SILAC-labelled HaCaT cells were generated in the lab by growing them for at least five cell doubling times. For this experiment, arginine (R) and Lysine (K) amino acids were labelled as R0K0, R6K4 and R10K8 for L-, M- and H- SILAC respectively. As outlined in Figure 4.2, SILAC-labelled cells were infected with HSV-1 WT (two M and one H), ΔgE (two H and one M) viruses or mock (three L) in three biological replicates. At 16 hpi the cells were lysed, the total protein concentration was measured by bicinchoninic acid (BCA) assay and equivalent amount of protein was used for IP with anti-gE/gI (MAb-3063) antibody. The immunoprecipitated samples from appropriately labelled WT, ΔgE and mock –infected cell lysates were mixed together in equal amount to generate 3 sample sets. The samples were then sent for MS analysis.

A fraction of the unmixed samples were kept to test the pull-down efficiency. The samples were run on SDS-PAGE and transferred on nitrocellulose membrane and tested for gE, tegument protein VP16 and housekeeping gene tubulin. As expected the anti-gE/gI antibody could pull down gE only from WT-infected samples but not from ΔgE and mock-infected samples (Figure 4.3). The IP sample shows approximately 20% of the total gE pull-down achieved by the antibody, whereas the supernatant and lysate show approximately 1% of the total gE present in the unbound and whole-cell lysates respectively. In the IP samples, tubulin and VP16 were not detected indicating the IP samples were not contaminated with non-specific proteins.

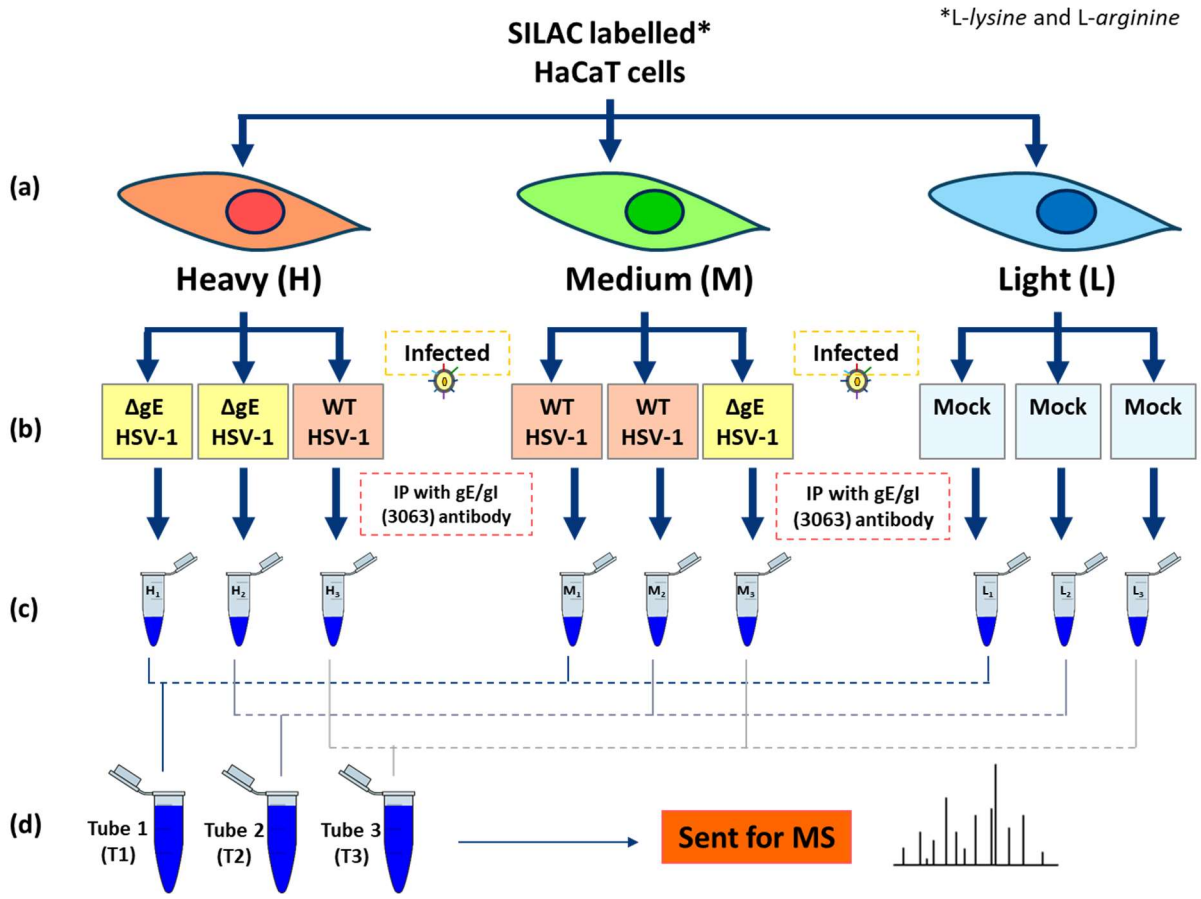

Figure 4.2 | Schematic representation of SILAC-labelling of HaCaT cells and pull down of HSV-1 gE/gI complex workflow. (a) HaCaT cells were either labelled with heavy or medium or unlabelled (light). (b) The cells were infected with either HSV-1 WT or HSV-1 ΔgE virus or mock-infected as shown in the flowchart. (c) At 16 hpi the cells were lysed and an IP was performed using gE/gI (MAb-3063) antibody. (d) The immunoprecipitated protein samples were mixed and sent for MS analysis.

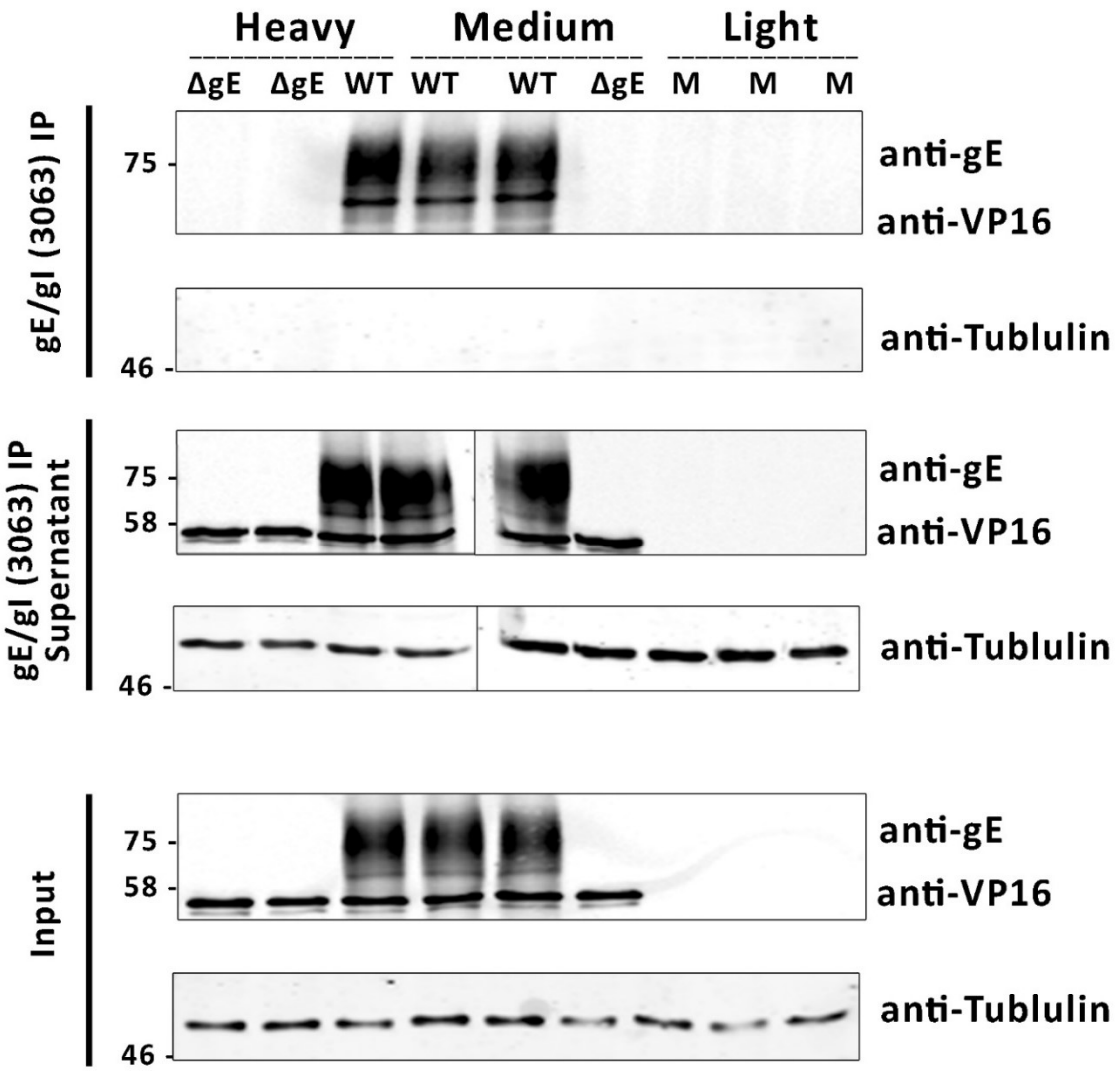

Figure 4.3 | SILAC-labelled HaCaT sample testing for protein expression. Heavy, medium and light SILAC HaCaT cells were infected with either HSV-1 WT or ΔgE virus or mock (M). After 16 hpi the cells were lysed and an IP was performed using anti-gE/gI (MAb-3063) antibody. The pull-down protein samples, their supernatant and whole cell lysates were separated by SDS-PAGE and analysed by WB using the antibodies indicated. Molecular mass markers (in KDa) are on the left.

4.2.2 Bioinformatics analysis of the MS data

Raw MS data were analysed in excel spread sheet and graph pad prism software for bioinformatics analysis based on the methodology described in the Materials and Methods section (8.6.4). A total of 26 common protein hits among all three sample sets (T1, T2 and T3) were identified, of which 20 were cellular (Table 4.1). Protein-protein interaction network information can help to identify involvement of particular cellular processes in the area of interest. In this context, STRING is very helpful. It is a web-based biological database which contains information from various sources, such as experimental results, computational prediction methods and public text input which allows the generation of networks of interacting proteins from raw proteomics data. A STRING analysis of the 20 cellular hits aligned 13 of them in a single cluster (Figure 4.3 a). Two other proteins i.e., Nipsnap1 and 2 though functionally linked to the cluster might carry out some other functions in the cell. The other five proteins were placed individually in the diagram showing no evidence of any functional linkage with any other proteins (Figure 4.3 a).

To broaden the list of candidate interactors of gE/gI additional hits that were common in at least two sample sets (T1 & T2, T2 & T3, and T1 & T3) were also considered (Table 4.2). This gave 21 additional cellular proteins in the list. However, further STRING analysis did not identify any additional clusters, but the previous cluster became enriched and some additional unconnected proteins were identified (Figure 4.3 b). From the STRING network, it was evident that the cluster contained proteins that are primarily mitochondrial and proteins that mediate cellular respiration. Of particular interest three proteins with putative roles in vesicle transport (Nipsnap1, Nipsnap2 and MYOF) an interferon inducible restriction factor (IFITM2), and a well characterised endo-lysosomal trafficking regulator (Rab7A) were identified in all three biological replicates (Figure 4.3 a). Some other well studied lysosome-associated membrane proteins with potential roles in lysosome biogenesis and autophagy (LAMP1 and LAMP2) (Eskelinen et al., 2002; Eskelinen, 2006) were present in duplicate sample hits (Figure 4.3 b). Careful consideration of the protein descriptions narrowed down the search and left us with few potential proteins that have predicted or established roles in endocytic pathway or vesicle transport in cells and therefore could be interesting in gE/gI mediated virion egress pathway to the cell junctions.

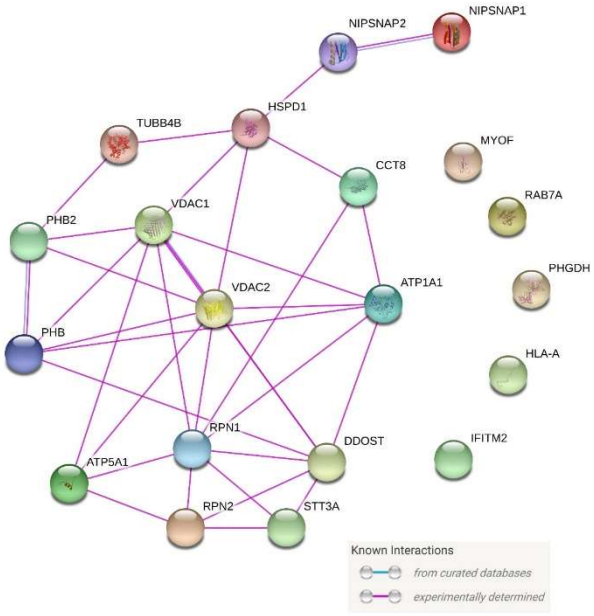

(a)

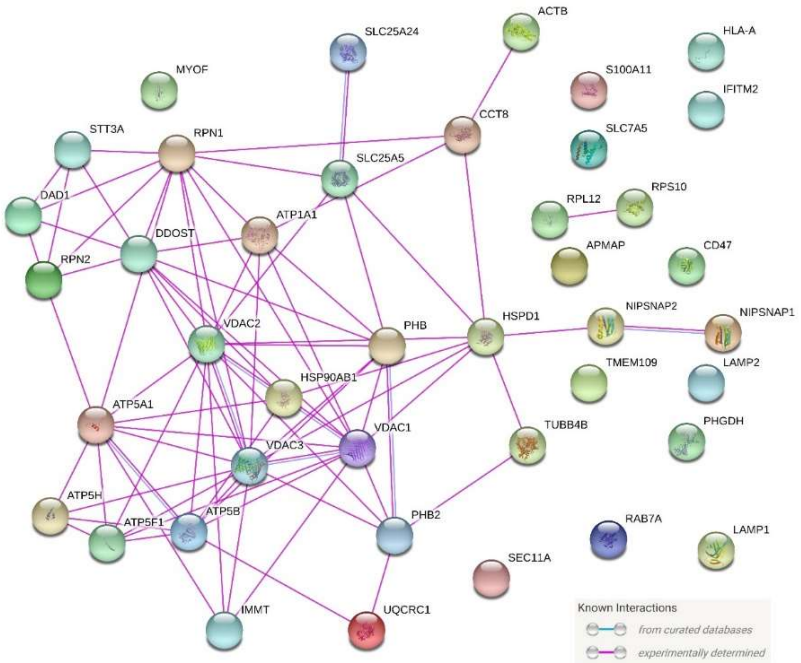

(b)

Figure 4.4 | STRING analysis of the potential interaction network of proteins identified as binding partners of gE/gI. (a) Network of interacting protein from three biological sample hits and (b) the same for two biological sample hits. Proteins clustered into sub-networks: mitochondrial proteins or proteins related to cellular respiration.

Table 4.1 | Common SILAC hits for cellular proteins in three biological replicates

			[a.]T1				[a.]T2				[a.]T3			
			[b.]Mean 0.054, [c.]SD 0.285, [c.]Threshold 0.596				[b.]Mean -0.0054, [c.]SD 0.258, [d.]Threshold 0.486				[b.]Mean 0.276, [c.]SD 0.637, [d.]Threshold 1.488			
Common in	String/Uniprot Name	Description	[e.]Unique Peptide	[f.]M/H	log2 M/H	[h.]Z score	[e.]Unique Peptide	[f.]M/H	log2 M/H	[h.]Z score	[e.]Unique Peptide	[f]H/M	log2 H/M	[h.]Z score
T1, T2 and T3	RPN2	cDNA FLJ60278, highly similar to Dolichyl-diphosphooligosaccharide--proteinglycosyltransferase 63 KDa subunit (EC 2.4.1.119) OS=Homo sapiens PE=2 SV=1 - [B4DJL0_HUMAN]	1.00	100.00	6.64	23.09	1.00	11.32	3.50	6.60	2.00	11.82	3.56	5.15
	MYOF	Myoferlin OS=Homo sapiens GN=MYOF PE=1 SV=1 - [MYOF_HUMAN]	2.00	2.97	1.57	5.30	5.00	2.43	1.28	2.08	1.00	23.39	4.55	6.70
	HLA-A	MHC class I antigen (Fragment) OS=Homo sapiens GN=HLA-A PE=3 SV=1 - [Q4QZC0_HUMAN]	1.00	8.10	3.02	10.39	4.00	2.01	1.01	1.53	1.00	3.13	1.65	2.15
	PHGDH	cDNA FLJ35987 fis, clone TESTI2014269, highly similar to D-3-phosphoglycerate dehydrogenase (EC 1.1.1.95) OS=Homo sapiens PE=2 SV=1 - [B3KSC3_HUMAN]	4.00	2.62	1.39	4.68	4.00	5.32	2.41	4.38	3.00	3.21	1.68	2.20
	TUBB4B	Tubulin beta-4B chain OS=Homo sapiens GN=TUBB4B PE=1 SV=1 - [TBB4B_HUMAN]	5.00	1.56	0.64	2.06	1.00	3.16	1.66	2.85	2.00	3.34	1.74	2.29
	RAB7A	Ras-related protein Rab-7a (Fragment) OS=Homo sapiens GN=RAB7A PE=1 SV=1 - [C9J592_HUMAN]	2.00	3.62	1.86	6.31	3.00	2.45	1.29	2.10	3.00	2.97	1.57	2.03
	PHB	Prohibitin OS=Homo sapiens GN=PHB PE=1 SV=1 - [PHB_HUMAN]	6.00	6.27	2.65	9.09	6.00	9.29	3.22	6.02	6.00	17.42	4.12	6.03
	VDAC1	Voltage-dependent anion-selective channel protein 1 OS=Homo sapiens GN=VDAC1 PE=1 SV=2 - [VDAC1_HUMAN]	2.00	2.72	1.45	4.88	6.00	2.64	1.40	2.32	3.00	5.02	2.33	3.22
	HSPD1	cDNA FLJ54373, highly similar to 60 KDa heat shock protein, mitochondrial OS=Homo sapiens PE=2 SV=1 - [B7Z597_HUMAN]	10.00	2.35	1.23	4.13	13.00	2.13	1.09	1.70	14.00	3.67	1.87	2.51
	CCT8	T-complex protein 1 subunit theta (Fragment) OS=Homo sapiens GN=CCT8 PE=1 SV=1 - [H7C4C8_HUMAN]	1.00	1.90	0.92	3.05	1.00	3.56	1.83	3.20	2.00	7.88	2.98	4.24
	Nipsnap2	Protein NipSnap homolog 2 (Fragment) OS=Homo sapiens GN=GBAS PE=1 SV=1 - [C9J7B1_HUMAN]	1.00	100.00	6.64	23.09	1.00	100.00	6.64	12.99	3.00	100.00	6.64	9.98

	IFITM2	Interferon-induced transmembrane protein 2 (Fragment) OS=Homo sapiens GN=IFITM2 PE=4 SV=1 - [H7BYV1_HUMAN]	1.00	10.27	3.36	11.58	1.00	5.26	2.39	4.34	1.00	5.34	2.42	3.35
	PHB2	Prohibitin-2 OS=Homo sapiens GN=PHB2 PE=1 SV=1 - [F5GY37_HUMAN]	5.00	8.19	3.03	10.44	6.00	9.08	3.18	5.95	10.00	10.81	3.43	4.95
	Nipsnap1	Protein NipSnap homolog 1 (Fragment) OS=Homo sapiens GN=Nipsnap1 PE=1 SV=1 - [H7C2U6_HUMAN]	3.00	100.00	6.64	23.09	1.00	100.00	6.64	12.99	4.00	100.00	6.64	9.98
	RPN1	Dolichyl-diphosphooligosaccharide--protein glycosyltransferase subunit 1 OS=Homo sapiens GN=RPN1 PE=1 SV=1 - [B7Z4L4_HUMAN]	3.00	3.44	1.78	6.06	5.00	4.59	2.20	3.94	6.00	6.98	2.80	3.96
	ATP5A1	ATP synthase subunit alpha, mitochondrial OS=Homo sapiens GN=ATP5A1 PE=1 SV=1 - [ATPA_HUMAN]	6.00	3.28	1.71	5.82	7.00	2.55	1.35	2.23	8.00	3.34	1.74	2.30
	ATP1A1	cDNA FLJ60077, highly similar to Sodium/potassium-transporting ATPase alpha-1 chain (EC 3.6.3.9) (Fragment) OS=Homo sapiens PE=2 SV=1 - [B7Z3V1_HUMAN]	3.00	12.48	3.64	12.57	6.00	6.12	2.61	4.79	4.00	61.35	5.94	8.88
	DDOST	Dolichyl-diphosphooligosaccharide--protein glycosyltransferase 48 KDa subunit OS=Homo sapiens GN=DDOST PE=1 SV=1 - [A0A0C4DGS1_HUMAN]	1.00	2.28	1.19	3.97	2.00	3.85	1.95	3.43	3.00	4.38	2.13	2.91
	VDAC2	Voltage-dependent anion-selective channel protein 2 (Fragment) OS=Homo sapiens GN=VDAC2 PE=1 SV=1 - [A0A0A0MR02_HUMAN]	4.00	4.10	2.04	6.95	4.00	3.98	1.99	3.52	4.00	8.40	3.07	4.38
	STT3A	HCG2032701, isoform CRA_a OS=Homo sapiens GN=hCG_2032701 PE=4 SV=1 - [A0A024R3J7_HUMAN]	2.00	4.17	2.06	7.03	1.00	3.66	1.87	3.28	1.00	8.53	3.09	4.41

[a.] T1 = tube 1, T2 = tube 2, T3 = tube 3
[b.] Mean = generated from a log2 ratios
[c.] SD = standard deviation generated from a log2 ratios
[d.] Threshold = represents the mean and standard deviations of the Gaussian distribution
[e.] Unique peptide = refers to the number of peptides used for identification of protein. When a protein is identified from several unique peptide spectra the confidence in identification of protein is improved.
[f.] M/H = the relative intensity of peptides in medium labelled sample, compared to heavy labelled sample
[g.] H/M = the relative intensity of peptides in heavy labelled sample, compared to medium labelled sample
[h.] z score = $(X - \mu) / \sigma$ where X is the value of the element, μ is the population mean, and σ is the standard deviation

Table 4.2 | Common SILAC hits for cellular proteins in two biological replicates

			[a.]T1				[a.]T2				[a.]T3			
			[b.]Mean 0.054, [c.]SD 0.285, [c.]Threshold 0.596				[b.]Mean -0.0054, [c.]SD 0.258, [d.]Threshold 0.486				[b.]Mean 0.276, [c.]SD 0.637, [d.]Threshold 1.488			
Common in	**String/Uniprot Name**	**Description**	**[c.]Unique Peptide**	**[f.]M/H**	**log2 M/H**	**[h.]Z score**	**Unique Peptide**	**[f.]M/H**	**Log2 M/H**	**[h.]Z score**	**Unique Peptide**	**[g.]H/M**	**Log2 H/M**	**[h.]Z score**
T1 and T2	SLC25A5	ADP/ATP translocase 2 OS=Homo sapiens GN=SLC25A5 PE=1 SV=7 - [ADT2_HUMAN]	4.00	1.53	0.61	1.96	4.00	2.76	1.46	2.45	x	x	x	x
	ATP5B	ATP synthase subunit beta (Fragment) OS=Homo sapiens GN=ATP5B PE=1 SV=1 - [H0YH81_HUMAN]	6.00	2.94	1.56	5.26	4.00	2.72	1.45	2.42	x	x	x	x
	APMAP	Adipocyte plasma membrane-associated protein (Fragment) OS=Homo sapiens GN=APMAP PE=1 SV=1 - [H0Y512_HUMAN]	1.00	4.58	2.19	7.50	1.00	4.15	2.05	3.65	x	x	x	x
	LAMP2	cDNA FLJ52540, highly similar to Lysosome-associated membrane glycoprotein 2 OS=Homo sapiens PE=2 SV=1 - [B7Z2R9_HUMAN]	1.00	2.07	1.05	3.49	1.00	2.50	1.32	2.16	x	x	x	x
	ACTB	cDNA FLJ52842, highly similar to Actin, cytoplasmic 1 OS=Homo sapiens PE=2 SV=1 - [B4E335_HUMAN]	8.00	1.82	0.86	2.83	4.00	2.02	1.01	1.53	x	x	x	x
	HSP90AB1	cDNA FLJ54023, highly similar to Heat shock protein HSP 90-beta OS=Homo sapiens PE=2 SV=1 - [B4DMA2_HUMAN]	3.00	3.80	1.93	6.56	2.00	1.82	0.87	1.24	x	x	x	x
	LAMP1	cDNA FLJ35079 fis, clone PLACE6005283, highly similar to Lysosome-associated membrane glycoprotein 1 OS=Homo sapiens PE=2 SV=1 - [B3KRY3_HUMAN]	1.00	1.91	0.93	3.08	2.00	1.60	0.68	0.85	x	x	x	x
	S100A11	Protein S100 OS=Homo sapiens PE=2 SV=1 - [B2R5H0_HUMAN]	1.00	14.17	3.82	13.21	1.00	1.70	0.76	1.02	x	x	x	x
	CD47	CD47 OS=Homo sapiens GN=CD47 PE=2 SV=1 - [A0A0A1TSG4_HUMAN]	1.00	3.27	1.71	5.79	1.00	2.48	1.31	2.14	x	x	x	x
T1 and T3	VDAC3	Voltage-dependent anion-selective channel protein 3 OS=Homo sapiens GN=VDAC3 PE=1 SV=1 - [VDAC3_HUMAN]	1.00	100.00	6.64	23.09	x	x	x	x	1.00	0.17	2.56	3.58
	ATP5F1	ATP synthase F(0) complex subunit B1, mitochondrial OS=Homo sapiens GN=ATP5F1 PE=1 SV=1 - [Q5QNZ2_HUMAN]	1.00	2.16	1.11	3.70	x	x	x	x	2.00	0.34	1.56	2.01

	RPS10	40S ribosomal protein S10 OS=Homo sapiens GN=RPS10 PE=1 SV=1 - [RS10_HUMAN]	1.00	1.75	0.81	2.65	x	x	x	x	2.00	0.21	2.26	3.12
	RPL12	60S ribosomal protein L12 OS=Homo sapiens GN=RPL12 PE=1 SV=1 - [RL12_HUMAN]	1.00	1.72	0.78	2.54	x	x	x	x	2.00	0.06	3.96	5.77
	SEC11A	Signal peptidase complex catalytic subunit SEC11 (Fragment) OS=Homo sapiens GN=SEC11A PE=1 SV=1 - [H0YNX5_HUMAN]	1.00	1.64	0.71	2.30	x	x	x	x	2.00	0.31	1.70	2.24
	DAD1	Dolichyl-diphosphooligosaccharide--protein glycosyltransferase subunit DAD1 OS=Homo sapiens GN=DAD1 PE=1 SV=1 - [F5H895_HUMAN]	1.00	3.18	1.67	5.66	x	x	x	x	1.00	0.25	1.99	2.69
	ATP5H	ATP synthase subunit d, mitochondrial OS=Homo sapiens GN=ATP5H PE=1 SV=2 - [F5H608_HUMAN]	1.00	4.14	2.05	6.99	x	x	x	x	1.00	0.29	1.79	2.38
	SLC25A24	cDNA FLJ50039, highly similar to Homo sapiens solute carrier family 25, member 24, transcript variant 1, mRNA OS=Homo sapiens PE=2 SV=1 - [B4E290_HUMAN]	2.00	2.36	1.24	4.16	x	x	x	x	1.00	0.01	6.25	9.37
	UQCRC1	cDNA FLJ51625, highly similar to Ubiquinol-cytochrome-c reductase complex coreprotein I, mitochondrial (EC 1.10.2.2) OS=Homo sapiens PE=2 SV=1 - [B4DUL5_HUMAN]	1.00	100.00	6.64	23.09	x	x	x	x	1.00	0.35	1.52	1.95
T2 and T3	SLC7A5	Large neutral amino acids transporter small subunit 1 OS=Homo sapiens GN=SLC7A5 PE=1 SV=2 - [LAT1_HUMAN]	x	x	x	x	3.00	2.09	1.07	1.64	3.00	0.20	2.29	3.16
	IMMT	MICOS complex subunit MIC60 (Fragment) OS=Homo sapiens GN=IMMT PE=1 SV=1 - [H7C463_HUMAN]	x	x	x	x	1.00	7.44	2.89	5.36	2.00	0.08	3.74	5.42
	TMEM109	cDNA FLJ57860, highly similar to Transmembrane protein 109 OS=Homo sapiens PE=2 SV=1 - [B4E1S3_HUMAN]	x	x	x	x	1.00	1.90	0.92	1.35	1.00	0.13	2.95	4.19

[a.] T1 = tube 1, T2 = tube 2, T3 = tube 3
[b.] Mean = generated from a log2 ratios
[c.] SD = standard deviation generated from a log2 ratios
[d.] Threshold = represents the mean and standard deviations of the Gaussian distribution
[e.] Unique peptide = refers to the number of peptides used for identification of protein. When a protein is identified from several unique peptide spectra the confidence in identification of protein is improved.
[f.] M/H = the relative intensity of peptides in medium labelled sample, compared to heavy labelled sample
[g.] H/M = the relative intensity of peptides in heavy labelled sample, compared to medium labelled sample
[h.] z score = $(X - \mu) / \sigma$ where X is the value of the element, μ is the population mean, and σ is the standard deviation

4.2.3 Validation of putative gE/gI binding partners identified from SILAC IP mass spectrometry

To validate some of the potential interactions of gE/gI with cellular proteins HaCaT cells were infected with WT, ΔgE virus or were mock-infected. After 16 h the cells were lysed and immunoprecipitations was performed with anti-gE/gI antibody (MAb-3063). The precipitated samples were run on SDS-PAGE for WB and tested initially for a small subset of cellular proteins. This included Nipsnap1, an evolutionary conserved but poorly characterised protein thought to have possible role in vesicular transport due to sequence homology with SNAP-25, a member of the SNARE family of vesicle fusion proteins (Seroussi et al., 1998). As can be seen from Figure 4.5, anti-gE/gI IP from WT-infected samples co-precipitated Nipsnap1, although the Nipsnap1 protein band ran close to the light chain band from the MAb-3063 antibody. Two other membrane traffic-related hits were tested: Rab7, a Ras-family member GTPase that is known to function in late endocytic trafficking pathways, especially downstream of multivesicular body biogenesis (Vanlandingham et al., 2009); and LAMP1, a transmembrane protein type-I found mostly in lysosome and to some extent late in endosomes (Harter et al., 1992; Rohrer et al., 1996). Faint signals of the correct approximate size were detected for both these proteins among all three IP samples with no increase in signal for WT-infected samples compared to ΔgE or mock, suggesting these proteins do not specifically interact with gE/gI. Alpha-tubulin was used as loading control and a negative control in this validation experiment. The anti-tubulin antibody used in this experiment is known to specifically recognise the tyrosylated form of alpha-tubulin (Wehland et al., 1983).

The interaction detected for gE/gI and Nipsnap1 was then further examined to test whether the interaction was dependent of gE, gI or the complex. HaCaT cells were infected with WT, gIG39R, ΔgE, ΔgI virus or mock. After 16 h the cells were lysed and immunoprecipitated with anti-gE/gI antibody, and the samples were tested by WB for gE, Nipsnap1 and tubulin. As demonstrated in the previous chapters the MAb-3063 antibody can efficiently pull down gE and gI from WT infection but only small amount of immature gE can be seen in the IP samples from gIG39R and ΔgI -infected cells. Interestingly even though predominantly immature gE was being pulled by the anti-gE/gI antibody from gIG39R and ΔgI -infected cell lysates, Nipsnap1 was also detected in these samples (Figure 4.6). This indicates Nipsnap1 interacts with gE and the interaction is neither dependent on the presence of gI nor on the gE/gI complex. The interaction with Nipsnap1 appears more efficient in WT-infected cells, which may reflect the greater gE expression levels from WT virus or could be due to changes in gE localisation that gives rise to more mature gE.

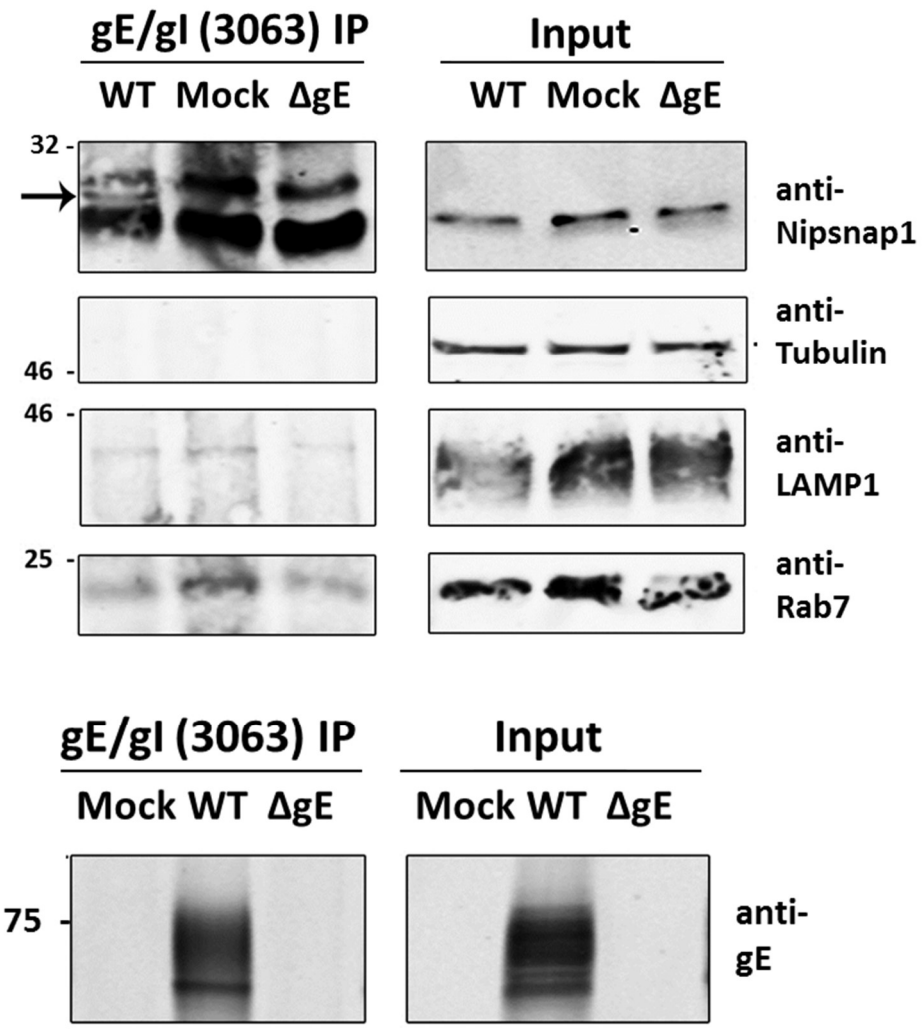

Figure 4.5 | Validation of SILAC hits by WB. HaCaT cells were infected with HSV-1 WT and ΔgE. After 16 h the cells were lysed and an IP was performed using anti-gE/gI (MAb-3063) antibody. The pulled protein samples and whole cell lysates were separated by SDS-PAGE and analysed by WB using the antibodies indicated. Molecular mass markers (in KDa) are on the left. The arrow on top left indicates position of Nipsnap1 on the membrane.

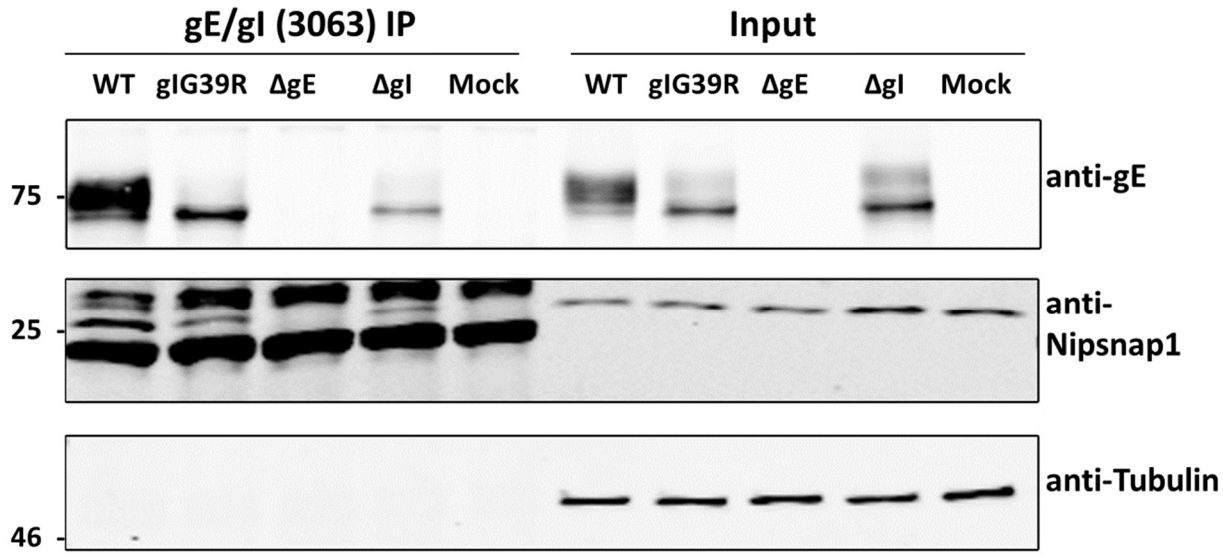

Figure 4.6 | Effect of gE and gI deletion or mutation on Nipsnap1 interaction. HaCaT cells were infected with HSV-1 WT, gIG39R, ΔgE, ΔgI or were mock infected. After 16 h the cells were lysed and an IP was performed using anti-gE/gI (MAb-3063) antibody. The pulled-down protein samples, their supernatant and whole cell lysates were separated by SDS-PAGE and analysed by WB using the antibodies indicated. Molecular mass markers (in KDa) are shown on the left.

4.2.4 Investigation of additional potential cellular interacting partners of gE/gI

Glycoprotein E (gE) has been reported to interact with many viral proteins, including pUL11, pUL16 and pUL49, and it is unclear whether gI is involved in these interactions. These data above also demonstrate that gE co-precipitates with a cellular protein Nipsnap1 during infection in the absence of gI, suggesting gE may be the main binding site for interactors of the gE/gI complex. Therefore, additional cellular proteins identified as gE/gI interactors in the SILAC-IP-MS analysis were tested for interaction by pulling down by gE alone using the anti-gE (MAb-3114) antibody. HaCaT cell were mock-infected or infected for 16 h with WT HSV-1 and lysed for IP with anti-gE antibody. The IP samples were run on SDS-PAGE followed by WB and tested for a range of antibodies as shown in Figure 4.7. A substantial amount of gE was seen in the pulled-down sample of WT HSV-1. However, the interaction with most of the proteins from the SILAC-IP-MS hit list were not seen. Mitochondrial proteins VDAC1, ATP5A1 or PHB all appeared as hits in the SILAC data but no specific bands of the correct molecular weight could be observed in the pull-down samples. Late endosomal marker protein Rab7, phosphoglycerate dehydrogenase enzyme PHGDH and cytoskeleton protein tubulin also could not be detected. Interestingly, besides Nipsnap1, Nipsnap2 was also detected in the pull-down sample. These proteins share ~66% sequence identity and are predicted to have similar functions. In addition to these two proteins, MYOF a member of the Ferlin protein family was detected. Interferon-induced antiviral protein IFITM2, while not detected in the IP sample, demonstrated a reduced protein level in infected cell lysates. The changes in IFITM2 expression and co-precipitation of Nipsnap1, 2 and MYOF were taken forward for further investigation.

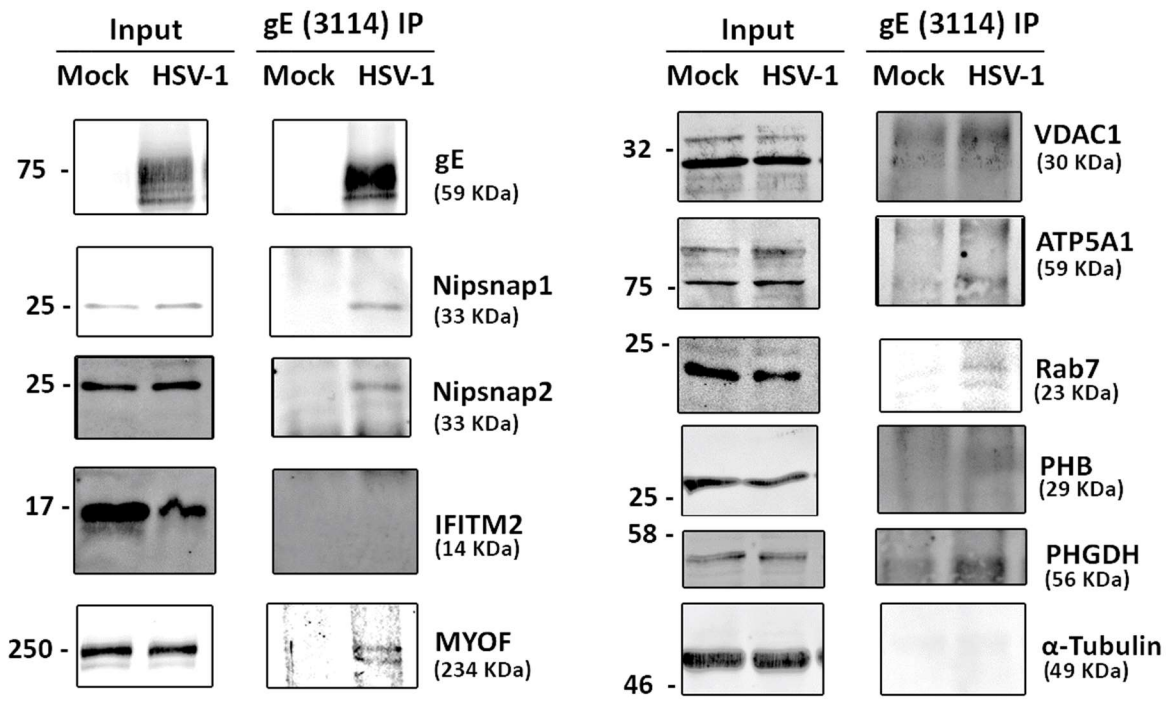

Figure 4.7 | Investigating potential cellular binding partner for gE by immunoprecipitation. HaCaT cells were infected with WT HSV-1. After 16 h the cells were lysed and an IP was done using gE (MAb-3114) antibody. The pull-down protein samples and whole cell lysates were separated by SDS-PAGE and analysed by WB using the antibodies indicated. Molecular mass markers (in KDa) are on the left and predicted molecular masses of target proteins indicated below protein names.

4.2.5 Investigation of gE-IFITM2 interaction during HSV-1 infection

IFITMs are known restriction factors of many RNA viruses and at least one DNA virus, namely African swine fever virus (Brass et al., 2009; Bailey et al., 2012; Lu et al., 2011; Muñoz-Moreno et al., 2016). HCMV on the other hand has been suggested to utilise IFITMs during morphogenesis although this publication demonstrated HSV-1 was unaffected by IFITM expression (Xie et al., 2015). Preliminary validation experiments for candidate gE interactors shown above demonstrated a reduction in IFITM2 expression in HSV-1-infected cells. To investigate this observation further, HaCaT cells were infected with either WT or gIG39R virus and cells were harvested at 6, 8, 12, 14 and 24 hpi and lysates were tested for expression of IFITM2 by WB. As can be seen in Figure 4.8 (a) in WT-infected cell lysate there were reduced amounts of IFITM2 at 12-24 hpi and in gIG39R there were reduced amounts of IFITM2 at 8-24 hpi. To understand whether the reduced expression of IFITM2 required the expression of gE and/or gI, or ICP0 (a ubiquitin ligase protein that promotes degradation of many cellular proteins and supress host immune responses), HaCaT cells were infected with WT, gIG39R, ΔgE, ΔgI, or ΔICP0 viruses. After 6 hpi the cells were lysed and IFITM2 expression was tested by WB. Figure 4.8 (b) shows lower expression of IFITM2 in all the infected cells and therefore it can be concluded that reduced IFITM2 was not caused by either gE, or gI or ICP0.

The reduced level of IFITM2 protein caused by HSV-1 infection could explain why the interaction between gE/gI and IFITM2 was detected by mass spectrometry because of the high sensitivity of this technique, but not by WB detection. To investigate whether a cell line stably expressing IFITM2 could supply enough protein to validate the potential interaction with gE/gI by WB, A549 cells stably transduced with an IFITM2-HA lentivirus expression vector were used (Smith et al., 2013). These cells should express IFITM2-HA in addition to native IFITM2 and therefore, gE/gI interaction may be observed taking place with both tagged and untagged IFITM2 in IP experiments. A549-IFITM2-HA cells were infected with WT, gIG39R, ΔgE, ΔgI viruses or mock-infected and lysed at 16 hpi. Immunoprecipitation was performed using anti-gE/gI antibody and samples tested by WB using antibodies specific for gE, IFITM2, and tubulin (Figure 4.9 a). IFITM2 and IFITM2-HA expression could be clearly observed in mock-infected lysates, with similar expression levels of HA-tagged and endogenous IFITM2. However, no signal could be observed for IFITM2-HA in infected cells, and endogenous IFITM2 was barely detectable in these samples. This suggests HSV-1 infection leads to the degradation of both endogenously and exogenously expressed IFITM2 in a gE/gI-independent

manner. Unsurprisingly, given the low levels of IFITM2, no pull-down of IFITM2 mediated by anti-gE/gI antibody was detected. To try and increase the amount of IFITM2 available for interaction with gE/gI this IP experiment was repeated at 6 hpi. At this time-point both endogenous expression of IFITM2 and exogenous expression of IFITM2-HA were observed in the lysates of both virus-infected and mock-infected samples. However, despite the higher IFITM2 protein levels, gE/gI mediated pull-down of IFITM2 could not be observed in any sample (Figure 4.9 b). Therefore, the potential interaction between gE/gI and IFITM2 could not be validated even in a cell line expressing additional IFITM2 protein. In addition, while HSV-1 infection causes depletion of IFITM2 from cells, this effect is not mediated by gE/gI and so no functional connection between gE/gI and IFITM2 can be interpreted from these data.

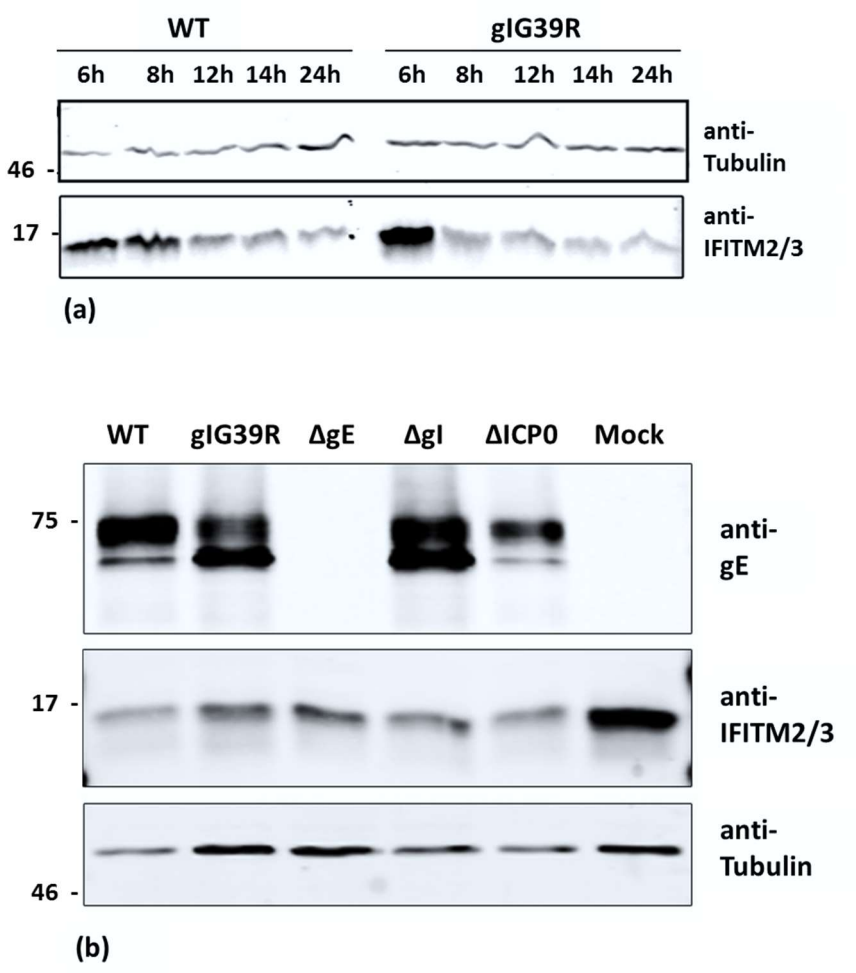

Figure 4.8 | IFITM2 expression in HSV-1-infected HaCaT cells. (a) HaCaT cells were infected with HSV-1 WT or gIG39R viruses and cell lysates were prepared at 6, 8, 12, 14 and 24 hpi and tested for IFITM2 and tubulin expression. (b) HaCaT cells were infected with either HSV-1 WT, gIG39R, ΔgE, ΔgI, ΔICP0 viruses or were mock infected and cell lysates were prepared at 6 hpi and tested for gE, IFITM2 and tubulin expression. Molecular mass markers (in KDa) are on the left.

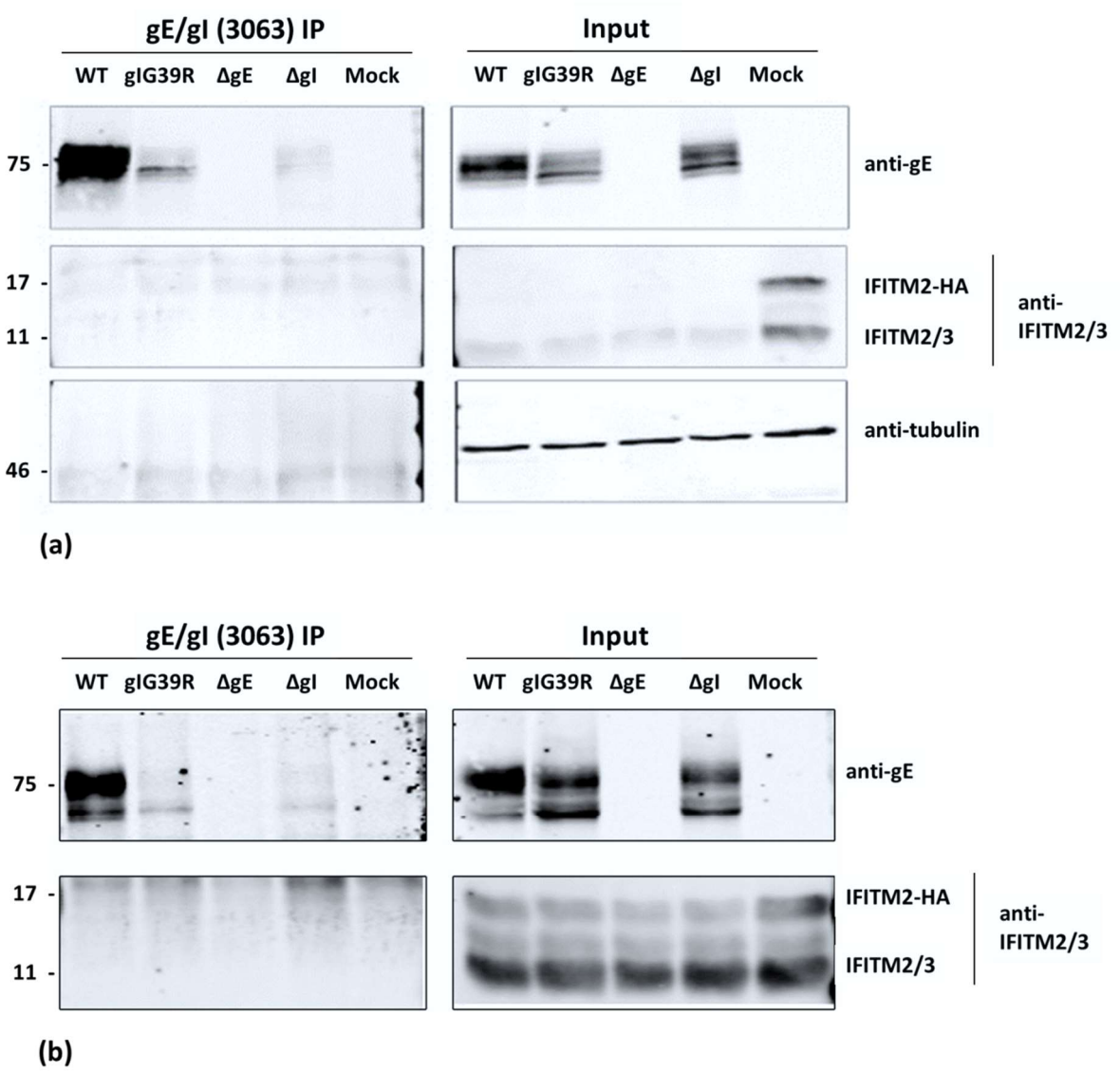

Figure 4.9 | IFITM2 interaction tests in HSV-1-infected A549-IFITM2-HA cells. A549-IFITM2-HA cells were infected with HSV-1 WT, ΔgE, ΔgI viruses or were mock infected. (a) At 16 hpi and (b) 6 hpi the cells were lysed and an IP was performed using gE/gI antibody (MAb-3063). Samples were separated by SDS-PAGE and analysed by WB using the antibodies indicated. Molecular mass markers (in KDa) are on the left.

4.2.6 gE-Nipsnap interaction in different strains of WT HSV-1-infected cells

During validation of the SILAC-IP-MS data pull-down of Nipsnap 1 and 2 with gE from HSV-1 WT (KOS strain) -infected HaCaT cells was observed. To understand whether such interaction also take place in other strains, HaCaT cells were infected with two different WT strains of HSV-1 (Sc16 and KOS) as well as the ΔgE virus (KOS backbone) as a control. After 16 hpi the cells were lysed and an IP was carried out using both anti- gE/gI (MAb-3063) and anti-gE (MAb-3114) antibodies. The pull-down samples were analysed in SDS-PAGE followed by WB and tested for gE, Nipsnap1, Nipsnap2, housekeeping gene tubulin and a mitochondrial chaperone HSP60. Figure 4.10 shows that both Nipsnap1 and 2 can be pulled-down by both anti- gE/gI and gE antibodies from both Sc16 and KOS-infected cells. The IP of Nipsnap1 and 2 was more efficient with anti-gE/gI than with anti-gE, although this is most likely explained by greater levels of gE immunoprecipitated by anti-gE/gI. No signal was observed for Nipsnap1 or 2 in mock or ΔgE virus IP samples. HSP60, which was one of the potential hits in all three samples in MS data, appeared to be non-specifically interacting with either antibodies or A/G beads as it was present at low levels in all samples. Overall these data suggest that Nipsnap1 and 2 interact with HSV-1 gE in a gI-independent manner during infection.

To understand whether the interaction can be seen in other cell lines HFF-hTERT cells were utilised beside HaCaT. The cells were infected with WT HSV-1 (KOS) and anti-gE (MAb-3114) pull-down experiment was carried out at 16 hpi. The samples were analysed by WB and tested for gE, Nipsnap1 and Nipsnap2 pull-down. As can be seen in Figure 4.11 both Nipsnap1 and 2 precipitations were seen along with gE from both cell lines.

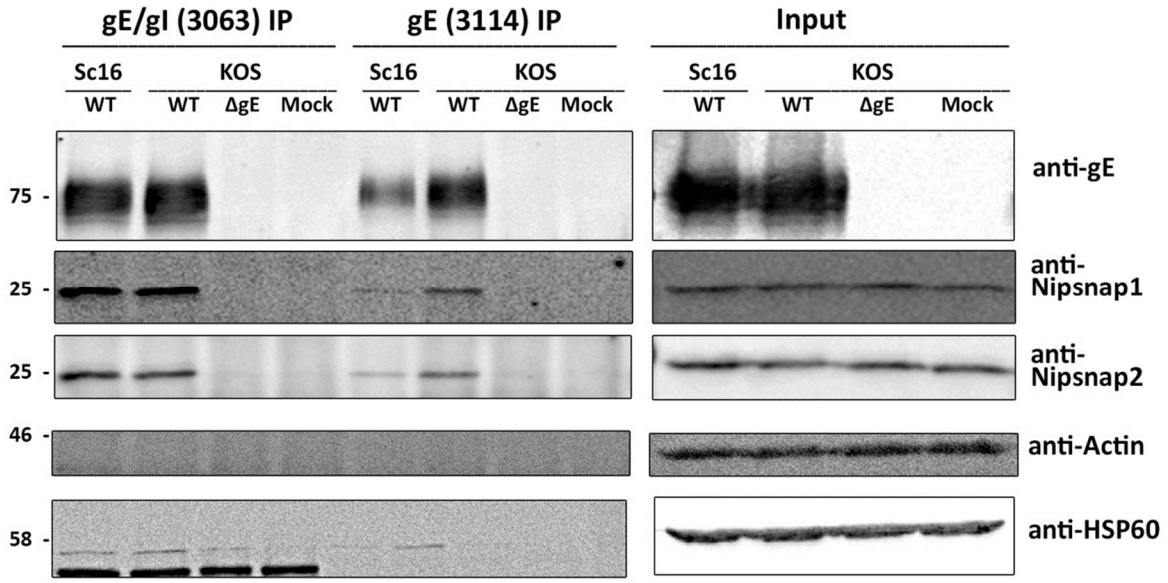

Figure 4.10 | Validation of gE and Nipsnap1 and 2 interactions in cells infected with different strains of WT HSV-1. HaCaT cells were infected with WT HSV-1 Sc16 or KOS strain, ΔgE (KOS backbone), or mock. At 16 hpi the cells were lysed and an IP was done using both anti- gE/gI (MAb-3063) and gE (MAb-3114) antibodies. The pull-down protein samples and whole cell lysates were separated by SDS-PAGE and analysed by WB using the antibodies indicated. Molecular mass markers (in KDa) are on the left.

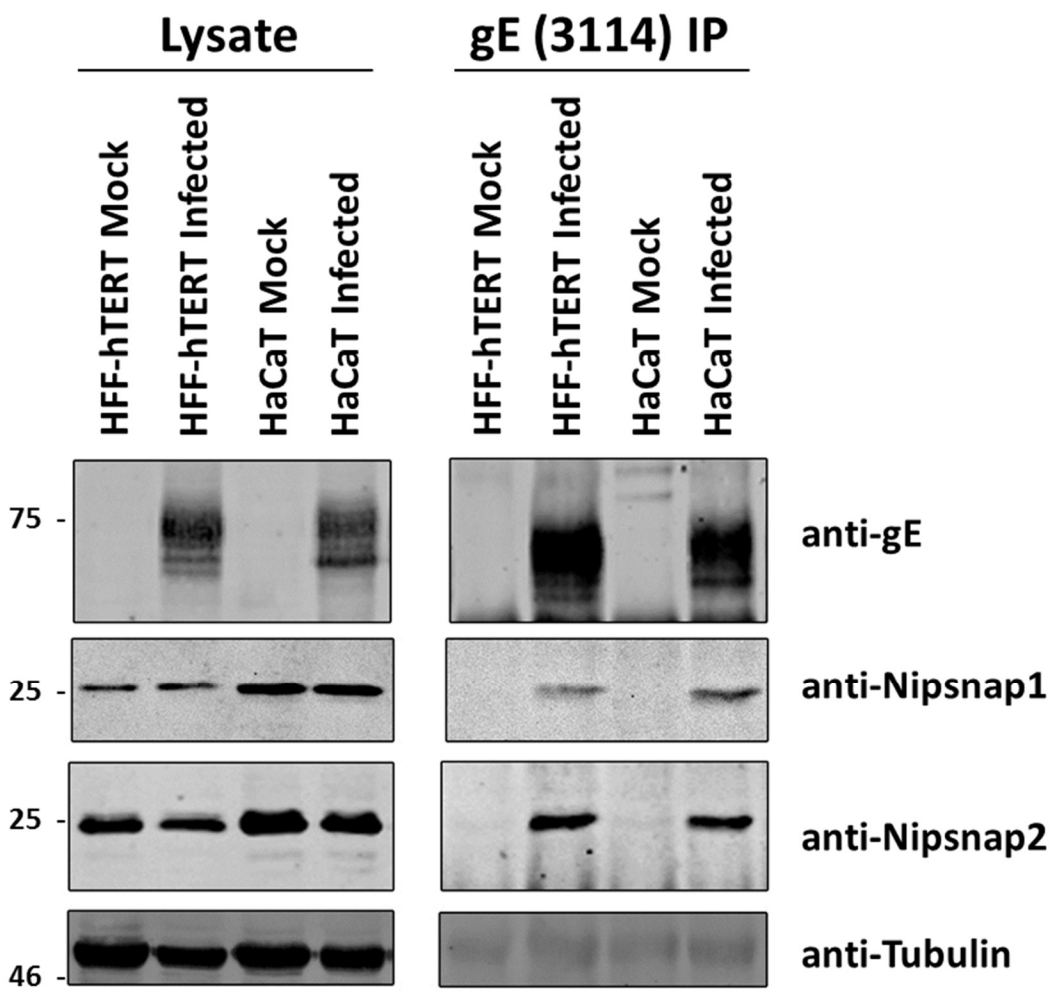

Figure 4.11 | Validation of gE and Nipsnap1 and 2 interactions in different cell line infected with HSV-1. HFF-hTERT and HaCaT cells were infected with WT HSV-1 (KOS). At 16 hpi the cells were lysed and an IP was done using anti-gE (MAb-3114) antibody. The pull-down protein samples and whole cell lysates were separated by SDS-PAGE and analysed by WB using the antibodies indicated. Molecular mass markers (in KDa) are on the left.

4.2.7 Analysis of viral interactome of gE/gI complex from SILAC-IP-MS data

The main focus of this thesis was to identify cellular proteins that function during HSV-1 egress processes. However, understanding which other viral protein binds to gE/gI is also of interest and might help us uncover more details of viral envelope and tegument interactions. To investigate the viral proteins that interact with gE/gI the raw SILAC-IP data were processed for viral proteins, applying the methodology used for cellular proteins in section 4.2.2. Table 4.3 presents all the viral interactome of gE/gI complex identified in either all three or in two of three biological replicates. As expected gE and gI are present in all the sample sets. Interestingly, glycoprotein B (gB) was also in all the sample sets. Surprisingly two of the nucleotide metabolism enzymes UL39 (ribonucleotide reductase subunit 1) and UL23 (thymidine kinase) were also identified, as well as major capsid protein VP5. Glycoproteins gD, gC, and gH, the nuclear egress protein UL34 and the tegument protein VP22 were found in at least two of the SILAC-MS data set.

To investigate some of these viral protein hits further the pull-down samples using anti-gE (MAb-3114) that was prepared for Figure 4.7 were analysed by WB with a subset of antibodies available to specific viral proteins. As shown in previous chapter the gE/gI complex cannot be pulled-down by anti-gE antibody, hence in the IP samples only gE was detected but not gI (Figure 4.12). Although VP22 was identified in the SILAC-IP data and has been shown to interact with gE in published IP experiments (Maringer et al., 2012) no VP22 was identified in these gE pull-down samples. This could be due to a sensitivity issue because the VP22 signals in the infected cell lysates were relatively weak. Interestingly, UL19 (VP5) and gB were both observed in the pull-down sample, although the VP5 reactive band appeared lower than the corresponding band in the lysate. It seems unlikely that gE would directly interact with VP5 and would more likely be indirect via a tegument protein, potentially pUL16 which has been shown to interact with both gE (Han et al., 2012; Yeh et al., 2011) and VP5 (Meckes et al., 2010). However, pUL16 was also not detected in the pull-down samples.

To understand whether gE-VP5 and gE-gB interaction is an experimental artefact the interactions were further verified in different cell lines. Vero, HFF-hTERT and HaCaT cell lines were infected with HSV-1 virus for 16 h. The cells were lysed and an anti-gE (MAb-3114) pull-down was conducted and analysed by WB for gE, gB and VP5 pull down. As can be seen in Figure 4.13 all of these proteins were pulled-down by gE in the HSV-1-infected Vero, HFF-hTERT and HaCaT cells. This supports the possibility that gE-gB and gE-VP5 interaction occurs during HSV-1 infection. However, whether such interactions are direct or indirect need further investigations.

Table 4.3 | Common SILAC hits for viral proteins

			[a.]T1				[a.]T2				[a.]T3			
			[b.]Mean 0.054, [c.]SD 0.285, [c.]Threshold 0.596				[b.]Mean -0.0054, [c.]SD 0.258, [d.]Threshold 0.486				[b.]Mean 0.276, [c.]SD 0.637, [d.]Threshold 1.488			
Common in	**Uniprot Name**	**Description**	**[e.]Unique Peptide**	**[f.]M/H**	**log2 M/H**	**[h.]Z score**	**[e.]Unique Peptide**	**[f.]M/H**	**log2 M/H**	**[h.]Z score**	**Unique Peptide**	**[g.]H/M**	**Log2 H/M**	**[h.]Z score**
T1, T2 and T3	US8 (2703448)	gE	12	100.00	6.64	23.09	9	100	6.64	25.77	13	71.75	6.16	9.24
	US7 (2703446)	gI	2	100.00	6.64	23.09	3	10	3.32	12.90	4	60.77	5.93	8.87
	UL39 (2703361)	Ribonucleotide reductase (RIR1)	5	2.30	1.20	4.03	5	18.79	4.23	16.42	9	6.79	2.76	3.90
	UL27 (24271469)	gB	5	3.06	1.61	5.47	6	25.27	4.66	18.08	5	3.89	1.96	2.64
	UL23 (24271467)	Thymidine kinase	2	2.42	1.28	4.28	4	100	6.64	25.77	2	7.2	2.85	4.04
	UL19 (2703368)	Major capsid protein VP5	3	5.76	1.28	4.28	2	100	6.64	25.77	6	4.98	2.32	3.20
T1 and T2	US6 (2703444)	gD	1	4.40	2.14	7.31	2	3.62	1.86	7.21	x	x	x	x
	UL44 (2703410)	gC	2	2.77	1.47	4.97	2	18.51	4.21	16.34	x	x	x	x
	UL22 (24271466)	gH	1	99.22	6.63	23.08	2	100	6.64	25.77	x	x	x	x
T1 and T3	x	x	x	x	x	x	x	x	x	x	x	x	x	x
T2 and T3	UL49 (2703417)	VP22	x	x	x	x	1	67.12	6.07	23.54	1	3.53	1.82	2.42
	UL34 (2703355)	Nuclear egress protein 2	x	x	x	x	1	5.84	2.55	9.89	3	6.81	2.77	3.91

[a.] T1 = tube 1, T2 = tube 2, T3 = tube 3
[b.] Mean = generated from a log2 ratios
[c.] SD = standard deviation generated from a log2 ratios
[d.] Threshold = represents the mean and standard deviations of the Gaussian distribution
[e.] Unique peptide = refers to the number of peptides used for identification of protein. When a protein is identified from several unique peptide spectra the confidence in identification of protein is improved.
[f.] M/H = the relative intensity of peptides in medium labelled sample, compared to heavy labelled sample
[g.] H/M = the relative intensity of peptides in heavy labelled sample, compared to medium labelled sample
[h.] z score = $(X - \mu) / \sigma$ where X is the value of the element, μ is the population mean, and σ is the standard deviation

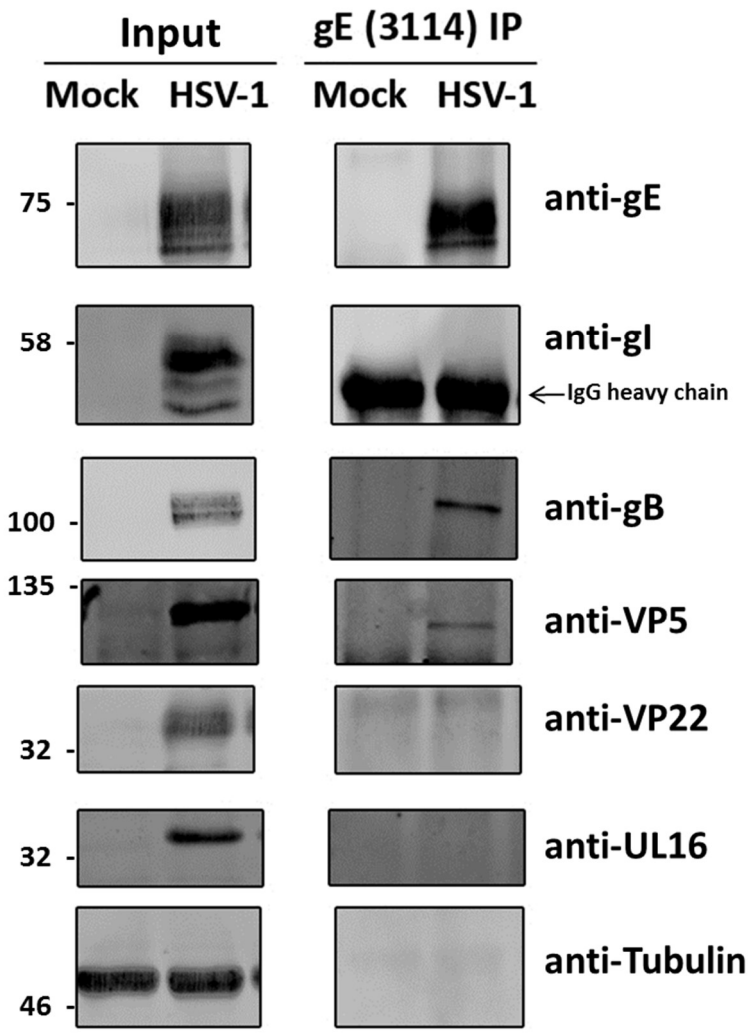

Figure 4.12 | Viral proteins immunoprecipitated by gE antibody. HaCaT cells were infected with WT HSV-1 virus. At 16 hpi the cells were lysed and an IP was done using gE (MAb-3114) antibody. The pulled-down protein samples and cell lysates were separated by SDS-PAGE and analysed by WB using the antibodies indicated. Molecular mass markers (in KDa) are on the left.

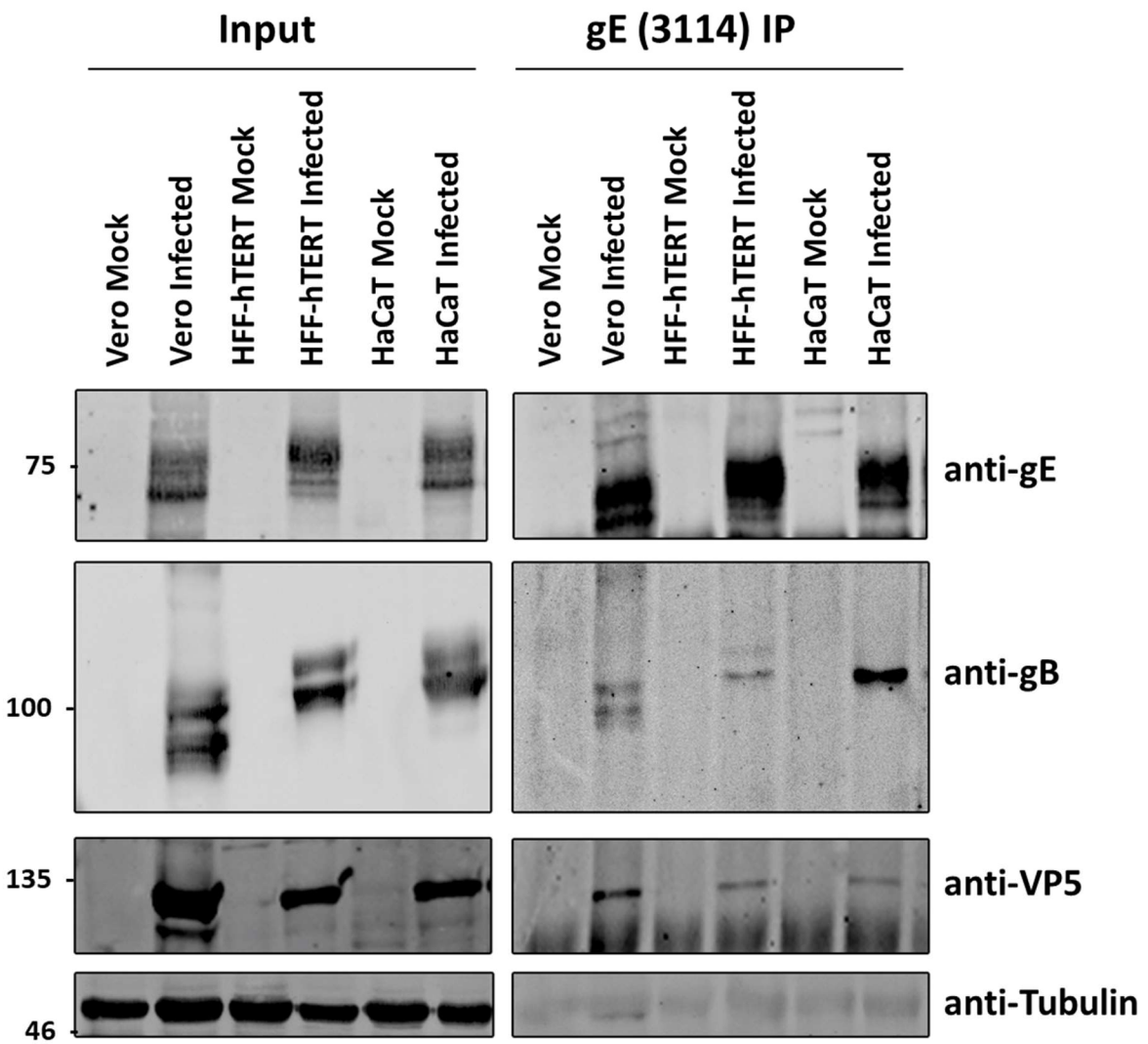

Figure 4.13 | Pull-down of gB and VP5 by anti-gE antibody from different cell lines. Vero, HFF-hTERT and HaCaT cells were infected with WT HSV-1 virus. At 16 hpi the cells were lysed and an IP was done using gE (MAb-3114) antibody. The pulled-down protein samples and whole cell lysates were separated by SDS-PAGE and analysed by WB using the antibodies indicated. Molecular mass markers (in KDa) are on the left.

4.3 Discussion

The aim of this chapter was to identify host proteins interacting with gE/gI complex during HSV-1 egress. Using SILAC-IP-MS data analysis a list of candidate cellular interaction partners of the gE/gI complex was generated. However, the majority of the cellular proteins were mitochondrial, and cellular proteins like TGN46, β-catenin, clathrin adaptors and PACS-1 that were previously been reported to co-localise with gE/gI were not present in the list. (Farnsworth et al., 2006; Wisner et al., 2004; McMillan and Johnson, 2001; Gu et al., 2001; Wan et al., 1998) There is no report suggesting gE/gI localises to the mitochondrion, and so the cluster of mitochondrial proteins identified as interaction partners seem more likely to be artefacts, which is supported by data showing HSP60 non-specific binding to the antibody or beads used for IP.

Initial validation of the SILAC-IP-MS data confirmed the interaction of gE with Nipnsnap1, Nipsnap2 and MYOF and also demonstrated a reduction in IFITM2 expression upon HSV-1 infection. The significance of these observations in HSV-1 egress is investigated in the next chapter.

Validation of the viral protein interactions with the gE/gI complex found co-precipitation of at least UL27 (gB) and UL19 (VP5) with gE. Pull-down of VP5 is somewhat unusual and may have resulted from an indirect interaction via tegument proteins. Surprisingly the well-established interaction with the tegument proteins VP22 and pUL16 were not observed in the IP WB validation experiments, although there may have been sensitivity issues with the antibodies used to detect these proteins. The potential interaction with TK could not be validated because a suitable antibody was not available in the lab. Possible interaction with the nuclear egress complex protein pUL34 could be of interest to follow up given the localisation of gE to the nuclear membrane observed in IF experiments. These data showing gB interaction with gE may suggest direct association with gE in a particular membrane compartment or potentially an indirect interaction via another viral or cellular protein. Investigation into gB localisation with potential cellular egress proteins is presented in the next chapter.

5. Validation of the potential hits in HSV-1 life cycle

5.1 Introduction

In the previous chapter, attempts were made to identify cellular binding partners for the HSV-1 gE/gI complex, which may be involved in mediating virion translocation to cell-to-cell contact points. SILAC-IP MS-based proteomics were used to identify a candidate cellular interactome for the gE/gI complex, which gave some interesting protein hits. As with any screening, hits need to be validated before conducting further research to determine the role of the candidate proteins in the context of study. During initial validation of the proteomics data detailed in Chapter 4 three intriguing observations were made: (1) degradation of IFITM2 in infected cells, (2) co-precipitation of Nipsnap1 and 2 with gE during infection, and (3) co-precipitation of MYOF with gE during HSV-1 infection. This chapter investigated these observations further.

5.2 Results

5.2.1 Observation of gE and IFITM interaction during transfection

Data in the previous chapter demonstrated that IFITM2 is degraded during HSV-1 infection (WT or ΔgE) both in normal and IFITM2 expressing stable cell lines possibly explaining why co-precipitation of IFITM2 with gE/gI or gE could not be detected. To investigate whether the interaction of IFITM2 and gE can be validated in the absence of other viral proteins, at least one of which is presumably causing IFITM2 degradation, HEK293T cells were co-transfected with plasmids expressing N-terminally HA-tagged human IFITM 1, 2 or 3 and a gE expression plasmid, or a gD expression plasmid as a control. When cells were incubated for 48 h post-transfection, the cell viability appeared to be severely compromised and so these experiments were conducted at 22 h post-transfection. The transfected cells were lysed and an IP with anti-gE antibody (MAb-3114) or anti-gD antibody (LP2) was performed and samples were analysed by WB using antibodies to gE or gD, HA-tag and IFITM2. Figure 5.1 shows clear co-precipitation of HA-IFITM1 with gE and faint signals for HA-IFITM2 and 3 were also observed in the gE IP samples with anti-HA staining. Probing with the anti-IFITM2 antibody demonstrated a slightly stronger signal for HA-IFITM2 in the gE pull-down sample. The

IFITM2 antibody also appears to efficiently recognise HA-IFITM3, but not HA-IFITM1 suggesting this antibody recognises a common epitope in IFITM2 and 3. These two proteins have ~90% identity in their amino acid sequence. Surprisingly, lower gE expression was observed when co-transfected with HA-IFITM1 and HA-IFITM2 compared with HA-IFITM3. However, IP samples demonstrated equivalent amounts of gE, suggesting sufficient expression in all samples to saturate the anti-gE antibodies in the IP reaction. In samples co-expressing gD with HA-IFITM1-3, there was little effect on gD expression levels, with only a slight reduction in gD in the HA-IFITM1 and 2 compared to HA-IFITM3. Reduced HA-IFITM3 expression, and to a lesser extent HA-IFITM2, was observed with gD co-expression. No specific pull down of HA-IFITM 1, 2 or 3 could be detected with gD. Taken together these data suggest IFITM1, and possibly IFITM2 and 3 can co-precipitate with gE when expressed in the absence of other viral proteins, and that the presence of IFITM1 and 2 may destabilise gE.

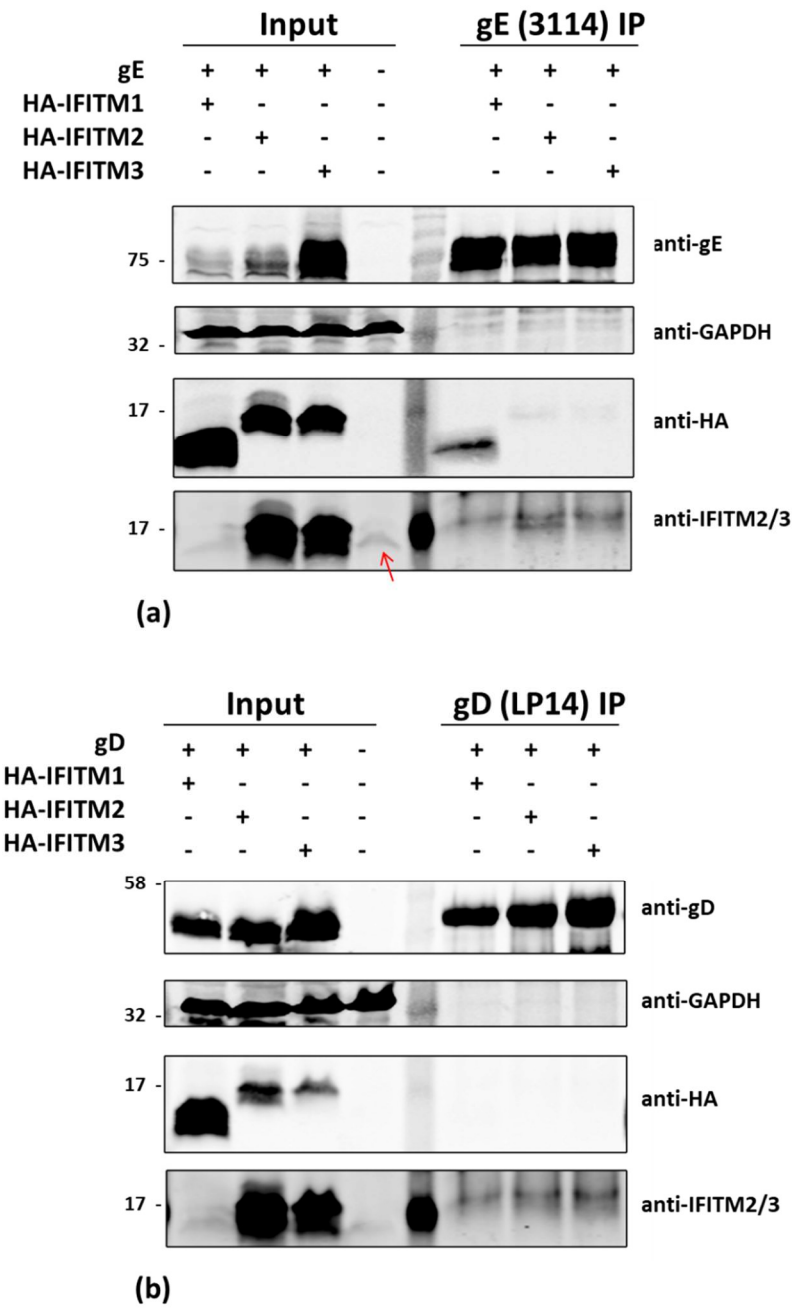

Figure 5.1 | Co-precipitation of IFITM proteins with gE or gD in transfected cells. HEK293T cells were transfected with plasmids expressing HSV-1 (a) gE or (b) gD together with HA-tagged IFITM1 or 2 or 3 expression plasmids. At 22 h post-transfection the cells were lysed and an IP was performed using gE or gD antibodies. IP samples and cell lysates were separated by SDS-PAGE and analysed by WB using the antibodies indicated. Molecular mass markers (in KDa) are on the left. Endogenous IFITM2/3 indicated by arrow.

5.2.2 Observation of gE and IFITM localisation in cells by immunofluorescence

To investigate the potential gE-IFITM interactions further, the localisation of these proteins when co-expressed was examined by IF microscopy. HFF-hTERT cells were transfected with gE and HA-IFITM1 or 2 or 3 expression plasmids and at 22 h post-transfection the cells were fixed and stained with anti-gE and anti-HA antibodies. As can be seen in Figure 5.2, HA-IFITM1, and 3 localised primarily to a juxta-nuclear compartment, similarly to gE. HA-IFITM1 showed a reasonable amount of overlapping signal with gE in some cells, whereas HA-IFITM2 demonstrated less co-localisation with gE, and IFITM3 showed little evidence of co-localisation with gE. These data support the co-IP data shown above, with Co-IP between gE and HA-IFITM1>HA-IFITM2>HA-IFITM3.

It is conceivable that the presence of a HA-tag on the N terminus of IFITM proteins may affect their subcellular localisation, as could aberrantly high expression levels that can occur during transient transfection assays. To investigate potential co-localisation between gE and IFITM proteins further, A549 cells stably expressing IFITM2-tagged with HA at the C terminus were transfected with plasmids expressing gE, gE^{GFP}, or gE and gI and after 22 h the cells were stained for HA and gE. However, no co-localisation of gE and IFITM2-HA could be observed in any of the samples (Figure 5.3). Surprisingly, cells that were positive for gE expression appeared negative for IFITM2-HA expression and vice versa. This cell line should constitutively express IFITM2-HA, although there appears to be heterogeneity in the cell population with some cells not expressing detectable IFITM2-HA. Therefore, it could be possible that gE expression was inhibited when IFITM2-HA was expressed and gE was only expressed at detectable levels in those cells in the population that did not express IFITM2-HA. However, whether a HA-tag at either the C terminus or N terminus of IFITM2 affects its subcellular localisation, and whether either tagged protein reflects the localisation of endogenous IFITM2 is unclear from these data.

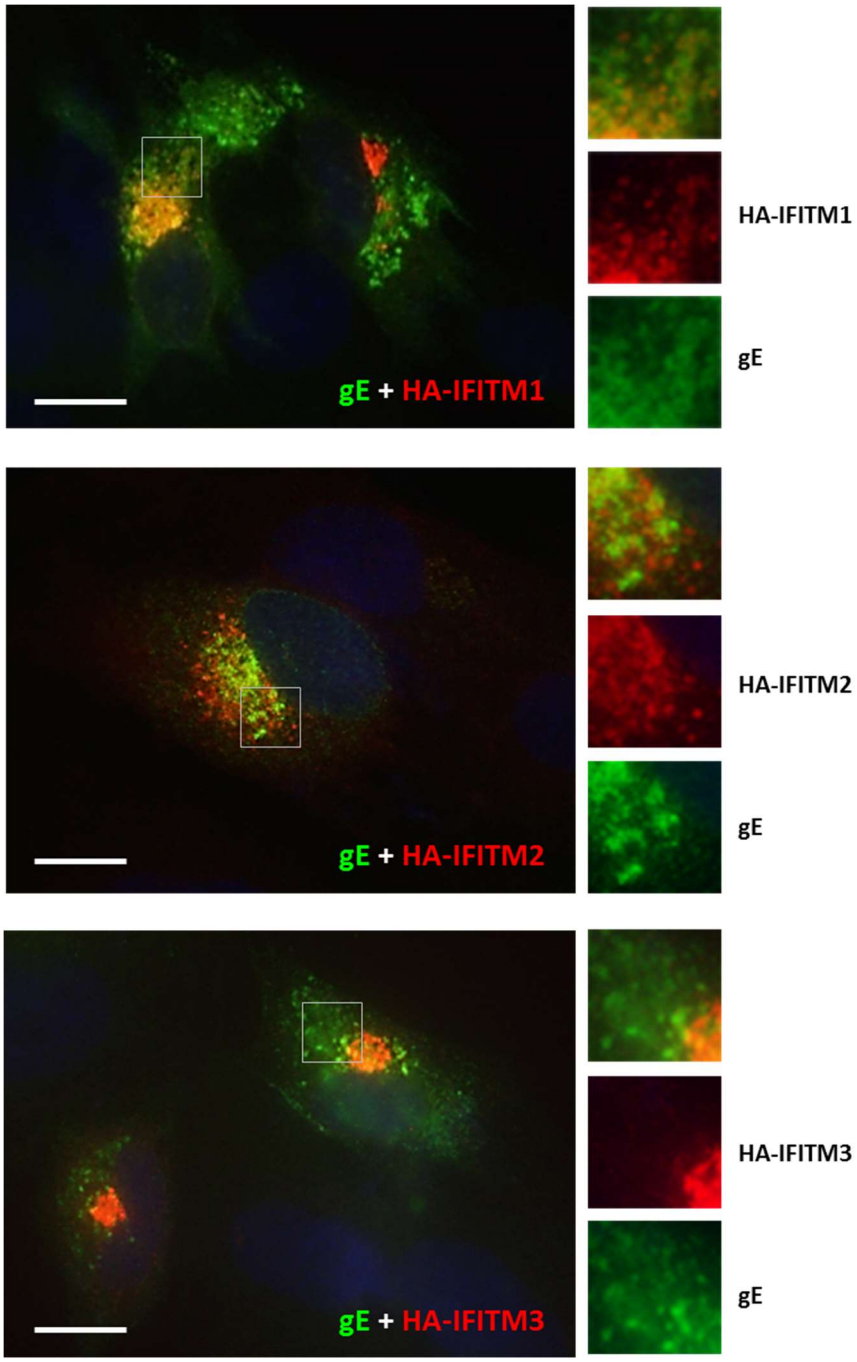

Figure 5.2 | Localisation of gE and IFITMs in transfected HFF-hTERT cells. HFF-hTERT cells were co-transfected with plasmids expression HSV-1 gE along with HA-tagged IFITM1 or 2 or 3. At 22 h post-transfection the cells were fixed and stained with anti-gE (MAb-3114) and HA antibodies. Images on the right panel indicate selected areas of the left image to show possible co-localisation of the two proteins. Images were taken using an Olympus IX-81 inverted fluorescence microscope using a 60x oil immersion lens. Blue: staining of nuclei with DAPI. Scale bar indicates 20 µm.

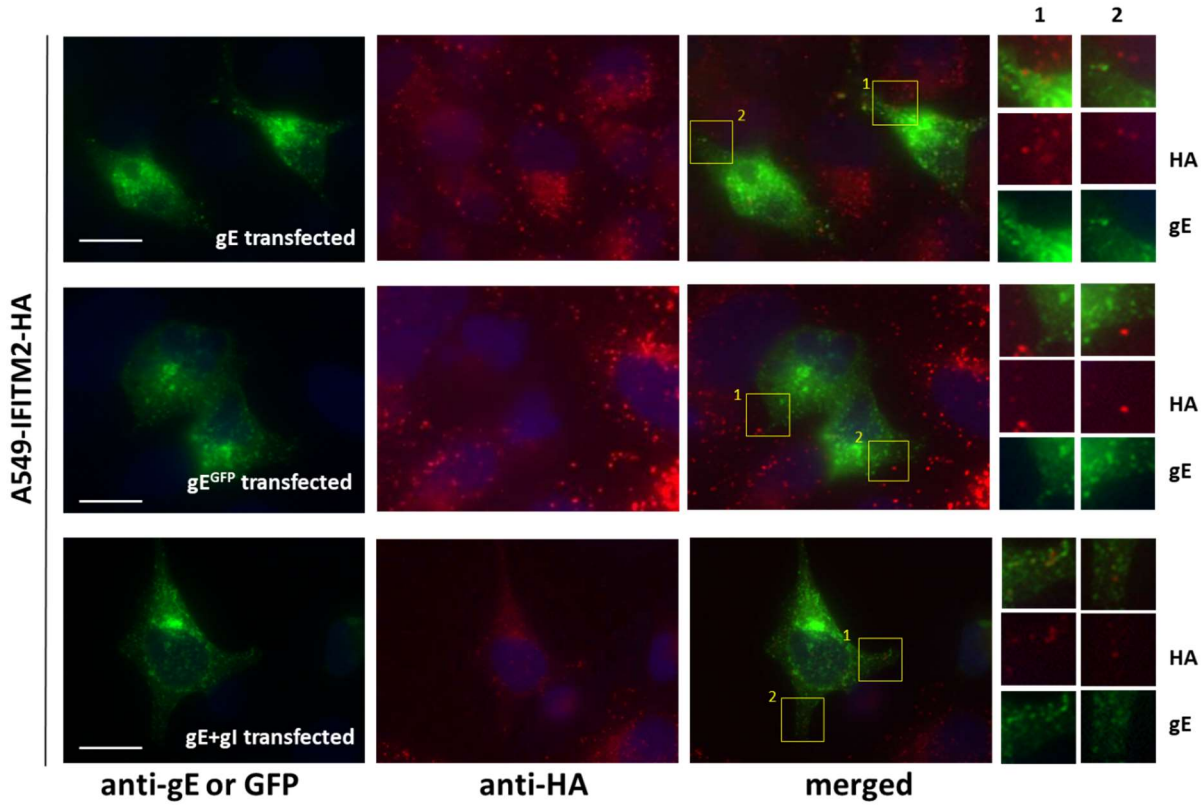

Figure 5.3 | Transfection of A549-IFITM2-HA cells with gE expression plasmids. A549-IFITM2-HA cells were transfected with plasmids expressing gE^{GFP} or untagged gE with or without gI. After 22 h post-transfection the cells were fixed and stained with anti-gE (MAb-3114) (for untagged gE only) and HA antibodies as required. Images on the right panel indicate selected areas of the merged panel to show possible co-localisation of the indicated proteins. Images were taken using an Olympus IX-81 inverted fluorescence microscope using a 60x oil immersion lens. Blue: staining of nuclei with DAPI. Scale bar indicates 10 µm.

To understand endogenous IFITM2 localisation in cells, Vero, HaCaT amd HFF-hTERT cells were incubated with mitotracker (to stain mitochondria) for 30 min prior to fixation, and subsequently stained with anti-IFITM2 antibody. As shown in Figure 5.4, IFITM2 antibody signal co-localised with mitotracker in Vero, HaCaT and HFF-hTERT cell lines, indicating endogenous IFITM2 (and/or IFITM3) primarily resides in mitochondria in these cell lines. Mitochondrial localisation of IFITM2 has been shown in a previous study although it has been also suggested that IFITM2 could also present in endosomal compartments which is mostly visible in over-expressing cell lines and cells that are treated with interferon (Muñoz-Moreno et al., 2016; Weston et al., 2014). Given that other mitochondrial proteins were pulled-down with gE/gI in the SILAC-IP experiments in this study, it is possible IFITM2 could be a false positive due to co-precipitation with other mitochondrial proteins. Alternatively, it could be also possible that the portion of IFITM2 present in endosomal compartments precipitated with gE/gI. It is also conceivable that the IFITM2 antibody non-specifically cross-reacts with a mitochondrial protein under the conditions used for IF. Additional antibodies that detect endogenous IFITM2 would be needed to investigate this further.

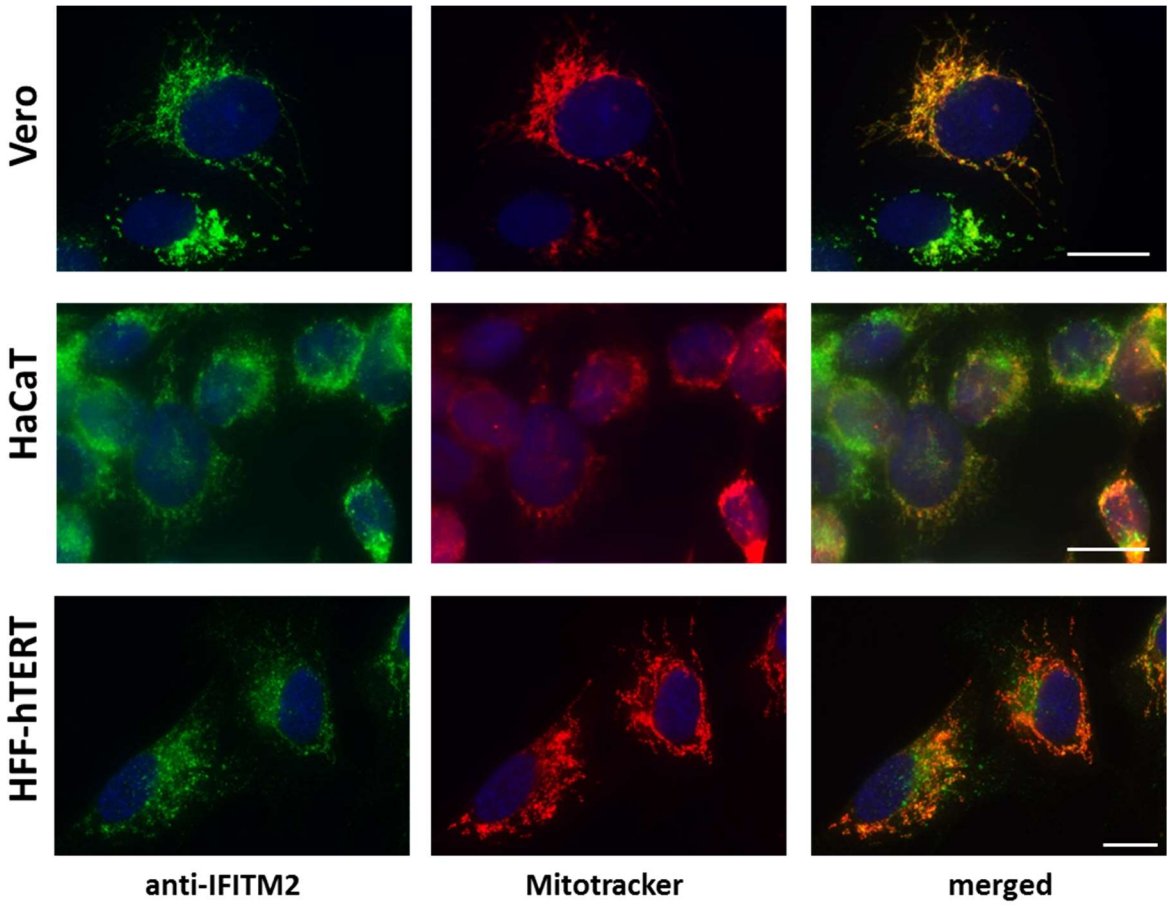

Figure 5.4 | IFITM2 antibody co-localises with a mitochondrial marker. Vero, HaCaT and HFF-hTERT cell lines were seeded on glass slides and incubated with mitotracker for 30 min prior to fixation. The cells were stained with anti-IFITM2 antibody. Images were taken using an Olympus IX-81 inverted fluorescence microscope using a 60x oil immersion lens. Blue: staining of nuclei with DAPI. Scale bar indicates 20 µm.

5.2.3 Observation of gE-Nipsnap1 interaction in transfected cells

Interaction between gE and Nipsnap1 was identified in HSV-1-infected cells, although it was unclear whether such interaction requires the presence of other viral proteins. To investigate the interaction of gE and Nipsnap1 in the absence of other viral proteins HEK293T cells were co-transfected with myc-Nipsnap1 (N-terminally tagged) together with either gE or gE^{GFP} or gE and gI expression plasmids. At 48 h post-transfection, cells were lysed and immunoprecipitated with either anti- gE (MAb-3114) or gE/gI (MAb-3063) or using GFP trap resin as required. Mock-transfected samples were incubated with anti-gE/gI pull-down only. The samples were then analysed by WB for gE and Nipsnap1. Figure 5.5 shows Nipsnap1 was co-precipitated in all the IP samples except mock. Lower levels of Nipsnap1 were co-precipitated with gE-GFP suggesting the presence of GFP fused to the cytoplasmic C terminus of gE may interfere with Nipsnap1 binding, although expression of myc-Nipsnap1 was also reduced in this sample. Myc-tagged Nipsnap1 ran at a higher molecular weight than endogenous Nipsnap1 as expected, with two individual bands detected in lysate samples using a Nipsnap1 antibody. These data suggest gE and Nipsnap1 interact in the absence of other HSV-1 proteins.

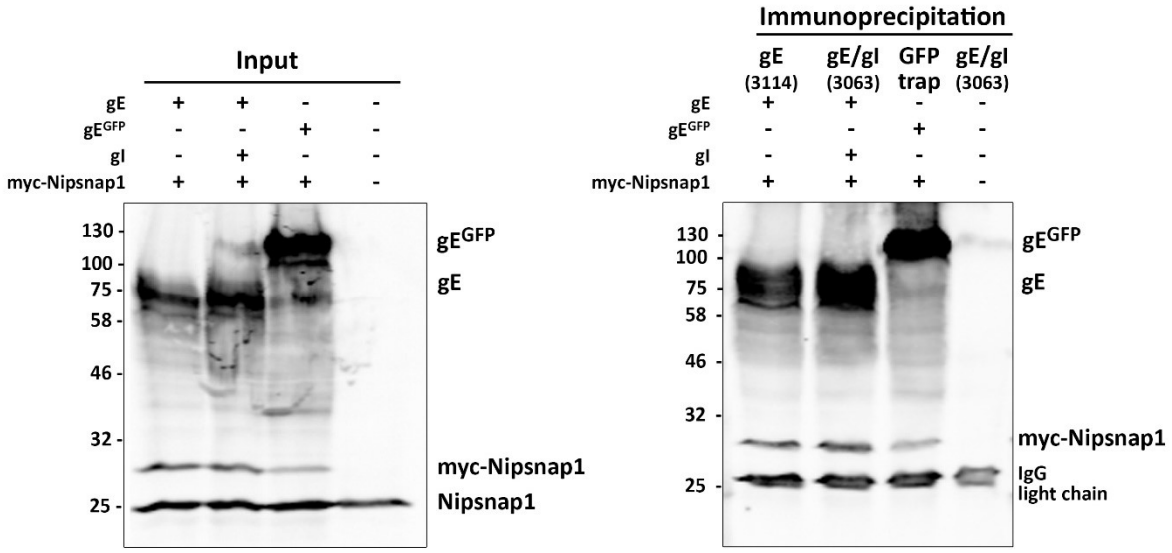

Figure 5.5 | Validation of gE and Nipsnap1 interaction in transfected cells. HEK293T cells were transfected with HSV-1 gE, gE and gI, or gE^{GFP} along with myc-Nipsnap1. After 48 h post-transfection the cells were lysed and an IP was done using gE or gE/gI antibody or GFP-trap. The pulled-down protein samples and cell lysates were separated by SDS-PAGE and analysed by WB using the antibodies indicated. Molecular mass markers (in KDa) are on the left.

5.2.4 Expression, purification and characterisation of gE C terminus tail

The cytoplasmic tail of gE has been proposed to interact with many viral proteins and is also the most likely domain to mediate interaction with cytoplasmic proteins such as Nipsnap1 and 2 during infection. gE is a type-I membrane protein with a signal sequence (spanning aa 1-20), a long N terminal ectodomain (aa 21-419), a transmembrane domain (aa 420-440) and C-terminal tail domain (aa 441-550) (discussed in Sprague et al., 2006 and Uniprot:P04488). Analysis of the CT domain of gE from the sequence of KOS strain using NetsurfP web-based tool suggested the region to be highly disordered (Appendix Figure 9.1). To understand whether the interaction of Nipsnap1 with gE can be observed in a cell free system, recombinant C-terminally GST-tagged gE cytoplasmic domain (gECT-GST) was constructed. The gECT(445-550) DNA fragment was cut and pasted from a previously constructed poPTnH (His-tagged) plasmid to poPTnG (GST-tagged) plasmid utilising NDE1 and BamH1 restriction sites. Pilot proteiAn expression tests were conducted in three different strains of *E. coli* (Rosetta, B834 and BL21) at two different temperatures (37ºC and 22ºC) with the highest yield of gECT-GST being observed from Rosetta cells at 37ºC (Appendix Figure 9.2), and so these conditions were chosen for scaling up gECT-GST production. Rosetta cells transformed with gECT-GST plasmid were induced with IPTG over night at 37ºC, the cells were then collected by centrifugation, lysed and the protein was purified by affinity chromatography using glutathione sepharose 4B resin followed by size exclusion (S200 16/600 column) chromatography (Figure 5.6 a and b). SDS-PAGE analysis of the fraction from the size exclusion column demonstrated reasonable separation of gECT-GST from higher and lower molecular mass contaminants that were visible in the sample after glutathione affinity purification. The exception was bands around 25 KDa, the expected size of GST, suggesting a modest level of cleavage of the gECT from GST. Fractions 30-35 were then concentrated by ultrafiltration and the measured protein concentration was 1.45mg/mL. The protein sample was then aliquoted and stored at -70ºC after snap freezing in liquid nitrogen.

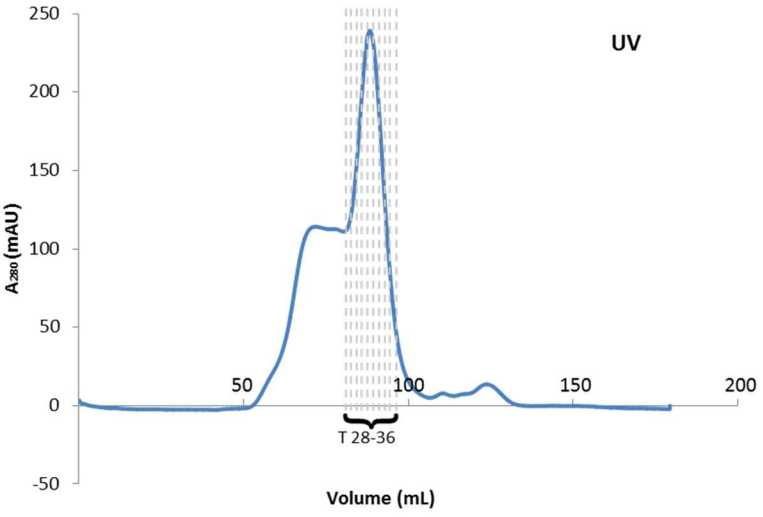

(a)

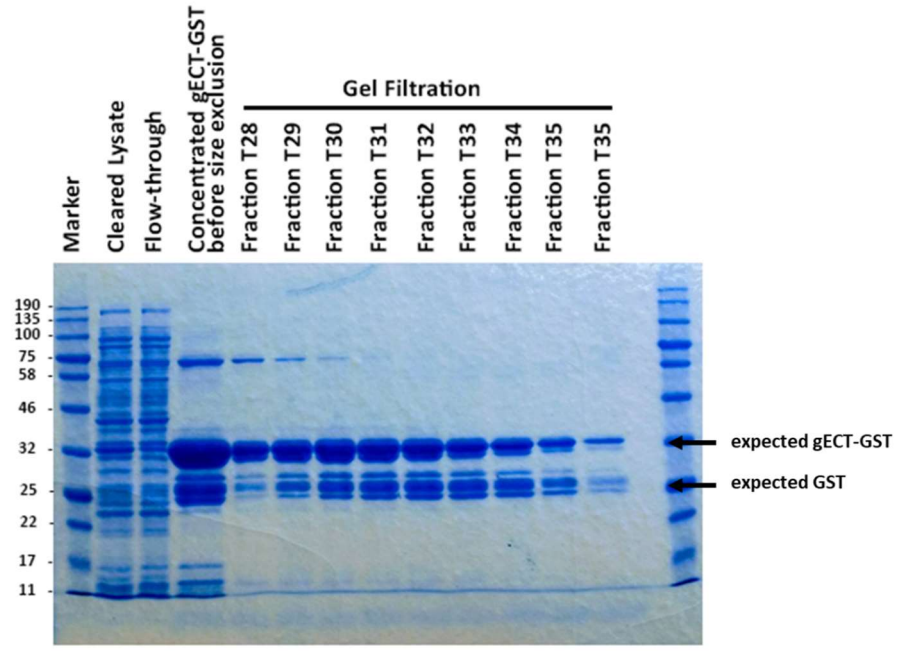

(b)

Figure 5.6 | Preparation of purified gECT-GST construct. gECT was expressed as a GST-tag fusion protein in Rosetta *E. coli* and first purified by affinity chromatography using glutathione sepharose 4B resin followed by size exclusion chromatography. (a) Size exclusion elution profile of gECT-GST on an S200 16/600 gel filtration column. (b) Coomassie-stained 12% polyacrylamide gel showing samples from key steps of the purification process and selected fractions from the size exclusion chromatography.

5.2.5 Interaction of gECT-GST and myc-Nipsnap1 in cell free system

While Nipsnap1 and gE co-precipitation could be demonstrated in the absence of other viral proteins it was unclear whether any cellular proteins are needed for this interaction. To test, whether gE can directly interact with Ninpsnap1 in a cell free system, Nipsnap1 N-terminally tagged with the myc epitope (myc-Nipsnap1) was expressed using the wheat-germ *in vitro* transcription/translation system and incubated with purified gECT-GST. As a control, purified GST was incubated with myc-Nipsnap1. After incubation for 1 h at 4˚C on a shaker, samples were incubated with glutathione 4b sepharose, for a GST pull-down assay. The samples were separated by SDS-PAGE and transferred to nitrocellulose membrane. The membrane was subsequently stained with ponceau-S and then destained for anti-Nipsnap1 antibody staining. As can be seen in Figure 5.7, Nipsnap1 was detected by antibody staining in the input and in the gECT-GST pull-down samples but not in the GST mock pull-down sample. However, it is worth noting the anti-Nipsnap1 antibody used in this experiment non-specifically bound to gECT-GST and GST bands, presumably because of high protein concentration in the purified protein samples. These data suggest that Nipsnap1 may directly interact with the cytoplasmic tail of gE and such interaction does not rely upon the presence of other mammalian or viral proteins.

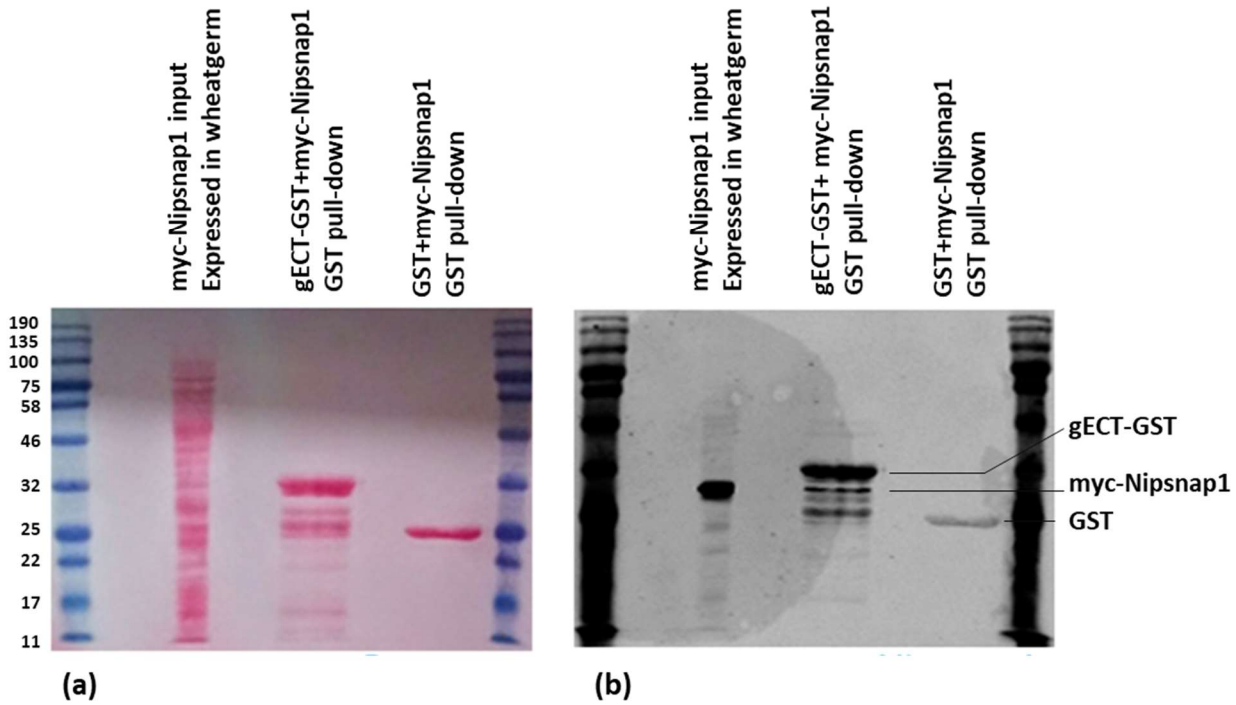

Figure 5.7 | Investigation of gECT-GST and Nipsnap1 interaction in a cell free system. Purified gECT-GST or GST were mixed with wheat-germ expressed myc-Nipsnap1 and a GST pull down was carried out. The pull-down samples and myc-Nipsnap1 input were run on SDS-PAGE and analysed by WB. The membrane was stained with (a) Ponceau before staining with (b) Nipsnap1 specific antibody.

5.2.6 Identification of Nipsnap1 and 2 binding sites in the cytoplasmic domain of gE

To identify the region within the gECT that binds Nipsnap1, a truncation analysis of the gE cytoplasmic domain was performed. Using full length gE as a template a series of C-terminally truncated constructs were generated by PCR and sub-cloned into a mammalian expression plasmid (pcDNA3) with the resulting proteins containing residues 1-440, 1-475, 1-510, 1-532, 1-537, 1-542 and 1-548 of gE (Figure 5.8). To understand where in the cell gE localises upon transfection and how truncation of the gE cytoplasmic domain affects localisation of the protein, Vero cells were transfected with all gE truncation constructs made in this study (1-440, 1-475, 1-510, 1-532, 1-537, 1-542 and 1-548) and full length gE (1-550). Cells were fixed and co-stained with antibodies for a Golgi marker (GM130) and gE at 36 h post-transfection. As can be seen in Figure 5.9 (a), full length gE and gE(1-548) seems to mainly accumulate near in a perinuclear structure that co-stained with GM130. The other gE constructs also demonstrated varying amounts of signal in a GM130-positive compartment but with greater signals with an ER-like pattern. This was particularly marked for the gE construct lacking any cytoplasmic tail (gE440) suggesting this construct cannot exit the endoplasmic reticulum either because of misfolding recognised by the ER quality control systems, or absence of sorting signals in the cytoplasmic tail that mediate ER exit. To investigate whether the presence of gI may alter the localisation of gE lacking a cytoplasmic tail, gE440 and gI were co-expressed and cells stained with anti-gE/gI (MAb-3063). These data showed greater localisation of gE to GM130-positive compartments and less ER-like signal, suggesting gE440 can form a complex with gI and this facilitates exit of gE from the ER to other cellular compartments (Figure 5.9 b).

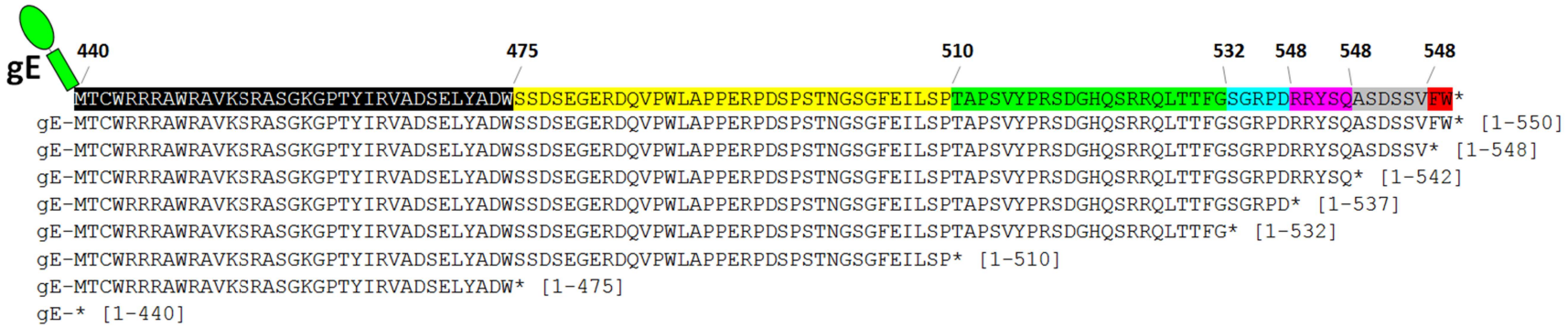

Figure 5.8 | Construction of gECT truncation plasmids. The cytoplasmic tail of gE was truncated to various lengths. The shortest one is 1-440 which ends with the transmembrane domain and does not contain any CT, the 1-475, 1-510 contains 30 and 65 amino acids of the CT respectively, and the 1-532, 1-537, 1-542 and 1-548 constructs are 18, 13, 8 and 2 amino acid shorter than the full length gE (1-550). All the constructs are in pCDNA3.1 vector.

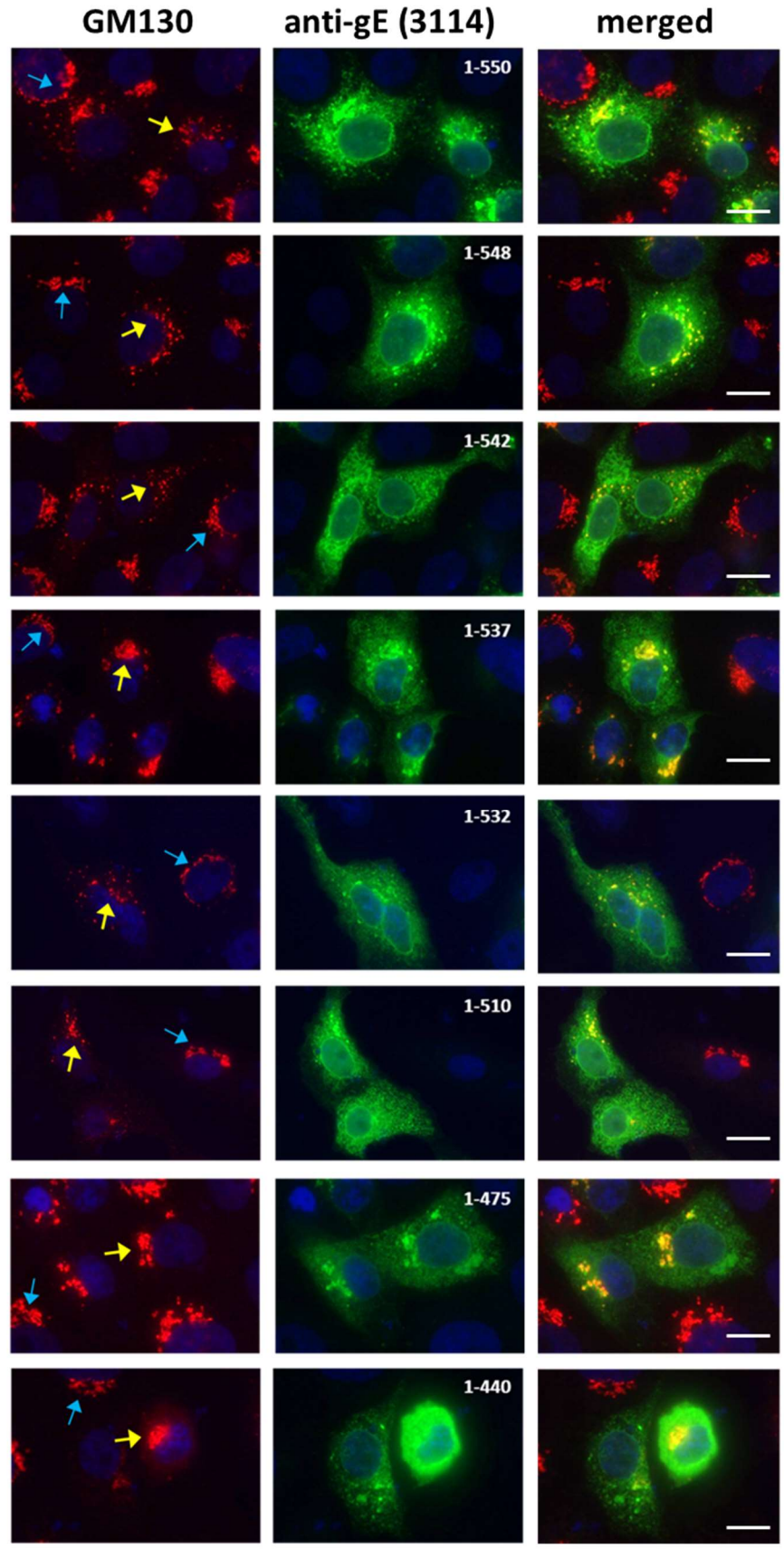
GM130
anti-gE (3114)
merged
1-550
1-548
1-542
1-537
1-532
1-510
1-475
1-440

(a)

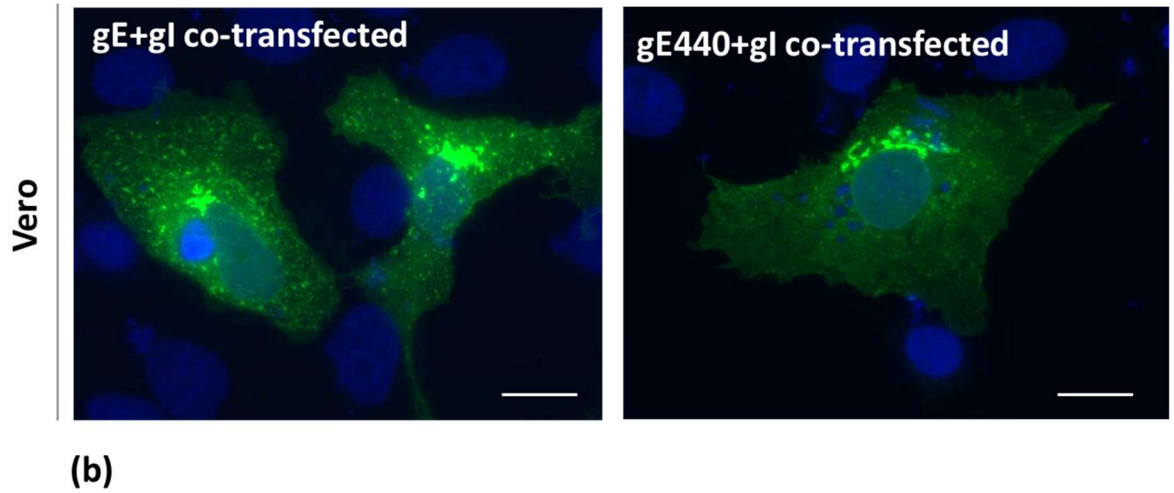

Figure 5.9 | Localisation of C terminal truncation mutants of gE in transfected Vero cell. (a) Vero cells were seeded on glass slides and transfected with the various gE expression plasmids (1-550, 1-548, 1-542, 1-537, 1-532, 1-510, 1-475 and 1-440). The cells were fixed at 36 h post-transfection and stained with anti-gE (MAb-3114) and GM130 antibodies. (b) Vero cells were cotransfected with gE and gI, or gE440 and gI for 22 h and were fixed and stained for gE/gI complex using MAb-3063. The blue and yellow arrows in (a) indicate Golgi staining in untransfected and transfected cells respectively. Images were taken using an Olympus IX-81 inverted fluorescence microscope using a 60x oil immersion lens. Blue: staining of nuclei with DAPI. Scale bar indicates 20 µm.

To investigate the interaction of these gE truncation constructs with Nipsnap1, HEK293T cells were co-transfected with plasmids expressing Nipsnap1-myc (C-terminally tagged) and either gECT 1-440, 1-475, 1-510, 1-532 or full length gE in the first instance. At 48 h post-transfection cells were lysed and an IPs were performed with anti-gE (3114) antibody, followed by WB analysis with anti-gE and anti-Nipsnap1 antibodies. Initially 12% SDS-PAGE was used and the membranes were blotted with secondary mouse antibody (H+L). However, under these conditions the Nipsnap1-specific band was difficult to distinguish from the strong signal from the IgG light chain present due to the immunoprecipitating antibody. Therefore, the samples were re-run on 15% SDS-PAGE and a mouse IgG1 heavy chain specific secondary antibody was used which should not recognise the light chain from the IgG2a isotype MAb-3114 antibody used for the IPs. These blots demonstrated a clear band for Nipsnap1 pull down for full length gE but not for the other gE constructs (Figure 5.10 a). Interestingly, only endogenous Nipsnap1, and not the plasmid expressed Nipsnap1-myc was coimmunoprecipitated with full length gE, suggesting the C terminal myc-tag on Nipsnap1 inhibits its binding to gE in transfection.

These co-transfection experiments were repeated using the gECT truncation constructs with fewer C terminal residues removed (1-537, 1-542, and 1-548) and co-transfection of Nipsnap1 or Nipsnap2 expression plasmids. Figure 5.10 (b) shows both Nipsnap1 and 2 are only pulled-down efficiently with full length gE and not with any of the truncated proteins. Only endogenous Nipsnap1 and 2 could be observed in the pull-down samples, again suggesting tagging at the C terminus of Nipsnap1, and also Nipsnap2, inhibits their interaction with gE. Further co-transfection experiment with gE and Nipsnap1 (untagged and myc-tagged at C- and N terminus) expression plasmid shows gE can pull down both endogenous and N-terminally myc-tagged Nipsnap1 but not C-terminally myc-tagged Nipsnap1 (Figure 5.12 c). Taken together, these data suggest that Nipsnap1 and 2 interact with the extreme C terminus of gE because deletion of just the last two amino acids (phenylalanine and tryptophan) inhibits this interaction. It also suggests that the C terminus portion of Nipsnap1 possibly interacts with gE and therefore, putting a myc-tag in this region abolishes gE-Nipsnap1-myc interaction. These data may explain the observation that gE-GFP, where the GFP is fused to the C terminus of gE, showed reduced pull-down of myc-Nipsnap1 (Figure 5.5).

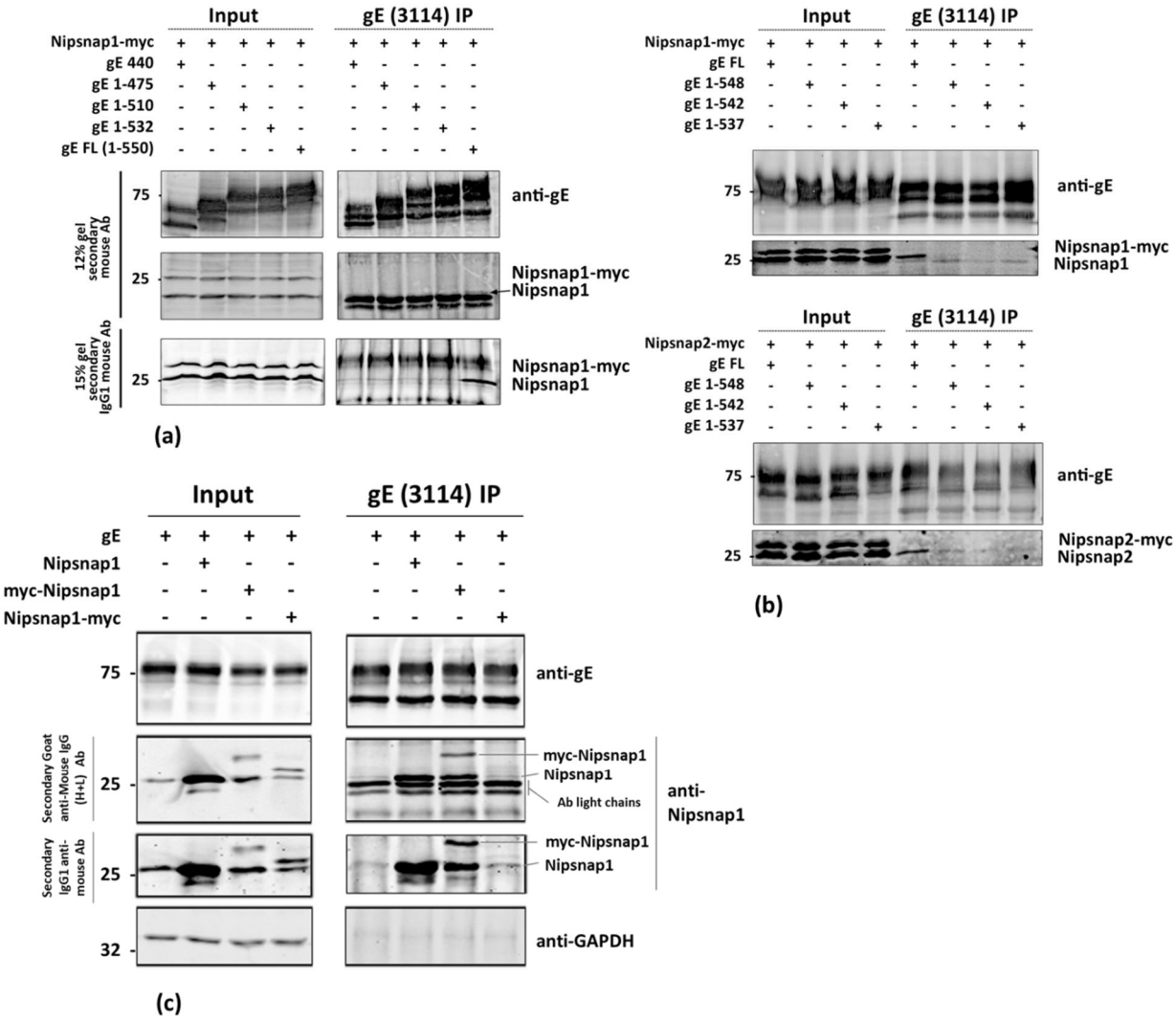

Figure 5.10 | Immunoprecipitation analysis of Nipsnap1 and 2 interaction with gE truncation constructs. HEK293T cells were co-transfected with expression plasmids encoding gE of various lengths (a) 1-440, 1-475, 1-510, 1-532 and FL or (b) 1-537, 1-542, 1-548, and FL along with Nipsnap1-myc or Nipsnap2-myc. (c) FL gE also co-transfected with Nipsnap1, myc-Nipsnap1 or Nipsnap1-myc. After 48 h the cells were lysed and an IP was carried out using anti-gE antibody. The samples were analysed by WB with the antibodies shown. Molecular mass markers (in KDa) are on the left.

5.2.7 Cellular localisation of Nipsnap1 and 2 and co-localisation with gE by immunofluorescence

Cellular location of Nipsnap1 and 2 could be highly diverse and dynamic depending on the nature and environment of the cell. Studies have suggested these proteins are localised in various compartments including the plasma membrane, cytoplasm and mitochondria (Seroussi et al., 1998; Nautiyal et al., 2010; Okuda-Ashitaka et al., 2012; Tummala et al., 2010; Yamamoto et al., 2017). The C terminus of Nipsnap1 and -2 contain a SNAP25-like domain whereas the N terminus of both proteins are predicted to have mitochondrial targeting sequences (Yamamoto et al., 2017). Given that Nipsnap1 and 2 have been proposed to localise to many subcellular compartments which may or may not enable interaction with the cytoplasmic domain of gE, the localisation of these proteins in cells was investigated. N- and C-terminally myc-tagged Nipsnap1 and 2, C-terminally GFP-tagged Nipsnap1 and untagged Nipsnap1 and 2 expression plasmids were constructed. Vero cells were transfected with these plasmids and fixed at 18 h post-transfection. Mock-transfected cells were used to compare the localisation of plasmid-expressed constructs with endogenous protein expression. The cells were stained with either anti-Nipsnap1 or 2 antibodies except for Nipsnap1-GFP expressing cells where no antibody staining was used. Figure 5.11 shows localisation of Nipsnap1 and 2 in Vero cells. The endogenous Nipsnap1 signal was relatively weak and difficult to interpret in Vero cells as most of the cells showed a broadly diffused signal, with some evidence of concentration near the nucleus. Endogenous Nipsnap2 however, showed clear cellular localisation to string-like structures concentrated around the nucleus, reminiscent of mitochondria staining. Overexpression of both untagged and C-terminally myc-tagged Nipsnap1 and Nipsnap2, as well as GFP-tagged Nipsnap1, showed a similar pattern to endogenous Nipsnap2 that looks like mitochondria staining. However, N-terminally myc-tagged Nipsnap1 showed a much more diffuse localisation throughout the cytoplasm, whereas and N-terminally myc-tagged Nipsnap2 showed no increase in signal above the endogenous protein. This suggest both Nipsnap1 and 2 are localised to mitochondria and that N terminal tagging of Nipsnap1 may interfere with mitochondrial targeting, whereas the N terminal tagging of Nipsnap2 may affect protein synthesis or stability.

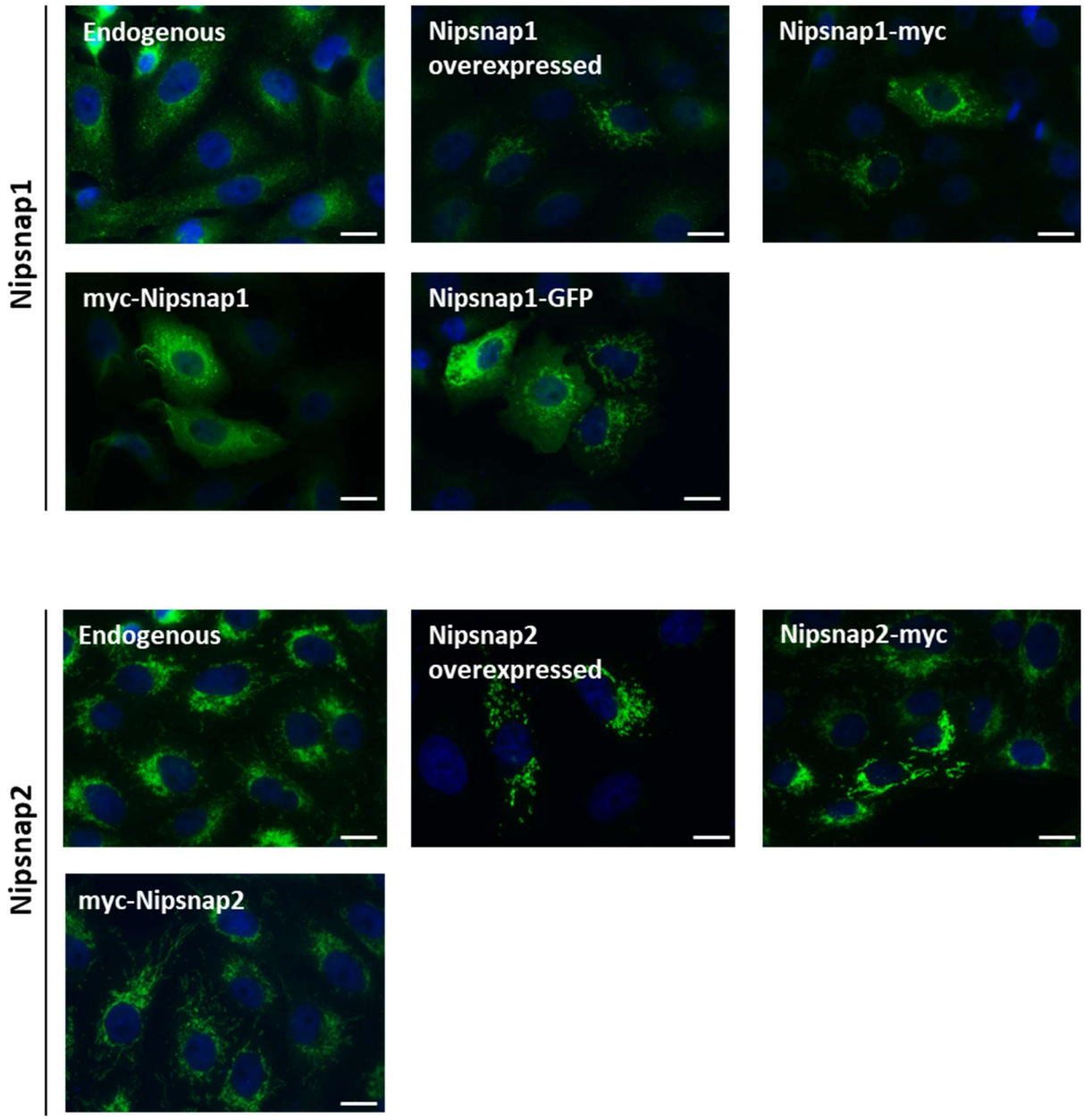

Figure 5.11 | Localisation of endogenous and transfected Nipsnap1 and 2 in Vero cells. Vero cells were transfected with either native or tagged Nipsnap1 (N-myc, C-myc or C-GFP) or Nipsnap2 (N-myc or C-myc) and after 18 h the cells were fixed, permeabilised and stained with Nipsnap1 or 2 specific antibodies (except for Nipsnap1-GFP expressing cells). Images were taken using an Olympus IX-81 inverted fluorescence microscope using a 60x oil immersion lens. Blue: staining of nuclei with DAPI. Scale bar indicates 20 µm.

To understand whether Nipsnap1 or 2 co-localises with gE in transfected cells, Vero cells were co-transfected with gE and untagged Nipsnap1 or Nipsnap2 encoding plasmids and after 18 h were stained for the respective proteins. Since the Nipsnap2 antibody was a rabbit polyclonal, to reduce non-specific interaction of the antibody with gE due to its Fc-receptor activity, cells were blocked with human IgG. Figure 5.12 (a) shows that both gE and Nipsnap1 localise to a relatively similar perinuclear location in the cell although with little evidence of co-localisation. On the other hand, gE and Nipsnap2 showed more distinctly different locations in the cell with no evidence of co-localisation. Potential co-localisation was also investigated in transfected HFF-hTERT for with either gE and Nipsnap1^{GFP} or gE and Nipsnap2. At 18 h post-transfection cells were stained with antibodies to gE together with mitochondrial markers Tom20 or HSP60 and Nipsnap2 antibodies as appropriate (Figure 5.12 b). Nipsnap1^{GFP} and Nipsnap2 showed extensive co-localisation with mitochondrial proteins Tom20 and HSP60 respectively. However, gE showed no co-localisation with either Nipsnap1 or 2 in these cells.

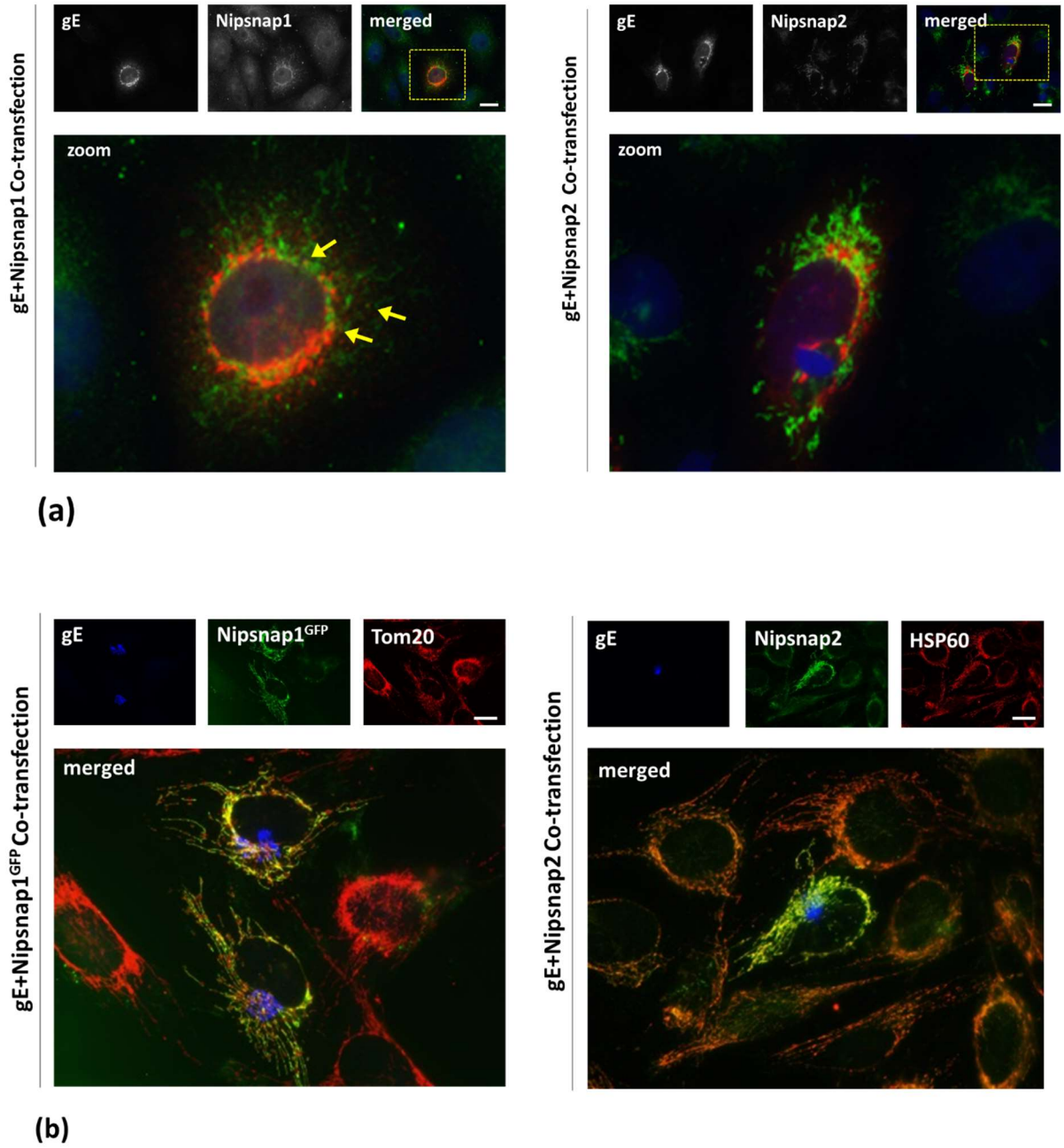

Figure 5.12 | Nipsnap1, 2 and gE localisation in cells. (a) Vero cells were co-transfected with gE and Nipsnap1 or Nipsnap2 and (b) HFF-hTERT cells were transfected with gE and Nipsnap1^{GFP} or Nipsnap2. At 18 h post-transfection the cells were fixed, permeabilised and stained with antibodies against (a) gE and Nipsnap1 or 2 or (b) gE, Tom20 or gE, Nipsnap2 and HSP60 as indicated. For (a) bottom panel shows selected areas (in yellow box) from the merged channel at higher magnification, blue indicates staining of nuclei with DAPI, and yellow arrow indicates possible Nipsnap1 and gE co-localisation. Images were taken using an Olympus IX-81 inverted fluorescence microscope using a 60x oil immersion lens. Scale bar indicates 20 μm.

5.2.8 Comparison of gE localisation and mitochondrial markers in infected cells

Although no clear co-localisation between gE and Nipsnap1, Nipsnap2, or mitochondrial markers was observed in transfected cells, the large number of mitochondrial protein that were identified in the SILAC-IP investigations for gE/gI interactors could indicate some interaction between gE and mitochondria. To investigate whether gE localises to mitochondria during infection, HFF-hTERT cells were infected with either HSV-1 WT or gIG39R and stained with mitotracker for 30 min before fixing, followed by staining with gE specific antibody. As can be seen in Figure 5.13, mitotracker-stained cellular mitochondria in virus-infected and mock-infected cells and at 10 hpi no obvious difference in the morphology of mitochondria was observed in the infected cells. Furthermore, no co-localisation between gE and mitotracker could be observed. This suggests that while gE may interact with proteins that localise to mitochondria, including Nipsnap1 or 2, gE itself does not appear to be present in mitochondria. Therefore, any interaction between gE and Nipsnap1 or 2 would presumably need to occur in another location, such as the cytoplasm where Nipsnap1 and 2 will be synthesised.

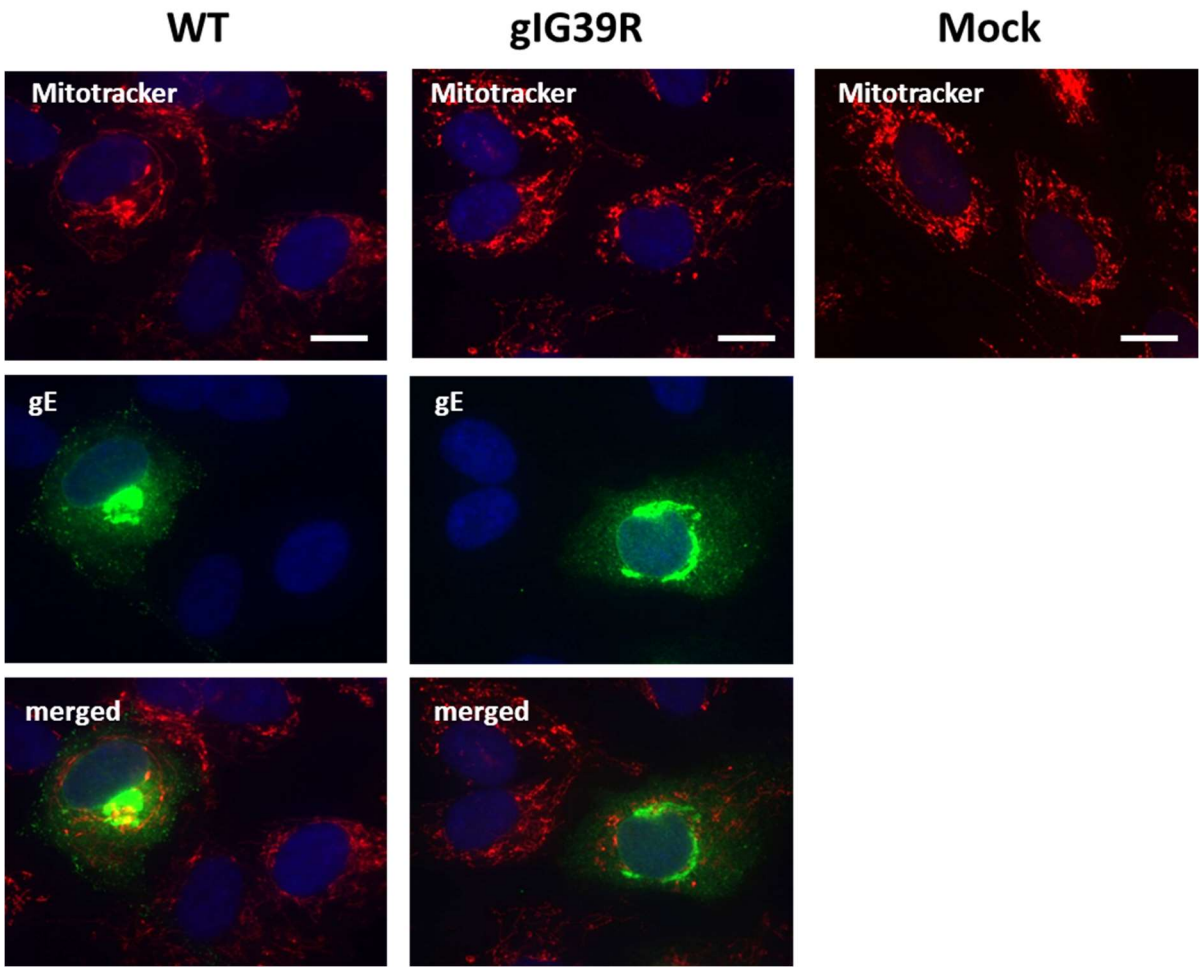

Figure 5.13 | HSV-1 gE and mitochondrial staining during infection. HFF-hTERT cells were infected with HSV-1 WT and gIG39R viruses (1 PFU/cell) and treated with mitotracker for 30 min before fixing at 10 hpi and staining with gE specific antibody. Images were taken using an Olympus IX-81 inverted fluorescence microscope using a 60x oil immersion lens. Blue: staining of nuclei with DAPI. Scale bar indicates 20 µm.

5.2.9 Localisation of MYOF in cells by immunofluorescence

Previous publications have shown endogenous MYOF to co-localise with endocytic recycling protein EHD2 at the plasma membrane in myoblast and with Golgi marker GM130 in airway epithelial cells (Doherty et al., 2008; Leung et al., 2012). However, when overexpressed MYOF was found at the plasma membrane of HEK293T and COS7 cells and appeared as vesicular puncta co-localising with secretory pathway markers (ER and Golgi) and more strongly with endosomal markers (Rab5 and Rab7) in HEK293T cells (Redpath et al., 2016; Bernatchez et al., 2007). To understand the potential roles of MYOF during HSV-1 replication, localisation of endogenous and overexpressed MYOF were tested in Vero and HFF-hTERT cells. The cells were seeded on glass slides and either left untreated or were transfected with an expression plasmid encoding C-terminally HA-tagged myoferlin (MYOF-HA). The cells were fixed at 18 h post-transfection and stained with antibodies to MYOF (Vero and HFF-hTERT cells) or HA (Vero cells only). The available antibodies against MYOF and HA were both IgG1 subtype therefore could not be used together. As can be seen in Figure 5.14 (a) staining of untransfected cells with the MYOF antibody produces mainly nuclear signals in Vero cells. Given that MYOF is thought to be primarily on cytoplasmic membrane compartments this may indicate that Vero cells have low expression levels, the antibody poorly recognises monkey MYOF, or there is cross reactivity of the antibody with a non-specific protein in these cells. The expected localisation pattern for MYOF is evident in HFF-hTERT cells, where the majority of the signal in untransfected cells appears on cytoplasmic puncta. In transfected cells MYOF-HA demonstrated a punctate cytoplasmic distribution in both HFF-hTERT and Vero cells, with some cells also showing more intense staining adjacent to the nucleus and around the nuclear rim.

To investigate whether MYOF shows any localisation to mitochondria, similar to Nipsnap1, Nipsnap2 and IFITM2 HFF-hTERT cells were co-stained with mitotracker (added 30 min prior to fixation) and stained with MYOF. As can be seen in Figure 5.14 (b) no co-localisation of MYOF with mitotracker could be observed, and thus, unlike other gE/gI interactome hits, MYOF does not appear to be a mitochondrial protein.

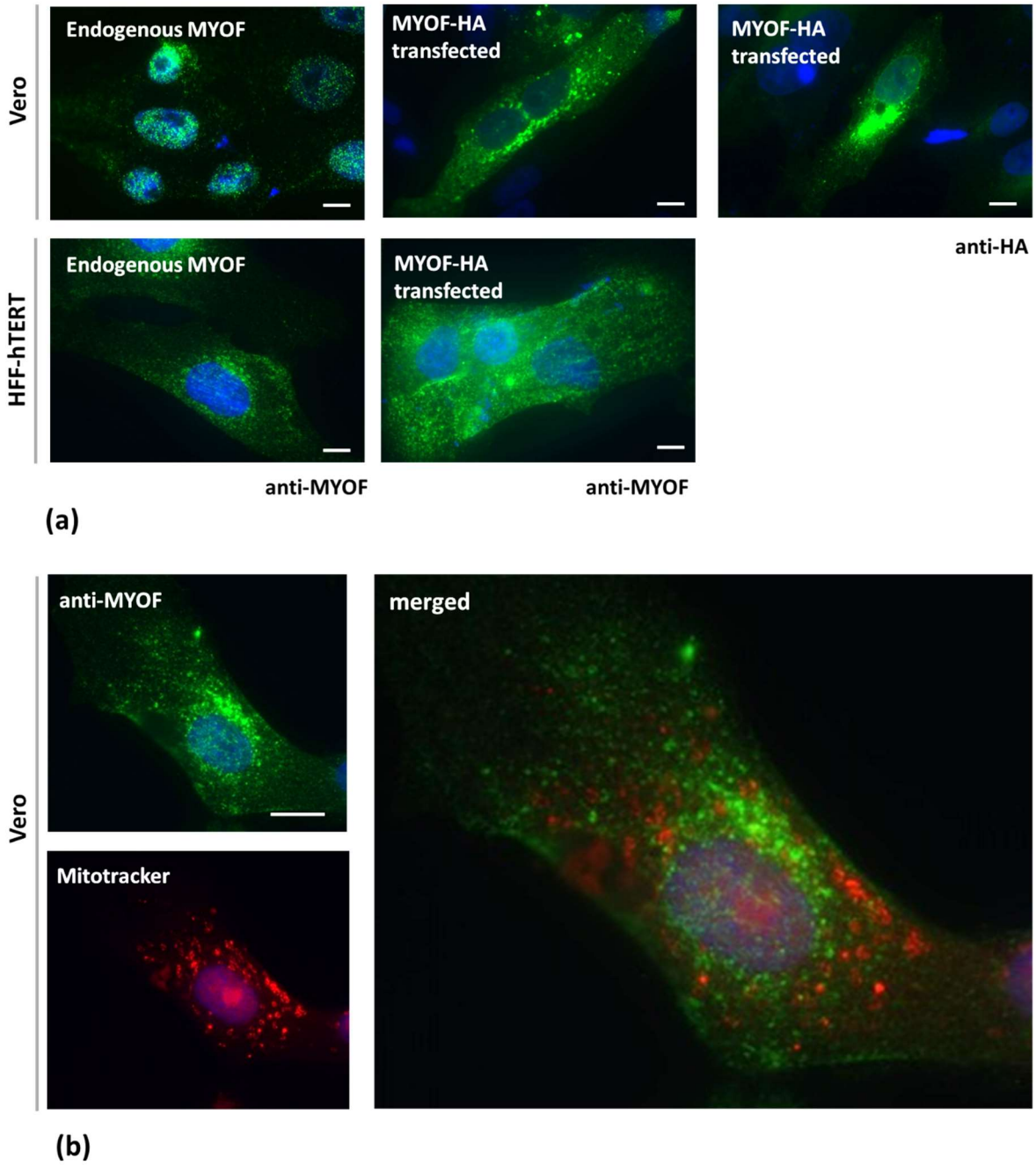

Figure 5.14 | Myoferlin (MYOF) localisation in transfected and untransfected cells. Vero and HFF-hTERT cells were seeded on glass slides and either transfected with MYOF-HA or mock transfected. (a) After 18 h the cells were fixed and stained for MYOF (for mock and transfected) or HA (for Vero cell only) or (b) after 18 h of MYOF-HA transfection Vero cells were added with mitotracker for 30 min and then the cells were fixed, permeabilised and stained for MYOF. Images were taken using an Olympus IX-81 inverted fluorescence microscope using a 60x oil immersion lens. Blue: staining of nuclei with DAPI. Scale bar indicates 20 µm.

5.2.10 gE and MYOF co-localisation in infected HFF-hTERT cells

To investigate whether gE and MYOF co-localise during infection HFF-hTERT cells were seeded on glass slide, infected with WT HSV-1 and then fixed and stained for gE and MYOF at 15 hpi. As can be seen in Figure 5.15, gE and MYOF demonstrated co-localisation in cytoplasmic puncta at various locations in the cell, although the majority of gE and MYOF signal did not show overlapping signals, particularly in the perinuclear region where the majority of gE localises. This suggests that during infection gE might recruit MYOF to a specific subset of membrane compartments during the HSV-1 replication cycle, such as specific cytoplasmic vesicles.

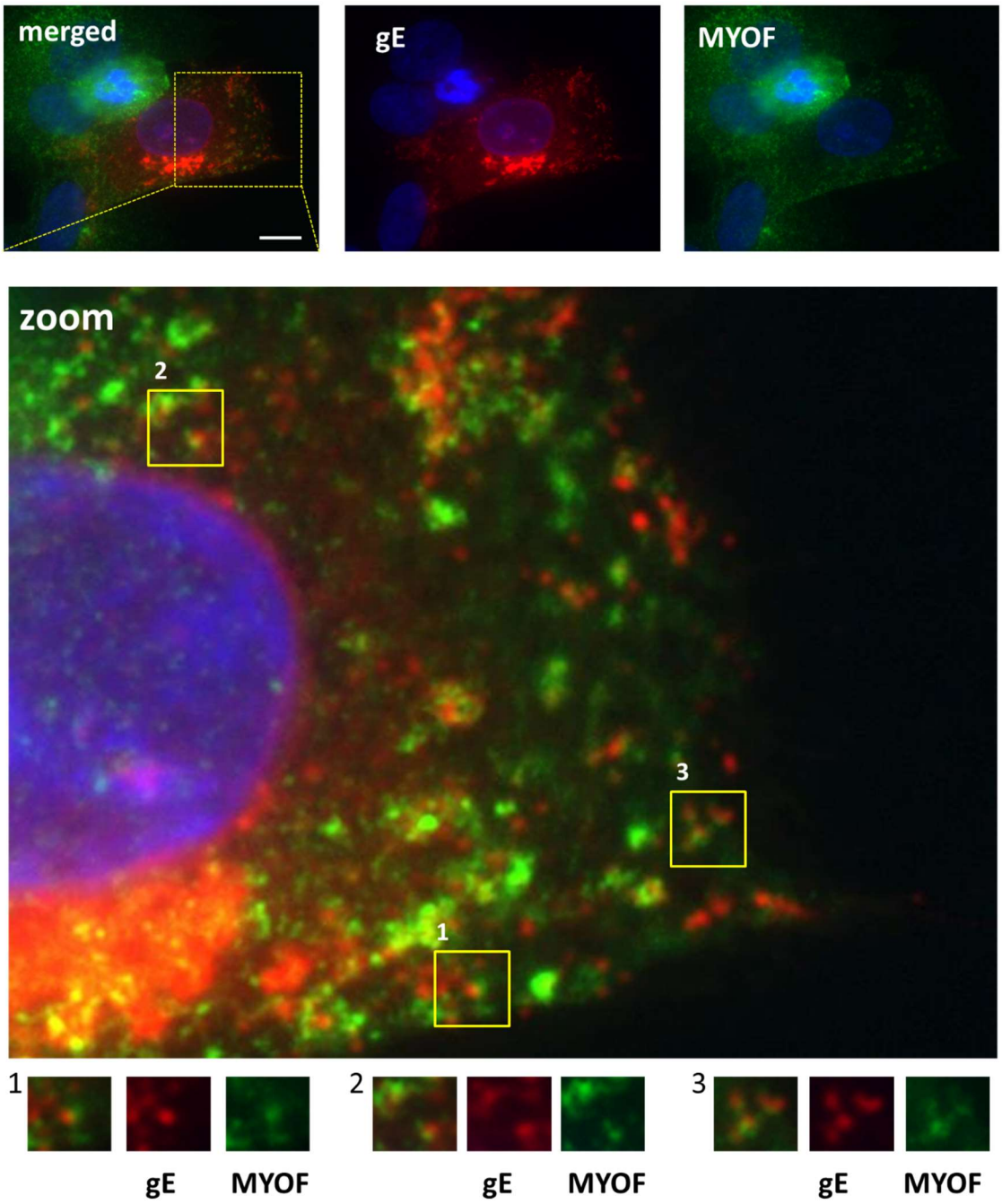

Figure 5.15 | Myoferlin (MYOF) and gE localisation in infected HFF-hTERT cell. HFF-hTERT cells were seeded on glass slides and infected with WT HSV-1 and the cells were fixed, permeabilised and stained for MYOF and gE (MAb-3114) at 15 hpi. The yellow boxes in the zoom panel indicate the possible MYOF and gE co-localisation (shown in separate channels in the bottom). Images were taken using an Olympus IX-81 inverted fluorescence microscope using a 60x oil immersion lens. Blue: staining of nuclei with DAPI. Scale bar indicates 20 µm.

5.2.11 MYOF-HA co-localisation with HSV-1 glycoproteins in transfected cells

To understand whether MYOF co-localises with gE, or other HSV-1 glycoproteins without the influence of other viral proteins, their localisation was analysed in transfected cells. Vero and HFF-hTERT cells were seeded on glass slides and co-transfected with MYOF-HA together with gE, gB or gD expression plasmids. Cells were fixed at 22 h post-transfection and stained with MYOF and HSV-1 glycoprotein specific antibodies. As shown in Figure 5.16 gE and MYOF-HA demonstrated substantial co-localisation in many cytoplasmic structures in both cell types. Furthermore, a similar level of co-localisation between MYOF-HA and both gD and gB were also observed in both cell types. This suggests over-expressed MYOF-HA localises to many endomembrane compartments where gE, gB and gD also localise in the absence of any other viral proteins. Interestingly, gB expression often appeared to induce the formation of large intracellular vacuole-like structures where both gB and MYOF localised.

To understand whether other viral glycoproteins localise to these large gB-induced structures, cells were co-transfected with a combination of gE, gB and MYOF-HA encoding plasmids. Cells were fixed at 22 h post-transfection and stained with gE, gB and MYOF antibodies. As can be seen in Figure 5.17 large cytoplasmic vacuole-like structures were observed that were positive for both MYOF and gE in some cells, presumably due to the co-expression of gB. This suggests gE is also recruited/retained in the gB-induced intracellular vacuoles.

Given three independent HSV-1 glycoproteins co-localised with MYOF when coexpressed, the tegument protein VP22 was tested for co-localisation with MYOF as a control viral protein that lacks a transmembrane domain. Vero cells were co-transfected with $VP22^{GFP}$ and MYOF-HA encoding plasmids and at 22 h post-transfection the cells were fixed and stained for MYOF. Little-to-no co-localisation of VP22 with MYOF could be detected in these cells (Figure 5.18). However, when a gE-encoding plasmid was included along with $VP22^{GFP}$ and MYOF-HA for Vero cell transfection, all three proteins were observed to co-localise together in cytoplasmic structures (Figure 5.18). Since VP22 has been previously shown to interact with gE (O'Regan et al., 2007; Farnsworth et al., 2007b), this suggests gE can recruit VP22 to MYOF-containing membrane compartments. However, whether the observed co-localisation between gE and MYOF reflects a potential interaction between these two proteins or is due to simply being present in the same limited number of membrane compartments is unclear.

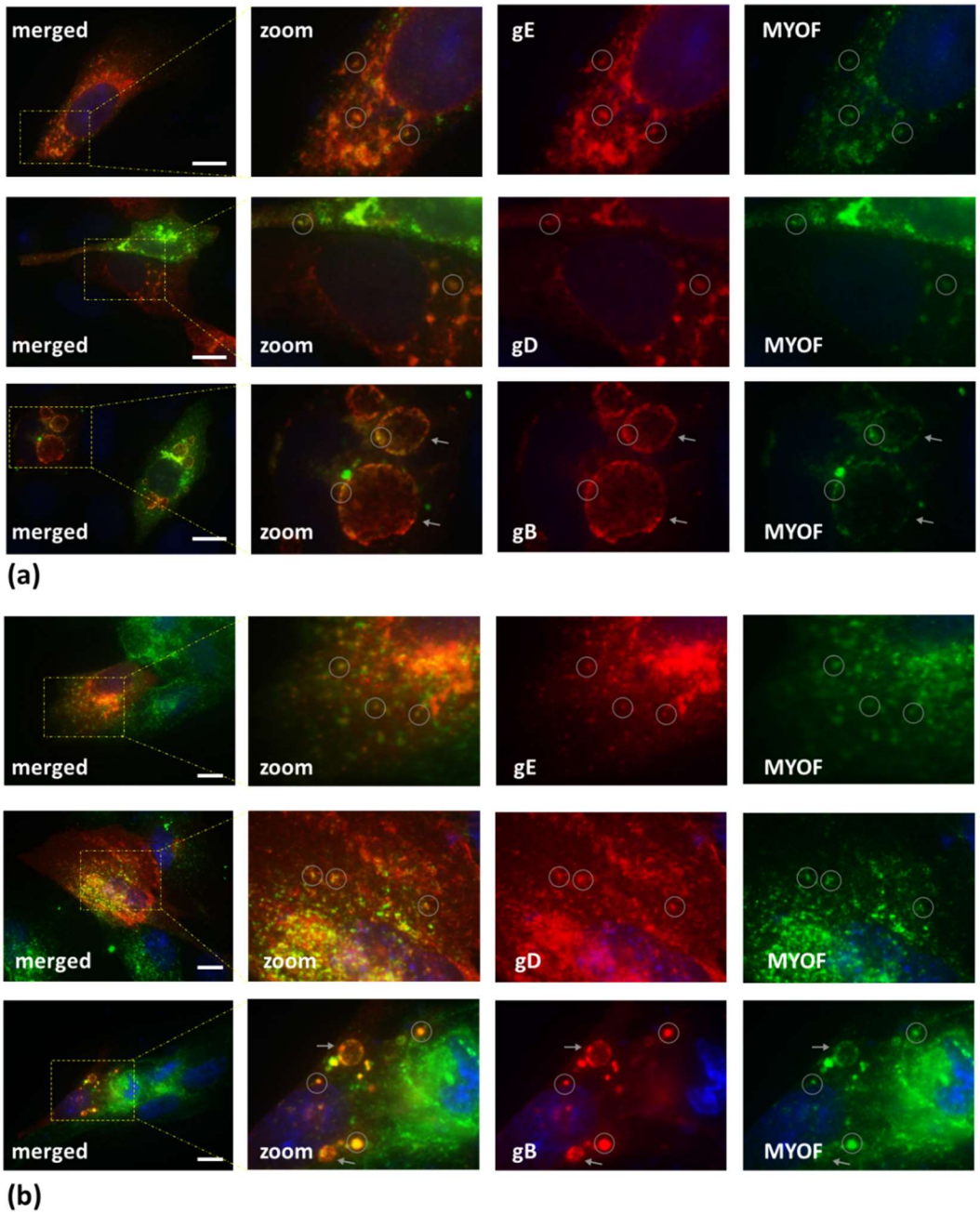

Figure 5.16 | MYOF co-localisation with gE, gD and gB in Vero and HFF-hTERT cells. (a) Vero and (b) HFF-hTERT cells were seeded on glass slides and transfected with HSV-1 MYOF-HA and glycoprotein gE or gD or gB encoding plasmids. At 22 h post-transfection the cells were fixed, permeabilised and stained for MYOF and gE or gD and gB as required. Images were taken using an Olympus IX-81 inverted fluorescence microscope using a 60x oil immersion lens. Blue: staining of nuclei with DAPI. Co-localising punctate are circled, white arrow shows gB-induced circular vacuole-like compartments in transfected cells. Scale bar indicates 20 µm.

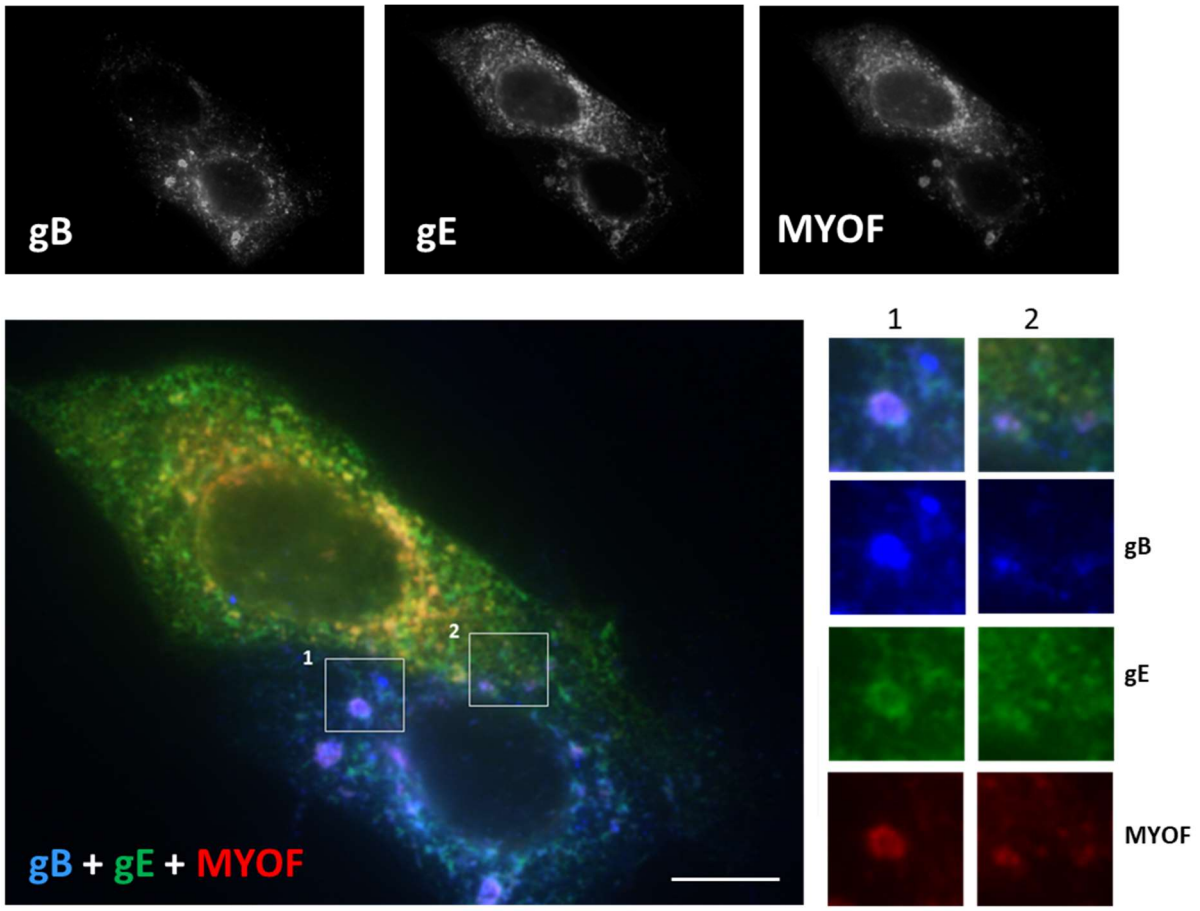

Figure 5.17 | MYOF co-localisation with gE and gB in Vero cells. Vero cells were seeded on glass slides and transfected with plasmids encoding HSV-1 gE, and gB along with and MYOF-HA. At 22 h post-transfection the cells were fixed, permeabilised and stained for MYOF, gB and gE. Images on the right panel indicate selected areas from the combined panel to show possible co-localisation of the indicated proteins. panel indicates selected section from the combined channel panel Images were taken using an Olympus IX-81 inverted fluorescence microscope using a 60x oil immersion lens. Scale bar indicates 20 µm.

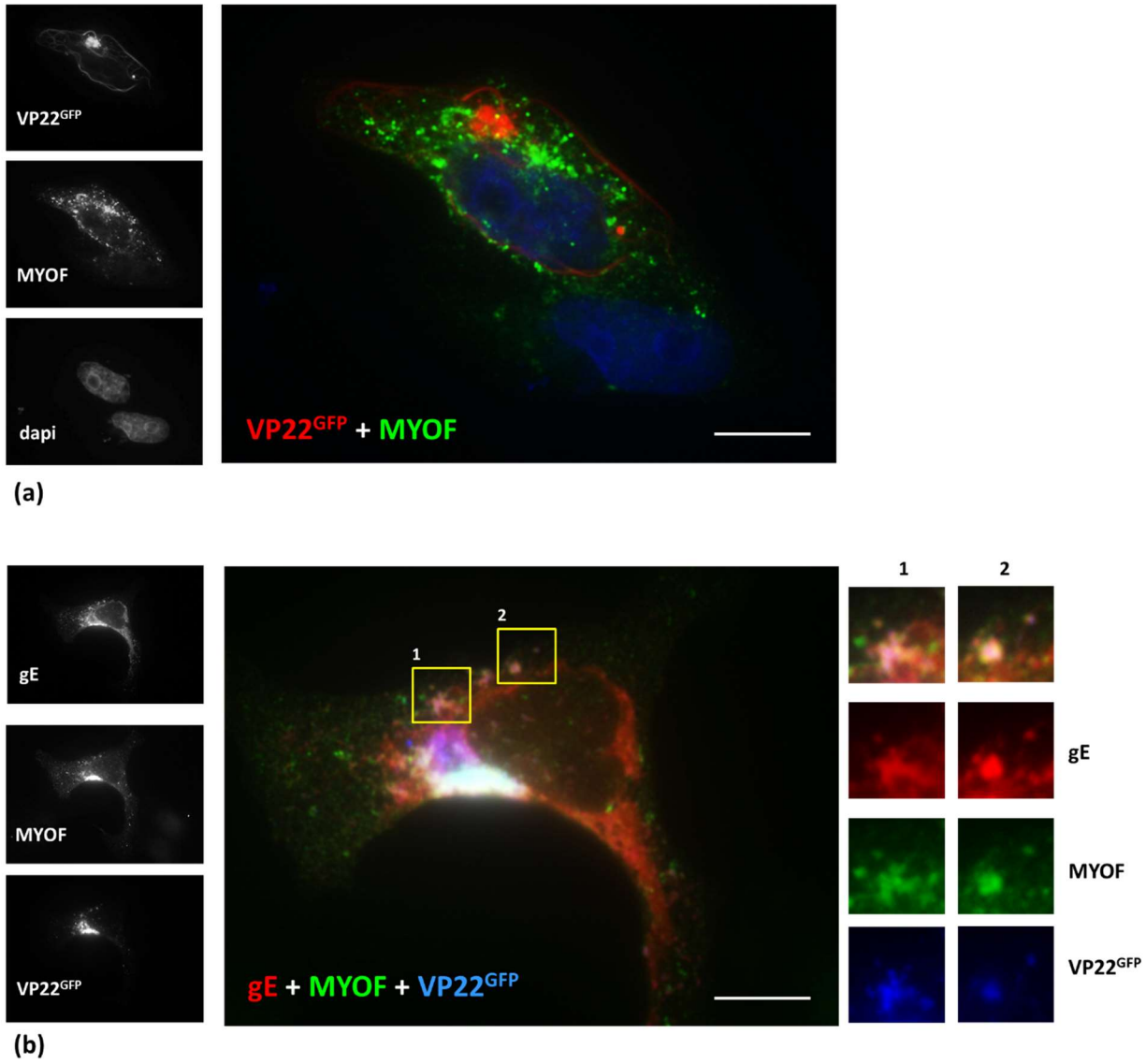

Figure 5.18 | MYOF co-localisation with gE and VP22 in Vero cells. Vero cells were seeded on glass slides and co-transfected with plasmids encoding for VP22^{GFP} and MYOF-HA with or without gE. At 22 h post-transfection the cells were fixed, permeabilised and stained for (a) MYOF or (b) MYOF and gE as indicated. For (b) images on the right panel indicate selected areas from the combined panel to show possible co-localisation of the indicated proteins. Images were taken using an Olympus IX-81 inverted fluorescence microscope using a 60x oil immersion lens. Blue: staining of nuclei with DAPI (top figure only). GFP shown in red colour in (a) and in blue colour in (b) of the composite images. Scale bar indicates 20 µm.

5.3 Discussion

The aim of this chapter was to further investigate the three main observations made from SILAC-IP-MS data analysis of the gE/gI complex. The observations are (i) reduction of IFITM2, and the interaction of gE with (ii) Nipsnap1 and 2, and (iii) MYOF during HSV-1 infection. This chapter showed a negative correlation between gE and IFITM (1 and 2) expression, predicted the binding site on gE for Nipsnap1 and identified MYOF as a potential interacting partner of gE or at least a host factor that is present in specific compartments of the endomembrane system that also contain HSV-1 glycoproteins.

IFITM1-3 are commonly known as restriction factors for many enveloped viruses. In this study it was found that HSV-1 causes the degradation of IFITM2, and presumably IFITM3 as the antibody used cross-reacts with both proteins, which may be to prevent chances of restriction of HSV-1 by these proteins. This finding is consistent with the previous observation where overexpression of IFITMs did not show any inhibitory effect on HSV-1 replication (Xie et al., 2015). Surprisingly, gE appeared to show some interaction with all three IFITM proteins tested in transfection assay, in particular IFITM1, even though only IFITM2 was detected in the SILAC-IP MS data. Furthermore, overexpression of IFITM1 and 2 reduced the expression levels of gE in co-transfection with the reduction correlating with the relative efficiency of pull down, e.g. IFITM1 showed the greatest reduction of gE expression and also the strongest signal for co-IP. It is possible that interaction between gE and IFITM proteins leads to their destruction in lysosomes, although at least for IFITM2 the reduced protein levels in infected cells did not appear to be gE-dependent. Staining for endogenous IFITM2 in IF demonstrated the majority of signal in mitochondria in normal cells, in distinct cytoplasmic punctate in IFITM2-HA- stably-expressing cells, and as an aggregated perinuclear signal in HA-IFITM2 transfected cells as has been reported previously (Muñoz-Moreno et al., 2016). Modification of IFITM proteins with -C or N- terminal tagging and over expression could influence subcellular localisation of the proteins and their restriction activity (Bailey et al., 2013; Bailey et al., 2014). Therefore, it is difficult to interpret data from overexpression of the proteins during IP and IF studies with gE because and further work will be needed to investigate the potential interaction of IFITM proteins with gE and the role this may play during HSV-1 infection. For example, it will be interesting to investigate whether expression of untagged IFITM proteins has different effects on the entry of WT and gE-deletion viruses.

Nipsnap1 was one of the strongest hits from the SILAC-IP MS screen and these studies have demonstrated it could be a direct binding partner of gE, interacting at the extreme CT domain of the glycoprotein. However, Nipsnap1 and 2 are both present in mitochondria (this chapter, Okuda-Ashitaka et al., 2012), although published data has suggested Nipsnap1 can be also found on plasma membrane (Okuda-Ashitaka et al., 2012; Schoeber et al., 2008). While localisation of gE within mitochondria was not observed, and there was little evidence of co-localisation of gE with Nipsnap1, the potential membrane trafficking activity of Nipsnap proteins warrants further investigation into the role of these proteins during HSV-1 replication (Chapter 6).

MYOF has previously been shown to localise in various endocytic compartments (Leung et al., 2012; Redpath et al., 2016; Bernatchez et al., 2007). This study found the punctate appearance of both endogenous and overexpressed MYOF in the cytoplasm, where it showed some co-localisation with gE. However, in co-transfected cells MYOF also co-localised with gD and gB, with high levels of gB expression inducing the formation of large vesicles, vacuoles or circular membrane ruffles in cell containing MYOF and gB. These aberrant membrane structures are reminiscent of those caused by inhibition of ESCRT proteins (Crump et al., 2007; Broniarczyk et al., 2017) and so may reflect disruption of endocytic trafficking by gB over-expression in the absence of other virus proteins. Additionally, gE costained with gB and MYOF in these compartments when all 3 proteins were co-expressed. Because MYOF is a transmembrane protein present within endocytic compartments and the Golgi, such co-localisation with viral glycoprotein could be simply because of their common sites of expression within cells. It will be important in the future to determine whether MYOF directly interacts with gE or another HSV-1 protein, and whether MYOF function plays any role in either virus secretion or transport of viral glycoproteins.

6. CRISPR-Cas9 knock-out of Nipsnap1 and 2 to understand their role in HSV-1 life cycle

6.1 Introduction

In the previous chapter, HSV-1 gE and Nipsnap1 and 2 interactions were validated and the possible site of interaction for Nipsnap1 on the gE cytoplasmic tail was identified. To understand the importance of specific cellular proteins in a virus life cycle, cellular genes can be either knocked down by siRNA or knocked out by CRISPR-Cas9 techniques. The siRNA technique involves silencing the expression of a target gene by depleting mRNA, whereas the CRISPR-Cas9 technique creates a double strand-break at target sites within the cellular genome which is then repaired by the non-homologous end joining (NHEJ) machinery. Because of the error prone nature of NHEJ frameshift mutations commonly occur that can result in disruption of gene function. The aim of this chapter was to utilise these techniques to investigate the possible roles of Nipsnap1 and 2 in the life cycle of HSV-1.

6.2 Results

6.2.1 Knock-down of Nipsnap1 and 2 by siRNA

To investigate the significance of gE interaction with Nipsnap1 and 2 in the HSV-1 life cycle the possibility of depleting Nipsnap1 and 2 from HaCaT and HEK293T cells using siRNA transfection was tested. Commercially available (QIAGEN) siRNA sequences designed for Nipsnap1 and Nipsnap2 (four for each gene) were tested by transfection. HaCaT and HEK293T cells were seeded and then transfected on the same day with 50 nM of each siRNA and then harvested at 3-days post-transfection. At this time point the cells were observed to have become detached and floating for many of the samples, and so they were collected by centrifugation of the culture medium. The cells were lysed and samples were tested for Nipsnap1 expression by WB. While there was some reduction in the band intensity for Nipsnap1 in all four Nipsnap1 siRNA-treated HaCaT samples, a reduction in the loading control (tubulin) was also observed from these samples suggesting some toxicity to the cells (Figure 6.1). However, no reduction in Nipsnap1 protein was observed in HEK293T cells. Given the little or no knock down of expression observed for Nipsnap1 and the potential toxicity problems, and successful application of CRISPR-Cas9 gene KO as detailed below, siRNA depletion of Nipsnap1 and 2 was not pursued further.

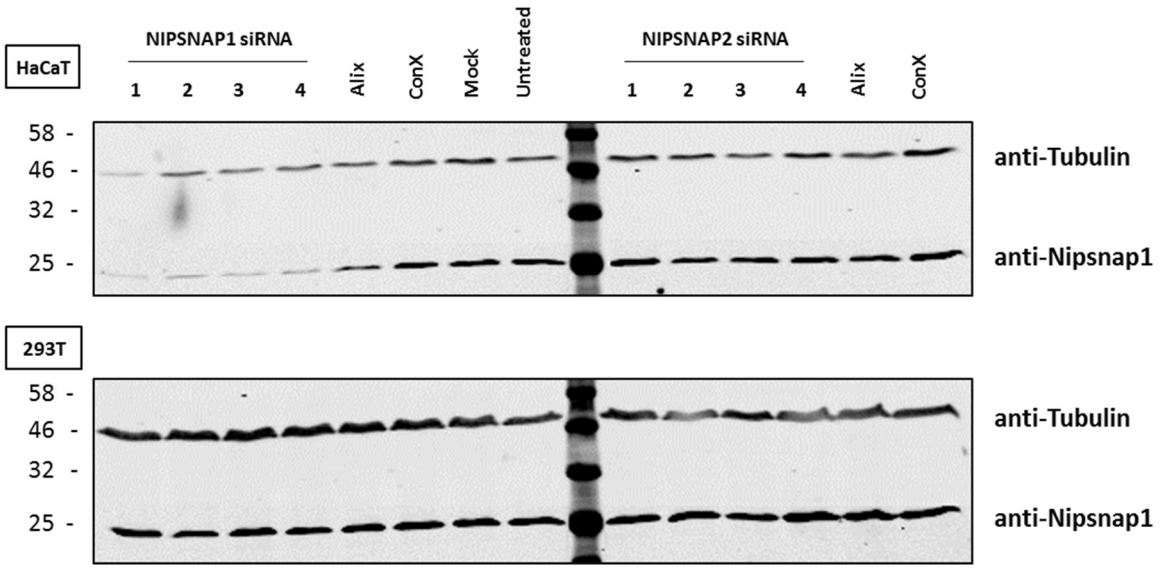

Figure 6.1 | Nipsnap1 knock down by siRNA in HaCaT and HEK293T cells. Wild type HaCaT and HEK293T cells were treated with four different siRNAs for both Nipsnap1 and Nipsnap2. siRNA for Alix and ConX was used as controls in the experiment. At 3 day post-transfection the cells were lysed and proteins were separated by SDS-PAGE and analysed by WB using the antibodies indicated. Molecular mass markers (in KDa) are shown on the left. Analysis of tubulin expression was included as loading control.

6.2.2 Generation of Nipsnap knock-out cells by CRISPR-Cas9 genome editing technology

Given the recent development of CRISPR-Cas9 based technology that enables relatively simple editing of the genome of cells, it was decided to attempt this approach to knock-out (KO) Nipsnap1 and 2 expression through generating mutations in the endogenous genes. Three independent guide RNAs (gRNAs) for both Nipsnap1 and 2 were designed. For guide RNA construction the target exons were put into an online CRISPR-gRNA designing tool (http://crispr.mit.edu) to calculate the gRNA scores and number of off-target sites for the guides. The target score for a gRNA reflects theoretical capacity of the gRNA to act on on-targets and not the off-targets. Candidates with high scores were chosen as a guide RNA against a target site on the chosen exon. For Nipsnap1 two independent target sites on exon 1 (NA and NB) and one on exon 4 (NC) were chosen and for Nipsnap2 (also called GBAS) independent sites on exon 1 (GA), exon 2 (GB) and exon 6 (GC) were chosen for the gRNA design. The gRNA oligonucleotides were annealed in a thermal cycler, phosphorylated utilising T4-PNK enzyme and inserted into pSpCas9(BB)-Puro(PX459) V2.0 plasmid (a gift from Feng Zhang) at the BbsI cloning sites. This plasmid contains two expression cassettes, a human codon-optimised SpCas9 (hSpCas9) – T2A StopGo site – PuroR cassette under a chicken β-actin promoter, and the single guide RNA under a U6 promoter. Upon transfection into a mammalian cell the plasmid expresses the guide RNA and Cas9 and also confers transient puromycin resistance to the cell.

For transfection, HaCaT cells were seeded at two different densities and transfected at 5-6 h post seeding with each of the Cas9/gRNA expressing plasmids. At 18 h post-transfection the cells were subjected to puromycin (2 µg/ml) selection. After 48 h of selection many of the PX459-derivative transfected cells were alive while control cells appeared dead. Cells were then washed with PBS and incubated in complete medium without puromycin until a sufficient cell population was obtained. Where possible, a sample of each cell population were lysed and tested for targeted gene expression by WB. From the population, cells were seeded at low density (~0.3 cells/well) in 96 well plates and wells scored for single cell clones. These were propagated until sufficient cell numbers were achieved to generate frozen stocks and test sample cell lysates by WB. Clones demonstrating loss of protein expression were further analysed by sequencing PCR products generated from the appropriate genetic locus for the target gRNAs used to confirm the nature of genetic lesion in each copy of the target genes.

This sequencing also serves as a test for clonal purity (schematic of approach shown in Figure 6.2).

Testing of the resulting populations after transfection with each gRNA and transient puromycin selection demonstrated that two Nipsnap1 KO populations obtained from NB and NC gRNAs showed substantial reduction in the Nipsnap1 band in WB, albeit the signal was very faint for control cells (Figure 6.3 a). The cell population derived from the other Nipsnap1 gRNA (NA) had insufficient cells to be examined in this initial test and so could not be included in the comparison. The three gRNAs (GA, GB and GC) utilised to KO Nipsnap2, appeared less successful at the population level, with only cells derived from GC gRNA treatment showing any reduction in the Nipsnap2 specific band, and this was only ~50% reduction in protein levels. From each of the Nipsnap1 gRNA populations and the GC Nipsnap2 gRNA population single cell clones were generated. Upon testing four clones from Nipsnap1 gRNAs (one from NA, one from NB and two from NC) and four clones from the Nipsnap2 gRNA GC, three clones demonstrating a complete loss of the Nipsnap1 protein band were identified (named NB1, NC1 and NC2) and one clone demonstrating a complete loss of the Nipsnap2 protein band (named GC1) was identified (Figure 6.3 b).

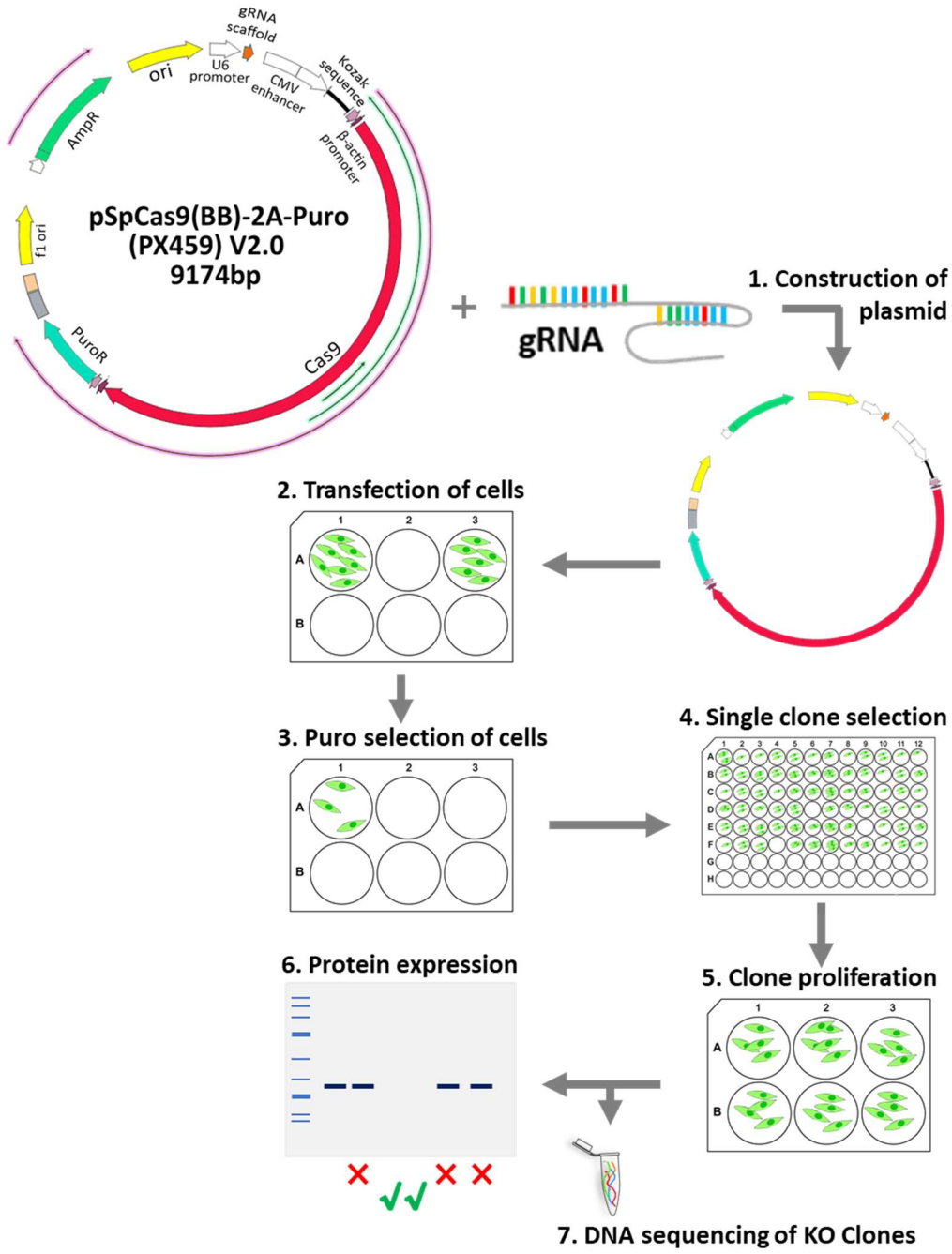

Figure 6.2 | Outline of procedure used to generate CRISPR-Cas9 KO cells. A Plasmid encoding both Cas9 and guide RNA was generated first. Sequence verified plasmids were used to transfect HaCaT cells. Cells were selected with puromycin for 48 h to remove untransfected cells. Single cell clones were isolated and amplified for WB testing followed by sequencing to confirm desired KO in the clones.

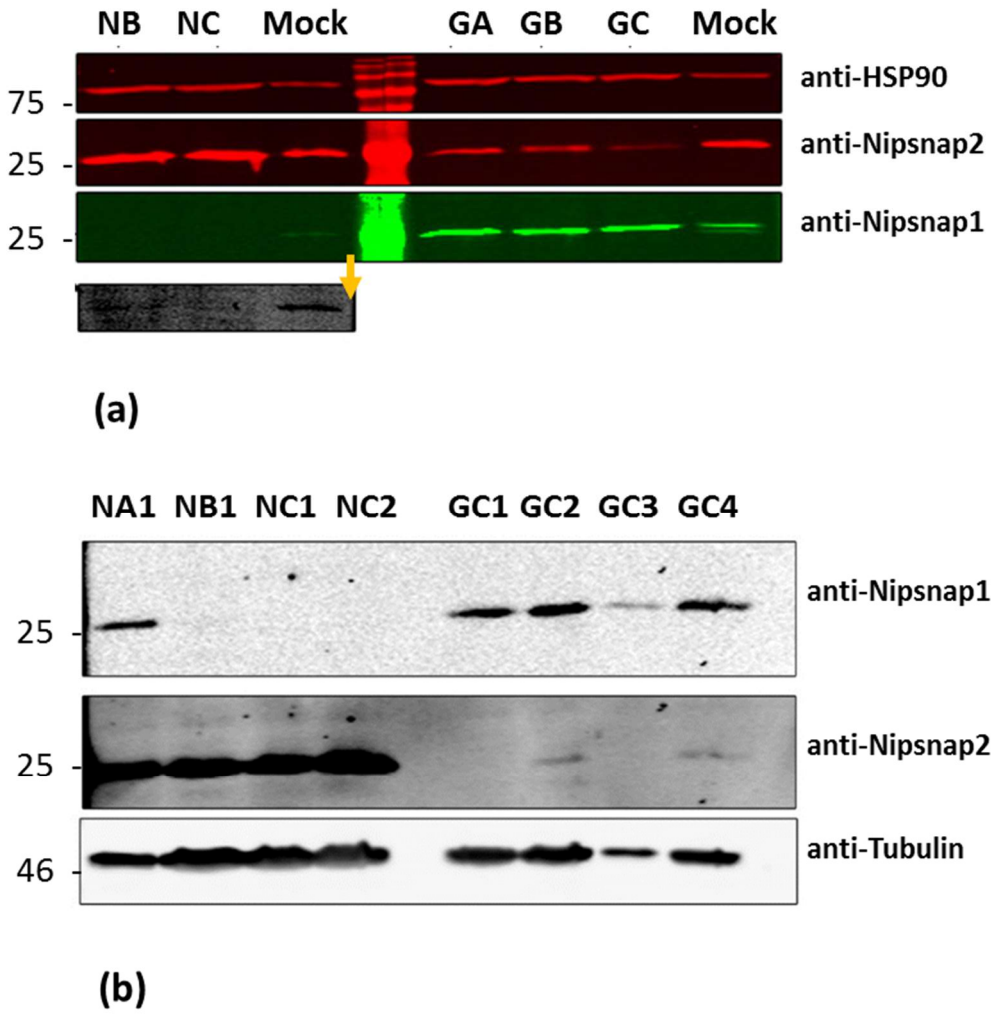

Figure 6.3 | Nipsnap1 and 2 expressions in WT- and CRISPR KO HaCaT cells. Wild type and CRISPR KO HaCaT cells were lysed and proteins were separated by SDS-PAGE and analysed by WB using the antibodies indicated. (a) NB, NC or GA, GB, GC indicates lysate from Nipsnap1 or 2 KO cell population respectively. (b) NA1, NB1, NC1, NC2 or GC1, GC2, GC3 GC4 indicates isolated single cell clones from Nipsnap1 or 2 KO cells. Molecular mass markers (in KDa) are shown on the left. HSP90 or tubulin was included as a loading control.

Once successful KO clones for Nipsnap1 and Nipsnap2 individually were obtained, these were used to try and generate double KO cells lacking both Nipsnap1 and Nipsnap2. Each of the three clones lacking Nipsnap1 (NB1, NC1 and NC2) were transfected with Nipsnap2 gRNA GC and two clones lacking Nipsnap2 (GC1 and GC2) were transfected with Nipsnap1 gRNA NC using the same procedure as above. The GC3 clone looked promising though eventually died off. Knocking out a second gene relies on the single cell clones having lost the original PX459 plasmid derivative so they will be puromycin sensitive again. After puromycin treatment and recovery the selected populations were tested by WB for both Nipsnap1 and Nipsnap2 expression. As can be seen in Figure 6.4 (a) the population derived from the NC2 clone that was transfected with the GC gRNA showed the most promise as it still had absence of Nipsnap1 and a substantially reduced Nipsnap2, although the loading of this sample was lower. Single cloning was conducted on the NC2+GC population and 7 clones were tested by WB. All clones looked promising with no detectable Nipsnap1 or Nipsnap2 bands, with the possible exception of clone 17 (Figure 6.4 b). Clones 4 and 6 were selected for further experiments.

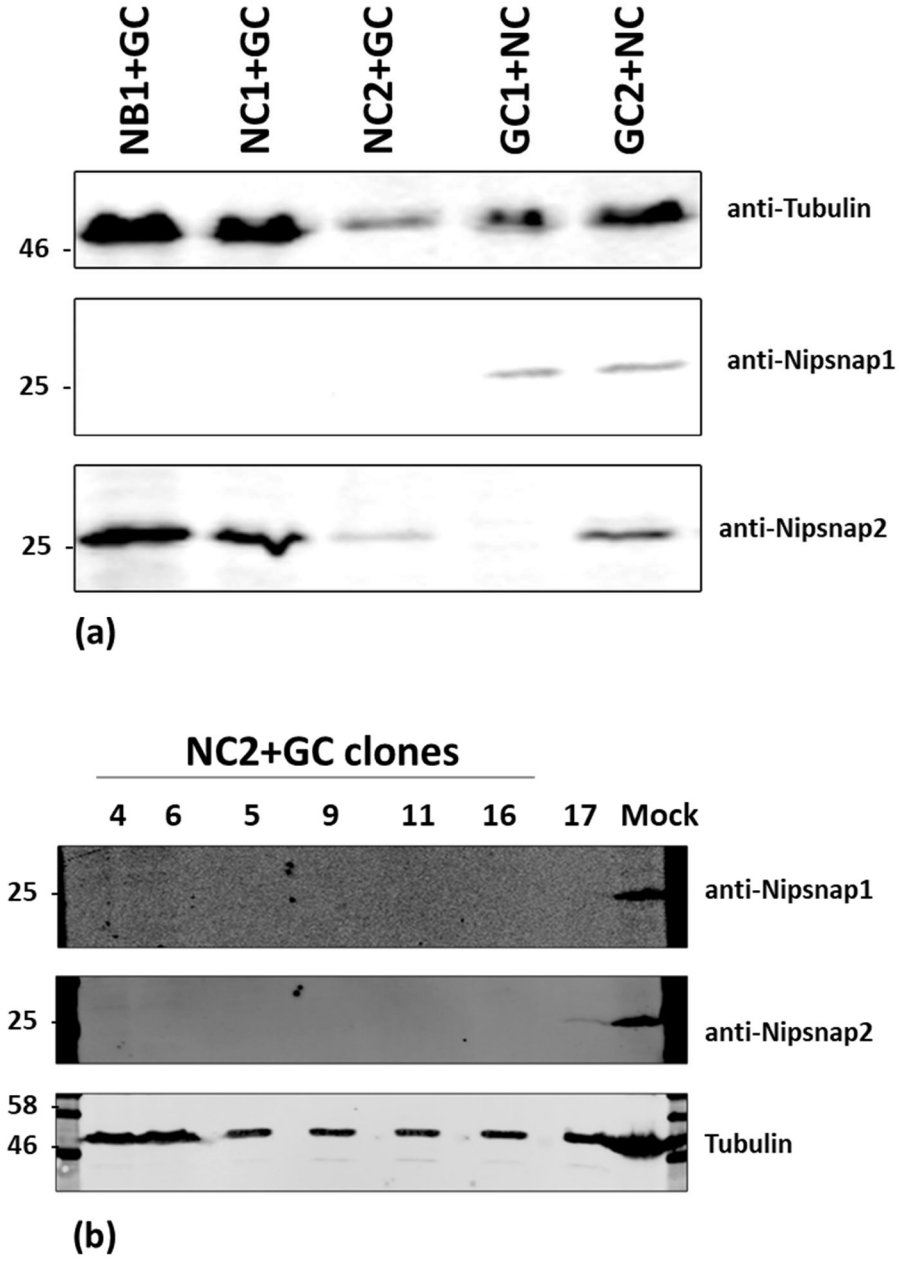

Figure 6.4 | Nipsnap1 and 2 expression in double CRISPR KO HaCaT cells. Double CRISPR KO HaCaT cells were lysed and proteins were separated by SDS-PAGE and analysed by WB using the antibodies indicated. Molecular mass markers (in KDa) are shown on the left. Tubulin was included as a loading control. (a) NB1+GC, NC1+GC and NC2+GC indicates population of cells where attempts were made to KO Nipsnap2 in the Nipsnap1 KO clones and GC1+NC and GC2+NC indicates population of cells where attempts were made to KO Nipsnap1 in the Nipsnap2 KO clones. (b) Number 4, 6, 5, 9, 11, 16 and 17 indicate isolated clones of NC2+GC population.

6.2.3 Sequencing of the Nipsnap KO clones

Selected clones from single and double KOs were then sequenced to identify the changes in targeted region of genome. Firstly, the target exons were amplified via PCR and then inserted into 'PCR-Blunt II-TOPO' vector as per manufacturer's instructions (Zero Blunt TOPO, Invitrogen). The resulting reaction mixtures were directly transformed into competent *E. coli* DH5α cells and plated on kanamycin agar plates. Colonies from the agar plates were subsequently grown and plasmid DNA was isolated by miniprep. The samples were sent for sequencing with M13 forward primer.

A total of 13 samples from NC1 clones were sent for sequencing of Nipsnap1 exon 4 of which 10 could be aligned to the parent sequence and the remaining 3 could not be aligned (Figure 6.5 a). The 10 sequences aligned as four different genetic variants (45, 35, 24 and 8 bases deletion) which matches the fact that HaCaT cells have been shown to be hypotetraploid (Boukamp et al., 1988). Of the four samples sent for NC2 clone sequencing, only two had alignable sequences and both had the same sequence as NC1 variant.1. This could possibly mean NC1 and NC2 are decendants of the same clone hence are not independent clones. For the Nipsnap2 exon 6 KO clones five out of nine samples for GC1 and one out of four samples for GC2 had alignable sequences to the parent exon sequence. The GC1 clones appeared as three different genetic variants (79 bases addition, 8 bases missing and 2 bases addition) (Figure 6.5 b). The GC2 clone had only one base deletion. A total of eleven and four samples were sent for sequencing of Nipsnap2 exon 6 from the double KO clone 4 and 6 respectively. Of these nine from clone 4 were aligned as three different genetic variants (1 base addition, 10 bases deletion and 8 bases deletion). Interestingly, the same variants were also seen in clone 6 sequences. This again suggests Clone 4 and 6 are not independent clones. Given that the original publication describing the HaCaT cell line showed that the chromosomes that contain the Nipsnap1 gene (chromosome 22) and Nipsnap2 gene (chromosome 7) are present in four copies, further sequencing will be required to confirm the nature of all genetic lesions in these single cell clones that lack protein expression of Nipsnap1 and Nipsnap2.

Nipsnap1 and 2 both have two predicted cellular variants where variant 2 of each protein is 20 and 39 amino acid shorter respectively. Both variants of Nipsnap1 have exo n4 and Nipsnap2 have exon 6 intact (Appendix Figure 9.3). The anti-Nipsnap1 antibody (sc-515197, Santa Cruz

Biotechnology) used in this study recognises protein sequences within the exon 4 region whereas the anti-Nipsnap2 antibody (ab204890, abcam) binds to protein sequences coming from around exon2 of the gene. Where 45 (variant 1) and 24 (variant 3) base pair deletions in exon 4 of Nipsnap1 were observed in the NC1 clone, the resulting gene sequence could be translated and give rise into slightly smaller version of the Nipsnap1 protein with internal deletions. Since both of these deletions are within exon 4 the anti-Nipsnap1 antibody used in the study may not recognise these variants, and so it is impossiblel to be certain that mutated forms of Nipsnap1 are still expressed but undetectable, which could be functional. The other two variants (2 and 4) of mutated Nipsnap1 gene in theNC1 clone have a frame-shift and would be translated into much smaller proteins (<15 KDa) with altered sequences near the antibody binding site (Appendix Figure 9.4 a). An antibody that recognises a different region of Nipsnap1 will be needed to confirm complete KO of gene expression. The deletion of Nipsnap2 was more convincing as the antibody binds to the region encoded by exon 2 upstream of the gRNA target region (exon6). All the sequence variants of Nipsnap2 identified in GC1, GC2 or double KO clone 4 and 6 would only be able to produce truncated Nipsnap2 protein (Appendix Figure 9.4 b and c).

The six final selected clones were renamed for simplicity: The two Nipsnap1 KO clones (NC1 and NC2) are termed N1a and N1b, the two Nipsnap2 KO clones (GC1 and GC2) are termed N2a and N2b, and the double KO clones (Clone 4 and Clone 6) are termed NNa and NNb in all subsequent data. Figure 6.6 shows WB data for all six of these KO cells in parallel with WT cell lysate control and with equivalent loading. As can be seen Nipsnap1 is absent in the N1a, N1b, NNa and NNb, and Nipsnap2 is absent in N2a, N2b, NNa and NNb. Tubulin indicates loading of the protein samples among different lanes. In the single KO cells, no obvious reduction in cell growth or viability was observed during cell passage and maintenance. While the GC2 clone appeared to expresse some Nipsnap2 during initial tests (Figure 6.3), after several passages the protein was undetectable in this clone by WB (Figure 6.6). The possible explanation for this could be overtime the KO population out-competed the WT cells. The double KO cells appeared to grow slightly slower at early stages after initial single cell cloning, although this seemed to recover after a few passages and the growth rate became close to the WT HaCaT. This suggests Nipsnap1 and 2 both are non-essential for HaCaT cell viability, although it is possible there was some minor adaptation in the double KO clones.

Nipsnap1 exon4

GGAGGCTGTGCTGCCCAAGCTTCACCTGGATGAGGACTACCCATGCTCACTCGTGGGCAACTGGAA
CACGTGGTATGGGGAGCAGGACCAGGCAG

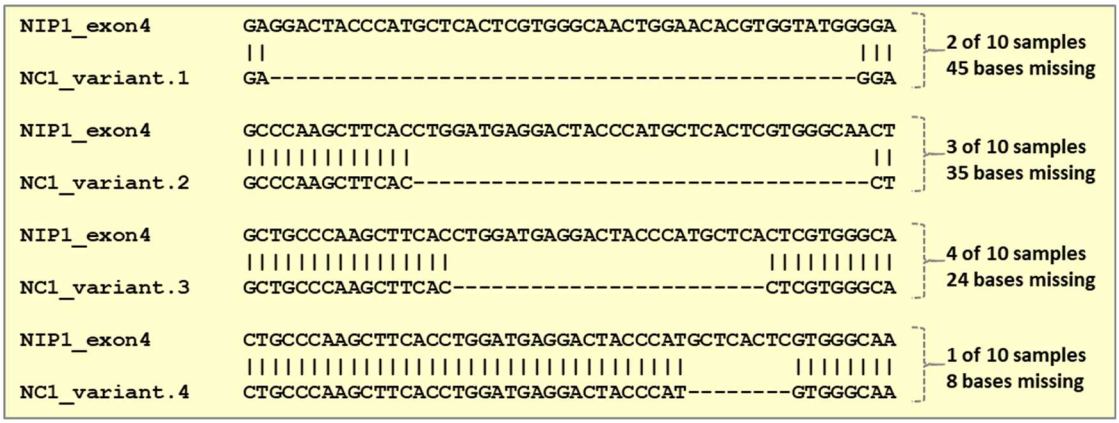

10 out of 13 samples sequenced could be aligned to the parent exon and 3 were unrelated sequences

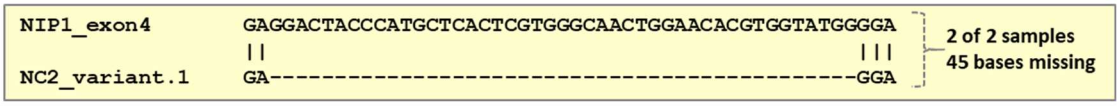

2 out of 2 samples sequenced could be aligned to the parent exon and 2 were unrelated sequences

(a)

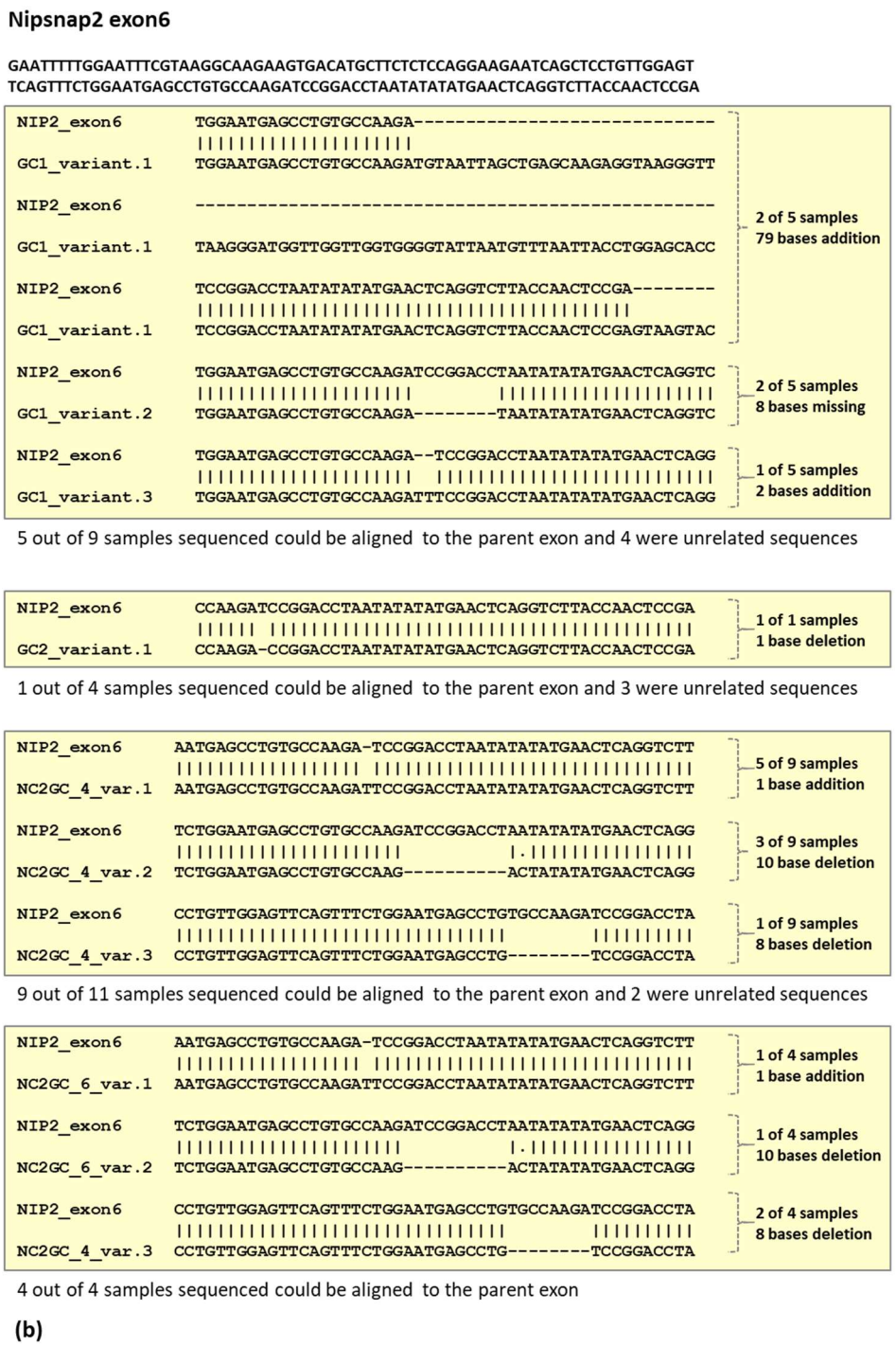

Figure 6.5 | Sequence alignment of Nipsnap1 and 2 genes between WT- and CRISPR KO HaCaT cells. Wild type and CRISPR KO HaCaT cells were lysed and whole cell DNA were extracted for sequencing of Nipsnap1 exon 4 and Nipsnap2 exon 6 as required. (a) Nipsnap1 exon 4 sequence alignment of NC1 and NC2 clones and (b) Nipsnap2 exon 6 sequence alignment of GC1, GC2 and double KO (NC2+GC) 4 and 6 clones are shown. Acquired changes in genes are indicated on right within a box.

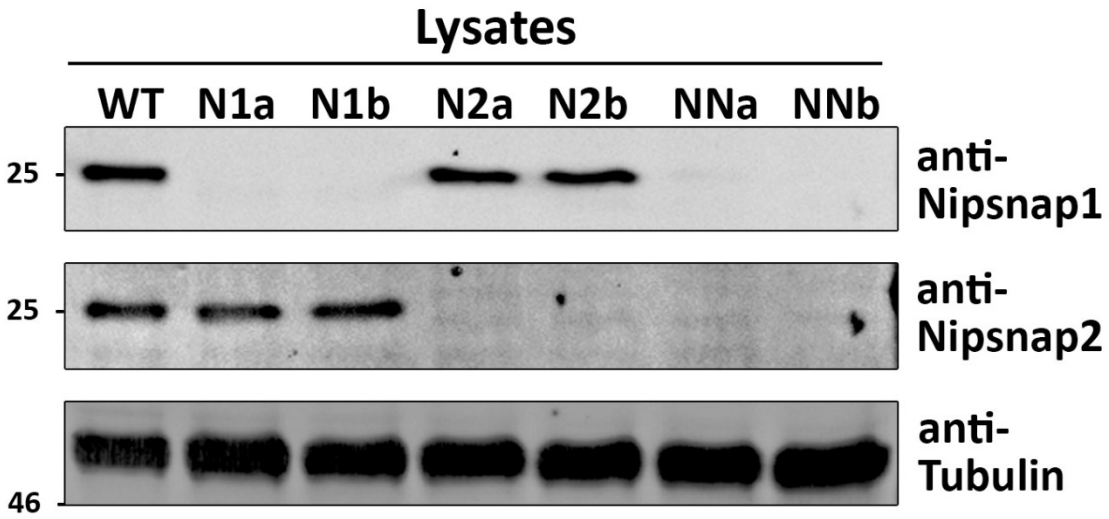

Figure 6.6 | Nipsnap1 and 2 expressions in WT- and CRISPR KO HaCaT cells. Wild type and CRISPR KO HaCaT cells were lysed and proteins were separated by SDS-PAGE and analysed by WB using the antibodies indicated. Molecular mass markers (in KDa) are on the left. Tubulin was included as a loading control. N1a and N1b indicates two independent clones of Nipsnap1 KO cells from a single gRNA (NC); N2a and N2b indicates two independent clones of Nipsnap2 KO cells from a single gRNA (GC); and NNa and NNb indicates two independent clones of both Nipsnap1 and Nipsnap2 KO cells, which are both derived from the N1b parent clone treated with a single gRNA (GC).

6.2.4 Analysis of Nipsnap2 expression by immunofluorescence

To further confirm successful KO and investigate effects on protein localisation CRISPR clones were fixed and stained with antibodies against Nipsnap1 and Nipsnap2. As can be seen in Figure 6.7 a Nipsnap2 antibody signal could be detected in a thread-like pattern, reminiscent of mitochondria, in WT, N1a and N1b HaCaT cells. Surprisingly, a faint signal with a similar pattern was also observed in both Nipsnap2 KO clones (N2a and N2b) despite the fact that no Nipsnap2 was detected in these cell lines by WB analysis. Since Nipsnap1 and 2 have high sequence similarity (75%), this could represent some cross-reactivity of the anti-Nipsnap2 antibody with endogenous Nipsnap1 in IF but not WB. In support of this, no signal for Nipsnap2 could be observed in the double KO cells (NNa and NNb). Unfortunately, loss of Nipsnap1 could not be confirmed by IF microscopy as only very weak signals were detected for the Nipsnap1 antibody, which did not appear to change in Nipsnap1 or double KO clones, suggesting this signal is background.

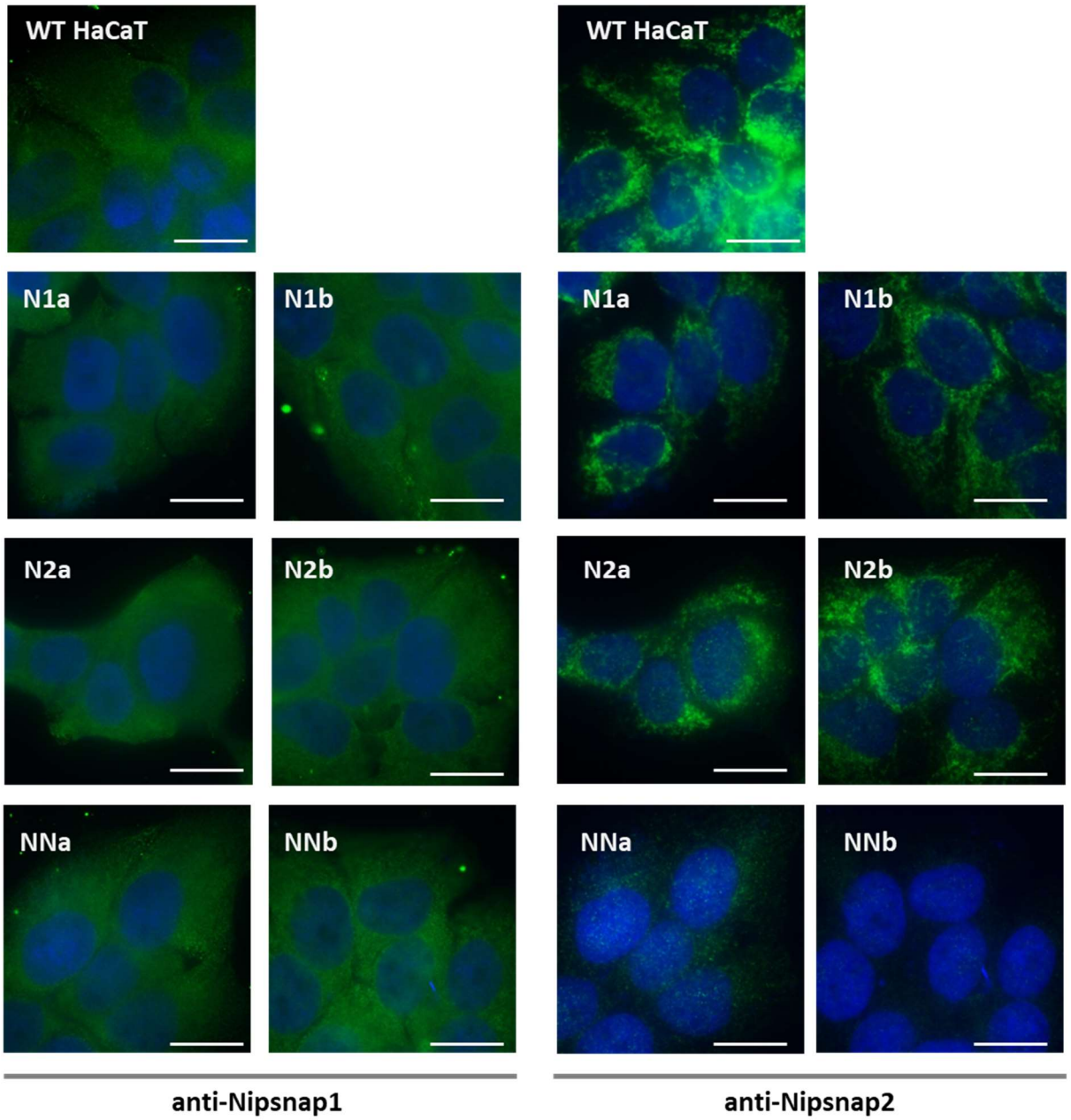

Figure 6.7 | Nipsnap1 and 2 expression in WT and CRISPR-Cas9 KO HaCaT cells. Wild type and CRISPR KO HaCaT cells were seeded on glass slides and fixed, permeabilised and stained with Nipsnap1 and Nipsnap2 specific antibodies followed by staining with relevant secondary antibodies. Images were taken using an Olympus IX-81 inverted fluorescence microscope using a 60x oil immersion lens. Blue: staining of nuclei with DAPI. Scale bar indicates 20 μm.

6.2.5 Protein expression and gE immunoprecipitation analysis of HSV-1-infected CRISPR-Cas9 KO cells

To investigate whether the interaction of gE with Nipsnap1 and 2 or protein expression is affected in the CRISPR-Cas9 KO cells, WT HaCaT and the single and double KO clones cells were infected with WT HSV-1 and immunoprecipitated with anti-gE (MAb-3114). Figure 6.8 shows Nipsnap1 can be precipitated from WT and both Nipsnap2 KO clones but not from single and double KO cells lacking Nipsnap1. However, while Nipsnap2 was co-precipitated with gE from WT HaCaT cells, this was substantially reduced in Nipsnap1 KO cells suggesting the interaction of Nipsnap2 with gE is dependent on Nipsnap1. Precipitation of all other proteins were consistent with previous observations with somewhat variable pull-down for gB and VP5 from all cell lines, potentially reflecting interaction of gE with these proteins or precipitation of virions. PHB, another mitochondrial localised protein that was a potential but un-validated hit from the gE/gI interactome screen, did not show any specific co-precipitation with gE from any sample.

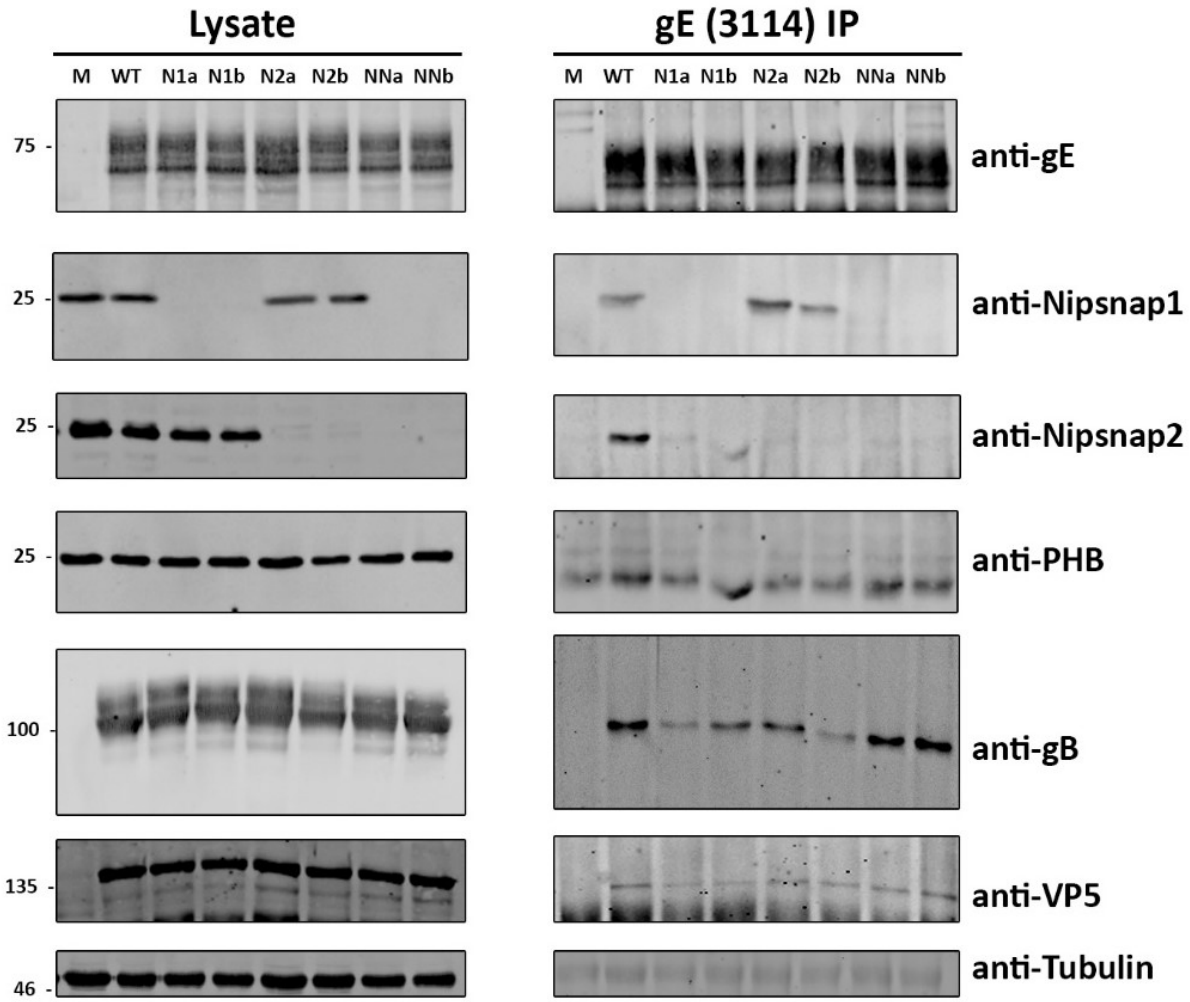

Figure 6.8 | Immunoprecipitation of gE from HSV-1-infected Nipsnap1 and 2 KO cells. WT and Nipsnap1 or 2 or double KO HaCaT cells were infected with WT HSV-1. At 16 hpi the cells were lysed and proteins were separated by SDS-PAGE and analysed by WB using the antibodies indicated. Molecular mass markers (in KDa) are on the left. Tubulin and PHB were included as loading controls.

6.2.6 Replication and release properties of WT and gE/gI mutant viruses on CRISPR-Cas9 KO cells

Given that Nipsnap1 and 2 contain SNAP25-like domains and thus have the potential to function in membrane trafficking, the potential role of these proteins in the control of HSV-1 secretion by gE/gI was investigated. The prediction was that deletion of Nipsnap1 and/or 2 may cause similar effects as the loss of gE/gI function on the secretion of HSV-1. To investigate this WT HaCaT, Nipsnap1 KO (N1a, N2a), Nipsnap2 KO (N2a, N2b) and double KO (NNa, NNb) cells were infected with WT and ΔgE HSV-1 and the CA and Sup samples were collected at 10 hpi, a time point that showed the greatest difference in virus release between WT and gE/gI mutant viruses (Chapter 2). However, contrary to expectations no noticeable effect of deletion of Nipsnap1 and/or 2 was observed on replication or release for the HSV-1 WT and ΔgE virus (Figure 6.9 a, b and c). Figure 6.9 (a) and (b) show CA and Sup titre and total virus titre were very similar in WT- and Nipsnap1- and 2- KO HaCaT cells, and Figure 6.9 (c) shows there was no effect of Nipsnap1 or 2 loss on the percentage of virus release for HSV-1 WT and ΔgE viruses. This could suggest that (1) Nipsnap1 and 2 interaction with gE might have functions other than targeted virion delivery, (2) other cellular protein/s may compensate for the loss of Nipsnap1 and 2 during HSV-1 virion release, and (3) the observed interactions of Nipsnap1 and 2 with gE does not normally occur in cells due to Nipsnap1 and 2's localisation to mitochondria and the interaction only occurs when the cells are detergent solubilised or in cell free preparations.

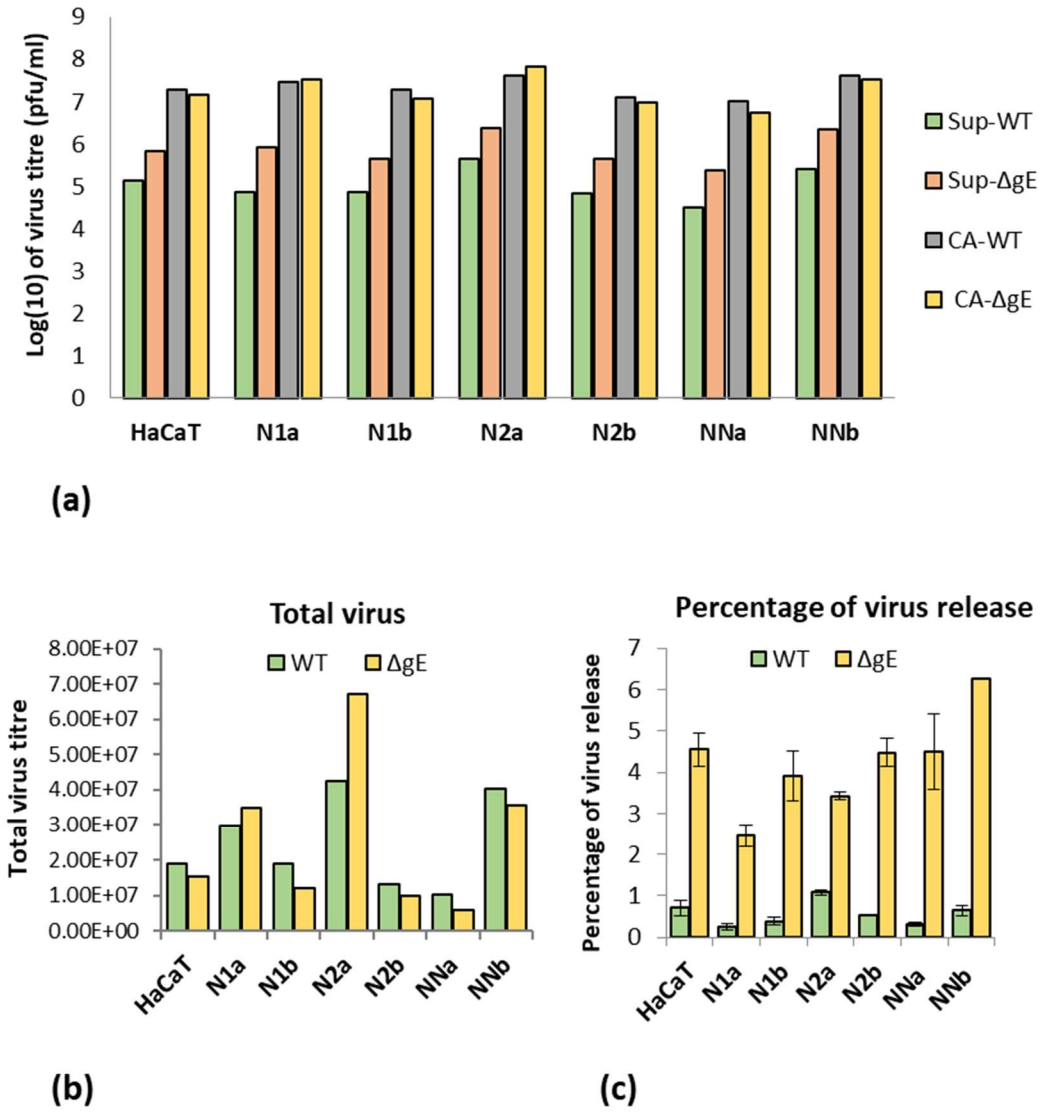

Figure 6.9 | Replication and release of HSV-1 WT and ΔgE in different CRISPR-Cas9 KO HaCaT cell lines. WT and Nipsnap1 (N1a and N1b) or Nipsnap2 (N2a and N2b) or Double (NNa and NNb) KO HaCaT cells were infected with HSV-1 WT and ΔgE viruses at 10 PFU/cell. At 10 hpi extracellular (Sup) and cell-associated (CA) viruses were collected and titred on Vero cell monolayers. (a) compares CA and Sup titre on log(10) scale (b) indicates total amount of infectious virus produced in the experimental cell lines and (c) indicates percentage of virus release. Each experiment was repeated at least three times. Data presented here is from a single representative experiment containing duplicate samples. Error bars indicate standard error of two biological replicates.

6.2.7 Localisation of gE and gE/gI in the Nipsnap KO cells by immunofluorescence

To investigate whether loss of Nipsnap1 and/or 2 alters gE localisation, WT and Nipsnap KO HaCaT cells were infected with WT HSV-1. At 15 hpi the cells were stained for gE and another HSV-1 glycoprotein gB. As can be seen in Figure 6.10 (a) gE demonstrated a punctate distribution showing some overlap with gB in the cytoplasm of all the cell lines and no obvious difference could be observed. These experiments were repeated on N1b, N2a, NNa and WT HaCaT cells and stained for the gE/gI complex and gB to understand Nipsnap1 or 2 has a specific role on the localisation of gE only when it is in complex with gI (Figure 6.10 b). However, as with gE staining, the localisation of the gE/gI complex in the KO cell lines looked similar to that in the WT HaCaT cells. This suggests gE or gE/gI localisation does not depend on Nipsnap1 or 2, although HaCaT cells are small with the cytoplasm appearing relatively compact in fluorescence microscopy, and so subtle effects on protein localisation may not be apparent.

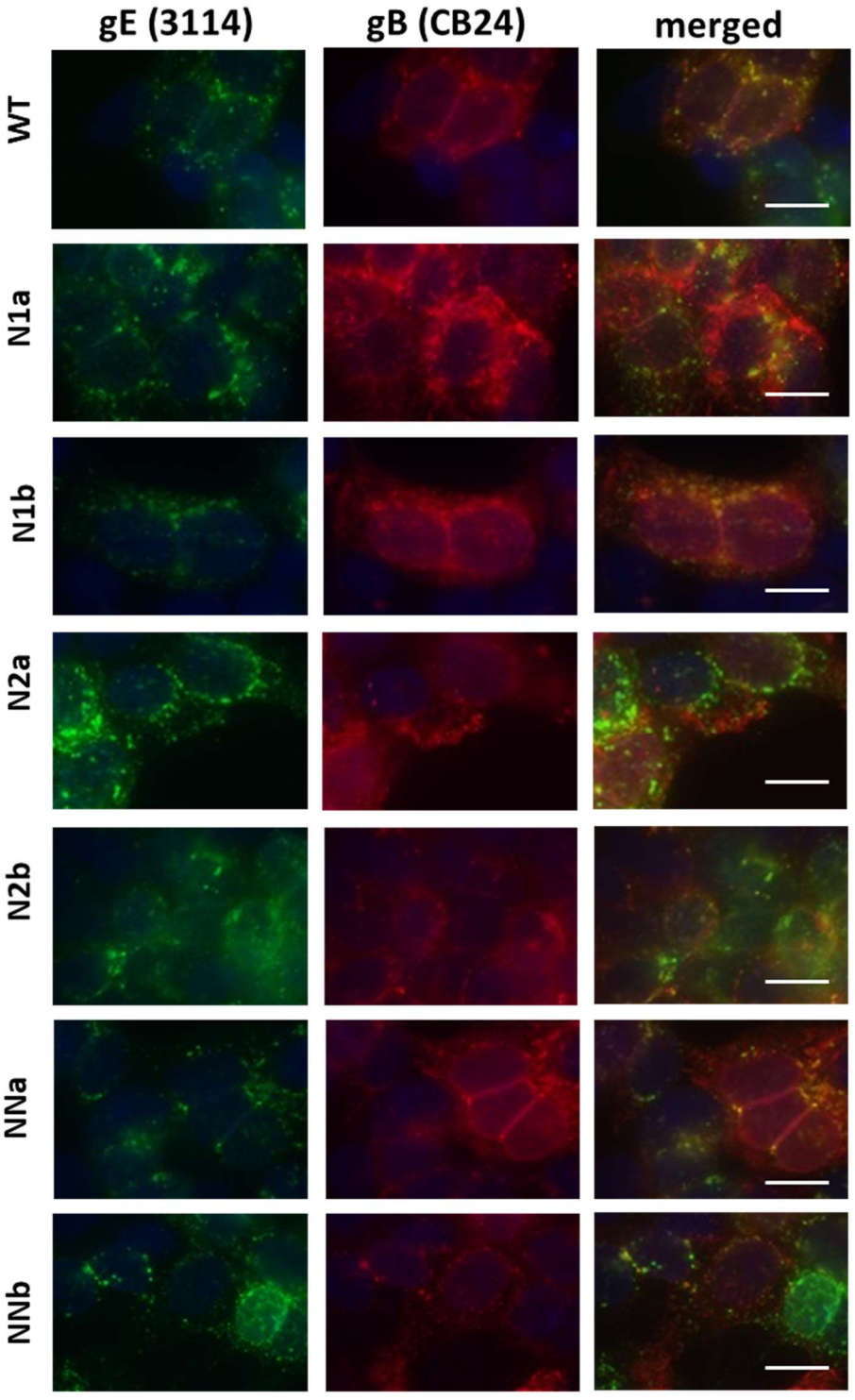

(a)

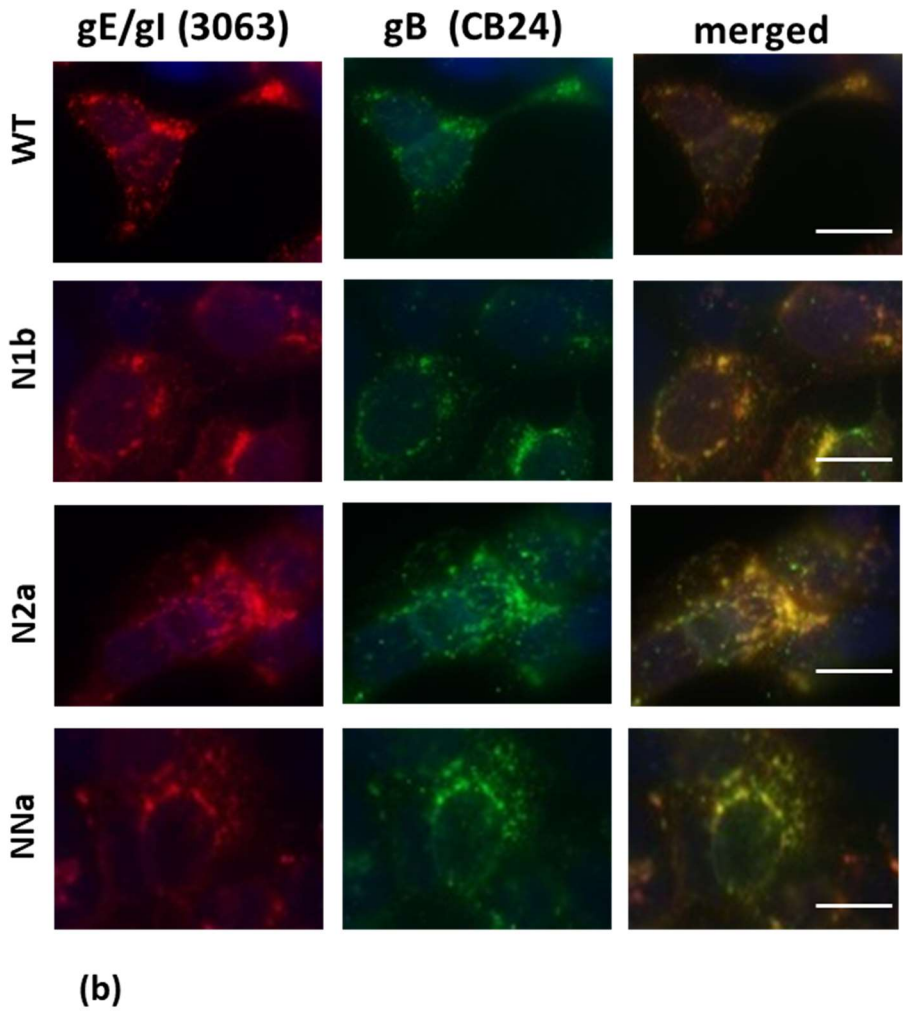

Figure 6.10 | Localisation of HSV-1 gE, gE/gI and gB in WT and CRISPR-Cas9 KO HaCaT cells. Wild type and CRISPR KO HaCaT cells were infected with WT HSV-1. At 15 hpi the cells were fixed, permeabilised and stained with (a) gE (MAb-3114; IgG2a) and gB (MAb-CB24; IgG2b) and (b) gE/gI (MAb-3063; IgG1) and gB (MAb-CB24; IgG2b) specific antibodies followed by staining with subtype-specific secondary antibodies. N1a and N1b indicate two independent clones of Nipsnap1 KO cells; N2a and N2b indicate two independent clones of Nipsnap2 KO cells; and NNa and NNb indicate two independent clones of both Nipsnap1 and Nipsnap2 KO cells. Images were taken using an Olympus IX-81 inverted fluorescence microscope using a 60x oil immersion lens. Blue: staining of nuclei with DAPI. Scale bar indicates 20 μm.

6.2.8 HSV-1 plaque morphology in CRISPR-Cas9 KO HaCaT cells

HSV-1 plaque assays are useful for monitoring the function of viral and cellular proteins in cell-to-cell spread of virus during infection. Plaques are thought to be generated primarily by delivery of virions to the cell-contacts which allows efficient penetration of the neighbouring cells. To investigate the potential roles of Nipsnap1 and 2 in HSV-1 cell-to-cell spread, the plaque size and morphology were analysed on the KO cell lines by infected the cell monolayers with < 50 PFU for 72 h under semi-solid media. Plaques formed by HSV-1 WT, gIG39R, ΔgE and ΔgI were analysed. The morphology of WT HSV-1 plaques on the WT HaCaT cell monolayers show a clearly defined large region of cytopathic effect (cpe) around the rim of the plaques with a hollow space within the centre using toluidine blue staining of cells (Figure 6.11 a). The morphology is clearer using a primary antibody to HSV-1 (gD monoclonal antibody LP2) followed by HRP-coupled secondary antibody staining and DAB reaction (6.11 b and c). For WT HSV-1, plaques on the Nipsnap1 or 2 KO cells were slightly different in appearance. The overall size appeared to be similar, although a slight variation in morphology was observed with the central hollow space appearing smaller with Nipsnap1 KO cells and larger on Nipsnap2 KO cells, with consequently wider or narrower antigen-positive areas of cpe at the plaque rims. Plaques on the double KO cell lines appeared to be much smaller in some experiments (6.11 a and b) but in other experiments such differences became negligible (Figure 6.11 c) and the plaques became more similar to the plaques on the parental HaCaT cells. The initial differences in plaque morpholgy could be linked to the seeded cell density during experimental setup. The plaques formed by gIG39R, ΔgE and ΔgI were smaller than those formed by WT HSV-1 as previously shown (Figure 2.18). Surprisingly, the plaque size of all three mutant viruses were bigger on the Nipsnap1, Nipsnap2 and double KO cell monolayers compared to the parental HaCaT cell line. This is particularly evident for the Nipsnap2 KO cell line. These data suggest that, contrary to expectations of a proviral role for Nipsnap1 or 2 in gE/gI-dependent virus transport, expression of Nipsnap1 and 2 may inhibit HSV-1 cell-to-cell spread in the absence gE/gI function.

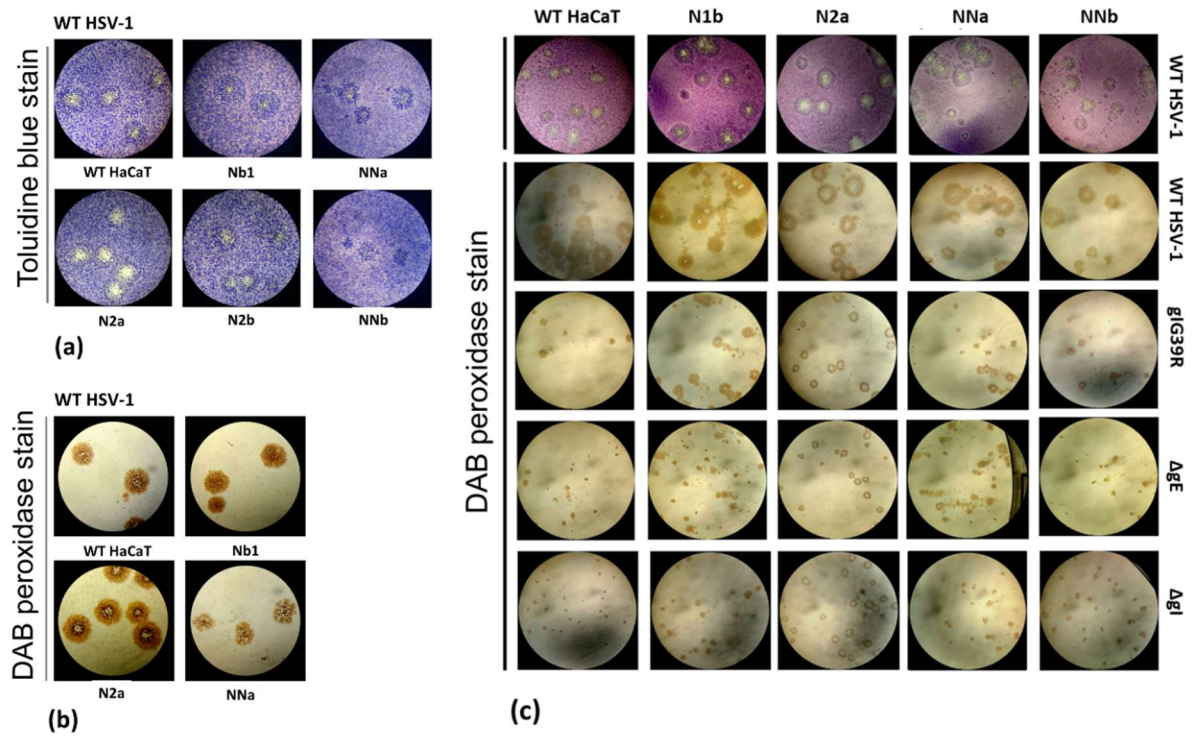

Figure 6.11 | Plaque morphology analysis on WT and CRISPR-Cas9 KO HaCaT cells. Representative images of plaques of (a) WT HSV-1 and (b) the indicated viruses on wild type, (c) Nipsnap1 KO, Nipsnap2 KO, and Nipsnap1+2 KO HaCaT cells. (a) and first row of (c) indicates toluidine blue staining and the rest of the images indicate DAB peroxidase staining of the plaques. For DAB peroxidase staining cells were fixed and treated with anti-gD antibody (MAb-LP2) followed by HRP-secondary anti-mouse antibody and developed with DAB kit.

6.3 Discussion

The functions of Nipsnap1 and 2 within cells are currently unclear, although they have been proposed to play roles in mitochondria-related signal transduction during innate immune responses, in the process of autophagosome and lysosome fusion and in the regulation of Ca^{2+} entry into the cells (Behrends et al., 2010; Schoeber et al., 2008; Brittain et al., 2012). The primary aim of this chapter was to understand the biological significance of Nipsnap1 and 2 in the HSV-1 life cycle by knocking out the protein coding genes utilising CRISPR-Cas9 technology. While the Nipsnap1 and double KO clones apparently lacked the Nipsnap1 protein band in WB analyses it can't be ruled out that some mutant variants of Nipsnap1 lacking the antibody epitopes are produced in these cell lines. Additionally, there was some mitochondria-like signal for Nipsnap2 in the Nipsnap2 KO clones. Given the fact that Nipsnap1 and 2 are very similar in terms of their amino acid sequence it is possible that the anti-Nipsnap2 antibody binds to Nipsnap1 when there is no Nipsnap2 present. The other alternative could be that these cells are still expressing some Nipsnap2 which were undetectable by WB, although this seems less likely because the genome sequence of the KO clones confirmed frame-shift mutations in the Nipsnap2 gene.

The single time point replication of HSV-1 WT and ΔgE virus did not show any difference between the WT-HaCaT and Nipsnap1 and 2 KO cell lines. This suggests that Nipsnap1 and 2 do not function during virus replication. However it may be also possible that other cellular proteins carry out similar functions in the absence of Nipsnap 1 and/or 2. Subtle differences in plaque morphology were observed on the KO cell lines compared to WT HaCaT cells, although it is unclear if these variations could be a consequence of single cell cloning and not directly related to Nipsnap1 or 2 functions. Interestingly, all three mutant viruses that lack functional gE/gI (gIG39R, ΔgE and ΔgI) demonstrated larger plaques on the KO cells than WT HaCaTs. This may suggest that Nipsnap1 and 2 have an inhibitory effect on HSV-1 spread, which is normally antagonised by gE/gI. While it is unclear how Nipsnap proteins may impact HSV-1 spread, and whether this is related to proposed mitochondrial or other functions of these cellular proteins, these will be interesting questions for future studies.

7. Concluding remarks

7.1 Complexity of HSV-1 envelopment and egress

Many aspects of the life cycle of HSV-1 depend on proper functioning of its envelope glycoproteins, including virus entry, secondary envelopment and cell-to-cell spread. The envelope glycoproteins work in a co-ordinated fashion and also exhibit some functional redundancy between them and therefore determining the role of an individual glycoprotein is often difficult. As an example, gC binds to host cell surface heparan sulphate proteoglycans (HSPGs) which is important for virion attachment, although gB also has HSPG-binding activity and so gC deletion viruses replicate in cell culture without any major defect (Cai et al., 1988; Herold et al., 1991; Shukla and Spear, 2001). Furthermore, gE and gD have both been shown to interact with tegument proteins and show functional redundancy during secondary envelopment, for example a gE deletion virus replicates as efficiently as the WT virus in culture and does not exhibit any defect in the secondary envelopment process (Farnsworth et al., 2003; this thesis). Therefore, often two or more glycoproteins need to be deleted to understand their role in the HSV-1 life cycle. For secondary envelopment to occur viral envelope glycoproteins must accumulate in the same intracellular membrane compartment(s) via membrane traffic pathways, which commonly pass via the plasma membrane (Hollinshead et al., 2012; Johns et al., 2014; Albecka et al., 2016), and within these compartments further interplay between tegument and capsid proteins is necessary to wrap the particles. Therefore, a balanced co-ordination is expected to occur among envelope-tegument-capsid protein interactions to facilitate efficient virion assembly. Mutation(s) of glycoproteins or tegument proteins could result in defective envelopment and eventually egress. HSV-1 egress most likely occurs after the completion of secondary envelopment, although some evidence suggests egress in neurons can begin before or during secondary envelopment (reviewed in Johnson and Baines, 2011). Controlled and directed virion egress is observed during HSV-1 infection until late time points of infection, after which the infected cells lose their integrity. In polarised cells virus egress is targeted to cell-cell junctions, whereas in non-polarised cells virions appear to be targeted to adherent points that are in contact with other cells or with the culture plate, as has been reported previously (Mingo et al., 2012) and also found in this thesis. Cellular proteins are undoubtedly important to transport the virion loaded vesicles towards the plasma membrane and also for specific targeting to cell junctions or cell-adherent sites. However, very little information regarding the host proteins utilised by HSV-1 to achieve this is available.

7.1.1 The role of the gE/gI complex during assembly and egress of HSV-1

The role of the gE/gI complex during HSV-1 replication can be divided into three main activities (i) during secondary envelopment (ii) during egress and (iii) after egress. Related to secondary envelopment, gE/gI has been shown to interact with pUL11, pUL13, pUL16, pUL21 and pUL49 (Fuchs et al., 2002; Han et al., 2012; Ng et al., 1998; Farnsworth et al., 2007). Deletion of either gE or gI does not seem to affect incorporation of pUL49 into purified virions as observed in this thesis and mentioned elsewhere (Fuchs et al., 2002), although pUL49 has also been shown to interact with gM (Maringer et al., 2012). pUL11, pUL16 and pUL21 have been shown to require each other and the cytoplasmic domain of gE for their proper localisation within cells (Han et al., 2012). Similarly, maturation of both gE and gI, and accumulation of pUL13 has been proposed to depend on each other (Ng et al., 1998). However, as demonstrated in this thesis gE and gI deletion mutants can replicate to WT level and no obvious defect in envelopment can be observed by electron microscopy studies, supporting the idea of a functional redundancy between gE/gI and other glycoproteins during envelopment, as has been proposed by other researchers (Farnsworth et al., 2003; Farnsworth and Johnson, 2006).

The requirement for gE/gI during directional HSV-1 egress is well established. Data in this thesis have demonstrated that deletion of either gE or gI, or a mutant of gI that cannot interact with gE, causes enhanced virion egress into the cell culture medium in addition to the reduced cell-to-cell spread (small plaques) phenotype previously observed (Farnsworth and Johnson, 2006; Wisner et al., 2000). The most likely explanation for these observations is the loss of gE/gI function causes more random egress of HSV-1 all over the plasma membrane, including the exposed cells surfaces not in contact with the culture dish or other cells, enabling more virions to detach into the culture medium.

While the importance of gE/gI for targeted HSV-1 egress is clear, exactly how gE/gI contributes to this is unknown and was the main focus of this thesis. The gE/gI ectodomains have been shown to be important for cell-to-cell spread (Wisner et al., 2000), although this may have had an impact on protein stability or targeting to assembling virions. The cytoplasmic tail of gE has TGN/endosome sorting motifs and has also been shown to be required for directed virion transport (Johnson et al., 2001; McMillan and Johnson, 2001). Since newly assembled HSV-1 virions are contained in vesicles prior delivery to the plasma membrane, viral membrane proteins that may be present in the membrane of those vesicles could function in the transport and targeted delivery of the virion inside. When the gE/gI complex is disrupted

the normal pathways of virion egress appear to be lost, suggesting gE/gI must be one of the viral factors that is present on these virion-transport vesicle membranes, with their cytoplasmic domains available to recruit and/or regulate cellular trafficking regulators. The work in this thesis suggests that the cytoplasmic domain of gE mediates interaction with putative cellular binding partners. Therefore, exactly how gI contributes to the function of gE/gI during virus egress is obscure. The expression of gI could help gE folding and maturation, as suggested from WB data in HaCaT cells during infection. The formation of the heterodimeric complex between the of gI and gE ecto-domains, which is important for the Fc-binding activity, as well as the extensive phosphorylation of the CT domains of both gE and gI that has previously been observed, may regulate the trafficking of gE/gI and therefore directed transport of the virion loaded vesicles (Edson, 1993; Alconada et al., 1996; Olson and Grose, 1997; Wisner et al., 2000).

The relative importance of gE and gI may vary in other alphaherpesviruses. In PrV the gI CT domain is necessary for efficient posttranslational modification of the gI protein, while the gE CT domain seems to be dispensable for the maturation of the gE protein. In addition, the gI CT domain appears to have a greater role in promoting *trans*-synaptic virion spread compared to the gE CT domain in PrV (Tirabassi and Enquist, 2000). In feline herpesvirus (FHV) gE was completely retained in the ER when gI was deleted, although the gI CT domain was non-essential for gE/gI mediated cell-to-cell spread (Mijnes et al., 1996).

In HSV-1 the interaction site(s) between gE and gI are poorly defined and no mutagenesis study with the gI ecto-domain that destabilises the gE/gI complex has been published. The work in this thesis has demonstrated that the G39R mutation in gI inhibits its ability to form a complex with gE, leading to a destabilisation of gI (in all cell lines) and in some cell types gE (in HaCaT cell line). The destabilising effect of the G39R mutation on gI appears to be more than just due to loss of interaction with gE however, as gI expression is greater in the gE deletion virus than the gIG39R virus. A previous study using insertional mutagenesis of the gE ectodomain demonstrated that inhibition of gE/gI complex formation caused loss of directional virion secretion and smaller plaques on cultured monolayer. Furthermore, a small plaque phenotype was also observed when for a virus where the gE/gI complex was retained, but which had lost FcR activity (Polcicova et al., 2005). These observations may suggest the presence of hypothetical receptors for gE/gI at the cell-cell junctions that could facilitate efficient virion spread to neighbouring cell.

7.1.2 The role of gC during virion release

HSV-1 gC is known for its HS binding activity on the surface of host cells during entry but it has functional redundancy with gB and is considered as non-essential, although gB-HS interaction is ~60% less efficient than gC-HS interaction (Cai et al., 1988; Herold et al., 1991). After egress HSV-1 is expected to exhibit some interaction with the infected cell surface due to the gC-HS interaction, which could reduce virus spread (Laquerre et al., 1998). Indeed, an HSV-1 gCΔmuc (deletion of the mucin-like region) virus, which displays increased HS binding, released 20-fold less virus from infected cells. Additionally, ΔgC viruses have been shown to produced bigger plaques than that of WT supporting the hypothesis that a lack of gC-HS interaction promotes release of virions from the surface of infeceted cells and enhances spread of virions to neighbouring uninfected cells (Laquerre et al., 1998; Mårdberg et al., 2004). Similar observations were made in this thesis, with all ΔgC viruses displaying increased plaque sizes. Additionally, a virus containing both ΔgC and gIG39R mutations showed increased release compared to gIG39R single mutants. This also supports the notion that gC-HS binding adheres the released virions to the surface of infected cells and loss of this HS binding after egress allows release of virions from the surface much more easily. Therefore, it may be concluded that gC is partly responsible for post-egress-cell-associated phenotype of HSV-1 and, at the same time, acts as an inhibitor of cell-to-cell spread. However, it is interesting to note that the enhanced release caused by deletion of gC was dependent on the gIG39R mutation as the single ΔgC mutant viruses release less infectious virus into the culture medium that WT.

7.1.3 The role of pUL43 in HSV-1 egress

The role of pUL43 in HSV-1 replication is unknown and no effect of pUL43 deletion either alone or in combination with ΔgC and/or gIG39R was observed in this study in virus replication, plaque formation or release. Previous studies also could not detect any effect of pUL43 deletion on HSV-1 *in vivo* or *in vitro* (Maclean et al., 1991; Powers et al., 1994). Studies with PrV have suggested that the pUL43 could have similar functions to gM and gK mostly because of their structural similarity in being multiple membrane spanning protein domains. Therefore, the effects of deletion of one or two of these proteins may be complemented by the others (Klupp et al., 2000 and 2005). In PrV-infected cells, pUL43 has been found to co-localise with gB in cytoplasmic vesicles and, upon pUL43 deletion, plaques were marginally reduced in size. Therefore, pUL43 was thought to contribute during membrane fusion (Klupp

et al., 2005). However, mouse pathogenesis studies with a large panel of PrV mutant viruses did not indicate an obvious role for pUL43 *in vivo* (Klopfleisch et al., 2006). Recently, equine herpesvirus-1 (EHV-1) pUL43 has been shown to promote lysosomal degradation of MHC-I molecules from the cell surface in co-operation with pUL56 (Huang and Osterrieder, 2015). Downregulation of MHC-I would allow the virus to hide from the deleterious effects of cytotoxic T lymphocytes (CTLs) during infection *in vivo*. However, pUL43-mediated downregulation of MHC-I or co-localisation with gB has not been shown for HSV-1.

7.1.4 Common cellular interaction partners of HSV-1 proteins or artefacts?

A recent proteomics study with HSV-1 gH in transiently expressing HEK293T cells identified 123 candidate cellular interacting partners for this viral glycopreotein (Hirohata et al., 2015). Interestingly, 10 of these potential gH interactors were also identified in the gE/gI interactome list of this study: ATP5A1, ATP5B, HSP90AB1, HSP90B1, TUBB4B, PHGDH, DDOST, PHB, PHB2, HSPD1. Furthermore, proteomic analysis of interactors of HSV-1 VP16 during infection also identified PHB2 (Oh and Knipe, 2015). One major caveat of the identification of these proteins as interactors for gE/gI, gH or VP16 is that they are all mitochondrial proteins. HSV-1 infection causes inhibition of mitochondrial Ca^{2+} influx and protein synthesis, mostly after 12 hpi, and therefore mitochondrial morphology can be substantially altered in infected cells at late time points (Kramer and Enquist, 2012), and this could result in protiens that are normally resident in the mitochondria becoming more accessible to viral protein domains in the cytoplasm. Studies have suggested at least two tegument proteins affect mitochondrial function; UL12.5 is thought to induce mitochondrial DNA degradation and UL7 has been shown to bind to the mitochondrial protein ANT2 but the function consequence of this is unknown (Tanaka et al., 2008; Corcoran et al., 2009). However, HSV-1 glycoproteins have not been reported to localise with mitochondrial proteins or play any role in affecting mitochondria function. Given the same proteins were identified as potential interactors for the gE/gI complex during infection in this thesis and for gH in a transient expression system (Hirohata et al., 2015), it could be speculated that these glycoproteins might directly modulate mitochondrial function. However, it seems more likely that these glycoproteins would not normally encounter these mitochondrial proteins until cells are artificially lysed in detergent, which would render both mitochondrial proteins and viral membrane proteins free in solution, and that these identified interactions are artefacts due to ‘stickiness’ of these particular mitochondrial proteins.

7.1.5 Interaction of viral proteins with gE/gI

Four other HSV-1 glycoproteins, gH, gB, gC, and gD, were identified as candidate gE/gI interaction partners in the SILAC-IP MS experiment, and gB interaction was confirmed during validation experiments. This could either indicate these proteins are directly interacting with gE/gI for a specific biological function, or these viral glycoproteins could have been identified simply because of localisation to a common membrane compartment that was pulled-down by virtue of gE/gI also being present in this membrane. Such indirect association is not likely to be due to IP of mature virions because although both capsid and tegument proteins were also identified, many high abundance structural proteins such as pUL47 (VP13/14) and VP16 were not present. Of the other potential viral protein interactors, VP5, pUL39 and pUL23 were also identified as interaction partners for GFP-tagged VP16 in HSV-1 infected cells in a published proteomics study, suggesting they could be artefacts (Oh and Knipe, 2015). Several previous studies have demonstrated gE and VP22 co-precipitation and showed the importance of a complex including gE, VP22, gM, gI and ICP0 for efficient virus morphogenesis and spread (Maringer et al., 2012; Farnsworth et al., 2007; O'Regan et al., 2007). Therefore, it was surprising that VP22 co-precipitation with gE from infected cell lysates was not observed in this thesis. One of the studies that established the gE-VP22 interaction utilised HSV-1 strain SC16 and used a commercial anti-gE antibody (ab6510) for pull down (Maringer et al., 2012), whereas this study used the KOS strain and utilised a different antibody (MAb-3114). Data in this thesis suggests MAb-3114 recognises the gE/gI complex poorly in IP experiments because virtually no gI is detected in IP samples with this antibody, and so it is possible that VP22 interacts preferentially with gE/gI rather than free gE, and perhaps the commercial ab6510 antibody does recognise gE/gI. Also, the VP22 antibody used here gave relatively weak signals in WB of lysate samples, and so the lack of detection of VP22 in gE IP samples may have been due to a sensitivity issue. Another study in this regard also utilised MAb-3114 and demonstrated gE-VP22 interaction, but concluded that binding of VP22 to gE was less extensive than with gD and suggested a stringent experimental setup before being able to conclude gE-VP22 interaction occurs (Farnsworth et al., 2007b). While several studies have demonstrated robust VP22-gE/gI interaction in transfected cells (Hafezi et al., 2005; O'Regan et al., 2007; Stylianou et al., 2009; Maringer et al., 2012), during infection such interactions could be more transient or weak and rely on the presence of other glycoproteins and tegument proteins (Farnsworth et al., 2007b; Fuchs et al., 2002).

The identification of pUL34 as a potential gE/gI interaction partner could be interesting for understanding the appearance gE in the nuclear membrane as observed in chapter 3 (section 3.2.3). Previous studies have shown the pUL31/pUL34 nuclear egress complex can recruit gD and gM to the nuclear membrane and have also proposed gB and gH are involved during virion egress from the nuclear membrane (Farnsworth et al., 2007a; Wills et al., 2009; Johnson et al., 2011). Since gB, gD, gH and pUL34 were all identified as potential gE/gI interaction partners, the gE/gI complex or gE alone could also be an interesting candidate protein to function during nuclear egress of nucleocapsids, albeit in a non-essential or redundant manner because a gE deletion virus does not appear to have any nuclear egress or other assembly defect.

A direct interaction of VP5 (the major capsid protein) with any glycoproteins has not been demonstrated previously. Data in this thesis identified VP5 in all biological replicates of the gE/gI SILAC-IP and pull-down of VP5 by gE/gI was also validated in subsequent experiments. It is possible this is due to an indirect interaction of gE/gI with viral capsids via a tegument protein. However it seems unlikely this is due simply to the IP of virus particles from infected-cell lysates due to the absence of other highly abundant virion proteins (e.g. VP13/14) and known binding partners for gE, namely gI, VP22 or pUL16. The tegument protein pUL16 has been proposed to act as a bridge between pUL11, gE and VP22 during envelopment of HSV-1 (Starkey et al., 2014; Baird et al., 2008; Yeh et al., 2008; reviewed in Owen et al., 2015). In addition, pUL16 has been proposed to interact with the major capsid protein (VP5) and small capsid protein (VP26) (Lee et al., 2008; Meckes et al., 2010). However, co-precipitation of gE and pUL16 is thought to be difficult to detect as previous studies showed pull-down of pUL16 with gE only when samples were incubated at 37°C overnight but not at 4ºC (Yeh et al., 2011). All the pull-down experiments in this thesis were performed at 4ºC, presumably causing the failure to detect pUL16 in gE pull-down samples. Clearly, further studies will be required to understand the interactions of gE/gI with other structural and non-structural viral proteins and the roles they play during HSV-1 infection.

7.2 The role of putative gE-interacting cellular proteins

HSV-1 can selectively utilise, inhibit or downregulate many cellular proteins for its own benefit. An important role of gE/gI appears to be sorting of nascent virions to cell junctions of epithelial cells, promoting virus spread (Johnson et al., 2011), and this presumably requires interaction with specific cytoplasmic cellular proteins. In support of this, viruses where the gE cytoplasmic domain was deleted showed virion trafficking to apical surfaces rather than to

lateral cell junctions (Farnsworth and Johnson, 2006). However, the cellular proteins interacting with gE and or gI that facilitate this process are not known. Within the virion loaded vesicles, any gE/gI remaining on the vesicle membrane would have their N terminal ecto-domains facing the lumen and their C terminal domains projecting from the cytoplasmic surface of the vesicle membrane. Therefore, cellular proteins providing directionality to the transport of the virion-containing vesicle would most likely interact with the CT domains of gE/gI. The proteomics study of gE/gI identified at least two novel cellular interaction partners of gE, Nipsnap1 and MYOF, that could be involved in the vesicle transport process, as well as, intriguingly, an interferon-inducible antiviral restriction factor IFITM2.

7.2.1 IFITM proteins

IFITMs are known restriction factors of many enveloped and non-enveloped viruses. In this thesis IFITM2 was identified as a potential gE/gI interaction partner, but was also found to be degraded upon infection, suggesting HSV-1 may target IFITM proteins to evade their antiviral activity. The reduced levels of IFITM2 made validation of the interaction with gE difficult, although a hint of IFITM2 interaction with gE was observed when both proteins were co-expressed by transfection. Interestingly, IFITM1 demonstrated a more robust interaction with gE in co-transfection experiments, and also high expression levels of IFITM1 and 2 were only observed in cells expressing low levels of gE, and vice versa. These data may suggest that gE can cause the degradation of IFITM proteins, although infection studies suggested infection-induced IFITM2 degradation did not depend on gE expression.

The cellular locations of IFITMs have been shown to be diverse depending on the type of IFITM protein and the nature of their induction. IFITM1 can be found on the plasma membrane. In contrast, IFITM3 appears to be primarily in intracellular compartments showing co-localisation with CD63, LAMP1 or Rab7, suggesting late endosome localisation (John et al., 2013; Yount et al., 2010; Feeley et al., 2011). Less is known about the localisation of IFITM2. A recent study has reported IFITM2 to be localised in mitochondria in Vero cells (Muñoz-Moreno et al., 2016), although a previous study with overexpressed IFITM2-HA demonstrated clustering near the nucleus in A549 cells (Muñoz-Moreno et al., 2016; Weston et al., 2014). IFITM proteins are thought to interfere with the entry mechanisms of at least some enveloped viruses, although this may be called into question if endogenous IFITM2 truly is a mitochondrial protein. Whether IFITM proteins can restrict the entry or replication of HSV-1 in the absence of gE, and how gE may antagonise IFITM function could be interesting topics

for future study. It would also be interesting to compare other herpesviruses because HCMV has been suggested to utilise IFITM proteins as pro-viral factors during virion assembly (Xie et al., 2015).

7.2.2 MYOF

MYOF has been shown to contribute to both clathrin-dependent and caveolin-mediated endocytosis and can co-localise with dynamin 2 and caveolin 1 (Doherty et al., 2008; Bernatchez et al., 2007). The C2 domains of MYOF have putative functions during docking or SNARE-mediated fusion at the plasma membrane (Chapman et al., 1998; Davis et al., 2002; Bansal and Campbell, 2004; Doherty and McNally, 2003; Therrien et al., 2009; Chapman, 2002). Therefore, MYOF could have a role in both membrane fission and fusion events.

Ferlins act as important regulators of bidirectional membrane turnover events (endocytosis and exocytosis) (Bernatchez et al., 2009). One role of MYOF in the HSV-1 life cycle could be to help recycling of viral glycoproteins through the endocytic pathway, as a part of its normal cellular process, helping to localise virion glycoproteins to the appropriate membrane compartments for envelopment and egress. However, it is also possible that MYOF could function during the secretion of newly assembled virions after the completion of secondary envelopment (Figure 7.1). It has been proposed that HSV-1 secondary envelopment occurs at recycling endosomes (Hollinshead et al., 2012), and so virus egress could be similar to the process of recycling endocytic vesicles to the plasma membrane. Myoferlin has been shown to be involved in recycling of transferrin (Posey et al., 2014). It co-stains with endosomal markers Rab5, Rab7, and Dynamin 2 (Bernatchez et al., 2009) but not with lysosomal marker LAMP-1 (Redpath et al., 2016). Additionally, disruption of ferlins were shown to cause defects in the endocytic pathway (Doherty et al., 2008; Posey et al., 2011). Therefore, MYOF and other ferlins would be interesting candidates to be involved in HSV-1 envelopment and egress, and the observations in this thesis suggests a potential role of this new family of cellular proteins that has not previously been identified for herpesviruses.

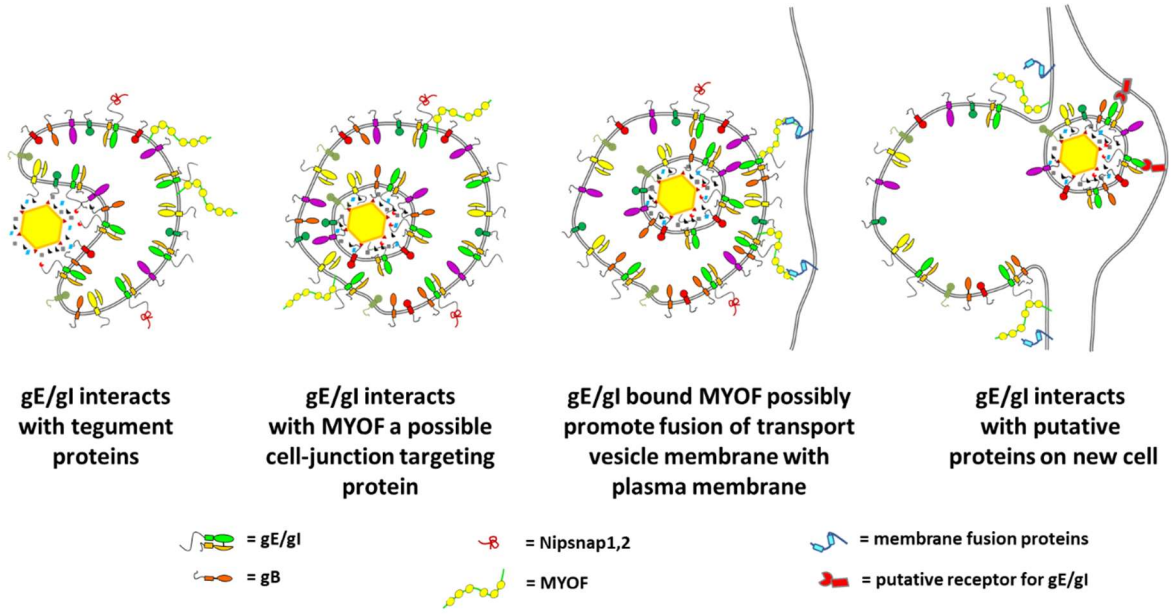

Figure 7.1 | Diagram of putative role of gE-MYOF interaction for mediating virion-loaded cargo delivery towards cell adhesion sites.

After envelopment, HSV-1 must travel to the cell-cell junctions or cell adherent contact points, which are target sites of virion delivery. Published data on MYOF indicate three possible ways this cellular proteins could be involved in HSV-1 egress: (1) MYOF co-localises with the tight junction marker ZO-1 in airway epithelial cells (Leung et al., 2012) and therefore, HSV-1 may recruit MYOF to facilitate virion targeting to tight juntions in infected cells, (2) MYOF regulates cell-substrate adhesion strength (Blackstone et al., 2015) and therefore the transport of virion-loaded vesicles to the plasma membrane may follow the pathway of host cargo delivery to adhesion contacts through MYOF activity, (3) MYOF is best known for its function during myoblast fusion and membrane repairing (Doherty et al., 2008; Bernatchez et al., 2007 and 2009; Demonbreunn et al., 2010) and so gE/gI may lead to activation of MYOF-mediated repair pathways and in doing so stimulate delivery of virus particles to the cell junctions. Future studies into the assembly and release of HSV-1 in the presence or absence of MYOF and other ferlins will shed more light on this.

7.2.3 Nipsnap1 and 2

Nipsnap proteins are thought to mediate vesicle trafficking in cells (Seroussi et al., 1998) although there is not any as direct evidence of this activity for Nipsnap1 and 2. A study of Nipsnap1-deficient mice revealed its importance in pain transmission, possibly indicating a role in pain-receptor trafficking (Okuda-Ashitaka et al., 2012). Nipsnap1 was one of the strongest binding partners of gE identified in the SILAC-IP data, and the interaction was validated for two different WT strains of HSV-1 and in at least two human cell lines; HaCaT and HFF-hTERT. A substantial amount of gE-Nipsnap1 interaction was seen with ΔgI and gIG39R-infected cells, even though less mature gE appears to be made by these viruses, suggesting gE could interreact with Nipsnap1 in the ER. At least four variants of Nipsnap1 with different molecular mass (27, 28, 29 and 33 KDa) have been suggested, with N-terminally truncated 29 KDa considered the mature form (Okuda-Ashitaka et al., 2012). However, in the work for this thesis only a single band for Nipsnap1 (~26 KDa) could be detected in all the cell lines tested. Tagging of the C terminus of Nipsnap1 and Nipsnap2 inhibited their interaction with gE as no precipitation of the tagged proteins were seen in the gE pull-down samples. This could indicate that the binding of these proteins gE is via their C-termini, or that the C terminus is important for correct Nipsnap folding. Endogenous Nipsnap1 or 2 and N-terminally myc-tagged Nipsnap1 were co-precipitated with gE effectively. In IF, C-terminally-tagged Nipsnap1 or 2 appeared to localise to mitochondria similarly to untagged proteins, while N-terminally-tagged proteins showed little or no localisation to mitochondria-like structures. Studies from different labs also detected Nipsnap1 and 2 in mitochondria either by IF or IP (Tummala et al., 2010; Okuda-Ashitaka et al., 2012; Yamamoto et al., 2017), and the N terminus of Nipsnap1 has been shown to contain a mitochondrial targeting sequence (MTS), which is important for the proper processing of this protein (Okuda-Ashitaka et al., 2012; Tummala at etl., 2010). Therefore, an N terminal myc-tag on Nipsnap1 or 2 is likely to inhibit mitochondrial targeting. Very little gE-Nipsnap1 co-localisation was observed and only when untagged Nipsnap1 was expressed (Figure 5.13 a). Despite several mitochondrial proteins being identified in the gE/gI SILAC-IP data gE showed no co-localisation with mitochondrial markers either in transfected or in infected cells. This was also true for various gE mutants lacking sections of the cytoplasmic domain. Despite altered gE localisation when much of the cytoplasmic domain was deleted (gE-1-475 and 1-440) none of the constructs seemed to localise in mitochondria. However, localisation of Nipsnap1 at the plasma membrane has been proposed by many authors and has been shown in transfected COS7 cells, which suggests a

function of Nipsnap1 outside the mitochondria (Okuda-Ashitaka et al., 2012; Schoeber et al., 2008).

Nipsnap1 and 2 KO cell lines were generated for this thesis by CRISPR-Cas9 technology. The deletion of Nipsnap1 and 2 were confirmed by WB although in IF experiments anti-Nipsnap2 antibody showed a signal in the Nipsnap2 KO cells, but not the double KO cells, suggesting the commercial Nipsnap2 antibody binds to Nipsnap1 presumably because of its high sequence similarity with Nipsnap2. Though the sequencing data for the Nipsnap2 gene from the KO clones demonstrated frameshift mutations had occured, data for the Nipsnap1 gene sequenced from KO clones showed some copies of the gene contained in-frame deletions. It is therefore possible that varying lengths of Nipsnap1 could be expressed in the Nipsnap1 KO clones, but not detected because the epitope for the Nipsnap1 antibdy used falls within the mutated region. Interestingly, pull-down assays from the KO cells suggested that interaction of Nipsnap2 with gE depends on Nipsnap1, which may indicate heterodimers of Nipsnap1 and 2 exist. However, HSV-1 replication and release were no different in the Nipsnap1 and 2 KO cell lines compared to the WT HaCaT cells, suggesting these cellular proteins are not essential for HSV-1 assembly or egress. The only noticeable difference was the size of the plaques which appeared to be slightly bigger in the KO cells than in the WT-HaCaT for the gE and gI mutants. This could suggest a potential antiviral function of Nipsnaps, which is normally antagonised by gE/gI during WT HSV-1 infection.

Some evidence of a role for Nipsnap1 and 2 in innate immune responses has been shown as knockdown of Nipsnap1 and 2 in various cell lines suppresses lipopolysaccharide-induced activation of NF-κB and IL-6 and IL-8 expression (Yamamoto et al., 2017). HSV-1 can activate NF-κB and induce the expression of antiviral factors IL-6 and IL-8 (Liu et al., 2013; Li et al., 2006) and IL-6 has been shown to contribute to resistance against HSV-1 infections (Paludan, 2001). Therefore, it is possible that gE/gI may normally antagonise this role of Nipsnap1 and 2 and the loss of this activity in gE and gI mutant viruses is compensated in the Nipsnap1/2 KO cell lines, leading to the partial rescue of plaque size. It will be interesting to follow up the potential antiviral role of Nipsnap proteins and the effect of gE/gI in the future.

Regarding the Nipsnap interactions, it should be taken into account that the observed binding of these proteins with gE could be an artefact of the experimental system. It may be that in a normal cell, gE localised in the secretory and endocytic pathway compartments and Nipsnap 1 and 2 in the mitochondria do not interact because they are not present in the same subcellular

compartments, but once a cell is lysed and the membranes are dissolved by detergent, they can interact. This would appear likely for the numerous other mitochondrial proteins identified in the SILAC-IP screen. An alternative method to identify putative gE/gI interaction partners, such as BioID or protein cross-linking approaches could help clarify the situation. Nevertheless, from data generated for this thesis, it seems highly unlikely that Nipsnap1 or 2 are involved in gE-mediated virus egress.

7.3 Future directions

The research of this thesis shows the importance of gE and gI in that HSV-1 life cycle and also identifies interesting cellular interactors of gE. However, a number of questions remained unanswered:

(1) How does the gIG39R mutation inhibit gE/gI complex formation and what amino acid residues in gI form a complex with gE?

This thesis suggests that the G39 residue on gI could be part of the interaction site for gE binding. It would be interesting to investigate whether the G39 is part of a specific gE binding site within gI or whether mutation of G39 to R results in a severe conformational change in gI ecto-domain, thereby preventing gE/gI heterodimer formation. Modification of G39 of gI with neutral or negatively charged amino acids, as well as mutagenesis of the surrounding residues, could help understand the gE/gI interaction.

(2) Is the cytoplasmic tail of gI necessary for gE/gI function and is there any role of gE or gI transmembrane domains for interactions with host factors?

Further screens for gE/gI interaction partners using a tailless gI together with full length gE, or a tailless gE together with full length gI, or IP of the individual proteins when expressed in the absence of each other, could help uncover genuine interactors of this complex and define host proteins that bind specifically to the gE/gI complex as opposed to either protein individually.

(3) What is the importance of nuclear rim appearance of gE?

The localisation of gE to the nuclear rim and the potential interaction with the nuclear egress protein pUL34 are intriguing but their significance is unknown. Investigating whether gE localises to perinuclear virions, and whether the localisation at the nuclear rim is connected to interaction of gE with gB should be investigated further.

(4) How do IFITM proteins get degraded during HSV-1 infection and do IFITM proteins have antiviral activity towards HSV-1 WT or ΔgE?

The disappearance of IFITM2 during HSV-1 infection would also be interesting to investigate further. Whether such inhibition occurs at the protein level due to activity of viral proteins or at mRNA level as a consequence of vhs activity needs to be clarified. The effect of IFITM1, 2 and 3 over expression on the entry and replication of HSV-1 in the presence or absence of gE/gI (and other potential antagonists such as vhs) will be an important area for further research.

(5) What significance do Nipsnap1/2-gE interactions have during HSV-1 infection?

There is seemingly no relevance for gE interaction with Nipsnap1/2 for HSV-1 replication or release in culture, although there may be some antiviral effect of Nipsnap1/2 in plaque formation when gE is absent. Whether gE and Nipsnap1 interact in the context of an intact cell is a key issue to address. The potential effect of gE-Nipsnap interactions on IL-6 or IL-8 production, and pathogenesis studies in Nipsnap1/2 deficient transgenic mice would be interesting avenues in the future.

(6) What is the role of MYOF or other ferlin proteins in HSV-1 life cycle?

The gE-MYOF interaction and its possible role in the transport of virions and/or viral glycoproteins is also intriguing. Other glycoproteins should be tested for interaction with MYOF and other ferlin proteins, and recapitulating gE-MYOF interactions with purified components could address whether the interaction is direct or indirect. Overexpression and deletion of MYOF and other ferlins will be needed to understand the role(s) of these cellular membrane traffic regulators during virion egress.

8. Materials and Methods

8.1 General reagents

The biochemical reagents and chemicals used in this research were supplied by the following companies unless otherwise stated; Amersham Bioscience, BDH Chemicals, Clontech, Fisher Scientific, Invitrogen, New England Biolabs (NEB), Promega, Roche, Sigma-Aldrich and Thermo Scientific. Tissue culture media were supplied by from Sigma-Aldrich and PAA laboratories. Molecular biology reagents were obtained from Invitrogen, NEB, Promega and Roche. Plastic plates, dishes and flasks were obtained from BD Bioscience and Gibco.

8.2 Cloning

The DNA constructs made in this study are listed in Table 8.1 and the primers used are listed in Table 8.2.

Table 8.1 | Viruses constructed and used in this study

Virus strain	*E. coli* strain	Description	Source
HSV-1 KOS-BAC	GS1783/ HSV-BAC	For Red-recombinant virus construction. GS1783 carring HSV-1 KOS BAC DNA. This bacterial strain contains a heat-shock inducible cassette for Red recombinase and arabinose inducible I-SceI. Utilised for construction of KOS ΔgC, ΔgE, ΔgI, gIG39R	KOS-BAC from David Leib (Gierasch et al., 2006), GS1783 from obtained from Gregory Smith (Tischer et al., 2010)
HSV-1 ΔpUL43	GS1783/ HSV-BAC ΔpUL43	Codons 54-56 of UL43 have been replaced with three tandem in-frame stop codons	Kathy Lau (CMC lab)
HSV-1 ΔgC	GS1783/ HSV-BAC ΔgC	Codons 37-39 of UL44 (gC) have been replaced with three tandem in-frame stop codons	This study
HSV-1 ΔgE	GS1783/ HSV-BAC ΔgE	Codons 21-24 of US8 (gE) have been replaced with three tandem in-frame stop codons	This study
HSV-1 ΔgI	GS1783/ HSV-BAC ΔgI	Codons 21-24 of US7 (gI) have been replaced with three tandem in-frame stop codons	This study
HSV-1 gIG39R	GS1783/ HSV-BAC gIG39R	gI has been modified with a point mutation in codon 39, causing glycine to be replaced with arginine (G39R)	This study
HSV-1 ΔgC-gIG39R	GS1783/ HSV-BAC	Codons 37-39 of UL44 (gC) have been replaced with three tandem in-frame	This study

	ΔgC-gIG39R	stop codons and the G39R mutation has been introduced in gI	
HSV-1 ΔpUL43-gIG39R	GS1783/ HSV-BAC ΔpUL43-gIG39R	Codons 54-56 of UL43 have been replaced with three tandem in-frame stop codons and the G39R mutation has been introduced in gI	This study
HSV-1 ΔpUL43-ΔgC	GS1783/ HSV-BAC ΔpUL43-ΔgC	Codons 37-39 of UL44 (gC) and codons 54-56 of UL43 have been replaced with three tandem in-frame stop codons	This study
HSV-1 ΔpUL43-ΔgC-gIG39R	GS1783/ HSV-BAC ΔpUL43-ΔgC-gIG39R	Codons 37-39 of UL44 (gC) and codons 54-56 of UL43 have been replaced with three tandem in-frame stop codons.and the G39R mutation has been introduced in gI	This study
HSV-1 gIG39R^{EYFP}	GS1783/ HSV-BAC gIG39R^{EYFP}	gIG39R has been tagged at the C terminus with EYFP (A206K) fluorescent protein	This study
HSV-1 gI^{EYFP}	GS1783/ HSV-BAC gI^{EYFP}	gI has been tagged at the C terminus with EYFP (A206K) fluorescent protein	This study
HSV-1 VP26^{TQ}	GS1783/ HSV-BAC VP26^{TQ}	VP26 has been tagged at the N terminus with mTurquoise fluorescent protein	CMC
HSV-1 VP26^{TQ}-gI^{EYFP}	GS1783/ HSV-BAC VP26^{TQ}-gI^{EYFP}	VP26 has been tagged at the N terminus with mTurquoise fluorescent protein and gI of the virus has been tagged at the C terminus with EYFP (A206K) fluorescent protein	This study

CMC: Dr Colin Crump (University of Cambridge)

Table 8.2 | Primers used in this study

Primer	Sequence (5'-3')	Details
COL400	CGGGGGCTCGGAAACTGCCTCCACCGGGCCCACGATCACCTGATAGTAAGCTTGTGACGAACGCGAGCGAGGCAGGATGACGACGATAAGTAGGG	F primer for gCstop
COL401	CGGGGGACCCCGATGTGGGGGCCTCGCTCGCGTTCGTCACAAGCTTACTATCAGGTGATCGTGGGCCCGGTGGCAACCAATTAACCAATTCTGATTAG	R primer for gCstop
COL517	CCCCACGGTCAGTCTGGTATCAAACTCATTTGTGGACGCCCGGGCCTTGGGGCCCGACGGCGTAGGATGACGACGATAAGTAGGG	F primer for gIG39R
COL518	TAAGCAGGTCTTCCTCCACTACGCCGTCGGGCCCCAAGGCCCGGGCGTCCACAAATGAGTTTGCAACCAATTAACCAATTCTGATTAG	R primer for gIG39R

COL521	TGGGGGCGCTGCTGTGCCCTCCGGGGTCAACGGGCGGGTGGTCGGGCGATGTGAGCAAGGGCGAGGAG	F primer for UL43^{EYFP}
COL522	CACACACCGGCGGTCTTCGGGACTAATGCCTTTTATTGAAAAATATATCACTTGTACAGCTCGTCCATG	R primer for UL43^{EYFP}
COL523	GGGGTTTCTTCTCGGTGTTTGTGTTGTATCGTGCTTGGCGTAGTGATAAGCTTCGTCCTGGAGACGGGTGAGTAGGATGACGACGATAAGTAGGG	F primer for gEstop
COL524	AACGAAACGTCCTCGCCGACACTCACCCGTCTCCAGGACGAAGCTTATCACTACGCCAAGCACGATACAACACCAACCAATTAACCAATTCTGATTAG	R primer for gEstop
COL525	GGGCCTGGTGCTCGTGGGCCTCTGGGTCTGTGCCACCAGCTAATAGTGAATTCGCCCCACGGTCAGTCTGGTAAGGATGACGACGATAAGTAGGG	F primer for gIstop
COL526	GCGTCCACAAATGAGTTTGATACCAGACTGACCGTGGGGCGAATTCACTATTAGCTGGTGGCACAGACCCAGACAACCAATTAACCAATTCTGATTAG	R primer for gIstop
COL527	CGCCCCCCGTGGACCCCACGACATCCACCCCAACGCCTCCCCTGTTGGTAGTGAGCAAGGGCGAGGAG	F primer for gI^{EYFP}
COL528	AGTGACTGCGGTCGGTTATGTGGTGCCCCCGGCCAGTGGCCGTGGACCTACTTGTACAGCTCGTCCATG	R primer for gI^{EYFP}
COL597	GGGGACAAGTTTGTACAAAAAAGCAGGCTTCACCATGCCGTGCCGCCCGTTG	F primer gI for pDONR207 insertion
COL598	GGGGACCACTTTGTACAAGAAAGCTGGGTTTTCTATACCAACAGGGGAGGCGT	R primer gI for pDONR207 insertion
COL599	GGGGACAAGTTTGTACAAAAAAGCAGGCTTCACCATGGATCGCGGGGCGGTG	F primer gE for pDONR207 insertion
COL600	GGGACCACTTTGTACAAGAAAGCTGGGTTTTCTACCAGAAGACGGACGAATC	R primer gE for pDONR207 insertion
COL615	CACC G GCATCTCTGTGACGGCGCGG	F primer for CRISPR sgRNA: Nipsnap1 exon1_1
COL616	AAAC CCGCGCCGTCACAGAGATGC C	R primer for CRISPR sgRNA: Nipsnap1 exon1_1
COL617	CACC G GACGCAACGTCCCCAGCGCG	F primer for CRISPR sgRNA: Nipsnap1 exon1_2
COL618	AAAC CGCGCTGGGGACGTTGCGTC C	R primer for CRISPR sgRNA: Nipsnap1 exon1_2
COL619	CACC G GACTACCCATGCTCACTCGT	F primer for CRISPR sgRNA: Nipsnap1 exon4_1
COL620	AAAC ACGAGTGAGCATGGGTAGTC C	R primer for CRISPR sgRNA: Nipsnap1 exon4_1
COL621	CACC G GCGCGAGTGCTGCGCGCCCG	F primer for CRISPR sgRNA: Nipsnap2 exon1_1

COL622	AAAC CGGGCGCGCAGCACTCGCGC C	R primer for CRISPR sgRNA: Nipsnap2 exon1_1
COL623	CACC G GTCTTCTCGAGATCTGTTGC	F primer for CRISPR sgRNA: Nipsnap2 exon2_1
COL624	AAAC GCAACAGATCTCGAGAAGAC C	R primer for CRISPR sgRNA: Nipsnap2 exon2_1
COL625	CACC G TATATATTAGGTCCGGATCT	F primer for CRISPR sgRNA: Nipsnap2 exon6_1
COL626	AAAC AGATCCGGACCTAATATATA C	R primer for CRISPR sgRNA: Nipsnap2 exon6_1
KL015	CTGAGAATTCGCCACCATGGATCGCGGGGCGGTG	gE F primer
MFA001	AGAACCCTGACTTCCGTCC	F primer for Nipsnap1 exon1
MFA002	ACAAAGACCCTACCCATCCC	R primer for Nipsnap1 exon1
MFA003	CTCTTGCCTAGCTTCTGCATTTT	F primer for Nipsnap1 exon4
MFA004	GACAGGTATTTGAGCAGGGG	R primer for Nipsnap1 exon4
MFA005	CATCAATGTTACTGAAATGGGCT	F primer for Nipsnap2 exon6
MFA006	GAGCTTAGCCTTGGTGACAGT	R primer for Nipsnap2 exon6
MFA007	AAAATCTAGATTAACACGCCCACACCGACAA	gE truncation 1-440 R primer
MFA008	AAAATCTAGATTACCAGTCCGCGTACAGCTC	gE truncation 1-475 R primer
MFA009	AAAATCTAGATTATGGTGATAAGATCTCAAAGCC	gE truncation 1-510 R primer
MFA010	AAAATCTAGATTATCCAAAGGTTGTGAGCTG	gE truncation 1-532 R primer
MFA014	AAAAGAATTCATGGCTCCGCGGCTGTGCAG	F primer Nipsnap1
MFA015	AAAAACCGGTAACTGCAGAGGCGAGATCTT	R primer Nipsnap1 for pEGFP-N1
MFA016	AAAATCTAGATTACAGGTCCTCCTCTGAGAT CAGCTTCTGCTCCTGCAGAGGCGAGATCTT	R primer Nipsnap1-myc for pCDNA3.1
MFA017	AAAATCTAGATTATCACTGCAGAGGCGA	R primer Nipsnap1
MFA018	AAAAGAATTCATGGCGGCGCGAGTGCTGC	F primer Nipsnap2
MFA019	AAAAGAATTCATGGAGCAGAAGCTGATCTCA GAGGAGGACCTGGCGGCGCGAGTGCTGC	F primer Nipsnap2-myc
MFA020	AAAATCTAGATTACTGGAGGGGCGAGGTC	R primer Nipsnap2
MFA021	AAAAACCGGTTTCTGGAGGGGCGAGGTC	R primer Nipsnap2 with AgeI for pmCherry-N1
MFA022	AAAATCTAGATTACAGGTCCTCCTCTGAGAT CAGCTTCTGCTCCTGGAGGGGCGAGGTC	R primer myc-Nipsnap2
MFA023	CCATGCTCACTCGTGGGC	F primer Nipsnap1 mRNA
MFA024	CTGGCTTGAGCTTGTATG	R primer Nipsnap1 mRNA
MFA025	AAAATCTAGATTAATCGGGCCTTCCGGATCC	R primer gE truncation 1-537
MFA026	AAAATCTAGATTACTGGGAGTAACGGCGATC	R primer gE truncation 1-542
MFA027	AAAATCTAGATTAGACGGACGAATCGGAGGC	R primer gE truncation 1-548
RU049	GACTATCATATGCTTACCGT	Human U6 promoter, F primer
COL642	ACGCTGAACTTGTGGCCGTTTACG	MG70 F primer for GFP sequencing
CMV f	CGCAAATGGGCGGTAGGCGTG	Human CMV immediate early promoter F primer
BGH r	TAGAAGGCACAGTCGAGG	Bovine growth hormone terminator R primer
M13 f	TGTAAAACGACGGCCAGT	Forward primer for M13
IGUC1906	ACAAGTTTGTACAAAAAAGCAGGCT	AttB1 F primer for pDONR sequencing
IGUC1906	ACCACTTTGTACAAGAAAGCTGGGT	AttB2 R primer for pDONR sequencing

Abbreviations: F primer = Forward primer, R primer = Reverse primer, Stop = With stop codons

8.2.1 Polymerase chain reaction (PCR)

PCR reactions were carried out in a total volume of 50µL containing 10µL 5x Phusion HF buffer, 1µL (10mM) dNTPs, 2.5µL (1µM) of each primer, 20ng template plasmid DNA, 25µL (2M) betaine, 0.5µL of Phusion HF DNA Polymerase (Finnzymes) and miliQ water (MQW; as required). The PCR conditions used are 98ºC denaturation for 30 sec, followed by 30 cycles of 98ºC for 10 sec, 56ºC annealing for 20 sec, and 72ºC elongation for 20 sec and final extension step at 72ºC for 10 min. A modified condition (58ºC annealing temperature) was used for the EYFP primers.

8.2.2 Agarose gel electrophoresis (AGE)

DNA fragments were mixed with 10X DNA loading buffer and separated in 0.8-2% agarose gel containing ethidium bromide dye. The gel was run in 1x TBE buffer with 100 v for appropriate time and was visualised by UV transilluminator (Table 8.3).

Table 8.3 | Gel electrophoresis buffers

Solution	Composition
DNA loading buffer (10x)	50% (v/v) glycerol, 100mM EDTA, pH 8.0, 1% (w/v) SDS, 0.25% (w/v) bromophenol blue
TBE (1x)	89m Tris base, 89mM sodium borate, 2.6mM EDTA, pH 8.0

8.2.3 DNA purification

DNA from the desired band on agarose gel was purified using in house reagents (details in the section 8.2.8).

8.2.4 Restriction digestion of plasmids and PCR products

DNA digestion was carried out in 50µL reaction mixture with 1µg PCR product or 2µg plasmid DNA, 1x buffer (as required by the enzyme), 1x BSA (if needed) and 20U of restriction enzyme(s). The reaction was carried out for a minimum 3 h in a 37ºC water bath.

Analytical restriction digestion of plasmids was carried out for 2 h at 37ºC in 20µL with 10U enzyme(s), 1x buffer and 1x BSA (if required) to check the correct insert. All the plasmid DNA constructs used in this study have been listed in table 8.4.

Table 8.4 | Plasmid DNA used in this experiment

Gene	DNA plasmid	Description	Source
Viral proteins			
UL27 (gB)	pCDNA3.1-gB	Untagged	CMC
US6 (gD)	pCDNA3.1-gD	Untagged	CMC
KOS US8 (gE)	pCDNA3.1-gE	Untagged	CMC
	pEGFP-N1-gE	C terminal GFP-tagged	CMC
	pmCherryFP-N1-gE	C terminal Cherry-tagged	CMC
	poPTnH-gECT	C terminal His-tagged gECT(445-550) fragment	Julia (SCG)
	poPTnG -gECT	C terminal GST-tagged gECT(445-550) fragment	This study
	pCDNA3.1-gE(1-440)	gE(1-440) truncated at CT domain after 440 residue	This study
	pCDNA3.1-gE(1-475)	gE(1-475) truncated at CT domain after 475 residue	This study
	pCDNA3.1-gE(1-510)	gE(1-510) truncated at CT domain after 510 residue	This study
	pCDNA3.1-gE(1-532)	gE(1-532) truncated at CT domain after 532 residue	This study
	pCDNA3.1-gE(1-537)	gE(1-537) truncated at CT domain after 538 residue	This study
	pCDNA3.1-gE(1-542)	gE(1-542) truncated at CT domain after 542 residue	This study
	pCDNA3.1-gE(1-548)	gE(1-548) truncated at CT domain after 548 residue	This study
KOS US7 (gI)	pCDNA3.1-gI	Untagged	This study
KOS VP22	pEGFP-N1-VP22	C terminal GFP-tagged	CMC
Cellular proteins			
HA-IFITM1	pCMV-HA-hIFITM1	IFITM1 with an N terminal HA-tag	Addgene (58399)
HA-IFITM2	pCMV-HA-hIFITM2	IFITM2 with an N terminal HA-tag	Addgene (58398)
HA-IFITM3	pCMV-HA-hIFITM3	IFITM3 with an N terminal HA-tag	Addgene (58397)
Myoferlin-HA	pCDNA3.1-Myoferlin-HA	Myoferlin with a C terminal HA-tag	Addgene (22443)
Nipsnap1	pCDNA3.1-Nipsnap1	Nipsnap1 amplified from pF5K-CMV-neo plasmid and cloned in pCDNA3.1	This study

Nipsnap1-myc	pCDNA3.1-Nipsnap1-myc	Nipsnap1 amplified from pF5K-CMV-neo plasmid and cloned in pCDNA3.1. R primer with myc.	This study
Nipsnap1-GFP	pEGFP-N1-Nipsnap1-GFP	Nipsnap1 amplified from pCDNA3.1 plasmid and cloned in pEGFP-N1.	This study
myc-Nipsnap1	pF5K-CMV-neo-myc-Nipsnap1	Copy pasted from pF3A WG (BYDV)-myc-Nipsnap1 plasmid to pF5K CMV-neo.	This study
Nipsnap2	pCDNA3.1-Nipsnap2	Nipsnap2 amplified from HaCaT cell-derived cDNA and cloned in to pCDNA3.1.	This study
Nipsnap2-myc	pCDNA3.1-Nipsnap2-myc	Nipsnap2 amplified from pCDNA3.1-Nipsnap2 using Nipsnap2-myc R primer	This study
myc - Nipsnap2	pCDNA3.1-myc-Nipsnap2	Nipsnap2 amplified from pCDNA3.1-Nipsnap2 using myc-Nipsnap2 F primer	This study
CRISPR-Cas9	pSpCas9(BB)-Puro(PX459)	V2.0 plasmid for CRISPR-Cas9 KO	FZ (Ran et al., 2013)

SG: Stephen Graham (University of Cambridge), FZ: Feng Zhang (MIT)

8.2.5 Dephosphorylation of cut vector

After restriction digestion, the cut vectors were dephosphorylated in a 50µL volume containing 1-2µg DNA, 1x Antarctic phosphatase buffer and 5U of Antarctic Phosphatase (NEB). The reaction was carried out for 15 min at 37ºC and then the enzyme was heat inactivated at 70ºC for 5 min.

8.2.6 Ligation of the DNA insert with the vector

The ligation reaction was carried out in 10µL volume containing 1µL DNA insert, 7µL vector DNA, 1x T4 DNA ligase buffer and 400U T4 DNA ligase (NEB). The reaction was incubated overnight at 14ºC before heat inactivation at 65ºC for 20 min in a preheated incubator.

8.2.7 Transforming DNA into competent *E. coli*

The *E. coli* DH5α strain (unless otherwise stated) was used for transformation of plasmid DNA by heat-shock method. 2-3µL of ligation reaction mixture or 100ng of plasmid DNA was mixed with 50µL of competent *E. coli,* thawed on ice. After 30 min incubation on ice the cells were heat-shocked for 30 sec at 42ºC and quickly transferred to ice for additional 2 min incubation. Pre-warmed 200µL Luria Broth (LB) medium was then added and incubated for 1 h at 37ºC

with shaking. The cells were then plated onto LB agar plates containing selective antibiotics as required and incubated overnight at 37ºC.

8.2.8 Plasmid DNA preparation

Purification of large amounts of plasmid DNA was conducted using NuceloBond Xtra Midi kit (Machere-Nagel) according to the manufacturer's instruction. For small amount of DNA, in house mini-prep reagents were used utilising all-in-one spin-columns (EconoSpin, Epoch Life Science). Transformed cells were grown in 4-5mL 2xTY culture for 12-16 h and centrifuged at 9000 x g for 1 min. Supernatant was discarded and the pellet was mixed by vortexing in 250µL of MX1 buffer containing RNase-A at a final concentration of 100µg/mL. Next 250µL of MX2 buffer was added and the reaction tubes were gently inverted 4-6 times and incubated at room temperature for 1-5 min until the solution became clear. 350µL of MX3 buffer was then added and the tubes were gently inverted 4-6 times and centrifuged at 14000 x g for 10 min. The supernatant was then transferred into a spin-column and centrifuge at 4000 x g for 1 min and the flow-through was discarded. Next the wash step was followed as described below (section 8.2.11). The buffers are listed in Table 8.5.

8.2.9 Gel extraction

After running on an agarose gel, the desired bands of DNA from the gel was excised and mixed with 3x volume of GEX buffer and kept at 55ºC with occasional shaking for 10 min or until the gel dissolved. The supernatant was then transferred to a spin-column and centrifuged at 4000 x g for 1 min, the flow thorough was discarded and the column was washed as described below (section 8.2.11).

8.2.10 PCR clean-up

Wherever required, the PCR products were added with distilled water to 100µL volume and 500 µL PEX buffer was added and mixed. The content was transferred to a spin-column and centrifuged at 4000 x g for 1 min, the flow thorough was discarded and column was washed as described below (section 8.2.11).

8.2.11 Wash step

On to each spin-column, 500µL of PB buffer or WS buffer (for PCR clean-up and gel extraction) was added and the column was centrifuged at 12000 x g for 1 min. The flow-through was discarded and 500µL of WS buffer was added to the spin-column and again was centrifuged at 12000 x g for 1 min. The flow-through was discarded again and the empty column was centrifuged at 12000 x g for 2 min to remove any residual ethanol. The flow-through collection tube was removed and the spin-column was placed into a new 1.5mL microcentrifuge tube. To elute the DNA, Nuclease-free water (for plasmid DNA50-100 µL and for gel extraction or PCR clean up 20µL) was added onto the column and left to stand for 2-5 min. Finally, the tube was centrifuged at 12000 x g for 1 min to elute the DNA. All the buffer compositions used in plasmid preperation are mentioned in the Table 8.5.

Table 8.5 | Gel electrophoresis buffers

Solution	Composition
Buffer MX1 (Suspension Buffer)	50mM Tris-HCl and 10mM EDTA, pH 8.0 (25°C), 100µg/ml RNase A
Buffer MX2 (Lysis Solution)	0.2M NaOH and 1% SDS
Buffer MX3 (Neutralisation and Binding Solution)	4M guanidine hydrochloride and 0.5M potassium acetate, pH 4.2
Buffer PB (Wash Buffer)	5M guanidine hydrochloride, 20mM Tris-HCl, pH 6.6 (25°C) (final concentration after addition of ethanol) with 38% ethanol.
Buffer WS (Wash Buffer)	10mM Tris-HCl, pH 7.5 (25°C) (final concentration after addition of ethanol) with 80% ethanol
Buffer EB (Elution Buffer)	10mM Tris-HCl, pH 8.5 (25°C)
Buffer GEX (Gel Solubilisation Buffer)	5.5M guanidine thiocyanate (GuSCN), 20mM Tris-HCl, pH 6.6 (25°C) Dissolve gel by adding 300ul of GEX for 100mg of gel
Buffer WS (Wash Buffer)	10mM Tris-HCl, pH 7.5 (25°C) (final concentration after addition of ethanol) with 80% ethanol
Buffer PEX (DNA absorption buffer)	5.5M guanidine hydrochloride (GuHCl), 20mM Tris-HCl, pH 6.6 (25°C)
Buffer WS (Wash Buffer)	10mM Tris-HCl, pH 7.5 (25°C) (final concentration after addition of ethanol) with 80% ethanol

Quick protocol for EconoSpin all-in-one mini spin-columns (#1910-250 and #1920-250)

8.2.12 DNA sequencing

Either for selecting a positive clone or for finding out a desired insert or mutation, DNA samples were sent to the Nucleotide sequencing facility at the Department of Biochemistry, University of Cambridge.

8.3 Protein expression analysis

8.3.1 Cell lysate preparation

Cells harvested by scraping were collected in 2mL eppendorf tubes and centrifuged at 5000 rpm for 5 min. The supernatant was discarded and the cell pellet was lysed by resuspending in mRIPA buffer containing protease inhibitor. The mixture was kept on ice for 20 min and then centrifuged at 13,300 rpm and 4^{o}C for 15 min to remove the cellular debris. The supernatant was transferred to a new tube and boiled for 5 min in presence of 5x Protein loading buffer containing β-mercaptoethanol. The sample was kept at -70^{o}C when not used immediately for SDS-PAGE analysis. For IP experiments, mRIPA buffer was replaced with NP-40 lysis buffer (IP buffer) (Table 8.6).

8.3.2 Immunoprecipitation (IP)

For IP, cell lysates were mixed with a particular antibody and incubated for 1 h at 4^{o}C on a rolling plate. Protein A/G beads (Santa cruz) were washed twice with ice cold IP buffer and pelleted at 8000 x g for 1 min at 4^{o}C before being added to the reaction tubes. The tubes were incubated in the same conditions for at least 3 h to over-night and finally the beads were collected by spinning down at 8000 x g for 1 min at 4^{o}C and washing 3 times with ice cold IP buffer.

Table 8.6 | Buffer used for cell lysate preparation

Name	Composition
IP buffer	25mM Tris pH 7.4, 150mM NaCl, 1mM EDTA, 1% NP-40, 5% glycerol
mRIPA buffer	50mM Tris pH 7.4, 150 mM NaCL, 1% Sodium deoxycholate, 1% Triton X-100

8.3.4 Protein estimation by BCA assay

On a 96-well flat bottom dish 200 µL of the samples (cell lysates), the standard and the blanks were added in duplicate. A 5x diluted sample was prepared by adding 12µL of samples to 48µL MQW. Then standards were prepared with known concentration of BSA starting from 2000µg/mL to 125µg/mL. To each well 200 µL of BCA reagents (BCA protein reagent kit A:B mixed at 50:1 ratio) was added and mixed well by tapping. The plate was incubated for 30 min at 37^{o}C and read in a plate reader at 570 nm. A standard curve was prepared from the values of standard samples and protein concentration of the samples were calculated. Table 8.7 shows the reagents used for BCA assay.

Table 8.7 | Reagents for BCA assay

Solution	Composition
Blank	200µL, 800µL MQW
Standard	40µL of sample lysis buffer, 40µL of 10µg/µL BSA, 120µL MQW
Reagent A	Sodium carbonate, sodium bicarbonate, bicinchoninic acid, sodium tartrate in 0.1M sodium hydroxide
Reagent B	Contain 4% cupric sulfate

8.3.5 SDS-PAGE

The protein samples were resolved in parallel with pre-stained protein markers using Mini-PROTEAN system (Bio-Rad) and SDS-polyacrylamide gels. The gel was run at 170 v for approximately 1 h.

8.3.6 WB analysis

Proteins separated by SDS-PAGE were transferred to nitrocellulose membrane (0.45 µm) using the Mini Trans-Blot Electrophoretic Transfer Cell (Bio-Rad). Protein transfer was carried out either at 70 v for 2 h or 18 v overnight at 4^{o}C. The nitrocellulose membranes were then blocked with 5% milk powder in PBS-T for 15 min. The membranes were the incubated with appropriate dilution of primary antibody in PBS-T containing 0.5% milk powder for 1 h, washed thress times with PBS-T (for 5 min each time), incubated with secondary antibodies in PBS-T for 1 h and finally washed six times with PBS-T (for 5 min each time). The membranes

were visualised using a LI-COR Odyssey CLx Infrared Imager. Buffers used for SDS-PAGE and WB are listed in Table 8.8.

Table 8.8 | SDS-PAGE and WB buffer solutions

Solution	Composition
SDS-PAGE sample loading buffer (5x)	250mM Tris base, pH 6.8, 10% (v/v) SDS, 50% glycerol, 0.01% (w/v) bromophenol blue, 3.5% (v/v) β-mercaptoethanol
SDS-PAGE running buffer (1x)	25mM Tris base, 200mM glycine, 0.1% (w/v) SDS
Western transfer buffer (1x)	25mM Tris base, 200mM glycine, 10% (v/v) ethanol
PBS-T	PBS containing 0.1% (v/v) Tween 20
Blocking buffer	5% (w/v) non-fat dehydrated milk in PBST

8.3.7 Immunofluorescence (IF) microscopic techniques

Cells were seeded on 13 mm coverslips at a density of $5x10^4$ well in a 24-well plate. Next day, the cells were either infected with HSV-1 strains at MOI of 1 PFU/cell or transfected (section 8.4.4). After incubation for a required time at 37ºC the cells were washed with PBS and fixed with 3% (v/v) formaldehyde in PBS for 10-15 min. Next, the cells were treated for 5 min with permeabilisation solution (1% FCS, 0.1% Triton X-100, in PBS) (Table 8.9) followed by appropriately diluted primary antibody (Table 8.10) for 1 h. The cells were washed three times with IF permeabilisation solution and incubated with AlexaFluor secondary antibodies for 1 h. Finally, the cells were washed three times in IF wash, three times in PBS and three times in water and mounted on glass slide with Prolong Gold antifade reagent containing DAPI (Invitrogen).

Table 8.9 | Immunofluorescence (IF) Microscopy solutions

Solution	Composition
Fixing solution	1x PBS, 3% EM-grade formaldehyde, dH_2O
Permeabilisation Solution	1% FCS, 0.1% Triton X-100, in 1x PBS

FCS: Fetal calf serum

Table 8.10 | Antibodies used in this study

Antigen	Name	Raised in	Isotype	Application and Dilution	Source
Cellular					
Actin	AC40	Mouse	IgG2a	WB (1:5000)	Sigma
Anti HSV-1	DAKO	Rabbit	-	IF (1:1000)	DAKO
ATP5A1	Sc-2020	Goat	-	WB (1:2000)	Santa cruz
HSP60	66041-1-Ig	Mouse	IgG1	IF (1:20), WB (1:5000)	proteintech
HSP90	sc-7947	Rabbit	-	WB (1:5000)	Santa cruz
Nipsnap1	sc-515197	Mouse	IgG1	IF (1:50), WB (1:1000)	Santa cruz
Nipsnap2	ab204890	Rabbit	IgG	IF (1:100), WB (1:500)	abcam
IFITM2	12769-1-AP	Rabbit	-	IF (1:50), WB (1:1000)	proteintech
LAMP1	H4A3	Mouse	-	WB (1:10000)	DSHB Hybridoma
Myoferlin	sc-376879	Mouse	IgG1	IF (1:50), WB (1:1000)	Santa cruz
PHGDH	sc-390610	Mouse	IgG1	IF (1:10), WB (1:500)	Santa cruz
PHB	ab55618	Mouse	IgG2a	WB (1:2000)	abcam
	ab75771	Rabbit	-	WB (1:2000)	abcam
RAB7	ab50533	Mouse	IgG2b	WB (1:2000)	abcam
Tubulin	MCA77G	Rat	-	WB (1:2000)	AbD Serotec
TOM20	sc-17764	Rabbit	-	IF (1:100)	Santa cruz
VDAC1	ab-14734	Mouse	IgG2b	WB (1:500)	abcam
Viral					
gB	CB24	Mouse	IgG2b	IF (1:6), WB (1:50)	CMC and SB (Zenner et al., 2011)
gC	CC6	Mouse	IgG2a	IF (1:6), WB (1:10)	CMC and SC
gD	AP12	Mouse	IgG1	IF (1:3)	AM (Minson et al., 1986)
	LP2	Mouse	IgG2a	IF (1:3)	
	LP14	Mouse	IgG2a	IF (1:6), WB (1:50)	
gE	3114	Mouse	IgG2a	IF (1:6), WB (1:50)	CMC (Cross et al., 1987)
gE/gI	3063	Mouse	IgG1	IF (1:6), WB (1:50)	CMC (described in Collins and Johnson, 2003)
gG	LP10	Mouse	IgG2a	IF (1:6), WB (1:10)	AM (Richman et al., 1986)
gH	BBH1	Mouse	IgG2a	IF (1:6), WB (1:10)	HB
gH/gL	LP11	Mouse	IgG2a	IF (1:6)	AM (Buckmaster et al., 1984)
gI	CC8	Mouse	IgG2a	IF (1:6), WB (1:10)	CMC
	CC7	Mouse	-	IF (1:6), WB (1:10)	CMC
	3104	Mouse	-	IF (1:6)	CMC (Cross et al., 1987)
pUL13/14	R220	Rabbit	-	WB (1:3000)	GE (Morrison et al., 1998)
pUL16	N-term	Rabbit	-	WB (1:2000)	JW
pUL19 (VP5)	AB6508	Mouse	IgG2b	WB (1:1000)	Abcam
	LP12	Mouse	IgG2a	IF (1:3)	AM
pU49 (VP22)	AGV30	Rabbit	-	WB (1:5000)	GE (Elliot and O'Hare, 1997)
	CC10	Mouse	IgG1	IF (1:6)	CMC
	CC11	Mouse	-	WB (1:10)	CMC
VP1/2	CB4	Mouse	IgG2b	IF (1:6)	CMC (Svobodova et al., 2011)

VP16	LP1	Mouse	IgG1	IF (1:6), WB (1:50)	AM (McLean et al., 1982)
Other					
GFP	JL-8	Mouse	IgG2a	IF (1:300), WB (1:5000)	Clontech
MYC	9E10	Mouse	IgG1	IF (1:100), WB (1:1000)	SC
HA (HA-11)	MMS 101R	Mouse	IgG1	WB (1:1000)	Biolegend

AM: Prof. Anthony Minson (University of Cambridge), CMC: Dr Colin Crump (University of Cambridge), HB: Dr Helena Browne (University of Cambridge), SB: Susanne Bell (University of Cambridge), SC: Susanna Colaco GE: Prof. Gill Elliott (University of Surrey), JW: Dr John Willis, University of Pennsylvania, DSHB: Developmental Studies Hybridoma Bank (H4A3 was deposited to the DSHB by August, J.T. / Hildreth, J.E.K),

8.4 Tissue culture techniques

8.4.1 Cell maintenance

The following cell lines A549, COS-7, HaCaT, HEK-293T, HeLa, HFF-hTERT and Vero cells (Table 8.11) were maintained in Dulbecco's modified Eagle's medium (DMEM) supplemented with 10% FCS, 2mM L-glutamine, 100U/mL penicillin and 100µg/mL streptomycin. All cell lines were maintained at 37ºC in a humidified incubator with 5% CO_2 supply.

8.4.2 Freezing of cells and resuscitation

For long term storage cells were harvested and resuspended in freezing medium (10% DMSO in FCS). Approximately $3x10^6$ cells were aliquoted per vial and slowly frozen in a cryogenic freezing chamber at -70ºC before transferring to liquid nitrogen. For resuscitation cells were thawed at 37ºC and transferred to tissue culture flasks containing pre-warmed medium. After 24 h incubation the medium was replaced with fresh medium.

8.4.3 Sub-culturing cells

Cells were subcultured twice a week. Firstly, the growth medium was removed from the flask and the monolayer was washed with PBS. Then the cells were detached from the flask by incubating with 0.05% (v/v) trypsin and 0.02% (v/v) EDTA in PBS for 5-15 min (depending on cell lines) at 37ºC. The cells were then re-suspended in fresh warm medium to neutralise the trypsin and a proportion of the cells were re-seeded back into a flask with fresh medium for continued culture.

8.4.4 Transfecting mammalian cells

Mammalian cells were either transfected for IF or IP experiments. For IF, $5x10^4$ cells were seeded on to 13mm coverslips in 24-well plates. Once the cells were attached (after 3-4 h) or the next day the cells were transfected. Initially, 0.6µL of TransIT-LT1 transfection reagent (Mirus) was diluted in 35µL of serum free Opti-Mem medium (Life Technologies) per transfection condition and incubated for 5 min at RT. Subsequently, 0.2µg of plasmid DNA was mixed with the TrasIT-LT1/media solution and incubated for 15 min at RT. Finally, the mixture was added to the cells and incubated at 37ºC for a preferred period of time and processed further.

For IP or relatively larger volume of transfection, HEK293T cells were seeded on 10cm dishes and incubated for 3 h or overnight. For the transfection, 10µg of DNA along with 40µL PEI in 1ml of Opti-Mem were incubated for 20 min at RT and added to the cell.

Table 8.11 | Cell lines used in this study

Cell line	Description
A549	Adenocarcinomic human alveolar basal epithelial cells
A549-IFITM2-HA	Adenocarcinomic human alveolar basal epithelial cells transduced with IFITM2-HA at C terminus
COS-7	African green monkey kidney cells
HaCaT	Immortalised human keratinocyte cells
HEK-293T	Human embryonic kidney cells
HeLa	Human cervical carcinoma cells
HFF-hTERT	Human foreskin fibroblast cells immortalised by stable expression of human telomerase
Vero	African green monkey kidney epithelial cells

8.5 Virus techniques

8.5.1 Virus release assay

Six-well dishes were seeded with $4x10^5$ cells/well (Vero/HFF-hTERT/HeLa/HaCaT/A549/ COS-7) and after overnight incubation at 37ºC the cells were infected with viruses (5 or 10 PFU per cell) to be assayed. At the required time point ~90% of the medium (supernatant) was removed and the cells were scraped into fresh medium and collected in separate tubes (cell associated). The supernatants were centrifuged at 5000 rpm for 5 min in a bench top microfuge

to remove any cell debris before transferring the supernatant to fresh tubes. This step was performed two consecutive times. All samples were stored at -70ºC until virus titration, and the harvested cell samples were freeze-thawed three times in total. The amount of virus present both in supernatant (released virus) and in cell scrapes (cell-associated virus) were determined by plaque assay. Table 8.12 listed the solutions used for virus growth analysis.

8.5.2 Determination of virus titre through plaque assay

Six-well dishes were seeded with $4x10^5$ Vero cells/well and incubated overnight at 37ºC. The virus samples were defrosted and 10-fold serially diluted. Medium from the Vero plates was aspirated and 500µL of the diluted virus samples was added to different wells and incubated at 37ºC to allow the virus to infect the cells. After 1 h incubation, 2 ml of overlaying medium (DMEM supplemented with 2% FCS, 2mM L-glutamine, 100U/mL penicillin and 100µg/mL streptomycin and 0.6% carboxymethylcellulose) was added to each well and the plates were incubated at 37ºC for 2-3 days. The infectious virus titre was determined by counting the plaques after formal saline fixation followed by 0.1% toludine blue staining.

8.5.3 Production of virus stocks

Virus stocks e.g., master, sub-master and working stocks were produced one after another. For generation of a master stock $2x10^6$ Vero cells (in a T75 flasks) were infected with pre-master virus (produced by transfection of Vero cells with HSV-1 BAC DNA and a Cre expression plasmid, pGS403) at 0.1-0.005 PFU/cell and incubated at 37ºC for 2-4 days. The cells were harvested after they started rounding and detaching from the flask by shaking or by scrapping. The cells were pelleted at 1400 rpm for 5 min at 4ºC. The pellet was resuspended in ~1ml medium, sonicated for 30 sec at 39% amplitude and aliquoted in to several tubes. The tubes were stored at -70ºC as master stock. The virus titre was determined by plaque assay as describe above (8.5.2). Subsequent virus stocks were made following the same procedure with greater numbers of cells. Experiments were all conducted with working stock virus for consistency.

Table 8.12 | Solutions used for virus growth analysis

Solution	Composition
PBS	138mM NaCl, 2.7mM KCl, 8mM Na_2HPO_4, 1.5mM KH_2PO_4, pH 7.4; Prepared by technical staff at the Department of Pathology, University of Cambridge.
Acid wash	40mM citric acid, 135mM NaCl, 10mM KCl, pH 3.0

CMC overlay	0.6% (v/v) CMC and 2% (v/v) FCS diluted in DMEM supplemented with glutamine and antibiotics
Formal Saline	3.7% (v/v) formaldehyde in PBS
Toludine Blue	0.1% (w/v) toludine blue in water

CMC: carboxymethylecellulose, PBS: phosphate buffered saline

8.5.4 Single step growth curve

Cells were seeded at $4x10^5$ cells/well on six-well plates or at $1x10^5$ on 24-well plates, except for HaCaT cells where twice as many cells were seeded. The next day, cells were infected with 10 PFU/cell of the appropriate viruses by incubation for 1 h at 37ºC and then incubated with acid wash for 1 min to inactivate residual viruses, followed by three PBS washes and then finally, growth medium was added to each well. At various time points the samples were collected and frozen at -70ºC. For cell free viruses, culture medium from the wells were collected prior to freezing and spun twice to remove cell debris as described above. The wells were topped up with the same volume of culture medium as was removed and cells were harvested by scraping. The cells were then lysed by three cycles of freeze thawing to release the cell-asociated viruses. The supernatant and cell-associated virus titres were determined by plaque assays.

8.5.5 Plaque size analysis

Plaque assay plates using Vero cells were fixed and stained with 0.1% toluidine blue solution and were scanned at 600 dpi. The diameter of the plaques was determined using Adobe Photoshop in pixels and the average plaque size was calculated from 60 plaques.

Plaques on HFF-hTERT and HaCaT cell monolayers were stained with DAB (3,3' Diaminobenzidine) peroxidase substrate kit. At first the cells were washed once with PBS and then fixed with 4% formaldehyde for 10 min. The cells were washed again with PBS and were blocked with Blocking buffer (5% FBS, 0.5% Tween in PBS) for 30 min. Next, the cells were incubated for 1 h with HSV-1 gD-specific antibody (LP2) and washed three times with Blocking buffer. Cells were then incubated with anti-mouse HRP antibody (1:1000) for 1 h and finally washed three times with Blocking buffer and once with PBS. To reveal the plaques,

samples were developed with DAB peroxidase substrate (ImmPACT DAB Vector, SK4105) where 1 mL of DAB diluent was mixed with 30 µL of DAB chromogen and added to the cell for 5-10 min and finally washed with water. The plates were scanned and plaque size was measured in Photoshop.

8.5.6 Virus purification by sucrose cushion

HaCaT cells were grown in 10 cm dishes and were infected with viruses at 5 PFU/cell for 1 h at 37ºC followed by acid wash for 1 min and three PBS washes and then incubated with complete growth medium. After, 24 h the culture supernatant was collected and centrifuged by two consecutive low speed centrifuge (912 x g for 20 min, 4ºC, Beckman GH-3.8 and then 1700 x g for 30 min, 4ºC, Beckman SW32Ti) to remove cellular debris. The clarified medium (3mL) was gently overlaid on top of 1mL of 33% (v/v) sucrose. Virus particles were then pelleted at 48600 x g for 3 h at 4ºC in a Beckman centrifuge TLA-100.3 rotor. The virus pellet was resuspended in 50 µL of 1x SDS-PAGE sample buffer and tested by WB for various proteins.

8.5.7 Virus purification by Ficoll gradient

HaCaT cells were grown in roller bottles and were infected with viruses at 0.01 PFU/cell for 1 h at 37ºC then the bottles were PBS washed three times and then incubated with fresh medium. After 72 h the culture medium was harvested and cell debris was removed by low speed centrifugation (912 x g for 12 min at 4ºC, Beckman GH-3.8). From the clarified supernatant virus particles were pelleted by centrifugation at 48300 x g for 2 h at 4ºC (Beckman Type 19 rotor). The pellet was resuspended in 2mL of 1% FCS/PBS and sonicated for 20 sec at 39% amplitude in a cup horn sonicator (Fisher Scientific). A 30mL 5% to 15% ficoll gradient was prepared onto which the resuspended virus was carefully added. The gradient was centrifuged at 26400 x g for 90 min at 4ºC (Beckman SW32Ti) and the light scattering band of virus particles was carefully aspirated using a syringe and needle. The samples were diluted to 30 mL with PBS and virus particles were pelleted by centrifugation at 68200 x g for 90 min at 4ºC

(Beckman SW32Ti) and finally dissolved in 100µL of sterile PBS. The virus preparation was aliquoted and stored at -70ºC, and the titre was determined by plaque assay.

8.5.8 Transmission electron microscopy (TEM)

Monolayers of HaCaT and HFF-hTERT cells were seeded on 35 mm culture dishes and infected at MOI of 3 PFU/cell. After 15 hpi the cells were washed with 0.9% (w/v) sodium chloride and fixed in 2% glutaraldehyde/2% formaldehyde in 0.5 M sodium cacodylate buffer (pH 7.4) for 4 h at 4ºC. The samples were sent to the Department of Pathology TEM Facility, University of Cambridge, for further processing and TEM imaging.

8.6 Construction of recombinant viruses

Recombinant viruses were constructed by two-step Red recombination technique (Tischer et al., 2010). Firstly, a liner DNA target cassette containing a resistance gene and an I-SceI recognition site with a flanking region (homologous to target site) was constructed by PCR. The cassette was then introduced into *E. coli* GS1783 strain bearing BAC-cloned HSV-1 genome (strain KOS) for homologous recombination. First Red recombination introduces the whole DNA construct in the target region of viral DNA and second Red recombination removes the selection markers from the insert leaving only the target gene in the viral DNA (Figure 8.1).

8.5.1 Construction of a targeting cassettes

A target DNA cassette was constructed using the appropriate primers as listed in Table 8.2 and according to the protocol as described in section 8.2.1. For most of the recombinant virus generation, where mutations were encoded in the primer sequences, pEPkan-S was used as the DNA template. However, for EYFP-tagging, pEP-EYFP(A206K)-in template DNA was used. After PCR, 50 µL of the product was treated with 2 µL DpnI in presence of 5.5 µL 10x buffer 4 (NEB) at 37ºC for 1 hr to remove the template DNA from the PCR amplicon. The mixture was then separated by agarose (0.8%) gel electrophoresis and purified using in house reagents. Concentration of the purified DNA was measured in Nanodrop (NanoDrop 1000, Thermo Scientific, USA).

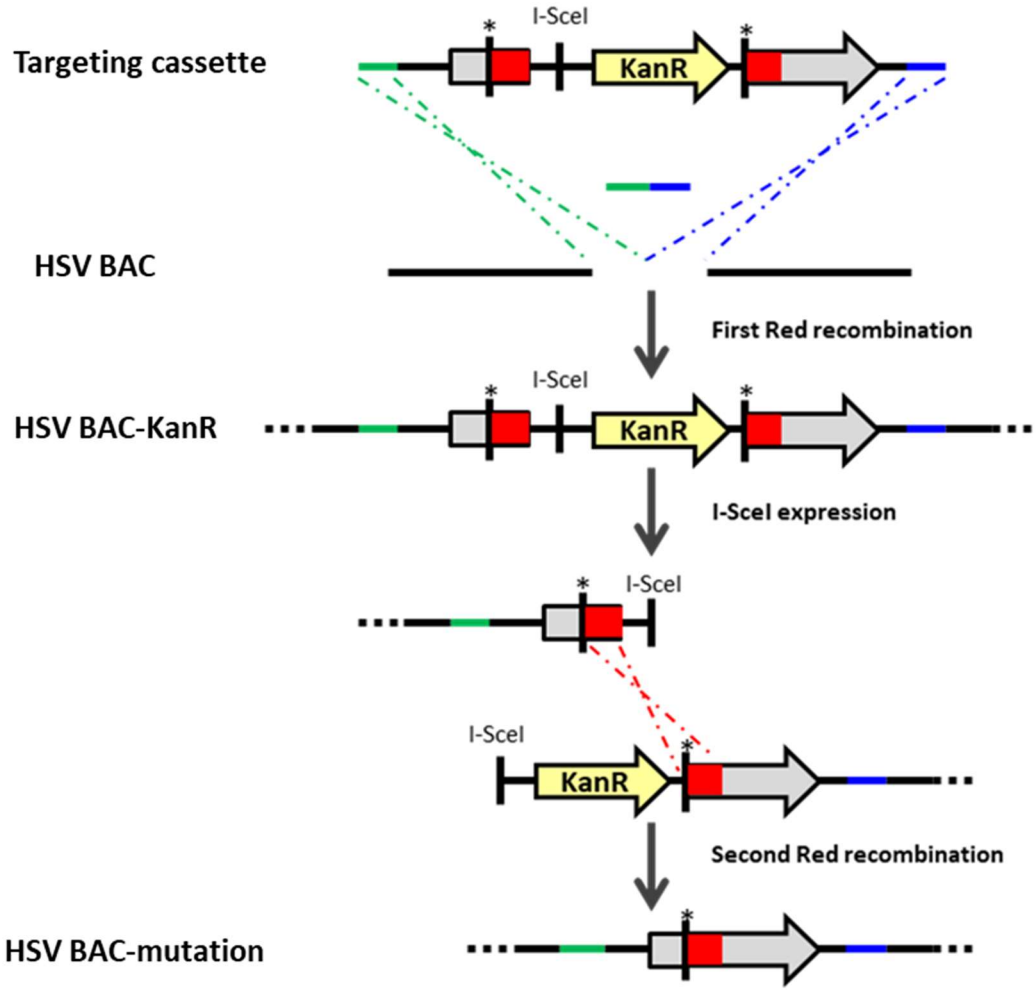

Figure 8.1 | Two-step Red recombination for mutant virus construction. A targeting cassette is first constructed using PCR and inserted by first Red recombination. Subsequently, expression of I-SceI cleaves the HSV BAC-KanR and second Red recombination removes the KanR gene from the construct. Coloured and dotted lines showing homologous recombination, asterisks are indicating unique restriction site. Lines (blue and green) or boxes (red) of identical colours are indicating same sequence. Image modified from Tishcher et al. (2006).

8.5.2 Competent cell preparation and electroporation

2ml of LB containing 34μg/ml chloramphenicol (CAM) was innoculated with *E. coli* GS1783/HSV-BAC and incubated at 30ºC with shaking overnight. Next day, 500 μL of the culture was transferred to 50 ml LB containing 34μg/ml CAM and incubated with shaking at 30ºC. When the cell density reached 0.5-0.7 nm at A_{600} the culture flask was transferred to 42ºC shaking water bath and incubated for 15 min to induce Red recombinase expression. The cells were immediately chilled in a shaking ice bath for 20 min. Subsequently, the cells were pelleted at 1200 x g at 4ºC for 5 min, the supernatant was discarded and the pellet was washed with ice-cold 10% (v/v) glycerol. Glycerol wash was repeated three times and finally the pellet was resuspended in 1 ml ice-cold 10% (v/v) glycerol. Electrocompetent cells were aliquoted in 100 μL aliquots and frozen in liquid N_2 before storing at -70ºC.

The electrocompetent cells (50 μL) were mixed with ~5μL (100 ng maximum) of purified PCR product. Electroporation was carried out in a 2mm ice-cold electroporation cuvette with 3000v, 25μF and 200Ω settings. The transformation mix was recovered in 1mL LB and incubated for 1-2 hr in a 30ºC shaking incubator. The cells were pelleted at 1200 x g for 5 min, resuspended in 100μL LB and plated on agar plate containing 34μg/mL chloramphenicol (CAM) (for BAC positive selection) and 30μg/mL kanamycin (KAN) (for targeting cassette selection). The plate was incubated overnight at 30ºC and selected colonies were checked by restriction digest assay.

8.5.3 Bacterial artificial chromosome (BAC) miniprep I and restriction digestion of BAC DNA

HSV-1 BAC DNA was isolated using plasmid DNA purification buffers from NucleoBondXtra Midi (Macherey-Nagel) commercial kit. Representative colony from KAN/CAM plates inoculated in to 10mL LB media containing 30μg/mL KAN and 34μg/mL CAM and incubated overnight in a 30ºC shaking incubator. The cells were pelleted at 1200 x g for 5 min at 4ºC. The pellet was resuspended in 200μL RES (resuspension) buffer and 200μL of the suspension was transferred to a fresh 2mL eppendorf tube. Residual cells were diluted with 1mL of LB containing KAN/CAM and stored at 4ºC for second Red recombination step and/or to create glycerol stocks. 300μL LYS (lysis) buffer was added and after 5 min incubation 300μL NEU (neutralising) buffer was added to stop lysis. The mixture was then centrifuged at 17,000 x g for 10 min in a 4ºC centrifuge. The supernatant was transferred to 600μL phenol:cholorform solution (1:1) and the tube was inverted several times to mix the phases. The tube was

centrifuged for 5 min at 17,000 x g and the top layer containing DNA was carefully transferred into fresh tubes, to which 800µL isopropanol was added. The tube was inverted several times and left on the bench to allow the DNA to be precipitated and spun at 17,000 x g for 5 min. The supernatant was poured off and the DNA pellet was washed with 500µL 70% ethanol, air dried and finally resuspended in 40µL EB (elution buffer, 10mM Tris at pH 8). Isolated BAC DNA was digested with appropriate restriction enzymes to confirm correct recombination had occurred.

8.5.4 Second Red recombination

Bacterial cultures found to be positive in the BAC miniprep I were grown overnight in a 30ºC shaking incubator. 100 µL of the culture was transferred to 2mL of LB containing 34µg/mL CAM and incubated at 30ºC with shaking. After 2-3 h of incubation 2mL of LB with 34µg/mL CAM and 2% (w/v) arabinose (final concentration 1%) was added and the culture was incubated for another 1 h at 30ºC with shaking to induce the expression of I-SceI. Next, the culture was heat-shocked at 42ºC in shaking water bath for 30 min to stimulate the expression of Red recombination system. The culture was then incubated further for 3-4 h at 30ºC in a shaking incubator. Samples were diluted and 10^{-3}-10^{-4} dilutions were plated on CAM (34µg/ml) + arabinose (1%) agar plates. The plates were incubated at 30ºC for 24-48 h. From these plates, several colonies were plated onto replica LB agar plates with 34µg/mL CAM and with or without 30µg/mL KAN to select the clones which are CAM resistant and KAN sensitive. Individual colony grown on CAM plate but not on KAN-CAM plate was selected for BAC miniprep II.

8.5.5 BAC miniprep II and restriction digestion of BAC DNA

Selected KAN sensitive clones from CAM only plates were grown and DNA isolaterd as described above. Subsequently, restriction digest analysis was performed to confirm deletion of the selection markers from the chosen colonies. At least one of the positive clones was selected and grown overnight at 30ºC with shaking and 1mL aliquots containing 15% (v/v) glycerol were snap frozen in the liquid N_2 and finally stored at -70ºC. BAC DNA of the selected clone was used for making recombinant virus and glycerol stock was used to generate additional modifications to the viral genome bu Red recombination.

8.5.6 BAC-excision and virus reconstitution

A six well dish was seeded with $2x10^5$ Vero cells/well. The following day, the cells were transfected with BAC DNA with pGS403 plasmid encoding Cre recombinase which excises the LoxP site flanked BAC cassette from the viral genome. Firstly, 100µL of serum free medium was thoroughly mixed with 3µL TransIT. After 5 min 2µL BAC DNA and 1µg pGS403 plasmid was added, mixed gently and incubated for 15-20 min. 100µL of the mixture was added drop by drop to the Vero cells. After 3-4 days incubation at 37ºC the cells were scraped and sonicated for 30 sec at 39% amplitude and stored at -70ºC as pre-master virus stock. Premaster stocks were titred and used for generating master stocks.

8.5.7 HSV-1 BAC DNA preparation from infected cells

Vero cells were seeded at $4x10^5$ cells per well in six well plate and next day the cells were infected with 1 MOI of the appropriate recombinant HSV-1. After 24 h incubation at 37ºC the cells were scraped, transferred to microcentrifuge tubes and spun down at 1200 x g for 5 mins in a refrigerated centrifuge (4ºC). The supernatant was removed, and the cell pellet was lysed in 500µL of Proteinase K lysis buffer for 3 h at 37ºC. The DNA was separated from protein by adding an equal mixture of chloroform and phenol (1:1) to the lysate and inverting gently several times before centrifuging at 1700 x g for 10 min at 4ºC. DNA containing top layers was removed and DNA precipitated in isopropanol as described above.

8.6 Stable isotope labelling with amino acids in cell culture (SILAC)

8.6.1 Maintenance of SILAC-labelled cell lines

HaCaT cells were grown in DMEM containing stable isotope of arginine (R) and Lysine (K) amino acid as R0K0, R6K4 and R10K8 for Light (L), Medium (M) and Heavy (H) respectively (Cambridge Isotope Laboratories). The cells were first grown in L-SILAC media containing no labelled amino acid for viability test. Next, the cells were grown in labelled media either M or H for a minimum of five cell doubling times. A brief trypsinisation was done to split the cells followed by 3x PBS washing to get rid of any residual trypsin.

8.6.2 SILAC:IP from infected cells

SILAC-labelled HaCaT cells ($2x10^6$ cells) were seeded to 9 cm dishes as in triplicate for Light, Medium, and Heavy labelled media. When the plates were 60-70% confluent the cells were infected with viruses at 37ºC for 1 h followed by acid wash (1 min) and three PBS washes and incubated with either Light, Medium or Heavy DMEM media as required. At 18 hpi the cells were scrapped and washed three times in cold PBS and resuspended in 1mL cold lysis buffer (with protease inhibitors) and transferred to low binding eppendorf tubes. Cell lysis was carried out for 30 min at 4ºC and spun at 14000rpm for 10 min at 4ºC and then the supernatant was transferred to pre-chilled tubes (Table 8.13). A BCA assay was performed to determine the protein concentration and equal amount of proteins (from mock, control and sample) were utilised for IP experiments with desired antibody.

Table 8.13 | Buffer for SILAC:IP

Buffer	Composition
Lysis buffer	10mM Tris-HCl pH 7.5, 150mM NaCl, 0.5mM EDTA, 0.5% NP-40, 1:100 Sigma Protease Inhibitor added freshly
Wash buffer	10mM Tris-HCl pH 7.5, 150mM NaCl, 0.5mM EDTA

8.6.3 Mass spectrometry of IP samples

The combined samples from SILAC-labelled HaCaT cells of three biological repeats were submitted for LCMS/MS analysis at proteomics facility unit in Bristol University.

8.6.4 Data analysis

Raw MS data were copied into a spreadsheet and parameters other than accession number, unique peptide number, ratios comparing samples (Sample/Mock), variability ratios and proteins description were deleted. For Mock/Sample ratio the values were converted to Sample/Mock using '=1/ratio' formula. In a new column of the spreadsheet log2 SILAC ratios for all Sample/Mock values were calculated. Since SILAC ratio results for protein data shows abundance between 0 and 1 the data is usually converted to a log2 SILAC ratio to make the abundance distribution wider on both positive and negative scale. Ideally, true interacting partners of the bait protein should have positive, environmental contaminants should have

negative and non-specific binding partners should have 0 log2 SILAC ratios. This transformation allows the data to fit a Gaussian distribution centred on a log2 SILAC ratio of 0. From the Excel spreadsheet log2 Sample/Mock ratio column was copied into graph pad prism file. A 'New analysis, was then run selecting 'Frequency distribution' mode to a generate histogram for the identified proteins at a given ratios. Next a 'Gaussian distribution' was generated for nonlinear regression which fits a curve on the previous histogram. This step also generated the mean and standard deviations of the Gaussian distribution. A threshold was then generated at the 95% confidence limit ($p \leq 0.05$) by adding 1.96 standard deviations to the mean. Threshold for other replica experiments were determined individually. Proteins having ratio variability above the threshold were considered as hits and proteins that were below the threshold may represent a contaminant. Proteins identified in at least two experiments represented a high confidence interaction. Across the replica experiments the identification of the same proteins via different or multiple accession numbers were sorted as the same (Emmott et al., 2014).

8.7 Protein purification and cell free protein expression

8.7.1 High-throughput grow-up of GST-tagged protein

Transformed bacterial colonies from culture plates were picked and grown overnight at 37ºC in 3mL of 2xTY medium with antibiotics as required. 35µL of the overnight culture was added to 3.5 mL of fresh 2xTY medium containing appropriate antibiotics. The culture was grown at 37ºC to an OD_{600} of 0.6-1.0. In a parallel set-up after adding 35 µL overnight culture, the media was transferred to 22ºC incubator and protein expression was then induced by adding 0.2 mM IPTG. The 37ºC induced cultures were grown for further 4 h whereas the 22ºC cultures were grown over night. After each incubation 1.5mL culture was transferred to eppendorf tube and centrifuged at 9000 x g for 5 min to collect cell pellet. The pellets were stored at -20ºC until required.

8.7.2 Magnetic Bead GST binding

For the cell pellets collected in the previous step, 250µL lysis buffer was added and the cells were lysed at RT for 30 min in an orbital shaker. The cell debris were pelleted at 14000 x g for 10 min and 200µL cell lysates were collected. Into a flat bottom 96-well ELISA plate 20 µL of GST magnetic bead was dispensed and washed twice in 100µL of wash buffer for 1 min on a

shaker. The plate was then placed on a magnet for 1 min to collect the beads to the side wall of the wells and the supernatant was discarded. The 200µL cell lysates was directly transferred on to washed magnetic beads. The contents were mixed for 30 min by shaking at 4ºC. Then the plate was placed on magnet for 1 min, the supernatant was removed, the beads were washed twice with 200µL wash buffer for 5 min and then separated on magnet for 1 min. Finally, 50µL elution buffer was added to each well and mixed on shaker for 1 min, placed on a magnet for 1 min and the supernatant collected. The supernatant was mixed with SDS-PAGE loading buffer and analysed by gel electrophoresis. Buffers for magnetic GST pull-down listed in Table 8.14.

Table 8.14 | Buffers for Magnetic GST pull-down

Buffer	Composition
Lysis	125mM Tris pH 7.4, 300mM NaCl, 1% (w/v) Tween20, 1.4mM 2-mercaptoethanol
Wash	125mM Tris pH 7.4, 300mM NaCl, 0.05% v/v Tween20
Elution	125mM Tris 7.4, 300mM NaCl, 0.05% v/v Tween20, 50mM reduced glutathione

8.7.3 GST Protein purification

GST-tagged protein encoding plasmid bearing *E. coli* Rosetta cells were grown in 2xTY with appropriate antibiotics at 37ºC for 4 h and transferred to 1 litre 2xTY media. After 2-3 h incubation at 37ºC shaker IPTG was added to the medium when OD_{600} of the media was between 0.8-1.0. The next day, cell pellets were collected by centrifugation at 6000 x g for 15 min at 4ºC and used immediately or stored at -80ºC. The pellets were resuspended in lysis buffer using a pre-cooled cell disruptor (Constant system) at 24 Kpsi. The lysates were clarified by centrifugation (40000 x g, 30 min at 4ºC) and purified by affinity chromatography using GSH beads (GE Healthcare). GSH beads are added to the column and washed with MQW followed by buffer. The beads were then mixed with clarified supernatant of cell lysates and incubated (4ºC, 1 h) on a rotating wheel. The mixture was added back to the column and washed with wash buffer. The protein was then extracted in elution buffer into various tubes. On a 96 well ELISA plate 200 µL Bradford reagents were added and 5 µL proteins from

different elution tubes were tested. Fractions shown to contain protein were purified by size exclusion (S200 16/600 column) chromatography and concentrated using a 10 KDa MWCO 4 mL Amicon concentrator by centrifugation at 4000 rpm for 5 min. Purified protein was tested by SDS-PAGE analysis, concentrated, mixed 1:1 with 100% v/v glycerol and stored at -20ºC. Table 8.15 shows the buffers used.

Table 8.15 | Buffers for GST protein purification

Buffer	Composition
Lysis buffer	20mM Tris pH 7.6, 300mM NaCl, 0.5mM $MgCl_2$, 1.4mM 2-ME, 0.05% Tween20, 400U DNAse, 200µL protease inhibitor
Wash buffer	20mM Tris pH 7.6, 300mM NaCl, 1mM DTT
Elution buffer	Wash buffer, 25mM GSH

8.7.4 Cell-free protein expression in Wheat-germ

Template DNA (2-4µg) containing desired insert in pF3A plasmid was dispensed on ice in 200µL PCR tubes. MQW was added to make the final volume 20µL. TNT SP6 high yield Wheat germ reaction mixture was quickly thawed from -70ºC and 30µL was added to the tube. The tube was incubated for 2 h at 25ºC in a thermal cycler for cell free protein production.

8.7.5 Magnetic GST pull-down with cell-free protein

In a flat bottom 96 well ELISA plate, 20 µL GST magnetic beads were dispensed. The beads were washed twice with 200 µL wash buffer with 1 min shaking followed by 15 sec on magnet to remove the supernatant. The bait protein was added to this 96 well plate with GST beads and was shaken for 10 min and placed on a magnet to remove the supernatant which was followed by three washes as described above. The beads were kept in 100µL buffer. Cell-free reaction mixture (from the previous section) was then added to the appropriate 96 wells and mixed for 1 h followed by 4x washes as described above. Finally, 48 µL elution buffer was added to each well and mixed on a shaker for 1 min and then placed on a magnet to collect the supernatant for SDS-PAGE analysis. Buffers used in this step is listed in Table 8.16.

Table 8.16 | Buffer for GST pull-down of bait protein

Buffer	Composition
Wash	20mM Tris pH 7.4, 200mM NaCl, 0.1% v/v NP-40, 1mM DTT, 1mM EDTA
Elution	Wash buffer, 50mM reduced glutathione

8.8 Lenti-transduction

8.8.1 Gateway system for pDONR vector construction

Gateway primers with necessary attP sites for recombining in to the pDONR (207) vector were constructed for the protein of interest. PCR reactions were perfomred from HSV-1 DNA template using the gateway primers and were purified by 'PCR cleanup'. 150ng of pDONR containing attP recombination sites were mixed with 150ng of the PCR product in presence of 2µL BP enzyme and MQW (up to 10 µL). The reaction mixture was incubated at 25ºC on a thermal cycler or left on a bench overnight. Recombination events will remove the ccdB gene located between attP sites in the pDONR plasmid which is toxic to *E. coli.* To stop the reaction 1 µL of Proteinase K was added and incubated at 37ºC for 20 min. The plasmid was then transformed into *E. coli* DH5α and plated onto Gentamycin containing agar plate. From the plate, selected colonies were picked for miniprep. 1µL of the plasmid DNA was then digested with HpaI and PstI enzymes (1µL each) to check the correct size PCR product insert. Positive samples were sent for sequencing with Forward AttB1 (IGUC1906) and Reverse AttB2 (IGUC1907) primers. Plasmid having the correct sequence was amplified by midiprep.

8.8.2 Putting the pDONR insert into the destination vector

150 ng pDONR was mixed with 150 ng Destination vector (pLenti CMV Puro Dest) in the presence of 2 µL LR clonase and MQW (up to 10 µL). The mixture was kept at 25ºC for 1 h in a thermal cycler, subsequently, the enzyme was neutralised by adding proteinase K at 37ºC for 20 minutes. 5µL of this mixture was used to transform *E. coli* strain DH5α and plated on ampicillin containing plate. Selected colony was further grown for amplifying the plasmid DNA construct.

8.8.3 Generating Lenti virus stocks

On a six well dish, HEK293T cells were seeded at $2x10^6$ cells/well density. After 4 h the cells were transfected with Lenti construct along with additional plasmids (pMDL, pRev and pVSVG) to provide the necessary trans-acting factors/packaging materials for the virus. A GFP-Lenti added in a separate well as a positive control of transfection. After 12 h the media was replaced with 2% serum containing DMEM. The next day, when the control GFP-Lenti well showed cells were mostly (90%) GFP expressing the viruses were harvested. The supernatants were collected in syringes and passed through 0.45 μm filters. The virus preparations were directly used for stable cell line construction or stored at -80ºC for future use.

8.8.4 Generating Lenti-transduced stable cell lines

A 24 well dish target cells was seeded at $2.5x10^5$ cells/well density. The next day, 500μL of the filtered Lenti-virus (test and GFP) was added to the well by replacing the growth medium. After 6 h the medium was replaced with fresh medium. The following day, when GFP expression was seen in the control well the cells were trypsinised and seeded to T-75 flasks. When GFP expression was seen in the T-75 flasks, the media was replaced with puromycin (at a concentration pre-determined by a killcurve of the cell line) containing DMEM. After 2-3 days, the culture medium was replaced again with normal DMEM and the cells were grown till confluency. At this stage part of the cells were frozen for storage in liquid Nitrogen and others were tested by WB and IF to detect desired gene insertion and were utilised for further research.

8.9 siRNA knock down system

Cells were seeded to a six well dish and were treated on the same day for transfection. A 50 nM siRNA (FlexiTube GeneSolutions from QIAGEN) was mixed with 100μL Opti-Mem and in a separate tube, DharmaFECT, a transfection reagent was mixed with 100μL Opti-Mem. After 5 min the contents were mixed together and incubated for 30-45 min and then mixed with 800μL antibiotic free DMEM medium. The cells on six well were washed 1x with optimem and the transfection reagent mixture was added. After overnight incubation a further 1mL of DMEM was added. The cells were incubated for 72 h and then lysed and tested by WB for silencing of the target gene expression. A positive control (Alix siRNA) and a negative control (ConX siRNA) were also added in the comparison. The siRNA sequences are shown in Table 8.17.

Table 8.17 | List of siRNA used in this study

Product name	Target sequence	Supplier
Hs_Nipsnap1_7	CTCACAGATAGGAGAGCTCTA	QIAGEN
Hs_Nipsnap1_6	CCGCTCCCTCTTTGTTCACAA	QIAGEN
Hs_Nipsnap1_5	CTGCGGCGCGTTTCTATTCCA	QIAGEN
Hs_Nipsnap1_1	CAGAATGGGTCCCAACATCTA	QIAGEN
Hs_GBAS_7	AAGATCCGGACCTAATATATA	QIAGEN
Hs_GBAS_6	AGCCCTCACAGAAGTCATGAA	QIAGEN
Hs_GBAS_5	CTCGAGAAGACAGCTGGCTAA	QIAGEN
Hs_GBAS_2	CTGGGAGGAATTGGTATATTA	QIAGEN
ConX	AUUCUAUCACUAGCGUGACUU	Dharmacon
Alix	GCC GCU GGU GAA GUU CAU CTT	CMC (Pawliczek and Crump, 2009)

8.10 CRISPR-Cas9 KO system

8.10.1 Construction of CRISPR-Cas9 plasmid

Oligos for sgRNA targeted against the desired sequence on the human genome were designed. The top and bottom oligos were mixed (100µM, 1µL each) with T4 ligation buffer (1µL) and T4 PNK (1µL) in MPW (6µL). The mixture was incubated in a thermal cycler at 37ºC for 30 min and then at 95ºC for 5 min, then the machine was turned off to let the samples cool down to room temperature (RT) on the cycler. The samples were diluted to 1:100 in MQW to be used for ligation reaction. A pSpCas9(BB)-2A-Puro (PX459) plasmid was cut with BbsI restriction enzyme at 37ºC for 2 h. For ligation, 1µL of the plasmid was mixed with 10 µL of the diluted Oligos along with T4 ligation buffer (2µL), T4 ligase (1µL) and MQW (4µL) and incubated for 1-2 h at RT. The ligated plasmid was then transformed into *E. coli* DH5α and platted on ampicillin containing agar plates. The next day, selected colonies were picked for plasmid miniprep followed by sequencing with the U6 primer.

8.10.2 Generation CRISPR-Cas9 KO cell

On a six well dish, HaCaT cells were seeded with 5 x10^6 cells per well (for ~50% confluency) and the cells were transfected with the CRISPR-Cas9 plasmid. In an eppendorf tube, 100µL DMEM was mixed with 6 L of Lipofectamine 2000 and was incubated for 5 min. Next, 2µg of the plasmid DNA was added to the tube. The mixture was then incubated at RT for 30 min and added to the cell. After 18-24 h incubation at 37ºC in a CO_2 incubator the culture medium was

replaced with DMEM containing 2µg/ml puromycin to kill the untransfected cells and incubated at the same condition. After 48 h the medium was replaced with normal DMEM added with 1 x non-essential amino acid to allow growth of the transfected cells that survived the puromycin selection. Once the cells became confluent they were transferred to a larger flask. The cells were tested by WB for the loss of desired gene expression and were stored in liquid Nitrogen as a population of KO cells. From the population, single cell clones were generated by limiting dilution on a 96 well dish. The KO clones were tested by WB for protein expression and were stored at liquid Nitrogen.

8.10.3 Sequencing of the KO clones

For genomic DNA extraction from a KO clone, some cells were transferred to a PCR tube and spun for 5 min at 300 xg. The supernatant was removed and to the cell pellet 10x Taq Buffer without Mg (1µL), 50mM $MgCl_2$ (0.3µL), Proteinase K 20mg/mL (0.5µL) and MQW (7.2µL) and incubated at 60ºC for 1 h and then at 95ºC for 15 min in a thermal cycler. 90 µL MQW was added to each sample and 2 µL of this gDNA was used for a PCR amplification reaction for the gene intended to be KO. The PCR amplified products were separated on a gel and cloned into the pTOPO-blunt vector using manufacturers protocol (Zero Blunt TOPO, Invitrogen). The vector was transformed into *E. coli* DH5α and plated on agar plates. Selected colonies were taken for plasmid DNA miniprep and were sent for sequencing using M13 forward primer. The sequence data was aligned against the parental gene sequence to understand the pattern of deletion(s)/mutation(s) acquired in the genome of the KO clone.

9. Appendix

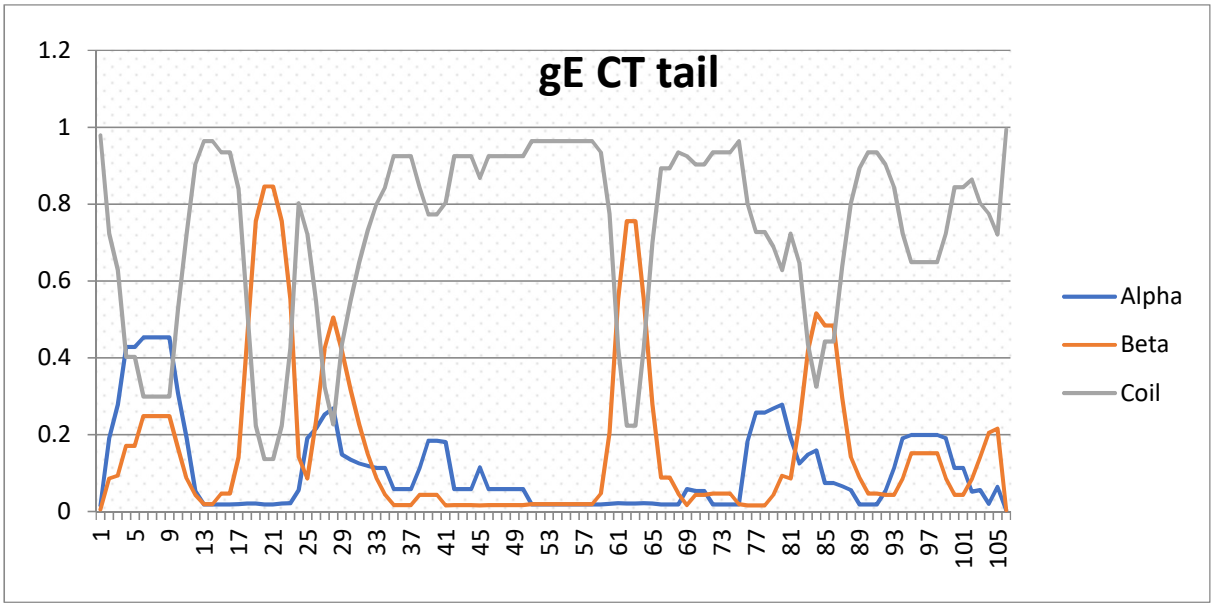

Appendix Figure 9.1 | Representation of disordered gE cytoplasmic tail. Secondary structure of gE cytoplasmic tail (445-550). Protein disorder and secondary structure were predicted using NetsurfP web-based tool.

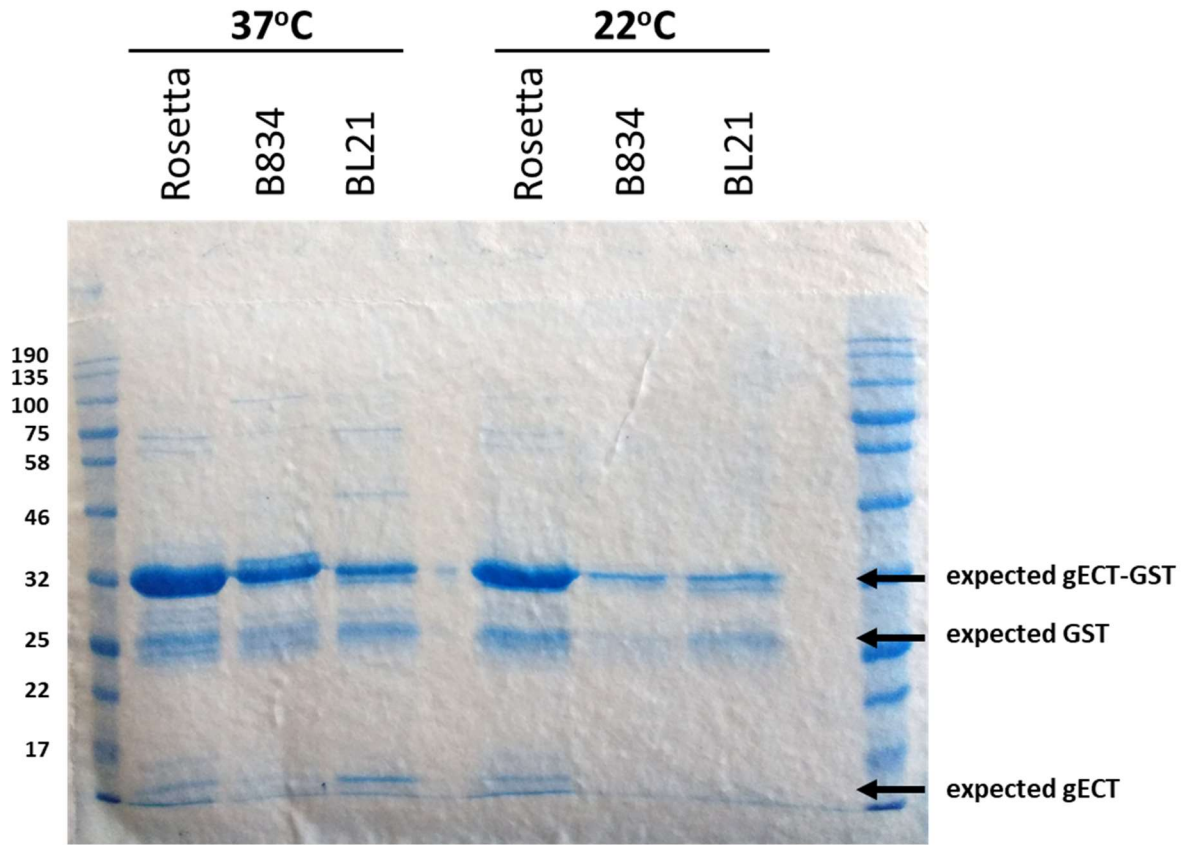

Appendix Figure 9.2 | Optimisation for gECT-GST production in different *E. coli*. Plasmid for gECT-GST was constructed and three different *E. coli* cells (Rosetta, B834 and BL21) were transformed. The cells were grown at two different temperatures (37°C and 22°C) and lysed to see protein expression of desired molecular weight. Protein markers are indicated on the left and expected protein positions on the right.

```
Nipsnap1_var1      1 MAPRLCSISVTARRLLGGPGPRAGDVASAAAARFYSKDNEGSWFRSLFVH   50
                     ||||||||||                    ||||||||||||||||||
Nipsnap1_var2      1 MAPRLCSISVT-------------------ARFYSKDNEGSWFRSLFVH   30

Nipsnap1_var1     51 KVDPRKDAHSTLLSKKETSNLYKIQFHNVKPEYLDAYNSLTEAVLPKLHL   100
                     ||||||||||||||||||||||||||||||||||||||||||||||||||
Nipsnap1_var2     31 KVDPRKDAHSTLLSKKETSNLYKIQFHNVKPEYLDAYNSLTEAVLPKLHL   80

Nipsnap1_var1    101 DEDYPCSLVGNWNTWYGEQDQAVHLWRFSGGYPALMDCMNKLKNNKEYLE   150
                     ||||||||||||||||||||||||||||||||||||||||||||||||||
Nipsnap1_var2     81 DEDYPCSLVGNWNTWYGEQDQAVHLWRFSGGYPALMDCMNKLKNNKEYLE   130

Nipsnap1_var1    151 FRRERSQMLLSRRNQLLLEFSFWNEPQPRMGPNIYELRTYKLKPGTMIEW   200
                     ||||||||||||||||||||||||||||||||||||||||||||||||||
Nipsnap1_var2    131 FRRERSQMLLSRRNQLLLEFSFWNEPQPRMGPNIYELRTYKLKPGTMIEW   180

Nipsnap1_var1    201 GNNWARAIKYRQENQEAVGGFFSQIGELYVVHHLWAYKDLQSREETRNAA   250
                     ||||||||||||||||||||||||||||||||||||||||||||||||||
Nipsnap1_var2    181 GNNWARAIKYRQENQEAVGGFFSQIGELYVVHHLWAYKDLQSREETRNAA   230

Nipsnap1_var1    251 WRKRGWDENVYYTVPLVRHMESRIMIPLKISPLQ    284
                     ||||||||||||||||||||||||||||||||
Nipsnap1_var2    231 WRKRGWDENVYYTVPLVRHMESRIMIPLKISPLQ    264
```

```
Nipsnap2_var1      1 MAARVLRARGAAWAGGLLQRAAPCSLLPRLRTWTSSSNRSREDSWLKSLF    50
                     ||||||||||||||||||||||||||||||||||||||||||||||||||
Nipsnap2_var2      1 MAARVLRARGAAWAGGLLQRAAPCSLLPRLRTWTSSSNRSREDSWLKSLF    50

Nipsnap2_var1     51 VRKVDPRKDAHSNLLAKKETSNLYKLQFHNVKPECLEAYNKICQEVLPKI    100
                     ||||||||||||||||||||||||||||    ..|.:.:.||
Nipsnap2_var2     51 VRKVDPRKDAHSNLLAKKETSNLYKLQF----KRCCQRFTKI--------    88

Nipsnap2_var1    101 HEDKHYPCTLVGTWNTWYGEQDQAVHLWRYEGGYPALTEVMNKLRENKEF    150
                           ..|||    .|:|...:          |..:.|::         ||
Nipsnap2_var2     89 ------NTTLV----LWWGLGTR---------GMASRTKL--------EF    111

Nipsnap2_var1    151 LEFRKARSDMLLSRKNQLLLEFSFWNEPVPRSGPNIYELRSYQLRPGTMI    200
                     ||||||||||||||||||||||||||||||||||||||||||||||||||
Nipsnap2_var2    112 LEFRKARSDMLLSRKNQLLLEFSFWNEPVPRSGPNIYELRSYQLRPGTMI    161

Nipsnap2_var1    201 EWGNYWARAIRFRQDGNEAVGGFFSQIGQLYMVHHLWAYRDLQTREDIRN    250
                     ||||||||||||||||||||||||||||||||||||||||||||||||||
Nipsnap2_var2    162 EWGNYWARAIRFRQDGNEAVGGFFSQIGQLYMVHHLWAYRDLQTREDIRN    211

Nipsnap2_var1    251 AAWHKHGWEELVYYTVPLIQEMESRIMIPLKTSPLQ    286
                     ||||||||||||||||||||||||||||||||||||
Nipsnap2_var2    212 AAWHKHGWEELVYYTVPLIQEMESRIMIPLKTSPLQ    247
```

Appendix Figure 9.3 | Protein sequence alignment of Nipsnap1 and 2 variants. The two variants of Nipsnap1 (top) and 2 (bottom) were aligned to understand structural similarity between them. Sequences in red indicate exon regions (4 for Nipsnap1 and 6 for Nipsnap2) targeted for CRISPR-Cas9 KO. Sequences underlined indicate the binding sites of the antibodies used in this thesis.

```
Nipsnap1          1 MAPRLCSISVTARRLLGGPGPRAGDVASAAAARFYSKDNEGSWFRSLFVH     50
                    ||||||||||||||||||||||||||||||||||||||||||||||||||
NC1_variant.1     1 MAPRLCSISVTARRLLGGPGPRAGDVASAAAARFYSKDNEGSWFRSLFVH     50

Nipsnap1         51 KVDPRKDAHSTLLSKKETSNLYKIQFHNVKPEYLDAYNSLTEAVLPKLHL    100
                    ||||||||||||||||||||||||||||||||||||||||||||||||||
NC1_variant.1    51 KVDPRKDAHSTLLSKKETSNLYKIQFHNVKPEYLDAYNSLTEAVLPKLH-     99

Nipsnap1        101 DEDYPCSLVGNWNTWYGEQDQAVHLWRFSGGYPALMDCMNKLKNNKEYLE    150
                            |||||||||||||||||||||||||||||||||||||||||||
NC1_variant.1   100 -------LVGNWNTWYGEQDQAVHLWRFSGGYPALMDCMNKLKNNKEYLE    142

Nipsnap1        151 FRRERSQMLLSRRNQLLLEFSFWNEPQPRMGPNIYELRTYKLKPGTMIEW    200
                    |||||:||||||||||||||||||||||||||||||||||||||||||||
NC1_variant.1   143 FRRERTQMLLSRRNQLLLEFSFWNEPQPRMGPNIYELRTYKLKPGTMIEW    192

Nipsnap1        201 GNNWARAIKYRQENQEAVGGFFSQIGELYVVHHLWAYKDLQSREETRNAA    250
                    ||||||||||||||||||||||||||||||||||||||||||||||||||
NC1_variant.1   193 GNNWARAIKYRQENQEAVGGFFSQIGELYVVHHLWAYKDLQSREETRNAA    242

Nipsnap1        251 WRKRGWDENVYYTVPLVRHMESRIMIPLKISPLQ*    285
                    |||||||||||||||||||||||||||||||||
NC1_variant.1   243 WRKRGWDENVYYTVPLVRHMESRIMIPLKISPLQ*    277
```

```
Nipsnap1          1 MAPRLCSISVTARRLLGGPGPRAGDVASAAAARFYSKDNEGSWFRSLFVH     50
                    ||||||||||||||||||||||||||||||||||||||||||||||||||
NC1_variant.2     1 MAPRLCSISVTARRLLGGPGPRAGDVASAAAARFYSKDNEGSWFRSLFVH     50

Nipsnap1         51 KVDPRKDAHSTLLSKKETSNLYKIQFHNVKPEYLDAYNSLTEAVLPKLHL    100
                    ||||||||||||||||||||||||||||||||||||||||||||||||||
NC1_variant.2    51 KVDPRKDAHSTLLSKKETSNLYKIQFHNVKPEYLDAYNSLTEAVLPKLHL    100

Nipsnap1        101 DEDYPCSLVGNWNTWYGEQDQAVHLWRFS--------------GGYPALM    136
                    :...       |....|....|:..|..|              .|.|...
NC1_variant.2   101 EHVV-------WGAGPGSAPVAILRWLPSPHGLHEQAQKQ*GVPGVPKGA    143

Nipsnap1        137 DCMNKL-----------------KNNKEYLEFRRERSQ------------    157
                    |....:                 :|..::|.....::|
NC1_variant.2   144 DADAAVQEKPAAP*VQLLE*ATAQNGSQHL*AEDIQAQARNHDRVGEQLG    193

Nipsnap1        158 ---------------MLLSRRNQLLLEFSFWNEPQPRMG---PNIYELRT    189
                              :||:.|..|        ...|.:|   |.:.
NC1_variant.2   194 SGHQVPAGEPGGSGRLLLTDRRAL--------RGAPSLGL*RPAVS----    231

Nipsnap1        190 YKLKPGTMIEWGNNWARAIKYRQENQEAVG---GFFSQIGELYVVHHLWA    236
                            |.:..|.::     :|.:|   ..:|..|..:.|.....
NC1_variant.2   232 -----------GGDSKRCLE-----EERLG*KCLLYSPPGATHGV*DHDP    265

Nipsnap1        237 YKDLQSREETRNAAWRKRGWDENVYYTVPLVRHMESRIMIPLKISPLQ*    285
                    .:||.|...
NC1_variant.2   266 LEDLASAVX-------------------------------------    274
```

Appendix Figure 9.4 a. continue overleaf

```
Nipsnap1          1 MAPRLCSISVTARRLLGGPGPRAGDVASAAAARFYSKDNEGSWFRSLFVH     50
                    ||||||||||||||||||||||||||||||||||||||||||||||||||
NC1_variant.3     1 MAPRLCSISVTARRLLGGPGPRAGDVASAAAARFYSKDNEGSWFRSLFVH     50

Nipsnap1         51 KVDPRKDAHSTLLSKKETSNLYKIQFHNVKPEYLDAYNSLTEAVLPKLHL    100
                    ||||||||||||||||||||||||||||||||||||||||||||||||||
NC1_variant.3    51 KVDPRKDAHSTLLSKKETSNLYKIQFHNVKPEYLDAYNSLTEAVLPKLHL    100

Nipsnap1        101 DEDYPCSLVGNWNTWYGEQDQAVHLWRFSGGYPALMDCMNKLKNNKEYLE    150
                    ||               ||||||||||||||||||||||||||||||||
NC1_variant.3   101 DE---------------EQDQAVHLWRFSGGYPALMDCMNKLKNNKEYLE    135

Nipsnap1        151 FRRERSQMLLSRRNQLLLEFSFWNEPQPRMGPNIYELRTYKLKPGTMIEW    200
                    |||||:||||||||||||||||||||||||||||||||||||||||||||
NC1_variant.3   136 FRRERTQMLLSRRNQLLLEFSFWNEPQPRMGPNIYELRTYKLKPGTMIEW    185

Nipsnap1        201 GNNWARAIKYRQENQEAVGGFFSQIGELYVVHHLWAYKDLQSREETRNAA    250
                    ||||||||||||||||||||||||||||||||||||||||||||||||||
NC1_variant.3   186 GNNWARAIKYRQENQEAVGGFFSQIGELYVVHHLWAYKDLQSREETRNAA    235

Nipsnap1        251 WRKRGWDENVYYTVPLVRHMESRIMIPLKISPLQ*    285
                    ||||||||||||||||||||||||||||||||||
NC1_variant.3   236 WRKRGWDENVYYTVPLVRHMESRIMIPLKISPLQ*    270
```

```
Nipsnap1          1 MAPRLCSISVTARRLLGGPGPRAGDVASAAAARFYSKDNEGSWFRSLFVH     50
                    ||||||||||||||||||||||||||||||||||||||||||||||||||
NC1_variant.4     1 MAPRLCSISVTARRLLGGPGPRAGDVASAAAARFYSKDNEGSWFRSLFVH     50

Nipsnap1         51 KVDPRKDAHSTLLSKKETSNLYKIQFHNVKPEYLDAYNSLTEAVLPKLHL    100
                    ||||||||||||||||||||||||||||||||||||||||||||||||||
NC1_variant.4    51 KVDPRKDAHSTLLSKKETSNLYKIQFHNVKPEYLDAYNSLTEAVLPKLHL    100

Nipsnap1        101 DEDYPCSLVGN--WNTWYGEQDQAVHLWRFS--------------GGYPA    134
                    ||||||..:.:  |....|....|:..|..|              .|.|.
NC1_variant.4   101 DEDYPCGQLEHVVWGAGPGSAPVAILRWLPSPHGLHEQAQKQ*GVPGVPK    150

Nipsnap1        135 LMDCMNKL-----------------KNNKEYLEFRRERSQ----------    157
                    ..|....:                 :|..::|.....::|
NC1_variant.4   151 GADADAAVQEKPAAP*VQLLE*ATAQNGSQHL*AEDIQAQARNHDRVGEQ    200

Nipsnap1        158 -----------------MLLSRRNQLLLEFSFWNEPQPRMG---PNIYEL    187
                                    :||:.|..|        ...|.:|   |.:.
NC1_variant.4   201 LGSGHQVPAGEPGGSGRLLLTDRRAL--------RGAPSLGL*RPAVS--    240

Nipsnap1        188 RTYKLKPGTMIEWGNNWARAIKYRQENQEAVG---GFFSQIGELYVVHHL    234
                              |.:..|.::     :|.:|   ..:|..|..:.|...
NC1_variant.4   241 -------------GGDSKRCLE-----EERLG*KCLLYSPPGATHGV*DH    272

Nipsnap1        235 WAYKDLQSREETRNAAWRKRGWDENVYYTVPLVRHMESRIMIPLKISPLQ    284
                    ...:||.|...
NC1_variant.4   273 DPLEDLASAVX-------------------------------------    283
```

(a)

```
Nipsnap2          1 MAARVLRARGAAWAGGLLQRAAPCSLLPRLRTWTSSSNRSREDSWLKSLF     50
                    ||||||||||||||||||||||||||||||||||||||||||||||||||
GC1_variant.1     1 MAARVLRARGAAWAGGLLQRAAPCSLLPRLRTWTSSSNRSREDSWLKSLF     50

Nipsnap2         51 VRKVDPRKDAHSNLLAKKETSNLYKLQFHNVKPECLEAYNKICQEVLPKI    100
                    ||||||||||||||||||||||||||||||||||||||||||||||||||
GC1_variant.1    51 VRKVDPRKDAHSNLLAKKETSNLYKLQFHNVKPECLEAYNKICQEVLPKI    100

Nipsnap2        101 HEDKHYPCTLVGTWNTWYGEQDQAVHLWRYEGGYPALTEVMNKLRENKEF    150
                    ||||||||||||||||||||||||||||||||||||||||||||||||||
GC1_variant.1   101 HEDKHYPCTLVGTWNTWYGEQDQAVHLWRYEGGYPALTEVMNKLRENKEF    150

Nipsnap2        151 LEFRKARSDMLLSRKNQLLLEFSFWNEPVPRSGPNIYELRSYQLRPGTMI    200
                    ||||||||||||||||||||||||||||||||
GC1_variant.1   151 LEFRKARSDMLLSRKNQLLLEFSFWNEPVPR----------------------    181

Nipsnap2        201 EWGNYWARAIRFRQDGNEAVG---------GFFS-QIGQLYMVHHLWAYR    240
                     |              ||.|.         ||.. .:|.:.|.::|...|
GC1_variant.1   182 -W--------------NEPVPRCN*LSKR*GFKGWLVGGVLMFNYLEHLR    216

Nipsnap2        241 D--LQTREDIRNAAWHKHGWEELVYYTVPLIQEMESRIMIPLKT------    282
                    .  :.|:                                  ::|..|
GC1_variant.1   217 T*YI*TQ-------------------------------VLPTPTRNHD*M    235

Nipsnap2        283 -------SPLQ---------------------------------------    286
                           :|||
GC1_variant.1   236 GQLLGSCNPLQTGW*RSRRRILLSDWAAVHGAPSLGLQGSSDQGRHTECS    285
```

```
Nipsnap2          1 MAARVLRARGAAWAGGLLQRAAPCSLLPRLRTWTSSSNRSREDSWLKSLF     50
                    ||||||||||||||||||||||||||||||||||||||||||||||||||
GC1_variant.2     1 MAARVLRARGAAWAGGLLQRAAPCSLLPRLRTWTSSSNRSREDSWLKSLF     50

Nipsnap2         51 VRKVDPRKDAHSNLLAKKETSNLYKLQFHNVKPECLEAYNKICQEVLPKI    100
                    ||||||||||||||||||||||||||||||||||||||||||||||||||
GC1_variant.2    51 VRKVDPRKDAHSNLLAKKETSNLYKLQFHNVKPECLEAYNKICQEVLPKI    100

Nipsnap2        101 HEDKHYPCTLVGTWNTWYGEQDQAVHLWRYEGGYPALTEVMNKLRENKEF    150
                    ||||||||||||||||||||||||||||||||||||||||||||||||||
GC1_variant.2   101 HEDKHYPCTLVGTWNTWYGEQDQAVHLWRYEGGYPALTEVMNKLRENKEF    150

Nipsnap2        151 LEFRKARSDMLLSRKNQLLLEFSFWNEPVPR---------SGPNIYELRS    191
                    ||||||||||||||||||||||||||||||||         :....::...
GC1_variant.2   151 LEFRKARSDMLLSRKNQLLLEFSFWNEPVPR*YI*TQVLPTPTRNHD*MG    200

Nipsnap2        192 YQLRPGTMIEWGNYWARAIR--FRQD-----GNEAVG--GFFSQ------    226
                    ..|.....::.|  |.|:.|  ...|     |..::|  |...|
GC1_variant.2   201 QLLGSCNPLQTG--W*RSRRRILLSDWAAVHGAPSLGLQGSSDQGRHTEC    248

Nipsnap2        227 ------IGQLYMVH-HLWAYRDLQTR---EDIRNAAWHKHGWEELVYYTV    266
                          :|.:.::| ..::...:|..   ||:.....
GC1_variant.2   249 SMAQTWLGGIGILHSSTYSGNGIQNHDPTEDLAPPVX-------------    285

Nipsnap2        267 PLIQEMESRIMIPLKTSPLQ    286

GC1_variant.2   286 --------------------    285
```

Appendix Figure 9.4 b. continue overleaf

```
Nipsnap2          1 MAARVLRARGAAWAGGLLQRAAPCSLLPRLRTWTSSSNRSREDSWLKSLF     50
                    ||||||||||||||||||||||||||||||||||||||||||||||||||
GC1_variant.3     1 MAARVLRARGAAWAGGLLQRAAPCSLLPRLRTWTSSSNRSREDSWLKSLF     50

Nipsnap2         51 VRKVDPRKDAHSNLLAKKETSNLYKLQFHNVKPECLEAYNKICQEVLPKI    100
                    ||||||||||||||||||||||||||||||||||||||||||||||||||||
GC1_variant.3    51 VRKVDPRKDAHSNLLAKKETSNLYKLQFHNVKPECLEAYNKICQEVLPKI    100

Nipsnap2        101 HEDKHYPCTLVGTWNTWYGEQDQAVHLWRYEGGYPALTEVMNKLRENKEF    150
                    ||||||||||||||||||||||||||||||||||||||||||||||||||||
GC1_variant.3   101 HEDKHYPCTLVGTWNTWYGEQDQAVHLWRYEGGYPALTEVMNKLRENKEF    150

Nipsnap2        151 LEFRKARSDMLLSRKNQLLLEFSFWNEPVPRSGPNIY---ELRSYQLRPG    197
                    ||||||||||||||||||||||||||||||....||   .|.:....|.
GC1_variant.3   151 LEFRKARSDMLLSRKNQLLLEFSFWNEPVPRFPDLIYMNSGLTNSDQEP*    200

Nipsnap2        198 TMIEWGNYWARAIRFRQDGNEAVGGFFSQIGQLYMVHHLWAYRDLQTRED    247
                    .                  |.|:.|
GC1_variant.3   201 L-----------------NGAITG-------------------------    207

Nipsnap2        248 IRNAAWHKHGWEELVYYTVPLIQEMESRIMI-PLKTSPLQ----------    286
                                      |:|....|::. |.:.|.|:
GC1_variant.3   208 -------------------LVQSASDRMVTKPSEDSSLRLGSCTWCTIF    237
```

```
Nipsnap2          1 MAARVLRARGAAWAGGLLQRAAPCSLLPRLRTWTSSSNRSREDSWLKSLF     50
                    ||||||||||||||||||||||||||||||||||||||||||||||||||
GC2_var.1_1       1 MAARVLRARGAAWAGGLLQRAAPCSLLPRLRTWTSSSNRSREDSWLKSLF     50

Nipsnap2         51 VRKVDPRKDAHSNLLAKKETSNLYKLQFHNVKPECLEAYNKICQEVLPKI    100
                    ||||||||||||||||||||||||||||||||||||||||||||||||||||
GC2_var.1_1      51 VRKVDPRKDAHSNLLAKKETSNLYKLQFHNVKPECLEAYNKICQEVLPKI    100

Nipsnap2        101 HEDKHYPCTLVGTWNTWYGEQDQAVHLWRYEGGYPALTEVMNKLRENKEF    150
                    ||||||||||||||||||||||||||||||||||||||||||||||||||||
GC2_var.1_1     101 HEDKHYPCTLVGTWNTWYGEQDQAVHLWRYEGGYPALTEVMNKLRENKEF    150

Nipsnap2        151 LEFRKARSDMLLSRKNQLLLEFSFWNEPVPRSGPNIYELRSYQLRPGTMI    200
                    ||||||||||||||||||||||||||||||||  |::
GC2_var.1_1     151 LEFRKARSDMLLSRKNQLLLEFSFWNEPVPR--PDL--------------    184

Nipsnap2        201 EWGNYWARAIRFRQDGNEAVGGFFSQIGQLYMVHHLWAYRDLQTREDIR-    249
                                          :||...|       |..|..
GC2_var.1_1     185 ----------------------------IYMNSGL-------TNSDQEP    198

Nipsnap2        250 --NAAWHKHGWEELVYYTVPLIQEMESRIMI-PLKTSPLQ----------    286
                      |.|            ...|:|....|::. |.:.|.|:
GC2_var.1_1     199 *LNGA------------ITGLVQSASDRMVTKPSEDSSLRLGSCTWCTIF    236
```

(b)

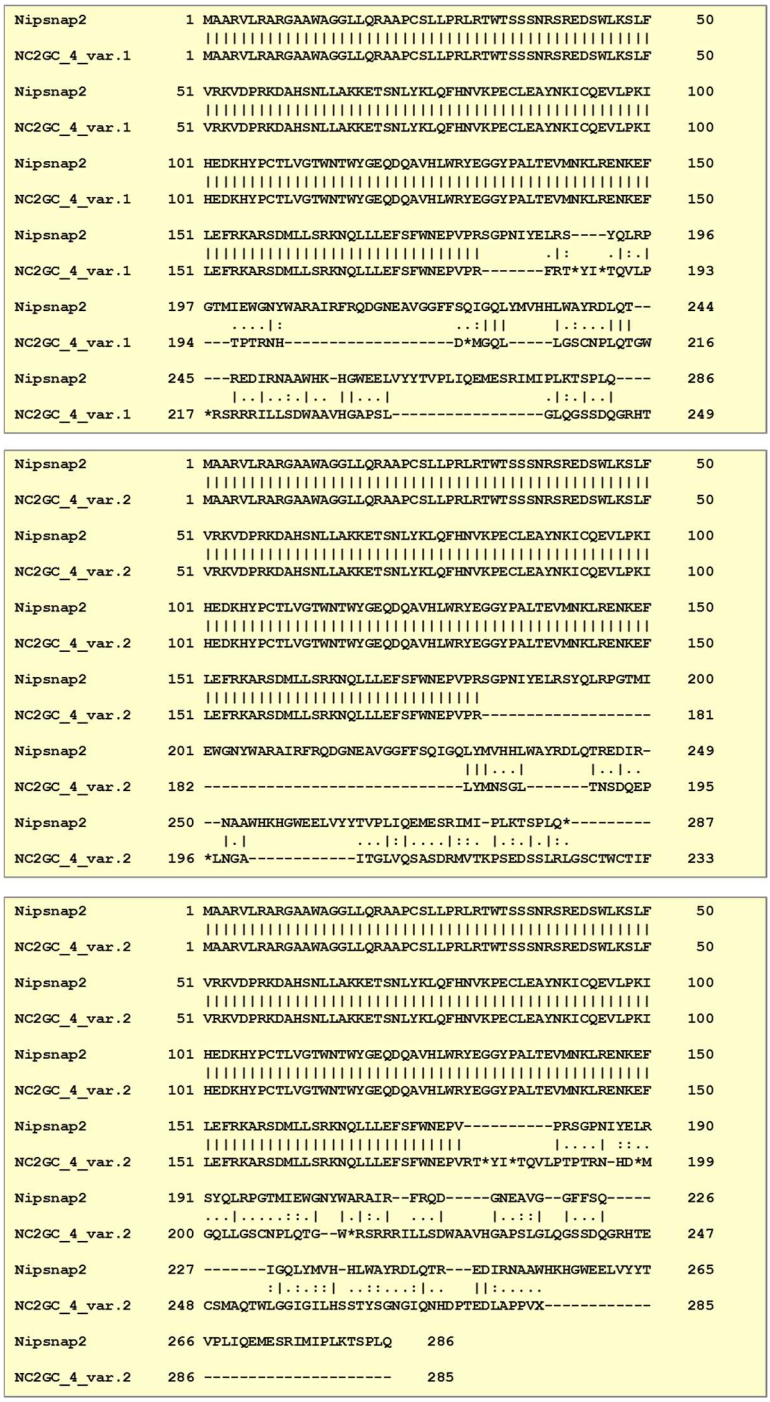

(c)

Appendix Figure 9.4 | Protein sequence alignment of Nipsnap (1 or 2 or both) KO clone variants. Predictive protein sequences generated from the Nipsnap (1 or 2 or both) KO clones DNA sequences were aligned with the parental protein sequence. Compared to the parental protein sequence variant 1 and 3 from NC1 clones were 8 and 15 amino acid shorter respectively. The rest of the clones had truncated protein sequences compared to their parents.

Appendix Table 9.1 | Raw data for all SILAC hits

Accession	Description	Unique Peptides	Heavy/Light	Medium/Heavy	Medium/Light
Tube 1					
H6VRF8	Keratin 1 OS=Homo sapiens GN=KRT1 PE=3 SV=1 - [H6VRF8_HUMAN]	25	0.010	1.000	0.010
P35908	Keratin, type II cytoskeletal 2 epidermal OS=Homo sapiens GN=KRT2 PE=1 SV=2 - [K22E_HUMAN]	23	0.010	1.000	0.010
B4DRR0	cDNA FLJ53910, highly similar to Keratin, type II cytoskeletal 6A OS=Homo sapiens PE=2 SV=1 - [B4DRR0_HUMAN]	4	0.223	0.414	0.088
P13645	Keratin, type I cytoskeletal 10 OS=Homo sapiens GN=KRT10 PE=1 SV=6 - [K1C10_HUMAN]	17	0.010	1.000	0.010
P13647	Keratin, type II cytoskeletal 5 OS=Homo sapiens GN=KRT5 PE=1 SV=3 - [K2C5_HUMAN]	16	0.090	0.537	0.037
P04259	Keratin, type II cytoskeletal 6B OS=Homo sapiens GN=KRT6B PE=1 SV=5 - [K2C6B_HUMAN]	3			
F6KPG5	Albumin (Fragment) OS=Homo sapiens PE=2 SV=1 - [F6KPG5_HUMAN]	15	0.010	1.000	0.010
P02533	Keratin, type I cytoskeletal 14 OS=Homo sapiens GN=KRT14 PE=1 SV=4 - [K1C14_HUMAN]	5	0.134	0.438	0.046
P08779	Keratin, type I cytoskeletal 16 OS=Homo sapiens GN=KRT16 PE=1 SV=4 - [K1C16_HUMAN]	10	0.188	0.593	0.112
P35527	Keratin, type I cytoskeletal 9 OS=Homo sapiens GN=KRT9 PE=1 SV=3 - [K1C9_HUMAN]	18	0.010	1.000	0.010
B7Z4V2	cDNA FLJ51907, highly similar to Stress-70 protein, mitochondrial OS=Homo sapiens PE=2 SV=1 - [B7Z4V2_HUMAN]	17	0.573	0.785	0.447
Q04695	Keratin, type I cytoskeletal 17 OS=Homo sapiens GN=KRT17 PE=1 SV=2 - [K1C17_HUMAN]	5	0.323	0.463	0.138
P11142	Heat shock cognate 71 kDa protein OS=Homo sapiens GN=HSPA8 PE=1 SV=1 - [HSP7C_HUMAN]	11	0.723	1.183	0.793
P11021	78 kDa glucose-regulated protein OS=Homo sapiens GN=HSPA5 PE=1 SV=2 - [GRP78_HUMAN]	13	0.647	0.949	0.583
US8	US8	12	1.000	100.000	100.000
P09211	Glutathione S-transferase P OS=Homo sapiens GN=GSTP1 PE=1 SV=2 - [GSTP1_HUMAN]	7	0.939	0.902	0.773
P0DMV8	Heat shock 70 kDa protein 1A OS=Homo sapiens GN=HSPA1A PE=1 SV=1 - [HS71A_HUMAN]	8	0.784	0.972	0.835
B4E335	cDNA FLJ52842, highly similar to Actin, cytoplasmic 1 OS=Homo sapiens PE=2 SV=1 - [B4E335_HUMAN]	8	0.933	1.818	1.584
P08727	Keratin, type I cytoskeletal 19 OS=Homo sapiens GN=KRT19 PE=1 SV=4 - [K1C19_HUMAN]	4	2.028	0.447	1.072
P07355	Annexin A2 OS=Homo sapiens GN=ANXA2 PE=1 SV=2 - [ANXA2_HUMAN]	9	0.395	1.353	0.596
P68104	Elongation factor 1-alpha 1 OS=Homo sapiens GN=EEF1A1 PE=1 SV=1 - [EF1A1_HUMAN]	7	0.960	0.914	0.941
A0A0A0MS14	Protein IGHV1-45 (Fragment) OS=Homo sapiens GN=IGHV1-45 PE=4 SV=1 - [A0A0A0MS14_HUMAN]	1			
B7Z597	cDNA FLJ54373, highly similar to 60 kDa heat shock protein, mitochondrial OS=Homo sapiens PE=2 SV=1 - [B7Z597_HUMAN]	10	0.820	2.348	1.851
Q0IIN1	Keratin 77 OS=Homo sapiens GN=KRT77 PE=1 SV=1 - [Q0IIN1_HUMAN]	3	0.010	1.000	0.010
A1A4E9	Keratin 13 OS=Homo sapiens GN=KRT13 PE=1 SV=1 - [A1A4E9_HUMAN]	5	0.015	1.000	0.015
B4DMA2	cDNA FLJ54023, highly similar to Heat shock protein HSP 90-beta OS=Homo sapiens PE=2 SV=1 - [B4DMA2_HUMAN]	3	0.466	3.803	1.804
C9J5D1	N-alpha-acetyltransferase 50 OS=Homo sapiens GN=NAA50 PE=1 SV=1 - [C9J5D1_HUMAN]	7	0.711	0.468	0.327
B4DJI2	cDNA FLJ53342, highly similar to Granulins OS=Homo sapiens PE=2 SV=1 - [B4DJI2_HUMAN]	9	0.244	0.879	0.230
P05787	Keratin, type II cytoskeletal 8 OS=Homo sapiens GN=KRT8 PE=1 SV=7 - [K2C8_HUMAN]	2	2.186	0.489	1.095
H0YH81	ATP synthase subunit beta (Fragment) OS=Homo sapiens GN=ATP5B PE=1 SV=1 - [H0YH81_HUMAN]	6	0.315	2.940	1.703
B3KY79	cDNA FLJ46620 fis, clone TLUNG2000654, highly similar to Keratin, type II cytoskeletal 7 OS=Homo sapiens PE=2 SV=1 - [B3KY79_HUMAN]	6	3.283	0.431	1.682
A0A0A0MSI0	Peroxiredoxin-1 (Fragment) OS=Homo sapiens GN=PRDX1 PE=1 SV=1 - [A0A0A0MSI0_HUMAN]	5	0.636	0.844	0.528

P35232	Prohibitin OS=Homo sapiens GN=PHB PE=1 SV=1 - [PHB_HUMAN]	6	0.559	6.275	3.518
F5GY37	Prohibitin-2 OS=Homo sapiens GN=PHB2 PE=1 SV=1 - [F5GY37_HUMAN]	5	0.572	8.193	4.845
F2Z2S8	40S ribosomal protein S3 OS=Homo sapiens GN=RPS3 PE=1 SV=1 - [F2Z2S8_HUMAN]	4	0.748	0.794	0.567
Q7RTS7	Keratin, type II cytoskeletal 74 OS=Homo sapiens GN=KRT74 PE=1 SV=2 - [K2C74_HUMAN]	1	0.010	1.000	0.010
B4E2Z3	cDNA FLJ54090, highly similar to 4F2 cell-surface antigen heavy chain OS=Homo sapiens PE=2 SV=1 - [B4E2Z3_HUMAN]	4	0.459	1.882	0.908
H7BYV1	Interferon-induced transmembrane protein 2 (Fragment) OS=Homo sapiens GN=IFITM2 PE=4 SV=1 - [H7BYV1_HUMAN]	1	0.530	10.266	8.608
P15924	Desmoplakin OS=Homo sapiens GN=DSP PE=1 SV=3 - [DESP_HUMAN]	9	0.010	1.000	0.010
P25705	ATP synthase subunit alpha, mitochondrial OS=Homo sapiens GN=ATP5A1 PE=1 SV=1 - [ATPA_HUMAN]	6	0.789	3.281	2.226
US7	US7	2	1.000	100.000	100.000
Q2VPJ6	HSP90AA1 protein (Fragment) OS=Homo sapiens GN=HSP90AA1 PE=1 SV=1 - [Q2VPJ6_HUMAN]	1			
P48047	ATP synthase subunit O, mitochondrial OS=Homo sapiens GN=ATP5O PE=1 SV=1 - [ATPO_HUMAN]	3	1.527	1.176	1.142
Q86YZ3	Hornerin OS=Homo sapiens GN=HRNR PE=1 SV=2 - [HORN_HUMAN]	3			
Q02413	Desmoglein-1 OS=Homo sapiens GN=DSG1 PE=1 SV=2 - [DSG1_HUMAN]	10	0.010	1.000	0.010
P68371	Tubulin beta-4B chain OS=Homo sapiens GN=TUBB4B PE=1 SV=1 - [TBB4B_HUMAN]	5	1.025	1.562	1.777
B3KSC3	cDNA FLJ35987 fis, clone TESTI2014269, highly similar to D-3-phosphoglycerate dehydrogenase (EC 1.1.1.95) OS=Homo sapiens PE=2 SV=1 - [B3KSC3_HUMAN]	4	0.808	2.618	1.902
A0A024R1X8	Junction plakoglobin, isoform CRA_a OS=Homo sapiens GN=JUP PE=4 SV=1 - [A0A024R1X8_HUMAN]	5	0.014	6.369	0.032
B3KTE3	cDNA FLJ38125 fis, clone D6OST2000127, moderately similar to RAS-RELATED PROTEIN RAB-8B OS=Homo sapiens PE=2 SV=1 - [B3KTE3_HUMAN]	1			
P05141	ADP/ATP translocase 2 OS=Homo sapiens GN=SLC25A5 PE=1 SV=7 - [ADT2_HUMAN]	4	0.673	1.529	1.188
P35579	Myosin-9 OS=Homo sapiens GN=MYH9 PE=1 SV=4 - [MYH9_HUMAN]	4	3.837	0.463	1.127
H7C2U6	Protein NipSnap homolog 1 (Fragment) OS=Homo sapiens GN=NIPSNAP1 PE=1 SV=1 - [H7C2U6_HUMAN]	3	1.000	100.000	100.000
A8K486	Peptidyl-prolyl cis-trans isomerase OS=Homo sapiens PE=2 SV=1 - [A8K486_HUMAN]	3	0.914	1.374	1.256
UL39	UL39	5	14.907	2.306	58.624
A0A024RA28	Heterogeneous nuclear ribonucleoprotein A2/B1, isoform CRA_d OS=Homo sapiens GN=HNRPA2B1 PE=4 SV=1 - [A0A024RA28_HUMAN]	3	0.666	0.569	0.349
B2DFV8	MHC class I antigen (Fragment) OS=Homo sapiens GN=HLA-A PE=3 SV=1 - [B2DFV8_HUMAN]	1			1.003
E5RJX2	40S ribosomal protein S20 OS=Homo sapiens GN=RPS20 PE=1 SV=1 - [E5RJX2_HUMAN]	2	0.586	0.924	0.541
P81605	Dermcidin OS=Homo sapiens GN=DCD PE=1 SV=2 - [DCD_HUMAN]	2			
P25311	Zinc-alpha-2-glycoprotein OS=Homo sapiens GN=AZGP1 PE=1 SV=2 - [ZA2G_HUMAN]	3	0.010	1.000	0.010
C8C504	Beta-globin OS=Homo sapiens GN=HBB PE=3 SV=1 - [C8C504_HUMAN]	4	0.010	1.000	0.010
P05109	Protein S100-A8 OS=Homo sapiens GN=S100A8 PE=1 SV=1 - [S10A8_HUMAN]	3	0.025	2.354	0.058
Q8N1N4	Keratin, type II cytoskeletal 78 OS=Homo sapiens GN=KRT78 PE=2 SV=2 - [K2C78_HUMAN]	3	0.010	1.000	0.010
H3BTN5	Pyruvate kinase (Fragment) OS=Homo sapiens GN=PKM PE=1 SV=1 - [H3BTN5_HUMAN]	4	0.642	1.203	0.797
M0R257	Ras-related protein Rab-3A (Fragment) OS=Homo sapiens GN=RAB3A PE=1 SV=1 - [M0R257_HUMAN]	1			1.819
B4DDU2	cDNA FLJ60097, highly similar to Tubulin alpha-ubiquitous chain OS=Homo sapiens PE=2 SV=1 - [B4DDU2_HUMAN]	1	1.037	1.230	1.276
B4E190	cDNA FLJ57770, moderately similar to ADP-ribosylation factor 3 OS=Homo sapiens PE=2 SV=1 - [B4E190_HUMAN]	2	0.645	2.097	1.353
B4DF70	cDNA FLJ60461, highly similar to Peroxiredoxin-2 (EC 1.11.1.15) OS=Homo sapiens PE=2 SV=1 - [B4DF70_HUMAN]	1	0.316	0.262	0.083
A8K6Q8	cDNA FLJ75881, highly similar to Homo sapiens transferrin receptor (p90, CD71) (TFRC), mRNA OS=Homo sapiens PE=2 SV=1 - [A8K6Q8_HUMAN]	2	0.010	1.000	0.010
B3KRY3	cDNA FLJ35079 fis, clone PLACE6005283, highly similar to Lysosome-associated membrane glycoprotein 1 OS=Homo sapiens PE=2 SV=1 - [B3KRY3_HUMAN]	1	0.557	1.907	1.063
P62269	40S ribosomal protein S18 OS=Homo sapiens GN=RPS18 PE=1 SV=3 - [RS18_HUMAN]	3	0.990	0.491	0.596
P30486	HLA class I histocompatibility antigen, B-48 alpha chain OS=Homo sapiens GN=HLA-B PE=1 SV=1 - [1B48_HUMAN]	3	0.400	1.962	0.784
A0A087X106	Keratin, type II cuticular Hb1 OS=Homo sapiens GN=KRT81 PE=1 SV=1 - [A0A087X106_HUMAN]	4	0.010	1.000	0.010

UL27	UL27	5	10.000	3.069	100.000
P27824	Calnexin OS=Homo sapiens GN=CANX PE=1 SV=2 - [CALX_HUMAN]	3	0.921	1.220	1.024
A0A087X2I6	Keratin, type I cuticular Ha3-II OS=Homo sapiens GN=KRT33B PE=1 SV=1 - [A0A087X2I6_HUMAN]	3	0.010	1.000	0.010
A0A0A0MR02	Voltage-dependent anion-selective channel protein 2 (Fragment) OS=Homo sapiens GN=VDAC2 PE=1 SV=1 - [A0A0A0MR02_HUMAN]	4	0.278	4.104	1.363
P21796	Voltage-dependent anion-selective channel protein 1 OS=Homo sapiens GN=VDAC1 PE=1 SV=2 - [VDAC1_HUMAN]	2	0.713	2.725	1.943
Q4QZC0	MHC class I antigen (Fragment) OS=Homo sapiens GN=HLA-A PE=3 SV=1 - [Q4QZC0_HUMAN]	1	0.351	8.100	2.839
P62805	Histone H4 OS=Homo sapiens GN=HIST1H4A PE=1 SV=2 - [H4_HUMAN]	3	0.481	0.390	0.163
A0A087X130	Ig kappa chain C region OS=Homo sapiens GN=IGKC PE=1 SV=1 - [A0A087X130_HUMAN]	3	0.010	1.000	0.010
X6RFL8	Ras-related protein Rab-14 (Fragment) OS=Homo sapiens GN=RAB14 PE=1 SV=1 - [X6RFL8_HUMAN]	1	0.412	2.942	1.212
UL23	UL23	2	8.939	2.426	21.687
P31944	Caspase-14 OS=Homo sapiens GN=CASP14 PE=1 SV=2 - [CASPE_HUMAN]	3	0.010	1.000	0.010
U3PXP0	Alpha globin chain (Fragment) OS=Homo sapiens GN=HBA2 PE=3 SV=1 - [U3PXP0_HUMAN]	1	0.010	1.000	0.010
B4DL14	ATP synthase subunit gamma OS=Homo sapiens PE=2 SV=1 - [B4DL14_HUMAN]	2	0.717	0.998	0.608
P01036	Cystatin-S OS=Homo sapiens GN=CST4 PE=1 SV=3 - [CYTS_HUMAN]	1			
A0A087WZH7	Myristoylated alanine-rich C-kinase substrate OS=Homo sapiens GN=MARCKS PE=1 SV=1 - [A0A087WZH7_HUMAN]	2	0.938		
A0A024R7P5	Similar to Laminin receptor 1, isoform CRA_a OS=Homo sapiens GN=LOC388524 PE=3 SV=1 - [A0A024R7P5_HUMAN]	3	0.731	0.947	0.802
P10599	Thioredoxin OS=Homo sapiens GN=TXN PE=1 SV=3 - [THIO_HUMAN]	2	0.454	0.932	0.406
UL34	UL34	2			
A0A024R3X7	Heat shock 10kDa protein 1 (Chaperonin 10), isoform CRA_d OS=Homo sapiens GN=HSPE1 PE=3 SV=1 - [A0A024R3X7_HUMAN]	1	1.643	0.612	1.006
P01621	Ig kappa chain V-III region NG9 (Fragment) OS=Homo sapiens PE=2 SV=1 - [KV303_HUMAN]	1			
P59665	Neutrophil defensin 1 OS=Homo sapiens GN=DEFA1 PE=1 SV=1 - [DEF1_HUMAN]	2	0.010	1.000	0.010
UL26.5	UL26.5	1		2.720	
B3KT34	cDNA FLJ37560 fis, clone BRCOC2000333, highly similar to Succinate dehydrogenase (ubiquinone) flavoprotein subunit, mitochondrial (EC 1.3.5.1) OS=Homo sapiens PE=2 SV=1 - [B3KT34_HUMAN]	2	0.072	1.216	0.634
Q53EW3	Regulatory factor X, 5 variant (Fragment) OS=Homo sapiens PE=2 SV=1 - [Q53EW3_HUMAN]	1			
UL44	UL44	2	10.070	2.774	27.936
C9JA05	Protein JCHAIN (Fragment) OS=Homo sapiens GN=JCHAIN PE=1 SV=1 - [C9JA05_HUMAN]	1	0.010	1.000	0.010
Q6KB66	Keratin, type II cytoskeletal 80 OS=Homo sapiens GN=KRT80 PE=1 SV=2 - [K2C80_HUMAN]	2			0.010
Q5T749	Keratinocyte proline-rich protein OS=Homo sapiens GN=KPRP PE=1 SV=1 - [KPRP_HUMAN]	2	0.010	1.000	0.010
H7C1V0	Cathepsin D (Fragment) OS=Homo sapiens GN=CTSD PE=1 SV=1 - [H7C1V0_HUMAN]	1	0.094	2.160	0.203
P31025	Lipocalin-1 OS=Homo sapiens GN=LCN1 PE=1 SV=1 - [LCN1_HUMAN]	2			
UL19	UL19	3	100.000	5.763	100.000
B4DTA2	cDNA FLJ60148, highly similar to Homo sapiens heterogeneous nuclear ribonucleoprotein D-like (HNRPDL), transcript variant 2, mRNA OS=Homo sapiens PE=2 SV=1 - [B4DTA2_HUMAN]	2	1.209	0.363	0.439
P04406	Glyceraldehyde-3-phosphate dehydrogenase OS=Homo sapiens GN=GAPDH PE=1 SV=3 - [G3P_HUMAN]	3	0.092	2.514	0.361
Q9Y509	VH3 protein (Fragment) OS=Homo sapiens GN=VH3 PE=2 SV=1 - [Q9Y509_HUMAN]	2			
O00483	Cytochrome c oxidase subunit NDUFA4 OS=Homo sapiens GN=NDUFA4 PE=1 SV=1 - [NDUA4_HUMAN]	2	0.197	4.396	0.831
UL18	UL18	2			
Q5CAQ5	Tumor rejection antigen (Gp96) 1 OS=Homo sapiens GN=TRA1 PE=2 SV=1 - [Q5CAQ5_HUMAN]	2	0.469	2.727	1.278
S6BAR0	IgG L chain OS=Homo sapiens PE=2 SV=1 - [S6BAR0_HUMAN]	1			
Q96P63	Serpin B12 OS=Homo sapiens GN=SERPINB12 PE=1 SV=1 - [SPB12_HUMAN]	3	0.010	1.000	0.010
Q08ES8	Cell growth-inhibiting protein 34 OS=Homo sapiens PE=2 SV=1 - [Q08ES8_HUMAN]	2	0.545	0.649	0.354

P05089	Arginase-1 OS=Homo sapiens GN=ARG1 PE=1 SV=2 - [ARGI1_HUMAN]	2	0.010	1.000	0.010
P25398	40S ribosomal protein S12 OS=Homo sapiens GN=RPS12 PE=1 SV=3 - [RS12_HUMAN]	1	0.728	1.407	1.024
G3V3U4	Proteasome subunit alpha type OS=Homo sapiens GN=PSMA6 PE=1 SV=1 - [G3V3U4_HUMAN]	2	0.785	1.384	1.087
P19105	Myosin regulatory light chain 12A OS=Homo sapiens GN=MYL12A PE=1 SV=2 - [ML12A_HUMAN]	1		0.826	
P63104	14-3-3 protein zeta/delta OS=Homo sapiens GN=YWHAZ PE=1 SV=1 - [1433Z_HUMAN]	1	0.928	2.152	1.996
B7ZAL5	cDNA, FLJ79229, highly similar to Lactotransferrin (EC 3.4.21.-) OS=Homo sapiens PE=2 SV=1 - [B7ZAL5_HUMAN]	5	0.010	1.000	0.010
K7EJT5	60S ribosomal protein L22 (Fragment) OS=Homo sapiens GN=RPL22 PE=1 SV=1 - [K7EJT5_HUMAN]	1	0.701	1.103	0.773
Q01650	Large neutral amino acids transporter small subunit 1 OS=Homo sapiens GN=SLC7A5 PE=1 SV=2 - [LAT1_HUMAN]	2			
F8VV32	Lysozyme OS=Homo sapiens GN=LYZ PE=1 SV=1 - [F8VV32_HUMAN]	1			
Q2F838	Eukaryotic translation elongation factor 1 gamma (Fragment) OS=Homo sapiens PE=2 SV=1 - [Q2F838_HUMAN]	1	0.010	1.000	0.010
P01833	Polymeric immunoglobulin receptor OS=Homo sapiens GN=PIGR PE=1 SV=4 - [PIGR_HUMAN]	1	0.010	1.000	0.010
C9JMH6	Alpha-2-antiplasmin (Fragment) OS=Homo sapiens GN=SERPINF2 PE=1 SV=1 - [C9JMH6_HUMAN]	1			
P62857	40S ribosomal protein S28 OS=Homo sapiens GN=RPS28 PE=1 SV=1 - [RS28_HUMAN]	1	0.552	0.776	0.428
C9J7B1	Protein NipSnap homolog 2 (Fragment) OS=Homo sapiens GN=GBAS PE=1 SV=1 - [C9J7B1_HUMAN]	1	1.000	100.000	100.000
B7Z556	cDNA FLJ56822, highly similar to Alpha-2-HS-glycoprotein OS=Homo sapiens PE=2 SV=1 - [B7Z556_HUMAN]	1			
P02656	Apolipoprotein C-III OS=Homo sapiens GN=APOC3 PE=1 SV=1 - [APOC3_HUMAN]	1	0.010	1.000	0.010
C9J0F2	Protein-L-isoaspartate(D-aspartate) O-methyltransferase (Fragment) OS=Homo sapiens GN=PCMT1 PE=1 SV=1 - [C9J0F2_HUMAN]	1		1.223	
H0Y512	Adipocyte plasma membrane-associated protein (Fragment) OS=Homo sapiens GN=APMAP PE=1 SV=1 - [H0Y512_HUMAN]	1	0.230	4.577	1.051
P31942	Heterogeneous nuclear ribonucleoprotein H3 OS=Homo sapiens GN=HNRNPH3 PE=1 SV=2 - [HNRH3_HUMAN]	1	0.010	1.000	0.010
P04083	Annexin A1 OS=Homo sapiens GN=ANXA1 PE=1 SV=2 - [ANXA1_HUMAN]	2	0.287	5.220	1.498
D6R904	Tropomyosin alpha-3 chain OS=Homo sapiens GN=TPM3 PE=1 SV=1 - [D6R904_HUMAN]	2	0.228	0.320	0.495
P09228	Cystatin-SA OS=Homo sapiens GN=CST2 PE=1 SV=1 - [CYTT_HUMAN]	1	0.010	1.000	0.010
H3BUH7	Fructose-bisphosphate aldolase (Fragment) OS=Homo sapiens GN=ALDOA PE=1 SV=1 - [H3BUH7_HUMAN]	1		1.108	
P12273	Prolactin-inducible protein OS=Homo sapiens GN=PIP PE=1 SV=1 - [PIP_HUMAN]	1			
M0QZK8	Uncharacterized protein OS=Homo sapiens PE=4 SV=1 - [M0QZK8_HUMAN]	1	0.011	1.000	0.011
Q4JFL9	Protein S100 (Fragment) OS=Homo sapiens GN=FLG PE=2 SV=1 - [Q4JFL9_HUMAN]	1	0.010	1.000	0.010
B7ZMD7	Alpha-amylase OS=Homo sapiens GN=AMY1A PE=2 SV=1 - [B7ZMD7_HUMAN]	4	0.010	1.000	0.010
B4DUL5	cDNA FLJ51625, highly similar to Ubiquinol-cytochrome-c reductase complex coreprotein I, mitochondrial (EC 1.10.2.2) OS=Homo sapiens PE=2 SV=1 - [B4DUL5_HUMAN]	1	1.000	100.000	100.000
Q15388	Mitochondrial import receptor subunit TOM20 homolog OS=Homo sapiens GN=TOMM20 PE=1 SV=1 - [TOM20_HUMAN]	1			
P03973	Antileukoproteinase OS=Homo sapiens GN=SLPI PE=1 SV=2 - [SLPI_HUMAN]	1	0.010	1.000	0.010
E9PMK8	Tripartite motif-containing protein 3 (Fragment) OS=Homo sapiens GN=TRIM3 PE=1 SV=5 - [E9PMK8_HUMAN]	1			
UL12	UL12	1	100.000	1.327	100.000
B3KM80	Nucleolin, isoform CRA_c OS=Homo sapiens GN=NCL PE=2 SV=1 - [B3KM80_HUMAN]	1	0.266	1.265	0.336
P05556	Integrin beta-1 OS=Homo sapiens GN=ITGB1 PE=1 SV=2 - [ITB1_HUMAN]	2	0.329	3.721	1.224
P01876	Ig alpha-1 chain C region OS=Homo sapiens GN=IGHA1 PE=1 SV=2 - [IGHA1_HUMAN]	2	0.010	1.000	0.010
A0A0A7M1X5	Lamin B2, isoform CRA_b OS=Homo sapiens GN=LMNB2 PE=2 SV=1 - [A0A0A7M1X5_HUMAN]	1			1.862
K7EIP6	Uncharacterized protein (Fragment) OS=Homo sapiens PE=4 SV=1 - [K7EIP6_HUMAN]	1	0.435	2.642	1.150
P19474	E3 ubiquitin-protein ligase TRIM21 OS=Homo sapiens GN=TRIM21 PE=1 SV=1 - [RO52_HUMAN]	2	0.068	1.051	0.072
H3BMH2	Ras-related protein Rab-11A (Fragment) OS=Homo sapiens GN=RAB11A PE=3 SV=1 - [H3BMH2_HUMAN]	1	0.511	0.629	0.321
B2R5H0	Protein S100 OS=Homo sapiens PE=2 SV=1 - [B2R5H0_HUMAN]	1	0.826	14.169	11.697

Q86WV2	COX4I1 protein OS=Homo sapiens GN=COX4I1 PE=1 SV=1 - [Q86WV2_HUMAN]	1			0.838
Q5HYD9	Putative uncharacterized protein DKFZp686M0619 (Fragment) OS=Homo sapiens GN=DKFZp686M0619 PE=2 SV=1 - [Q5HYD9_HUMAN]	1	0.635	2.184	1.387
C5IX07	Tumor-associated calcium signal transducer 2 OS=Homo sapiens GN=TACSTD2 PE=4 SV=1 - [C5IX07_HUMAN]	1	0.264	2.749	0.725
A0A059QFD5	Cytochrome c oxidase subunit 2 OS=Homo sapiens GN=COX2 PE=3 SV=1 - [A0A059QFD5_HUMAN]	1			2.122
P36955	Pigment epithelium-derived factor OS=Homo sapiens GN=SERPINF1 PE=1 SV=4 - [PEDF_HUMAN]	1	0.019	1.000	0.019
Q8NAV1	Pre-mRNA-splicing factor 38A OS=Homo sapiens GN=PRPF38A PE=1 SV=1 - [PR38A_HUMAN]	1			
Q0ZCF6	Immunglobulin heavy chain variable region (Fragment) OS=Homo sapiens PE=4 SV=1 - [Q0ZCF6_HUMAN]	1			
A0A087WWY3	Filamin-A OS=Homo sapiens GN=FLNA PE=1 SV=1 - [A0A087WWY3_HUMAN]	3	0.280	1.000	0.119
Q9NYE4	Cervical mucin MUC5B (Fragment) OS=Homo sapiens PE=2 SV=1 - [Q9NYE4_HUMAN]	1			
B4DE30	cDNA FLJ51711, highly similar to T-complex protein 1 subunit epsilon OS=Homo sapiens PE=2 SV=1 - [B4DE30_HUMAN]	1		3.461	
V9HWC6	Peptidyl-prolyl cis-trans isomerase OS=Homo sapiens GN=HEL-S-39 PE=2 SV=1 - [V9HWC6_HUMAN]	1			
Q5D862	Filaggrin-2 OS=Homo sapiens GN=FLG2 PE=1 SV=1 - [FILA2_HUMAN]	1			
B7Z3V1	cDNA FLJ60077, highly similar to Sodium/potassium-transporting ATPase alpha-1 chain (EC 3.6.3.9) (Fragment) OS=Homo sapiens PE=2 SV=1 - [B7Z3V1_HUMAN]	3	0.274	12.484	1.548
A0A0C4DGS1	Dolichyl-diphosphooligosaccharide--protein glycosyltransferase 48 kDa subunit OS=Homo sapiens GN=DDOST PE=1 SV=1 - [A0A0C4DGS1_HUMAN]	1	1.149	2.278	2.618
E5RJH3	60S ribosomal protein L30 OS=Homo sapiens GN=RPL30 PE=1 SV=1 - [E5RJH3_HUMAN]	1		1.762	
Q08188	Protein-glutamine gamma-glutamyltransferase E OS=Homo sapiens GN=TGM3 PE=1 SV=4 - [TGM3_HUMAN]	2	0.010	1.000	0.010
Q5QNZ2	ATP synthase F(0) complex subunit B1, mitochondrial OS=Homo sapiens GN=ATP5F1 PE=1 SV=1 - [Q5QNZ2_HUMAN]	1	0.670	2.158	1.445
F6RFD5	Destrin OS=Homo sapiens GN=DSTN PE=1 SV=1 - [F6RFD5_HUMAN]	1	0.462	0.809	0.374
E9PLA2	Rho-related GTP-binding protein RhoC OS=Homo sapiens GN=RHOC PE=4 SV=1 - [E9PLA2_HUMAN]	1			1.387
P62851	40S ribosomal protein S25 OS=Homo sapiens GN=RPS25 PE=1 SV=1 - [RS25_HUMAN]	1			
H7C547	Sodium/potassium-transporting ATPase subunit beta-3 (Fragment) OS=Homo sapiens GN=ATP1B3 PE=1 SV=1 - [H7C547_HUMAN]	1	0.223	6.592	1.469
B4DZG7	ADP-ribosylation factor-like protein 1 OS=Homo sapiens GN=ARL1 PE=1 SV=1 - [B4DZG7_HUMAN]	1	1.000	34.746	34.746
B4E290	cDNA FLJ50039, highly similar to Homo sapiens solute carrier family 25, member 24, transcript variant 1, mRNA OS=Homo sapiens PE=2 SV=1 - [B4E290_HUMAN]	2	0.791	2.362	0.827
M0R3H0	40S ribosomal protein S16 OS=Homo sapiens GN=RPS16 PE=1 SV=1 - [M0R3H0_HUMAN]	1	1.505	0.671	1.010
H7C4C8	T-complex protein 1 subunit theta (Fragment) OS=Homo sapiens GN=CCT8 PE=1 SV=1 - [H7C4C8_HUMAN]	1	1.250	1.897	2.372
B4DL55	cDNA FLJ61309, highly similar to Laminin beta-3 chain OS=Homo sapiens PE=2 SV=1 - [B4DL55_HUMAN]	1	0.010	23.682	0.186
Q6W6M8	Antigen MLAA-42 (Fragment) OS=Homo sapiens PE=2 SV=1 - [Q6W6M8_HUMAN]	1	1.000	26.066	26.066
P27348	14-3-3 protein theta OS=Homo sapiens GN=YWHAQ PE=1 SV=1 - [1433T_HUMAN]	1	1.000	100.000	100.000
H3BNP9	Sulfide:quinone oxidoreductase, mitochondrial (Fragment) OS=Homo sapiens GN=SQRDL PE=1 SV=1 - [H3BNP9_HUMAN]	1	0.211	3.653	0.769
B3KUZ8	Aspartate aminotransferase OS=Homo sapiens PE=2 SV=1 - [B3KUZ8_HUMAN]	1	0.810	0.983	0.797
Q9UBI6	Guanine nucleotide-binding protein G(I)/G(S)/G(O) subunit gamma-12 OS=Homo sapiens GN=GNG12 PE=1 SV=3 - [GBG12_HUMAN]	1	0.543	2.655	1.441
Q70T18	BBF2H7/FUS protein (Fragment) OS=Homo sapiens PE=2 SV=1 - [Q70T18_HUMAN]	2	0.397	0.348	0.138
I3L3U9	Ribosomal L1 domain-containing protein 1 (Fragment) OS=Homo sapiens GN=RSL1D1 PE=1 SV=1 - [I3L3U9_HUMAN]	1			
A0A075B6K9	Ig lambda-2 chain C regions (Fragment) OS=Homo sapiens GN=IGLC2 PE=4 SV=1 - [A0A075B6K9_HUMAN]	1	0.010	1.000	0.010
H7BY36	RNA-binding protein EWS (Fragment) OS=Homo sapiens GN=EWSR1 PE=1 SV=1 - [H7BY36_HUMAN]	1	0.010	1.000	0.010
E5RJR5	S-phase kinase-associated protein 1 OS=Homo sapiens GN=SKP1 PE=1 SV=1 - [E5RJR5_HUMAN]	1	0.503		
B4DRV1	cDNA FLJ51536, highly similar to Protein-glutamine gamma-glutamyltransferase K (EC 2.3.2.13) OS=Homo sapiens PE=2 SV=1 - [B4DRV1_HUMAN]	1	0.010	1.000	0.010
P09669	Cytochrome c oxidase subunit 6C OS=Homo sapiens GN=COX6C PE=1 SV=2 - [COX6C_HUMAN]	1	0.571	4.387	2.505
J3KSC4	Ras-related C3 botulinum toxin substrate 3 (Fragment) OS=Homo sapiens GN=RAC3 PE=1 SV=1 - [J3KSC4_HUMAN]	1	0.341	1.674	0.572

Q9Y277	Voltage-dependent anion-selective channel protein 3 OS=Homo sapiens GN=VDAC3 PE=1 SV=1 - [VDAC3_HUMAN]	1	1.000	100.000	100.000
A0A024RC29	Desmocollin 3, isoform CRA_b OS=Homo sapiens GN=DSC3 PE=4 SV=1 - [A0A024RC29_HUMAN]	1	0.010	1.000	0.010
F8VS58	60S acidic ribosomal protein P0 (Fragment) OS=Homo sapiens GN=RPLP0 PE=1 SV=1 - [F8VS58_HUMAN]	1	0.681		
B4DV51	GTP-binding nuclear protein Ran OS=Homo sapiens GN=RAN PE=1 SV=1 - [B4DV51_HUMAN]	1	0.228	8.660	1.976
P31151	Protein S100-A7 OS=Homo sapiens GN=S100A7 PE=1 SV=4 - [S10A7_HUMAN]	2			
A2VCQ4	PRKCSH protein (Fragment) OS=Homo sapiens GN=PRKCSH PE=2 SV=1 - [A2VCQ4_HUMAN]	1			5.190
R4GMX5	Basigin (Fragment) OS=Homo sapiens GN=BSG PE=1 SV=1 - [R4GMX5_HUMAN]	1	0.782	2.122	1.660
Q9NZM1	Myoferlin OS=Homo sapiens GN=MYOF PE=1 SV=1 - [MYOF_HUMAN]	2	0.442	2.965	1.312
H0YNX5	Signal peptidase complex catalytic subunit SEC11 (Fragment) OS=Homo sapiens GN=SEC11A PE=1 SV=1 - [H0YNX5_HUMAN]	1	0.698	1.637	1.143
A0A087WYY6	Plakophilin-1 OS=Homo sapiens GN=PKP1 PE=1 SV=1 - [A0A087WYY6_HUMAN]	1			
F8WCK2	Elongation factor Ts, mitochondrial OS=Homo sapiens GN=TSFM PE=1 SV=1 - [F8WCK2_HUMAN]	1			
C9J0H3	Phospholipid scramblase 1 (Fragment) OS=Homo sapiens GN=PLSCR1 PE=1 SV=1 - [C9J0H3_HUMAN]	1	1.000	100.000	100.000
E9PJY4	Puromycin-sensitive aminopeptidase (Fragment) OS=Homo sapiens GN=NPEPPS PE=1 SV=2 - [E9PJY4_HUMAN]	1			2.253
UL40	UL40	2	1.620	32.042	51.902
A0A0A1TSG4	CD47 OS=Homo sapiens GN=CD47 PE=2 SV=1 - [A0A0A1TSG4_HUMAN]	1	0.762	3.265	2.489
P80188	Neutrophil gelatinase-associated lipocalin OS=Homo sapiens GN=LCN2 PE=1 SV=2 - [NGAL_HUMAN]	1	0.408		
H7BZJ3	Protein disulfide-isomerase A3 (Fragment) OS=Homo sapiens GN=PDIA3 PE=1 SV=1 - [H7BZJ3_HUMAN]	1	0.784	1.918	1.504
E5RFX3	WD repeat-containing protein 6 OS=Homo sapiens GN=WDR6 PE=1 SV=2 - [E5RFX3_HUMAN]	1			
P29508	Serpin B3 OS=Homo sapiens GN=SERPINB3 PE=1 SV=2 - [SPB3_HUMAN]	2	0.015	1.000	0.015
B4DZ85	Nuclear receptor coactivator 4 OS=Homo sapiens GN=NCOA4 PE=1 SV=1 - [B4DZ85_HUMAN]	1			
UL51	UL51	1			
UL37	UL37	2		8.302	
F8WE04	Heat shock protein beta-1 OS=Homo sapiens GN=HSPB1 PE=1 SV=1 - [F8WE04_HUMAN]	1	0.503	1.543	0.775
P01597	Ig kappa chain V-I region DEE OS=Homo sapiens PE=1 SV=1 - [KV105_HUMAN]	1			
H0Y5E8	GTP-binding protein SAR1a (Fragment) OS=Homo sapiens GN=SAR1A PE=1 SV=1 - [H0Y5E8_HUMAN]	1	1.359	1.266	1.721
J3QKQ5	Importin subunit beta-1 (Fragment) OS=Homo sapiens GN=KPNB1 PE=1 SV=1 - [J3QKQ5_HUMAN]	1	1.000	56.464	56.464
C9J592	Ras-related protein Rab-7a (Fragment) OS=Homo sapiens GN=RAB7A PE=1 SV=1 - [C9J592_HUMAN]	2	0.130	3.619	0.590
H7C125	Ras-related protein Rab-2A (Fragment) OS=Homo sapiens GN=RAB2A PE=1 SV=1 - [H7C125_HUMAN]	1	0.627	2.149	1.348
A0A024R085	UDP glycosyltransferase 3 family, polypeptide A1, isoform CRA_b OS=Homo sapiens GN=UGT3A1 PE=4 SV=1 - [A0A024R085_HUMAN]	1			
I6L8B7	Fatty acid-binding protein, epidermal OS=Homo sapiens GN=FABP5 PE=1 SV=1 - [I6L8B7_HUMAN]	2	0.010	1.000	0.010
V9GZN0	Histone H2A gene (lambda-HHG55) (Fragment) OS=Homo sapiens PE=4 SV=1 - [V9GZN0_HUMAN]	1	0.249		
P04431	Ig kappa chain V-I region Walker OS=Homo sapiens PE=1 SV=1 - [KV123_HUMAN]	1			
C9JLE9	Kelch-like protein 22 (Fragment) OS=Homo sapiens GN=KLHL22 PE=1 SV=1 - [C9JLE9_HUMAN]	1			
B7Z462	cDNA FLJ58016, highly similar to Polypeptide N-acetylgalactosaminyltransferase2 (EC 2.4.1.41) OS=Homo sapiens PE=2 SV=1 - [B7Z462_HUMAN]	1	0.359	4.192	1.506
US6	US6	1	3.467	4.402	15.264
A0A075B6Z2	Protein TRAJ56 (Fragment) OS=Homo sapiens GN=TRAJ56 PE=4 SV=1 - [A0A075B6Z2_HUMAN]	1			
A0A087WUL7	Nuclear receptor-binding factor 2 OS=Homo sapiens GN=NRBF2 PE=1 SV=1 - [A0A087WUL7_HUMAN]	1	0.010	1.000	0.010
B7Z4L4	Dolichyl-diphosphooligosaccharide--protein glycosyltransferase subunit 1 OS=Homo sapiens GN=RPN1 PE=1 SV=1 - [B7Z4L4_HUMAN]	3	0.678	3.440	12.575
P04040	Catalase OS=Homo sapiens GN=CAT PE=1 SV=3 - [CATA_HUMAN]	1			

P63173	60S ribosomal protein L38 OS=Homo sapiens GN=RPL38 PE=1 SV=2 - [RL38_HUMAN]	1			
P31947	14-3-3 protein sigma OS=Homo sapiens GN=SFN PE=1 SV=1 - [1433S_HUMAN]	1		1.236	
P05090	Apolipoprotein D OS=Homo sapiens GN=APOD PE=1 SV=1 - [APOD_HUMAN]	1	0.010	1.000	0.010
Q9BYJ0	Fibroblast growth factor-binding protein 2 OS=Homo sapiens GN=FGFBP2 PE=1 SV=1 - [FGFP2_HUMAN]	1			
Q9C010	cAMP-dependent protein kinase inhibitor beta OS=Homo sapiens GN=PKIB PE=3 SV=1 - [IPKB_HUMAN]	1			
Q8WVV4	Protein POF1B OS=Homo sapiens GN=POF1B PE=1 SV=3 - [POF1B_HUMAN]	1			
Q9BXM0	Periaxin OS=Homo sapiens GN=PRX PE=1 SV=2 - [PRAX_HUMAN]	1			
P30050	60S ribosomal protein L12 OS=Homo sapiens GN=RPL12 PE=1 SV=1 - [RL12_HUMAN]	1	0.504	1.716	0.865
P46783	40S ribosomal protein S10 OS=Homo sapiens GN=RPS10 PE=1 SV=1 - [RS10_HUMAN]	1	1.096	1.753	1.922
Q9HCY8	Protein S100-A14 OS=Homo sapiens GN=S100A14 PE=1 SV=1 - [S10AE_HUMAN]	1	0.010	100.000	0.427
O75556	Mammaglobin-B OS=Homo sapiens GN=SCGB2A1 PE=1 SV=1 - [SG2A1_HUMAN]	1			
Q5JUK2	Spermatogenesis- and oogenesis-specific basic helix-loop-helix-containing protein 1 OS=Homo sapiens GN=SOHLH1 PE=1 SV=4 - [SOLH1_HUMAN]	1			
Q8IW75	Serpin A12 OS=Homo sapiens GN=SERPINA12 PE=1 SV=1 - [SPA12_HUMAN]	1			
Q9UKZ4	Teneurin-1 OS=Homo sapiens GN=TENM1 PE=1 SV=2 - [TEN1_HUMAN]	1	1.000	100.000	100.000
Q96IX5	Up-regulated during skeletal muscle growth protein 5 OS=Homo sapiens GN=USMG5 PE=1 SV=1 - [USMG5_HUMAN]	1			
Q5T750	Skin-specific protein 32 OS=Homo sapiens GN=XP32 PE=1 SV=1 - [XP32_HUMAN]	1			
Q8N823	Zinc finger protein 611 OS=Homo sapiens GN=ZNF611 PE=2 SV=2 - [ZN611_HUMAN]	1			
Q96EG3	Zinc finger protein 837 OS=Homo sapiens GN=ZNF837 PE=2 SV=2 - [ZN837_HUMAN]	1	0.010	1.000	0.010
B4DGW0	E3 SUMO-protein ligase PIAS2 OS=Homo sapiens GN=PIAS2 PE=1 SV=1 - [B4DGW0_HUMAN]	1			
D9MZN6	ATP synthase protein 8 OS=Homo sapiens GN=ATP8 PE=3 SV=1 - [D9MZN6_HUMAN]	1			
A0A024R3J7	HCG2032701, isoform CRA_a OS=Homo sapiens GN=hCG_2032701 PE=4 SV=1 - [A0A024R3J7_HUMAN]	2	0.308	4.170	1.285
Q8TBT6	Putative uncharacterized protein (Fragment) OS=Homo sapiens PE=2 SV=1 - [Q8TBT6_HUMAN]	1	1.597	2.561	4.091
B4DP51	cDNA FLJ54533, highly similar to Heterogeneous nuclear ribonucleoprotein H OS=Homo sapiens PE=2 SV=1 - [B4DP51_HUMAN]	1		59.504	
B4DHR1	cDNA FLJ53009, highly similar to Calreticulin OS=Homo sapiens PE=2 SV=1 - [B4DHR1_HUMAN]	1			4.730
F8W1N5	Nascent polypeptide-associated complex subunit alpha (Fragment) OS=Homo sapiens GN=NACA PE=1 SV=1 - [F8W1N5_HUMAN]	1	0.801	0.362	0.290
M0QZ36	Occludin/ELL domain-containing protein 1 OS=Homo sapiens GN=OCEL1 PE=4 SV=1 - [M0QZ36_HUMAN]	1			
B2R4M6	Protein S100 OS=Homo sapiens PE=2 SV=1 - [B2R4M6_HUMAN]	2			
A0A087WWA5	Tenascin-X OS=Homo sapiens GN=TNXB PE=1 SV=1 - [A0A087WWA5_HUMAN]	1	0.021	1.000	0.021
Q59H27	Hydroxysteroid (17-beta) dehydrogenase 4 variant (Fragment) OS=Homo sapiens PE=2 SV=1 - [Q59H27_HUMAN]	1	0.445	2.562	1.140
F8W0V3	Extracellular glycoprotein lacritin OS=Homo sapiens GN=LACRT PE=1 SV=1 - [F8W0V3_HUMAN]	1	0.010	1.000	0.010
A0A087WTT6	40S ribosomal protein S29 OS=Homo sapiens GN=RPS29 PE=1 SV=1 - [A0A087WTT6_HUMAN]	1			
E5RK64	Vesicle-associated membrane protein-associated protein B/C OS=Homo sapiens GN=VAPB PE=1 SV=1 - [E5RK64_HUMAN]	1			
Q6PJM8	RRP1B protein (Fragment) OS=Homo sapiens GN=RRP1B PE=2 SV=1 - [Q6PJM8_HUMAN]	1	0.010	1.000	0.010
H0YE40	CD44 antigen (Fragment) OS=Homo sapiens GN=CD44 PE=1 SV=1 - [H0YE40_HUMAN]	1	0.392	1.354	0.531
C9JYN0	Synaptophysin-like protein 1 OS=Homo sapiens GN=SYPL1 PE=1 SV=1 - [C9JYN0_HUMAN]	1			
Q15898	(clone XP6A11B) mRNA, partial EST (Fragment) OS=Homo sapiens PE=2 SV=1 - [Q15898_HUMAN]	1			
A0A075B6N7	Ig alpha-2 chain C region (Fragment) OS=Homo sapiens GN=IGHA2 PE=1 SV=1 - [A0A075B6N7_HUMAN]	1			
V9GY25	ATP-dependent 6-phosphofructokinase, platelet type (Fragment) OS=Homo sapiens GN=PFKP PE=1 SV=1 - [V9GY25_HUMAN]	1			
F5H1S8	Malectin (Fragment) OS=Homo sapiens GN=MLEC PE=1 SV=1 - [F5H1S8_HUMAN]	2	0.102	3.887	0.575
C9J3L8	Translocon-associated protein subunit alpha OS=Homo sapiens GN=SSR1 PE=1 SV=1 - [C9J3L8_HUMAN]	1	0.258	4.909	1.267

F8WDN2	Thioredoxin, mitochondrial OS=Homo sapiens GN=TXN2 PE=1 SV=1 - [F8WDN2_HUMAN]	1			
F5H895	Dolichyl-diphosphooligosaccharide--protein glycosyltransferase subunit DAD1 OS=Homo sapiens GN=DAD1 PE=1 SV=1 - [F5H895_HUMAN]	1		3.181	
H0YDD8	60S acidic ribosomal protein P2 (Fragment) OS=Homo sapiens GN=RPLP2 PE=1 SV=1 - [H0YDD8_HUMAN]	1	0.650	1.420	0.924
A0A075B6E2	40S ribosomal protein S19 OS=Homo sapiens GN=RPS19 PE=1 SV=1 - [A0A075B6E2_HUMAN]	1	2.126	0.471	1.002
X6RJP6	Transgelin-2 (Fragment) OS=Homo sapiens GN=TAGLN2 PE=1 SV=1 - [X6RJP6_HUMAN]	1	0.582	2.681	1.561
B2RA57	cDNA, FLJ94708 OS=Homo sapiens PE=2 SV=1 - [B2RA57_HUMAN]	1			
A8K251	cDNA FLJ77884 OS=Homo sapiens PE=2 SV=1 - [A8K251_HUMAN]	1			
H0YH80	Heterogeneous nuclear ribonucleoprotein A1 (Fragment) OS=Homo sapiens GN=HNRNPA1 PE=1 SV=1 - [H0YH80_HUMAN]	2	0.611	0.306	0.187
H0YLS6	Proteasome subunit alpha type OS=Homo sapiens GN=PSMA4 PE=1 SV=1 - [H0YLS6_HUMAN]	1	0.363	0.936	0.340
M0R0Y3	RuvB-like 2 OS=Homo sapiens GN=RUVBL2 PE=1 SV=1 - [M0R0Y3_HUMAN]	1		0.768	
H7C4H2	Signal recognition particle receptor subunit beta (Fragment) OS=Homo sapiens GN=SRPRB PE=1 SV=1 - [H7C4H2_HUMAN]	1			
B1AKQ8	Guanine nucleotide-binding protein G(I)/G(S)/G(T) subunit beta-1 (Fragment) OS=Homo sapiens GN=GNB1 PE=1 SV=5 - [B1AKQ8_HUMAN]	1	0.850	1.258	1.070
A6NKZ9	Nucleolysin TIAR OS=Homo sapiens GN=TIAL1 PE=1 SV=1 - [A6NKZ9_HUMAN]	1	0.341	0.579	0.198
E9PD35	Receptor protein-tyrosine kinase OS=Homo sapiens GN=FLT4 PE=1 SV=1 - [E9PD35_HUMAN]	1			
E5RFS3	Alpha-1,3-mannosyl-glycoprotein 4-beta-N-acetylglucosaminyltransferase B (Fragment) OS=Homo sapiens GN=MGAT4B PE=1 SV=1 - [E5RFS3_HUMAN]	1			
E9PHM2	Probable leucine--tRNA ligase, mitochondrial OS=Homo sapiens GN=LARS2 PE=1 SV=1 - [E9PHM2_HUMAN]	1			
B6DU66	Estrogen receptor alpha delta 2*,3,4,5,6,7*/834 hypothalamic isoform (Fragment) OS=Homo sapiens GN=ESR1 PE=2 SV=1 - [B6DU66_HUMAN]	1			
F5H608	ATP synthase subunit d, mitochondrial OS=Homo sapiens GN=ATP5H PE=1 SV=2 - [F5H608_HUMAN]	1	0.568	4.140	2.353
J3QSA3	Polyubiquitin-B (Fragment) OS=Homo sapiens GN=UBB PE=1 SV=1 - [J3QSA3_HUMAN]	1			0.471
J3KRG2	Gasdermin-A (Fragment) OS=Homo sapiens GN=GSDMA PE=1 SV=5 - [J3KRG2_HUMAN]	1	0.010	1.000	0.010
A2NZL8	Tcell beta chain (Fragment) OS=Homo sapiens GN=TCR PE=2 SV=1 - [A2NZL8_HUMAN]	1	0.013	1.000	0.013
Q9P0C3	HSPC258 (Fragment) OS=Homo sapiens PE=2 SV=1 - [Q9P0C3_HUMAN]	1			
B7Z2R9	cDNA FLJ52540, highly similar to Lysosome-associated membrane glycoprotein 2 OS=Homo sapiens PE=2 SV=1 - [B7Z2R9_HUMAN]	1	0.190	2.070	0.393
Q8TD79	Protein tyrosine phosphatase receptor type C (Fragment) OS=Homo sapiens PE=4 SV=1 - [Q8TD79_HUMAN]	1			
Q53T40	Putative uncharacterized protein FHL2 (Fragment) OS=Homo sapiens GN=FHL2 PE=4 SV=1 - [Q53T40_HUMAN]	1	0.759		
H0YLU2	Proteasome activator complex subunit 1 (Fragment) OS=Homo sapiens GN=PSME1 PE=1 SV=1 - [H0YLU2_HUMAN]	1	0.018	1.000	0.018
K7ESE8	Bleomycin hydrolase (Fragment) OS=Homo sapiens GN=BLMH PE=1 SV=1 - [K7ESE8_HUMAN]	1			
A4QMX9	C2orf16 protein (Fragment) OS=Homo sapiens GN=C2orf16 PE=2 SV=1 - [A4QMX9_HUMAN]	1			
Q96IE3	Similar to plectin 1, intermediate filament binding protein, 500kD (Fragment) OS=Homo sapiens PE=2 SV=1 - [Q96IE3_HUMAN]	1			
B4DNY1	cDNA FLJ60318, highly similar to RNA-binding protein 6 OS=Homo sapiens PE=2 SV=1 - [B4DNY1_HUMAN]	1	0.013	1.000	0.013
C9JQM9	Aspartate--tRNA ligase, cytoplasmic (Fragment) OS=Homo sapiens GN=DARS PE=1 SV=1 - [C9JQM9_HUMAN]	1	0.541	3.537	1.914
G3V3H8	Tryptophan--tRNA ligase, cytoplasmic (Fragment) OS=Homo sapiens GN=WARS PE=1 SV=5 - [G3V3H8_HUMAN]	1	0.975	0.998	0.973
B4DSR0	cDNA FLJ60080, highly similar to 130 kDa leucine-rich protein (LRP 130) (Fragment) OS=Homo sapiens PE=2 SV=1 - [B4DSR0_HUMAN]	2	0.224	2.059	0.461
Q6AI22	Putative uncharacterized protein DKFZp686H16106 (Fragment) OS=Homo sapiens GN=DKFZp686H16106 PE=2 SV=1 - [Q6AI22_HUMAN]	1			
A0JLQ2	Kinesin-like protein (Fragment) OS=Homo sapiens GN=KIF13B PE=2 SV=1 - [A0JLQ2_HUMAN]	1			
I3L1H9	Zymogen granule protein 16 homolog B (Fragment) OS=Homo sapiens GN=ZG16B PE=1 SV=1 - [I3L1H9_HUMAN]	1			
Q9H834	cDNA FLJ13966 fis, clone Y79AA1001394, weakly similar to CELL DIVISION PROTEIN FTSH HOMOLOG (EC 3.4.24.-) OS=Homo sapiens PE=2 SV=1 - [Q9H834_HUMAN]	1	0.333	1.483	0.494

Q86W20	Protease serine 1 (Fragment) OS=Homo sapiens GN=PRSS1 PE=3 SV=1 - [Q86W20_HUMAN]	1	0.010	1.000	0.010
K7ENK9	Vesicle-associated membrane protein 2 OS=Homo sapiens GN=VAMP2 PE=4 SV=1 - [K7ENK9_HUMAN]	1			
A4UCS8	Enolase (Fragment) OS=Homo sapiens PE=2 SV=1 - [A4UCS8_HUMAN]	1	0.010		
H7C3P7	Ras-related protein Ral-A (Fragment) OS=Homo sapiens GN=RALA PE=1 SV=1 - [H7C3P7_HUMAN]	1	0.355	1.008	0.358
Q7L4N0	CAPZB protein (Fragment) OS=Homo sapiens GN=CAPZB PE=2 SV=1 - [Q7L4N0_HUMAN]	1			0.449
B4DJL0	cDNA FLJ60278, highly similar to Dolichyl-diphosphooligosaccharide--proteinglycosyltransferase 63 kDa subunit (EC 2.4.1.119) OS=Homo sapiens PE=2 SV=1 - [B4DJL0_HUMAN]	1	1.000	100.000	100.000
L8ECA8	Alternative protein MCM3AP OS=Homo sapiens GN=MCM3AP PE=4 SV=1 - [L8ECA8_HUMAN]	1			
V9GZL3	GBP OS=Homo sapiens PE=4 SV=1 - [V9GZL3_HUMAN]	1			0.960
B7Z867	cDNA FLJ52293, moderately similar to Microtubule-associated protein RP/EB family member 3 OS=Homo sapiens PE=2 SV=1 - [B7Z867_HUMAN]	1	0.026	1.000	0.026
L8EAK9	Alternative protein ABCB8 OS=Homo sapiens GN=ABCB8 PE=4 SV=1 - [L8EAK9_HUMAN]	1			
B2R8A2	cDNA, FLJ93804, highly similar to Homo sapiens gp25L2 protein (HSGP25L2G), mRNA OS=Homo sapiens PE=2 SV=1 - [B2R8A2_HUMAN]	1			2.300
S6BGF5	IgG H chain OS=Homo sapiens PE=2 SV=1 - [S6BGF5_HUMAN]	1			
A8KAD2	cDNA FLJ77477, highly similar to Homo sapiens zinc finger protein 484 (ZNF484), transcript variant 2, mRNA OS=Homo sapiens PE=2 SV=1 - [A8KAD2_HUMAN]	1			
L8EC50	Alternative protein LCE1E OS=Homo sapiens GN=LCE1E PE=4 SV=1 - [L8EC50_HUMAN]	1			
B2RDI6	cDNA, FLJ96628, highly similar to Homo sapiens mitogen-activated protein kinase kinase kinase 11(MAP3K11), mRNA OS=Homo sapiens PE=2 SV=1 - [B2RDI6_HUMAN]	1	0.010	1.000	0.010
B2RA91	cDNA, FLJ94773, highly similar to Homo sapiens splicing factor, arginine/serine-rich 2, interacting protein (SFRS2IP), mRNA OS=Homo sapiens PE=2 SV=1 - [B2RA91_HUMAN]	1			
A1L407	Histone cluster 1, H1t OS=Homo sapiens GN=HIST1H1T PE=2 SV=1 - [A1L407_HUMAN]	1	0.013	41.111	0.547
UL22	UL22	1	1.000	99.223	99.223
UL24	UL24	1			
US2	US2	1			
A0A090N8G0	Glycyl-tRNA synthetase OS=Homo sapiens GN=GARS PE=3 SV=1 - [A0A090N8G0_HUMAN]	1	1.000	47.172	47.172
A0A0F7G8J1	Plasminogen OS=Homo sapiens GN=PLG PE=2 SV=1 - [A0A0F7G8J1_HUMAN]	1	0.010	1.000	0.010
A0A0A0MRR2	Sphingomyelin synthase-related protein 1 OS=Homo sapiens GN=SAMD8 PE=1 SV=1 - [A0A0A0MRR2_HUMAN]	1			
Tube 2					
H6VRF8	Keratin 1 OS=Homo sapiens GN=KRT1 PE=3 SV=1 - [H6VRF8_HUMAN]	29	0.010	1.000	0.010
P35908	Keratin, type II cytoskeletal 2 epidermal OS=Homo sapiens GN=KRT2 PE=1 SV=2 - [K22E_HUMAN]	29	0.010	1.000	0.010
F6KPG5	Albumin (Fragment) OS=Homo sapiens PE=2 SV=1 - [F6KPG5_HUMAN]	18	0.010	1.000	0.010
B4DRR0	cDNA FLJ53910, highly similar to Keratin, type II cytoskeletal 6A OS=Homo sapiens PE=2 SV=1 - [B4DRR0_HUMAN]	2	0.092	0.810	0.074
P48668	Keratin, type II cytoskeletal 6C OS=Homo sapiens GN=KRT6C PE=1 SV=3 - [K2C6C_HUMAN]	1			
P04259	Keratin, type II cytoskeletal 6B OS=Homo sapiens GN=KRT6B PE=1 SV=5 - [K2C6B_HUMAN]	1			
P13647	Keratin, type II cytoskeletal 5 OS=Homo sapiens GN=KRT5 PE=1 SV=3 - [K2C5_HUMAN]	13	0.142	0.995	0.100
P09211	Glutathione S-transferase P OS=Homo sapiens GN=GSTP1 PE=1 SV=2 - [GSTP1_HUMAN]	12	0.732	0.881	0.629
B7Z4V2	cDNA FLJ51907, highly similar to Stress-70 protein, mitochondrial OS=Homo sapiens PE=2 SV=1 - [B7Z4V2_HUMAN]	21	0.595	0.875	0.510
P35527	Keratin, type I cytoskeletal 9 OS=Homo sapiens GN=KRT9 PE=1 SV=3 - [K1C9_HUMAN]	18	0.010	1.000	0.010
P13645	Keratin, type I cytoskeletal 10 OS=Homo sapiens GN=KRT10 PE=1 SV=6 - [K1C10_HUMAN]	16	0.010	1.000	0.010
P02533	Keratin, type I cytoskeletal 14 OS=Homo sapiens GN=KRT14 PE=1 SV=4 - [K1C14_HUMAN]	6	0.043	0.695	0.025
P08779	Keratin, type I cytoskeletal 16 OS=Homo sapiens GN=KRT16 PE=1 SV=4 - [K1C16_HUMAN]	7	0.010	1.000	0.010
Q04695	Keratin, type I cytoskeletal 17 OS=Homo sapiens GN=KRT17 PE=1 SV=2 - [K1C17_HUMAN]	4	0.221	0.858	0.190

P0DMV8	Heat shock 70 kDa protein 1A OS=Homo sapiens GN=HSPA1A PE=1 SV=1 - [HS71A_HUMAN]	9	0.757	1.046	0.799
B4E335	cDNA FLJ52842, highly similar to Actin, cytoplasmic 1 OS=Homo sapiens PE=2 SV=1 - [B4E335_HUMAN]	4	0.735	2.017	1.343
US8	US8	9	1.000	100.000	100.000
B7Z597	cDNA FLJ54373, highly similar to 60 kDa heat shock protein, mitochondrial OS=Homo sapiens PE=2 SV=1 - [B7Z597_HUMAN]	13	0.613	2.134	0.925
P68104	Elongation factor 1-alpha 1 OS=Homo sapiens GN=EEF1A1 PE=1 SV=1 - [EF1A1_HUMAN]	7	0.769	1.174	0.808
A0A0A0MS14	Protein IGHV1-45 (Fragment) OS=Homo sapiens GN=IGHV1-45 PE=4 SV=1 - [A0A0A0MS14_HUMAN]	1			
Q53HF2	Heat shock 70kDa protein 8 isoform 2 variant (Fragment) OS=Homo sapiens PE=1 SV=1 - [Q53HF2_HUMAN]	6	0.496	1.399	0.624
B7Z6P1	cDNA FLJ53662, highly similar to Actin, alpha skeletal muscle OS=Homo sapiens PE=2 SV=1 - [B7Z6P1_HUMAN]	1			
P08729	Keratin, type II cytoskeletal 7 OS=Homo sapiens GN=KRT7 PE=1 SV=5 - [K2C7_HUMAN]	5	4.697	0.573	2.721
A8K872	cDNA FLJ77849, highly similar to Homo sapiens keratin, hair, basic, 6 (monilethrix) (KRTHB6), mRNA OS=Homo sapiens PE=2 SV=1 - [A8K872_HUMAN]	4	0.010	1.000	0.010
Q0IIN1	Keratin 77 OS=Homo sapiens GN=KRT77 PE=1 SV=1 - [Q0IIN1_HUMAN]	3			
Q15323	Keratin, type I cuticular Ha1 OS=Homo sapiens GN=KRT31 PE=1 SV=3 - [K1H1_HUMAN]	6	0.010	1.000	0.010
P11021	78 kDa glucose-regulated protein OS=Homo sapiens GN=HSPA5 PE=1 SV=2 - [GRP78_HUMAN]	7	0.685	0.946	0.744
P78386	Keratin, type II cuticular Hb5 OS=Homo sapiens GN=KRT85 PE=1 SV=1 - [KRT85_HUMAN]	2	0.021	1.000	0.010
P07355	Annexin A2 OS=Homo sapiens GN=ANXA2 PE=1 SV=2 - [ANXA2_HUMAN]	10	0.404	0.926	0.421
US7	US7	3	0.100	10.000	14.845
Q86Y46	Keratin, type II cytoskeletal 73 OS=Homo sapiens GN=KRT73 PE=1 SV=1 - [K2C73_HUMAN]	1	0.010	1.000	0.010
F5GZS6	4F2 cell-surface antigen heavy chain OS=Homo sapiens GN=SLC3A2 PE=1 SV=1 - [F5GZS6_HUMAN]	10	0.462	2.007	0.955
P05787	Keratin, type II cytoskeletal 8 OS=Homo sapiens GN=KRT8 PE=1 SV=7 - [K2C8_HUMAN]	6	2.814	0.733	2.027
K7ERE3	Keratin, type I cytoskeletal 13 OS=Homo sapiens GN=KRT13 PE=1 SV=1 - [K7ERE3_HUMAN]	3	0.010	1.000	0.010
P08727	Keratin, type I cytoskeletal 19 OS=Homo sapiens GN=KRT19 PE=1 SV=4 - [K1C19_HUMAN]	1	1.719	1.044	1.796
B4DJI2	cDNA FLJ53342, highly similar to Granulins OS=Homo sapiens PE=2 SV=1 - [B4DJI2_HUMAN]	7	0.252	1.069	0.282
B3KML9	cDNA FLJ11352 fis, clone HEMBA1000020, highly similar to Tubulin beta-2C chain OS=Homo sapiens PE=2 SV=1 - [B3KML9_HUMAN]	1	0.960	2.168	2.082
B4DRW1	cDNA FLJ55805, highly similar to Keratin, type II cytoskeletal 4 OS=Homo sapiens PE=2 SV=1 - [B4DRW1_HUMAN]	1	0.010	8.486	0.049
H0YH81	ATP synthase subunit beta (Fragment) OS=Homo sapiens GN=ATP5B PE=1 SV=1 - [H0YH81_HUMAN]	4	0.443	2.725	1.106
Q96B85	TUBB protein (Fragment) OS=Homo sapiens GN=TUBB PE=2 SV=1 - [Q96B85_HUMAN]	1	0.296	3.158	0.934
B3KT06	cDNA FLJ37398 fis, clone BRAMY2027467, highly similar to Tubulin alpha-ubiquitous chain OS=Homo sapiens PE=2 SV=1 - [B3KT06_HUMAN]	2	1.000	100.000	100.000
P25705	ATP synthase subunit alpha, mitochondrial OS=Homo sapiens GN=ATP5A1 PE=1 SV=1 - [ATPA_HUMAN]	7	0.483	2.554	1.370
B3KSC3	cDNA FLJ35987 fis, clone TESTI2014269, highly similar to D-3-phosphoglycerate dehydrogenase (EC 1.1.1.95) OS=Homo sapiens PE=2 SV=1 - [B3KSC3_HUMAN]	4	0.644	5.322	14.854
Q9BQE3	Tubulin alpha-1C chain OS=Homo sapiens GN=TUBA1C PE=1 SV=1 - [TBA1C_HUMAN]	1			
A0A0A0MR02	Voltage-dependent anion-selective channel protein 2 (Fragment) OS=Homo sapiens GN=VDAC2 PE=1 SV=1 - [A0A0A0MR02_HUMAN]	4	0.576	3.976	2.817
Q8TAS0	ATP synthase subunit gamma (Fragment) OS=Homo sapiens PE=2 SV=1 - [Q8TAS0_HUMAN]	5	0.697	1.231	0.930
O76013	Keratin, type I cuticular Ha6 OS=Homo sapiens GN=KRT36 PE=2 SV=1 - [KRT36_HUMAN]	2	0.010	1.000	0.010
B4DMA2	cDNA FLJ54023, highly similar to Heat shock protein HSP 90-beta OS=Homo sapiens PE=2 SV=1 - [B4DMA2_HUMAN]	2	0.479	1.823	0.873
Q8N1N4	Keratin, type II cytoskeletal 78 OS=Homo sapiens GN=KRT78 PE=2 SV=2 - [K2C78_HUMAN]	3	0.010	1.000	0.010
F5GY37	Prohibitin-2 OS=Homo sapiens GN=PHB2 PE=1 SV=1 - [F5GY37_HUMAN]	6	0.627	9.078	6.132
P01876	Ig alpha-1 chain C region OS=Homo sapiens GN=IGHA1 PE=1 SV=2 - [IGHA1_HUMAN]	4	0.010	1.000	0.010
P21796	Voltage-dependent anion-selective channel protein 1 OS=Homo sapiens GN=VDAC1 PE=1 SV=2 - [VDAC1_HUMAN]	6	0.682	2.636	1.458

H7BYV1	Interferon-induced transmembrane protein 2 (Fragment) OS=Homo sapiens GN=IFITM2 PE=4 SV=1 - [H7BYV1_HUMAN]	1	0.844	5.256	18.240
Q01650	Large neutral amino acids transporter small subunit 1 OS=Homo sapiens GN=SLC7A5 PE=1 SV=2 - [LAT1_HUMAN]	3	0.165	2.094	1.066
Q2VPJ6	HSP90AA1 protein (Fragment) OS=Homo sapiens GN=HSP90AA1 PE=1 SV=1 - [Q2VPJ6_HUMAN]	1			0.570
I6L8B7	Fatty acid-binding protein, epidermal OS=Homo sapiens GN=FABP5 PE=1 SV=1 - [I6L8B7_HUMAN]	4	0.010	1.000	0.010
C9JZ20	Prohibitin (Fragment) OS=Homo sapiens GN=PHB PE=1 SV=1 - [C9JZ20_HUMAN]	6	0.548	9.292	5.474
Q6NSB3	Alpha-amylase (Fragment) OS=Homo sapiens GN=AMY1A PE=2 SV=1 - [Q6NSB3_HUMAN]	6	0.010	1.000	0.010
E7EQ69	N-alpha-acetyltransferase 50 OS=Homo sapiens GN=NAA50 PE=1 SV=1 - [E7EQ69_HUMAN]	4	0.771	0.496	0.299
Q96HX3	Dolichyl-diphosphooligosaccharide--protein glycosyltransferase subunit 1 (Fragment) OS=Homo sapiens PE=2 SV=1 - [Q96HX3_HUMAN]	5	0.712	4.587	2.245
E7EQB2	Lactotransferrin (Fragment) OS=Homo sapiens GN=LTF PE=1 SV=1 - [E7EQB2_HUMAN]	8	0.010	1.000	0.010
S6BAR0	IgG L chain OS=Homo sapiens PE=2 SV=1 - [S6BAR0_HUMAN]	1			
P04406	Glyceraldehyde-3-phosphate dehydrogenase OS=Homo sapiens GN=GAPDH PE=1 SV=3 - [G3P_HUMAN]	6	0.099	1.076	0.034
B7Z3V1	cDNA FLJ60077, highly similar to Sodium/potassium-transporting ATPase alpha-1 chain (EC 3.6.3.9) (Fragment) OS=Homo sapiens PE=2 SV=1 - [B7Z3V1_HUMAN]	6	0.552	6.125	5.213
C9J0F2	Protein-L-isoaspartate(D-aspartate) O-methyltransferase (Fragment) OS=Homo sapiens GN=PCMT1 PE=1 SV=1 - [C9J0F2_HUMAN]	1			2.878
Q02413	Desmoglein-1 OS=Homo sapiens GN=DSG1 PE=1 SV=2 - [DSG1_HUMAN]	3	0.010	1.000	0.010
P01833	Polymeric immunoglobulin receptor OS=Homo sapiens GN=PIGR PE=1 SV=4 - [PIGR_HUMAN]	3	0.010	1.000	0.010
Q5T749	Keratinocyte proline-rich protein OS=Homo sapiens GN=KPRP PE=1 SV=1 - [KPRP_HUMAN]	2			
P05141	ADP/ATP translocase 2 OS=Homo sapiens GN=SLC25A5 PE=1 SV=7 - [ADT2_HUMAN]	4	0.740	2.759	2.931
B3KRY3	cDNA FLJ35079 fis, clone PLACE6005283, highly similar to Lysosome-associated membrane glycoprotein 1 OS=Homo sapiens PE=2 SV=1 - [B3KRY3_HUMAN]	2	0.594	1.599	0.950
F2Z2S8	40S ribosomal protein S3 OS=Homo sapiens GN=RPS3 PE=1 SV=1 - [F2Z2S8_HUMAN]	3	0.589	1.830	1.294
P81605	Dermcidin OS=Homo sapiens GN=DCD PE=1 SV=2 - [DCD_HUMAN]	1			
B2DFV8	MHC class I antigen (Fragment) OS=Homo sapiens GN=HLA-A PE=3 SV=1 - [B2DFV8_HUMAN]	4	0.335	2.014	0.910
UL23	UL23	4	1.000	100.000	100.000
B4DNK4	Pyruvate kinase OS=Homo sapiens GN=PKM PE=1 SV=1 - [B4DNK4_HUMAN]	4	0.311	1.114	0.411
Q6UWP8	Suprabasin OS=Homo sapiens GN=SBSN PE=1 SV=2 - [SBSN_HUMAN]	2			
P05109	Protein S100-A8 OS=Homo sapiens GN=S100A8 PE=1 SV=1 - [S10A8_HUMAN]	3	0.010	1.000	0.010
Q6PIQ7	IGL@ protein OS=Homo sapiens GN=IGL@ PE=1 SV=1 - [Q6PIQ7_HUMAN]	0			
P27824	Calnexin OS=Homo sapiens GN=CANX PE=1 SV=2 - [CALX_HUMAN]	5	0.852	1.396	1.091
P04083	Annexin A1 OS=Homo sapiens GN=ANXA1 PE=1 SV=2 - [ANXA1_HUMAN]	4	0.398	1.198	0.477
A0A087WYR4	Immunoglobulin lambda-like polypeptide 5 OS=Homo sapiens GN=IGLL5 PE=1 SV=1 - [A0A087WYR4_HUMAN]	1			
A0A024R7P5	Similar to Laminin receptor 1, isoform CRA_a OS=Homo sapiens GN=LOC388524 PE=3 SV=1 - [A0A024R7P5_HUMAN]	2	0.651	0.737	0.479
P02765	Alpha-2-HS-glycoprotein OS=Homo sapiens GN=AHSG PE=1 SV=1 - [FETUA_HUMAN]	2			
A0A0C4DGN4	Zymogen granule protein 16 homolog B OS=Homo sapiens GN=ZG16B PE=1 SV=1 - [A0A0C4DGN4_HUMAN]	4	0.010	1.000	0.010
S6AWD9	IgG H chain OS=Homo sapiens PE=2 SV=1 - [S6AWD9_HUMAN]	1	0.010	1.000	0.010
UL27	UL27	6	2.400	25.277	60.655
Q4LE79	DSP variant protein (Fragment) OS=Homo sapiens GN=DSP variant protein PE=2 SV=1 - [Q4LE79_HUMAN]	3	0.010	1.000	0.010
B2R4M6	Protein S100 OS=Homo sapiens PE=2 SV=1 - [B2R4M6_HUMAN]	3	0.010	1.000	0.010
B3KT34	cDNA FLJ37560 fis, clone BRCOC2000333, highly similar to Succinate dehydrogenase (ubiquinone) flavoprotein subunit, mitochondrial (EC 1.3.5.1) OS=Homo sapiens PE=2 SV=1 - [B3KT34_HUMAN]	2	0.498	0.621	0.309
P05089	Arginase-1 OS=Homo sapiens GN=ARG1 PE=1 SV=2 - [ARGI1_HUMAN]	2			
S6C4S4	IgG H chain OS=Homo sapiens PE=2 SV=1 - [S6C4S4_HUMAN]	1			
P61626	Lysozyme C OS=Homo sapiens GN=LYZ PE=1 SV=1 - [LYSC_HUMAN]	3	0.010	1.000	0.010

P31025	Lipocalin-1 OS=Homo sapiens GN=LCN1 PE=1 SV=1 - [LCN1_HUMAN]	2	0.010	1.000	0.010
P12273	Prolactin-inducible protein OS=Homo sapiens GN=PIP PE=1 SV=1 - [PIP_HUMAN]	3	0.010	1.000	0.010
A0A024R1X8	Junction plakoglobin, isoform CRA_a OS=Homo sapiens GN=JUP PE=4 SV=1 - [A0A024R1X8_HUMAN]	6	0.010	1.000	0.010
P09228	Cystatin-SA OS=Homo sapiens GN=CST2 PE=1 SV=1 - [CYTT_HUMAN]	2	0.010	1.000	0.010
P25311	Zinc-alpha-2-glycoprotein OS=Homo sapiens GN=AZGP1 PE=1 SV=2 - [ZA2G_HUMAN]	2			
P59665	Neutrophil defensin 1 OS=Homo sapiens GN=DEFA1 PE=1 SV=1 - [DEF1_HUMAN]	1			
E1B2D1	Hemoglobin alpha-1 globin chain variant (Fragment) OS=Homo sapiens GN=HBA1 PE=3 SV=1 - [E1B2D1_HUMAN]	2			
A0A0C4DGS1	Dolichyl-diphosphooligosaccharide--protein glycosyltransferase 48 kDa subunit OS=Homo sapiens GN=DDOST PE=1 SV=1 - [A0A0C4DGS1_HUMAN]	2	0.367	3.851	1.415
C8C504	Beta-globin OS=Homo sapiens GN=HBB PE=3 SV=1 - [C8C504_HUMAN]	4	0.010	1.000	0.010
Q9NZM1	Myoferlin OS=Homo sapiens GN=MYOF PE=1 SV=1 - [MYOF_HUMAN]	5	1.000	2.429	3.132
A8K6Q8	cDNA FLJ75881, highly similar to Homo sapiens transferrin receptor (p90, CD71) (TFRC), mRNA OS=Homo sapiens PE=2 SV=1 - [A8K6Q8_HUMAN]	2			1.445
P10599	Thioredoxin OS=Homo sapiens GN=TXN PE=1 SV=3 - [THIO_HUMAN]	2			
A9UFC0	Caspase 14 OS=Homo sapiens GN=CASP14 PE=2 SV=1 - [A9UFC0_HUMAN]	2	0.010	1.000	0.010
C9IZZ0	Ras-related protein Rab-7a (Fragment) OS=Homo sapiens GN=RAB7A PE=1 SV=1 - [C9IZZ0_HUMAN]	3	0.244	2.446	0.490
P01834	Ig kappa chain C region OS=Homo sapiens GN=IGKC PE=1 SV=1 - [IGKC_HUMAN]	1			
B5BUB1	RuvB-like 1 (Fragment) OS=Homo sapiens GN=RUVBL1 PE=2 SV=1 - [B5BUB1_HUMAN]	3	0.631	3.388	2.137
Q9GZZ8	Extracellular glycoprotein lacritin OS=Homo sapiens GN=LACRT PE=1 SV=1 - [LACRT_HUMAN]	2	0.010	1.000	0.010
UL39	UL39	5	4.702	18.791	100.000
P16615	Sarcoplasmic/endoplasmic reticulum calcium ATPase 2 OS=Homo sapiens GN=ATP2A2 PE=1 SV=1 - [AT2A2_HUMAN]	2	0.233	11.691	1.735
Q45KI0	Trypsin I (Fragment) OS=Homo sapiens GN=PRSS1 PE=3 SV=1 - [Q45KI0_HUMAN]	1	0.010	1.000	0.010
P01037	Cystatin-SN OS=Homo sapiens GN=CST1 PE=1 SV=3 - [CYTN_HUMAN]	2	0.010	1.000	0.010
Q86YZ3	Hornerin OS=Homo sapiens GN=HRNR PE=1 SV=2 - [HORN_HUMAN]	3			
Q4JFL9	Protein S100 (Fragment) OS=Homo sapiens GN=FLG PE=2 SV=1 - [Q4JFL9_HUMAN]	1	0.010	1.000	0.010
Q9BYT5	Keratin-associated protein 2-2 OS=Homo sapiens GN=KRTAP2-2 PE=2 SV=3 - [KRA22_HUMAN]	1			
C9J7B1	Protein NipSnap homolog 2 (Fragment) OS=Homo sapiens GN=GBAS PE=1 SV=1 - [C9J7B1_HUMAN]	1	1.000	100.000	100.000
Q5D862	Filaggrin-2 OS=Homo sapiens GN=FLG2 PE=1 SV=1 - [FILA2_HUMAN]	2			
P01621	Ig kappa chain V-III region NG9 (Fragment) OS=Homo sapiens PE=2 SV=1 - [KV303_HUMAN]	1			
UL34	UL34	1	3.335	5.844	19.491
P03973	Antileukoproteinase OS=Homo sapiens GN=SLPI PE=1 SV=2 - [SLPI_HUMAN]	1			
H3BQZ5	UPF0235 protein C15orf40 OS=Homo sapiens GN=C15orf40 PE=1 SV=1 - [H3BQZ5_HUMAN]	1			
Q701L7	Type II hair keratin 2 OS=Homo sapiens GN=KRTHB2 PE=2 SV=1 - [Q701L7_HUMAN]	1			
A0A087WYY6	Plakophilin-1 OS=Homo sapiens GN=PKP1 PE=1 SV=1 - [A0A087WYY6_HUMAN]	1			
H0YDD8	60S acidic ribosomal protein P2 (Fragment) OS=Homo sapiens GN=RPLP2 PE=1 SV=1 - [H0YDD8_HUMAN]	1	0.700	0.962	0.673
A0A0A0MRQ5	Peroxiredoxin-1 OS=Homo sapiens GN=PRDX1 PE=1 SV=1 - [A0A0A0MRQ5_HUMAN]	1	0.582	0.745	0.434
C9JA05	Protein JCHAIN (Fragment) OS=Homo sapiens GN=JCHAIN PE=1 SV=1 - [C9JA05_HUMAN]	1	0.010	1.000	0.010
A0A087WU05	C-Maf-inducing protein OS=Homo sapiens GN=CMIP PE=1 SV=1 - [A0A087WU05_HUMAN]	1			
Q8NF17	FLJ00385 protein (Fragment) OS=Homo sapiens GN=FLJ00385 PE=1 SV=1 - [Q8NF17_HUMAN]	1	0.010	1.000	0.010
B7Z2R9	cDNA FLJ52540, highly similar to Lysosome-associated membrane glycoprotein 2 OS=Homo sapiens PE=2 SV=1 - [B7Z2R9_HUMAN]	1	0.268	2.501	0.670
P09758	Tumor-associated calcium signal transducer 2 OS=Homo sapiens GN=TACSTD2 PE=1 SV=3 - [TACD2_HUMAN]	2	0.332	3.520	1.515
A0A024R3V9	HCG37498, isoform CRA_b OS=Homo sapiens GN=hCG_37498 PE=4 SV=1 - [A0A024R3V9_HUMAN]	1	0.938	0.891	0.836
O75556	Mammaglobin-B OS=Homo sapiens GN=SCGB2A1 PE=1 SV=1 - [SG2A1_HUMAN]	1	0.010	1.000	0.010

A0A0F7G8J1	Plasminogen OS=Homo sapiens GN=PLG PE=2 SV=1 - [A0A0F7G8J1_HUMAN]	1	0.010	1.000	0.010
C9JYN0	Synaptophysin-like protein 1 OS=Homo sapiens GN=SYPL1 PE=1 SV=1 - [C9JYN0_HUMAN]	1	0.010	1.000	0.010
P04431	Ig kappa chain V-I region Walker OS=Homo sapiens PE=1 SV=1 - [KV123_HUMAN]	1			
B4DT53	cDNA FLJ52905, highly similar to Runt-related transcription factor 3 OS=Homo sapiens PE=2 SV=1 - [B4DT53_HUMAN]	1			
F5H5G7	L-lactate dehydrogenase OS=Homo sapiens GN=LDHC PE=1 SV=1 - [F5H5G7_HUMAN]	1	0.010	1.000	0.010
Q3LI55	Keratin associated protein OS=Homo sapiens GN=KRTAP11-1 PE=2 SV=1 - [Q3LI55_HUMAN]	1			
Q08188	Protein-glutamine gamma-glutamyltransferase E OS=Homo sapiens GN=TGM3 PE=1 SV=4 - [TGM3_HUMAN]	2	0.010	1.000	0.010
A0A087WTB6	Guanine nucleotide-binding protein G(o) subunit alpha OS=Homo sapiens GN=GNAO1 PE=1 SV=1 - [A0A087WTB6_HUMAN]	1			
Q9H9K5	Endogenous retrovirus group MER34 member 1 Env polyprotein OS=Homo sapiens GN=ERVMER34-1 PE=2 SV=1 - [MER34_HUMAN]	1			
I6L957	HNRNPA2B1 protein OS=Homo sapiens GN=HNRNPA2B1 PE=2 SV=1 - [I6L957_HUMAN]	1	0.760	0.584	0.443
C9JDV8	Protein NipSnap homolog 1 (Fragment) OS=Homo sapiens GN=NIPSNAP1 PE=1 SV=4 - [C9JDV8_HUMAN]	1	1.000	100.000	100.000
A0A024R3X7	Heat shock 10kDa protein 1 (Chaperonin 10), isoform CRA_d OS=Homo sapiens GN=HSPE1 PE=3 SV=1 - [A0A024R3X7_HUMAN]	2	0.478	0.726	0.347
B4DRV1	cDNA FLJ51536, highly similar to Protein-glutamine gamma-glutamyltransferase K (EC 2.3.2.13) OS=Homo sapiens PE=2 SV=1 - [B4DRV1_HUMAN]	1			
E9PQ63	Carbonyl reductase [NADPH] 1 OS=Homo sapiens GN=CBR1 PE=1 SV=1 - [E9PQ63_HUMAN]	1	0.764	1.323	1.011
B4DJL0	cDNA FLJ60278, highly similar to Dolichyl-diphosphooligosaccharide--proteinglycosyltransferase 63 kDa subunit (EC 2.4.1.119) OS=Homo sapiens PE=2 SV=1 - [B4DJL0_HUMAN]	1	0.095	11.319	1.071
A0A0A1TSG4	CD47 OS=Homo sapiens GN=CD47 PE=2 SV=1 - [A0A0A1TSG4_HUMAN]	1	0.509	2.477	1.262
UL40	UL40	1			
Q8TBZ8	Zinc finger protein 564 OS=Homo sapiens GN=ZNF564 PE=1 SV=1 - [ZN564_HUMAN]	1	1.000	100.000	100.000
UL44	UL44	2	3.494	18.511	64.674
Q0PHS5	Glucose-6-phosphate dehydrogenase (Fragment) OS=Homo sapiens GN=G6PD PE=4 SV=1 - [Q0PHS5_HUMAN]	1			
D6R9C3	Cytochrome c oxidase subunit 7A2, mitochondrial OS=Homo sapiens GN=COX7A2 PE=1 SV=1 - [D6R9C3_HUMAN]	1	0.598	3.580	2.140
H0YKQ5	Kinesin-like protein (Fragment) OS=Homo sapiens GN=KIF23 PE=1 SV=1 - [H0YKQ5_HUMAN]	1			
B4DZ87	cDNA FLJ57240, highly similar to Mitochondrial proteins import receptor OS=Homo sapiens PE=2 SV=1 - [B4DZ87_HUMAN]	1			0.331
Q96P63	Serpin B12 OS=Homo sapiens GN=SERPINB12 PE=1 SV=1 - [SPB12_HUMAN]	2			
R4GN98	Protein S100 (Fragment) OS=Homo sapiens GN=S100A6 PE=1 SV=1 - [R4GN98_HUMAN]	1			
Q01813	ATP-dependent 6-phosphofructokinase, platelet type OS=Homo sapiens GN=PFKP PE=1 SV=2 - [PFKAP_HUMAN]	2		12.687	
A8K9J7	Histone H2B OS=Homo sapiens PE=2 SV=1 - [A8K9J7_HUMAN]	1	0.010	1.000	0.010
A8K651	cDNA FLJ75700, highly similar to Homo sapiens complement component 1, q subcomponent binding protein (C1QBP), nuclear gene encoding mitochondrial protein, mRNA OS=Homo sapiens PE=2 SV=1 - [A8K651_HUMAN]	1	0.165	5.724	0.944
P22531	Small proline-rich protein 2E OS=Homo sapiens GN=SPRR2E PE=2 SV=2 - [SPR2E_HUMAN]	1			
A8K1M0	cDNA FLJ75297, highly similar to Homo sapiens inositol hexakisphosphate kinase 3 mRNA OS=Homo sapiens PE=2 SV=1 - [A8K1M0_HUMAN]	1			
B4E1S3	cDNA FLJ57860, highly similar to Transmembrane protein 109 OS=Homo sapiens PE=2 SV=1 - [B4E1S3_HUMAN]	1	0.586	1.897	1.112
UL22	UL22	2	1.000	100.000	100.000
C9K0M0	Trifunctional enzyme subunit beta, mitochondrial (Fragment) OS=Homo sapiens GN=HADHB PE=1 SV=5 - [C9K0M0_HUMAN]	1			
Q59FC6	Tumor rejection antigen (Gp96) 1 variant (Fragment) OS=Homo sapiens PE=2 SV=1 - [Q59FC6_HUMAN]	1	0.221	3.353	0.742
H7C4C8	T-complex protein 1 subunit theta (Fragment) OS=Homo sapiens GN=CCT8 PE=1 SV=1 - [H7C4C8_HUMAN]	1	0.509	3.560	1.811
Q9UGM3	Deleted in malignant brain tumors 1 protein OS=Homo sapiens GN=DMBT1 PE=1 SV=2 - [DMBT1_HUMAN]	1			
US6	US6	2	3.076	3.629	11.163
A0A075B6Z2	Protein TRAJ56 (Fragment) OS=Homo sapiens GN=TRAJ56 PE=4 SV=1 - [A0A075B6Z2_HUMAN]	1			

I3NI03	Protein disulfide-isomerase (Fragment) OS=Homo sapiens GN=P4HB PE=1 SV=1 - [I3NI03_HUMAN]	1			0.617
E7EQR6	T-complex protein 1 subunit alpha OS=Homo sapiens GN=TCP1 PE=1 SV=1 - [E7EQR6_HUMAN]	1	0.341	4.208	1.434
A2J1M5	Rheumatoid factor RF-IP4 (Fragment) OS=Homo sapiens PE=2 SV=1 - [A2J1M5_HUMAN]	1			
P35579	Myosin-9 OS=Homo sapiens GN=MYH9 PE=1 SV=4 - [MYH9_HUMAN]	4	0.901	0.988	1.179
B4DI70	cDNA FLJ53509, highly similar to Galectin-3-binding protein OS=Homo sapiens PE=2 SV=1 - [B4DI70_HUMAN]	1	0.010	1.000	0.010
A0A024R3J7	HCG2032701, isoform CRA_a OS=Homo sapiens GN=hCG_2032701 PE=4 SV=1 - [A0A024R3J7_HUMAN]	1	0.448	3.662	1.641
G3GAU4	Anti-H1N1 influenza HA kappa chain variable region (Fragment) OS=Homo sapiens PE=2 SV=1 - [G3GAU4_HUMAN]	1			
Q9H834	cDNA FLJ13966 fis, clone Y79AA1001394, weakly similar to CELL DIVISION PROTEIN FTSH HOMOLOG (EC 3.4.24.-) OS=Homo sapiens PE=2 SV=1 - [Q9H834_HUMAN]	1	0.668	3.053	2.039
Q6KB66	Keratin, type II cytoskeletal 80 OS=Homo sapiens GN=KRT80 PE=1 SV=2 - [K2C80_HUMAN]	2	0.010	1.000	0.010
H0Y512	Adipocyte plasma membrane-associated protein (Fragment) OS=Homo sapiens GN=APMAP PE=1 SV=1 - [H0Y512_HUMAN]	1	0.452	4.154	1.877
P01861	Ig gamma-4 chain C region OS=Homo sapiens GN=IGHG4 PE=1 SV=1 - [IGHG4_HUMAN]	2	0.010	1.000	0.010
Q9BZ93	Prosomal P27K protein (Fragment) OS=Homo sapiens GN=PSMA6 PE=4 SV=1 - [Q9BZ93_HUMAN]	1	0.020	1.000	0.020
P62857	40S ribosomal protein S28 OS=Homo sapiens GN=RPS28 PE=1 SV=1 - [RS28_HUMAN]	1	0.554	0.877	0.485
Q15758	Neutral amino acid transporter B(0) OS=Homo sapiens GN=SLC1A5 PE=1 SV=2 - [AAAT_HUMAN]	1			1.199
P02656	Apolipoprotein C-III OS=Homo sapiens GN=APOC3 PE=1 SV=1 - [APOC3_HUMAN]	1			
Q9NZT1	Calmodulin-like protein 5 OS=Homo sapiens GN=CALML5 PE=1 SV=2 - [CALL5_HUMAN]	1			
Q5JTW2	Centrosomal protein of 78 kDa OS=Homo sapiens GN=CEP78 PE=1 SV=1 - [CEP78_HUMAN]	1			
Q9P1W3	Calcium permeable stress-gated cation channel 1 OS=Homo sapiens GN=TMEM63C PE=2 SV=1 - [CSC1_HUMAN]	1			
P01040	Cystatin-A OS=Homo sapiens GN=CSTA PE=1 SV=1 - [CYTA_HUMAN]	1	0.010	1.000	0.010
P49411	Elongation factor Tu, mitochondrial OS=Homo sapiens GN=TUFM PE=1 SV=2 - [EFTU_HUMAN]	1	0.232	1.444	0.335
P31994	Low affinity immunoglobulin gamma Fc region receptor II-b OS=Homo sapiens GN=FCGR2B PE=1 SV=2 - [FCG2B_HUMAN]	1			
P01765	Ig heavy chain V-III region TIL OS=Homo sapiens PE=1 SV=1 - [HV304_HUMAN]	1			
Q96AG4	Leucine-rich repeat-containing protein 59 OS=Homo sapiens GN=LRRC59 PE=1 SV=1 - [LRC59_HUMAN]	1			
Q9Y2I6	Ninein-like protein OS=Homo sapiens GN=NINL PE=1 SV=2 - [NINL_HUMAN]	1			
P12004	Proliferating cell nuclear antigen OS=Homo sapiens GN=PCNA PE=1 SV=1 - [PCNA_HUMAN]	1			
P30048	Thioredoxin-dependent peroxide reductase, mitochondrial OS=Homo sapiens GN=PRDX3 PE=1 SV=3 - [PRDX3_HUMAN]	1	0.017	1.000	0.017
Q9NVN3	Synembryn-B OS=Homo sapiens GN=RIC8B PE=1 SV=2 - [RIC8B_HUMAN]	1			
Q9HCY8	Protein S100-A14 OS=Homo sapiens GN=S100A14 PE=1 SV=1 - [S10AE_HUMAN]	1	0.010	1.000	0.010
Q96FQ6	Protein S100-A16 OS=Homo sapiens GN=S100A16 PE=1 SV=1 - [S10AG_HUMAN]	1	0.016	1.000	0.016
O95969	Secretoglobin family 1D member 2 OS=Homo sapiens GN=SCGB1D2 PE=2 SV=1 - [SG1D2_HUMAN]	1			
P29508	Serpin B3 OS=Homo sapiens GN=SERPINB3 PE=1 SV=2 - [SPB3_HUMAN]	1			
Q562E7	WD repeat-containing protein 81 OS=Homo sapiens GN=WDR81 PE=1 SV=2 - [WDR81_HUMAN]	1			
Q6UXN9	WD repeat-containing protein 82 OS=Homo sapiens GN=WDR82 PE=1 SV=1 - [WDR82_HUMAN]	1	0.010	1.000	0.010
Q5T750	Skin-specific protein 32 OS=Homo sapiens GN=XP32 PE=1 SV=1 - [XP32_HUMAN]	1	0.010	1.000	0.010
Q6S9W8	Kallikrein 5 isoform 3 preproprotein OS=Homo sapiens GN=KLK5 PE=2 SV=1 - [Q6S9W8_HUMAN]	1			
Q6B823	Histone H4 (Fragment) OS=Homo sapiens PE=3 SV=1 - [Q6B823_HUMAN]	1	0.146	2.035	0.297
F5H163	Mevalonate kinase OS=Homo sapiens GN=MVK PE=1 SV=1 - [F5H163_HUMAN]	1			
G3V210	60S acidic ribosomal protein P0 OS=Homo sapiens GN=RPLP0 PE=1 SV=1 - [G3V210_HUMAN]	3	0.877	1.397	1.226
F2Z2H1	Putative helicase Mov10l1 OS=Homo sapiens GN=MOV10L1 PE=4 SV=1 - [F2Z2H1_HUMAN]	1			

B3KM80	Nucleolin, isoform CRA_c OS=Homo sapiens GN=NCL PE=2 SV=1 - [B3KM80_HUMAN]	1			
D3DUJ3	Protein tyrosine phosphatase, non-receptor type 2, isoform CRA_d OS=Homo sapiens GN=PTPN2 PE=4 SV=1 - [D3DUJ3_HUMAN]	1			
Q6NVI1	MARCKS protein (Fragment) OS=Homo sapiens GN=MARCKS PE=2 SV=1 - [Q6NVI1_HUMAN]	1	0.588	1.478	0.869
C9JA68	Serpin B7 (Fragment) OS=Homo sapiens GN=SERPINB7 PE=1 SV=5 - [C9JA68_HUMAN]	1			
B4DWK8	Catalase OS=Homo sapiens PE=2 SV=1 - [B4DWK8_HUMAN]	1			
E7EU96	Casein kinase II subunit alpha OS=Homo sapiens GN=CSNK2A1 PE=1 SV=1 - [E7EU96_HUMAN]	1			
Q5VVC9	60S ribosomal protein L11 (Fragment) OS=Homo sapiens GN=RPL11 PE=1 SV=1 - [Q5VVC9_HUMAN]	1	0.329	0.794	0.261
Q9Y355	Apolipoprotein A1 (Fragment) OS=Homo sapiens PE=4 SV=1 - [Q9Y355_HUMAN]	1			
C9JCA9	Leucine-rich PPR motif-containing protein, mitochondrial (Fragment) OS=Homo sapiens GN=LRPPRC PE=1 SV=1 - [C9JCA9_HUMAN]	1			
E5RFQ7	Protein FAM135B (Fragment) OS=Homo sapiens GN=FAM135B PE=4 SV=1 - [E5RFQ7_HUMAN]	1			
A0A077H155	LTR2-FABP7 OS=Homo sapiens PE=2 SV=1 - [A0A077H155_HUMAN]	1			
B4E1S8	cDNA FLJ59147, highly similar to Cysteine-rich secretory protein 3 OS=Homo sapiens PE=2 SV=1 - [B4E1S8_HUMAN]	1	0.013	1.000	0.013
K7EJZ9	Microtubule-associated serine/threonine-protein kinase 1 (Fragment) OS=Homo sapiens GN=MAST1 PE=1 SV=1 - [K7EJZ9_HUMAN]	1			
A6NLD2	cDNA FLJ11885 fis, clone HEMBA1007203, highly similar to Transmembrane GTPase MFN2 (EC 3.6.5.-) OS=Homo sapiens PE=2 SV=4 - [A6NLD2_HUMAN]	1			
M0QZK8	Uncharacterized protein OS=Homo sapiens PE=4 SV=1 - [M0QZK8_HUMAN]	1			
H0YE40	CD44 antigen (Fragment) OS=Homo sapiens GN=CD44 PE=1 SV=1 - [H0YE40_HUMAN]	1	0.166	3.392	0.563
U3KPT8	Histone H2B type 1-J (Fragment) OS=Homo sapiens GN=HIST1H2BJ PE=4 SV=1 - [U3KPT8_HUMAN]	1			
B4DWN1	cDNA FLJ52285, highly similar to Vesicular integral-membrane protein VIP36 OS=Homo sapiens PE=2 SV=1 - [B4DWN1_HUMAN]	2	0.544	1.263	0.298
S4R460	Protein IGHV3OR16-9 OS=Homo sapiens GN=IGHV3OR16-9 PE=1 SV=2 - [S4R460_HUMAN]	1			
M0QYC8	Complement C3 (Fragment) OS=Homo sapiens GN=C3 PE=1 SV=1 - [M0QYC8_HUMAN]	1			
V9GZN0	Histone H2A gene (lambda-HHG55) (Fragment) OS=Homo sapiens PE=4 SV=1 - [V9GZN0_HUMAN]	1			
A8K0T9	cDNA FLJ75422, highly similar to Homo sapiens capping protein (actin filament) muscle Z-line, alpha 1, mRNA OS=Homo sapiens PE=2 SV=1 - [A8K0T9_HUMAN]	1			
B3KU93	cDNA FLJ39390 fis, clone PLACE6004219, highly similar to Puromycin-sensitive aminopeptidase OS=Homo sapiens PE=2 SV=1 - [B3KU93_HUMAN]	2	1.472	0.762	2.371
H7C4M0	Filamin A-interacting protein 1-like (Fragment) OS=Homo sapiens GN=FILIP1L PE=1 SV=1 - [H7C4M0_HUMAN]	1			
E5RGE1	14-3-3 protein zeta/delta (Fragment) OS=Homo sapiens GN=YWHAZ PE=1 SV=5 - [E5RGE1_HUMAN]	1	0.368	0.957	0.352
F2Z2I8	Stomatin-like protein 2, mitochondrial OS=Homo sapiens GN=STOML2 PE=1 SV=1 - [F2Z2I8_HUMAN]	1	1.000	100.000	100.000
A0A087WVZ4	Cytochrome b-c1 complex subunit 2, mitochondrial (Fragment) OS=Homo sapiens GN=UQCRC2 PE=1 SV=1 - [A0A087WVZ4_HUMAN]	1	0.333	5.134	1.711
Q2XN56	(S)-mephenytoin hydroxylase associated cytochrome P450 (Fragment) OS=Homo sapiens GN=CYP2C18 PE=4 SV=1 - [Q2XN56_HUMAN]	1			
Q6RK68	Fibroblast growth factor (Fragment) OS=Homo sapiens GN=FGF7 PE=3 SV=1 - [Q6RK68_HUMAN]	1			
A2VCQ4	PRKCSH protein (Fragment) OS=Homo sapiens GN=PRKCSH PE=2 SV=1 - [A2VCQ4_HUMAN]	1			2.740
F2Z393	Transaldolase OS=Homo sapiens GN=TALDO1 PE=1 SV=1 - [F2Z393_HUMAN]	1	0.012	1.000	0.012
B4E1V1	Anoctamin (Fragment) OS=Homo sapiens PE=2 SV=1 - [B4E1V1_HUMAN]	1			
F8WF65	Elongation factor 1-beta OS=Homo sapiens GN=EEF1B2 PE=1 SV=1 - [F8WF65_HUMAN]	1			
H7C463	MICOS complex subunit MIC60 (Fragment) OS=Homo sapiens GN=IMMT PE=1 SV=1 - [H7C463_HUMAN]	1		7.438	
E2DRY6	Enolase OS=Homo sapiens PE=2 SV=1 - [E2DRY6_HUMAN]	1	0.460	1.122	0.516
C9JLM5	Serpin B5 (Fragment) OS=Homo sapiens GN=SERPINB5 PE=1 SV=1 - [C9JLM5_HUMAN]	1	0.438	2.810	1.230
Q6AI22	Putative uncharacterized protein DKFZp686H16106 (Fragment) OS=Homo sapiens GN=DKFZp686H16106 PE=2 SV=1 - [Q6AI22_HUMAN]	1			
J3KS13	Clathrin heavy chain 1 OS=Homo sapiens GN=CLTC PE=1 SV=1 - [J3KS13_HUMAN]	1	0.783	1.618	1.266
B2R5H0	Protein S100 OS=Homo sapiens PE=2 SV=1 - [B2R5H0_HUMAN]	1	0.597	1.696	1.012

B4DT78	cDNA FLJ59975, highly similar to Homo sapiens nuclear prelamin A recognition factor-like (NARFL), mRNA OS=Homo sapiens PE=2 SV=1 - [B4DT78_HUMAN]	1			
B4DNS0	cDNA FLJ59234, highly similar to Phosphate-regulating neutral endopeptidase (EC 3.4.24.-) OS=Homo sapiens PE=2 SV=1 - [B4DNS0_HUMAN]	1			
O14992	HS24/P52 OS=Homo sapiens GN=HS24/p52 PE=2 SV=1 - [O14992_HUMAN]	1	0.087	1.000	0.087
B4DN39	cDNA FLJ53065, highly similar to T-complex protein 1 subunit zeta OS=Homo sapiens PE=2 SV=1 - [B4DN39_HUMAN]	1	0.380	5.273	2.003
B4DL87	cDNA FLJ52243, highly similar to Heat-shock protein beta-1 OS=Homo sapiens PE=2 SV=1 - [B4DL87_HUMAN]	1	0.010	1.000	0.010
B4DJ98	cDNA FLJ53558, highly similar to Protein disulfide-isomerase A3 (EC 5.3.4.1) OS=Homo sapiens PE=2 SV=1 - [B4DJ98_HUMAN]	2	0.093	0.683	0.064
Q7Z587	Putative uncharacterized protein OS=Homo sapiens PE=2 SV=1 - [Q7Z587_HUMAN]	1			
B4E3Q9	cDNA FLJ59659, highly similar to Vinculin OS=Homo sapiens PE=2 SV=1 - [B4E3Q9_HUMAN]	1			
Q0EFA5	S protein OS=Homo sapiens GN=S PE=4 SV=1 - [Q0EFA5_HUMAN]	1			
L0R5F6	Alternative protein TNS4 OS=Homo sapiens GN=TNS4 PE=4 SV=1 - [L0R5F6_HUMAN]	1			
S6B2A1	IgG L chain OS=Homo sapiens PE=2 SV=1 - [S6B2A1_HUMAN]	1			
B4DS32	cDNA FLJ56236, highly similar to Exportin-2 OS=Homo sapiens PE=2 SV=1 - [B4DS32_HUMAN]	1	1.161	0.832	0.966
UL19	UL19	2	1.000	100.000	100.000
UL37	UL37	1			
UL49	UL49	1	1.000	67.125	67.125
A0A0A0MSD6	Teneurin-3 OS=Homo sapiens GN=TENM3 PE=1 SV=1 - [A0A0A0MSD6_HUMAN]	1			
A0A0C4DFV9	Protein SET OS=Homo sapiens GN=SET PE=1 SV=1 - [A0A0C4DFV9_HUMAN]	1		0.640	
Tube 3					
F6KPG5	Albumin (Fragment) OS=Homo sapiens PE=2 SV=1 - [F6KPG5_HUMAN]	26	0.010	1.000	0.010
P09211	Glutathione S-transferase P OS=Homo sapiens GN=GSTP1 PE=1 SV=2 - [GSTP1_HUMAN]	11	0.939	0.981	0.925
H6VRF8	Keratin 1 OS=Homo sapiens GN=KRT1 PE=3 SV=1 - [H6VRF8_HUMAN]	20	0.010	1.000	0.010
B7Z4V2	cDNA FLJ51907, highly similar to Stress-70 protein, mitochondrial OS=Homo sapiens PE=2 SV=1 - [B7Z4V2_HUMAN]	22	0.698	0.852	0.557
P35908	Keratin, type II cytoskeletal 2 epidermal OS=Homo sapiens GN=KRT2 PE=1 SV=2 - [K22E_HUMAN]	22	0.010	1.000	0.010
B4DRR0	cDNA FLJ53910, highly similar to Keratin, type II cytoskeletal 6A OS=Homo sapiens PE=2 SV=1 - [B4DRR0_HUMAN]	2	0.088	2.462	0.200
A1A4E9	Keratin 13 OS=Homo sapiens GN=KRT13 PE=1 SV=1 - [A1A4E9_HUMAN]	13	0.010	1.000	0.010
B2R853	cDNA, FLJ93744, highly similar to Homo sapiens keratin 6E (KRT6E), mRNA OS=Homo sapiens PE=2 SV=1 - [B2R853_HUMAN]	1	0.010	1.000	0.010
P13647	Keratin, type II cytoskeletal 5 OS=Homo sapiens GN=KRT5 PE=1 SV=3 - [K2C5_HUMAN]	14	0.042	2.123	0.135
B4DRW1	cDNA FLJ55805, highly similar to Keratin, type II cytoskeletal 4 OS=Homo sapiens PE=2 SV=1 - [B4DRW1_HUMAN]	21	0.010	1.000	0.010
P04259	Keratin, type II cytoskeletal 6B OS=Homo sapiens GN=KRT6B PE=1 SV=5 - [K2C6B_HUMAN]	1			
P13645	Keratin, type I cytoskeletal 10 OS=Homo sapiens GN=KRT10 PE=1 SV=6 - [K1C10_HUMAN]	18	0.010	1.000	0.010
P11021	78 kDa glucose-regulated protein OS=Homo sapiens GN=HSPA5 PE=1 SV=2 - [GRP78_HUMAN]	19	0.716	0.599	0.439
P35527	Keratin, type I cytoskeletal 9 OS=Homo sapiens GN=KRT9 PE=1 SV=3 - [K1C9_HUMAN]	17	0.010	1.000	0.010
P02533	Keratin, type I cytoskeletal 14 OS=Homo sapiens GN=KRT14 PE=1 SV=4 - [K1C14_HUMAN]	7	0.010	1.000	0.051
Q9HC84	Mucin-5B OS=Homo sapiens GN=MUC5B PE=1 SV=3 - [MUC5B_HUMAN]	30	0.010	1.000	0.010
P11142	Heat shock cognate 71 kDa protein OS=Homo sapiens GN=HSPA8 PE=1 SV=1 - [HSP7C_HUMAN]	11	0.883	0.530	0.418
P19012	Keratin, type I cytoskeletal 15 OS=Homo sapiens GN=KRT15 PE=1 SV=3 - [K1C15_HUMAN]	1	0.115	5.372	0.616
Q04695	Keratin, type I cytoskeletal 17 OS=Homo sapiens GN=KRT17 PE=1 SV=2 - [K1C17_HUMAN]	5	0.454	2.701	0.813
P08779	Keratin, type I cytoskeletal 16 OS=Homo sapiens GN=KRT16 PE=1 SV=4 - [K1C16_HUMAN]	6	0.010	1.000	0.010
US8	US8	13	20.535	0.014	0.277
B7ZMD7	Alpha-amylase OS=Homo sapiens GN=AMY1A PE=2 SV=1 - [B7ZMD7_HUMAN]	14	0.010	1.000	0.010

P0DMV8	Heat shock 70 kDa protein 1A OS=Homo sapiens GN=HSPA1A PE=1 SV=1 - [HS71A_HUMAN]	9	0.866	0.535	0.449
P08727	Keratin, type I cytoskeletal 19 OS=Homo sapiens GN=KRT19 PE=1 SV=4 - [K1C19_HUMAN]	6	1.158	1.791	1.973
P08729	Keratin, type II cytoskeletal 7 OS=Homo sapiens GN=KRT7 PE=1 SV=5 - [K2C7_HUMAN]	12	1.840	1.567	3.985
B4E335	cDNA FLJ52842, highly similar to Actin, cytoplasmic 1 OS=Homo sapiens PE=2 SV=1 - [B4E335_HUMAN]	3	1.170	0.400	0.467
P61626	Lysozyme C OS=Homo sapiens GN=LYZ PE=1 SV=1 - [LYSC_HUMAN]	6	0.010	1.000	0.010
F5GY37	Prohibitin-2 OS=Homo sapiens GN=PHB2 PE=1 SV=1 - [F5GY37_HUMAN]	10	4.697	0.092	0.434
B7Z597	cDNA FLJ54373, highly similar to 60 kDa heat shock protein, mitochondrial OS=Homo sapiens PE=2 SV=1 - [B7Z597_HUMAN]	14	1.172	0.273	0.346
B7Z6P1	cDNA FLJ53662, highly similar to Actin, alpha skeletal muscle OS=Homo sapiens PE=2 SV=1 - [B7Z6P1_HUMAN]	1	1.180	0.345	0.407
P05787	Keratin, type II cytoskeletal 8 OS=Homo sapiens GN=KRT8 PE=1 SV=7 - [K2C8_HUMAN]	8	2.099	1.494	2.948
P68104	Elongation factor 1-alpha 1 OS=Homo sapiens GN=EEF1A1 PE=1 SV=1 - [EF1A1_HUMAN]	7	1.022	0.375	0.353
Q86Y46	Keratin, type II cytoskeletal 73 OS=Homo sapiens GN=KRT73 PE=1 SV=1 - [K2C73_HUMAN]	1	0.010	1.000	0.010
E7EQB2	Lactotransferrin (Fragment) OS=Homo sapiens GN=LTF PE=1 SV=1 - [E7EQB2_HUMAN]	17	0.010	1.000	0.010
B2R4M6	Protein S100 OS=Homo sapiens PE=2 SV=1 - [B2R4M6_HUMAN]	4	0.010	1.000	0.010
Q5FWF9	IGL@ protein OS=Homo sapiens GN=IGL@ PE=1 SV=1 - [Q5FWF9_HUMAN]	0			
Q6ZW64	cDNA FLJ41552 fis, clone COLON2004478, highly similar to Protein Tro alpha1 H,myeloma OS=Homo sapiens PE=2 SV=1 - [Q6ZW64_HUMAN]	4			
P07355	Annexin A2 OS=Homo sapiens GN=ANXA2 PE=1 SV=2 - [ANXA2_HUMAN]	11	0.292	0.667	0.213
US7	US7	4	15.306	0.016	0.257
Q0KKI6	Immunoblobulin light chain (Fragment) OS=Homo sapiens PE=1 SV=1 - [Q0KKI6_HUMAN]	5	0.010	1.000	0.010
E7EQ69	N-alpha-acetyltransferase 50 OS=Homo sapiens GN=NAA50 PE=1 SV=1 - [E7EQ69_HUMAN]	9	0.509	1.005	0.516
Q2VPJ6	HSP90AA1 protein (Fragment) OS=Homo sapiens GN=HSP90AA1 PE=1 SV=1 - [Q2VPJ6_HUMAN]	4	0.501	0.445	0.133
B4DMA2	cDNA FLJ54023, highly similar to Heat shock protein HSP 90-beta OS=Homo sapiens PE=2 SV=1 - [B4DMA2_HUMAN]	3	0.870	0.514	0.150
P23396	40S ribosomal protein S3 OS=Homo sapiens GN=RPS3 PE=1 SV=2 - [RS3_HUMAN]	9	0.805	0.305	0.267
Q06830	Peroxiredoxin-1 OS=Homo sapiens GN=PRDX1 PE=1 SV=1 - [PRDX1_HUMAN]	6	0.629	0.760	0.489
Q0IIN1	Keratin 77 OS=Homo sapiens GN=KRT77 PE=1 SV=1 - [Q0IIN1_HUMAN]	2			
B4E2Z3	cDNA FLJ54090, highly similar to 4F2 cell-surface antigen heavy chain OS=Homo sapiens PE=2 SV=1 - [B4E2Z3_HUMAN]	8	1.068	0.382	0.344
P01036	Cystatin-S OS=Homo sapiens GN=CST4 PE=1 SV=3 - [CYTS_HUMAN]	2	0.010	1.000	0.010
Q8N1N4	Keratin, type II cytoskeletal 78 OS=Homo sapiens GN=KRT78 PE=2 SV=2 - [K2C78_HUMAN]	7	0.010	1.000	0.010
Q9NPP6	Immunoglobulin heavy chain variant (Fragment) OS=Homo sapiens PE=2 SV=1 - [Q9NPP6_HUMAN]	4			
Q8NEJ1	Uncharacterized protein OS=Homo sapiens PE=2 SV=1 - [Q8NEJ1_HUMAN]	1			
P07437	Tubulin beta chain OS=Homo sapiens GN=TUBB PE=1 SV=2 - [TBB5_HUMAN]	2	1.006	0.146	0.196
Q8N355	IGL@ protein OS=Homo sapiens GN=IGL@ PE=1 SV=1 - [Q8N355_HUMAN]	2	0.010	1.000	0.010
P01591	Immunoglobulin J chain OS=Homo sapiens GN=JCHAIN PE=1 SV=4 - [IGJ_HUMAN]	6	0.010	1.000	0.010
A5A3E0	POTE ankyrin domain family member F OS=Homo sapiens GN=POTEF PE=1 SV=2 - [POTEF_HUMAN]	1			
P68371	Tubulin beta-4B chain OS=Homo sapiens GN=TUBB4B PE=1 SV=1 - [TBB4B_HUMAN]	2	1.195	0.300	0.358
P25705	ATP synthase subunit alpha, mitochondrial OS=Homo sapiens GN=ATP5A1 PE=1 SV=1 - [ATPA_HUMAN]	8	1.593	0.299	0.417
B4DL14	ATP synthase subunit gamma OS=Homo sapiens PE=2 SV=1 - [B4DL14_HUMAN]	4	0.826	0.762	0.759
K7EKL3	Granulins (Fragment) OS=Homo sapiens GN=GRN PE=1 SV=1 - [K7EKL3_HUMAN]	6	0.141	1.412	0.290
S6BAR0	IgG L chain OS=Homo sapiens PE=2 SV=1 - [S6BAR0_HUMAN]	1			
P03973	Antileukoproteinase OS=Homo sapiens GN=SLPI PE=1 SV=2 - [SLPI_HUMAN]	3	0.010	1.000	0.010
P05109	Protein S100-A8 OS=Homo sapiens GN=S100A8 PE=1 SV=1 - [S10A8_HUMAN]	5	0.010	1.000	0.010
P0CF74	Ig lambda-6 chain C region OS=Homo sapiens GN=IGLC6 PE=4 SV=1 - [LAC6_HUMAN]	1			

A0A087WYR4	Immunoglobulin lambda-like polypeptide 5 OS=Homo sapiens GN=IGLL5 PE=1 SV=1 - [A0A087WYR4_HUMAN]	1			
Q6GMX6	IGH@ protein OS=Homo sapiens GN=IGH@ PE=1 SV=1 - [Q6GMX6_HUMAN]	6	0.010	1.000	0.010
A0A0A0MS14	Protein IGHV1-45 (Fragment) OS=Homo sapiens GN=IGHV1-45 PE=4 SV=1 - [A0A0A0MS14_HUMAN]	1			
A0A024R609	Pyruvate kinase OS=Homo sapiens GN=PKM2 PE=3 SV=1 - [A0A024R609_HUMAN]	6	0.078	0.453	0.011
A0A0C4DGN4	Zymogen granule protein 16 homolog B OS=Homo sapiens GN=ZG16B PE=1 SV=1 - [A0A0C4DGN4_HUMAN]	5	0.010	1.000	0.010
P01833	Polymeric immunoglobulin receptor OS=Homo sapiens GN=PIGR PE=1 SV=4 - [PIGR_HUMAN]	8	0.010	1.000	0.010
UL39	UL39	9	100.000	0.147	100.000
P27482	Calmodulin-like protein 3 OS=Homo sapiens GN=CALML3 PE=1 SV=2 - [CALL3_HUMAN]	5	0.010	1.000	0.010
P22061	Protein-L-isoaspartate(D-aspartate) O-methyltransferase OS=Homo sapiens GN=PCMT1 PE=1 SV=4 - [PIMT_HUMAN]	5	3.612	0.781	2.257
S6C4S4	IgG H chain OS=Homo sapiens PE=2 SV=1 - [S6C4S4_HUMAN]	1	0.010	1.000	0.010
P62805	Histone H4 OS=Homo sapiens GN=HIST1H4A PE=1 SV=2 - [H4_HUMAN]	5	0.087	0.910	0.063
Q02413	Desmoglein-1 OS=Homo sapiens GN=DSG1 PE=1 SV=2 - [DSG1_HUMAN]	7	0.010	1.000	0.010
P35579	Myosin-9 OS=Homo sapiens GN=MYH9 PE=1 SV=4 - [MYH9_HUMAN]	8	3.137	0.342	1.191
P35232	Prohibitin OS=Homo sapiens GN=PHB PE=1 SV=1 - [PHB_HUMAN]	6	6.468	0.057	0.417
Q96HX3	Dolichyl-diphosphooligosaccharide--protein glycosyltransferase subunit 1 (Fragment) OS=Homo sapiens PE=2 SV=1 - [Q96HX3_HUMAN]	6	1.563	0.143	0.178
P09228	Cystatin-SA OS=Homo sapiens GN=CST2 PE=1 SV=1 - [CYTT_HUMAN]	2	0.034	1.000	0.034
P04083	Annexin A1 OS=Homo sapiens GN=ANXA1 PE=1 SV=2 - [ANXA1_HUMAN]	7	0.045	0.495	0.021
P12273	Prolactin-inducible protein OS=Homo sapiens GN=PIP PE=1 SV=1 - [PIP_HUMAN]	6			
UL34	UL34	3	17.333	0.147	2.665
Q01469	Fatty acid-binding protein, epidermal OS=Homo sapiens GN=FABP5 PE=1 SV=3 - [FABP5_HUMAN]	5	0.010	1.000	0.010
UL19	UL19	6	100.000	0.200	73.996
P05164	Myeloperoxidase OS=Homo sapiens GN=MPO PE=1 SV=1 - [PERM_HUMAN]	6	0.010	1.000	0.010
H7BYV1	Interferon-induced transmembrane protein 2 (Fragment) OS=Homo sapiens GN=IFITM2 PE=4 SV=1 - [H7BYV1_HUMAN]	1	3.110	0.187	0.799
I6L965	KRT18 protein (Fragment) OS=Homo sapiens GN=KRT18 PE=2 SV=1 - [I6L965_HUMAN]	2	5.425	0.715	3.878
Q6IVJ6	MHC class I antigen precusor (Fragment) OS=Homo sapiens GN=HLA-A PE=3 SV=1 - [Q6IVJ6_HUMAN]	4	0.644	0.253	0.260
P62269	40S ribosomal protein S18 OS=Homo sapiens GN=RPS18 PE=1 SV=3 - [RS18_HUMAN]	5	0.826	0.458	0.358
A8K486	Peptidyl-prolyl cis-trans isomerase OS=Homo sapiens PE=2 SV=1 - [A8K486_HUMAN]	4	0.236	0.503	0.093
Q9HCY8	Protein S100-A14 OS=Homo sapiens GN=S100A14 PE=1 SV=1 - [S10AE_HUMAN]	5	0.010	1.000	0.010
P04080	Cystatin-B OS=Homo sapiens GN=CSTB PE=1 SV=2 - [CYTB_HUMAN]	4	0.010	1.000	0.010
H0YH81	ATP synthase subunit beta (Fragment) OS=Homo sapiens GN=ATP5B PE=1 SV=1 - [H0YH81_HUMAN]	7	0.970	0.426	0.399
D6RHX1	Mucin-7 (Fragment) OS=Homo sapiens GN=MUC7 PE=1 SV=1 - [D6RHX1_HUMAN]	2	0.010	1.000	0.010
P06733	Alpha-enolase OS=Homo sapiens GN=ENO1 PE=1 SV=2 - [ENOA_HUMAN]	6	0.566	0.351	0.217
A0A087X2I6	Keratin, type I cuticular Ha3-II OS=Homo sapiens GN=KRT33B PE=1 SV=1 - [A0A087X2I6_HUMAN]	1			
W8QEH3	Lamin A/C OS=Homo sapiens GN=LMNA PE=3 SV=1 - [W8QEH3_HUMAN]	5	0.383	0.350	0.202
P51149	Ras-related protein Rab-7a OS=Homo sapiens GN=RAB7A PE=1 SV=1 - [RAB7A_HUMAN]	3	0.646	0.337	0.209
I3L0K7	Heat shock protein 75 kDa, mitochondrial OS=Homo sapiens GN=TRAP1 PE=1 SV=1 - [I3L0K7_HUMAN]	1	1.036		
P05141	ADP/ATP translocase 2 OS=Homo sapiens GN=SLC25A5 PE=1 SV=7 - [ADT2_HUMAN]	2	1.169	0.399	0.467
P31947	14-3-3 protein sigma OS=Homo sapiens GN=SFN PE=1 SV=1 - [1433S_HUMAN]	1	0.165	0.695	0.115
A0A0F7DDK1	MHC class I antigen (Fragment) OS=Homo sapiens GN=HLA-B PE=3 SV=1 - [A0A0F7DDK1_HUMAN]	1			
B3KPS3	cDNA FLJ32131 fis, clone PEBLM2000267, highly similar to Tubulin alpha-ubiquitous chain OS=Homo sapiens PE=2 SV=1 - [B3KPS3_HUMAN]	5	0.884	0.197	0.211
P31025	Lipocalin-1 OS=Homo sapiens GN=LCN1 PE=1 SV=1 - [LCN1_HUMAN]	3	0.010	1.000	0.010

Q4LE79	DSP variant protein (Fragment) OS=Homo sapiens GN=DSP variant protein PE=2 SV=1 - [Q4LE79_HUMAN]	7	0.010	1.000	0.010
P63104	14-3-3 protein zeta/delta OS=Homo sapiens GN=YWHAZ PE=1 SV=1 - [1433Z_HUMAN]	1	0.287	0.359	0.103
UL27	UL27	5	100.000	0.257	46.716
H7C3P7	Ras-related protein Ral-A (Fragment) OS=Homo sapiens GN=RALA PE=1 SV=1 - [H7C3P7_HUMAN]	2	0.860	0.597	0.513
P27824	Calnexin OS=Homo sapiens GN=CANX PE=1 SV=2 - [CALX_HUMAN]	3	2.145	0.350	0.758
P04406	Glyceraldehyde-3-phosphate dehydrogenase OS=Homo sapiens GN=GAPDH PE=1 SV=3 - [G3P_HUMAN]	5	0.198	0.383	0.041
V9HWC6	Peptidyl-prolyl cis-trans isomerase OS=Homo sapiens GN=HEL-S-39 PE=2 SV=1 - [V9HWC6_HUMAN]	3	0.254	0.244	0.010
Q01650	Large neutral amino acids transporter small subunit 1 OS=Homo sapiens GN=SLC7A5 PE=1 SV=2 - [LAT1_HUMAN]	3	1.031	0.205	0.225
P19105	Myosin regulatory light chain 12A OS=Homo sapiens GN=MYL12A PE=1 SV=2 - [ML12A_HUMAN]	3	0.963	0.565	0.703
P25311	Zinc-alpha-2-glycoprotein OS=Homo sapiens GN=AZGP1 PE=1 SV=2 - [ZA2G_HUMAN]	3	0.010	1.000	0.010
A0A024R1X8	Junction plakoglobin, isoform CRA_a OS=Homo sapiens GN=JUP PE=4 SV=1 - [A0A024R1X8_HUMAN]	7	0.010	1.000	0.010
B4DI57	cDNA FLJ54111, highly similar to Serotransferrin OS=Homo sapiens PE=2 SV=1 - [B4DI57_HUMAN]	5			
H7C2U6	Protein NipSnap homolog 1 (Fragment) OS=Homo sapiens GN=NIPSNAP1 PE=1 SV=1 - [H7C2U6_HUMAN]	4	28.121	0.010	0.045
E9PK01	Elongation factor 1-delta (Fragment) OS=Homo sapiens GN=EEF1D PE=1 SV=1 - [E9PK01_HUMAN]	2		0.189	
P31942	Heterogeneous nuclear ribonucleoprotein H3 OS=Homo sapiens GN=HNRNPH3 PE=1 SV=2 - [HNRH3_HUMAN]	2	0.291	2.638	0.459
P27348	14-3-3 protein theta OS=Homo sapiens GN=YWHAQ PE=1 SV=1 - [1433T_HUMAN]	1	1.083	0.881	0.954
P61019	Ras-related protein Rab-2A OS=Homo sapiens GN=RAB2A PE=1 SV=1 - [RAB2A_HUMAN]	3	1.219	0.672	0.888
P10599	Thioredoxin OS=Homo sapiens GN=TXN PE=1 SV=3 - [THIO_HUMAN]	3	0.035	0.370	0.013
P48047	ATP synthase subunit O, mitochondrial OS=Homo sapiens GN=ATP5O PE=1 SV=1 - [ATPO_HUMAN]	3	0.772	0.114	0.081
B3KSC3	cDNA FLJ35987 fis, clone TESTI2014269, highly similar to D-3-phosphoglycerate dehydrogenase (EC 1.1.1.95) OS=Homo sapiens PE=2 SV=1 - [B3KSC3_HUMAN]	3	1.150	0.312	0.359
P07737	Profilin-1 OS=Homo sapiens GN=PFN1 PE=1 SV=2 - [PROF1_HUMAN]	3	0.010	1.000	0.010
P12236	ADP/ATP translocase 3 OS=Homo sapiens GN=SLC25A6 PE=1 SV=4 - [ADT3_HUMAN]	1	1.276	0.012	0.015
H7C333	Protein NipSnap homolog 2 (Fragment) OS=Homo sapiens GN=GBAS PE=1 SV=1 - [H7C333_HUMAN]	3	17.680	0.010	0.010
B4DHC4	cDNA FLJ51843, highly similar to 14-3-3 protein gamma OS=Homo sapiens PE=2 SV=1 - [B4DHC4_HUMAN]	1	2.836	0.148	0.419
A8K5I6	cDNA FLJ78643, highly similar to Homo sapiens cornulin (CRNN), mRNA OS=Homo sapiens PE=2 SV=1 - [A8K5I6_HUMAN]	6	0.010	1.000	0.010
H7BZJ3	Protein disulfide-isomerase A3 (Fragment) OS=Homo sapiens GN=PDIA3 PE=1 SV=1 - [H7BZJ3_HUMAN]	1	0.249	0.454	0.113
C8C504	Beta-globin OS=Homo sapiens GN=HBB PE=3 SV=1 - [C8C504_HUMAN]	5	0.010	1.000	0.010
B0YJC4	Vimentin OS=Homo sapiens GN=VIM PE=1 SV=1 - [B0YJC4_HUMAN]	4			
A8K739	cDNA FLJ77339 OS=Homo sapiens PE=2 SV=1 - [A8K739_HUMAN]	5			
A0A0A0MR02	Voltage-dependent anion-selective channel protein 2 (Fragment) OS=Homo sapiens GN=VDAC2 PE=1 SV=1 - [A0A0A0MR02_HUMAN]	4	7.030	0.119	0.569
P47929	Galectin-7 OS=Homo sapiens GN=LGALS7 PE=1 SV=2 - [LEG7_HUMAN]	3	0.010	1.000	0.010
P51148	Ras-related protein Rab-5C OS=Homo sapiens GN=RAB5C PE=1 SV=2 - [RAB5C_HUMAN]	3	1.072	0.518	0.555
P78386	Keratin, type II cuticular Hb5 OS=Homo sapiens GN=KRT85 PE=1 SV=1 - [KRT85_HUMAN]	2	0.010	1.000	0.010
P02765	Alpha-2-HS-glycoprotein OS=Homo sapiens GN=AHSG PE=1 SV=1 - [FETUA_HUMAN]	2			
P04792	Heat shock protein beta-1 OS=Homo sapiens GN=HSPB1 PE=1 SV=2 - [HSPB1_HUMAN]	2	0.051	0.348	0.033
Q9UL91	Myosin-reactive immunoglobulin heavy chain variable region (Fragment) OS=Homo sapiens PE=2 SV=1 - [Q9UL91_HUMAN]	2	0.010	1.000	0.010
Q5HYD9	Putative uncharacterized protein DKFZp686M0619 (Fragment) OS=Homo sapiens GN=DKFZp686M0619 PE=2 SV=1 - [Q5HYD9_HUMAN]	1	1.770	0.438	0.775
P28325	Cystatin-D OS=Homo sapiens GN=CST5 PE=1 SV=1 - [CYTD_HUMAN]	2	0.010	1.000	0.010
P23280	Carbonic anhydrase 6 OS=Homo sapiens GN=CA6 PE=1 SV=3 - [CAH6_HUMAN]	3	0.010	1.000	0.010
UL23	UL23	2	16.232	0.139	2.656

H3BMH2	Ras-related protein Rab-11A (Fragment) OS=Homo sapiens GN=RAB11A PE=3 SV=1 - [H3BMH2_HUMAN]	2	0.794	0.274	0.217
Q08ES8	Cell growth-inhibiting protein 34 OS=Homo sapiens PE=2 SV=1 - [Q08ES8_HUMAN]	3	0.812	0.383	0.305
I6L957	HNRNPA2B1 protein OS=Homo sapiens GN=HNRNPA2B1 PE=2 SV=1 - [I6L957_HUMAN]	2		0.330	
P81605	Dermcidin OS=Homo sapiens GN=DCD PE=1 SV=2 - [DCD_HUMAN]	2	0.010	1.000	0.010
P21796	Voltage-dependent anion-selective channel protein 1 OS=Homo sapiens GN=VDAC1 PE=1 SV=2 - [VDAC1_HUMAN]	3	2.347	0.199	0.467
P59665	Neutrophil defensin 1 OS=Homo sapiens GN=DEFA1 PE=1 SV=1 - [DEF1_HUMAN]	2			
D6RF44	Heterogeneous nuclear ribonucleoprotein D0 (Fragment) OS=Homo sapiens GN=HNRNPD PE=1 SV=5 - [D6RF44_HUMAN]	1	0.010	1.000	0.010
A0A0F7G8J1	Plasminogen OS=Homo sapiens GN=PLG PE=2 SV=1 - [A0A0F7G8J1_HUMAN]	2	0.010	1.000	0.010
H7C4C8	T-complex protein 1 subunit theta (Fragment) OS=Homo sapiens GN=CCT8 PE=1 SV=1 - [H7C4C8_HUMAN]	2	2.035	0.127	0.258
P35321	Cornifin-A OS=Homo sapiens GN=SPRR1A PE=1 SV=2 - [SPR1A_HUMAN]	1	0.010	1.000	0.010
F8VPE8	60S acidic ribosomal protein P0 (Fragment) OS=Homo sapiens GN=RPLP0 PE=1 SV=1 - [F8VPE8_HUMAN]	2	0.742	0.489	0.322
Q16610	Extracellular matrix protein 1 OS=Homo sapiens GN=ECM1 PE=1 SV=2 - [ECM1_HUMAN]	3	0.010	1.000	0.010
D6R9P3	Heterogeneous nuclear ribonucleoprotein A/B OS=Homo sapiens GN=HNRNPAB PE=1 SV=1 - [D6R9P3_HUMAN]	1			
Q6UWP8	Suprabasin OS=Homo sapiens GN=SBSN PE=1 SV=2 - [SBSN_HUMAN]	2	0.010	1.000	0.010
P49411	Elongation factor Tu, mitochondrial OS=Homo sapiens GN=TUFM PE=1 SV=2 - [EFTU_HUMAN]	2			0.121
U3PXP0	Alpha globin chain (Fragment) OS=Homo sapiens GN=HBA2 PE=3 SV=1 - [U3PXP0_HUMAN]	2			
P35325	Small proline-rich protein 2B OS=Homo sapiens GN=SPRR2B PE=2 SV=1 - [SPR2B_HUMAN]	1	0.010	1.000	0.010
UL12	UL12	3	100.000	0.712	100.000
Q6FIG4	RAB1B protein OS=Homo sapiens GN=RAB1B PE=2 SV=1 - [Q6FIG4_HUMAN]	2	1.224	0.475	0.545
P35326	Small proline-rich protein 2A OS=Homo sapiens GN=SPRR2A PE=1 SV=1 - [SPR2A_HUMAN]	1	0.011	1.000	0.011
B7Z3V1	cDNA FLJ60077, highly similar to Sodium/potassium-transporting ATPase alpha-1 chain (EC 3.6.3.9) (Fragment) OS=Homo sapiens PE=2 SV=1 - [B7Z3V1_HUMAN]	4	0.852	0.016	0.021
P62857	40S ribosomal protein S28 OS=Homo sapiens GN=RPS28 PE=1 SV=1 - [RS28_HUMAN]	2	0.434	0.735	0.319
Q9UGM3	Deleted in malignant brain tumors 1 protein OS=Homo sapiens GN=DMBT1 PE=1 SV=2 - [DMBT1_HUMAN]	3	0.010	1.000	0.010
P04208	Ig lambda chain V-I region WAH OS=Homo sapiens PE=1 SV=1 - [LV106_HUMAN]	1			
Q5CAQ5	Tumor rejection antigen (Gp96) 1 OS=Homo sapiens GN=TRA1 PE=2 SV=1 - [Q5CAQ5_HUMAN]	3	0.574	1.533	0.881
P31949	Protein S100-A11 OS=Homo sapiens GN=S100A11 PE=1 SV=2 - [S10AB_HUMAN]	2	0.131	1.215	0.159
M0R2L9	40S ribosomal protein S19 (Fragment) OS=Homo sapiens GN=RPS19 PE=1 SV=1 - [M0R2L9_HUMAN]	1	0.010	1.000	0.055
A8K651	cDNA FLJ75700, highly similar to Homo sapiens complement component 1, q subcomponent binding protein (C1QBP), nuclear gene encoding mitochondrial protein, mRNA OS=Homo sapiens PE=2 SV=1 - [A8K651_HUMAN]	2	1.135	0.462	0.524
A0A087WZ27	Zinc finger protein 90 OS=Homo sapiens GN=ZNF90 PE=4 SV=2 - [A0A087WZ27_HUMAN]	3	1.746	0.408	0.713
H0Y2W2	ATPase family AAA domain-containing protein 3A (Fragment) OS=Homo sapiens GN=ATAD3A PE=1 SV=1 - [H0Y2W2_HUMAN]	3	0.498	0.199	0.099
H7C463	MICOS complex subunit MIC60 (Fragment) OS=Homo sapiens GN=IMMT PE=1 SV=1 - [H7C463_HUMAN]	2	14.475	0.075	1.087
B3KUZ8	Aspartate aminotransferase OS=Homo sapiens PE=2 SV=1 - [B3KUZ8_HUMAN]	2	0.239	0.807	0.155
Q9NQ38	Serine protease inhibitor Kazal-type 5 OS=Homo sapiens GN=SPINK5 PE=1 SV=2 - [ISK5_HUMAN]	2			
H3BUH7	Fructose-bisphosphate aldolase (Fragment) OS=Homo sapiens GN=ALDOA PE=1 SV=1 - [H3BUH7_HUMAN]	2	0.170	0.210	0.036
A0A0C4DGS1	Dolichyl-diphosphooligosaccharide--protein glycosyltransferase 48 kDa subunit OS=Homo sapiens GN=DDOST PE=1 SV=1 - [A0A0C4DGS1_HUMAN]	3	1.551	0.229	0.355
P22528	Cornifin-B OS=Homo sapiens GN=SPRR1B PE=1 SV=2 - [SPR1B_HUMAN]	1			
X6RFL8	Ras-related protein Rab-14 (Fragment) OS=Homo sapiens GN=RAB14 PE=1 SV=1 - [X6RFL8_HUMAN]	1			0.131
Q9Y355	Apolipoprotein A1 (Fragment) OS=Homo sapiens PE=4 SV=1 - [Q9Y355_HUMAN]	2	0.010	1.000	0.010
A9UFC0	Caspase 14 OS=Homo sapiens GN=CASP14 PE=2 SV=1 - [A9UFC0_HUMAN]	1			

H0YDD8	60S acidic ribosomal protein P2 (Fragment) OS=Homo sapiens GN=RPLP2 PE=1 SV=1 - [H0YDD8_HUMAN]	1	0.430	0.473	0.203
P00738	Haptoglobin OS=Homo sapiens GN=HP PE=1 SV=1 - [HPT_HUMAN]	2	0.010	1.000	0.010
A0A024R7P5	Similar to Laminin receptor 1, isoform CRA_a OS=Homo sapiens GN=LOC388524 PE=3 SV=1 - [A0A024R7P5_HUMAN]	3	0.369	0.507	0.187
F5H6Q2	Polyubiquitin-C (Fragment) OS=Homo sapiens GN=UBC PE=1 SV=5 - [F5H6Q2_HUMAN]	3	1.196	0.197	0.134
A0A087WYY6	Plakophilin-1 OS=Homo sapiens GN=PKP1 PE=1 SV=1 - [A0A087WYY6_HUMAN]	4	0.010	1.000	0.010
G3GAU4	Anti-H1N1 influenza HA kappa chain variable region (Fragment) OS=Homo sapiens PE=2 SV=1 - [G3GAU4_HUMAN]	2	0.010	1.000	0.010
Q6KB66	Keratin, type II cytoskeletal 80 OS=Homo sapiens GN=KRT80 PE=1 SV=2 - [K2C80_HUMAN]	2	0.010	1.000	0.010
E5RJX2	40S ribosomal protein S20 OS=Homo sapiens GN=RPS20 PE=1 SV=1 - [E5RJX2_HUMAN]	2	0.664	0.547	0.317
P01621	Ig kappa chain V-III region NG9 (Fragment) OS=Homo sapiens PE=2 SV=1 - [KV303_HUMAN]	2			
B4DDV4	cDNA FLJ52530, highly similar to Tumor protein D54 OS=Homo sapiens PE=2 SV=1 - [B4DDV4_HUMAN]	2	1.692		
UL42	UL42	3	12.311	0.293	3.604
P21397	Amine oxidase [flavin-containing] A OS=Homo sapiens GN=MAOA PE=1 SV=1 - [AOFA_HUMAN]	1	1.357	0.416	0.564
O75594	Peptidoglycan recognition protein 1 OS=Homo sapiens GN=PGLYRP1 PE=1 SV=1 - [PGRP1_HUMAN]	1			
I3NI03	Protein disulfide-isomerase (Fragment) OS=Homo sapiens GN=P4HB PE=1 SV=1 - [I3NI03_HUMAN]	2	0.265	0.282	0.092
A0N5G5	Rheumatoid factor D5 light chain (Fragment) OS=Homo sapiens GN=V<kappa>3 PE=2 SV=1 - [A0N5G5_HUMAN]	2			
P25398	40S ribosomal protein S12 OS=Homo sapiens GN=RPS12 PE=1 SV=3 - [RS12_HUMAN]	2	0.435	0.269	0.125
Q5T6W2	Heterogeneous nuclear ribonucleoprotein K (Fragment) OS=Homo sapiens GN=HNRNPK PE=1 SV=1 - [Q5T6W2_HUMAN]	2			
B4DUR8	T-complex protein 1 subunit gamma OS=Homo sapiens GN=CCT3 PE=1 SV=1 - [B4DUR8_HUMAN]	2	4.103	0.010	0.027
UL44	UL44	3	95.250	0.391	61.201
Q9Y277	Voltage-dependent anion-selective channel protein 3 OS=Homo sapiens GN=VDAC3 PE=1 SV=1 - [VDAC3_HUMAN]	1	3.294	0.170	0.559
B4DJL0	cDNA FLJ60278, highly similar to Dolichyl-diphosphooligosaccharide--proteinglycosyltransferase 63 kDa subunit (EC 2.4.1.119) OS=Homo sapiens PE=2 SV=1 - [B4DJL0_HUMAN]	2	0.993	0.085	0.084
Q5T0H8	Gelsolin OS=Homo sapiens GN=GSN PE=1 SV=1 - [Q5T0H8_HUMAN]	2	0.010	1.000	0.010
M0QZN2	40S ribosomal protein S5 OS=Homo sapiens GN=RPS5 PE=1 SV=1 - [M0QZN2_HUMAN]	2	1.378	0.539	0.380
C9J0D1	Histone H2A OS=Homo sapiens GN=H2AFV PE=3 SV=1 - [C9J0D1_HUMAN]	2	0.037	0.698	0.026
P30050	60S ribosomal protein L12 OS=Homo sapiens GN=RPL12 PE=1 SV=1 - [RL12_HUMAN]	2	0.464	0.064	0.044
Q9HB00	Desmocollin 1, isoform CRA_b OS=Homo sapiens GN=DSC1 PE=4 SV=1 - [Q9HB00_HUMAN]	5	0.010	1.000	0.010
H0YH80	Heterogeneous nuclear ribonucleoprotein A1 (Fragment) OS=Homo sapiens GN=HNRNPA1 PE=1 SV=1 - [H0YH80_HUMAN]	2	0.013	0.597	0.013
Q6IBG5	MYL6 protein OS=Homo sapiens GN=MYL6 PE=2 SV=1 - [Q6IBG5_HUMAN]	1	0.730	0.165	0.121
B4DJI1	L-lactate dehydrogenase OS=Homo sapiens PE=2 SV=1 - [B4DJI1_HUMAN]	2	0.069	0.450	0.031
H0Y512	Adipocyte plasma membrane-associated protein (Fragment) OS=Homo sapiens GN=APMAP PE=1 SV=1 - [H0Y512_HUMAN]	2	1.148	0.702	0.640
P06312	Ig kappa chain V-IV region (Fragment) OS=Homo sapiens GN=IGKV4-1 PE=4 SV=1 - [KV401_HUMAN]	2	0.010	1.000	0.010
B4DEB9	cDNA FLJ61099, highly similar to ADP-ribosylation factor 1 OS=Homo sapiens PE=2 SV=1 - [B4DEB9_HUMAN]	2	1.022	0.397	0.405
B3KM80	Nucleolin, isoform CRA_c OS=Homo sapiens GN=NCL PE=2 SV=1 - [B3KM80_HUMAN]	2	0.255	0.685	0.309
F6RFD5	Destrin OS=Homo sapiens GN=DSTN PE=1 SV=1 - [F6RFD5_HUMAN]	1	0.869	0.597	0.518
Q96FQ6	Protein S100-A16 OS=Homo sapiens GN=S100A16 PE=1 SV=1 - [S10AG_HUMAN]	2			
O43760	Synaptogyrin-2 OS=Homo sapiens GN=SYNGR2 PE=1 SV=1 - [SNG2_HUMAN]	2	0.273		0.314
P36952	Serpin B5 OS=Homo sapiens GN=SERPINB5 PE=1 SV=2 - [SPB5_HUMAN]	2	0.065	0.760	0.050
O95292	Vesicle-associated membrane protein-associated protein B/C OS=Homo sapiens GN=VAPB PE=1 SV=3 - [VAPB_HUMAN]	2	3.033	0.010	0.010
B3KQT9	Protein disulfide-isomerase OS=Homo sapiens PE=2 SV=1 - [B3KQT9_HUMAN]	1			

B7Z2I6	cDNA FLJ57106, highly similar to Transferrin receptor protein 1 OS=Homo sapiens PE=2 SV=1 - [B7Z2I6_HUMAN]	2	0.887	0.250	0.222
D6RAE9	Sideroflexin-1 OS=Homo sapiens GN=SFXN1 PE=1 SV=1 - [D6RAE9_HUMAN]	1			
Q9BRX8	Redox-regulatory protein FAM213A OS=Homo sapiens GN=FAM213A PE=1 SV=3 - [F213A_HUMAN]	1	0.852	0.585	0.498
A8K7T4	cDNA FLJ75774, highly similar to Homo sapiens lectin, mannose-binding 2 (LMAN2), mRNA OS=Homo sapiens PE=2 SV=1 - [A8K7T4_HUMAN]	2	0.010	1.000	0.010
Q05CF8	KNG1 protein OS=Homo sapiens GN=KNG1 PE=2 SV=1 - [Q05CF8_HUMAN]	1			
US2	US2	2	100.000	0.081	17.644
X2J4X7	Kallikrein 7 (Fragment) OS=Homo sapiens GN=KLK7 PE=2 SV=1 - [X2J4X7_HUMAN]	1	0.010	1.000	0.010
P26641	Elongation factor 1-gamma OS=Homo sapiens GN=EEF1G PE=1 SV=3 - [EF1G_HUMAN]	4	0.010	1.000	0.010
B3KT34	cDNA FLJ37560 fis, clone BRCOC2000333, highly similar to Succinate dehydrogenase (ubiquinone) flavoprotein subunit, mitochondrial (EC 1.3.5.1) OS=Homo sapiens PE=2 SV=1 - [B3KT34_HUMAN]	1	0.010	1.000	0.010
Q53EW3	Regulatory factor X, 5 variant (Fragment) OS=Homo sapiens PE=2 SV=1 - [Q53EW3_HUMAN]	1			
O95873	Uncharacterized protein C6orf47 OS=Homo sapiens GN=C6orf47 PE=2 SV=2 - [CF047_HUMAN]	1			
US11	US11	1			
UL26.5	UL26.5	1			10.459
E5RGH4	Heterogeneous nuclear ribonucleoprotein H (Fragment) OS=Homo sapiens GN=HNRNPH1 PE=1 SV=1 - [E5RGH4_HUMAN]	1	0.328	0.841	0.276
Q5D862	Filaggrin-2 OS=Homo sapiens GN=FLG2 PE=1 SV=1 - [FILA2_HUMAN]	1	0.010	1.000	0.010
P31151	Protein S100-A7 OS=Homo sapiens GN=S100A7 PE=1 SV=4 - [S10A7_HUMAN]	1			
P32320	Cytidine deaminase OS=Homo sapiens GN=CDA PE=1 SV=2 - [CDD_HUMAN]	1	0.010	1.000	0.010
Q70T18	BBF2H7/FUS protein (Fragment) OS=Homo sapiens PE=2 SV=1 - [Q70T18_HUMAN]	1	0.220	0.502	0.110
Q0QF37	Malate dehydrogenase (Fragment) OS=Homo sapiens GN=MDH2 PE=2 SV=1 - [Q0QF37_HUMAN]	2	0.022	1.616	0.036
H0YD14	Myoferlin (Fragment) OS=Homo sapiens GN=MYOF PE=1 SV=1 - [H0YD14_HUMAN]	1		0.043	
P08493	Matrix Gla protein OS=Homo sapiens GN=MGP PE=1 SV=2 - [MGP_HUMAN]	1			
V9GY25	ATP-dependent 6-phosphofructokinase, platelet type (Fragment) OS=Homo sapiens GN=PFKP PE=1 SV=1 - [V9GY25_HUMAN]	1			
P01596	Ig kappa chain V-I region CAR OS=Homo sapiens PE=1 SV=1 - [KV104_HUMAN]	1	0.010	1.000	0.010
O00151	PDZ and LIM domain protein 1 OS=Homo sapiens GN=PDLIM1 PE=1 SV=4 - [PDLI1_HUMAN]	1	0.010	1.000	0.010
H0YJF9	Dihydrolipoyllysine-residue succinyltransferase component of 2-oxoglutarate dehydrogenase complex, mitochondrial (Fragment) OS=Homo sapiens GN=DLST PE=1 SV=1 - [H0YJF9_HUMAN]	1	0.395	0.801	0.316
UL25	UL25	1	4.959		
D3DPF9	Titin, isoform CRA_b OS=Homo sapiens GN=TTN PE=4 SV=1 - [D3DPF9_HUMAN]	1			
P00742	Coagulation factor X OS=Homo sapiens GN=F10 PE=1 SV=2 - [FA10_HUMAN]	1	0.010	1.000	0.010
H0YNX5	Signal peptidase complex catalytic subunit SEC11 (Fragment) OS=Homo sapiens GN=SEC11A PE=1 SV=1 - [H0YNX5_HUMAN]	2	0.993	0.307	0.305
Q8NAG3	cDNA FLJ35393 fis, clone SKNSH2000971, highly similar to TROPOMYOSIN, CYTOSKELETAL TYPE OS=Homo sapiens PE=2 SV=1 - [Q8NAG3_HUMAN]	2	0.010	1.000	0.010
A0A024RC29	Desmocollin 3, isoform CRA_b OS=Homo sapiens GN=DSC3 PE=4 SV=1 - [A0A024RC29_HUMAN]	1			
UL31	UL31	1			
Q5QNZ2	ATP synthase F(0) complex subunit B1, mitochondrial OS=Homo sapiens GN=ATP5F1 PE=1 SV=1 - [Q5QNZ2_HUMAN]	2	0.807	0.339	0.273
F5H895	Dolichyl-diphosphooligosaccharide--protein glycosyltransferase subunit DAD1 OS=Homo sapiens GN=DAD1 PE=1 SV=1 - [F5H895_HUMAN]	1	0.644	0.252	0.162
P02656	Apolipoprotein C-III OS=Homo sapiens GN=APOC3 PE=1 SV=1 - [APOC3_HUMAN]	1			
H7C1V0	Cathepsin D (Fragment) OS=Homo sapiens GN=CTSD PE=1 SV=1 - [H7C1V0_HUMAN]	1			
B3KRY3	cDNA FLJ35079 fis, clone PLACE6005283, highly similar to Lysosome-associated membrane glycoprotein 1 OS=Homo sapiens PE=2 SV=1 - [B3KRY3_HUMAN]	1	0.811	0.557	0.452
Q0VGA3	SUPT16H protein (Fragment) OS=Homo sapiens GN=SUPT16H PE=2 SV=1 - [Q0VGA3_HUMAN]	1			
A0A087WVQ2	PHD finger protein 23 OS=Homo sapiens GN=PHF23 PE=1 SV=1 - [A0A087WVQ2_HUMAN]	1			

A2VCT2	OGDH protein (Fragment) OS=Homo sapiens GN=OGDH PE=2 SV=1 - [A2VCT2_HUMAN]	1			
P25815	Protein S100-P OS=Homo sapiens GN=S100P PE=1 SV=2 - [S100P_HUMAN]	1			
Q53H37	Calmodulin-like skin protein variant (Fragment) OS=Homo sapiens PE=2 SV=1 - [Q53H37_HUMAN]	1	0.010	1.000	0.010
B2MUD5	Neutrophil elastase (Fragment) OS=Homo sapiens GN=ELA2 PE=3 SV=1 - [B2MUD5_HUMAN]	1			
Q8TAK2	Similar to catalase (Fragment) OS=Homo sapiens PE=2 SV=1 - [Q8TAK2_HUMAN]	1	0.010	1.000	0.010
C9J0H3	Phospholipid scramblase 1 (Fragment) OS=Homo sapiens GN=PLSCR1 PE=1 SV=1 - [C9J0H3_HUMAN]	1			
E5RGS7	Uncharacterized protein OS=Homo sapiens PE=4 SV=1 - [E5RGS7_HUMAN]	1			
B4DFL1	Dihydrolipoyl dehydrogenase OS=Homo sapiens PE=2 SV=1 - [B4DFL1_HUMAN]	1	0.297	0.495	0.147
H0YLF3	Beta-2-microglobulin (Fragment) OS=Homo sapiens GN=B2M PE=1 SV=1 - [H0YLF3_HUMAN]	1		0.373	
Q5JPJ9	Putative uncharacterized protein DKFZp686D0114 OS=Homo sapiens GN=DKFZp686D0114 PE=4 SV=1 - [Q5JPJ9_HUMAN]	1			
K7EJT5	60S ribosomal protein L22 (Fragment) OS=Homo sapiens GN=RPL22 PE=1 SV=1 - [K7EJT5_HUMAN]	1	0.465	0.567	0.264
B4DQ44	cDNA FLJ51274, highly similar to NACHT, LRR and PYD-containing protein 7 OS=Homo sapiens PE=2 SV=1 - [B4DQ44_HUMAN]	1			
A1L407	Histone cluster 1, H1t OS=Homo sapiens GN=HIST1H1T PE=2 SV=1 - [A1L407_HUMAN]	1	0.010	13.712	0.011
F8VTZ0	Poly(rC)-binding protein 2 (Fragment) OS=Homo sapiens GN=PCBP2 PE=1 SV=1 - [F8VTZ0_HUMAN]	1			
P05089	Arginase-1 OS=Homo sapiens GN=ARG1 PE=1 SV=2 - [ARGI1_HUMAN]	1			
Q5M9N0	Coiled-coil domain-containing protein 158 OS=Homo sapiens GN=CCDC158 PE=1 SV=2 - [CD158_HUMAN]	1			
UL40	UL40	2			
Q5S4N1	Putative uncharacterized protein (Fragment) OS=Homo sapiens PE=2 SV=1 - [Q5S4N1_HUMAN]	2	0.921	0.055	0.071
Q68DY8	Putative uncharacterized protein DKFZp686I11137 OS=Homo sapiens GN=DKFZp686I11137 PE=2 SV=1 - [Q68DY8_HUMAN]	1			
Q6P5S2	Protein LEG1 homolog OS=Homo sapiens GN=LEG1 PE=1 SV=2 - [LEG1H_HUMAN]	2			
P05090	Apolipoprotein D OS=Homo sapiens GN=APOD PE=1 SV=1 - [APOD_HUMAN]	2	0.010	1.000	0.010
B4DPN7	cDNA FLJ57553, highly similar to SPFH domain-containing protein 1 OS=Homo sapiens PE=2 SV=1 - [B4DPN7_HUMAN]	1			
P01040	Cystatin-A OS=Homo sapiens GN=CSTA PE=1 SV=1 - [CYTA_HUMAN]	2			
Q59GN1	Proteasome subunit beta type (Fragment) OS=Homo sapiens PE=2 SV=1 - [Q59GN1_HUMAN]	1			
H0YEP8	Serpin H1 (Fragment) OS=Homo sapiens GN=SERPINH1 PE=1 SV=1 - [H0YEP8_HUMAN]	1			
A4ZU86	Truncated nucleolar phosphoprotein B23 OS=Homo sapiens GN=NPM1 PE=2 SV=1 - [A4ZU86_HUMAN]	2	0.098	0.725	0.071
C9JMD7	B-cell receptor-associated protein 31 (Fragment) OS=Homo sapiens GN=BCAP31 PE=1 SV=1 - [C9JMD7_HUMAN]	1	0.341	0.155	0.053
D6CHE9	Proteinase 3 OS=Homo sapiens GN=PRTN3 PE=2 SV=1 - [D6CHE9_HUMAN]	1			
B4DJW9	cDNA FLJ55029, highly similar to Creatine kinase, ubiquitous mitochondrial (EC 2.7.3.2) OS=Homo sapiens PE=2 SV=1 - [B4DJW9_HUMAN]	1	0.330		
P25788	Proteasome subunit alpha type-3 OS=Homo sapiens GN=PSMA3 PE=1 SV=2 - [PSA3_HUMAN]	1	0.010	1.000	0.010
K7EKI8	Periplakin OS=Homo sapiens GN=PPL PE=1 SV=1 - [K7EKI8_HUMAN]	2	0.014	1.000	0.014
E5RJR5	S-phase kinase-associated protein 1 OS=Homo sapiens GN=SKP1 PE=1 SV=1 - [E5RJR5_HUMAN]	1	0.370	0.359	0.133
B3KPA6	Acyl-Coenzyme A dehydrogenase, very long chain, isoform CRA_e OS=Homo sapiens GN=ACADVL PE=2 SV=1 - [B3KPA6_HUMAN]	2	0.774	0.024	0.014
K7EMN2	6-phosphogluconate dehydrogenase, decarboxylating (Fragment) OS=Homo sapiens GN=PGD PE=1 SV=1 - [K7EMN2_HUMAN]	1	0.010	1.000	0.010
B7Z478	Proteasome (Prosome, macropain) subunit, beta type, 2, isoform CRA_b OS=Homo sapiens GN=PSMB2 PE=2 SV=1 - [B7Z478_HUMAN]	1			
RL2	RL2	1			
F5H018	GTP-binding nuclear protein Ran (Fragment) OS=Homo sapiens GN=RAN PE=1 SV=5 - [F5H018_HUMAN]	2	1.457	0.255	0.372
Q96AG4	Leucine-rich repeat-containing protein 59 OS=Homo sapiens GN=LRRC59 PE=1 SV=1 - [LRC59_HUMAN]	1			
X2D3Z6	Cytochrome c oxidase subunit 2 (Fragment) OS=Homo sapiens GN=cox2 PE=3 SV=1 - [X2D3Z6_HUMAN]	3			

F2Z2I8	Stomatin-like protein 2, mitochondrial OS=Homo sapiens GN=STOML2 PE=1 SV=1 - [F2Z2I8_HUMAN]	1	2.939		
A8K313	cDNA FLJ78249, highly similar to Homo sapiens RAD51 associated protein 1, mRNA OS=Homo sapiens PE=2 SV=1 - [A8K313_HUMAN]	1			
B4DUL5	cDNA FLJ51625, highly similar to Ubiquinol-cytochrome-c reductase complex coreprotein I, mitochondrial (EC 1.10.2.2) OS=Homo sapiens PE=2 SV=1 - [B4DUL5_HUMAN]	1	0.720	0.349	0.252
E5KN59	Peptidyl-prolyl cis-trans isomerase D OS=Homo sapiens PE=4 SV=1 - [E5KN59_HUMAN]	1			
S0BE06	BTB and CNC homology 1, basic leucine zipper transcription factor 2 (Fragment) OS=Homo sapiens GN=Bach2 PE=2 SV=1 - [S0BE06_HUMAN]	1			
P62851	40S ribosomal protein S25 OS=Homo sapiens GN=RPS25 PE=1 SV=1 - [RS25_HUMAN]	1	0.699	0.406	0.284
Q9H3M1	Airway lactoperoxidase (Fragment) OS=Homo sapiens PE=2 SV=1 - [Q9H3M1_HUMAN]	1			
H3BMQ0	Tuberin OS=Homo sapiens GN=TSC2 PE=1 SV=1 - [H3BMQ0_HUMAN]	1	0.010	1.000	0.010
B3KPM4	Zinc finger protein 185 (LIM domain), isoform CRA_a OS=Homo sapiens GN=ZNF185 PE=2 SV=1 - [B3KPM4_HUMAN]	1			
Q0EFA5	S protein OS=Homo sapiens GN=S PE=4 SV=1 - [Q0EFA5_HUMAN]	1			
B4E1S3	cDNA FLJ57860, highly similar to Transmembrane protein 109 OS=Homo sapiens PE=2 SV=1 - [B4E1S3_HUMAN]	1	2.553	0.130	0.331
D6R9A6	High mobility group protein B2 (Fragment) OS=Homo sapiens GN=HMGB2 PE=1 SV=1 - [D6R9A6_HUMAN]	1	0.010	1.000	0.010
E9PQ63	Carbonyl reductase [NADPH] 1 OS=Homo sapiens GN=CBR1 PE=1 SV=1 - [E9PQ63_HUMAN]	2	0.829	0.354	0.293
V9HW35	Epididymis secretory protein Li 55 OS=Homo sapiens GN=HEL-S-55 PE=2 SV=1 - [V9HW35_HUMAN]	1	0.010	1.000	0.010
Q53GB0	Mitochondrial import receptor Tom22 variant (Fragment) OS=Homo sapiens PE=2 SV=1 - [Q53GB0_HUMAN]	1			
Q04941	Proteolipid protein 2 OS=Homo sapiens GN=PLP2 PE=1 SV=1 - [PLP2_HUMAN]	1			
A0A024R3J7	HCG2032701, isoform CRA_a OS=Homo sapiens GN=hCG_2032701 PE=4 SV=1 - [A0A024R3J7_HUMAN]	1	1.653	0.117	0.194
B4DUI5	Triosephosphate isomerase OS=Homo sapiens PE=2 SV=1 - [B4DUI5_HUMAN]	2	0.010	1.000	0.010
Q15758	Neutral amino acid transporter B(0) OS=Homo sapiens GN=SLC1A5 PE=1 SV=2 - [AAAT_HUMAN]	2	1.880	0.367	0.184
B4DHR1	cDNA FLJ53009, highly similar to Calreticulin OS=Homo sapiens PE=2 SV=1 - [B4DHR1_HUMAN]	1	0.106	1.880	0.200
B4DZ87	cDNA FLJ57240, highly similar to Mitochondrial proteins import receptor OS=Homo sapiens PE=2 SV=1 - [B4DZ87_HUMAN]	1	0.683	0.169	0.115
A4UCS6	Peroxiredoxin 6 (Fragment) OS=Homo sapiens PE=2 SV=1 - [A4UCS6_HUMAN]	1	0.149	0.339	0.050
O95969	Secretoglobin family 1D member 2 OS=Homo sapiens GN=SCGB1D2 PE=2 SV=1 - [SG1D2_HUMAN]	1	0.010	1.000	0.010
A2NKM6	NANUC-1 heavy chain (Fragment) OS=Homo sapiens PE=2 SV=1 - [A2NKM6_HUMAN]	1			
P60903	Protein S100-A10 OS=Homo sapiens GN=S100A10 PE=1 SV=2 - [S10AA_HUMAN]	1	0.695		
E7EQG2	Eukaryotic initiation factor 4A-II OS=Homo sapiens GN=EIF4A2 PE=1 SV=1 - [E7EQG2_HUMAN]	2	0.675	0.021	0.014
P35754	Glutaredoxin-1 OS=Homo sapiens GN=GLRX PE=1 SV=2 - [GLRX1_HUMAN]	1	0.010	1.000	0.010
P80188	Neutrophil gelatinase-associated lipocalin OS=Homo sapiens GN=LCN2 PE=1 SV=2 - [NGAL_HUMAN]	1			
Q6LER6	Cytochrome c (Fragment) OS=Homo sapiens PE=2 SV=1 - [Q6LER6_HUMAN]	1	0.052		
B4DS32	cDNA FLJ56236, highly similar to Exportin-2 OS=Homo sapiens PE=2 SV=1 - [B4DS32_HUMAN]	1			
B1AN48	Small proline-rich protein 3 (Fragment) OS=Homo sapiens GN=SPRR3 PE=1 SV=5 - [B1AN48_HUMAN]	1			
J3KS17	Beta-2-glycoprotein 1 (Fragment) OS=Homo sapiens GN=APOH PE=1 SV=1 - [J3KS17_HUMAN]	1			
Q15084	Protein disulfide-isomerase A6 OS=Homo sapiens GN=PDIA6 PE=1 SV=1 - [PDIA6_HUMAN]	1	0.011	1.000	0.011
Q8NGM9	Olfactory receptor 8D4 OS=Homo sapiens GN=OR8D4 PE=2 SV=1 - [OR8D4_HUMAN]	1			
B7ZBI5	Collagen alpha-1(XX) chain (Fragment) OS=Homo sapiens GN=COL20A1 PE=4 SV=1 - [B7ZBI5_HUMAN]	1			
Q6NVI1	MARCKS protein (Fragment) OS=Homo sapiens GN=MARCKS PE=2 SV=1 - [Q6NVI1_HUMAN]	1	0.022	1.000	0.022
US6	US6	1	9.718	0.487	4.733
M0QZK8	Uncharacterized protein OS=Homo sapiens PE=4 SV=1 - [M0QZK8_HUMAN]	1			
F8W1N5	Nascent polypeptide-associated complex subunit alpha (Fragment) OS=Homo sapiens GN=NACA PE=1 SV=1 - [F8W1N5_HUMAN]	1	0.135	0.603	0.082
Q03252	Lamin-B2 OS=Homo sapiens GN=LMNB2 PE=1 SV=3 - [LMNB2_HUMAN]	1			0.180

B4DSR0	cDNA FLJ60080, highly similar to 130 kDa leucine-rich protein (LRP 130) (Fragment) OS=Homo sapiens PE=2 SV=1 - [B4DSR0_HUMAN]	1	0.025	1.000	0.025
H0YB22	40S ribosomal protein S14 (Fragment) OS=Homo sapiens GN=RPS14 PE=1 SV=1 - [H0YB22_HUMAN]	1	0.688	1.489	1.025
Q4QZC0	MHC class I antigen (Fragment) OS=Homo sapiens GN=HLA-A PE=3 SV=1 - [Q4QZC0_HUMAN]	1	0.655	0.320	0.209
Q4G168	CPNE4 protein OS=Homo sapiens GN=CPNE4 PE=2 SV=1 - [Q4G168_HUMAN]	1	0.529		
A0A075B6Z2	Protein TRAJ56 (Fragment) OS=Homo sapiens GN=TRAJ56 PE=4 SV=1 - [A0A075B6Z2_HUMAN]	1			
P30048	Thioredoxin-dependent peroxide reductase, mitochondrial OS=Homo sapiens GN=PRDX3 PE=1 SV=3 - [PRDX3_HUMAN]	1	0.022	7.274	0.160
Q9BZ93	Prosomal P27K protein (Fragment) OS=Homo sapiens GN=PSMA6 PE=4 SV=1 - [Q9BZ93_HUMAN]	1	0.410	0.563	0.231
UL38	UL38	2	100.000	0.170	18.975
P12724	Eosinophil cationic protein OS=Homo sapiens GN=RNASE3 PE=1 SV=2 - [ECP_HUMAN]	1			
J3KSC4	Ras-related C3 botulinum toxin substrate 3 (Fragment) OS=Homo sapiens GN=RAC3 PE=1 SV=1 - [J3KSC4_HUMAN]	1	0.217	0.978	0.212
B4DVE1	cDNA FLJ53478, highly similar to Galectin-3-binding protein OS=Homo sapiens PE=2 SV=1 - [B4DVE1_HUMAN]	2	0.010	1.000	0.010
C9J191	Kelch-like protein 22 (Fragment) OS=Homo sapiens GN=KLHL22 PE=1 SV=1 - [C9J191_HUMAN]	1	0.538	0.334	0.180
P62266	40S ribosomal protein S23 OS=Homo sapiens GN=RPS23 PE=1 SV=3 - [RS23_HUMAN]	1	1.233		
B1AKQ8	Guanine nucleotide-binding protein G(I)/G(S)/G(T) subunit beta-1 (Fragment) OS=Homo sapiens GN=GNB1 PE=1 SV=5 - [B1AKQ8_HUMAN]	1	0.721	0.083	0.059
E9PLJ3	Cofilin-1 (Fragment) OS=Homo sapiens GN=CFL1 PE=1 SV=1 - [E9PLJ3_HUMAN]	1	0.010	1.000	0.010
F8VP99	ADP-ribosylation factor-like protein 1 (Fragment) OS=Homo sapiens GN=ARL1 PE=1 SV=1 - [F8VP99_HUMAN]	1			
Q6UW32	Insulin growth factor-like family member 1 OS=Homo sapiens GN=IGFL1 PE=1 SV=1 - [IGFL1_HUMAN]	1			
F8VY02	Endoplasmic reticulum resident protein 29 OS=Homo sapiens GN=ERP29 PE=1 SV=1 - [F8VY02_HUMAN]	1			
B4E2A4	cDNA FLJ53275, highly similar to Homo sapiens spectrin domain with coiled-coils 1 (SPECC1), transcript variant, mRNA OS=Homo sapiens PE=2 SV=1 - [B4E2A4_HUMAN]	1			
Q96P63	Serpin B12 OS=Homo sapiens GN=SERPINB12 PE=1 SV=1 - [SPB12_HUMAN]	1			
P01008	Antithrombin-III OS=Homo sapiens GN=SERPINC1 PE=1 SV=1 - [ANT3_HUMAN]	1			
L0R4T3	Histone H2B OS=Homo sapiens GN=ABCF2 PE=3 SV=1 - [L0R4T3_HUMAN]	1	0.074	0.515	0.038
H0YNQ3	Aldehyde dehydrogenase family 1 member A3 OS=Homo sapiens GN=ALDH1A3 PE=1 SV=1 - [H0YNQ3_HUMAN]	1			
F2Z393	Transaldolase OS=Homo sapiens GN=TALDO1 PE=1 SV=1 - [F2Z393_HUMAN]	2	0.010	1.000	0.010
Q9HBB2	Aconitate hydratase OS=Homo sapiens GN=IRP1 PE=2 SV=1 - [Q9HBB2_HUMAN]	1			
Q7Z4Q5	Heterogeneous nuclear ribonucleoprotein U (Scaffold attachment factor A), isoform CRA_a OS=Homo sapiens GN=HNRPU PE=2 SV=1 - [Q7Z4Q5_HUMAN]	1			
UL22	UL22	2	4.638	0.386	1.789
H0YFD6	Trifunctional enzyme subunit alpha, mitochondrial (Fragment) OS=Homo sapiens GN=HADHA PE=1 SV=1 - [H0YFD6_HUMAN]	2		0.145	
Q49AG2	TMED5 protein OS=Homo sapiens GN=TMED5 PE=2 SV=1 - [Q49AG2_HUMAN]	1	81.443	0.275	22.376
R4GN98	Protein S100 (Fragment) OS=Homo sapiens GN=S100A6 PE=1 SV=1 - [R4GN98_HUMAN]	1	0.086	0.484	0.042
Q9GZZ8	Extracellular glycoprotein lacritin OS=Homo sapiens GN=LACRT PE=1 SV=1 - [LACRT_HUMAN]	1	0.010	1.000	0.010
E9PDK7	Plasminogen activator inhibitor 2 (Fragment) OS=Homo sapiens GN=SERPINB2 PE=1 SV=1 - [E9PDK7_HUMAN]	1	0.616	0.010	0.010
F5H3C5	Superoxide dismutase [Mn], mitochondrial (Fragment) OS=Homo sapiens GN=SOD2 PE=1 SV=1 - [F5H3C5_HUMAN]	1	0.010	1.000	0.010
K7ERY7	60S ribosomal protein L27 OS=Homo sapiens GN=RPL27 PE=1 SV=1 - [K7ERY7_HUMAN]	1			
F5H608	ATP synthase subunit d, mitochondrial OS=Homo sapiens GN=ATP5H PE=1 SV=2 - [F5H608_HUMAN]	1	2.523	0.289	0.728
Q9H2U9	Disintegrin and metalloproteinase domain-containing protein 7 OS=Homo sapiens GN=ADAM7 PE=1 SV=3 - [ADAM7_HUMAN]	1			
B4DKZ9	cDNA FLJ55705, highly similar to Threonyl-tRNA synthetase, cytoplasmic (EC 6.1.1.3) OS=Homo sapiens PE=2 SV=1 - [B4DKZ9_HUMAN]	1			
B7Z7I4	cDNA FLJ54568, highly similar to T-complex protein 1 subunit eta OS=Homo sapiens PE=2 SV=1 - [B7Z7I4_HUMAN]	3	0.888	0.080	0.030
UL49	UL49	1	7.763	0.283	2.193

B7Z2R9	cDNA FLJ52540, highly similar to Lysosome-associated membrane glycoprotein 2 OS=Homo sapiens PE=2 SV=1 - [B7Z2R9_HUMAN]	1	0.432	0.444	0.192
G3V2K7	Transmembrane emp24 domain-containing protein 10 OS=Homo sapiens GN=TMED10 PE=1 SV=1 - [G3V2K7_HUMAN]	1	1.371	0.150	0.206
Q9UHS8	PRO1975 OS=Homo sapiens PE=2 SV=1 - [Q9UHS8_HUMAN]	2	0.203	0.644	0.131
Q08188	Protein-glutamine gamma-glutamyltransferase E OS=Homo sapiens GN=TGM3 PE=1 SV=4 - [TGM3_HUMAN]	1	0.010	1.000	0.010
C9JKY3	Epithelial cell adhesion molecule (Fragment) OS=Homo sapiens GN=EPCAM PE=1 SV=1 - [C9JKY3_HUMAN]	1	0.020	1.000	0.020
Q0PHS5	Glucose-6-phosphate dehydrogenase (Fragment) OS=Homo sapiens GN=G6PD PE=4 SV=1 - [Q0PHS5_HUMAN]	1			
Q16821	Protein phosphatase 1 regulatory subunit 3A OS=Homo sapiens GN=PPP1R3A PE=1 SV=3 - [PPR3A_HUMAN]	1			
O14828	Secretory carrier-associated membrane protein 3 OS=Homo sapiens GN=SCAMP3 PE=1 SV=3 - [SCAM3_HUMAN]	1	1.234	0.481	0.594
B4E290	cDNA FLJ50039, highly similar to Homo sapiens solute carrier family 25, member 24, transcript variant 1, mRNA OS=Homo sapiens PE=2 SV=1 - [B4E290_HUMAN]	1	1.587	0.013	0.021
P46783	40S ribosomal protein S10 OS=Homo sapiens GN=RPS10 PE=1 SV=1 - [RS10_HUMAN]	2	0.542	0.208	0.113
Q8N3X5	Similar to ATPase, Ca++ transporting, cardiac muscle, fast twitch 1 (Fragment) OS=Homo sapiens PE=2 SV=1 - [Q8N3X5_HUMAN]	1	0.961	0.121	0.116
P50238	Cysteine-rich protein 1 OS=Homo sapiens GN=CRIP1 PE=1 SV=3 - [CRIP1_HUMAN]	1	0.010	1.000	0.010
UL18	UL18	1		1.150	
P52597	Heterogeneous nuclear ribonucleoprotein F OS=Homo sapiens GN=HNRNPF PE=1 SV=3 - [HNRPF_HUMAN]	1	0.017	1.000	0.017
A8MUD9	60S ribosomal protein L7 OS=Homo sapiens GN=RPL7 PE=1 SV=1 - [A8MUD9_HUMAN]	1	0.270		
B4DNY1	cDNA FLJ60318, highly similar to RNA-binding protein 6 OS=Homo sapiens PE=2 SV=1 - [B4DNY1_HUMAN]	1			
Q5IWS5	Intelectin 1 OS=Homo sapiens GN=ITLN1 PE=2 SV=1 - [Q5IWS5_HUMAN]	1	0.014	1.000	0.014
N0E466	Casein kinase II subunit beta OS=Homo sapiens GN=CSNK2B PE=2 SV=1 - [N0E466_HUMAN]	1	8.360	0.010	0.052
B7Z1V9	cDNA FLJ53310, highly similar to Puromycin-sensitive aminopeptidase (EC 3.4.11.-) OS=Homo sapiens PE=2 SV=1 - [B7Z1V9_HUMAN]	1			
P12004	Proliferating cell nuclear antigen OS=Homo sapiens GN=PCNA PE=1 SV=1 - [PCNA_HUMAN]	2	1.294	0.334	0.432
Q53T09	Putative uncharacterized protein XRCC5 (Fragment) OS=Homo sapiens GN=XRCC5 PE=4 SV=1 - [Q53T09_HUMAN]	1			
P07954	Fumarate hydratase, mitochondrial OS=Homo sapiens GN=FH PE=1 SV=3 - [FUMH_HUMAN]	1	0.010	1.000	0.010
H3BRM5	Cytochrome c oxidase subunit 5A, mitochondrial OS=Homo sapiens GN=COX5A PE=1 SV=1 - [H3BRM5_HUMAN]	1	0.810	0.457	0.370
O15269	Serine palmitoyltransferase 1 OS=Homo sapiens GN=SPTLC1 PE=1 SV=1 - [SPTC1_HUMAN]	1			
Q5T6L6	Argininosuccinate synthase (Fragment) OS=Homo sapiens GN=ASS1 PE=1 SV=1 - [Q5T6L6_HUMAN]	1			
P62330	ADP-ribosylation factor 6 OS=Homo sapiens GN=ARF6 PE=1 SV=2 - [ARF6_HUMAN]	1			
P05091	Aldehyde dehydrogenase, mitochondrial OS=Homo sapiens GN=ALDH2 PE=1 SV=2 - [ALDH2_HUMAN]	1	0.010	1.000	0.010
P49703	ADP-ribosylation factor-like protein 4D OS=Homo sapiens GN=ARL4D PE=1 SV=2 - [ARL4D_HUMAN]	1			
A2VCL2	Coiled-coil domain-containing protein 162 OS=Homo sapiens GN=CCDC162P PE=2 SV=3 - [CC162_HUMAN]	1			
O43866	CD5 antigen-like OS=Homo sapiens GN=CD5L PE=1 SV=1 - [CD5L_HUMAN]	1			
Q14677	Clathrin interactor 1 OS=Homo sapiens GN=CLINT1 PE=1 SV=1 - [EPN4_HUMAN]	1			
Q86YZ3	Hornerin OS=Homo sapiens GN=HRNR PE=1 SV=2 - [HORN_HUMAN]	1			
Q9Y573	Actin-binding protein IPP OS=Homo sapiens GN=IPP PE=2 SV=1 - [IPP_HUMAN]	1			
Q8NCM2	Potassium voltage-gated channel subfamily H member 5 OS=Homo sapiens GN=KCNH5 PE=1 SV=3 - [KCNH5_HUMAN]	1			
P04431	Ig kappa chain V-I region Walker OS=Homo sapiens PE=1 SV=1 - [KV123_HUMAN]	1			
P11226	Mannose-binding protein C OS=Homo sapiens GN=MBL2 PE=1 SV=2 - [MBL2_HUMAN]	1			
Q5VYS4	Mesenteric estrogen-dependent adipogenesis protein OS=Homo sapiens GN=MEDAG PE=2 SV=1 - [MEDAG_HUMAN]	1			
Q9Y623	Myosin-4 OS=Homo sapiens GN=MYH4 PE=1 SV=2 - [MYH4_HUMAN]	1			
Q7Z494	Nephrocystin-3 OS=Homo sapiens GN=NPHP3 PE=1 SV=1 - [NPHP3_HUMAN]	1			

O60285	NUAK family SNF1-like kinase 1 OS=Homo sapiens GN=NUAK1 PE=1 SV=1 - [NUAK1_HUMAN]	1			
Q96PD5	N-acetylmuramoyl-L-alanine amidase OS=Homo sapiens GN=PGLYRP2 PE=1 SV=1 - [PGRP2_HUMAN]	1			
Q8TC12	Retinol dehydrogenase 11 OS=Homo sapiens GN=RDH11 PE=1 SV=2 - [RDH11_HUMAN]	1	3.642		
Q9ULI2	Beta-citrylglutamate synthase B OS=Homo sapiens GN=RIMKLB PE=2 SV=2 - [RIMKB_HUMAN]	1			
Q9NQZ2	Something about silencing protein 10 OS=Homo sapiens GN=UTP3 PE=1 SV=1 - [SAS10_HUMAN]	1			14.971
P29508	Serpin B3 OS=Homo sapiens GN=SERPINB3 PE=1 SV=2 - [SPB3_HUMAN]	1			
Q86TG1	Transmembrane protein 150A OS=Homo sapiens GN=TMEM150A PE=1 SV=1 - [T150A_HUMAN]	1			1.854
Q96PF1	Protein-glutamine gamma-glutamyltransferase Z OS=Homo sapiens GN=TGM7 PE=2 SV=1 - [TGM7_HUMAN]	1			
Q7Z7H5	Transmembrane emp24 domain-containing protein 4 OS=Homo sapiens GN=TMED4 PE=1 SV=1 - [TMED4_HUMAN]	1	2.169	0.138	0.300
Q6ZT12	E3 ubiquitin-protein ligase UBR3 OS=Homo sapiens GN=UBR3 PE=2 SV=2 - [UBR3_HUMAN]	1			
A4D1P6	WD repeat-containing protein 91 OS=Homo sapiens GN=WDR91 PE=1 SV=2 - [WDR91_HUMAN]	1			
K7ELT6	Cold-inducible RNA-binding protein OS=Homo sapiens GN=CIRBP PE=1 SV=1 - [K7ELT6_HUMAN]	1			
B2RNT0	EBF2 protein OS=Homo sapiens GN=EBF2 PE=2 SV=1 - [B2RNT0_HUMAN]	1			
A0A024R0N6	Spectrin, beta, non-erythrocytic 4, isoform CRA_e OS=Homo sapiens GN=SPTBN4 PE=4 SV=1 - [A0A024R0N6_HUMAN]	1			
Q86WV2	COX4I1 protein OS=Homo sapiens GN=COX4I1 PE=1 SV=1 - [Q86WV2_HUMAN]	1	0.850	0.428	0.364
B2R894	Mitochondrial ribosomal protein L38, isoform CRA_b OS=Homo sapiens GN=MRPL38 PE=1 SV=1 - [B2R894_HUMAN]	1	0.010	1.000	0.010
A6NHH0	Prostaglandin E synthase 2 OS=Homo sapiens GN=PTGES2 PE=1 SV=2 - [A6NHH0_HUMAN]	1			
J3KQN4	60S ribosomal protein L36a OS=Homo sapiens GN=RPL36A PE=3 SV=1 - [J3KQN4_HUMAN]	1			
G3V121	Coiled-coil domain containing 25, isoform CRA_b OS=Homo sapiens GN=CCDC25 PE=1 SV=1 - [G3V121_HUMAN]	1			
A0A024R6R1	SHC SH2-domain binding protein 1, isoform CRA_a OS=Homo sapiens GN=SHCBP1 PE=4 SV=1 - [A0A024R6R1_HUMAN]	1			
A0A024RC30	Desmoglein 3 (Pemphigus vulgaris antigen), isoform CRA_a OS=Homo sapiens GN=DSG3 PE=4 SV=1 - [A0A024RC30_HUMAN]	1	0.017	1.000	0.017
C5HTY9	Amiloride-sensitive sodium channel subunit alpha OS=Homo sapiens GN=SCNN1A PE=3 SV=1 - [C5HTY9_HUMAN]	1			
A2KBC1	Anti-(ED-B) scFV (Fragment) OS=Homo sapiens PE=2 SV=2 - [A2KBC1_HUMAN]	1	0.010	1.000	0.010
H0YE40	CD44 antigen (Fragment) OS=Homo sapiens GN=CD44 PE=1 SV=1 - [H0YE40_HUMAN]	2			
D6RB21	Testican-1 (Fragment) OS=Homo sapiens GN=SPOCK1 PE=1 SV=1 - [D6RB21_HUMAN]	1			
Q01991	Dihydrolipoamide S-acetyltransferase (Fragment) OS=Homo sapiens PE=2 SV=1 - [Q01991_HUMAN]	1	0.621	0.599	0.372
B4DS58	cDNA FLJ57834, moderately similar to Mus musculus NHS-like 1 (Nhsl1), mRNA OS=Homo sapiens PE=2 SV=1 - [B4DS58_HUMAN]	1	0.010	1.000	0.010
Q53QP3	Putative uncharacterized protein FHL2 (Fragment) OS=Homo sapiens GN=FHL2 PE=4 SV=1 - [Q53QP3_HUMAN]	1	1.649	0.379	0.625
Q86SR2	AZU1 protein (Fragment) OS=Homo sapiens GN=AZU1 PE=2 SV=1 - [Q86SR2_HUMAN]	1			
M0QX45	Protein Smaug homolog 2 (Fragment) OS=Homo sapiens GN=SAMD4B PE=1 SV=1 - [M0QX45_HUMAN]	1			
E9PR82	Ribonuclease inhibitor OS=Homo sapiens GN=RNH1 PE=1 SV=1 - [E9PR82_HUMAN]	1			
Q5R207	Carbamoylphosphate synthetase I OS=Homo sapiens GN=CPS1 PE=2 SV=1 - [Q5R207_HUMAN]	1			
M0R0Y6	Heterogeneous nuclear ribonucleoprotein M OS=Homo sapiens GN=HNRNPM PE=1 SV=1 - [M0R0Y6_HUMAN]	1	1.896	0.015	0.028
Q4W5P3	Transmembrane protease serine (Fragment) OS=Homo sapiens GN=DESC1 PE=3 SV=1 - [Q4W5P3_HUMAN]	1			
G3V3W6	Putative acyl-coenzyme A thioesterase 6 (Fragment) OS=Homo sapiens GN=ACOT6 PE=4 SV=1 - [G3V3W6_HUMAN]	1			
Q8TES4	FLJ00119 protein (Fragment) OS=Homo sapiens GN=FLJ00119 PE=2 SV=1 - [Q8TES4_HUMAN]	1	0.010	1.000	0.010
H0YJM8	Proteasome subunit beta type-5 (Fragment) OS=Homo sapiens GN=PSMB5 PE=1 SV=1 - [H0YJM8_HUMAN]	1	0.331		
H0Y721	CDK5 regulatory subunit-associated protein 1 (Fragment) OS=Homo sapiens GN=CDK5RAP1 PE=1 SV=1 - [H0Y721_HUMAN]	1			

H7BY49	Nucleolysin TIA-1 isoform p40 (Fragment) OS=Homo sapiens GN=TIA1 PE=1 SV=1 - [H7BY49_HUMAN]	1	0.490		
B4DFB8	cDNA FLJ60468, weakly similar to Synaptonemal complex protein 2 OS=Homo sapiens PE=2 SV=1 - [B4DFB8_HUMAN]	1			
K7EQW4	Tropomodulin-4 (Fragment) OS=Homo sapiens GN=TMOD4 PE=1 SV=1 - [K7EQW4_HUMAN]	1			
B7Z577	cDNA FLJ60780, highly similar to Carboxypeptidase A4 (EC 3.4.17.-) OS=Homo sapiens PE=2 SV=1 - [B7Z577_HUMAN]	1			
H0YLU2	Proteasome activator complex subunit 1 (Fragment) OS=Homo sapiens GN=PSME1 PE=1 SV=1 - [H0YLU2_HUMAN]	1	0.010	1.000	0.010
G3V2H3	Purine nucleoside phosphorylase (Fragment) OS=Homo sapiens GN=PNP PE=1 SV=1 - [G3V2H3_HUMAN]	1	0.014	1.000	0.014
Q86TZ0	Full-length cDNA clone CS0DC023YN15 of Neuroblastoma of Homo sapiens (human) (Fragment) OS=Homo sapiens PE=2 SV=1 - [Q86TZ0_HUMAN]	1	0.010	1.000	0.010
H7C5C3	Phosphatidylinositol 4,5-bisphosphate 3-kinase catalytic subunit beta isoform (Fragment) OS=Homo sapiens GN=PIK3CB PE=4 SV=1 - [H7C5C3_HUMAN]	1			
F8WF65	Elongation factor 1-beta OS=Homo sapiens GN=EEF1B2 PE=1 SV=1 - [F8WF65_HUMAN]	1	0.257	0.614	0.158
Q7KYT6	Type I phosphatidylinositol-4-phosphate 5-kinase beta (Fragment) OS=Homo sapiens GN=STM7 PE=2 SV=1 - [Q7KYT6_HUMAN]	1			
B4DNG2	cDNA FLJ59357, highly similar to Probable ATP-dependent RNA helicase DDX5 (EC 3.6.1.-) OS=Homo sapiens PE=2 SV=1 - [B4DNG2_HUMAN]	2	0.661	0.526	0.364
K7EQB6	DNA ligase 3 (Fragment) OS=Homo sapiens GN=LIG3 PE=1 SV=1 - [K7EQB6_HUMAN]	1			
A8K9I1	cDNA FLJ78035, highly similar to Homo sapiens serine/threonine protein kinase OS=Homo sapiens PE=2 SV=1 - [A8K9I1_HUMAN]	1			
Q5TBN3	Plastin-2 (Fragment) OS=Homo sapiens GN=LCP1 PE=1 SV=1 - [Q5TBN3_HUMAN]	1			
B4E2Z7	cDNA FLJ61562, highly similar to Asporin OS=Homo sapiens PE=2 SV=1 - [B4E2Z7_HUMAN]	1			
Q96AG1	ZSCAN29 protein (Fragment) OS=Homo sapiens GN=ZSCAN29 PE=2 SV=2 - [Q96AG1_HUMAN]	1			
B3KNK7	cDNA FLJ14806 fis, clone NT2RP4001753, highly similar to Zinc finger protein 268 OS=Homo sapiens PE=2 SV=1 - [B3KNK7_HUMAN]	1	0.020	1.000	0.020
B3KY88	Transmembrane channel-like protein OS=Homo sapiens PE=2 SV=1 - [B3KY88_HUMAN]	1			
B3KMB2	cDNA FLJ10625 fis, clone NT2RP2005540, highly similar to Homo sapiens KIAA0494 protein OS=Homo sapiens PE=2 SV=1 - [B3KMB2_HUMAN]	1			
B4DMW1	cDNA FLJ58268, highly similar to Homo sapiens nischarin (NISCH), mRNA OS=Homo sapiens PE=2 SV=1 - [B4DMW1_HUMAN]	1			
B4DJD3	cDNA FLJ55077, highly similar to Ectonucleotidepyrophosphatase/phosphodiesterase 2 OS=Homo sapiens PE=2 SV=1 - [B4DJD3_HUMAN]	1			
B4DIR5	cDNA FLJ56026 OS=Homo sapiens PE=2 SV=1 - [B4DIR5_HUMAN]	1			
L8E8F9	Alternative protein FAM21B OS=Homo sapiens GN=FAM21B PE=4 SV=1 - [L8E8F9_HUMAN]	1	0.020	1.000	0.020
B4DNB5	cDNA FLJ58082, highly similar to Myosin-binding protein C, cardiac-type OS=Homo sapiens PE=2 SV=1 - [B4DNB5_HUMAN]	1			
Q8NC73	cDNA FLJ90439 fis, clone NT2RP3000907, weakly similar to PROBABLE CALCIUM-TRANSPORTING ATPASE 6 (EC 3.6.1.38) OS=Homo sapiens PE=2 SV=1 - [Q8NC73_HUMAN]	1			
B4DPU6	cDNA FLJ50605, moderately similar to Plastin-3 OS=Homo sapiens PE=2 SV=1 - [B4DPU6_HUMAN]	1			
B7Z3Y0	cDNA FLJ61305, highly similar to Voltage-dependent L-type calcium channel subunit beta-2 OS=Homo sapiens PE=2 SV=1 - [B7Z3Y0_HUMAN]	1	1.000	66.627	66.627
B4DWQ3	Phosphoglycerate kinase OS=Homo sapiens PE=2 SV=1 - [B4DWQ3_HUMAN]	1			
B7Z4R9	cDNA FLJ59037 OS=Homo sapiens PE=2 SV=1 - [B7Z4R9_HUMAN]	1			
B4DZB4	cDNA FLJ51707, highly similar to Heat-shock protein 105 kDa OS=Homo sapiens PE=2 SV=1 - [B4DZB4_HUMAN]	1			
UL7	UL7	1			
A0A0B4J213	60S ribosomal protein L30 OS=Homo sapiens GN=RPL30 PE=1 SV=1 - [A0A0B4J213_HUMAN]	1	0.242	0.667	0.162
A0A0C4DGU3	Minor histocompatibility antigen H13 OS=Homo sapiens GN=HM13 PE=1 SV=1 - [A0A0C4DGU3_HUMAN]	1			
A0A0B4J2E0	Protein TRBV12-4 (Fragment) OS=Homo sapiens GN=TRBV12-4 PE=4 SV=2 - [A0A0B4J2E0_HUMAN]	1			
A0A0F6MTF4	MHC class II antigen (Fragment) OS=Homo sapiens PE=4 SV=1 - [A0A0F6MTF4_HUMAN]	1			

10. Bibliography

1. Abaitua, F., Zia, F.R., Hollinshead, M. and O'Hare, P., 2013. Polarized cell migration during cell-to-cell transmission of herpes simplex virus in human skin keratinocytes. Journal of virology, 87(14), pp.7921-7932.
2. Achanzar, W.E. and Ward, S., 1997. A nematode gene required for sperm vesicle fusion. Journal of cell science, 110(9), pp.1073-1081.
3. Albecka, A., Laine, R.F., Janssen, A.F., Kaminski, C.F. and Crump, C.M., 2016. HSV-1 Glycoproteins Are Delivered to Virus Assembly Sites Through Dynamin-Dependent Endocytosis. Traffic, 17(1), pp.21-39.
4. Albecka, A., Owen, D.J., Ivanova, L., Brun, J., Liman, R., Davies, L., Ahmed, M.F., Colaco, S., Hollinshead, M., Graham, S.C. and Crump, C.M., 2016. Dual function of the pUL7-pUL51 tegument protein complex in HSV-1 infection. Journal of virology, pp.JVI-02196.
5. Alber, D. and Staeheli, P., 1996. Partial inhibition of vesicular stomatitis virus by the interferon-induced human 9-27 protein. Journal of interferon & cytokine research, 16(5), pp.375-380.
6. Alconada, A., Bauer, U. and Hoflack, B., 1996. A tyrosine-based motif and a casein kinase II phosphorylation site regulate the intracellular trafficking of the varicella-zoster virus glycoprotein I, a protein localized in the trans-Golgi network. The EMBO journal, 15(22), pp.6096-6110.
7. Alconada, A., Bauer, U., Sodeik, B. and Hoflack, B., 1999. Intracellular Traffic of Herpes Simplex Virus Glycoprotein gE: Characterization of the Sorting Signals Required for Its *trans*-Golgi Network Localization. Journal of virology, 73(1), pp.377-387.
8. Al-Mubarak, A., Zhou, Y. and Chowdhury, S.I., 2004. A glycine-rich bovine herpesvirus 5 (BHV-5) gE-specific epitope within the ectodomain is important for BHV-5 neurovirulence. Journal of virology, 78(9), pp.4806-4816.
9. Alwine, J.C., Steinhart, W.L. and Hill, C.W., 1974. Transcription of herpes simplex type 1 DNA in nuclei isolated from infected HEp-2 and KB cells. Virology, 60(1), pp.302-307.
10. Atanasiu, D., Saw, W.T., Cohen, G.H. and Eisenberg, R.J., 2010. Cascade of events governing cell-cell fusion induced by herpes simplex virus glycoproteins gD, gH/gL, and gB. Journal of virology, 84(23), pp.12292-12299.
11. Atanasiu, D., Whitbeck, J.C., Cairns, T.M., Reilly, B., Cohen, G.H. and Eisenberg, R.J., 2007. Bimolecular complementation reveals that glycoproteins gB and gH/gL of herpes simplex virus interact with each other during cell fusion. Proceedings of the National Academy of Sciences, 104(47), pp.18718-18723.
12. Bailey, C.C., Huang, I.C., Kam, C. and Farzan, M., 2012. Ifitm3 limits the severity of acute influenza in mice. PLoS pathogens, 8(9), p.e1002909.
13. Bailey, C.C., Kondur, H.R., Huang, I.C. and Farzan, M., 2013. Interferon-induced transmembrane protein 3 is a type II transmembrane protein. Journal of Biological Chemistry, 288(45), pp.32184-32193.
14. Bailey, C.C., Zhong, G., Huang, I.C. and Farzan, M., 2014. IFITM-family proteins: the cell's first line of antiviral defense. Annual review of virology, 1, pp.261-283.
15. Baines, J.D., Wills, E., Jacob, R.J., Pennington, J. and Roizman, B., 2007. Glycoprotein M of herpes simplex virus 1 is incorporated into virions during budding at the inner nuclear membrane. Journal of virology, 81(2), pp.800-812.

16. Baird, N.L., Yeh, P.C., Courtney, R.J. and Wills, J.W., 2008. Sequences in the UL11 tegument protein of herpes simplex virus that control association with detergent-resistant membranes. Virology, 374(2), pp.315-321.
17. Balan, P., Davis-Poynter, N., Bell, S., Atkinson, H., Browne, H. and Minson, T., 1994. An analysis of the in vitro and in vivo phenotypes of mutants of herpes simplex virus type 1 lacking glycoproteins gG, gE, gI or the putative gJ. Journal of General Virology, 75(6), pp.1245-1258.
18. Balliet, J.W. and Schaffer, P.A., 2006. Point mutations in herpes simplex virus type 1 oriL, but not in oriS, reduce pathogenesis during acute infection of mice and impair reactivation from latency. Journal of virology, 80(1), pp.440-450.
19. Bansal, D. and Campbell, K.P., 2004. Dysferlin and the plasma membrane repair in muscular dystrophy. Trends in cell biology, 14(4), pp.206-213.
20. Basu, S., Dubin, G., Basu, M., Nguyen, V. and Friedman, H.M., 1995. Characterization of regions of herpes simplex virus type 1 glycoprotein E involved in binding the Fc domain of monomeric IgG and in forming a complex with glycoprotein I. The Journal of Immunology, 154(1), pp.260-267.
21. Basu, S., Dubin, G., Nagashunmugam, T., Basu, M., Goldstein, L.T., Wang, L., Weeks, B. and Friedman, H.M., 1997. Mapping regions of herpes simplex virus type 1 glycoprotein I required for formation of the viral Fc receptor for monomeric IgG. The Journal of Immunology, 158(1), pp.209-215.
22. Baucke, R.B. and Spear, P.G., 1979. Membrane proteins specified by herpes simplex viruses. V. Identification of an Fc-binding glycoprotein. Journal of Virology, 32(3), pp.779-789.
23. Beauman, J.G., 2005. Genital herpes: a review. American family physician, 72(8), pp.1527-1534.
24. Behrends, C., Sowa, M.E., Gygi, S.P. and Harper, J.W., 2010. Network organization of the human autophagy system. Nature, 466(7302), p.68.
25. Bell, S., Cranage, M., Borysiewicz, L. and Minson, T., 1990. Induction of immunoglobulin G Fc receptors by recombinant vaccinia viruses expressing glycoproteins E and I of herpes simplex virus type 1. Journal of virology, 64(5), pp.2181-2186.
26. Bernatchez, P.N., Acevedo, L., Fernandez-Hernando, C., Murata, T., Chalouni, C., Kim, J., Erdjument-Bromage, H., Shah, V., Gratton, J.P., McNally, E.M. and Tempst, P., 2007. Myoferlin regulates vascular endothelial growth factor receptor-2 stability and function. Journal of Biological Chemistry, 282(42), pp.30745-30753.
27. Bernatchez, P.N., Sharma, A., Kodaman, P. and Sessa, W.C., 2009. Myoferlin is critical for endocytosis in endothelial cells. American Journal of Physiology-Cell Physiology, 297(3), pp.C484-C492.
28. Blackstone, B.N., Li, R., Ackerman 4th, W.E., Ghadiali, S.N., Powell, H.M. and Kniss, D.A., 2015. Myoferlin depletion elevates focal adhesion kinase and paxillin phosphorylation and enhances cell-matrix adhesion in breast cancer cells. American Journal of Physiology-Cell Physiology, 308(8), pp.C642-C649.
29. Boehmer, P.E. and Lehman, I.R. 1997. Herpes simplex virus DNA replication. Annu.Rev.Biochem., 66, 347-384.
30. Bonifacino, J.S. and Glick, B.S., 2004. The mechanisms of vesicle budding and fusion. cell, 116(2), pp.153-166.

31. Boukamp, P., Petrussevska, R.T., Breitkreutz, D., Hornung, J., Markham, A. and Fusenig, N.E., 1988. Normal keratinization in a spontaneously immortalized aneuploid human keratinocyte cell line. The Journal of cell biology, 106(3), pp.761-771.
32. Brass, A.L., Huang, I.C., Benita, Y., John, S.P., Krishnan, M.N., Feeley, E.M., Ryan, B.J., Weyer, J.L., Van Der Weyden, L., Fikrig, E. and Adams, D.J., 2009. The IFITM proteins mediate cellular resistance to influenza A H1N1 virus, West Nile virus, and dengue virus. Cell, 139(7), pp.1243-1254.
33. Brittain, J.M., Wang, Y., Wilson, S.M. and Khanna, R., 2012. Regulation of CREB signaling through L-type Ca2+ channels by Nipsnap-2. Channels, 6(2), pp.94-102.
34. Britton, S., Freeman, T., Vafiadaki, E., Keers, S., Harrison, R., Bushby, K. and Bashir, R., 2000. The third human FER-1-like protein is highly similar to dysferlin. Genomics, 68(3), pp.313-321.
35. Broniarczyk, J., Pim, D., Massimi, P., Bergant, M., Goździcka-Józefiak, A., Crump, C. and Banks, L., 2017. The VPS4 component of the ESCRT machinery plays an essential role in HPV infectious entry and capsid disassembly. Scientific reports, 7, p.45159.
36. Brown, S.M. and MacLean, A.R. eds., 1998. Herpes simplex virus protocols (Vol. 10). Humana Press.
37. Bucks, M.A., O'Regan, K.J., Murphy, M.A., Wills, J.W. and Courtney, R.J., 2007. Herpes simplex virus type 1 tegument proteins VP1/2 and UL37 are associated with intranuclear capsids. Virology, 361(2), pp.316-324.
38. Buechler, C., Bodzioch, M., Bared, S.M., Sigruener, A., Boettcher, A., Lapicka-Bodzioch, K., Aslanidis, C., Duong, C.Q., Grandl, M., Langmann, T. and Dembinska-Kiec, A., 2004. Expression pattern and raft association of Nipsnap3 and Nipsnap4, highly homologous proteins encoded by genes in close proximity to the ATP-binding cassette transporter A1. Genomics, 83(6), pp.1116-1124.
39. Cai, W.H., Gu, B., and Person, S. 1988. Role of glycoprotein B of herpes simplex virus type 1 in viral entry and cell fusion. J.Virol., 62, (8) 2596-2604.
40. Calistri, A., Sette, P., Salata, C., Cancellotti, E., Forghieri, C., Comin, A., Göttlinger, H., Campadelli-Fiume, G., Palù, G. and Parolin, C., 2007. Intracellular trafficking and maturation of herpes simplex virus type 1 gB and virus egress require functional biogenesis of multivesicular bodies. Journal of virology, 81(20), pp.11468-11478.
41. Campadelli, G., Brandimarti, R., Di Lazzaro, C., Ward, P.L., Roizman, B. and Torrisi, M.R., 1993. Fragmentation and dispersal of Golgi proteins and redistribution of glycoproteins and glycolipids processed through the Golgi apparatus after infection with herpes simplex virus 1. Proceedings of the National Academy of Sciences, 90(7), pp.2798-2802.
42. Campadelli-Fiume, G. 2007, "The egress of alphaherpesviruses from the cell," In (ed.), Human herpesviruses: biology, therapy, and immunoprophylaxis, A. Arvin; G. Campadelli-Fiume; E. Mocarski; P. S. Moore; B. Roizman; R. Whitley; K. Yamanishi ed. Cambridge University Press, Cambridge, United Kingdom., pp. 151-163.
43. Cardone, G., Newcomb, W.W., Cheng, N., Wingfield, P.T., Trus, B.L., Brown, J.C. and Steven, A.C., 2012. The UL36 tegument protein of herpes simplex virus 1 has a composite binding site at the capsid vertices. Journal of virology, 86(8), pp.4058-4064.
44. Carmichael, J.C., Yokota, H., Craven, R.C., Schmitt, A. and Wills, J.W., 2018. The HSV-1 mechanisms of cell-to-cell spread and fusion are critically dependent on host PTP1B. PLoS pathogens, 14(5), p.e1007054.

45. Chadha, P., Han, J., Starkey, J.L. and Wills, J.W., 2012. Regulated interaction of tegument proteins UL16 and UL11 from herpes simplex virus. Journal of virology, 86(21), pp.11886-11898.
46. Chang, Y.E., Van Sant, C., Krug, P.W., Sears, A.E. and Roizman, B., 1997. The null mutant of the U (L) 31 gene of herpes simplex virus 1: construction and phenotype in infected cells. Journal of virology, 71(11), pp.8307-8315.
47. Chapman, E.R., 2002. Synaptotagmin: A Ca 2+ sensor that triggers exocytosis?. Nature Reviews Molecular Cell Biology, 3(7), p.498.
48. Chapman, T.L., You, I., Joseph, I.M., Bjorkman, P.J., Morrison, S.L. and Raghavan, M., 1999. Characterization of the interaction between the herpes simplex virus type I Fc receptor and immunoglobulin G. Journal of Biological Chemistry, 274(11), pp.6911-6919.
49. Cheng, S.B., Ferland, P., Webster, P. and Bearer, E.L., 2011. Herpes simplex virus dances with amyloid precursor protein while exiting the cell. PLoS One, 6(3), p.e17966.
50. Cheshenko, N., Del, R.B., Woda, C., Marcellino, D., Satlin, L.M., and Herold, B.C. 2003. Herpes simplex virus triggers activation of calcium-signaling pathways. J.Cell Biol., 163, (2) 283-293.
51. Ch'ng, T.H. and Enquist, L.W., 2005. Efficient axonal localization of alphaherpesvirus structural proteins in cultured sympathetic neurons requires viral glycoprotein E. Journal of virology, 79(14), pp.8835-8846.
52. Cho, W. and Stahelin, R.V., 2006. Membrane binding and subcellular targeting of C2 domains. Biochimica et Biophysica Acta (BBA)-Molecular and Cell Biology of Lipids, 1761(8), pp.838-849.
53. Clement, C., Tiwari, V., Scanlan, P.M., Valyi-Nagy, T., Yue, B.Y. and Shukla, D., 2006. A novel role for phagocytosis-like uptake in herpes simplex virus entry. The Journal of cell biology, 174(7), pp.1009-1021.
54. Cockrell, S.K., Huffman, J.B., Toropova, K., Conway, J.F. and Homa, F.L., 2011. Residues of the UL25 protein of herpes simplex virus that are required for its stable interaction with capsids. Journal of virology, 85(10), pp.4875-4887.
55. Coller, K.E., Joy, I., Lee, H., Ueda, A. and Smith, G.A., 2007. The capsid and tegument of the alphaherpesviruses are linked by an interaction between the UL25 and VP1/2 proteins. Journal of virology, 81(21), pp.11790-11797.
56. Collins, W.J. and Johnson, D.C., 2003. Herpes simplex virus gE/gI expressed in epithelial cells interferes with cell-to-cell spread. Journal of virology, 77(4), pp.2686-2695.
57. Copeland, A.M., Newcomb, W.W., and Brown, J.C. 2009. Herpes simplex virus replication: roles of viral proteins and nucleoporins in capsid-nucleus attachment. J.Virol., 83, (4) 1660-1668.
58. Corcoran, J.A., Saffran, H.A., Duguay, B.A. and Smiley, J.R., 2009. Herpes simplex virus UL12. 5 targets mitochondria through a mitochondrial localization sequence proximal to the N terminus. Journal of virology, 83(6), pp.2601-2610.
59. Cross, A.M., Hope, R.G. and Marsden, H.S., 1987. Generation and properties of the glycoprotein E-related 32K/34K/35K and 55K/57K polypeptides encoded by herpes simplex virus type 1. Journal of general virology, 68(8), pp.2093-2104.
60. Crump, C.M., Yates, C. and Minson, T., 2007. Herpes simplex virus type 1 cytoplasmic envelopment requires functional Vps4. Journal of virology, 81(14), pp.7380-7387.
61. Cunningham, A.L., Taylor, R., Taylor, J., Marks, C., Shaw, J. and Mindel, A., 2006. Prevalence of infection with herpes simplex virus types 1 and 2 in Australia: a nationwide population based survey. Sexually transmitted infections, 82(2), pp.164-168.

62. Dargan, D.J. and Subak-Sharpe, J.H., 1997. The effect of herpes simplex virus type 1 L-particles on virus entry, replication, and the infectivity of naked herpesvirus DNA. Virology, 239(2), pp.378-388.
63. Davis, D.B., Delmonte, A.J., Ly, C.T. and McNally, E.M., 2000. Myoferlin, a candidate gene and potential modifier of muscular dystrophy. Human molecular genetics, 9(2), pp.217-226.
64. Davis, D.B., Doherty, K.R., Delmonte, A.J. and McNally, E.M., 2002. Calcium-sensitive phospholipid binding properties of normal and mutant ferlin C2 domains. Journal of Biological Chemistry, 277(25), pp.22883-22888.
65. Delboy, M.G. and Nicola, A.V., 2011. A pre-immediate early role for tegument ICP0 in the proteasome-dependent entry of herpes simplex virus. Journal of virology.
66. Demonbreun, A.R., Posey, A.D., Heretis, K., Swaggart, K.A., Earley, J.U., Pytel, P. and McNally, E.M., 2010. Myoferlin is required for insulin-like growth factor response and muscle growth. The FASEB Journal, 24(4), pp.1284-1295.
67. Desai, T.M., Marin, M., Chin, C.R., Savidis, G., Brass, A.L. and Melikyan, G.B., 2014. IFITM3 restricts influenza A virus entry by blocking the formation of fusion pores following virus-endosome hemifusion. PLoS pathogens, 10(4), p.e1004048.
68. Dingwell, K.S. and Johnson, D.C., 1998. The herpes simplex virus gE-gI complex facilitates cell-to-cell spread and binds to components of cell junctions. Journal of virology, 72(11), pp.8933-8942.
69. Dingwell, K.S., Brunetti, C.R., Hendricks, R.L., Tang, Q., Tang, M., Rainbow, A.J. and Johnson, D.C., 1994. Herpes simplex virus glycoproteins E and I facilitate cell-to-cell spread in vivo and across junctions of cultured cells. Journal of virology, 68(2), pp.834-845.
70. Dingwell, K.S., Doering, L.C., and Johnson, D.C. 1995. Glycoproteins E and I facilitate neuron-to-neuron spread of herpes simplex virus. J Virol, 69, (11) 7087-7098.
71. Doherty, G.J. and McMahon, H.T., 2009. Mechanisms of endocytosis. Annual review of biochemistry, 78, pp.857-902.
72. Doherty, K.R. and McNally, E.M., 2003. Repairing the tears: dysferlin in muscle membrane repair. Trends in molecular medicine, 9(8), pp.327-330.
73. Doherty, K.R., Demonbreun, A.R., Wallace, G.Q., Cave, A., Posey, A.D., Heretis, K., Pytel, P. and McNally, E.M., 2008. The endocytic recycling protein EHD2 interacts with myoferlin to regulate myoblast fusion. Journal of Biological Chemistry, 283(29), pp.20252-20260.
74. Dubin, G., Basu, S., Mallory, D.L., Basu, M., Tal-Singer, R., and Friedman, H.M. 1994. Characterization of domains of herpes simplex virus type 1 glycoprotein E involved in Fc binding activity for immunoglobulin G aggregates. J Virol, 68, (4) 2478-2485.
75. Duffy, C., LaVail, J.H., Tauscher, A.N., Wills, E.G., Blaho, J.A. and Baines, J.D., 2006. Characterization of a UL49-null mutant: VP22 of herpes simplex virus type 1 facilitates viral spread in cultured cells and the mouse cornea. Journal of virology, 80(17), pp.8664-8675.
76. Edson, C.M., 1993. Phosphorylation of neurotropic alphaherpesvirus envelope glycoproteins: Herpes simplex virus type 2 gE2 and pseudorabies virus gl. Virology, 195(1), pp.268-270.
77. Eisenberg, R.J., Atanasiu, D., Cairns, T.M., Gallagher, J.R., Krummenacher, C. and Cohen, G.H., 2012. Herpes virus fusion and entry: a story with many characters. Viruses, 4(5), pp.800-832.

78. El Kasmi, I. and Lippé, R., 2015. Herpes simplex virus 1 gN partners with gM to modulate the viral fusion machinery. Journal of virology, 89(4), pp.2313-2323.
79. Emmott, E. and Goodfellow, I., 2014. Identification of protein interaction partners in mammalian cells using SILAC-immunoprecipitation quantitative proteomics. Journal of visualized experiments: JoVE, (89).
80. Enquist, L.W., Husak, P.J., Banfield, B.W. and Smith, G.A., 1998. Infection and spread of alphaherpesviruses in the nervous system. In Advances in virus research (Vol. 51, pp. 237-347). Academic Press.
81. Esclatine, A., Taddeo, B., and Roizman, B. 2004. The UL41 protein of herpes simplex virus mediates selective stabilization or degradation of cellular mRNAs. Proc.Natl.Acad.Sci.U.S.A, 101, (52) 18165-18170.
82. Eskelinen, E.L., 2006. Roles of LAMP-1 and LAMP-2 in lysosome biogenesis and autophagy. Molecular aspects of medicine, 27(5-6), pp.495-502.
83. Eskelinen, E.L., Illert, A.L., Tanaka, Y., Schwarzmann, G., Blanz, J., Von Figura, K. and Saftig, P., 2002. Role of LAMP-2 in lysosome biogenesis and autophagy. Molecular biology of the cell, 13(9), pp.3355-3368.
84. Farnsworth, A. and Johnson, D.C., 2006. Herpes simplex virus gE/gI must accumulate in the *trans*-Golgi network at early times and then redistribute to cell junctions to promote cell-cell spread. Journal of virology, 80(7), pp.3167-3179.
85. Farnsworth, A., Goldsmith, K. and Johnson, D.C., 2003. Herpes simplex virus glycoproteins gD and gE/gI serve essential but redundant functions during acquisition of the virion envelope in the cytoplasm. Journal of virology, 77(15), pp.8481-8494.
86. Farnsworth, A., Wisner, T.W. and Johnson, D.C., 2007 (b). Cytoplasmic residues of herpes simplex virus glycoprotein gE required for secondary envelopment and binding of tegument proteins VP22 and UL11 to gE and gD. Journal of virology, 81(1), pp.319-331.
87. Farnsworth, A., Wisner, T.W., Webb, M., Roller, R., Cohen, G., Eisenberg, R. and Johnson, D.C., 2007 (a). Herpes simplex virus glycoproteins gB and gH function in fusion between the virion envelope and the outer nuclear membrane. Proceedings of the National Academy of Sciences, 104(24), pp.10187-10192.
88. Feeley, E.M., Sims, J.S., John, S.P., Chin, C.R., Pertel, T., Chen, L.M., Gaiha, G.D., Ryan, B.J., Donis, R.O., Elledge, S.J. and Brass, A.L., 2011. IFITM3 inhibits influenza A virus infection by preventing cytosolic entry. PLoS pathogens, 7(10), p.e1002337.
89. Feng, P., Everly, D.N. and Read, G.S., 2001. mRNA decay during herpesvirus infections: interaction between a putative viral nuclease and a cellular translation factor. Journal of virology, 75(21), pp.10272-10280.
90. Fernandez-Chacon, R., Königstorfer, A., Gerber, S.H., García, J., Matos, M.F., Stevens, C.F., Brose, N., Rizo, J., Rosenmund, C. and Südhof, T.C., 2001. Synaptotagmin I functions as a calcium regulator of release probability. Nature, 410(6824), p.41.
91. Forrester, A., Farrell, H., Wilkinson, G., Kaye, J., Davis-Poynter, N., and Minson, T. 1992. Construction and properties of a mutant of herpes simplex virus type 1 with glycoprotein H coding sequences deleted. J.Virol., 66, (1) 341-348.
92. Foster, T.P., Melancon, J.M., Olivier, T.L. and Kousoulas, K.G., 2004. Herpes simplex virus type 1 glycoprotein K and the UL20 protein are interdependent for intracellular trafficking and *trans*-Golgi network localization. Journal of virology, 78(23), pp.13262-13277.

93. Fox, H.L., Dembowski, J.A. and DeLuca, N.A., 2017. A Herpesviral Immediate Early Protein Promotes Transcription Elongation of Viral Transcripts. mBio, 8(3), pp.e00745-17.
94. Fuchs, W., Klupp, B.G., Granzow, H., Hengartner, C., Brack, A., Mundt, A., Enquist, L.W. and Mettenleiter, T.C., 2002. Physical interaction between envelope glycoproteins E and M of pseudorabies virus and the major tegument protein UL49. Journal of virology, 76(16), pp.8208-8217.
95. Fuchs, W., Klupp, B.G., Granzow, H., Osterrieder, N. and Mettenleiter, T.C., 2002. The interacting UL31 and UL34 gene products of pseudorabies virus are involved in egress from the host-cell nucleus and represent components of primary enveloped but not mature virions. Journal of virology, 76(1), pp.364-378.
96. Ghosh, P., Dahms, N.M. and Kornfeld, S., 2003. Mannose 6-phosphate receptors: new twists in the tale. Nature reviews Molecular cell biology, 4(3), p.202.
97. Gierasch, W.W., Zimmerman, D.L., Ward, S.L., VanHeyningen, T.K., Romine, J.D. and Leib, D.A., 2006. Construction and characterization of bacterial artificial chromosomes containing HSV-1 strains 17 and KOS. Journal of virological methods, 135(2), pp.197-206.
98. Glover, L. and Brown, R.H., 2007. Dysferlin in membrane trafficking and patch repair. Traffic, 8(7), pp.785-794.
99. Granzow, H., Klupp, B.G., Fuchs, W., Veits, J., Osterrieder, N., and Mettenleiter, T.C. 2001. Egress of alphaherpesviruses: comparative ultrastructural study. J.Virol, 75, (8) 3675-3684.
100. Griffiths, S.J., Koegl, M., Boutell, C., Zenner, H.L., Crump, C.M., Pica, F., Gonzalez, O., Friedel, C.C., Barry, G., Martin, K. and Craigon, M.H., 2013. A systematic analysis of host factors reveals a Med23-interferon-λ regulatory axis against herpes simplex virus type 1 replication. PLoS pathogens, 9(8), p.e1003514.
101. Gross, S.T., Harley, C.A. and Wilson, D.W., 2003. The cytoplasmic tail of herpes simplex virus glycoprotein H binds to the tegument protein VP16 in vitro and in vivo. Virology, 317(1), pp.1-12.
102. Grünewald, K., Desai, P., Winkler, D.C., Heymann, J.B., Belnap, D.M., Baumeister, W. and Steven, A.C., 2003. Three-dimensional structure of herpes simplex virus from cryo-electron tomography. Science, 302(5649), pp.1396-1398.
103. Gu, F., Crump, C.M. and Thomas, G., 2001. Trans-Golgi network sorting. Cellular and Molecular Life Sciences CMLS, 58(8), pp.1067-1084.
104. Haanes, E.J., Nelson, C.M., Soule, C.L. and Goodman, J.L., 1994. The UL45 gene product is required for herpes simplex virus type 1 glycoprotein B-induced fusion. Journal of virology, 68(9), pp.5825-5834.
105. Hafezi, W., Bernard, E., Cook, R. and Elliott, G., 2005. Herpes simplex virus tegument protein VP22 contains an internal VP16 interaction domain and a C-terminal domain that are both required for VP22 assembly into the virus particle. Journal of virology, 79(20), pp.13082-13093.
106. Hagen, C., Dent, K.C., Zeev-Ben-Mordehai, T., Grange, M., Bosse, J.B., Whittle, C., Klupp, B.G., Siebert, C.A., Vasishtan, D., Bäuerlein, F.J. and Cheleski, J., 2015. Structural basis of vesicle formation at the inner nuclear membrane. Cell, 163(7), pp.1692-1701.
107. Han, J., Chadha, P., Starkey, J.L. and Wills, J.W., 2012. Function of glycoprotein E of herpes simplex virus requires coordinated assembly of three tegument proteins on its

cytoplasmic tail. Proceedings of the National Academy of Sciences, 109(48), pp.19798-19803.
108. Hanke, T., Graham, F.L., Lulitanond, V. and Johnson, D.C., 1990. Herpes simplex virus IgG Fc receptors induced using recombinant adenovirus vectors expressing glycoproteins E and I. Virology, 177(2), pp.437-444.
109. Hansen, C.G. and Nichols, B.J., 2009. Molecular mechanisms of clathrin-independent endocytosis. Journal of cell science, 122(11), pp.1713-1721.
110. Harland, J. and Brown, S.M., 1998. HSV growth, preparation, and assay. In Herpes simplex virus protocols (pp. 1-8). Humana Press.
111. Harley, C.A., Dasgupta, A. and Wilson, D.W., 2001. Characterization of herpes simplex virus-containing organelles by subcellular fractionation: role for organelle acidification in assembly of infectious particles. Journal of virology, 75(3), pp.1236-1251.
112. Harter, C. and Mellman, I., 1992. Transport of the lysosomal membrane glycoprotein lgp120 (lgp-A) to lysosomes does not require appearance on the plasma membrane. The Journal of Cell Biology, 117(2), pp.311-325.
113. Herold, B.C., WuDunn, D., Soltys, N. and Spear, P.G., 1991. Glycoprotein C of herpes simplex virus type 1 plays a principal role in the adsorption of virus to cells and in infectivity. Journal of virology, 65(3), pp.1090-1098.
114. Hirohata, Y., Kato, A., Oyama, M., Kozuka-Hata, H., Koyanagi, N., Arii, J. and Kawaguchi, Y., 2015. Interactome analysis of herpes simplex virus 1 envelope glycoprotein H. Microbiology and immunology, 59(6), pp.331-337.
115. Hofemeister, H. and O'Hare, P., 2008. Nuclear pore composition and gating in herpes simplex virus-infected cells. Journal of virology, 82(17), pp.8392-8399.
116. Hogue, I.B., Bosse, J.B., Hu, J.R., Thiberge, S.Y. and Enquist, L.W., 2014. Cellular mechanisms of alpha herpesvirus egress: live cell fluorescence microscopy of pseudorabies virus exocytosis. PLoS pathogens, 10(12), p.e1004535.
117. Hollinshead, M., Johns, H.L., Sayers, C.L., Gonzalez-Lopez, C., Smith, G.L., and Elliott, G. 2012. Endocytic tubules regulated by Rab GTPases 5 and 11 are used for envelopment of herpes simplex virus. EMBO J., 31, (21) 4204-4220.
118. Howard, P.W., Howard, T.L. and Johnson, D.C., 2013. Herpes simplex virus membrane proteins gE/gI and US9 act cooperatively to promote transport of capsids and glycoproteins from neuron cell bodies into initial axon segments. Journal of virology, 87(1), pp.403-414.
119. Howard, P.W., Wright, C.C., Howard, T. and Johnson, D.C., 2014. Herpes simplex virus gE/gI extracellular domains promote axonal transport and spread from neurons to epithelial cells. Journal of virology, 88(19), pp.11178-11186.
120. Huang, I.C., Bailey, C.C., Weyer, J.L., Radoshitzky, S.R., Becker, M.M., Chiang, J.J., Brass, A.L., Ahmed, A.A., Chi, X., Dong, L. and Longobardi, L.E., 2011. Distinct patterns of IFITM-mediated restriction of filoviruses, SARS coronavirus, and influenza A virus. PLoS pathogens, 7(1), p.e1001258.
121. Huang, T. and Osterrieder, N., 2015. The herpesvirus stealth program. Oncotarget, 6(26), p.21761.
122. Igarashi, K., Fawl, R., Roller, R.J. and Roizman, B., 1993. Construction and properties of a recombinant herpes simplex virus 1 lacking both S-component origins of DNA synthesis. Journal of virology, 67(4), pp.2123-2132.

123. Jambunathan, N., Chouljenko, D., Desai, P., Charles, A.S., Subramanian, R., Chouljenko, V.N. and Kousoulas, K.G., 2014. Herpes simplex virus 1 protein UL37 interacts with viral glycoprotein gK and membrane protein UL20 and functions in cytoplasmic virion envelopment. Journal of virology, 88(11), pp.5927-5935.
124. Jayachandra, S., Baghian, A. and Kousoulas, K.G., 1997. Herpes simplex virus type 1 glycoprotein K is not essential for infectious virus production in actively replicating cells but is required for efficient envelopment and translocation of infectious virions from the cytoplasm to the extracellular space. Journal of virology, 71(7), pp.5012-5024.
125. Jerome, K.R., Chen, Z., Lang, R., Torres, M.R., Hofmeister, J., Smith, S., Fox, R., Froelich, C.J. and Corey, L., 2001. HSV and glycoprotein J inhibit caspase activation and apoptosis induced by granzyme B or Fas. The Journal of Immunology, 167(7), pp.3928-3935.
126. John, S.P., Chin, C.R., Perreira, J.M., Feeley, E.M., Aker, A.M., Savidis, G., Smith, S.E., Elia, A.E., Everitt, A.R., Vora, M. and Pertel, T., 2013. The CD225 domain of IFITM3 is required for both IFITM protein association and inhibition of influenza A virus and dengue virus replication. Journal of virology, 87(14), pp.7837-7852.
127. Johns, H.L., Gonzalez-Lopez, C., Sayers, C.L., Hollinshead, M. and Elliott, G., 2014. Rab6 dependent post-golgi trafficking of HSV1 envelope proteins to sites of virus envelopment. Traffic, 15(2), pp.157-178.
128. Johnson, D.B., Puzanov, I. and Kelley, M.C., 2015. Talimogene laherparepvec (T-VEC) for the treatment of advanced melanoma. Immunotherapy, 7(6), pp.611-619.
129. Johnson, D.C. and Baines, J.D., 2011. Herpesviruses remodel host membranes for virus egress. Nature Reviews Microbiology, 9(5), p.382.
130. Johnson, D.C. and Feenstra, V., 1987. Identification of a novel herpes simplex virus type 1-induced glycoprotein which complexes with gE and binds immunoglobulin. Journal of Virology, 61(7), pp.2208-2216.
131. Johnson, D.C. and Huber, M.T., 2002. Directed egress of animal viruses promotes cell-to-cell spread. Journal of virology, 76(1), pp.1-8.
132. Johnson, D.C., Frame, M.C., Ligas, M.W., Cross, A.M. and Stow, N.D., 1988. Herpes simplex virus immunoglobulin G Fc receptor activity depends on a complex of two viral glycoproteins, gE and gI. Journal of Virology, 62(4), pp.1347-1354.
133. Johnson, D.C., Webb, M., Wisner, T.W. and Brunetti, C., 2001. Herpes simplex virus gE/gI sorts nascent virions to epithelial cell junctions, promoting virus spread. Journal of virology, 75(2), pp.821-833.
134. Johnson, D.C., Wisner, T.W. and Wright, C.C., 2011. Herpes simplex virus glycoproteins gB and gD function in a redundant fashion to promote secondary envelopment. Journal of virology, 85(10), pp.4910-4926.
135. Kamen, D.E., Gross, S.T., Girvin, M.E. and Wilson, D.W., 2005. Structural basis for the physiological temperature dependence of the association of VP16 with the cytoplasmic tail of herpes simplex virus glycoprotein H. Journal of virology, 79(10), pp.6134-6141.
136. Kato, Akihisa, Michiko Tanaka, Mayuko Yamamoto, Risa Asai, Tetsutaro Sata, Yukihiro Nishiyama, and Yasushi Kawaguchi. "Identification of a physiological phosphorylation site of the herpes simplex virus 1-encoded protein kinase Us3 which regulates its optimal catalytic activity in vitro and influences its function in infected cells." Journal of virology 82, no. 13 (2008): 6172-6189.

137. Killock, D., 2015. Skin cancer: T-VEC oncolytic viral therapy shows promise in melanoma. Nature Reviews Clinical Oncology, 12(8), p.438.
138. Kim, I.J., Chouljenko, V.N., Walker, J.D. and Kousoulas, K.G., 2013. Herpes simplex virus 1 glycoprotein M and the membrane-associated protein UL11 are required for virus-induced cell fusion and efficient virus entry. Journal of virology, 87(14), pp.8029-8037.
139. Klopfleisch, R., Klupp, B.G., Fuchs, W., Kopp, M., Teifke, J.P. and Mettenleiter, T.C., 2006. Influence of pseudorabies virus proteins on neuroinvasion and neurovirulence in mice. Journal of virology, 80(11), pp.5571-5576.
140. Klupp, B., Altenschmidt, J., Granzow, H., Fuchs, W. and Mettenleiter, T.C., 2008. Glycoproteins required for entry are not necessary for egress of pseudorabies virus. Journal of virology, 82(13), pp.6299-6309.
141. Klupp, B.G., Altenschmidt, J., Granzow, H., Fuchs, W. and Mettenleiter, T.C., 2005. Identification and characterization of the pseudorabies virus UL43 protein. Virology, 334(2), pp.224-233.
142. Klupp, B.G., Granzow, H. and Mettenleiter, T.C., 2000. Primary envelopment of pseudorabies virus at the nuclear membrane requires the UL34 gene product. Journal of virology, 74(21), pp.10063-10073.
143. Klupp, B.G., Granzow, H., Fuchs, W., Keil, G.M., Finke, S., and Mettenleiter, T.C. 2007. Vesicle formation from the nuclear membrane is induced by coexpression of two conserved herpesvirus proteins. Proc.Natl.Acad.Sci.U.S.A, 104, (17) 7241-7246.
144. Koyama, A.H. and Uchida, T., 1987. The mode of entry of herpes simplex virus type 1 into Vero cells. Microbiology and immunology, 31(2), pp.123-130.
145. Kramer, T. and Enquist, L.W., 2012. Alphaherpesvirus infection disrupts mitochondrial transport in neurons. Cell host & microbe, 11(5), pp.504-514.
146. Kratchmarov, R., Taylor, M.P. and Enquist, L.W., 2013. Role of Us9 phosphorylation in axonal sorting and anterograde transport of pseudorabies virus. PloS one, 8(3), p.e58776.
147. Krummenacher, C., Supekar, V.M., Whitbeck, J.C., Lazear, E., Connolly, S.A., Eisenberg, R.J., Cohen, G.H., Wiley, D.C. and Carfí, A., 2005. Structure of unliganded HSV gD reveals a mechanism for receptor-mediated activation of virus entry. The EMBO journal, 24(23), pp.4144-4153.
148. La, B.S., Hughes, T. and O'Hare, P. 1999. HCF-dependent nuclear import of VP16. EMBO J., 18, (2) 480-489.
149. Laine, R.F., Albecka, A., Van De Linde, S., Rees, E.J., Crump, C.M. and Kaminski, C.F., 2015. Structural analysis of herpes simplex virus by optical super-resolution imaging. Nature communications, 6, p.5980.
150. Lam, Q., Smibert, C.A., Koop, K.E., Lavery, C., Capone, J.P., Weinheimer, S.P. and Smiley, J.R., 1996. Herpes simplex virus VP16 rescues viral mRNA from destruction by the virion host shutoff function. The EMBO journal, 15(10), pp.2575-2581.
151. Lamberti, C. and Weller, S.K., 1998. The herpes simplex virus type 1 cleavage/packaging protein, UL32, is involved in efficient localization of capsids to replication compartmentsn. Journal of virology, 72(3), pp.2463-2473.
152. Laquerre, S., Argnani, R., Anderson, D.B., Zucchini, S., Manservigi, R. and Glorioso, J.C., 1998. Heparan sulfate proteoglycan binding by herpes simplex virus type 1 glycoproteins B and C, which differ in their contributions to virus attachment, penetration, and cell-to-cell spread. Journal of virology, 72(7), pp.6119-6130.
153. Lau, S.Y.K. and Crump, C.M., 2015. HSV-1 gM and the gK/pUL20 complex are important for the localization of gD and gH/L to viral assembly sites. Viruses, 7(3), pp.915-938.

154. Leach, N., Bjerke, S.L., Christensen, D.K., Bouchard, J.M., Mou, F., Park, R., Baines, J., Haraguchi, T. and Roller, R.J., 2007. Emerin is hyperphosphorylated and redistributed in herpes simplex virus type 1-infected cells in a manner dependent on both UL34 and US3. Journal of virology, 81(19), pp.10792-10803.
155. Leach, N.R. and Roller, R.J., 2010. Significance of host cell kinases in herpes simplex virus type 1 egress and lamin-associated protein disassembly from the nuclear lamina. Virology, 406(1), pp.127-137.
156. Lee, A.H., Zareei, M.P. and Daefler, S., 2002. Identification of a Nipsnap homologue as host cell target for Salmonella virulence protein SpiC. Cellular microbiology, 4(11), pp.739-750.
157. Lee, J.H., Vittone, V., Diefenbach, E., Cunningham, A.L. and Diefenbach, R.J., 2008. Identification of structural protein–protein interactions of herpes simplex virus type 1. Virology, 378(2), pp.347-354.
158. Leege, T., Fuchs, W., Granzow, H., Kopp, M., Klupp, B.G. and Mettenleiter, T.C., 2009. Effects of simultaneous deletion of pUL11 and glycoprotein M on virion maturation of herpes simplex virus type 1. Journal of virology, 83(2), pp.896-907.
159. Lehman, I.R. and Boehmer, P.E. 1999. Replication of herpes simplex virus DNA. J Biol.Chem., 274, (40) 28059-28062.
160. Lehmann, M.J., Sherer, N.M., Marks, C.B., Pypaert, M., and Mothes, W. 2005. Actin- and myosin-driven movement of viruses along filopodia precedes their entry into cells. J.Cell Biol., 170, (2) 317-325.
161. Leung, C., Shaheen, F., Bernatchez, P. and Hackett, T.L., 2012. Expression of myoferlin in human airway epithelium and its role in cell adhesion and zonula occludens-1 expression. PloS one, 7(7), p.e40478.
162. Leuzinger, H., Ziegler, U., Schraner, E.M., Fraefel, C., Glauser, D.L., Heid, I., Ackermann, M., Mueller, M., and Wild, P. 2005. Herpes simplex virus 1 envelopment follows two diverse pathways. J.Virol., 79, (20) 13047-13059.
163. Li, H., Zhang, J., Kumar, A., Zheng, M., Atherton, S.S. and Yu, F.S.X., 2006. Herpes simplex virus 1 infection induces the expression of proinflammatory cytokines, interferons and TLR7 in human corneal epithelial cells. Immunology, 117(2), pp.167-176.
164. Li, M.L., Guo, H., Ding, Q. and Zheng, C.F., 2009. A multiple functional protein: the herpes simplex virus type 1 tegument protein VP22. Virologica Sinica, 24(3), pp.153-161.
165. Ligas, M.W. and Johnson, D.C. 1988. A herpes simplex virus mutant in which glycoprotein D sequences are replaced by beta-galactosidase sequences binds to but is unable to penetrate into cells. J.Virol., 62, (5) 1486-1494.
166. Liu, Z., Guan, Y., Sun, X., Shi, L., Liang, R., Lv, X. and Xin, W., 2013. HSV-1 activates NF-kappaB in mouse astrocytes and increases TNF-alpha and IL-6 expression via Toll-like receptor 3. Neurological research, 35(7), pp.755-762.
167. Longnecker, R., Chatterjee, S., Whitley, R.J. and Roizman, B., 1987. Identification of a herpes simplex virus 1 glycoprotein gene within a gene cluster dispensable for growth in cell culture. Proceedings of the National Academy of Sciences, 84(12), pp.4303-4307.
168. Loret, S. and Lippé, R., 2012. Biochemical analysis of infected cell polypeptide (ICP) 0, ICP4, UL7 and UL23 incorporated into extracellular herpes simplex virus type 1 virions. Journal of General Virology, 93(3), pp.624-634.
169. Loret, S., Guay, G., and Lippe, R. 2008. Comprehensive characterization of extracellular herpes simplex virus type 1 virions. J.Virol., 82, (17) 8605-8618.

170. Lu, J., Pan, Q., Rong, L., Liu, S.L. and Liang, C., 2011. The IFITM proteins inhibit HIV-1 infection. Journal of virology, 85(5), pp.2126-2137.
171. Lubinski, J.M., Wang, L., Soulika, A.M., Burger, R., Wetsel, R.A., Colten, H., Cohen, G.H., Eisenberg, R.J., Lambris, J.D. and Friedman, H.M., 1998. Herpes simplex virus type 1 glycoprotein gC mediates immune evasion in vivo. Journal of virology, 72(10), pp.8257-8263.
172. Lyman, M.G., Feierbach, B., Curanovic, D., Bisher, M. and Enquist, L.W., 2007. Pseudorabies virus Us9 directs axonal sorting of viral capsids. Journal of virology, 81(20), pp.11363-11371.
173. Mach, M., Osinski, K., Kropff, B., Schloetzer-Schrehardt, U., Krzyzaniak, M. and Britt, W., 2007. The carboxy-terminal domain of glycoprotein N of human cytomegalovirus is required for virion morphogenesis. Journal of virology, 81(10), pp.5212-5224.
174. MacLean, C.A., Efstathiou, S., Elliott, M.L., Jamieson, F.E. and McGeoch, D.J., 1991. Investigation of herpes simplex virus type 1 genes encoding multiply inserted membrane proteins. Journal of General Virology, 72(4), pp.897-906.
175. Makhov, A.M., Lee, S.S., Lehman, I.R., and Griffith, J.D. 2003. Origin-specific unwinding of herpes simplex virus 1 DNA by the viral UL9 and ICP8 proteins: visualization of a specific preunwinding complex. Proc.Natl.Acad.Sci.U.S.A, 100, (3) 898-903.
176. Mårdberg, K., Nyström, K., Tarp, M.A., Trybala, E., Clausen, H., Bergström, T. and Olofsson, S., 2004. Basic amino acids as modulators of an O-linked glycosylation signal of the herpes simplex virus type 1 glycoprotein gC: functional roles in viral infectivity. Glycobiology, 14(7), pp.571-581.
177. Maringer, K., Stylianou, J. and Elliott, G., 2012. A network of protein interactions around the herpes simplex virus tegument protein VP22. Journal of virology, 86(23), pp.12971-12982.
178. Maurer, U.E., Sodeik, B. and Grünewald, K., 2008. Native 3D intermediates of membrane fusion in herpes simplex virus 1 entry. Proceedings of the National Academy of Sciences, 105(30), pp.10559-10564.
179. McGraw, H.M. and Friedman, H.M. 2009. Herpes simplex virus type 1 glycoprotein E mediates retrograde spread from epithelial cells to neurites. J Virol, 83, (10) 4791-4799.
180. McLauchlan, J. and Rixon, F.J., 1992. Characterization of enveloped tegument structures (L particles) produced by alphaherpesviruses: integrity of the tegument does not depend on the presence of capsid or envelope. Journal of general virology, 73(2), pp.269-276.
181. McLean, C., Buckmaster, A., Hancock, D., Buchan, A., Fuller, A. and Minson, A., 1982. Monoclonal antibodies to three non-glycosylated antigens of herpes simplex virus type 2. Journal of General Virology, 63(2), pp.297-305.
182. McMillan, T.N. and Johnson, D.C., 2001. Cytoplasmic domain of herpes simplex virus gE causes accumulation in the *trans*-Golgi network, a site of virus envelopment and sorting of virions to cell junctions. Journal of virology, 75(4), pp.1928-1940.
183. McNeil, P.L. and Kirchhausen, T., 2005. An emergency response team for membrane repair. Nature Reviews Molecular Cell Biology, 6(6), p.499.
184. Meckes, D.G. and Wills, J.W., 2008. Structural rearrangement within an enveloped virus upon binding to the host cell. Journal of virology, 82(21), pp.10429-10435.
185. Meckes, D.G., Marsh, J.A. and Wills, J.W., 2010. Complex mechanisms for the packaging of the UL16 tegument protein into herpes simplex virus. Virology, 398(2), pp.208-213.

186. Melancon, J.M., Luna, R.E., Foster, T.P. and Kousoulas, K.G., 2005. Herpes simplex virus type 1 gK is required for gB-mediated virus-induced cell fusion, while neither gB and gK nor gB and UL20p function redundantly in virion de-envelopment. Journal of virology, 79(1), pp.299-313.
187. Mettenleiter, T.C. and Minson, T. 2006. Egress of alphaherpesviruses. J.Virol., 80, (3) 1610-1611.
188. Mettenleiter, T.C., 2002. Herpesvirus assembly and egress. Journal of virology, 76(4), pp.1537-1547.
189. Mettenleiter, T.C., 2004. Budding events in herpesvirus morphogenesis. Virus research, 106(2), pp.167-180.
190. Mettenleiter, T.C., Klupp, B.G. and Granzow, H., 2009. Herpesvirus assembly: an update. Virus research, 143(2), pp.222-234.
191. Mijnes, J.D., Van der Horst, L.M., Van Anken, E., Horzinek, M.C., Rottier, P.J. and De Groot, R.J., 1996. Biosynthesis of glycoproteins E and I of feline herpesvirus: gE-gI interaction is required for intracellular transport. Journal of virology, 70(8), pp.5466-5475.
192. Mingo, R.M., Han, J., Newcomb, W.W. and Brown, J.C., 2012. Replication of herpes simplex virus: egress of progeny virus at specialized cell membrane sites. Journal of virology, 86(13), pp.7084-7097.
193. Minson, A. C., Davison, A., Eberle, R., Desrosiers, R. C., Fleckenstein, B., McGeoch, D. J., Pellett, P. E., Roizman, B. and Studdert, M. J., 2000. Family Herpesviridae. In Virus Taxonomy. Seventh Report of the International Committee on Taxonomy of Viruses, San Diego: Academic Press, pp. 203–225.
194. Minson, A.C., Hodgman, T.C., Digard, P., Hancock, D.C., Bell, S.E. and Buckmaster, E.A., 1986. An analysis of the biological properties of monoclonal antibodies against glycoprotein D of herpes simplex virus and identification of amino acid substitutions that confer resistance to neutralization. Journal of general virology, 67(6), pp.1001-1013.
195. Montgomery, R.I., Warner, M.S., Lum, B.J., and Spear, P.G. 1996. Herpes simplex virus-1 entry into cells mediated by a novel member of the TNF/NGF receptor family. Cell, 87, (3) 427-436.
196. Mootha, V.K., Bunkenborg, J., Olsen, J.V., Hjerrild, M., Wisniewski, J.R., Stahl, E., Bolouri, M.S., Ray, H.N., Sihag, S., Kamal, M. and Patterson, N., 2003. Integrated analysis of protein composition, tissue diversity, and gene regulation in mouse mitochondria. Cell, 115(5), pp.629-640.
197. Morris, J.B., Hofemeister, H. and O'Hare, P., 2007. Herpes simplex virus infection induces phosphorylation and delocalization of emerin, a key inner nuclear membrane protein. Journal of virology, 81(9), pp.4429-4437.
198. Morrison, E.E., Stevenson, A.J., Wang, Y.F. and Meredith, D.M., 1998. Differences in the intracellular localization and fate of herpes simplex virus tegument proteins early in the infection of Vero cells. Journal of general virology, 79(10), pp.2517-2528.
199. Mostov, K.E., Verges, M. and Altschuler, Y., 2000. Membrane traffic in polarized epithelial cells. Current opinion in cell biology, 12(4), pp.483-490.
200. Mou, F., Forest, T., and Baines, J.D. 2007. US3 of herpes simplex virus type 1 encodes a promiscuous protein kinase that phosphorylates and alters localization of lamin A/C in infected cells. J.Virol., 81, (12) 6459-6470.
201. Mou, F., Wills, E. and Baines, J.D., 2009. Phosphorylation of the UL31 protein of herpes simplex virus 1 by the US3-encoded kinase regulates localization of the nuclear

envelopment complex and egress of nucleocapsids. Journal of virology, 83(10), pp.5181-5191.
202. Mudhasani, R., Tran, J.P., Retterer, C., Radoshitzky, S.R., Kota, K.P., Altamura, L.A., Smith, J.M., Packard, B.Z., Kuhn, J.H., Costantino, J. and Garrison, A.R., 2013. IFITM-2 and IFITM-3 but not IFITM-1 restrict Rift Valley fever virus. Journal of virology, 87(15), pp.8451-8464.
203. Muñoz-Moreno, R., Cuesta-Geijo, M.Á., Martínez-Romero, C., Barrado-Gil, L., Galindo, I., García-Sastre, A. and Alonso, C., 2016. Antiviral role of IFITM proteins in African swine fever virus infection. PloS one, 11(4), p.e0154366.
204. Muylaert, I., Tang, K.W., and Elias, P. 2011. Replication and recombination of herpes simplex virus DNA. J Biol.Chem., 286, (18) 15619-15624.
205. Nautiyal, M., Sweatt, A.J., MacKenzie, J.A., Mark Payne, R., Szucs, S., Matalon, R., Wallin, R. and Hutson, S.M., 2010. Neuronal localization of the mitochondrial protein Nipsnap1 in rat nervous system. European Journal of Neuroscience, 32(4), pp.560-569.
206. Ndjamen, B., Farley, A.H., Lee, T., Fraser, S.E. and Bjorkman, P.J., 2014. The herpes virus Fc receptor gE-gI mediates antibody bipolar bridging to clear viral antigens from the cell surface. PLoS pathogens, 10(3), p.e1003961.
207. Newcomb, W.W. and Brown, J.C., 2010. Structure and capsid association of the herpesvirus large tegument protein UL36. Journal of virology, 84(18), pp.9408-9414.
208. Newcomb, W.W. and Brown, J.C., 2012. Internal catalase protects herpes simplex virus from inactivation by hydrogen peroxide. Journal of virology, 86(21), pp.11931-11934.
209. Newcomb, W.W., Homa, F.L. and Brown, J.C., 2006. Herpes simplex virus capsid structure: DNA packaging protein UL25 is located on the external surface of the capsid near the vertices. Journal of virology, 80(13), pp.6286-6294.
210. Newcomb, W.W., Homa, F.L., Thomsen, D.R., Booy, F.P., Trus, B.L., Steven, A.C., Spencer, J.V. and Brown, J.C., 1996. Assembly of the herpes simplex virus capsid: characterization of intermediates observed during cell-free capsid formation. Journal of molecular biology, 263(3), pp.432-446.
211. Newcomb, W.W., Juhas, R.M., Thomsen, D.R., Homa, F.L., Burch, A.D., Weller, S.K. and Brown, J.C., 2001. The UL6 gene product forms the portal for entry of DNA into the herpes simplex virus capsid. Journal of virology, 75(22), pp.10923-10932.
212. Newcomb, W.W., Trus, B.L., Booy, F.P., Steven, A.C., Wall, J.S., and Brown, J.C. 1993. Structure of the herpes simplex virus capsid. Molecular composition of the pentons and the triplexes. J.Mol.Biol., 232, (2) 499-511.
213. Ng, T.I., Ogle, W.O. and Roizman, B., 1998. UL13 protein kinase of herpes simplex virus 1 complexes with glycoprotein E and mediates the phosphorylation of the viral Fc receptor: glycoproteins E and I. Virology, 241(1), pp.37-48.
214. Oh, H.S. and Knipe, D.M., 2015. Proteomic analysis of the herpes simplex virus 1 virion protein 16 transactivator protein in infected cells. Proteomics, 15(12), pp.1957-1967.
215. Okuda-Ashitaka, E., Minami, T., Tsubouchi, S., Kiyonari, H., Iwamatsu, A., Noda, T., Handa, H. and Ito, S., 2012. Identification of Nipsnap1 as a nocistatin-interacting protein involving pain transmission. Journal of Biological Chemistry, 287(13), pp.10403-10413.
216. Olson, J.K. and Grose, C., 1997. Endocytosis and recycling of varicella-zoster virus Fc receptor glycoprotein gE: internalization mediated by a YXXL motif in the cytoplasmic tail. Journal of virology, 71(5), pp.4042-4054.

217. Olson, J.K. and Grose, C., 1998. Complex formation facilitates endocytosis of the varicella-zoster virus gE: gI Fc receptor. Journal of virology, 72(2), pp.1542-1551.
218. Ong, S.E. and Mann, M., 2005. Mass spectrometry–based proteomics turns quantitative. Nature chemical biology, 1(5), p.252.
219. O'Regan, K.J., Bucks, M.A., Murphy, M.A., Wills, J.W. and Courtney, R.J., 2007. A conserved region of the herpes simplex virus type 1 tegument protein VP22 facilitates interaction with the cytoplasmic tail of glycoprotein E (gE). Virology, 358(1), pp.192-200.
220. Owen, D.J., Crump, C.M. and Graham, S.C., 2015. Tegument assembly and secondary envelopment of alphaherpesviruses. Viruses, 7(9), pp.5084-5114.
221. Padula, M.E., Sydnor, M.L. and Wilson, D.W., 2009. Isolation and preliminary characterization of herpes simplex virus 1 primary enveloped virions from the perinuclear space. Journal of virology, 83(10), pp.4757-4765.
222. Paludan, S.R., 2001. Requirements for the induction of interleukin-6 by herpes simplex virus-infected leukocytes. Journal of virology, 75(17), pp.8008-8015.
223. Pangršič, T., Reisinger, E. and Moser, T., 2012. Otoferlin: a multi-C2 domain protein essential for hearing. Trends in neurosciences, 35(11), pp.671-680.
224. Panté, N. and Kann, M., 2002. Nuclear pore complex is able to transport macromolecules with diameters of~ 39 nm. Molecular biology of the cell, 13(2), pp.425-434.
225. Pawliczek, T. and Crump, C.M., 2009. Herpes simplex virus type 1 production requires a functional ESCRT-III complex but is independent of TSG101 and ALIX expression. Journal of virology, 83(21), pp.11254-11264.
226. Perdue, M.L., Cohen, J.C., Randall, C.C., and O'Callaghan, D.J. 1976. Biochemical studies of the maturation of herpesvirus nucleocapsid species. Virology, 74, (1) 194-208.
227. Polcicova, K., Biswas, P.S., Banerjee, K., Wisner, T.W., Rouse, B.T. and Johnson, D.C., 2005. Herpes keratitis in the absence of anterograde transport of virus from sensory ganglia to the cornea. Proceedings of the National Academy of Sciences of the United States of America, 102(32), pp.11462-11467.
228. Polvino-Bodnar, M.., Orberg, P.K. and Schaffer, P.A., 1987. Herpes simplex virus type 1 oriL is not required for virus replication or for the establishment and reactivation of latent infection in mice. Journal of virology, 61(11), pp.3528-3535.
229. Posey, A.D., Pytel, P., Gardikiotes, K., Demonbreun, A.R., Rainey, M., George, M., Band, H. and McNally, E.M., 2011. Endocytic recycling proteins EHD1 and EHD2 interact with fer-1-like-5 (Fer1L5) and mediate myoblast fusion. Journal of Biological Chemistry, 286(9), pp.7379-7388.
230. Posey, A.D., Swanson, K.E., Alvarez, M.G., Krishnan, S., Earley, J.U., Band, H., Pytel, P., McNally, E.M. and Demonbreun, A.R., 2014. EHD1 mediates vesicle trafficking required for normal muscle growth and transverse tubule development. Developmental biology, 387(2), pp.179-190.
231. Powers, L., Wilkinson, K.S. and Ryan, P., 1994. Characterization of the prv43 gene of pseudorabies virus and demonstration that it is not required for virus growth in cell culture. Virology, 199(1), pp.81-88.
232. Radtke, K., Kieneke, D., Wolfstein, A., Michael, K., Steffen, W., Scholz, T., Karger, A. and Sodeik, B., 2010. Plus-and minus-end directed microtubule motors bind simultaneously to herpes simplex virus capsids using different inner tegument structures. PLoS pathogens, 6(7), p.e1000991.

233. Ran, F.A., Hsu, P.D., Wright, J., Agarwala, V., Scott, D.A. and Zhang, F., 2013. Genome engineering using the CRISPR-Cas9 system. Nature protocols, 8(11), p.2281.
234. Read, G.S. and Patterson, M., 2007. Packaging of the virion host shutoff (Vhs) protein of herpes simplex virus: two forms of the Vhs polypeptide are associated with intranuclear B and C capsids, but only one is associated with enveloped virions. Journal of virology, 81(3), pp.1148-1161.
235. Redpath, G.M., Sophocleous, R.A., Turnbull, L., Whitchurch, C.B. and Cooper, S.T., 2016. Ferlins Show Tissue-Specific Expression and Segregate as Plasma Membrane/Late Endosomal or Trans-Golgi/Recycling Ferlins. Traffic, 17(3), pp.245-266.
236. Rémillard-Labrosse, G., Mihai, C., Duron, J., Guay, G. and Lippé, R., 2009. Protein kinase D-dependent trafficking of the large Herpes simplex virus type 1 capsids from the TGN to plasma membrane. Traffic, 10(8), pp.1074-1083.
237. Ren, Y., Bell, S., Zenner, H.L., Lau, S.Y.K. and Crump, C.M., 2012. Glycoprotein M is important for the efficient incorporation of glycoprotein H–L into herpes simplex virus type 1 particles. Journal of general virology, 93(2), pp.319-329.
238. Reynolds, A.E., Liang, L. and Baines, J.D., 2004. Conformational changes in the nuclear lamina induced by herpes simplex virus type 1 require genes UL31 and UL34. Journal of virology, 78(11), pp.5564-5575.
239. Reynolds, A.E., Wills, E.G., Roller, R.J., Ryckman, B.J. and Baines, J.D., 2002. Ultrastructural localization of the herpes simplex virus type 1 UL31, UL34, and US3 proteins suggests specific roles in primary envelopment and egress of nucleocapsids. Journal of virology, 76(17), pp.8939-8952.
240. Richman, D.D., Buckmaster, A., Bell, S., Hodgman, C. and Minson, A.C., 1986. Identification of a new glycoprotein of herpes simplex virus type 1 and genetic mapping of the gene that codes for it. Journal of virology, 57(2), pp.647-655.
241. Rigbolt, K.T., Zarei, M., Sprenger, A., Becker, A.C., Diedrich, B., Huang, X., Eiselein, S., Kristensen, A.R., Gretzmeier, C., Andersen, J.S. and Zi, Z., 2014. Characterization of early autophagy signaling by quantitative phosphoproteomics. Autophagy, 10(2), pp.356-371.
242. Rizo, J. and Südhof, T.C., 1998. C2-domains, structure and function of a universal Ca2+-binding domain. Journal of Biological Chemistry, 273(26), pp.15879-15882.
243. Rizvi, S.M. and Raghavan, M. 2001. An N-terminal domain of herpes simplex virus type Ig E is capable of forming stable complexes with gI. J Virol, 75, (23) 11897-11901.
244. Roberts, K.L. and Baines, J.D., 2010. Myosin Va enhances secretion of herpes simplex virus 1 virions and cell surface expression of viral glycoproteins. Journal of virology, 84(19), pp.9889-9896.
245. Rohrer, J., Schweizer, A., Russell, D. and Kornfeld, S., 1996. The targeting of Lamp1 to lysosomes is dependent on the spacing of its cytoplasmic tail tyrosine sorting motif relative to the membrane. The Journal of cell biology, 132(4), pp.565-576.
246. Roizman B., and Sears A. E., 1996. Herpes simplex viruses and their replication. in Fields virology, eds Fields B. N., Knipe D. M., Howley P. M. (Lippincott-Raven Publishers, Philadelphia, Pa), 3rd ed. 2:2231–2295.
247. Roizman, B., Jacob, R.J., Knipe, D.M., Morse, L.S. and Ruyechan, W.T., 1979, January. On the structure, functional equivalence, and replication of the four arrangements of herpes simplex virus DNA. In Cold Spring Harbor symposia on quantitative biology (Vol. 43, pp. 809-826). Cold Spring Harbor Laboratory Press.
248. Roizman, B., Knipe, D.M. and Whitley, R.J., 2013. Herpes simplex viruses, p 1823–1897. Fields virology, 6th ed. Lippincott Williams & Wilkins, Philadelphia, PA.

249. Roller, R.J., Bjerke, S.L., Haugo, A.C. and Hanson, S., 2010. Analysis of a charge cluster mutation of herpes simplex virus type 1 UL34 and its extragenic suppressor suggests a novel interaction between pUL34 and pUL31 that is necessary for membrane curvature around capsids. Journal of virology, 84(8), pp.3921-3934.
250. Roller, R.J., Zhou, Y., Schnetzer, R., Ferguson, J. and DeSalvo, D., 2000. Herpes simplex virus type 1 UL34 gene product is required for viral envelopment. Journal of Virology, 74(1), pp.117-129.
251. Roop, C., Hutchinson, L., and Johnson, D.C. 1993. A mutant herpes simplex virus type 1 unable to express glycoprotein L cannot enter cells, and its particles lack glycoprotein H. J.Virol., 67, (4) 2285-2297.
252. Roos, W.H., Radtke, K., Kniesmeijer, E., Geertsema, H., Sodeik, B., and Wuite, G.J. 2009. Scaffold expulsion and genome packaging trigger stabilization of herpes simplex virus capsids. Proc.Natl.Acad.Sci.U.S.A, 106, (24) 9673-9678.
253. Ryckman, B.J. and Roller, R.J., 2004. Herpes simplex virus type 1 primary envelopment: UL34 protein modification and the US3-UL34 catalytic relationship. Journal of virology, 78(1), pp.399-412.
254. Saksena, M. M., Boadle, R.A., Aggarwal, A., Tijono, B., Rixon, F.J., Diefenbach, R.J. and Cunningham, A.L., 2009. Herpes simplex virus utilizes the large secretory vesicle pathway for anterograde transport of tegument and envelope proteins and for viral exocytosis from growth cones of human fetal axons. Journal of Virology, 83(7), pp.3187-3199.
255. Saksena, M.M., Boadle, R.A., Diefenbach, R.J. and Cunningham, A.L., 2015. Dual role of HSV-1 pUS9 in virus anterograde axonal transport and final assembly in growth cones in distal axons. Journal of virology, pp.JVI-03023.
256. Saldanha, C.E., Lubinski, J., Martin, C., Nagashunmugam, T., Wang, L., van Der, K.H., Tal-Singer, R., and Friedman, H.M. 2000. Herpes simplex virus type 1 glycoprotein E domains involved in virus spread and disease. J Virol, 74, (15) 6712-6719.
257. Sanchala, D.S., Bhatt, L.K. and Prabhavalkar, K.S., 2017. Oncolytic herpes simplex viral therapy: a stride toward selective targeting of cancer cells. Frontiers in pharmacology, 8, p.270.
258. Savidis, G., Perreira, J.M., Portmann, J.M., Meraner, P., Guo, Z., Green, S. and Brass, A.L., 2016. The IFITMs inhibit Zika virus replication. Cell reports, 15(11), pp.2323-2330.
259. Schoeber, J.P., Topala, C.N., Lee, K.P., Lambers, T.T., Ricard, G., van der Kemp, A.W., Huynen, M.A., Hoenderop, J.G. and Bindels, R.J., 2008. Identification of Nipsnap1 as a novel auxiliary protein inhibiting TRPV6 activity. Pflügers Archiv-European Journal of Physiology, 457(1), pp.91-101.
260. Schrag, J.D., Prasad, B.V., Rixon, F.J., and Chiu, W. 1989. Three-dimensional structure of the HSV1 nucleocapsid. Cell, 56, (4) 651-660.
261. Sciortino, M.T., Taddeo, B., Poon, A.P., Mastino, A., and Roizman, B. 2002. Of the three tegument proteins that package mRNA in herpes simplex virions, one (VP22) transports the mRNA to uninfected cells for expression prior to viral infection. Proc.Natl.Acad.Sci.U.S.A, 99, (12) 8318-8323.
262. Seroussi, E., Pan, H.Q., Kedra, D., Roe, B.A. and Dumanski, J.P., 1998. Characterization of the human Nipsnap1 gene from 22q12: a member of a novel gene family. Gene, 212(1), pp.13-20.
263. Shanmughapriya, S., Rajan, S., Hoffman, N.E., Higgins, A.M., Tomar, D., Nemani, N., Hines, K.J., Smith, D.J., Eguchi, A., Vallem, S. and Shaikh, F., 2015. SPG7 is an essential

and conserved component of the mitochondrial permeability transition pore. Molecular cell, 60(1), pp.47-62.
264. Sheaffer, A.K., Newcomb, W.W., Brown, J.C., Gao, M., Weller, S.K., and Tenney, D.J. 2000. Evidence for controlled incorporation of herpes simplex virus type 1 UL26 protease into capsids. J.Virol., 74, (15) 6838-6848.
265. Sheaffer, A.K., Newcomb, W.W., Gao, M., Yu, D., Weller, S.K., Brown, J.C. and Tenney, D.J., 2001. Herpes simplex virus DNA cleavage and packaging proteins associate with the procapsid prior to its maturation. Journal of virology, 75(2), pp.687-698.
266. Sheldrick, P. and Berthelot, N., 1974, January. Inverted repetitions in the chromosome of herpes simplex virus. In Cold Spring Harbor symposia on quantitative biology (Vol. 39, pp. 667-678). Cold Spring Harbor Laboratory Press.
267. Shukla, D. and Spear, P.G., 2001. Herpesviruses and heparan sulfate: an intimate relationship in aid of viral entry. The Journal of clinical investigation, 108(4), pp.503-510.
268. Shukla, D., Dal Canto, M.C., Rowe, C.L. and Spear, P.G., 2000. Striking similarity of murine nectin-1α to human nectin-1α (HveC) in sequence and activity as a glycoprotein D receptor for alphaherpesvirus entry. Journal of virology, 74(24), pp.11773-11781.
269. Shukla, D., Liu, J., Blaiklock, P., Shworak, N.W., Bai, X., Esko, J.D., Cohen, G.H., Eisenberg, R.J., Rosenberg, R.D. and Spear, P.G., 1999. A novel role for 3-O-sulfated heparan sulfate in herpes simplex virus 1 entry. Cell, 99(1), pp.13-22.
270. Skaliter, R. and Lehman, I.R., 1994. Rolling circle DNA replication in vitro by a complex of herpes simplex virus type 1-encoded enzymes. Proceedings of the National Academy of Sciences, 91(22), pp.10665-10669.
271. Skepper, J.N., Whiteley, A., Browne, H. and Minson, A., 2001. Herpes simplex virus nucleocapsids mature to progeny virions by an envelopment→ deenvelopment→ reenvelopment pathway. Journal of virology, 75(12), pp.5697-5702.
272. Smith, K.O., 1964. Relationship between the envelope and the infectivity of herpes simplex virus. Proceedings of the Society for Experimental Biology and Medicine, 115(3), pp.814-816.
273. Smith, S.E., Gibson, M.S., Wash, R.S., Ferrara, F., Wright, E., Temperton, N., Kellam, P. and Fife, M., 2013. Chicken interferon-inducible transmembrane protein 3 restricts influenza viruses and lyssaviruses in vitro. Journal of virology, 87(23), pp.12957-12966.
274. Snyder, A., Polcicova, K. and Johnson, D.C., 2008. Herpes simplex virus gE/gI and US9 proteins promote transport of both capsids and virion glycoproteins in neuronal axons. Journal of virology, 82(21), pp.10613-10624.
275. Sodeik, B., Ebersold, M.W. and Helenius, A., 1997. Microtubule-mediated transport of incoming herpes simplex virus 1 capsids to the nucleus. The Journal of cell biology, 136(5), pp.1007-1021.
276. Spear, P.G. and Longnecker, R., 2003. Herpesvirus entry: an update. Journal of virology, 77(19), pp.10179-10185.
277. Spear, P.G., 1993. Membrane fusion induced by herpes simplex virus. Viral fusion mechanisms. CRC Press, Inc., Boca Raton, Fla, pp.201-232.
278. Sprague, E.R., Martin, W.L., and Bjorkman, P.J. 2004. pH dependence and stoichiometry of binding to the Fc region of IgG by the herpes simplex virus Fc receptor gE-gI. J Biol.Chem., 279, (14) 14184-14193.
279. Sprague, E.R., Wang, C., Baker, D. and Bjorkman, P.J., 2006. Crystal structure of the HSV-1 Fc receptor bound to Fc reveals a mechanism for antibody bipolar bridging. PLoS biology, 4(6), p.e148.

280. Stannard, L.M., Himmelhoch, S. and Wynchank, S., 1996. Intra-nuclear localization of two envelope proteins, gB and gD, of herpes simplex virus. Archives of virology, 141(3-4), pp.505-524.
281. Starkey, J.L., Han, J., Chadha, P., Marsh, J.A. and Wills, J.W., 2014. Elucidation of the block to herpes simplex virus egress in the absence of tegument protein UL16 reveals a novel interaction with VP22. Journal of virology, 88(1), pp.110-119.
282. Stegen, C., Yakova, Y., Henaff, D., Nadjar, J., Duron, J., and Lippe, R. 2013. Analysis of virion-incorporated host proteins required for herpes simplex virus type 1 infection through a RNA interference screen. PLoS.One., 8, (1) e53276.
283. Stenmark, H., 2009. Rab GTPases as coordinators of vesicle traffic. Nature reviews Molecular cell biology, 10(8), p.513.
284. Stoorvogel, W., Kleijmeer, M.J., Geuze, H.J. and Raposo, G., 2002. The biogenesis and functions of exosomes. Traffic, 3(5), pp.321-330.
285. Strauss, J.H., and Strauss, E.G., 2008. Chapter 7 – DNA-containing viruses. In Viruses and Human Disease, J.H. Strauss, and E.G. Strauss, eds. (London: Academic Press), pp. 261-323.
286. Striebinger, H., Funk, C., Raschbichler, V. and Bailer, S.M., 2016. Subcellular trafficking and functional relationship of the HSV-1 glycoproteins N and M. Viruses, 8(3), p.83.
287. Stylianou, J., Maringer, K., Cook, R., Bernard, E. and Elliott, G., 2009. Virion incorporation of the herpes simplex virus type 1 tegument protein VP22 occurs via glycoprotein E-specific recruitment to the late secretory pathway. Journal of virology, 83(10), pp.5204-5218.
288. Sullivan, V. and Smith, G.L., 1988. The herpes simplex virus type 1 US7 gene product is a 66K glycoprotein and is a target for complement-dependent virus neutralization. Journal of general virology, 69(4), pp.859-867.
289. Svobodova, S., Bell, S. and Crump, C.M., 2011. Analysis of the interaction between the essential HSV-1 tegument proteins VP16 and VP1/2. Journal of virology, pp.JVI-05981.
290. Szilagyi, J.F. and Cunningham, C., 1991. Identification and characterization of a novel non-infectious herpes simplex virus-related particle. Journal of general virology, 72(3), pp.661-668.
291. Taddeo, B. and Roizman, B. 2006. The virion host shutoff protein (UL41) of herpes simplex virus 1 is an endoribonuclease with a substrate specificity similar to that of RNase A. J.Virol., 80, (18) 9341-9345.
292. Taddeo, B., Sciortino, M.T., Zhang, W. and Roizman, B., 2007. Interaction of herpes simplex virus RNase with VP16 and VP22 is required for the accumulation of the protein but not for accumulation of mRNA. Proceedings of the National Academy of Sciences, 104(29), pp.12163-12168.
293. Tanaka, M., Sata, T. and Kawaguchi, Y., 2008. The product of the Herpes simplex virus 1 UL7 gene interacts with a mitochondrial protein, adenine nucleotide translocator 2. Virology journal, 5(1), p.125.
294. Tatman, J.D., Preston, V.G., Nicholson, P., Elliott, R.M. and Rixon, F.J., 1994. Assembly of herpes simplex virus type 1 capsids using a panel of recombinant baculoviruses. Journal of General Virology, 75(5), pp.1101-1113.
295. Therrien, C., Di Fulvio, S., Pickles, S. and Sinnreich, M., 2009. Characterization of lipid binding specificities of dysferlin C2 domains reveals novel interactions with phosphoinositides. Biochemistry, 48(11), pp.2377-2384.
296. Tirabassi, R.S. and Enquist, L.W., 2000. Role of the pseudorabies virus gI cytoplasmic domain in neuroinvasion, virulence, and posttranslational N-linked glycosylation. Journal of virology, 74(8), pp.3505-3516.

297. Tischer, B.K., Smith, G.A. and Osterrieder, N., 2010. En passant mutagenesis: a two step markerless red recombination system. In In vitro mutagenesis protocols (pp. 421-430). Humana Press, Totowa, NJ.
298. Tokarev, A.A., Alfonso, A. and Segev, N., 2009. Overview of intracellular compartments and trafficking pathways. In Trafficking Inside Cells (pp. 3-14). Springer, New York, NY.
299. Torrisi, M.R., Di Lazzaro, C., Pavan, A., Pereira, L. and Campadelli-Fiume, G., 1992. Herpes simplex virus envelopment and maturation studied by fracture label. Journal of virology, 66(1), pp.554-561.
300. Tran, L.C., Kissner, J.M., Westerman, L.E. and Sears, A.E., 2000. A herpes simplex virus 1 recombinant lacking the glycoprotein G coding sequences is defective in entry through apical surfaces of polarized epithelial cells in culture and in vivo. Proceedings of the National Academy of Sciences, 97(4), pp.1818-1822.
301. Tummala, H., Li, X. and Homayouni, R., 2010. Interaction of a novel mitochondrial protein, 4-nitrophenylphosphatase domain and non-neuronal SNAP25-like protein homolog 1 (Nipsnap1), with the amyloid precursor protein family. European Journal of Neuroscience, 31(11), pp.1926-1934.
302. Turtoi, A., Blomme, A., Bellahcene, A., Gilles, C., Hennequière, V., Peixoto, P., Bianchi, E., Noel, A., De Pauw, E., Lifrange, E. and Delvenne, P., 2013. Myoferlin is a key regulator of EGFR activity in breast cancer. Cancer research, 73(17), pp.5438-5448.
303. van Genderen, I.L., Brandimarti, R., Torrisi, M.R., Campadelli, G., and van, M.G. 1994. The phospholipid composition of extracellular herpes simplex virions differs from that of host cell nuclei. Virology, 200, (2) 831-836.
304. Vanlandingham, P.A. and Ceresa, B.P., 2009. Rab7 regulates late endocytic trafficking downstream of multivesicular body biogenesis and cargo sequestration. Journal of Biological Chemistry, 284(18), pp.12110-12124.
305. Viejo-Borbolla, A., Martinez-Martín, N., Nel, H.J., Rueda, P., Martín, R., Blanco, S., Arenzana-Seisdedos, F., Thelen, M., Fallon, P.G. and Alcamí, A., 2012. Enhancement of chemokine function as an immunomodulatory strategy employed by human herpesviruses. PLoS pathogens, 8(2), p.e1002497.
306. Wan, L., Molloy, S.S., Thomas, L., Liu, G., Xiang, Y., Rybak, S.L. and Thomas, G., 1998. PACS-1 defines a novel gene family of cytosolic sorting proteins required for *trans*-Golgi network localization. Cell, 94(2), pp.205-216.
307. Wang, X.Y., Smith, D.I., Liu, W. and James, C.D., 1998. GBAS, a Novel Gene Encoding a Protein with Tyrosine Phosphorylation Sites and a Transmembrane Domain, Is Co-amplified withEGFR. Genomics, 49(3), pp.448-451.
308. Watson, D.H., Russell, W.C. and Wildy, P., 1963. Electron microscopic particle counts on herpes virus using the phosphotungstate negative staining technique. Virology, 19(3), pp.250-260.
309. Wehland, J., Willingham, M.C. and Sandoval, I.V., 1983. A rat monoclonal antibody reacting specifically with the tyrosylated form of alpha-tubulin. I. Biochemical characterization, effects on microtubule polymerization in vitro, and microtubule polymerization and organization in vivo. The Journal of cell biology, 97(5), pp.1467-1475.
310. Weller, S.K. and Coen, D.M., 2012. Herpes simplex viruses: mechanisms of DNA replication. Cold Spring Harbor perspectives in biology, 4(9), p.a013011.
311. Weston, S., Czieso, S., White, I.J., Smith, S.E., Kellam, P. and Marsh, M., 2014. A membrane topology model for human interferon inducible transmembrane protein 1. PloS one, 9(8), p.e104341.
312. Wilkinson, D. and Weller, S., 2003. The role of DNA recombination in herpes simplex virus DNA replication. IUBMB life, 55(8), pp.451-458.

313. Wills, E., Mou, F. and Baines, J.D., 2009. The UL31 and UL34 gene products of herpes simplex virus 1 are required for optimal localization of viral glycoproteins D and M to the inner nuclear membranes of infected cells. Journal of virology, 83(10), pp.4800-4809.
314. Wisner, T., Brunetti, C., Dingwell, K. and Johnson, D.C., 2000. The extracellular domain of herpes simplex virus gE is sufficient for accumulation at cell junctions but not for cell-to-cell spread. Journal of virology, 74(5), pp.2278-2287.
315. Wisner, T.W. and Johnson, D.C., 2004. Redistribution of cellular and herpes simplex virus proteins from the *trans*-Golgi network to cell junctions without enveloped capsids. Journal of virology, 78(21), pp.11519-11535.
316. Wisner, T.W., Wright, C.C., Kato, A., Kawaguchi, Y., Mou, F., Baines, J.D., Roller, R.J. and Johnson, D.C., 2009. Herpesvirus gB-induced fusion between the virion envelope and outer nuclear membrane during virus egress is regulated by the viral US3 kinase. Journal of virology, 83(7), pp.3115-3126.
317. Wittels, M. and Spear, P.G., 1991. Penetration of cells by herpes simplex virus does not require a low pH-dependent endocytic pathway. Virus research, 18(2-3), pp.271-290.
318. Xie, M., Xuan, B., Shan, J., Pan, D., Sun, Y., Shan, Z., Zhang, J., Yu, D., Li, B. and Qian, Z., 2015. Human cytomegalovirus exploits interferon-induced transmembrane proteins to facilitate morphogenesis of the virion assembly compartment. Journal of virology, 89(6), pp.3049-3061.
319. Yamamoto, S., Ogasawara, N., Yamamoto, K., Uemura, C., Takaya, Y., Shiraishi, T., Sato, T., Hashimoto, S., Tsutsumi, H., Takano, K. and Himi, T., 2017 (a). Mitochondrial proteins NIP-SNAP-1 and-2 are a target for the immunomodulatory activity of clarithromycin, which involves NF-κB-mediated cytokine production. Biochemical and biophysical research communications, 483(3), pp.911-916.
320. Yamamoto, S., Okamoto, T., Ogasawara, N., Hashimoto, S., Shiraishi, T., Sato, T., Yamamoto, K., Tsutsumi, H., Takano, K., Himi, T. and Itoh, H., 2017 (b). NIP-SNAP-1 and-2 mitochondrial proteins are maintained by heat shock protein 60. Biochemical and biophysical research communications, 483(3), pp.917-922.
321. Yang, K. and Baines, J.D., 2011. Selection of HSV capsids for envelopment involves interaction between capsid surface components pUL31, pUL17, and pUL25. Proceedings of the National Academy of Sciences, 108(34), pp.14276-14281.
322. Yang, K., Wills, E., Lim, H.Y., Zhou, Z.H. and Baines, J.D., 2014. Association of herpes simplex virus pUL31 with capsid vertices and components of the capsid vertex-specific complex. Journal of virology, 88(7), pp.3815-3825.
323. Ye, G.J. and Roizman, B., 2000. The essential protein encoded by the UL31 gene of herpes simplex virus 1 depends for its stability on the presence of UL34 protein. Proceedings of the National Academy of Sciences, 97(20), pp.11002-11007.
324. Yeh, P.C., Han, J., Chadha, P., Meckes, D.G., Ward, M.D., Semmes, O.J. and Wills, J.W., 2011. Direct and specific binding of the UL16 tegument protein of herpes simplex virus to the cytoplasmic tail of glycoprotein E. Journal of virology, 85(18), pp.9425-9436.
325. Yeh, P.C., Meckes, D.G. and Wills, J.W., 2008. Analysis of the interaction between the UL11 and UL16 tegument proteins of herpes simplex virus. Journal of virology, 82(21), pp.10693-10700.
326. Yount, J.S., Moltedo, B., Yang, Y.Y., Charron, G., Moran, T.M., López, C.B. and Hang, H.C., 2010. Palmitoylome profiling reveals S-palmitoylation–dependent antiviral activity of IFITM3. Nature chemical biology, 6(8), p.610.
327. Zeev-Ben-Mordehai, T., Weberruß, M., Lorenz, M., Cheleski, J., Hellberg, T., Whittle, C., El Omari, K., Vasishtan, D., Dent, K.C., Harlos, K. and Franzke, K., 2015. Crystal structure of the herpesvirus nuclear egress complex provides insights into inner nuclear membrane remodeling. Cell reports, 13(12), pp.2645-2652.

328. Zenner, H.L., Yoshimura, S.I., Barr, F.A. and Crump, C.M., 2011. Analysis of Rab GTPase-activating proteins indicates that Rab1a/b and Rab43 are important for HSV-1 secondary envelopment. Journal of virology, pp.JVI-00500.
329. Zhou, G., Avitabile, E., Campadelli-Fiume, G. and Roizman, B., 2003. The domains of glycoprotein D required to block apoptosis induced by herpes simplex virus 1 are largely distinct from those involved in cell-cell fusion and binding to nectin1. Journal of virology, 77(6), pp.3759-3767.
330. Zhu, H. and Liu, C., 2003. Interleukin-1 inhibits hepatitis C virus subgenomic RNA replication by activation of extracellular regulated kinase pathway. Journal of virology, 77(9), pp.5493-5498.
331. Zhu, Q. and Courtney, R.J., 1994. Chemical cross-linking of virion envelope and tegument proteins of herpes simplex virus type 1. Virology, 204(2), pp.590-599.